

**ELECTROCHEMICALLY CONTROLLED ATOM
TRANSFER RADICAL POLYMERIZATION AND
SYNTHESIS OF POLYMERS WITH COMPLEX
ARCHITECTURES**

Sangwoo Park

Carnegie Mellon University

Department of Chemistry

June 2016

in partial fulfillment of the requirements for a Ph.D. in Chemistry

ABSTRACT

Atom transfer radical polymerization (ATRP) is one of the most broadly applied reversible deactivation radical polymerization (RDRP) technique that provide well-defined polymers with predetermined molecular weight (MW) and narrow molecular weight distribution (MWD). The functional polymers synthesized by ATRP showed a potential promise in the fields of biomedical applications such as smart drug delivery, tissue engineering, and diagnostic sensors. In general, conventional ATRP requires a large amount of transition metal catalysts (> 1000 parts per million (ppm) versus molar ratio of monomers) and removal of the residual catalysts is necessary for use of advanced materials in bio-applications. The advent of catalysts (re)generation from the oxidized transition metal/ligand catalysts allows for the use of ppm level of catalysts in an ATRP, and offers more environmentally benign and industrially favorable reaction conditions for the synthesis of polymers. This work mainly explores electrochemically controlled atom transfer radical polymerization (*e*ATRP) with diminished catalysts conditions as one of many catalysts regeneration ATRP systems being examined in the past decade.

This dissertation is composed of nine chapters. Chapter I reviews recent progress in electrochemically controlled chemical reaction and polymerization. Chapter II provides an in-depth study of *e*ATRP and serves as a basis for the discussions in Chapter III on developing a simplified *e*ATRP reaction (*se*ATRP). Chapters II and III cover six appendices, which include related collaborations, explanations on catalysts development and characterization, polymerization mechanism, and evaluation of new polymerization procedures. Chapter IV and V address related aqueous *e*ATRP techniques. Chapter IV

details optimization of polymerization conditions for acrylamides and minimization of side reactions. Chapter V explores miniemulsion polymerization of *n*-butyl acrylate which requires optimization of aqueous-organic phase catalyst communication. Chapter VI addresses development of electrochemically mediated reversible addition-fragmentation chain transfer (*e*RAFT) polymerization of methyl methacrylate. Chapters VII to IX discuss the synthesis of copolymers with complex polymeric architectures, *i.e.*, star polymers. Specifically in Chapter VII procedures for achieving high yield for the synthesis of stars by combining arm-first methods and *e*ATRP to reduce initial intermolecular termination reactions. Chapter VII also contains an appendix on star synthesis by the core-first method via *e*ATRP. Chapter VIII and IX elucidate applications of the functional star polymers. In Chapter VIII, the preparation and application of light induced crosslinkable star polymers in surface patterning are discussed and extended to biomedical applications. Lastly, Chapter IX encompasses temperature responsive surfaces, that were prepared by star polymers upon UV irradiation, as smart cell cultivate substrates.

ACKNOWLEDGEMENTS

First and foremost, I would like to express my deep gratitude to my advisor, Professor Krzysztof (Kris) Matyjaszewski. His encouragement to continue doctoral studies in the field of polymer chemistry when I was a visiting student at the Matyjaszewski Lab has given me the opportunities to hone my research skills and develop an interest in the area that I could pursue for life.

I would also like to thank my committee members, Professors Newell Washburn and Christopher (Chris) Bettinger, for supporting my studies during the Ph. D. program. In addition, I would like to thank my committee members, Professor Kevin Noonan, and Professor Tomislav Pintauer for sharing their time to review my work and provide constructive feedback. My gratitude goes to Dr. Rea Freeland and Valerie Bridge for their help and accommodations throughout the program. I am grateful to Professor Hyun-jong Paik, my advisor from Pusan National University (PNU), for his continued support and valuable ideas.

None of the research included in this dissertation would have been possible without the help of my former and present group members. In particular, I would like to thank Dr. Yungwan Kwak, Dr. Jeong Ae Yoon, Dr. Mingjiang Zhong, and Dr. Valerie Williams for their well-thought discussions. I would also like to show appreciation to Dr. Wojtek Jakubowski, Dr. Renaud Nicolay, Dr. Patricia Golas, Dr. Andrea Elsen, Dr. Saadyah Averick, Dr. Joanna Burdyńska, Dr. Antonina Simakova, Dr. Andrew Magenau, Dr. Melissa Lamson, Dr. Antoine Beziau, Dr. Hangjun Ding, Dr. Maciek Kopec, Dr. Ryan Fanyves, Pawel Kryszewski, and Yi Wang for their help and friendship. I am especially thankful

to Dr. James (Jim) Spanswick, for numerous reviews and corrections he has done for all my paper drafts without any hesitance. I would also like to thank Dr. Hong Cho who was always willing to share his invaluable time on the discussions for my research.

Last but not least, I would like to thank my family who has always been the source of inspirations. I am forever indebted to Kihyun Park and Youngsook Choi, my parents, Youngmi Choi, my aunt, Gaesung Kim, my grandmother, Yunwon Hwang and Inkyung Yoon, my parents-in-law, Jimin Hwang, my brother-in-law, and Carolyn Heil, my aunt and the closest neighbor. I am thankful to my wife, Seyeon Hwang who has supported me in every way possible. Without her devotion and patience, this journey would have never ended. I dedicate this dissertation to my wife.

TABLE OF CONTENTS

LIST OF ABBREVIATIONS.....	x
LIST OF SCHEMES.....	xviii
LIST OF TABLES.....	xxi
LIST OF FIGURES	xxiii
Chapter I Recent Progress in Electrochemically Mediated Polymerization and Controlled Reaction	2
I. 1. Introduction	2
I. 2. Progress on ATRP: Conventional to low catalysts loading ATRP	6
I. 3. Development of <i>e</i> ATRP	16
I. 4. Architectural control by <i>e</i> ATRP.....	19
I. 5. Electrochemically controlled reaction for surface modification to form a biosensor, and a conducting elastomer	29
I. 6. Summary.....	36
I. 7. Thesis goal	37
I. 8. References	39
Chapter II Investigation of Electrochemically Mediated Atom Transfer Radical*	2
II. 1. Preface.....	2
II. 2. Introduction	6
II. 3. Results and discussion.....	9
II. 4. Summary	28
II. 5. Experimental section.....	29
II. 6. References	31
Chapter III Simplified Electrochemically Mediated Atom Transfer Radical Polymerization using Sacrificial Counter Electrode*	34
III. 1. Preface	34
III. 2. Introduction.....	36
III. 3. Results and Discussion	38
III. 4. Summary	50
III. 5. Experimental section.....	51
III. 6. References.....	56
Chapter IV Electrochemically Mediated ATRP of Acrylamides in Water*	58
IV. 1. Preface	58
IV. 2. Introduction.....	60
IV. 3. Results and Discussion	63
IV. 4. Summary.....	76
IV. 5. Experimental Section.....	77
IV. 6. References.....	80
Chapter V Miniemulsion Polymerization of n-Butyl Acrylate by Electrochemically Mediated Atom Transfer Radical Polymerization*	84
V. 1. Preface.....	84
V. 2. Introduction.....	86
V. 3. Results and discussion	89

V. 4. Summary	103
V. 5. Experimental section.....	104
V. 6. References.....	109
Chapter VI Electrochemically Mediated Reversible Addition-Fragmentation Chain Transfer Polymerization of Methyl Methacrylate*	113
VI. 1. Preface	113
VI. 2. Introduction.....	115
VI. 3. Results and Discussion	117
VI. 4. Summary	147
VI. 5. Experimental Section.....	147
VI. 6. References.....	150
Chapter VII Star Synthesis Using Macroinitiators <i>via</i> Electrochemically Mediated Atom Transfer Radical Polymerization*	153
VII. 1. Preface	153
VII. 2. Introduction	156
VII. 3. Results and Discussion.....	158
VII. 4. Summary	172
VII. 5. Experimental Section	172
VII. 6. References	175
Chapter VIII Modification of the Surface of Silicon Wafers with Temperature Responsive Crosslinkable Poly((Oligo Ethylene Oxide) Methacrylate) Based Star Polymers*	177
VIII. 1. Preface.....	177
VIII. 2. Introduction.....	179
VIII. 3. Results and Discussion.....	181
VIII. 4. Summary	192
VIII. 5. Experimental Section	192
VIII. 6. References	196
Chapter IX Photo-cross-linkable Thermoresponsive Star Polymers Designed for Control of Cell-Surface Interactions*	198
IX. 1. Preface	198
IX. 2. Introduction.....	201
IX. 3. Results and Discussion	203
IX. 4. Summary	216
IX. 5. Experimental Section.....	217
IX. 6. References.....	222
Chapter X Summary and Outlook	226
Appendix I Active Ligands for Low PPM Miniemulsion Atom Transfer Radical Polymerizations*	232
A-I. 1. Introduction	232
A-I. 2. Results and Discussion.....	236
A-I. 3. Summary	247
A-I. 4. Experimental Section	248
A-I. 5. References	252
Appendix II ARGET ATRP in Miniemulsion with 50 PPM of Copper Catalyst*.....	254

A-II. 1. Introduction.....	254
A-II. 2. Results and Discussion.....	256
A-II. 3. Summary	262
A-II. 4. Experimental Section	262
A-II. 5. References	267
Appendix III Initiators for Continuous Activator Regeneration Atom Transfer Radical Polymerization of Methyl Methacrylate and Styrene with <i>N</i> -Heterocyclic Carbene as Ligands for Fe-Based Catalysts*	269
A-III. 1. Introduction.....	269
A-III. 2. Results and Discussion	270
A-III. 3. Summary	279
A-III. 4. Experimental Section.....	279
A-III. 5. References.....	281
Appendix IV Bioinspired Fe-Based Catalyst for Atom Transfer Radical Polymerization*	284
A-IV. 1. Introduction	284
A-IV. 2. Results and Discussion	287
A-IV. 3. Summary.....	299
A-IV. 4. Experimental Section.....	300
A-IV. 5. References	303
Appendix V Reversible-Deactivation Radical Polymerization in the Presence of Metallic Copper. Activation of Alkyl Halides by Cu ⁰ *	305
A-V. 1. Introduction.....	305
A-V. 2. Results and Discussion	310
A-V. 3. Summary.....	344
A-V. 4. Experimental Section.....	345
A-V. 5. References.....	351
Appendix VI A Silver Bullet: Elemental Silver as an Efficient Reducing Agent for Atom Transfer Radical Polymerization of Acrylates*	354
A-VI. 1. Introduction	354
A-VI. 2. Results and Discussion	356
A-VI. 3. Summary.....	367
A-VI. 4. Experimental Section.....	368
A-VI. 5. References	376
Appendix VII Synthesis of β -cyclodextrin-based star polymers <i>via</i> a simplified electrochemically mediated ATRP*	379
A-VII. 1. Introduction	379
A-VII. 2. Results and Discussion.....	382
A-VII. 3. Summary	407
A-VII. 4. Experimental Section	408
A-VII. 5. References	415
Appendix VIII Phototunable Supersoft Elastomers using Coumarin Functionalized Molecular Bottlebrushes for Cell-Surface Interactions Study*	419
A-VIII. 1. Introduction.....	419
A-VIII. 2. Results and Discussion	420

A-VIII. 3. Summary	439
A-VIII. 4. Experimental Section	439
A-VIII. 5. References	444

LIST OF ABBREVIATIONS

<i>A</i>	surface area (cm ²)
AA	L-ascorbic acid (or Asc. A)
AAm	acrylamide
AFM	atomic force microscopy
Ag	silver
AGET	activators generated by electron transfer
AIBN	2,2'-azobis(2-methylpropionitrile)
Al	aluminum
Al ₂ O ₃	aluminum oxide
ARGET	activators regenerated by electron transfer
ATR-IR	attenuated total reflectance infrared spectroscopy
ATRP	atom transfer radical polymerization
BA	<i>n</i> -butyl acrylate
BBDA	4-bromobenzyl diazonium
BMA	<i>n</i> -butyl methacrylate
BPE	bipolar electrode
BPED	<i>N,N'</i> -dimethyl- <i>N,N'</i> -bis(2-pyridylmethyl)ethane-1,2-diamine
BPMEA	<i>N,N</i> -bis(2-pyridylmethyl)-2-hydroxyethylamine
BPMODA	bis(2-pyridylmethyl)-octadecylamine
BPMODA *	bis[2-(4-methoxy-3,5-dimethyl)pyridylmethyl]octadecylamine
BPPMA	<i>N,N</i> -bis(2-pyridinylmethyl)-1-propanamine
BPO	benzoyl peroxide
bpy	2,2'-bipyridine
BriBBBr	2-bromoisobutryl bromide
Brij 98	polyoxyethylene(20) oleyl ether
Bzp	benzophenone
C ₁₈	octadecyl

CA	chronoamperometry
CDCl ₃	chloroform-d
CE	counter electrode or current efficiency
CEC	click electrochemistry
CF	carbon fiber
CoPc	cobalt phthalocyanine
CP	chronopotentiometry
CPPA	4-cyano-4-(phenylcarbonothioylthio)pentanoic acid
CRP	controlled/living radical polymerization
CTA	chain-transfer agent
Cu	copper
CuAAC	Cu-catalyzed azide–alkyne cycloaddition
CuBr	copper(I) bromide
CuBr ₂	copper (II) bromide
CuCl ₂	copper(II) chloride
CuDC ₂	copper (II) diethyldithiocarbamate
CuOTf ₂	copper(II) trifluoromethanesulfonate
CV	cyclic voltammetry
<i>D</i>	diffusion coefficient
D ₂ O	deuterium oxide
DC	dithiocarbamate
DCM	dichloromethane
DLS	dynamic light scattering
DMA	dynamical mechanical analysis
DMAP	4-dimethylaminopyridine
DMEM	Dulbecco's Modified Eagle Medium
DMF	dimethylformamide
DMSO	dimethyl sulfoxide
dNbpy	4,4'-dinonyl-2,2'-bipyridine
DOD-	<i>N',N''</i> -dioctadecyl- <i>N',N''</i> -bis(2-pyridylmethyl)ethane-1,2-diamine

BPED	
DOD-	<i>N',N''</i> -dioctadecyl- <i>N',N''</i> -bis[2-(4-methoxy-3,5-dimethyl)pyridylmethyl]
BPED*	ethane-1,2-diamine
DP	degree of polymerization
DVB	divinylbenzene
<i>E</i>	potential (V)
<i>E</i> _{1/2}	half of the sum of anodic and cathodic peak potential values ($E_{1/2} = (E_{pa} + E_{pc})/2$)
<i>E</i> _{app}	applied potential
<i>e</i> ATRP	electrochemically mediated atom transfer radical polymerization
EBiB	ethyl α -bromoisobutyrate
EBP	ethyl 2-bromopropionate
EBPA	ethyl- α -bromophenylacetate
<i>EC'</i>	electrochemical catalytic process
ECM	extracellular matrix
EDC·HCl	<i>N</i> -(3-dimethylaminopropyl)- <i>N</i> -(ethylcarbodiimide hydrochloride)
EDG	electron donating group
EDGA	ethylene glycol diacrylate
EGDMA	ethylene glycol dimethacrylate
<i>E</i> ^o	standard potential
<i>E</i> _{pa}	anodic peak potential
<i>E</i> _{pc}	cathodic peak potential
eq	equation
ET	electron transfer
<i>F</i>	Faraday's constant (96485 C/mol)
FBS	fetal bovine serum
Fe	iron
FeSalen	<i>N,N'</i> -bis(3,5-di- <i>tert</i> -butylsalicylidene)-1,2-ethyldiimine
FT-IR	Fourier transform infrared spectroscopy
<i>G'</i>	storage modulus

G''	loss modulus
GC	glassy carbon or gas chromatography
GMA	glycidyl methacrylate
G°	Gibbs free energy
GPC	gel permeation chromatography
Gr	graphite rod
H ₂ SO ₄	sulfuric acid
Hb	hemoglobin
HCl	hydrogen chloride
HD	hexadecane
HEBiB	2-hydroxyethyl-2-bromoisobutyrate
HEMA	2-hydroxyethyl methacrylate
HEMA-TMS	2-(trimethylsilyloxy)ethyl methacrylate
HIDipp	1,3-bis(2,6-di- <i>i</i> -propylphenyl)imidazolidin-2-ylidene
HPLC	high-performance liquid chromatography
HRP	horseradish peroxidase
I	(electrical) current (A)
I	initiator
ICAR	initiators for continuous activator regeneration
ICP-MS	inductively coupled plasma–mass spectrometry
IDA	iminodiacetic acid
IDipp	1,3-bis(2,6-di- <i>i</i> -propylphenyl)imidazol-2-ylidene
ISSET	inner sphere electron transfer
k_a	activation rate constant
K_{ATRP}	ATRP equilibrium constant ($= k_a/k_{\text{da}}$)
KBr	potassium bromide
k_{da}	deactivation rate constant
k_p	propagation rate constant
k_p^{app}	apparent propagation rate constant

k_{red}	reduction rate constant
k_t	termination rate constant
K_X	halidophilicity
L	ligand
l	length (cm)
LCST	lower critical solution temperature
LiAlH_4	lithium aluminum hydride
LSV	linear sweep voltammogram
M	molar concentration (mol/L)
MA	methyl acrylate
MALLS	multi angle laser light scattering
MANDC	1-cyano-1-methylethyldiethyl dithiocarbamate
MBrP	methyl 2-bromopropionate
Me_6TREN	tris(2-(dimethylamino)ethyl)amine
MeCN	acetonitrile
MEO_2MA	2-(2-methoxyethoxy)ethyl methacrylate
METAC	2-(methacryloyloxy)ethyl trimethylammonium chloride
MgSO_4	magnesium sulfate anhydrous
MI	macroinitiator
MMA	methyl methacrylate
M_n	number average molecular weight
$M_{n,\text{GPC}}$	number average molecular weight by GPC
$M_{n,\text{th}}$	theoretical number average molecular weight
MW	molecular weight
M_w	weight average molecular weight
MWD	molecular weight distribution ($= M_w/M_n$ or D)
N_2	nitrogen
NaBr	sodium bromide
NaCl	sodium chloride
NaHCO_3	sodium bicarbonate

NaOH	sodium hydroxide
NHC	<i>N</i> -heterocyclic carbene
NMP	nitroxide mediated polymerization
NMR	nuclear magnetic resonance spectroscopy
OEOA	oligo(ethylene oxide) monomethyl ether acrylate
OEOMA	oligo(ethylene oxide) monomethyl ether methacrylate
OMRP	organometallic mediated radical polymerization
OSET	outer sphere electron transfer
<i>p</i>	conversion
p/s	penicillin/streptomycin
PANI	polyaniline
PBA	poly(<i>n</i> -butyl acrylate)
PBS	phosphate buffer saline
PEDOT	poly(3,4-ethylenedioxythiophene)
PEDOT- N ₃	poly(3,4-(1-azidomethylethylene) dioxothiophene)
PEG-BPA	poly(ethylene glycol) bromophenyl acetate
PEG-iBBr	poly(ethylene oxide) isobutyryl bromide
PEO	poly(ethylene oxide)
PGMA	poly(glycidyl methacrylate)
PHEMA	poly(2-hydroxyethyl methacrylate)
PMA	poly(methyl acrylate)
PMDETA	<i>N,N,N',N',N''</i> -pentamethyldiethylenetriamine
PMETAC	poly(2-(methacryloyloxy)ethyl trimethylammonium chloride)
PMMA	poly(methyl methacrylate)
PNIPAAm	<i>N</i> -isopropylacrylamide
POEOMA	poly(oligo(ethylene oxide) monomethyl ether methacrylate)
ppm	parts per million
PRE	persistent radical effect
PSBMA	poly(sulfobetaine methacrylate)

PSPMA	poly(potassium 3-sulfopropyl methacrylate)
Pt	Platinum
PtBA	poly(<i>tert</i> -butyl acrylate)
Py-HCl	2-(chloromethyl)pyridine hydrochloride
Py-HCl*	2-chloromethyl-4-methoxy-3,5-dimethylpyridine hydrochloride
Q	total passed charge (C)
RAFT	reversible addition-fragmentation chain transfer
RDE	rotating disk electrode
RDRP	reversible deactivation radical polymerization
RE	reference electrode
RI	refractive index
ROMP	ring-opening metathesis polymerization
R_p	rate of polymerization
R-X	alkyl halide
S	surface area (cm ²)
SARA	supplemental activator and reducing agent
SBMA	sulfobetaine methacrylate
SCE	saturated-calomel electrode
SDS	sodium dodecyl sulfate
<i>se</i> ATRP	simplified electrochemically mediated atom transfer radical polymerization
SECM	scanning electrochemical microscopy
SEM	scanning electron microscope
SET-LRP	single electron transfer living radical polymerization
SFRP	stable free radical polymerization
Si	silicon
SI-ATRP	surface initiated atom transfer radical polymerization
SI- <i>e</i> ATRP	surface initiated electrochemically mediated atom transfer radical polymerization
Sn ^{II} (EH) ₂	tin(II) 2-ethylhexanoate

SPMA	potassium 3-sulfopropyl methacrylate
Sty	styrene
T	temperature
t	time
t BA	<i>tert</i> -butyl acrylate
TBABF ₄	tetrabutylammonium tetrafluoroborate
TBABr	tetrabutylammonium bromide
TBACl	tetrabutylammonium chloride
TBAClO ₄	tetrabutylammonium perchlorate
TBAPF ₆	tetrabutylammonium hexafluorophosphate
T_c	critical temperature
TEA	triethylamine
TEABr	tetraethylammonium bromide
TEMPO	2,2,6,6-tetramethylpiperidin-1-yl)oxyl
TETDF	tetraethylthiuram disulfide
THF	tetrahydrofuran
TPMA	tris(2-pyridylmethyl)amine
TPMA*2	bis(4-methoxy-3,5-dimethyl-pyridin-2-ylmethyl)-pyridin-2-ylmethyl-amine
WE	working electrode
β -CD	beta-cyclodextrin
β^j	stability constant of the complex of Cu ^j
η	overpotential ($\eta = E_{app} - E_{1/2}$)
ν	scan rate (mV/s)

LIST OF SCHEMES

Scheme I-1. Proposed mechanism of <i>e</i> ATRP. Polymerization can be (re)initiated or ceased by switching the applied current. ¹⁰	5
Scheme I-2. ATRP processes (k_a = activation rate constant, k_{da} = deactivation rate constant, k_p = propagation rate constant, k_t = termination rate constant, M = monomer, L = ligand, X = halogen, and P_n-X = alkyl halide).	6
Scheme I-3. ATRP processes with a generation or/and regeneration of the catalyst (k_{red} = reduction rate constant).	9
Scheme I-4. Catalytic electrochemical process occurring at the working electrode surface. ¹¹	13
Scheme II-1. Electrochemically Mediated ATRP (<i>e</i> ATRP).	8
Scheme II-2. Catalytic Electrochemical-chemical Reaction. [*formal charges have been omitted in this Chapter]	12
Scheme III-1. Mechanism of <i>e</i> ATRP.	36
Scheme III-2. Galvanostatic condition of <i>se</i> ATRP.	48
Scheme IV-1. Mechanism of <i>e</i> ATRP.....	62
Scheme IV-2. (A) Synthesis of PEO- <i>b</i> -PAAm diblock copolymers <i>via e</i> ATRP; (B) Synthesis of PEO- <i>b</i> -PAAm- <i>b</i> -P(NIPAAm- <i>stat</i> -AAm)) pseudo-triblock copolymers <i>via e</i> ATRP.....	63
Scheme V-1. Mechanism of electrochemically mediated atom transfer radical polymerization (<i>e</i> ATRP).....	87
Scheme V-2. Proposed mechanism of miniemulsion polymerization by <i>e</i> ATRP.....	93

Scheme VI-1. General mechanism for RAFT polymerization.....	115
Scheme VI-2. Concurrent ATRP/RAFT polymerization (red box) and electrochemically mediated ATRP/RAFT polymerization (blue box).....	117
Scheme VI-3. CuDC ₂ /TPMA formation.	119
Scheme VI-4. Proposed mechanism of <i>e</i> RAFT. Radical species are introduced from a direct electrolysis of conventional initiator or CTA.	128
Scheme VII-1. Mechanism of <i>e</i> ATRP.	157
Scheme VII-2. Synthesis of PEO star polymers <i>via</i> macroinitiator method.....	158
Scheme VII-3. Synthesis of PEO MI. Reaction conditions: [HO-PEO]/[BriBBr]/[TEA]=1/2/2, V _{tot} =500 mL, [HO-PEO] ₀ =0.04M in dichloromethane..	158
Scheme VII-4. Catalytic electrochemical-chemical reaction. [[*] formal charges have been omitted in this chapter]	161
Scheme VII-5. Synthesis of PEO Star Polymers using Multi-step <i>E</i> _{app}	170
Scheme VIII-1. Preparation of benzophenone functionalized POEOMA and PBMA linear and star polymers.	182
Scheme VIII-2. Surface patterning by Bzp-dual functionalized POEOMA star polymers.	190
Scheme IX-1. Synthetic pathway to benzophenone-P(MEO ₂ MA- <i>co</i> -OEOMA ₃₀₀) _n -PEGDMA star polymers and preparation of modified surface using UV irradiation.....	203
Scheme A-I-1. Low ppm catalyst ATRP mechanisms.....	233
Scheme A-II-1. Low ppm catalyst ATRP mechanisms.	255
Scheme A-IV-1. AGET ATRP of OEOMA ₄₇₅	287
Scheme A-IV-2. Hemin and its modification to mesohemin-(MPEG ₅₅₀) ₂	287

Scheme A-IV-3. Hemin modification scheme with PEG.	292
Scheme A-IV-4. Catalytic Electrochemical-chemical Reaction.	295
Scheme A-V-1. Schematic illustration of possible reactions between P_n-X , P_n^\bullet radicals, Cu^0 , $Cu^I X/L$, and $Cu^{II} X_2/L$ species in the RDRP in the presence of Cu^0 . The proposed SET-LRP mechanism is shown as the left panel, and the proposed SARA ATRP mechanism is shown as the right panel. Bold arrows illustrate major (dominating) reactions, regular solid line represent contributing reactions and dash lines represent minor reactions that could be neglected.	307
Scheme A-V-2. Reactions involving Cu species and the derivation of dimensions of rate coefficients.	311
Scheme A-VI-1. Proposed mechanism of ATRP in the presence of Ag^0	355
Scheme A-VII-1. Mechanism of <i>e</i> ATRP. Reprinted with permission from reference. ¹¹	381
Scheme A-VII-2. Synthesis of β -CD-PBA star polymers <i>via se</i> ATRP.	382
Scheme A-VII-3. Synthesis of β -CD-(PBA- <i>b</i> -PtBA) ₂₁ star block copolymers <i>via se</i> ATRP.	382
Scheme A-VII-4. Synthesis of β -CD-Br ₁₄ ATRP initiator. Reaction conditions: [β -CD (per -OH)]/[BrIBr] = 1/1, V_{tot} = 59 mL, [β -CD] ₀ = 0.04 M in NMP.	383
Scheme A-VII-5. Synthesis of β -CD-Br ₂₁ ATRP initiator. Reaction conditions: [β -CD (per -OH)]/[BrIBr] = 1/3.5, V_{tot} = 90 mL, [β -CD] ₀ = 0.03 M in NMP.	384
Scheme A-VIII-1. Schematic illustration of synthesis of molecular bottlebrushes with coumarin chain end functionality.	421

LIST OF TABLES

Table III-1. Summary of <i>se</i> ATRP of BA. ^a	43
Table III-2. Weight loss of Al wires after <i>se</i> ATRP.....	44
Table IV-1. Summary of PEO- <i>b</i> -PAAm Synthesis by <i>e</i> ATRP.	64
Table V-1. Partition experiments of CuBr ₂ /BPMEA catalysts with aqueous/BA solution.	91
Table V-2. Results from CV analysis of various CuBr ₂ /L complexes.....	94
Table V-3. Composition of organic and aqueous phases in miniemulsion polymerization.	94
Table V-4. Control polymerization of BA by miniemulsion <i>e</i> ATRP.	96
Table V-5. Summary of catalysts combination for miniemulsion polymerization.	98
Table V-6. Polymerization with different E_{app} s and targeting DPs.....	102
Table VI-1. Summary of MMA polymerization by concurrent <i>e</i> ATRP/RAFT	119
Table VI-2. Summary of direct electrolysis for free radical polymerization.....	129
Table VI-3. Summary of <i>e</i> RAFT polymerization of MMA.....	134
Table VII-1. Summary of Star Synthesis by <i>e</i> ATRP.....	162
Table VIII-1. Summary of the Bzp functionalized polymers.....	184
Table VIII-2. Thicknesses and stabilities of the polymer modified surfaces.	186
Table VIII-3. Summaries of contact angle measurements and film thicknesses.....	189
Table IX-1. Characterization of Prepared Macroinitiators and Star Polymers.	204
Table A-I-1. Normal ATRP of <i>n</i> -BA with BPMODA and BPMODA*.....	238

Table A-I-2. Partitioning of CuBr ₂ /BPMODA and CuBr ₂ /BPMODA* in BA/Water (w/w) = 30/100.	242
Table A-I-3. A(R)GET ATRP of BA in miniemulsion with BPMODA and BPMODA*. ^a	244
Table A-II-1. ARGET ATRP of BMA with TPMA and DOD-BPED*	259
Table A-II-2. ARGET ATRP of BMA in Miniemulsion with DOD-BPED* ^a	260
Table A-III-1. Summaries of ICAR ATRP of MMA with 50 ppm of catalysts.....	274
Table A-III-2. ICAR ATRP of MMA using FeX ₃ (X = Cl, Br) with or without additives.	275
Table A-III-3. Summaries of ICAR ATRP of Sty with 50 ppm of catalysts. ^a	278
Table A-IV-1. Experimental conditions and results of ATRP of OEO(M)A ₄₇₅	291
Table A-V-1. Kinetic model and rate constants for model reactions at 25 °C.....	312
Table A-V-2. Rate coefficient of activation of PMA-Br by Cu ⁰ . ^a	332
Table A-V-3. Summary of all measured rate coefficient of activation of MBrP/PMA-Br by Cu ⁰ at 25 °C.....	338
Table A-VII-1. Summary of β-CD-PBA synthesis by <i>e</i> ATRP and <i>se</i> ATRP.	385
Table A-VII-2. Calculation of Dead Chain Fraction (DCF) for <i>e</i> ATRP/ <i>se</i> ATRP of BA and <i>t</i> BA.....	400
Table A-VII-3. Results from the arms cleaved from the star (co)polymers in order to investigate initiation efficiency (<i>f_i</i>).	406
Table A-VIII-1. Molecular weight and molecular weight distribution characterization of bottlebrushes.	421

LIST OF FIGURES

Figure I-1. Polymers synthesized by ATRP and potential applications. ⁴	3
Figure I-2. (Left) CV of Cl-Cu/L complexes in MeCN at scan rate (ν) = 0.5 V s ⁻¹ , showing the reversible oxidation of the catalysts; (Right) correlation of $E_{1/2}$ with the ATRP apparent equilibrium constant (initiator = ethyl 2-bromopropionate (EBP)), which is an index of catalyst activity. ⁹	11
Figure I-3. Cyclic voltammetry of (a) Cu ^{II} Me ₆ TREN ²⁺ , (b) Cu ^{II} TPMA ²⁺ , and (c) Cu ^{II} PMDETA ²⁺ in DMF in the absence (black line) and presence (red line) of ethyl 2-bromoisobutyrate (EBiB). ¹¹	14
Figure I-4. (a) Chronoamperometry recording the decay of oxidation current of Cu ^I TPMA ⁺ during its disproportionation in H ₂ O; Comparison between (b) experimental and (c) simulated CV of Br-Cu ^{II} Me ₆ TREN in MeCN in the absence and presence of EBiB. ^{31a}	16
Figure I-5. Five necked flask with three electrodes used for <i>e</i> ATRP. The WE, CE, and a RE, are a platinum (Pt) disk, a Pt mesh, and a silver ion/silver (Ag ⁺ /Ag), respectively. The CE and RE were separated from the working solutions by a porous Vycor tip. ¹⁰	18
Figure I-6. Synthesis of star polymers by (a) arm-first method and (b) core-first method. ^{42c}	20
Figure I-7. PSPMA brush generation on an electrode by <i>e</i> ATRP using a grafting-from approach. ^{23a}	21

Figure I-8. A monolayer of ATRP-initiator (bis[2-(2'-bromoisobutyryloxy)ethyl]disulfide) on a flat gold substrate which is used as the WE in the electrochemical setup. Cu^{II} was reduced to Cu^{I} which initiates the reaction on the electrode surface. ^{43a}	22
Figure I-9. Illustration of fabrication of gradient polymer brushes by SI- <i>e</i> ATRP. ^{23b}	23
Figure I-10. Gradient polymeric brushes. (a) Ellipsometry analysis of polymer thickness versus position and time. (b) AFM image of a part of patterned gradients grown on gold surfaces. ^{23b}	23
Figure I-11. Illustration of the electrochemical apparatus used for <i>e</i> ATRP, applying a glassy carbon (GC) as the BPE set between Pt driving electrodes. ^{43c}	25
Figure I-12. Illustration of the apparatus employed for polymer brush patterning. (a) Side view of the system in which a Pt mesh electrode was placed under the cylinder without a gap and a glass substrate was placed 130 mm apart from the Pt mesh. (b) SI- <i>e</i> ATRP of NIPAAm generating a bipolar electrochemical patterning. (c) Optical micrograph of a water droplet adsorbed on the patterned PNIPAAm brush. ^{43c}	25
Figure I-13. Strategy for the preparation of chelating carbon fibers (CFs). ^{43b}	27
Figure I-14. Antifouling surfaces prepared by SI- <i>e</i> ATRP. ^{43d}	28
Figure I-15. Hb imprinted polymers by SI- <i>e</i> ATRP for biosensor. ⁴⁵	29
Figure I-16. Electrochemical attachment of 4-phenylacetic diazonium salt and its subsequent use as initiator for generating polymer brushes. ⁴⁹	30
Figure I-17. Structure formation by surface-initiated polymerizations using an ammonium persulfate as redox-sensitive initiator (a) without RAFT agent and (b) with RAFT agent, leading to a homogeneous hydrogel PNIPAAm film on the surface. ^{38b}	31

Figure I-18. Functionalization of PEDOT-N ₃ electrodes using electrochemically mediated CuAAC. Optical microscopy bright-field image of dried PEDOT-N ₃ electrodes after electrochemically mediated CuAAC with alkynated fluorescein (yellow color) or rhodamine (purple color): (a) without potential (non-modified), (b) cathodic current to electrode <i>set 1</i> , and (c) using (b) electrodes and switching current (cathode = <i>set 2</i>) in presence of alkynated rhodamine. ^{52a}	32
Figure I-19. Gradient surface modification using electrochemically mediated CuAAC. The concentration of Cu ^I /L ⁺ was gradually decreased far from cathode. ⁵³	33
Figure I-20. Locally reduction of deactivators to activators at a gold microelectrode and functionalization of a glass substrate through “click chemistry”. ^{54a}	34
Figure I-21. Electrode modification <i>via</i> “click chemistry” and CEC to use of electrochemical pesticide sensors. ⁵⁵	34
Figure I-22. Schematic illustration of the fabrication of a conducting polymer/hydrogel electrode. (a) A melted agarose solution was poured onto a Pt microelectrode substrate. (b) Electropolymerization of the PEDOT into the gel (c) repeat electrochemically actuation for nondestructively peeling. (d) Photograph of the PEDOT microelectrode array on the gel sheet. ⁵⁶	35
Figure I-23. Photographs of the conductive and flexible electrodes with various hydrogels (collagen, glucomannan, PAAm, and commercially available contact lens (PHEMA)). Scale bar: 5 mm. ⁵⁷	36
Figure II-1. CV of 1.17 mM Br-Cu ^{II} /TPMA in 56% (v/v) BA/DMF ([BA] ₀ = 3.9 M) containing 0.2 M TBAClO ₄ recorded at a scan rate (<i>v</i>) of 50 mV/s in the absence (dashed black) and presence (solid black) of 12.9 mM EBiB. LSV (solid red) using an identical	

formulation to those in CV containing EBiB under convection. Hollow black dots correspond to applied potential values (E_{app}), expressed as overpotential (η) values, used in subsequent *e*ATRP experiments. $E_{1/2}$ values of 0.322 and -0.166 V were determined using Ag/AgI/I⁻ and SCE, respectively..... 11

Figure II-2. Electrolysis of Cu^{II}/TPMA at E_{app} of $\eta = 0$ (blue) and -165 mV in the absence (black) or presence of EBiB (red). (A) Current as a function of time, and (B) first order plot of current versus time. Determined k_{red} values are reported in Figure II-2B..... 14

Figure II-3. (A) First order kinetic plot versus time as a function of stirring rate and (B) M_n and M_w/M_n versus monomer conversion for *e*ATRP of BA in DMF as a function of stirring rate. Reaction condition: $[BA]_0/[EBiB]_0/[Br-Cu^{II}/TPMA]_0 = 300/1/0.03$, $[BA]_0 = 3.9$ M, $[TBAClO_4]_0 = 0.2$ M, $T = 45$ °C. The E_{app} of $\eta = -125$ mV at each stir rate..... 15

Figure II-4. Kinetics of *e*ATRP as a function of E_{app} at a η ranging from 0 to -0.180 V. (A) First-order plot of monomer conversion versus time, (B) M_n and M_w/M_n versus conversion, and (C) current versus time, (D) Semi-logarithmic plot of apparent polymerization rate coefficient (k_{app}) versus the overpotential ($\eta = 0, -45, -85, -125, -165$, and -180 mV). Reaction conditions: $[BA]_0/[EBiB]_0/[Br-Cu^{II}/TPMA]_0 = 300/1/0.09$, $[TBAClO_4]_0 = 0.2$ M, $[BA]_0 = 3.9$ M in DMF, $T = 44$ °C, $V_{tot} = 23$ mL, and stirring rate (f) = 875 rpm. For clarity $\eta_6 = -0.180$ V was omitted from (A), (B), and (C)..... 17

Figure II-5. *e*ATRP as a function of $[Br-Cu^{II}/L]_0$ with a $\eta_4 = -0.125$ V. (A) First-order kinetic plot of monomer consumption, (B) M_n and M_w/M_n versus conversion, and (C) current versus time. Reaction conditions: $[BA]_0/[EBiB]_0/[Br-Cu^{II}/TPMA]_0 = 300/1/X$, $[TBAClO_4]_0 = 0.2$ M, $[BA]_0 = 3.9$ M in DMF, $T = 44$ °C, $V_{tot} = 23$ mL, and $f = 875$ rpm. $X = 0.9, 0.3$, and 0.15 corresponding to 300, 100, and 50 ppm, respectively. 18

Figure II-6. Cyclic voltammetry of (A) Me₆TREN, (B) TPMA, and (C) PMDETA in the absence (black line) and presence (red line) of EBiB. Experimental condition: [BA]₀/[EBiB]₀/[Br-Cu^{II}/L]₀ = 300/1/0.09, [BA]₀ = 3.9 M in DMF, [TBAClO₄]₀ = 0.2 M, *T* = 44 °C, L = Me₆TREN, TPMA, or PMDETA. 20

Figure II-7. *e*ATRP as a function of ligand (L = Me₆TREN, TPMA, and PMDETA) with a η = -0.180 V and 100 ppm catalyst. Note: the second instance of PMDETA (magenta squares) was conducted instead with a η = -0.125 V and 300 ppm catalyst. (A) First-order kinetic plot of monomer conversion versus time, (B) *M_n* and *M_w*/*M_n* versus conversion, and (C) current versus time. Reaction conditions: [BA]₀/[EBiB]₀/[Br-Cu^{II}/L]₀ = 300/1/0.03, [TBAClO₄]₀ = 0.2 M, [BA]₀ = 3.9 M in DMF, *T* = 44 °C, *V*_{tot} = 23 mL, and *f* = 875 rpm. 21

Figure II-8. Galvanostatic versus potentiostatic *e*ATRP. (A) Current versus time for a potentiostatic polymerization (black) using an *E*_{app} at a η_4 = -0.125 V and galvanostatic polymerization (red) using an *I*_{app} of -1 mA (*t* = 2800 s) and -0.3 mA (*t* = 9800 s). Red hashes represent integrated area to calculate *Q* for current determination. (B) First-order kinetic plot of a potentiostatic and galvanostatic *e*ATRP. (C) *M_n* and *M_w*/*M_n* versus conversion for potentiostatic (black) and galvanostatic (red) *e*ATRP. (D) Monitored applied potential versus time during a galvanostatic *e*ATRP. Reaction conditions: [BA]₀/[EBiB]₀/[Br-Cu^{II}/TPMA]₀ = 300/1/0.09, [TBAClO₄]₀ = 0.2 M, [BA]₀ = 3.9 M in DMF, *T* = 44 °C, *V*_{tot} = 23 mL, and *f* = 875 rpm. 23

Figure II-9. Recycling of copper via electrodeposition and stripping for sequential *e*ATRP polymerizations. (A) *M_n* and *M_w*/*M_n* versus conversion for fresh (black) and recycled (green) catalyst. (B) Current versus time plot during copper deposition with an *E*_{app} at -

0.283 V vs. Ag/AgI/I⁻ (inset: CV after first polymerization conducted with $\nu = 250$ mV/s and $T = 65$ °C). (C) Images of crude polymerization mixture and Pt working electrode, before and after deposition. (D) Current versus time during copper stripping with an E_{app} at 0.800 V vs. Ag/AgI/I⁻ (inset: CV before (dashed line) and after (solid line) copper stripping). (E) Cyclic voltammograms of Cu^{II}/TPMA prior to the first (black) and second (green) polymerization at $\nu = 100$ mV/s and $T = 44$ °C. (F) First order kinetic versus time plot of two sequential polymerizations with fresh (black) and recycled (green) copper catalyst. Reaction conditions: $[BA]_0/[EBiB]_0/[Br-Cu^{II}/TPMA]_0 = 300/1/0.09$, $[TBAClO_4]_0 = 0.2$ M, $[BA]_0 = 3.9$ M in DMF, $T = 44$ °C, $V_{tot} = 23$ mL, $\eta_6 = -0.180$ V, and $f = 875$ rpm. 25

Figure II-10. (A) CV of Cu^{II}/TPMA after polymerization at 25, 44, and 60 °C, and (B) a UV-Vis calibration curve of Cu/TPMA absorbance versus concentration. 27

Figure III-1. ATRP with 10 cm metal wires ($d = 1$ mm). Pt mesh = *e*ATRP carried out with a Pt mesh cathode and a directly immersed Pt mesh counter electrode). 39

Figure III-2. *se*ATRP of BA with different E_{app} s; reaction condition: $[BA]/[EBiB]/[CuBr_2/TPMA] = 160/1/0.02$, $[BA] = 3.49$ M in DMF (50% solution polymerization), $[TBAClO_4] = 0.2$ M, $T = 50$ °C, WE = Pt mesh, CE = Al wire, RE = Ag/AgI/I⁻; (A) CV of CuBr₂/TPMA with and without initiator (dot lines indicate E_{app}); (B) Chronopotentiometry of the BA polymerizations, the reported charges correspond to the total charge passed after 3 h; (C) first-order kinetic plot with different E_{app} s; and (D) M_n and M_w/M_n versus conversion of BA polymerizations by *se*ATRP; (E)-(H) GPC traces of BA polymerization under different E_{app} s; (I) Normalized applied potential $\eta = E_{app} - E_{1/2}$ 41

Figure III-3. Surface morphologies of Al wires by SEM; (A) pristine, (B) used for <i>se</i> ATRP 1 time, and (C) used for <i>se</i> ATRP 10 times.	43
Figure III-4. High MW of PBA by <i>se</i> ATRP; (A) Conversion of monomers versus reaction time and (B) MW evolution and MWD results by GPC with PMMA standards.	45
Figure III-5. Chain extension by <i>se</i> ATRP; (A) GPC trace of PBA with low DP by <i>se</i> ATRP; (B) ^1H NMR spectra of purified sample (in CDCl_3); (C) Conversion of monomers versus reaction time; (D) MW evolution and MWD results from GPC with PMMA standards; (E) GPC results of block copolymerization.	46
Figure III-6. Galvanostatic <i>se</i> ATRP; (A) chronoamperometry results from potentiostatic condition (exponentially drop) and applied current (dot line); (B) MW and MWD results from GPC with PMMA standards; (C) monomer conversion versus time; (D) GPC traces of BA polymerization; (E) UV-vis spectra of post-polymerization solution; (F) copper deposited on Pt mesh WE.	49
Figure III-7. Multi-step chronoamperometry for galvanostatic <i>se</i> ATRP; (A) chronoamperometry results from potentiostatic conditions (exponential drop) and applied current (dot line), (B) first-order kinetic plots by potentiostatic and galvanostatic conditions, and (C) MW and MWD results from GPC with PMMA standards.	50
Figure IV-1. Kinetics of <i>e</i> ATRP of acrylamide as a function of polymerization temperature and monomer concentration. (A) First-order kinetic plot of monomer conversion versus time, (B) M_n versus monomer conversion, (C) CA results of acrylamides polymerization. General reaction conditions: $[\text{AAm}]/[\text{PEO MI}]/[\text{CuBr}_2/2\text{TPMA}] = 200/1/0.1$, $[\text{TEABr}]_0 = 0.1 \text{ M}$, $E_{\text{app}} = E_{\text{pc}} - 120 \text{ mV}$ (vs. $\text{Ag}/\text{AgI}/\text{I}$).	66

Figure IV-2. *e*ATRP of acrylamide as a function of ligand (L = TPMA, TPMA*2, and Me₆TREN). (A) First-order kinetic plot of monomer conversion versus time, and (B) M_n and M_w/M_n versus monomer conversion. Reaction conditions: [AAm]/[PEO MI]/[CuBr₂/2L] = 100/1/0.05, [AAm] = 1.3 M, [CuBr₂/2L] = 0.64 mM, $T = 0\text{ }^\circ\text{C}$, [TEABr]₀ = 0.1 M, $E_{app} = E_{pc} - 120\text{ mV}$ (vs. Ag/AgI/I). 68

Figure IV-3. GPC traces during the *e*ATRP of acrylamides as a function of ligand (A, B and F, DP = 100) and as a function of DP (for TPMA*2: B-E; for Me₆TREN: F-I). 70

Figure IV-4. Cyclic voltammetry results of (A) TPMA, (B) TPMA*2, and (C) Me₆TREN in the absence (black) and presence of PEO MI (red). Arrows indicate applied potential. (D) Current profile versus time. Reaction conditions: [AAm]/[PEO MI]/[CuBr₂/2L] = 100/1/0.05, [AAm] = 1.3 M, [CuBr₂/2L] = 0.64 mM, $T = 0\text{ }^\circ\text{C}$, [TEABr]₀ = 0.1 M, $E_{app} = E_{pc} - 120\text{ mV}$ (vs. Ag/AgI/I). 71

Figure IV-5. *e*ATRP of acrylamide as a function of targeted DP (100, 200, 400, and 1000). (A) First-order kinetic plot of monomer conversion versus time, (B) M_n and M_w/M_n versus monomer conversion, (C) Current profile versus time during the *e*ATRP, and (D) The apparent propagation rate constant (k_p^{app}) versus the PEO MI concentration. Reaction conditions: [AAm] = 1.3 M, [CuBr₂/2TPMA*2] = 0.64 mM, $T = 0\text{ }^\circ\text{C}$, [TEABr]₀ = 0.1 M, $E_{app} = E_{pc} - 120\text{ mV}$ (vs. Ag/AgI/I). 73

Figure IV-6. *e*ATRP of acrylamide as a function of targeted DP (100, 200, 400, and 1000). (A) First-order kinetic plot of monomer conversion versus time, (B) M_n and M_w/M_n versus monomer conversion, (C) Current profile versus time during the *e*ATRP, (D) The apparent propagation rate constant (k_p^{app}) versus the PEO MI concentration. Reaction conditions:

[AAm] = 1.3 M, [CuBr₂/2Me₆TREN] = 0.64 mM, $T = 0\text{ }^{\circ}\text{C}$, [TEABr]₀ = 0.1 M, $E_{\text{app}} = E_{\text{pc}} - 120\text{ mV}$ (vs. Ag/AgI/I⁻). 74

Figure IV-7. *In situ* chain extension by *e*ATRP; (A) M_n and M_w/M_n versus monomer conversion, (B) First-order kinetic plot of monomer conversion versus time, and (C) GPC results of block copolymerization. Reaction conditions: [NIPAAm]/[PEO-*b*-PAAm-Br]/[CuBr₂/2Me₆TREN] = 200/1/0.1, [NIPAAm] = 1.1 M, [CuBr₂/2Me₆TREN] = 0.55 mM, [TEABr]₀ = 0.1 M, $E_{\text{app}} = E_{\text{pc}} - 120\text{ mV}$ (vs. Ag/AgI/I⁻). 76

Figure V-1. Conventional *e*ATRP of BA with CuBr₂/BPMODA*. (A) Monomer conversion vs. time, (B) MW and MWD vs. monomer conversion, and (C) GPC traces. Reaction condition: [BA]/[EBiB]/[CuBr₂]/[BPMODA*] = 283/1/0.3/0.3; [BA]₀ = 4.19 M (in DMF); 5 wt% of HD (vs. wt of BA); [TBAClO₄] = 0.2 M; $E_{\text{app}} = E_{\text{pc}} - 80\text{ mV}$ 90

Figure V-2. (A) UV-Vis spectra of CuBr₂/BPMEA at different concentrations (0.1 to 20 mM). (B) Calibration curve (absorbance vs. concentration) obtained from the UV-Vis spectra ($R^2 = 0.99986$). 92

Figure V-3. Partition experiments of CuBr₂/BPMEA in (A) 50/50 and (B) 70/30 water/BA mixtures (by v/v). $T = \text{ambient}$ ($\sim 20\text{ }^{\circ}\text{C}$) or $60\text{ }^{\circ}\text{C}$. Calibration curve was obtained from Figure V-2. 92

Figure V-4. Particle sizes of miniemulsion polymerization. (A) Before polymerization and (B) after polymerization (Figure V-5 entry 4). 95

Figure V-5. Miniemulsion *e*ATRP with different catalysts combination. (A) MW and MWD evolution vs. monomer conversion. GPC traces obtained during *e*ATRP with different catalysts combination and (B) kinetic plots of miniemulsion *e*ATRP. (C-F) GPC traces of the polymerization with catalysts of (C) BPMODA_{oil}-BPMEA_{aq}, (D)

BPMODA_{oil}-TPMA_{aq}, (E) BPMODA*_{oil}-bpy_{aq}, and (F) BPMODA*_{oil}-BPMEA_{aq} (Table V-5). 99

Figure V-6. Effects of E_{app} s on miniemulsion polymerization. (A) CV of polymerization mixture, (B) MW evolution and MWD vs. conversion, (C) kinetic plots of the polymerizations, (D-E) GPC trace with various E_{app} s: (D) $E_{1/2}$ and (E) $E_{pc} - 80$ mV.... 101

Figure V-7. Polymerization under different target DP. (A) MW and MWD vs. monomer conversion, (B) kinetics plot of miniemulsion *e*ATRP with different target DP: $[M]/[R-X] = 150$ (red), 283 (orange), and 500 (blue), and GPC traces for target DP = (C) 150 and (D) 500..... 103

Figure VI-1. Polymerization of MMA by concurrent *e*ATRP/RAFT under $E_{app} = E_{pc}$ (Table VI-1, entry 1). (A) CV spectra of CuBr₂/TPMA without or with MANDC (red and blue, respectively); (B) CA curve for MMA polymerization; (C) monomer consumption vs. reaction time; (D) MW and MWD vs. monomer conversion; (E) GPC trace of the polymerization; (F) CV spectra of before and after polymerization..... 120

Figure VI-2. Polymerization of MMA by concurrent *e*ATRP/RAFT under $E_{app} = E_{1/2}$ (Table VI-1, entry 2). (A) CV spectra of CuBr₂/TPMA without or with MANDC (black and red, respectively); (B) CA curve for MMA polymerization; (C) monomer consumption vs. reaction time; (D) MW and MWD vs. monomer conversion; (E) GPC trace of the polymerization. 122

Figure VI-3. Polymerization of MMA by concurrent *e*ATRP/RAFT under $E_{app} = E_{1/2}$ in anisole (Table VI-1, entry 3) (A) CV spectra of CuBr₂/TPMA without or with MANDC (black and red, respectively); (B) CA curve for MMA polymerization; (C) monomer

consumption vs. reaction time; (D) MW and MWD vs. monomer conversion; (E) GPC trace of the polymerization. (F) CV spectra of before and after polymerization..... 123

Figure VI-4. Polymerization of MMA by concurrent *e*ATRP/RAFT with CuDC₂/TPMA (Table VI-1, entry 4) (A) comparing CV spectra of CuDC₂/TPMA (red) and after polymerization with CuBr₂/TPMA/MANDC (black); (B) CA curve for MMA polymerization; (C) monomer consumption vs. reaction time; (D) MW and MWD vs. monomer conversion; (E) GPC trace of the polymerization. 126

Figure VI-5. Polymerization of MMA by concurrent *e*ATRP/RAFT with CuBr₂/bpy catalysts (Table VI-1, entry 5) (A) CV spectra of CuBr/bpy (red) and CuDC/bpy (black); (B) monomer consumption vs. reaction time; (C) MW and MWD vs. monomer conversion; (D) GPC eluogram of the polymerization..... 126

Figure VI-6. Electrolysis of CPPA in the presence of MMA. (A) CV analysis of CPPA ($E_{app} = E_{pc,CPPA} - 80$ mV) and (B) CA result of electrolysis..... 129

Figure VI-7. Electrolysis of 1 mM of CPPA in DMF. (A) CV of CPPA ($E_{app} = E_{pc,CPPA} - 80$ mV) and (B) CA result of electrolysis. 130

Figure VI-8. Electrolysis of BPO in the presence of MMA. (A) CV analysis of BPO ($E_{app} = E_{pc,BPO} - 80$ mV), (B) CA result of electrolysis, (C) monomer consumption vs. reaction time, and (D) GPC trace of final sample..... 131

Figure VI-9. Electrolysis of BBDA in the presence of MMA. (A) CV analysis of BBDA ($E_{app} = E_{pc,BBDA} - 80$ mV), (B) CA result of electrolysis, (C) monomer consumption vs. reaction time, and (D) GPC trace of final sample..... 132

Figure VI-10. *e*RAFT of MMA with CPPA/BPO combination. (A) CV of pure BPO and CTA (1 mM concentration in pure DMF at RT), (B) CV of BPO and BPO/CPPA in

polymerization mixture, (C) monomer consumption vs. reaction time (Table VI-3, entry 2), (D) MW and MWD vs. conversion (Table VI-3, entry 2), and (E) GPC traces of PMMA.

..... 135

Figure VI-11. *e*RAFT polymerization of MMA with BBDA/CPPA combination. (A) CV of BBDA/CPPA with 3 consecutive cycles, (B) CA result of the polymerization, (C) monomer consumption vs. reaction time (9 eq. of BBDA was additionally introduced at 20 h), (D) MW and MWD vs. conversion, and (E) MW evolutions by THF GPC. 137

Figure VI-12. *e*RAFT polymerization of MMA with [CPPA]/[BBDA] = 10/1. (A) CV of BBDA/CPPA, (B) CA result of the polymerization, (C) monomer consumption vs. reaction time, (D) MW and MWD vs. conversion, and (E) MW evolutions by THF GPC. 138

Figure VI-13. *e*RAFT polymerization of MMA with Cu WE. (A) CV of BBDA/CPPA with 3 consecutive cycles (by Cu microelectrode, $A = 0.008 \text{ cm}^2$), (B) CA result of the polymerization, (C) monomer consumption vs. reaction time, (D) MW and MWD vs. conversion, and (E) MW evolutions by THF GPC..... 140

Figure VI-14. *e*RAFT polymerization of MMA with Gr WE. (A) CV of BBDA/CPPA with 3 consecutive cycles (by GC electrode, $A = 0.071 \text{ cm}^2$), (B) CA result of the polymerization, (C) monomer consumption vs. reaction time, (D) MW and MWD vs. conversion, and (E) MW evolutions by THF GPC..... 142

Figure VI-15. *e*RAFT polymerization of MMA with CF WE. (A) CV of BBDA/CPPA in 3 consecutive cycles (by GC electrode, $A = 0.071 \text{ cm}^2$), (B) CA result of the polymerization, (C) monomer consumption vs. reaction time, (D) MW and MWD vs. conversion, and (E) MW evolutions by THF GPC. 143

Figure VI-16. <i>e</i> RAFT polymerization of MMA under $E_{app} = E_{pc} - 120$ mV. (A) CV of BBDA/CPPA with 3 consecutive cycles, (B) CA result of the polymerization, (C) monomer consumption vs. reaction time, (D) MW and MWD vs. conversion, and (E) MW evolutions by THF GPC.....	145
Figure VI-17. <i>e</i> RAFT polymerization of MMA under Galvanostatic condition ($I = -12$ μ A). (A) monomer consumption vs. reaction time, (B) MW and MWD vs. conversion, and (C) MW evolutions by THF GPC.	146
Figure VI-18. <i>e</i> RAFT polymerization of MMA with different target DP. [MMA]/[CPPA] = 200, 500, and 1000 (red, blue, and green, respectively).....	147
Figure VII-1. ^1H NMR spectrum of PEO MI ($\text{DP}_{average} = 44$).....	159
Figure VII-2. Chain extension of PEO with BA; (A) Conversion and first-order kinetic plot versus time; (B) Number average molecular weights and molecular weight distributions versus the monomer conversion; (C) GPC traces for the molecular weight evolution; (D) CV of $\text{CuBr}_2/\text{TPMA}$ (black, dot) and addition of initiator (red), blue circle indicates E_{app}	160
Figure VII-3. CV of $\text{CuBr}_2/\text{TPMA}$ alone (red) and in the presence of PEO MI (blue). 161	
Figure VII-4. PEO star synthesis (Table VII-1, entry 1); (A) CV (black circle: applied potential); (B) CA results, total passed charge = 5.48 C; (C) crosslinker conversion and log plot; (D) GPC traces.....	163
Figure VII-5. PEO star synthesis (Table VII-1, entry 2); (A) CV (red line: applied potential); (B) CA results, total passed charge = 7.67 C; (C) crosslinker conversion and log plot; (D) GPC traces; (E) eluograms of star polymers (20 h).	164

Figure VII-6. PEO star synthesis (Table VII-1, entry 3); (A) CA results, total passed charge=8.11 C; (B) crosslinker conversion and log plot; (C) GPC traces; (D) eluograms of star polymers (20 h).	165
Figure VII-7. PEO star synthesis (Table VII-1, entry 4); (A) CA results, total passed charge=8.65 C; (B) crosslinker conversion and log plot; (C) GPC traces; (D) eluograms of star polymers (20 h).	166
Figure VII-8. PEO star synthesis (Table VII-1, entry 5); (A) CV (red circle: applied potential); (B) CA results, total passed charge = 12.26 C; (C) crosslinker conversion and log plot; (D) GPC traces; (E) eluograms of star polymers (20 h).	167
Figure VII-9. PEO Star polymerization (Table 1, entry 7); (A) CA results, total passed charge = 14.61 C; (B) GPC trace; (C) eluograms of star polymers (20 h).	169
Figure VII-10. PEO star synthesis (Table VII-1, entry 6); (A) CV (E_{app} s from 0.340 to 0.189 V); (B) CA results, total passed charge = 11.37 C; (C) crosslinker conversion and E_{app} s versus time; (D) GPC traces; (E) GPC eluograms of star polymers (20 h).	171
Figure VIII-1. (A) ^1H NMR spectrum of Bzp-initiator; 300 MHz ^1H NMR spectrum and GPC trace of (B-C) Bzp-POEOMA MI, and (D-E) Bzp-PBMA MI. The MW of each polymer was determined by PMMA standards.....	183
Figure VIII-2. GPC traces of (A) Bzp-POEOMA star, (B) Bzp-dual functional POEOMA star and (C) Bzp-PBMA star polymers; (D) 300 MHz ^1H NMR spectra of (a) Bzp-POEOMA star, (b) Bzp-dual functionalized POEOMA star, and (c) Bzp-PBMA star polymers.....	184
Figure VIII-3. Photograph of star polymers modified surfaces; (A) Bzp-POEOMA star polymers and (B) Bzp-dual functionalized POEOMA star polymers.	187

Figure VIII-4. Variation in polymer film thicknesses when using different concentrations of polymer solution. The average values were determined by averaging 5 ellipsometry measurements with standard deviations.....	188
Figure VIII-5. Temperature response behavior of (A) Bzp-POEOMA star and (B) Bzp-dual functionalized POEOMA star. Concentration of solutions were 1 mg/mL and heating rates were 1 °C/min.....	189
Figure VIII-6. Optical microscopic images of polymer patterned surfaces; (A) Scale bars correspond to 200 µm (magnification 5x), (B) 50 µm (magnification 20x).....	191
Figure VIII-7. AFM analysis of stripe patterned surface (100 µm width) – (A) height image and (B) height profile (blue line); AFM analysis for 50 µm square patterned surface – (C) Height image, (D) height profile.	192
Figure IX-1. (A) ¹ H NMR spectra of (a) MI, (b) Bzp-MI, and (c) Star Polymers in CDCl ₃ . (B) Evolution of GPC traces during synthesis of benzophenone-P(MEO ₂ MA- <i>co</i> -OEOMA ₃₀₀) _n -PEGDMA star polymers. (C) Plots of transmittance as a function of temperature measured for aqueous solutions (1 mg/mL) of MI, Bzp-MI, and star polymers (cloud points: 37, 36 and 27 °C, respectively).....	206
Figure IX-2. (A) DLS analysis of benzophenone-(P(MEO ₂ MA- <i>co</i> -OEOMA ₃₀₀)) _n -PEGDMA star polymers in cold water: average particle size <i>ca.</i> 15 nm (by volume distribution), (B) AFM image of the individual star polymer on the mica substrate.....	207
Figure IX-3. (A) ATR-IR spectra of (a) untreated PS surface, (b) PS surface coated with star polymers before UV irradiation, (c) PS surface coated with star polymers <i>without</i> UV irradiation and washed with methanol, and (d) PS surface coated with star polymers <i>with</i> UV irradiation and washed with methanol. Star polymer solution concentration: 0.2% (by	

wt/v, in methanol); (B) AFM image of thin (*ca.* 30nm) films of star polymers coated on the silicon wafer. (C) ATR-IR spectra of modified surfaces; unmodified polystyrene (a), star polymer modified surfaces (b-d, 0.2-0.4% (wt/v), respectively each)..... 209

Figure IX-4. (A) Calibration curve from a known amount of star polymers deposited films, (B) relative peak intensity values from variable thickness stars modified PS surfaces. The thickness of films: 0.2% - 31 nm, 0.3% - 39 nm and 0.4% - 53 nm. Calibration curve was made based on a known amount of star polymer casted both Si wafer and PS surfaces. The equation for calibration was as follows; (i) Relative peak intensity (by ATR-IR): $A_{\text{standard}} = A_{\text{sample}} - A_{\text{control}}$, where A = area of peak, $A_{\text{sample}} = A_{[1750\sim1700]} / A_{[1500\sim1400]}$, and $A_{\text{control}} = A_{[1750\sim1700]} / A_{[1500\sim1400]}$; Peak area from star polymers was ignored ($1500 \sim 1400 \text{ cm}^{-1}$), (ii) Film thickness (by ellipsometry): The film thicknesses of star polymers were determined by ellipsometry and each measurement was repeated more than 5 times..... 210

Figure IX-5. Temperature-dependent contact angle changes (20 to 38 °C) for star polymers modified PS surface (●: Uncoated PS, ○: Star Polymers modified PS) by sessile drop methods (data from five separate experiments with standard deviations)...... 211

Figure IX-6. *In-vitro* cell viability assay of MC3T3-E1.4 cells mixed in suspension with (1) Bzp-MI, (2) star polymers, and (3) cells only (control experiment). The live cells fluoresce green and the dead cells fluoresce red. Scale bars correspond to 100 μm (magnification: 10x)..... 212

Figure IX-7. (top) Phase contrast microscopic images of NIH 3T3 (mouse fibroblast cell) on PS modified with star polymers: after 48 h of incubation at 37 °C and cooling the sample by adding cold media (4 °C). (bottom) high magnification of 0 and 69 min. This estimated

thickness of star polymer film was 30.5 nm. Scale bars correspond to 200 μm , respectively each. 214

Figure IX-8. Phase contrast microscopic images of NIH 3T3 on PS modified with star polymers and unmodified PS: (a, b) after 48 h of incubation at 37 °C and 70 min after cooling the sample by adding cold media (4 °C) from stars modified surface (0.3% star solution was used), (c, d) after 48 h of incubation at 37 °C and 70 min after cooling the sample by adding cold media (4 °C) from stars modified surface (0.4% star solution was used), and (e, f) after 48 h of incubation at 37 °C and 70 min after cooling the sample by adding cold media (4 °C) from unmodified surface. Scale bars correspond to 200 μm (magnification 5x). This estimated thickness of star polymer films were 39 nm (a, b) and 53 nm (c, d). 215

Figure A-I-1. First order kinetic plots (a-c) and evolution of M_n and M_w/M_n with conversion (d-f) for the normal ATRP of BA at = 80/20; 99/5; and 99/1 for BPMODA and BPMODA*. All polymerizations were conducted with $[\text{BA}]/[\text{EBiB}]/[\text{CuBr}]/[\text{CuBr}_2]/[\text{Ligand}] = 200/1/X/Y/1$ ($X = 0.80, 0.95, 0.99$ and $Y = 0.20, 0.05, 0.01$) in 20% (v/v) anisole at 60 °C. 239

Figure A-I-2. First-order kinetic plots (a) and evolution of M_n and M_w/M_n with monomer conversion (b) for the SARA ATRP of BA with BPMODA, BPMODA*, or TPMA. All polymerizations were conducted with $[\text{BA}]/[\text{EBiB}]/[\text{CuBr}_2]/[\text{Ligand}]/[\text{Cu}^0 \text{ wire}] = 200/1/0.01/0.03/1 \text{ cm}$ in 20% (v/v) anisole at 60 °C. 240

Figure A-I-3. 500 ppm catalyst solutions in BA with BPMODA* and BPMODA..... 243

Figure A-I-4. First-order kinetic plots (a-c) and evolution of molecular weights and M_w/M_n with conversion (d-f) of AGET ATRP of BA with BPMODA and BPMODA* in

mini-emulsion. ^a [BA]/[EBiB] = 200/1, [Brij98]/[Hexadecane] = 2.3/3.6 wt% vs. BA, <i>T</i> = 80 °C.	245
Figure A-I-5. First-order kinetic plot (a-c) and evolution of molecular weight and M_w/M_n with conversion (d-f) of AGET ATRP of BA with BPMODA and BPMODA* in mini-emulsion. ^a [BA]/[EBiB] = 200/1, [Brij98]/[Hexadecane] = 2.3/3.6 wt% vs. BA, <i>T</i> = 80 °C.	247
Figure A-II-1. Structure of DOD-BPED*.	257
Figure A-II-2. First-order kinetic plots (a) and evolution of M_n and M_w/M_n with monomer conversion (b) for the AGET ATRP of BMA with DOD-BPED*, TPMA, or BPMODA. All polymerizations were conducted with [BMA]/[EBPA]/[CuBr ₂]/[Ligand]/[Sn ^{II} (EH) ₂] = 200/1/0.01/0.03/0.1, 20% (v/v) anisole, <i>T</i> = 60 °C.	259
Figure A-II-3. First-order kinetic plots (a, c) and evolution of M_n and M_w/M_n with monomer conversion (b, d) for the AGET ATRP of BMA DOD-BPED* under mini-emulsion conditions. All polymerizations were conducted with [Brij 98]/[hexadecane] = 2.3/3.6 wt% vs. BMA, <i>T</i> = 80 °C. Specific reaction conditions in Table A-II-2.	261
Figure A-III-1. Structures of FeX ₃ (NHC) catalysts.	271
Figure A-III-2. Cyclic voltammograms of I-Cl, H-Cl, I-Br, H-Br, FeCl ₃ /TBACl, and FeBr ₃ /TBABr; Measurement condition: working electrode = glassy carbon electrode, counter electrode = platinum meshed electrode, reference electrode = Ag/AgI/I ⁻ and externally referred by Fc ^{0/+} , supporting electrolyte = 0.2 M Bu ₄ NPF ₆ in CH ₂ Cl ₂ . ([Cat.] = 1.0 mM, scan rate 50 mV/s).	272

Figure A-III-3. (A) Plot of M_n and M_w/M_n vs. conversion; (B) kinetic plots of $\ln([M]_0/[M])$ vs. time with iron complexes; Reaction condition: $[MMA]/[EBPA]/[Cat.]/[AIBN] = 200/1/0.01/0.2$, $[MMA] = 4.7$ M in 50% (v/v) anisole at 60 °C for 24 h.	274
Figure A-III-4. Cyclic voltammograms of I-Br with various ratio of TBABr (Br ⁻); Measurement condition: working electrode = glassy carbon electrode, counter electrode = platinum meshed electrode, reference electrode = Ag/AgI/I ⁻ and externally referred by Fc ^{0/+} , supporting electrolyte = 0.2 M Bu ₄ NPF ₆ in CH ₂ Cl ₂ . ([Cat.] = 1.0 mM, scan rate 50 mV/s).	276
Figure A-III-5. (A) Plot of M_n and M_w/M_n vs. conversion; (B) kinetic plots of $\ln([M]_0/[M])$ vs. time; Reaction conditions: $[Sty]/[EBPA]/[Cat.]/[AIBN] = 200/1/0.01/0.2$; $[Sty] = 4.4$ M in 50% (v/v) anisole at 60 °C for 72 h.	278
Figure A-IV-1. GPC traces for ATRP reaction catalyzed by catalase. $[OEOMA_{480}]_0 = 0.5$ M; $[OEOMA_{480}]/[PEG_{2000}iBBr]/[Asc. A]/[Catalase] = 78/1/15/0.007$, 100 mM NaCl, water, 30 °C.	289
Figure A-IV-2. GPC traces for ATRP reaction catalyzed by hemin. $[OEOMA_{475}]_0 = 0.45$ M; $[OEOMA_{475}]/[I]/[Asc. A]/[Hemin] = 227/1/10/1$, water/DMF (3/1), 30 °C.	289
Figure A-IV-3. First-order kinetic plots (a), evolution of M_n and M_w/M_n with conversion (b). $[OEOMA_{475}]_0 = 0.45$ M; $[OEOMA_{475}]/[I]/[Asc. A]/[Hemin] = 227/1/10/1$, 100 mM NaCl/KBr, water, 30 °C.	290
Figure A-IV-4. GPC traces for ATRP reaction catalyzed by hemin in the presence of 100 mM KBr (A) and NaCl (B). $[OEOMA_{475}]_0 = 0.45$ M; $[OEOMA_{475}]/[I]/[Asc. A]/[Hemin] = 227/1/10/1$, 100 mM NaCl/KBr, water, 30 °C.	290

Figure A-IV-5. First-order kinetic plots (a), evolution of M_n and M_w/M_n with conversion (b), GPC traces. $[OEOMA_{475}]_0 = 0.45$ M; $[OEOMA_{475}]/[I]/[Asc. A]/[Hemin-(PEG_{1000})_2] = 227/1/n/1$, $n = 1, 10$, water, $30\text{ }^\circ\text{C}$, 100 mM KBr.	293
Figure A-IV-6. GPC traces for ATRP reaction catalyzed by hemin-(PEG ₁₀₀₀) ₂ . $[OEOMA_{475}]_0 = 0.45$ M; $[OEOMA_{475}]/[I]/[Asc. A]/[Hemin-(PEG_{1000})_2] = 227/1/10/1$, 100 mM KBr, water, $30\text{ }^\circ\text{C}$	293
Figure A-IV-7. UV-Vis spectra of the purified polymer after AGET ATRP catalyzed by hemin-PEG and mesohemin-PEG (1 wt. %).	294
Figure A-IV-8. UV-Vis spectra of mesohemin-(MPEG ₅₅₀) ₂ in CH ₃ Cl.	296
Figure A-IV-9. ESI of mesohemin-(MPEG ₅₅₀) ₂ : 250 μM in water:methanol = 1:3.....	296
Figure A-IV-10. Cyclic voltammogram of (A) Hemin and (B) Mesohemin-(MPEG ₅₅₀) ₂ , scan rate = 100 mV/s, supporting electrolyte=TBAPF ₆ (0.1 M in DMF).	297
Figure A-IV-11. First-order kinetic plots (a), evolution of MW and MWD with conversion (b), GPC traces with conversion (c). $[OEOMA_{475}]_0 = 0.45$ M; $[OEOMA_{475}]/[I]/[Asc. A]/[Mesohemin-(MPEG_{550})_2] = 227/1/1n/1$, $n = 1, 5, 10$, water, $30\text{ }^\circ\text{C}$, 100 mM KBr..	298
Figure A-IV-12. (A) First-order kinetic plot, (B) evolution of molecular weight and molecular weight distribution with conversion, (C) GPC traces with conversion. $[OEOMA_{475}]_0 = 0.45$ M; $[OEOMA_{475}]/[I]/[Sn(EH)_2]/[Mesohemin-(MPEG_{550})_2] = 227/1/1/1$, anisole, $60\text{ }^\circ\text{C}$	299
Figure A-V-1. Time resolved conversion of $[Cu^I]$ to $[Cu^{II}]$, ($[Cu/Me_6TREN]_0 = 0.33$ mM), due to activation of MBrP (13.3 mM) and trapping of the generated radicals with TEMPO (13.3 mM) followed at 350 nm. Blue: experimental data; red: mono-exponential fit to the	

experimental data. The function, $\text{absorbance} = c + (a-c)\text{Exp}^{(-k \text{ time})}$ was fitted to the decay profile, with fitted parameters of $a = -0.484$, $c = -0.282$, and $k = 4.22 \text{ s}^{-1}$ 315

Figure A-V-2. Results of several stopped flow experiments followed at 780 nm in MA/DMSO = 2/1 (v/v). Stock solutions of $[\text{MBrP}]_0 = 142.7 \text{ mM}$, $[\text{CuBr}]_0 = 6.34 \text{ mM}$ were used with an excess of TEMPO. Results of fitting gave $k_{a1}^{\text{app}} = 2.0 \times 10^2 \text{ M}^{-1} \text{ s}^{-1}$. Here k_{a1}^{fit} is the value of k fitted to the data. 316

Figure A-V-3. (a) Time-evolution of $[\text{Cu}^{\text{II}}]$ and $[\text{MBrP}]$ measured by UV/Vis/NIR spectrum and GC, respectively $[\text{MBrP}] + [\text{Cu}^{\text{I}}]$ was calculated as $[\text{MBrP}]_0 - 2[\text{Cu}^{\text{II}}]$ because of halogen conservation. (b) Plot of $\ln([\text{MBrP}]_0/[\text{MBrP}]_t)$ vs. time and $\ln([\text{MBrP}]_0/([\text{MBrP}]_0 - 2[\text{Cu}^{\text{II}}\text{Br}_2/\text{Me}_6\text{TREN}]))$ vs. time. Conditions: 25°C ; $[\text{Me}_6\text{TREN}]_0/[\text{MBrP}]_0 = 15 \text{ mM}/10 \text{ mM}$ in DMSO; $V = 7 \text{ mL}$; Cu^0 wire $l = 4 \text{ cm}$, $S = 1.27 \text{ cm}^2$, $S/V = 0.18 \text{ cm}^{-1}$ 319

Figure A-V-4. Plots of (a) $[\text{Cu}^{\text{II}}]$ with time; and (b) $d[\text{Cu}^{\text{II}}]/dt$ vs. Cu^0 wire surface area for model reaction between Cu^0 wire ($d = 1 \text{ mm}$) and 10 mM MBrP in the presence of 15 mM Me_6TREN in 7 mL DMSO at 25°C . The lengths of Cu^0 wire were $2, 4$ and 16 cm ($S = 0.64, 1.3, 5.0 \text{ cm}^2$, $S/V = 0.091, 0.18, 0.72 \text{ cm}^{-1}$), giving $k_{a0}^{\text{app}} = 2.1 \times 10^{-4}, 2.4 \times 10^{-4}$ and $1.9 \times 10^{-4} \text{ cm s}^{-1}$, respectively. 325

Figure A-V-5. Plots of $[\text{Cu}^{\text{II}}]$ vs. time for model reaction between Cu^0 wire ($d = 1 \text{ mm}$) and 10 mM MBrP in the presence of 15 mM Me_6TREN in 7 mL DMSO. The lengths of Cu^0 wire were $2, 4$ and 16 cm ($S = 0.64, 1.27, 5.04 \text{ cm}^2$). 325

Figure A-V-6. Model reactions of 4 cm Cu^0 wire ($S = 1.27 \text{ cm}^2$) with 10 mM MBrP in the presence of different concentration of Me_6TREN ($1 \sim 20 \text{ mM}$) in 7 mL DMSO at 25°C

($S/V = 0.18 \text{ cm}^{-1}$). (a) Evolution of $[\text{Cu}^{\text{II}}]$ in all six experiments. (b) The initial plots of the three experiments with highest $[\text{Me}_6\text{TREN}]_0$, giving $k_{a0}^{\text{app}} = 1.3 \times 10^{-4}$, 1.4×10^{-4} and $1.4 \times 10^{-4} \text{ cm s}^{-1}$ 328

Figure A-V-7. Plots of (a) $[\text{Cu}^{\text{II}}]$ with time; and (b) $\ln([\text{M}]_0/[\text{M}])$ vs. time in SARA ATRP in MA/DMSO = 1/1 (v/v) with the ratio of reagents $[\text{MA}]_0/[\text{MBrP}]_0/[\text{Me}_6\text{TREN}]_0 = 200/1/0.1$, at 25 °C, in the presence of Cu^0 wire ($d = 0.25 \text{ mm}$, $l = 1 \text{ cm}$), the total volume 10 mL, $[\text{MBrP}]_0 = 0.0278 \text{ M}$, $S = 7.95 \times 10^{-2} \text{ cm}^2$, and $S/V = 7.95 \times 10^{-3} \text{ cm}^{-1}$ 330

Figure A-V-8. Plots of (a) $[\text{Cu}^{\text{II}}]$ with time; and (b) $d[\text{Cu}^{\text{II}}]/dt$ vs. Cu^0 wire surface area for SARA ATRP of MA in 10 mL MA/DMSO = 1/1 (v/v) with the ratio of reagents $[\text{MA}]_0/[\text{MBrP}]_0/[\text{Me}_6\text{TREN}]_0 = 200/1/0.1$, at 25 °C, in the presence of different length of Cu^0 wire ($d = 0.5 \text{ mm}$, $l = 0.5, 1 \text{ and } 2 \text{ cm}$, $S = 0.082, 0.16 \text{ and } 0.32 \text{ cm}^2$, $S/V = 0.0082, 0.016, \text{ and } 0.032 \text{ cm}^{-1}$). $k_{a0}^{\text{app}} = 1.0 \times 10^{-4}, 9.1 \times 10^{-5} \text{ and } 1.2 \times 10^{-4} \text{ cm s}^{-1}$, respectively. The average value of k_{a0}^{app} for the four experiments in Table A-V-2 and Figure 8 is $1.0 \times 10^{-4} \text{ cm s}^{-1}$ 333

Figure A-V-9. Pt foil electrode of area 4.5 cm^2 before (left) and after Cu^0 deposition (right) under the conditions: $[\text{Cu}^{\text{II}}\text{Br}_2/\text{Me}_6\text{TREN}]_0 = 15 \text{ mM}$, $[\text{TBAClO}_4] = 0.2 \text{ M}$ in a total volume 25 mL (30 mL of DMF used as internal standard for NMR), at $T = 60 \text{ °C}$ in DMSO. .. 334

Figure A-V-10. Electrochemical measurement of the activation of alkyl halides by Cu^0 . (a) Cyclic voltammogram of a DMSO solution of $[\text{Cu}^{\text{II}}\text{Br}_2/\text{Me}_6\text{TREN}]_0 = 15 \text{ mM}$, $[\text{TBAClO}_4] = 0.2 \text{ M}$ in a total volume of 25 mL (30 μL of DMF was used as internal standard for NMR), at $T = 60 \text{ °C}$, with sweep rate $\nu = 100 \text{ mV/s}$. The continuous trace illustrates the $\text{Cu}^{\text{I/II}}$ couple only, the dashed trace shows a wider sweep range, including the $\text{Cu}^{0/\text{I}}$ couple. The

potential used in the Cu^0 activation experiment is highlighted. (b) Semilogarithmic plot for the consumption of the initiator over time at the applied potential of -0.7 V (vs. Ag/AgI/I⁻), $[\text{MBrP}]_0 = 11 \text{ mM}$, $[\text{Me}_6\text{TREN}]_0 = 15 \text{ mM}$, $T = 25 \text{ }^\circ\text{C}$, using a 4.5 cm^2 Cu deposited electrode, $S/V = 0.18 \text{ cm}^{-1}$ 336

Figure A-V-11. Polymerization of MA under electrochemical conditions, with activation of alkyl halides by Cu^0 . Cu^0 was deposited onto the Pt electrode ($A = 4.5 \text{ cm}^2$): $[\text{Cu}^{\text{II}}\text{Br}_2/\text{Me}_6\text{TREN}]_0 = 15 \text{ mM}$, $[\text{TBAClO}_4] = 0.2 \text{ M}$ in a total volume 25 mL, at $T = 40 \text{ }^\circ\text{C}$, $E_{\text{app}} = -0.6 \text{ V}$ (vs. Ag/AgI/I⁻) for 22 h. Polymerization conditions: $[\text{MA}]_0/[\text{MBP}]_0/[\text{Me}_6\text{TREN}]_0 = 200/1/0.5$, $[\text{TBAClO}_4] = 0.2 \text{ M}$ in a total volume 21 mL ($[\text{MA}]_0 = 7.4 \text{ M}$), $T = 25 \text{ }^\circ\text{C}$, $E_{\text{app}} = -0.5 \text{ V}$ (vs. Ag/AgI/I⁻). (a) M_n and M_w/M_n values vs. conversion, solid red line shows predicted M_n with complete initiation (b) evolution of MWD, (c) monomer conversion and $\ln([M]_0/[M])$ vs. time (solid points are conversion and hollow points are $\ln([M]_0/[M])$)..... 337

Figure A-V-12. Experimental and simulation results for a model reaction between 4 cm Cu^0 wire ($S = 1.27 \text{ cm}^2$) and 10 mM MBrP in the presence of 15 mM Me_6TREN in 7 mL DMSO ($S/V = 0.18 \text{ cm}^{-1}$). Solid points represent experimental data and dash lines follow simulation results. (a) concentrations of MBrP, Cu^{I} and Cu^{II} ; (b) rates of all relevant reactions from 0 to 10000 s, and the inset showing the comproportionation/disproportionation rates from 0 to 40000 s. 344

Figure A-VI-1. (A) UV-Vis-NIR spectra and (B) semi-log plot of $[\text{Cu}^{\text{II}}]$ in the reduction of CuBr_2 with Ag^0 in the absence of alkyl halide initiator. Reaction conditions: $[\text{BA}]_0/[\text{CuBr}_2]_0/[\text{TPMA}]_0 = 200/0.04/0.08$ with $[\text{BA}]_0 = 3.49 \text{ M}$ in DMF at $25 \text{ }^\circ\text{C}$, in the presence of 2 cm Ag^0 wire ($d = 2 \text{ mm}$, $A = 1.3 \text{ cm}^2$; $V_{\text{tot}} = 10 \text{ mL}$). 358

Figure A-VI-2. (A) Kinetics, (B) evolution of M_n and M_w/M_n with conversion, and (C) GPC traces for the polymerization of BA in DMF. Reaction conditions: $[BA]_0/[EBiB]_0/[CuBr_2]_0/[TPMA]_0 = 200/1/0.04/0.08$ with $[BA]_0 = 3.49$ M in DMF at 50 °C, in the presence of 5 cm Ag^0 wire ($d = 2$ mm, $SA = 3.2$ cm²; $V_{tot} = 10$ mL; $S/V = 0.32$ cm⁻¹). 359

Figure A-VI-3. (A) Kinetics, (B) evolution of M_n and M_w/M_n with conversion, and (C) GPC traces for the polymerization of BA in DMF, run to long reaction times. Reaction conditions: $[BA]_0/[EBiB]_0/[CuBr_2]_0/[TPMA]_0 = 200/1/0.04/0.08$ with $[BA]_0 = 3.49$ M in DMF at 50 °C, in the presence of 5 cm Ag^0 wire ($d = 2$ mm, $SA = 3.2$ cm²; $V_{tot} = 10$ mL; $S/V = 0.32$ cm⁻¹). 360

Figure A-VI-4. (a) Kinetics and (b) evolution of M_n and M_w/M_n with conversion in the ATRP of BA with various S/V of silver. Reaction conditions: $[BA]_0/[EBiB]_0/[CuBr_2]_0/[TPMA]_0 = 200/1/0.04/0.08$ with $[BA]_0 = 3.49$ M in DMF at 50 °C, in the presence of 0.5-10 cm Ag^0 wire ($d = 2$ mm, $SA = 0.4 - 6.4$ cm²; $V_{tot} = 10$ mL; $S/V = 0.04 - 0.64$ cm⁻¹). 361

Figure A-VI-5. (A) Kinetics, (B) evolution of M_n and M_w/M_n with conversion in the ATRP of BA, and (C) GPC traces at ~67% conversion for 5 sequential polymerizations with reused silver wire. Reaction conditions: $[BA]_0/[EBiB]_0/[CuBr_2]_0/[TPMA]_0 = 200/1/0.04/0.08$ with $[BA]_0 = 3.49$ M in DMF at 50 °C, in the presence of 5 cm Ag^0 wire ($d = 2$ mm, $SA = 3.2$ cm²; $V_{tot} = 10$ mL). 362

Figure A-VI-6. Evolution of M_n and M_w/M_n with conversion in the ATRP of BA with various initial concentrations of $Cu^{II}Br_2$. Reaction conditions: $[BA]_0/[EBiB]_0/[CuBr_2]_0/[TPMA]_0 = 200/1/x/2x$ ($x = 0.04, 0.02, 0.01, 0.005, 0.002$) with

$[BA]_0 = 3.49$ M in DMF at 50 °C, in the presence of 5 cm Ag^0 wire ($d = 2$ mm, $SA = 3.2$ cm²; $V_{tot} = 10$ mL). 363

Figure A-VI-7. (A) Kinetics and (B) evolution of M_n and M_w/M_n with conversion for the polymerization of MA in DMF and (C) kinetics and (D) evolution of M_n and M_w/M_n with conversion for the polymerization of *t*BA in DMF. Reaction conditions: $[M]_0/[EBiB]_0/[CuBr_2]_0/[TPMA]_0 = 200/1/0.04/0.08$ with $[M]_0 = 3.49$ M in DMF at 50 °C, in the presence of 5 cm Ag^0 wire ($d = 2$ mm, $SA = 3.2$ cm²; $V_{tot} = 10$ mL), $M = MA$ or *t*BA. 365

Figure A-VI-8. ¹H NMR spectrum of PtBA ($M_n = 3,600$, $\bar{D} = 1.17$) in CD₃CN. Inset: Regions containing resonances of interest. Conditions: 500 MHz, acquisition time = 5.5 s (sweep width = 12 ppm, centered at 5 ppm), delay = 15 s, number of scans = 128. 366

Figure A-VI-9. (A) Kinetics (B) evolution of M_n and M_w/M_n with conversion for the chain extension of *t*BA from PBA-Br. Reaction conditions: $[tBA]_0/[PBA-Br]_0/[CuBr_2]_0/[TPMA]_0 = 1000/1/0.2/0.4$ with $[tBA]_0 = 3.49$ M in DMF at 50 °C, in the presence of 5 cm Ag^0 wire ($d = 2$ mm, $SA = 3.2$ cm²; $V_{tot} = 10$ mL). 366

Figure A-VI-10. GPC traces for the chain extension from PBA-Br with *t*BA. Reaction conditions: $[tBA]_0/[PBA-Br]_0/[CuBr_2]_0/[TPMA]_0 = 1000/1/0.2/0.4$ with $[tBA]_0 = 3.49$ M in DMF at 50 °C, in the presence of 5 cm Ag^0 wire ($d = 2$ mm, $SA = 3.2$ cm²; $V_{tot} = 10$ mL). 367

Figure A-VI-11. Polymerization of BA in the presence (RA) and absence (SARA) of $CuBr_2$ catalyst. Reaction conditions: SARA: $[BA]_0/[EBiB]_0/[TPMA]_0 = 160/1/0.018/0.036$ with $[BA]_0 = 3.49$ M in DMF at 50 °C, in the presence of 10 cm Ag^0 wire ($d = 1$ mm, SA

= 3.2 cm²); RA: [BA]₀/[EBiB]₀/[CuBr₂]₀/[TPMA]₀ = 160/1/0.018/0.036 with [BA]₀ = 3.49 M in DMF at 50 °C, in the presence of 10 cm Ag⁰ wire (*d* = 1 mm, SA = 3.2 cm²)...... 372

Figure A-VI-12. GPC traces as a function of reaction progress for the polymerization of BA in DMF with low S/*V* of silver. Reaction conditions: [BA]₀/[EBiB]₀/[CuBr₂]₀/[TPMA]₀ = 200/1/0.04/0.08 with [BA]₀ = 3.49 M in DMF at 50 °C, in the presence of 0.5 cm Ag⁰ wire (*d* = 2 mm, SA = 0.4 cm²; *V*_{tot} = 10 mL; S/*V* = 0.04 cm⁻¹). 373

Figure A-VI-13. Photographs of Ag⁰ before reaction (1) and after each polymerization (2 – End). Reaction conditions: [BA]₀/[EBiB]₀/[CuBr₂]₀/[TPMA]₀ = 200/1/0.04/0.08 with [BA]₀ = 3.49 M in DMF at 50 °C, in the presence of 5 cm Ag⁰ wire (*d* = 2 mm, SA = 3.2 cm²; *V*_{tot} = 10 mL). 374

Figure A-VI-14. (A) Kinetic data for the polymerization of BA in DMF with various initial concentrations of Cu^{II}Br₂ and (B) GPC traces for the polymerization of BA with 10 ppm catalyst loading. Reaction conditions: [BA]₀/[EBiB]₀/[CuBr₂]₀/[TPMA]₀ = 200/1/*x*/2*x* (*x* = 0.04, 0.02, 0.01, 0.005, 0.002) with [BA]₀ = 3.49 M in DMF at 50 °C, in the presence of 5 cm Ag⁰ wire (*d* = 2 mm, SA = 3.2 cm²; *V*_{tot} = 10 mL). 375

Figure A-VI-15. ¹H-NMR spectrum of PBA-*b*-PtBA block copolymer after purification. 376

Figure A-VII-1. ¹H-NMR analysis of β-CD-Br₁₄ (*M*_n = 2,930, *D* = 1.05, 90% purity) after purification (in CDCl₃). 384

Figure A-VII-2. ¹H-NMR analysis of β-CD-Br₂₁ (*M*_n = 4,260, *D* = 1.06, 98% purity) after purification (in CDCl₃). 385

Figure A-VII-3. Multi-step preparative electrolysis for galvanostatic *e*ATRP; (a) preparative electrolysis results from potentiostatic conditions (grey line) and applied

current (red line), and (b) M_n and M_w/M_n versus monomer conversion by potentiostatic and galvanostatic conditions..... 388

Figure A-VII-4. Cyclic voltammetry results of $\text{Cu}^{\text{II}}\text{Br}_2/2\text{TPMA}$ alone (black) and in the presence of $\beta\text{-CD-Br}_{14}$ (green). The arrow indicates the applied potential during electrolysis. Measurement conditions: $[\text{BA}]/[\beta\text{-CD-Br}_{14} \text{ (per -Br)}]/[\text{Cu}^{\text{II}}\text{Br}_2/2\text{TPMA}] = 85/1/0.0085$, $[\text{BA}] = 3.6 \text{ M}$, $[\text{Cu}^{\text{II}}\text{Br}_2/2\text{TPMA}] = 0.36 \text{ mM}$, $T = 50 \text{ }^\circ\text{C}$, $[\text{TBAP}]_0 = 0.2 \text{ M}$, $V_{\text{tot}} = 20 \text{ mL}$ 389

Figure A-VII-5. GPC traces of BA polymerization in the presence of $\beta\text{-CD-Br}_{14}$ under different conditions: potentiostatic *e*ATRP (a), galvanostatic *e*ATRP (b), potentiostatic *se*ATRP (c), galvanostatic *se*ATRP (d); GPC traces during the potentiostatic *se*ATRP as a function of $[\text{Br-Cu}^{\text{II}}/2\text{TPMA}]$ concentration ((c) 100 ppm, (e) 75 ppm, and (f) 50 ppm). GPC traces of BA polymerization in the presence of $\beta\text{-CD-Br}_{21}$ under different conditions: potentiostatic *se*ATRP as a function of E_{app} ((g) $E_{\text{pc}}-80 \text{ mV}$, (h) $E_{\text{pc}}-50 \text{ mV}$, and (i) $E_{\text{pc}}-20 \text{ mV}$); galvanostatic *se*ATRP (j). GPC traces of *t*BA polymerization in the presence of $\beta\text{-CD-(PBA-Br)}_{21}$ under different conditions: potentiostatic *se*ATRP (k); galvanostatic *se*ATRP (l). 391

Figure A-VII-6. First-order kinetic plots by potentiostatic and galvanostatic *e*ATRP. Reaction conditions: $[\text{BA}]/[\beta\text{-CD-Br}_{14} \text{ (per -Br)}]/[\text{Cu}^{\text{II}}\text{Br}_2/2\text{TPMA}] = 85/1/0.0085$, $[\text{BA}] = 3.6 \text{ M}$, $[\text{Cu}^{\text{II}}\text{Br}_2/2\text{TPMA}] = 0.36 \text{ mM}$, $T = 50 \text{ }^\circ\text{C}$, $[\text{TBAP}]_0 = 0.2 \text{ M}$, $V_{\text{tot}} = 20 \text{ mL}$, $E_{\text{app}} = E_{\text{pc}}-80 \text{ mV (vs. SCE)}$ 392

Figure A-VII-7. Multi-step preparative electrolysis for galvanostatic *se*ATRP; (a) preparative electrolysis results from potentiostatic conditions (grey line) and applied

current (red line), and (b) M_n and M_w/M_n versus monomer conversion by potentiostatic and galvanostatic conditions..... 393

Figure A-VII-8. First-order kinetic plots by potentiostatic and galvanostatic *se*ATRP.

Reaction conditions: $[BA]/[\beta\text{-CD-Br}_{14} \text{ (per -Br)}]/[\text{Cu}^{\text{II}}\text{Br}_2/2\text{TPMA}] = 85/1/0.0085$, $[BA] = 3.6 \text{ M}$, $[\text{Cu}^{\text{II}}\text{Br}_2/2\text{TPMA}] = 0.36 \text{ mM}$, $T = 50 \text{ }^\circ\text{C}$, $[\text{TBAP}]_0 = 0.2 \text{ M}$, $V_{\text{tot}} = 20 \text{ mL}$, $E_{\text{app}} = E_{\text{pc}} - 80 \text{ mV (vs. SCE)}$ 393

Figure A-VII-9. $^1\text{H-NMR}$ spectrum of CD star homopolymers with PBA arms ($\beta\text{-CD-(PBA}_{68})_{14}$); $M_n = 124,700$, $D = 1.10$) after purification (in CDCl_3). Table A-VII-1, entry 4.

..... 394

Figure A-VII-10. Synthesis of $\beta\text{-CD-PBA}$ star polymers as a function of

$[\text{Br-Cu}^{\text{II}}/2\text{TPMA}]$. (a) First-order kinetic plot of monomer conversion versus time, (b)

evolution of M_n and M_w/M_n versus monomer conversion, (c) Current profile versus time,

and (d) apparent polymerization rate coefficient (k_p^{app}) versus the square root of the X-

$\text{Cu}^{\text{II}}/\text{L}$ concentration ($[\text{X-Cu}^{\text{II}}/\text{L}] = 0.36, 0.27, \text{ and } 0.18 \text{ mM}$). Reaction conditions:

$[BA]/[14\text{Br-}\beta\text{-CD (per -Br)}]/[\text{Cu}^{\text{II}}\text{Br}_2/2\text{TPMA}] = 85/1/x$, $[BA] = 3.6 \text{ M}$, $T = 50 \text{ }^\circ\text{C}$,

$[\text{TBAP}]_0 = 0.2 \text{ M}$, $V_{\text{tot}} = 20 \text{ mL}$, $E_{\text{app}} = E_{\text{pc}} - 80 \text{ mV (vs. SCE)}$, $x = 0.0085, 0.0064, \text{ and}$

0.0043 corresponding to 100, 75, and 50 ppm, respectively. 396

Figure A-VII-11. R_p as a function of applied potential during synthesis of $\beta\text{-CD-PBA}$ star

polymers. (a) Cyclic voltammetry of $\text{Cu}^{\text{II}}\text{Br}_2/2\text{TPMA}$ with and without initiator (lines

indicate E_{app}), (b) first-order kinetic plots for different E_{app} values, (c) Current profile

versus time, (d) M_n and M_w/M_n versus monomer conversion, and (e) apparent

polymerization rate coefficient (k_p^{app}) versus the overpotential (η). Reaction conditions:

$[BA]/[21\text{Br-}\beta\text{-CD (per -Br)}]/[\text{Cu}^{\text{II}}\text{Br}_2/2\text{TPMA}] = 85/1/0.0043$, $[BA] = 3.6 \text{ M}$,

$[\text{Cu}^{\text{II}}\text{Br}_2/2\text{TPMA}] = 0.18 \text{ mM}$, $T = 50 \text{ }^\circ\text{C}$, $[\text{TBAP}]_0 = 0.2 \text{ M}$, $V_{\text{tot}} = 20 \text{ mL}$, $E_{\text{app}} = E_{\text{pc}} - 80 \text{ mV}$, $E_{\text{pc}} - 50 \text{ mV}$, and $E_{\text{pc}} - 20 \text{ mV}$ (vs. SCE)..... 398

Figure A-VII-12. ^1H -NMR spectrum of CD star homopolymers with PBA arms ($\beta\text{-CD-(PBA}_{41})_{21}$); $M_n = 115,000$, $D = 1.18$) after purification (in CDCl_3). Table A-VII-1, entry 10..... 402

Figure A-VII-13. Multi-step preparative electrolysis for galvanostatic *se*ATRP; (a) preparative electrolysis results from potentiostatic conditions (grey line) and applied current (red line), (b) first-order kinetic plot of monomer conversion versus time, and (c) M_n and M_w/M_n versus monomer conversion by potentiostatic and galvanostatic conditions. Reaction conditions: $[\text{BA}]/[21\text{Br-}\beta\text{-CD (per -Br)}]/[\text{Cu}^{\text{II}}\text{Br}_2/2\text{TPMA}] = 85/1/0.0043$, $[\text{BA}] = 3.6 \text{ M}$, $[\text{Cu}^{\text{II}}\text{Br}_2/2\text{TPMA}] = 0.18 \text{ mM}$, $T = 50 \text{ }^\circ\text{C}$, $[\text{TBAP}]_0 = 0.2 \text{ M}$, $V_{\text{tot}} = 20 \text{ mL}$ 403

Figure A-VII-14. ^1H -NMR spectrum of star block copolymer ($\beta\text{-CD-(PBA}_{41}\text{-PtBA}_{35})_{21}$); $M_n = 212,900$, $D = 1.23$) after purification (in CDCl_3)..... 404

Figure A-VII-15. Multi-step chronoamperometry for galvanostatic *se*ATRP; (a) chronoamperometry results from potentiostatic conditions (grey line) and applied current (red line), (b) first-order kinetic plot of monomer conversion versus time, and (c) M_n and M_w/M_n versus monomer conversion by potentiostatic and galvanostatic conditions. Reaction conditions: $[t\text{BA}]/[\beta\text{-CD-(PBA-Br)}_{21} \text{ (per -Br)}]/[\text{Cu}^{\text{II}}\text{Br}_2/2\text{TPMA}] = 60/1/0.003$, $[t\text{BA}] = 3.4 \text{ M}$, $[\text{Cu}^{\text{II}}\text{Br}_2/2\text{TPMA}] = 0.17 \text{ mM}$, $T = 50 \text{ }^\circ\text{C}$, $[\text{TBAP}]_0 = 0.2 \text{ M}$, $V_{\text{tot}} = 20 \text{ mL}$ 405

Figure A-VII-16. GPC traces of (a) $\beta\text{-CD-(PBA)}_{14}$ and the corresponding cleaved PBA arms (Table A-VII-1 and Table A-VII-3, entry 4), (b) $\beta\text{-CD-(PBA)}_{21}$ and the corresponding cleaved PBA arms (Table A-VII-1 and Table A-VII-3, entry 11), (c) $\beta\text{-CD-(PBA-PtBA)}_{21}$

and the corresponding cleaved PBA-PtBA arms (Table A-VII-1 and Table A-VII-3, entry 13).	407
Figure A-VIII-1. GPC traces of the backbone and the resulting molecular bottlebrushes.	422
Figure A-VIII-2. FT-IR spectra of coumarin functionalized PBA bottlebrush (CB-100, red line) and azide functionalized PBA bottlebrushes (N ₃ -PBA, black line).	423
Figure A-VIII-3. ¹ H NMR spectra of (red) the purified alkyne coumarin and (blue) 7-(6-hydroxyhexyl)oxycoumarin.	424
Figure A-VIII-4. GPC traces and ¹ H NMR spectra of the PHEMA-TMS and PBiBEM.	425
Figure A-VIII-5. GPC trace and ¹ H NMR spectrum of PBA bottlebrushes.	426
Figure A-VIII-6. ¹ H NMR spectra of CB-100 and CB-10.	427
Figure A-VIII-7. UV-vis spectra of CB-100 (A) and CB-10 (B) as thin films after irradiation with UV light (320 nm), arrows indicate progressive decreasing coumarin peak intensities.	428
Figure A-VIII-8. UV-vis spectra of CB-100 (A) and CB-10 (B) as thin films after irradiation with UV light (254 nm) after the sample was irradiated with UV light at 320 nm, arrows indicate progressive increasing coumarin peak intensities.	429
Figure A-VIII-9. Normalized absorbance at 320 nm of CB-100 as a function of irradiation time with UV of 320 nm and 254 nm.	430
Figure A-VIII-10. Temperature dependence of the shear moduli G' and G'' of the CB-100 molecular bottlebrushes. Effect of (A) photocrosslinking time and (B) comparison of photocrosslinking and photoscission on mechanical properties.	431

Figure A-VIII-11. Reduced frequency plots for the shear storage G' and loss G'' moduli of the CB-100 molecular bottlebrushes. Comparison of photocrosslinking (A, C, and E), and photoscission (B, E, and F). The reference temperature was 20 °C.	432
Figure A-VIII-12. Temperature dependence of the shear storage and loss moduli G' and G'' of the CB-100 molecular bottlebrushes. Effect of photocrosslinking time (A, C, and E) and comparison of photocrosslinking and photoscission (B, D, and F) on mechanical properties.....	433
Figure A-VIII-13. Representative fluorescent images of NIH 3T3 fibroblasts cultured on pristine (left) and photocrosslinked (right) CB-100 coated substrates. The cytotoxicity of the cells was determined through a live/dead assay where the cells that show green fluorescence are living cells and the cells are dead with red fluorescence.	435
Figure A-VIII-14. NIH 3T3 fibroblasts growth on the CB-100 compared to controls. Normalized cell count based on the absorbance readings from the MTT assay for cells grown on cover slips (control-blue), and soft (orange) and stiff (grey) CB-100 coated glass cover slips, 1 and 2 days after cell seeding. The values were normalized with respect to the well with the highest absorbance reading in the control on Day 2. Bars denote standard deviation ($n = 24$). Using student's t-tests, the differences between the controls and the coumarin brushes were not statistically significant (N.S.) ($P > 0.1$). The cell growth was the same on the CB-100 as the controls showing their ability to enable cell growth.	435
Figure A-VIII-15. Cell adhesion behavior on the softer surface (pristine brushes, A and B) and stiffer surface (crosslinked brushes, C and D).	437

Figure A-VIII-16. Differential interference contrast microscopy images of the NIH 3T3 cells on the pristine (A, arrows indicate aggregating cells) and photocrosslinked (B) CB-100 coated substrates.	438
Figure A-VIII-17. SEM images of the NIH3T3 cells on glass substrate (control experiments).....	438
Figure A-VIII-18. Differential interference contrast microscopy images of the NIH 3T3 cells on polystyrene (petri dish) substrate (control experiments).	439

Section I.

Introduction

Chapter I

Recent Progress in Electrochemically Mediated Polymerization and Controlled Reaction

I. 1. Introduction

Atom transfer radical polymerization (ATRP) is one of the most rapidly developing synthetic methods in polymer science, allowing for effective control over molecular weights (MW), preparation of polymers with narrow molecular weight distributions (MWD), incorporation of site-specific functionalities, fabrication of polymers with various architectures and synthesis of well-defined hybrids, Figure I-1.¹ ATRP has been successfully used for the preparation of various (co)polymers with essentially any desired complex macromolecular architecture. This includes polymers with controlled topology, ranging from linear chains with precisely controlled dimensions and controlled dispersity to various branched structures formed by copolymerization of macromonomers, grafting onto functional backbones, grafting from multifunctional backbones, copolymers formed using inimers, di- and multi-functional initiators, and even encompassing cyclic structures.^{1d, 1f, 2} ATRP was also used to precisely control chain composition and prepare segmented, block and grafted copolymers as well as periodic and gradient systems.^{1e} The list of monomers successfully homopolymerized by ATRP includes substituted styrenes, (meth)acrylates, (meth)acrylamides, and acrylonitrile as well as vinyl chloride.³

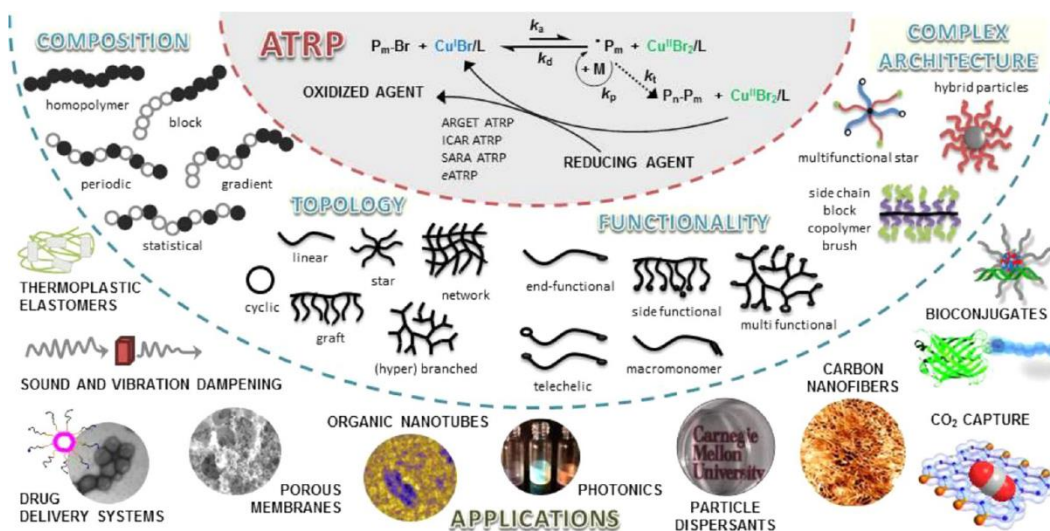


Figure I-1. Polymers synthesized by ATRP and potential applications.⁴

The advent of procedures that provide (re)generation of the oxidized transition metal/ligand catalysts allows the use of parts per million (ppm) of catalysts in an ATRP and offers more environmentally benign and industrially favorable reaction conditions for the synthesis of polymers. These procedures include activators regenerated by electron transfer (ARGET) ATRP,⁵ initiators for continuous activator regeneration (ICAR) ATRP,⁶ supplemental activator and reducing agent (SARA) ATRP,⁷ and photoinduced ATRP (photoATRP).⁸ In addition, the polymerization techniques provide an option to prepare polymers with designed dispersity, defined by the catalyst content.^{1e}

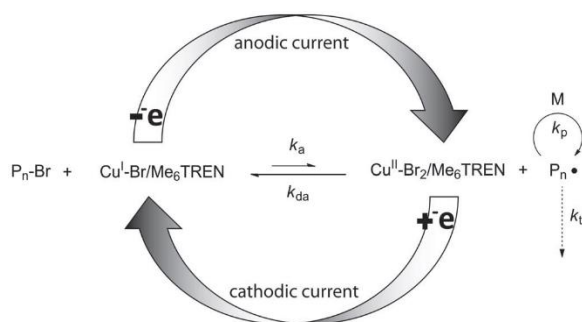
Several analytical techniques, for example, UV-Vis, NMR, and electrochemistry have been employed for characterization of various catalysts and elucidation of the mechanism of ATRP. In the case of electrochemical studies, cyclic voltammetry (CV) was used to determine the half-sum of anodic (E_{pa}) and cathodic peak (E_{pc}) potential value ($E_{1/2} = (E_{pa} + E_{pc})/2$) of various catalyst complexes used in an ATRP. The observed $E_{1/2}$ is directly

correlated to the ATRP equilibrium constant ($K_{\text{ATRP}} = k_a/k_{\text{da}}$) when $\text{Cu}^{\text{II}}/\text{L}$ halidophilicity constants.^{1b,9} Briefly, a catalyst that has a more negative $E_{1/2}$ shows higher catalytic activity ($\ln K_{\text{ATRP}} = nFE/RT$, $E = 0.061 \log K_{\text{ATRP}}$).⁹ Furthermore, by combining with CV and chronoamperometry (CA) analysis, the energy required for activation of ATRP catalysts in the presence of different alkyl halide (R-X) initiators can be calculated.

In 2011, an article on electrochemically mediated ATRP (*e*ATRP) was published.¹⁰ The concept of *e*ATRP is that a controlled reduction of deactivators to activators can be induced by electrical current so that the (re)generated activators can react with initiators in an ATRP as shown in Scheme I-1. The advantages of *e*ATRP is the ability to control the rate of polymerization (R_p) by applied electrical potential, current, or total passed charge, using ppm levels of catalysts, and remove transition metal species when the polymerization ends.¹¹ The detailed mechanism of *e*ATRP is discussed in Chapter 2.

An additional advantage of controlling R_p by *e*ATRP is that the procedure can also be used in aqueous polymerization. K_{ATRP} values are significantly higher in aqueous media than in organic media, *e. g.*, 1000 greater than in acetonitrile. Such a high value for K_{ATRP} can result in loss of control over the polymerization because of excessively high radical concentrations. Another limitation is that low halidophilicity (K_X , $\text{Cu}^{\text{II}}/\text{L}^{2+} + \text{X}^- \xrightleftharpoons{K_X} \text{X-Cu}^{\text{II}}/\text{L}^+$) of the cupric complex could result in loss of deactivators in aqueous media. In *e*ATRP, the ratio of activator/deactivator can be tuned by the selected applied potential, thereby reducing the rate of activation and hence diminishing termination reactions resulting from a high radical concentration. Moreover, the addition of halides as supporting electrolytes reduces loss of deactivators by increasing the concentration of stable

deactivator.¹²



Scheme I-1. Proposed mechanism of *e*ATRP. Polymerization can be (re)initiated or ceased by switching the applied current.¹⁰

Although *e*ATRP has many advantages in developing conditions for a controlled radical polymerization, the complexity of its reaction setup is an obstacle to the wide spread use of *e*ATRP in polymer science. Therefore, a simplified *e*ATRP (*se*ATRP) procedure was developed, in order to simplify the reaction setup. One limitation present in the initial *e*ATRP was to overcome the use of a sacrificial counter electrode (anode) and a further simplification was attained when successful galvanostatic conditions were developed. The detailed investigation of conditions required for *se*ATRP is discussed in Chapter 3.

Polymers with more complex architectures, such as star-shaped polymers, were prepared by (*s*)*e*ATRP.¹³ A high yield of star polymers was obtained by controlling the *R_p* using electrochemical methods. Detailed discussions on star synthesis are provided in Chapter 7 and Appendix 7.

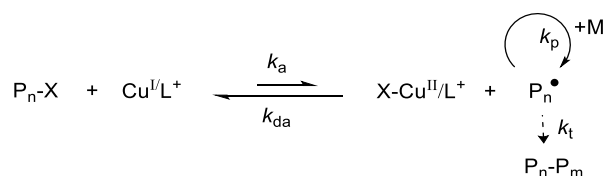
*e*ATRP also can be used for the preparation of functional surfaces. Polymer modified surfaces were prepared by surface-initiated *e*ATRP (SI-*e*ATRP), including gradient polymeric surfaces, and on-demand polymerization using a bipolar electrode. Functional

surfaces are potentially useful in a number of biomedical applications, for example, as biosensors and antifouling surfaces. Section I. 4 discusses some of the examples.

I. 2. Progress on ATRP: Conventional to low catalysts loading ATRP

I. 2. 1. General Mechanism of ATRP

ATRP is controlled by forming an equilibrium (K_{ATRP}) between a low concentration of active propagating species and a larger number of dormant chains, in the form of alkyl (pseudo)halides/macromolecular species ($\text{P}_n\text{-X}$). This dormant species periodically reacts with a transition metal complex in its lower oxidation state ($\text{Cu}^{\text{I}}/\text{L}^+$) at a rate constant of activation k_a . The activation of $\text{P}_n\text{-X}$ generates growing radicals (P_n^\bullet) and the transition metal complexes in its higher oxidation state, coordinated with the transferred (pseudo)halide ($\text{X-Cu}^{\text{II}}/\text{L}^+$), Scheme I-2.^{1e} The ternary complex $\text{X-Cu}^{\text{II}}/\text{L}^+$ reacts with the propagating radical in the deactivation reaction (k_{da}), where the radical is trapped to re-form both a dormant species and the activating catalyst complex $\text{Cu}^{\text{I}}/\text{L}^+$.



Scheme I-2. ATRP processes (k_a = activation rate constant, k_{da} = deactivation rate constant, k_p = propagation rate constant, k_t = termination rate constant, M = monomer, L = ligand, X = halogen, and $\text{P}_n\text{-X}$ = alkyl halide).

Since ATRP is a catalytic process, it can be mediated by many redox-active transition metal complexes including Cu, Fe, Ru, Ni, Ti, Re, Mo, Co, and Os.^{1a, 1c, 2c, 14} The radicals

P_n^\bullet , intermittently generated by the fast activation/deactivation process, add monomers during each repetitive activation procedure and all polymer chains grow at a constant rate of propagation. Termination reactions (k_t) also occur in ATRP, mainly through radical coupling (P_n-P_m) or disproportionation. In the latter case, a chain terminated with a double bond (P_n^-) and a saturated chain (P_m-H) are formed *via* hydrogen abstraction. However, in a well-controlled ATRP, only a very small fraction of polymer chains undergo termination. This is due to generating conditions that provide a low concentration of active propagating radicals and a suitable higher concentration of deactivator species, which minimizes termination.

The rate of polymerization (R_p) depends on the rate constant of propagation (k_p) and the concentrations of monomer ($[M]$) and growing radicals ($[P_n^\bullet]$). The radical concentration depends on the ATRP equilibrium constant ($K_{ATRP} = k_a/k_{da}$) and the concentration of dormant species ($[P_n-X]$), activators ($[Cu^I/L^+]$), and deactivators ($[X-Cu^{II}/L^+]$, equation (I-1)).¹⁵ Typically, generating conditions where $K_{ATRP} \ll 1$.

$$R_p = k_p[M][P_n^\bullet] = k_p K_{ATRP} \frac{[P_n - X][Cu^I/L^+][M]}{[X - Cu^{II}/L^+]} \quad (I-1)$$

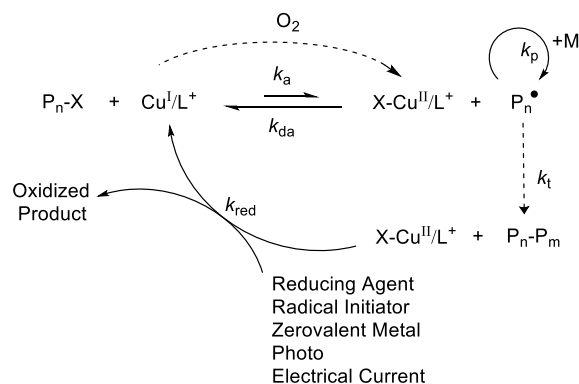
The structures of ligand, monomer, dormant species, as well as reaction conditions (solvent, temperature and pressure) strongly influence the values of the rate constants (k_a , k_{da} and K_{ATRP}) attained in the polymerization reaction.^{1e, 1f, 16} Polymerization rate increases with more active catalysts (higher K_{ATRP}), however, under a particular set of conditions, it may decrease. For instance, a low $[Cu^I/L^+]/[X-Cu^{II}/L^+]$ ratio can be established as a result of excessive radical termination due the buildup in the concentration of Cu^{II} deactivator *via*

the persistent radical effect (PRE).¹⁷ Typically, higher concentrations of deactivator ($[X-Cu^{II}/L^+]$) and higher monomer conversion (p) enables more uniform polymer chains^{1e} and a narrow molecular weight distribution (\mathcal{D} or M_w/M_n) is obtained by ATRP (equation (I-2)).

$$\frac{M_w}{M_n} = 1 + \frac{1}{DP_n} + \left(\frac{k_p[P_n - X]}{k_{da}[X - Cu^{II}/L^+]} \right) \left(\frac{2}{p} - 1 \right) \quad (I-2)$$

I. 2. 2. Evolution from “normal” ATRP to ATRP with ppm levels of catalysts loading.

One limitation of the “early” ATRP procedures was associated with use of a relatively high concentration of catalyst, often equimolar to the initiator ($[Cu/L] \approx [I]$).^{1e, 15} This high concentration of catalyst was required to overcome both radical termination reactions and the low activity of the initial catalyst complexes.^{1c} Purification methods included: precipitation of polymers into a non-solvent; passing the polymer solution through silica, neutral alumina, or clay columns; stirring with an ion-exchange resin; or the use of a heterogeneous catalyst that could be isolated after polymerization was complete.¹⁸ In recent years, various activator (Cu^I/L^+) (re)generation methods have been developed, which allow conducting ATRP reactions with low concentrations of catalyst, typically at or below 100 ppm.^{5a, 19} In addition, these ATRP systems, with low levels of ppm of catalyst usually begin by addition of the stable oxidized catalyst complex (deactivator) to the reaction and subsequent activation in the presence of reducing agents. The fraction of activators (Cu^I/L^+) are generated by reduction of the initially present deactivators ($X-Cu^{II}/L^+$) and the Cu^I/L^+ is continuously regenerated from $X-Cu^{II}/L^+$ accumulated in solution by the occurrence of radical termination reactions, as indicated in Scheme I-3.



Scheme I-3. ATRP processes with a generation or/and regeneration of the catalyst (k_{red} = reduction rate constant).

The reducing/reactivating cycles can also be employed to eliminate air from the system.^{1e} Various methods can be employed for the reduction of deactivators; including introducing a chemical reducing agent (ARGET ATRP),^{5a, 5b, 5d-f, 20} adding an external radical initiator (ICAR ATRP),⁶ using zerovalent metals or sulfite compounds as supplemental activators and reducing agents (SARA ATRP).^{7a-c, 7e, 7f, 21} In addition external stimulation can be applied to generate the active Cu^{I} species *e.g.* the Cu^{I} can be generated by light (photo-ATRP),^{8a, 8c-f, 8h, 8j-l, 22} or by applying a reducing current as in *e*ATRP.^{10-12,}

23

In ARGET ATRP, chemical reducing agents include organo tin compounds, glucose, ascorbic acid, hydrazine, sulfites, or even functional monomers.^{5a, 24} In ICAR ATRP, standard free radical initiators (*e.g.*, azobisisobutyronitrile (AIBN)) are used to spontaneously regenerate $\text{Cu}^{\text{I}}/\text{L}^+$ from $\text{X-Cu}^{\text{II}}/\text{L}^+$.^{6e} In SARA ATRP, zerovalent metals (Cu^0 , Fe^0 or Ag^0) act as mild reducing agents in addition to supplemental activators.²⁵ In case of *e*ATRP, a selected electric potential is applied to adjust the ratio between $\text{Cu}^{\text{I}}/\text{L}^+$

and $X-Cu^{II}/L^+$ throughout the course the reaction.¹⁰

However ARGET, ICAR, and SARA ATRP processes all generate by-products, some of which are undesired. For instance, in ARGET ATRP, products of the oxidized reducing agents, *e.g.*, dehydroascorbic acid or Sn^{IV} compounds, may be toxic.²⁶ Polymers prepared by ICAR ATRP, contain a certain fraction of polymer chains initiated by the added free radical initiator rather than solely from the ATRP initiator, which can result in formation of homopolymer impurity for certain applications.^{5a} In SARA ATRP, copper halides and higher concentration of catalyst complexes accumulate throughout the polymerization process.²⁷ In contrast, *e*ATRP can eliminate the formation of any by-products, producing purer and more environmentally friendly materials.

I. 2. 3. Electrochemical techniques for analysis of ATRP catalysts

Cyclic voltammetry (CV) has been used for over a decade to measure the relative activity of ATRP copper catalysts.^{1b, 9} One of the earliest studies determined that the $E_{1/2}$ value generated by CV provided an estimate of the catalytic activity based on the redox coupling of Cu/L and that $E_{1/2}$ strongly depended on the nature of the ligands (Figure I-2).⁹

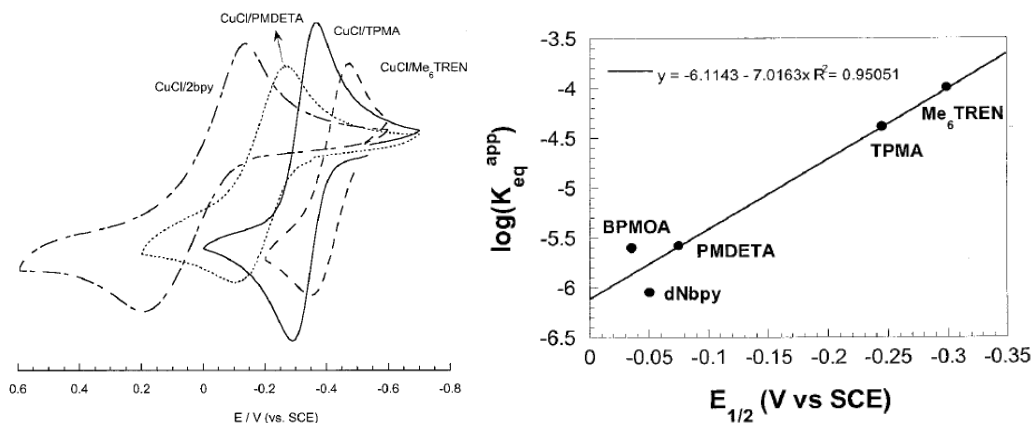


Figure I-2. (Left) CV of Cl-Cu/L complexes in MeCN at scan rate (ν) = 0.5 V s⁻¹, showing the reversible oxidation of the catalysts; (Right) correlation of $E_{1/2}$ with the ATRP apparent equilibrium constant (initiator = ethyl 2-bromopropionate (EBP)), which is an index of catalyst activity.⁹

The ATRP equilibrium, an indication of the activity of an ATRP catalyst, can be formally expressed as a combination of simpler equilibria:²⁸



where ΔG_{R-X} is the Gibbs free energy of R-X bond dissociation and K_X^{II} is the stability constant of the association reaction between an halide ion and the binary Cu^{II}/L complex, the halidophilicity. In a stable 1:1 metal:ligand complex, the standard redox potential of the $Cu^{II}/L^{2+}/Cu^I/L^+$ couple depends on the relative stability of Cu^{2+} and Cu^+ complexes, according to:

$$E_{\text{Cu}^{\text{II}}\text{L}^{2+}/\text{Cu}^{\text{I}}\text{L}^+}^{\ominus} = E_{\text{Cu}^{2+}/\text{Cu}^+}^{\ominus} + \frac{RT}{F} \ln \frac{\beta^{\text{I}}}{\beta^{\text{II}}} \quad (\text{I-7})$$

thus, ligands forming very stable complexes with Cu^{2+} lead to generation of a high $\beta^{\text{II}}/\beta^{\text{I}}$ ratio (β^{j} is the stability constant of the complex of Cu^{j}), high K_{ATRP} and to a strongly reducing $\text{Cu}^{\text{II}}/\text{L}^{2+}/\text{Cu}^{\text{I}}/\text{L}^+$ couple, equation (I-5). These mechanistic considerations infer that one can approximately predict the catalytic activity of metal complexes in ATRP by simply knowing the $\beta^{\text{II}}/\beta^{\text{I}}$ ratio.

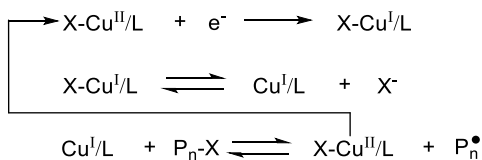
The redox potential of the ternary complexes, in turn, depends upon the relative stability of the higher and lower oxidation state of the metal complex with the ligands (K_{X}^{II} and K_{X}^{I}).^{14c}

$$E_{\text{X-Cu}^{\text{II}}\text{L}^+/\text{X-Cu}^{\text{I}}\text{L}}^{\ominus} = E_{\text{Cu}^{\text{II}}\text{L}^{2+}/\text{Cu}^{\text{I}}\text{L}^+}^{\ominus} + \frac{RT}{F} \ln \frac{K_{\text{X}}^{\text{I}}}{K_{\text{X}}^{\text{II}}} \quad (\text{I-8})$$

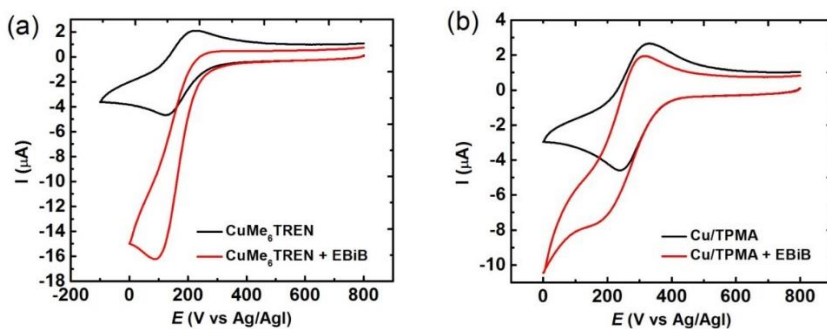
Typically, in an organic solvent, $E_{\text{X-Cu}^{\text{II}}\text{L}^+/\text{X-Cu}^{\text{I}}\text{L}}^{\ominus} < E_{\text{Cu}^{\text{II}}\text{L}^{2+}/\text{Cu}^{\text{I}}\text{L}^+}^{\ominus}$ therefore $K_{\text{X}}^{\text{II}} > K_{\text{X}}^{\text{I}}$. This is desirable because a stable $\text{X-Cu}^{\text{II}}/\text{L}^+$ complex is necessary for efficient deactivation. Conversely, a high $\text{X-Cu}^{\text{I}}/\text{L}$ concentration slows down the rate of polymerization because this ternary Cu^{I} complex is less active than $\text{Cu}^{\text{I}}/\text{L}^+$.²⁹ It was observed that when the same ligand was used, CuCl complexes had a more negative potential *i.e.*, they are more reducing than CuBr complexes.⁹ However, the R_{p} using CuCl/L catalysts is lower than that of CuBr/L because *i)* the activity of the catalyst is directly correlated to the redox potential of the binary Cu/L complexes, not to the ternary $\text{X-Cu}/\text{L}^+$, *ii)* C-Cl bonds are stronger than C-Br bonds, and *iii)* K_{ATRP} is lower for R-Cl than for R-Br . Moreover, the higher C-Cl bond energy could overcompensate for a higher reducing power of Cu-Cl vs. Cu-Br .^{9, 30}

The possibility of using CV electrochemistry as a screening method for selecting ATRP catalysts is subsequently discussed.

When alkyl halide initiators were added to the solution of monomer, Cu/L, and solvent, a cathodic current enhancement was observed in the CV analysis due to the occurrence of the catalytic electrochemical (EC'') process, Scheme I-4 and Figure I-3.¹¹ At the same time, the anodic current decreased because most of $\text{Cu}^{\text{I}}/\text{L}$ complex near the electrode surface was already oxidized by its reaction with R-X .¹⁰⁻¹¹ A more intense cathodic current was obtained with more active Cu ligands, in the order of $\text{Me}_6\text{TREN} > \text{TPMA} > \text{PMDETA}$. Subsequently, a higher anodic current was recorded for the oxidation of residual $\text{Cu}^{\text{I}}/\text{L}$ species. The results indicated that more active catalysts can react faster with the alkyl halide and form radical species and $\text{X-Cu}^{\text{II}}/\text{L}^+$.



Scheme I-4. Catalytic electrochemical process occurring at the working electrode surface.¹¹



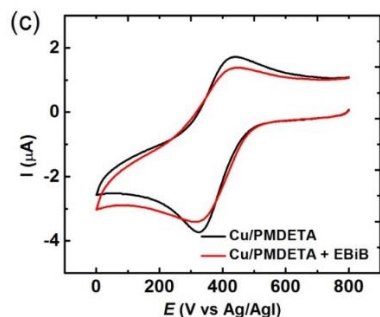


Figure I-3. Cyclic voltammetry of (a) $\text{Cu}^{\text{II}}\text{Me}_6\text{TREN}^{2+}$, (b) $\text{Cu}^{\text{II}}\text{TPMA}^{2+}$, and (c) $\text{Cu}^{\text{II}}\text{PMDETA}^{2+}$ in DMF in the absence (black line) and presence (red line) of ethyl 2-bromoisobutyrate (EBiB).¹¹

Electrochemical techniques were also successfully applied to accurately evaluate activation/deactivation rate constants, k_a/k_{da} , of various catalyst-initiator systems.³¹ Chronoamperometry utilizing a rotating disk electrode (RDE) enabled a facile determination of k_a in a large number of solvents.^{29, 32} Experiments were carried out in the presence of the stable radical 2,2,6,6-tetramethylpiperidin-1-yl)oxyl (TEMPO), which trapped the radicals generated by ATRP activation and made the ATRP equilibrium irreversible, providing a reliable information on the activation kinetics. The limit of detection of this technique is approximately $k_a = 5 \times 10^3 \text{ M}^{-1} \text{ s}^{-1}$. The same technique was also used for the determination of the disproportionation rate constant of Cu^{I} complexes (Figure I-4a).²⁸

CV measurements were also used to determine k_a of active ATRP systems in aqueous media.³³ The ratio between the cathodic peak currents of Cu/L in the absence and presence of initiator RX were recorded at different scan rates in the presence of a radical scavenger (TEMPO). These values were compared to the theoretical data obtained by digital

simulation of the same catalytic process. As a result, exceptionally high values for k_a were measured, up to $2.7 \times 10^7 \text{ M}^{-1} \text{ s}^{-1}$, for the activation of 2-hydroxyethyl-2-bromoisobutyrate (HEBiB) by $\text{Cu}^{\text{I}}/\text{Me}^6\text{TREN}^+$ in pure water.

Bernhardt and coworkers determined both k_a and k_{da} of ATRP catalysts by the combination of CV measurements and simulations of the whole voltammetric curve. The enhanced cathodic current observed during a CV cathodic scan in the presence of Cu/L and alkyl halide initiators provided a direct measurement on the overall activation/deactivation rates. For example, a fast activation between ethyl 2-bromoisobutyrate and $\text{CuBr}/\text{Me}_6\text{TREN}$ was measured providing values of $k_a = 3.7 \times 10^4$ in MeCN and $8.7 \times 10^4 \text{ M}^{-1} \text{ s}^{-1}$ in DMSO.^{31a} The direct determination of k_{da} is one advantage of this technique. The accurate measurement of k_{da} is usually more difficult than that of k_a or K_{ATRP} , because the bimolecular deactivation reaction approaches diffusion-controlled limits ($k_{da} \approx 10^7\text{--}10^8 \text{ M}^{-1} \text{ s}^{-1}$) and the propagating radical (P_n^\bullet) cannot be isolated.³⁴ Accuracy of the rate constants obtained with this method may be limited because precise simulation of the voltammetric curve requires exact knowledge of the $\text{Cu}^{\text{II}}/\text{L}$ halidophilicity constants. Using simulation of the CV patterns, Bernhardt and coworkers determined k_{da} , using a resting solution of $\text{X-Cu}^{\text{II}}/\text{L}^+$ which was reduced *in situ* to produce the active form of the catalyst $\text{Cu}^{\text{I}}\text{PMDETA}^+$ in DMSO.^{31b}

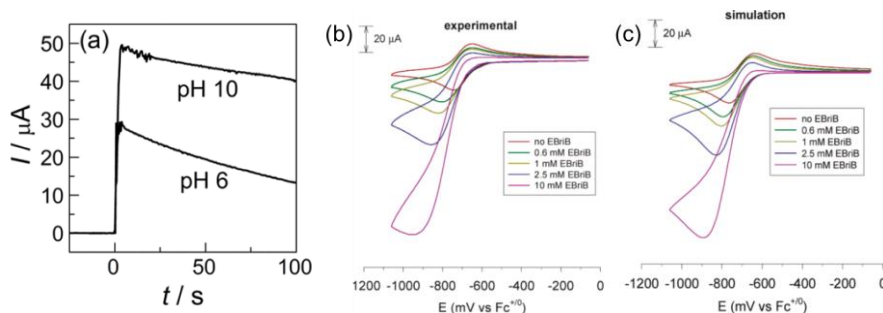


Figure I-4. (a) Chronoamperometry recording the decay of oxidation current of $\text{Cu}^{\text{I}}\text{TPMA}^+$ during its disproportionation in H_2O ; Comparison between (b) experimental and (c) simulated CV of $\text{Br-Cu}^{\text{II}}\text{Me}_6\text{TREN}$ in MeCN in the absence and presence of EBiB.^{31a}

I. 3. Development of *e*ATRP

Many synthetic chemistry reactions are based on the use of redox-active metal catalysts as part of the initiation system. One example is cerium-based oxidation of alcohols, obtained through the controlled formation of radicals.³⁵ The use of electrochemistry to provide radicals and initiate polymerizations on the electrode surface was established in the literature³⁶ and electro-polymerizations have been extensively used to generate thin films³⁷ and/or hydrogel layers on the WE surface,³⁸ *via* free radical or RAFT polymerization.

A paper on electrochemically-triggered controlled polymerization occurring in bulk or in solution was published in 2009 by Amatore and coworkers.³⁹ In this study, alkyl- or benzyl halide initiators were activated by electro-generated N,N' -bis(3,5-di-*tert*-butylsalicylidene)-1,2-ethyldiimine ($\text{Fe}^{\text{II}}\text{Salen}$) catalysts in the presence of styrene (Sty) or methyl methacrylate (MMA) monomers.³⁹ For instance, PSty was obtained by activation

of 1-chloro-1-phenylethane in the presence of Sty. Notably, PSty with a relatively narrow molecular-weight distribution ($\bar{D} = 1.43$) was obtained when a 1/1 ratio of $\text{Fe}^{\text{III}}\text{Salen}/\text{Fe}^{\text{II}}\text{Salen}$ was electro-generated.

In an *e*ATRP, the desired amount of catalytic complex ($\text{X-Cu}^{\text{II}}/\text{L}^+$) is electrochemically reduced to the active complex ($\text{Cu}^{\text{I}}/\text{L}^+$), which triggers a controlled radical polymerization.¹⁰ Typically, the reaction mixture initially contains solvent, monomer, initiator, supporting electrolyte and $\text{X-Cu}^{\text{II}}/\text{L}^+$. In the absence of $\text{Cu}^{\text{I}}/\text{L}^+$ activators, polymerization does not occur. The polymerization begins when a sufficiently negative potential (E_{app}) is applied at the working electrode (WE). The reduction of $\text{X-Cu}^{\text{II}}/\text{L}^+$ to $\text{Cu}^{\text{I}}/\text{L}^+$ occurs at the WE surface, then the reduced activators can be spread out into the bulk reaction mixture by vigorous stirring where the $\text{Cu}^{\text{I}}/\text{L}^+$ reacts with initiators (*e.g.*, alkyl halide, $\text{P}_n\text{-X}$) to form radicals (P_n^\bullet) and is oxidized back to the deactivating complex ($\text{X-Cu}^{\text{II}}/\text{L}^+$). The radical species propagate to form polymeric chains by reacting with monomers (M), and/or are deactivated back to dormant species ($\text{P}_n\text{-X}$) by $\text{X-Cu}^{\text{II}}/\text{L}^+$ (Scheme I-1). Continuous (re)generation of activators ($\text{Cu}^{\text{I}}/\text{L}^+$) and modulation of the rate of polymerization (R_p) can be achieved by selecting the appropriate E_{app} . More detailed investigations on mechanisms including effects of E_{app} s, stirring, and catalysts are provided in Chapter 2.

A specially designed reactor is needed for electrochemical ATRP reactions. Figure I-5 represents the three-electrode set-up typically used for both the electrochemical characterization of the catalytic system and the *e*ATRP electrolysis process.¹⁰ The applied potential is determined between the working (WE) and reference electrode (RE), while

electrical current flows between WE and counter electrode (CE).

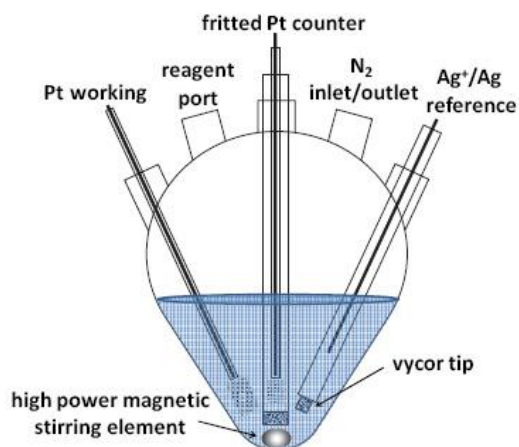


Figure I-5. Five necked flask with three electrodes used for *e*ATRP. The WE, CE, and a RE, are a platinum (Pt) disk, a Pt mesh, and a silver ion/silver (Ag^+/Ag), respectively. The CE and RE were separated from the working solutions by a porous Vycor tip.¹⁰

A pear-shaped five-neck jacketed flask was equipped with a magnetic stirring element, a N_2 purge, and a condenser. The flask necks were fitted with: a silver/silver ion (Ag/Ag^+ , for organic solution) ion or saturated-calomel (SCE, for aqueous condition) as the reference electrode, a Pt mesh/disk working electrode, a Pt mesh counter electrode, and an inlet/outlet port for extraction of samples and addition of reagents. In the case of silver/silver ion RE, a Pleskov electrode is well suited for electrochemistry in organic media, especially with MeCN as a solvent.⁴⁰ The CE should be placed in a separate fritted compartment (glass frit). A methylcellulose gel was placed over the glass frit in order to minimize the diffusion of oxidized species formed at the CE and further isolate the two compartments. For *e*ATRP electrolysis, the working electrode should be a Pt mesh, because of its larger surface area and easy accessible by the convection of the solution. A Pt disc WE should be used for all

analytical CV measurements. The complexity of the reaction setup requires simplification in order to generate wider application of *e*ATRP and a simplified *e*ATRP (*se*ATRP) procedure was successfully implemented using a sacrificial counter electrode (or anode). Further details are explained in Chapter 3.

I. 4. Architectural control by *e*ATRP

I. 4. 1. Homopolymers, block copolymers and star polymers

*e*ATRP can be used to prepare homopolymers (PBA, poly(*tert*-butyl acrylate) (PtBA), poly(methyl acrylate) (PMA), poly(oligo(ethylene oxide) monomethyl ether methacrylate) (POEOMA), poly(acrylamide) (PAAm), poly(*N*-isopropylacrylamide) (PNIPAAm)), and block copolymers (PBA-*b*-PtBA, PEO-*b*-PBA, PEO-*b*-PAAm, PEO-*b*-PNIPAAm, PEO-*b*-PAAm-*b*-P(NIPAAm-*stat*-AAm))^{10-12, 23a, 23b, 23d, 41} and polymers with more complex architecture.^{13b}

Indeed, *e*ATRP has several potential advantages for the synthesis of materials with complex polymeric architectures, such as star polymers which consist of multiple arms linked to a central core. Star copolymers combine interesting properties of a branched architecture, globular shape, and chemically cross-linked structure.⁴² One approach to preparing star polymers by *e*ATRP is the macroinitiator (MI) method, or arm-first method, where the chain-end functionalized linear MIs reacts with divinyl- or multi vinyl-compounds (crosslinkers) to form a dense core (from chain extension with a crosslinker) and stretched arms (Figure I-6a). The preparation of well-defined star polymers in high yield by the arm-first method *via e*ATRP is discussed in Chapter 7. The other approach is the core-first method (Figure I-6b) where multiple initiating groups present at a preformed

core can be used for chain extension with monomers. Appendix 7 discusses an example of star synthesis using functional initiators and preparation of star polymers with block arms.

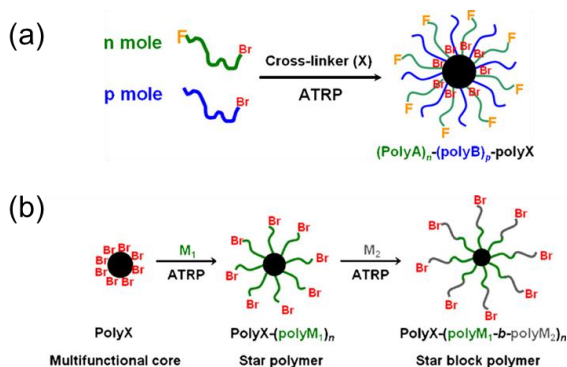


Figure I-6. Synthesis of star polymers by (a) arm-first method and (b) core-first method.^{42c}

I. 4. 2. Surface modification by *e*ATRP

One example of an industrially interesting application of *e*ATRP is the direct growth of polymeric brushes from initiator modified surfaces. Several polymers including POEOMA, poly(2-hydroxyethyl methacrylate) (PHEMA), poly(potassium 3-sulfopropyl methacrylate) (PSPMA), poly(sulfobetaine methacrylate) (PSBMA), poly(glycidyl methacrylate) (PGMA), PMMA, PNIPAAm and poly(2-(methacryloyloxy)ethyl trimethylammonium chloride) (PMETAC), were successfully grafted from solid surfaces, such as gold surfaces, with tethered ATRP initiators.^{23a, 23b, 41a, 43} The influence of the length of linkers between thiol group and ATRP initiator moiety was also investigated by Huck and coworkers.^{23a} Microcontact printing techniques allows for the preparation of thiol-based ATRP initiator monolayers on certain locations of the WE. The *e*ATRP was carried out by reduction of deactivators under cathodic current generating well-defined polymeric surfaces, Figure I-7.

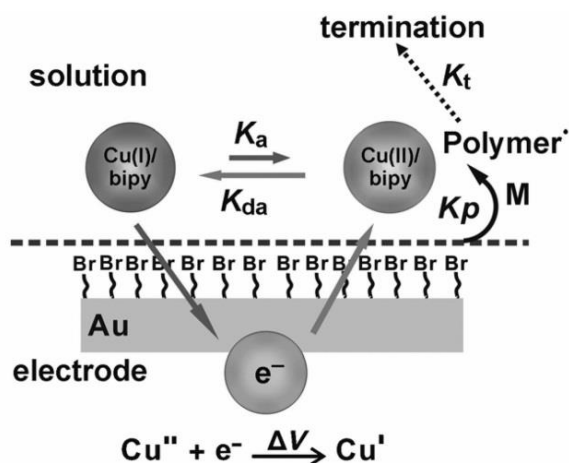


Figure I-7. PSPMA brush generation on an electrode by *e*ATRP using a grafting-from approach.^{23a}

Subsequently, van Rijn and coworkers described surface modification with water soluble polymers such as PHEMA or POEOMA by conducting an *e*ATRP in an aqueous solution, without additional supporting electrolyte, Figure I-8.^{43a} The use of an electrochemical quartz crystal microbalance displayed a highly regular increase in surface confined mass only after the addition of the pre-copper catalyst which was reduced *in situ* and transformed into the catalyst. Reinitiation of the polymerization process was achieved even after isolation and washing of the modified electrode surface thereby confirming retention of chain end functionality in the controlled electrochemical ATRP reaction. This approach brings an interesting perspective to the synthesis of smart thin film materials and also offers the possibility of post-modification *via* additional electrochemical induced reactions. Atomic force microscopy (AFM), confirmed the direct growth of the water-soluble polymeric chains by *e*ATRP by visualization of the PSPMA or PMETAC brushes. Surfaces modified with polyelectrolyte brushes have the potential to be used in applications

such as biosensors and “smart” coatings.^{41a}

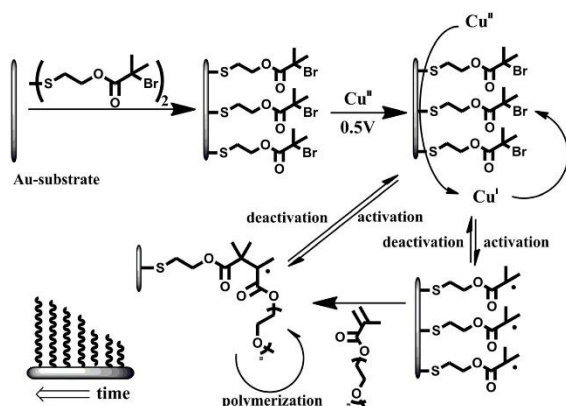


Figure I-8. A monolayer of ATRP-initiator (bis[2-(2'-bromoisobutyryloxy)ethyl]disulfide) on a flat gold substrate which is used as the WE in the electrochemical setup. Cu^{II} was reduced to Cu^{I} which initiates the reaction on the electrode surface.^{43a}

Another advantage of surface initiated *e*ATRP (SI-*e*ATRP) is the ability to prepare a gradient polymeric surface simply by manipulating/controlling the distance between the WE and ATRP initiator modified substrates. Huck and coworkers have successfully exploited the concentration gradients originating from $\text{Cu}^{\text{I}}/\text{L}^+$ diffusion from an electrode surface to initiate ATRP on nonconducting substrates to accomplish this task.^{23b} Briefly, initiator moieties close to the WE are exposed to a higher concentration of the Cu^{I} species and thus, experience a higher rate of polymerization which leads to increased brush thicknesses, Figure I-9.^{23b} For example, when a silicon (Si) wafer, modified with ATRP initiators, is placed at a tilted angle with respect to the WE, the $\text{Cu}^{\text{II}}/\text{Cu}^{\text{I}}$ ratio will vary with the distance from WE to the substrate surface. Therefore, the polymerization rates would differ leading to a gradient in the MW of the formed brushes. In addition, the steepness of the gradient can easily be tuned by changing the tilt angle between WE and substrate. A

linear continuous increase in the thickness of the PGMA gradient layer along one direction (*i.e.*, x-axis) can be achieved, Figure I-10. Pre-patterning the initiator areas allows a “wedge” or “stair” shaped gradient pattern to be formed, Figure I-10. The current approach of using the $[X-Cu^{II}/L^+]/[Cu^I/L^+]$ concentration gradient for tailored gradient slopes can potentially be used to prepare very complex surface topographies in a straightforward way.

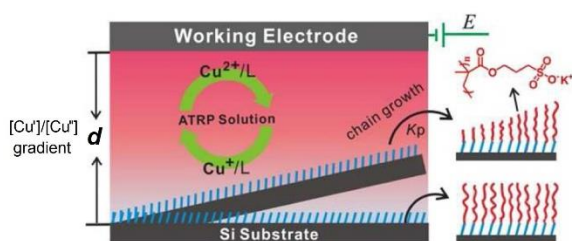


Figure I-9. Illustration of fabrication of gradient polymer brushes by SI-eATRP.^{23b}

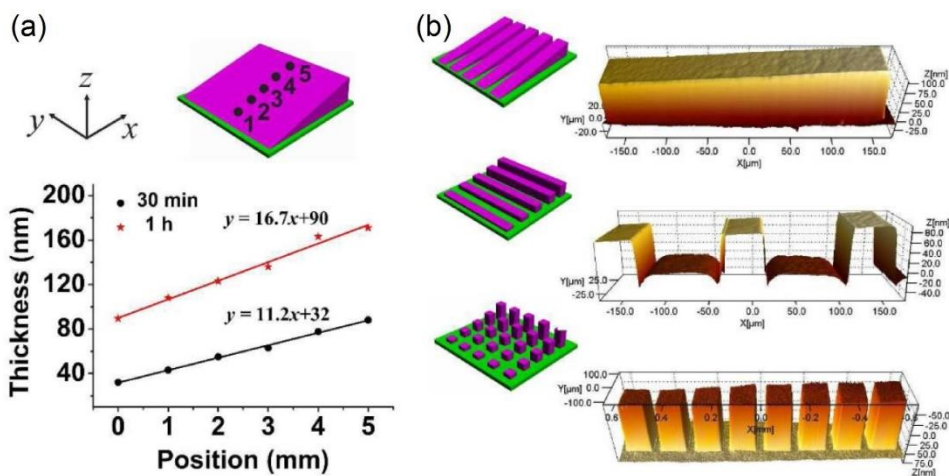


Figure I-10. Gradient polymeric brushes. (a) Ellipsometry analysis of polymer thickness versus position and time. (b) AFM image of a part of patterned gradients grown on gold surfaces.^{23b}

Gradient polymeric surfaces can also be fabricated using a bipolar electrochemical method. A bipolar electrode (BPE) is a wireless electrode produced from the polarization of a conducting material in an external electric field generated by driving electrodes in a low concentration of a supporting electrolyte. BPE have several unique characteristics, including multiple polarities and the ability to generate a gradient potential.⁴⁴ A potential gradient generated on a bipolar electrode (BPE) allowed the formation of a concentration gradient of a $\text{Cu}^{\text{I}}/\text{L}^+$ polymerization catalyst through the one-electron reduction of $\text{X-Cu}^{\text{II}}/\text{L}^+$, resulting in the gradient growth of PNIPAAm and PMMA brushes from an initiator-modified substrate surface set close to a BPE, Figure I-11.^{43c} These polymer brushes could be fabricated in three-dimensional gradient shapes with control over thickness, steepness, and modified area simply by varying the electrolytic conditions. A polymer brush with a circular pattern was successfully formed by site-selective application of potential during bipolar electrolysis by using this same electrolytic apparatus in conjunction with an insulating cylinder (Figure I-12).^{43c} Since the BPE system requires a low concentration of supporting salts, it is possible to be flexible in the selection of the electrolytic media and monomers, as well as providing the ability to fabricate more complex architectures within the polymer brush, such as block copolymers.

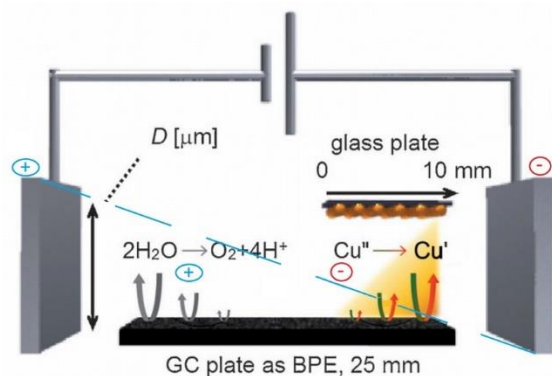


Figure I-11. Illustration of the electrochemical apparatus used for *e*ATRP, applying a glassy carbon (GC) as the BPE set between Pt driving electrodes.^{43c}

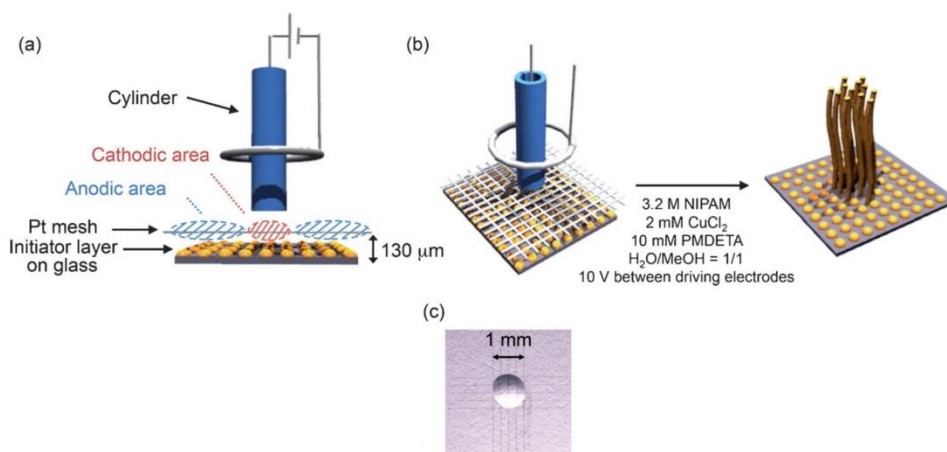


Figure I-12. Illustration of the apparatus employed for polymer brush patterning. (a) Side view of the system in which a Pt mesh electrode was placed under the cylinder without a gap and a glass substrate was placed 130 mm apart from the Pt mesh. (b) SI-*e*ATRP of NIPAAm generating a bipolar electrochemical patterning. (c) Optical micrograph of a water droplet adsorbed on the patterned PNIPAAm brush.^{43c}

One interesting example of the application of *e*ATRP for surface modification is grafting PGMA from carbon fibers (CFs) and post-modification to introduce iminodiacetic

acid-functionalities. The modified CFs can be used for nano-nickel recovery from spent electroless nickel plating (EN) baths, Figure I-13.^{43b} In this example, the first stage includes electro-grafting of aryl layers from a diazonium salt bearing ATRP initiating groups while the second step involves surface-initiated *e*ATRP followed by post-functionalization of the PGMA grafts by iminodiacetic acid (IDA), which reacts with the epoxy groups in the presence of sodium hydroxide. The final step includes absorption of Ni^{2+} on the CFs from spent electroless nickel plating baths. The CFs containing the absorbed Ni^{2+} were then used as a WE at a potential of -0.7 V in sulfuric acid to obtain nano-nickel coated CFs. These chelating carbon fibers may also be used in a treatment of wastewater containing other heavy metals, such as Ni, Pd, and Cu.

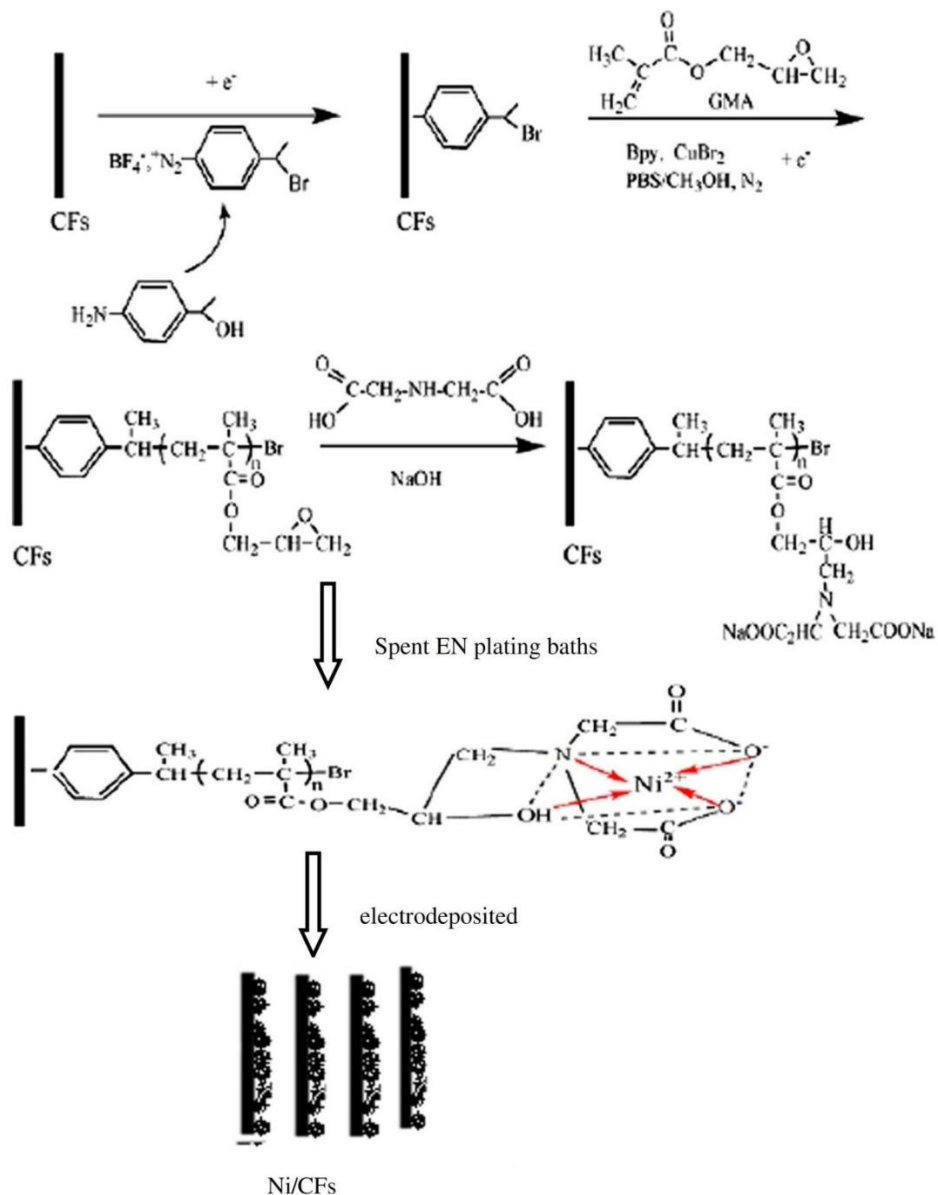


Figure I-13. Strategy for the preparation of chelating carbon fibers (CFs).^{43b}

Super-low protein absorption polymeric surfaces can be produced by SI-*e*ATRP.^{43d} A well-defined zwitterionic polymer hydrogel (PSBMA) was introduced onto a gold substrate under potentiostatic conditions, Figure I-14. *In vitro* and *in vivo* impedance–time scans showed that the PSBMA coating effectively delayed the sensitivity decay of the

electrodes. The ability to prepare zwitterionic polymer surfaces generates the possibility of forming materials for multiple applications, especially in the development of biocompatible materials for implantable devices such as neural and biosensor electrodes.^{43d}

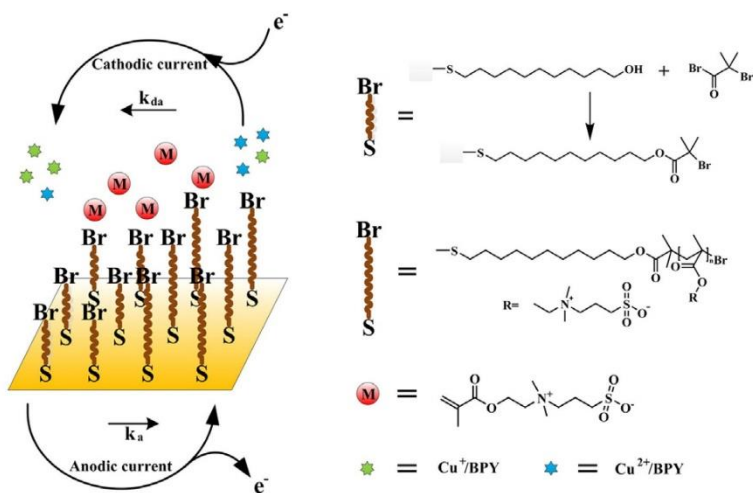


Figure I-14. Antifouling surfaces prepared by SI-*e*ATRP.^{43d}

Hemoglobin (Hb) imprinted polymer/electrodes were prepared by SI-*e*ATRP. Sun and coworkers modified gold (Au) electrode with ATRP initiators⁴⁵ then Hb was used as a template material and catalyst for the polymerization, Figure I-15. The polymerizations were carried out under the reduction potential of Hb in the presence of AAm and crosslinkers. Throughout the SI-*e*ATRP, Hb molecules were embedded in the polymer layer and Hbs were removed from the polymer/electrode. The final polymer layer showed a porous morphology. This porosity was successfully used for the detection of Hb over a Hb range of 1.0×10^{-10} to 1.0×10^1 mg/L. Similarly, Sun and coworkers prepared a lead (Pb^{2+}) detective electrode by SI-*e*ATRP. The electrode detected Pb^{2+} in a range of 3.0×10^{-3} to 2.0×10^3 $\mu\text{g/L}$, and provided a broader range of Pb^{2+} detection than the sensors (typical detection range = 10^{-1} to 2×10^1 $\mu\text{g/L}$) that had already been reported.⁴⁶



Several electropolymerization methods have been studied in recent years in the area of surface modification. Typically, monomers were oxidized or reduced at a working electrode, often forming insoluble electrode coatings that can prevent corrosion.⁴⁷ Encapsulation of several chemical agents can be accomplished during electropolymerization forming materials that can be used as biosensors, and drug release systems. Indeed, due to its practicality, the field of classical electropolymerization is a very active area of research.⁴⁸ In addition, electrochemical processes can change the composition of agents closer to the electrode interface and electrochemical manipulation of reactions is best suited for modifying the electrode surface itself.⁴⁷

29

aryl diazonium (Ar-N_2^+) groups present on the tethered molecule were reduced to form radical species (Ar^\bullet) followed by growth of polymers from the surfaces. In the presence of ATRP catalysts and suitable applied reduction potential for copper catalysts, well-defined polymeric surfaces were obtained. Such a simple strategy provides a versatile approach to surface modification.

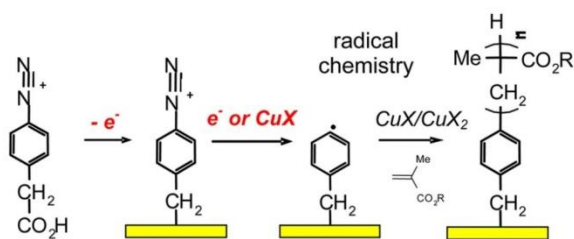


Figure I-16. Electrochemical attachment of 4-phenylacetic diazonium salt and its subsequent use as initiator for generating polymer brushes.⁴⁹

Recently, Johannsmann and coworkers investigated surface-initiated polymerizations for the preparation of hydrogel films, Figure I-17.^{38, 50} A redox-active initiator modified substrate was used and the initiators were electrochemically decomposed to form radical species that were used to activate a reversible addition-fragmentation chain transfer (RAFT) polymerization in the presence of chain-transfer agents (CTA). When the polymerization was conducted in the presence of a crosslinker, hydrogel-modified electrodes were obtained. The addition of RAFT agents (CTA) had an influence on the polymer film thickness and the surface morphology – more uniform surfaces were obtained when polymerized in the presence of the CTA.^{38b}

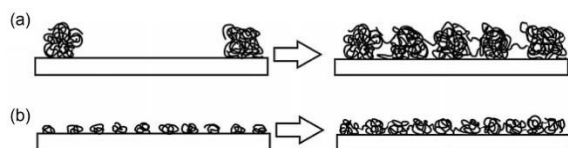


Figure I-17. Structure formation by surface-initiated polymerizations using an ammonium persulfate as redox-sensitive initiator (a) without RAFT agent and (b) with RAFT agent, leading to a homogeneous hydrogel PNIPAAm film on the surface.^{38b}

A widely used example of an electrochemically controlled “click reaction” is protein modification using Cu^{I} -catalyzed azide–alkyne cycloaddition (CuAAC).⁵¹ The concentration of the active species (Cu^{I}) was maintained electrochemically and the click reaction was performed even in the presence of air. In another example Larsen and coworkers proposed a synthetic route for the preparation of a post-modifiable conducting poly(3,4-(1-azidomethylethylene) dioxothiophene) (PEDOT- N_3) by CuAAC.⁵² A CuAAC reaction between an array of PEDOT- N_3 units on an electrode and alkyne moieties present in the contacting solution was carried out. Multiple PEDOT- N_3 electrodes were prepared and CuAAC occurred only on the cathode due to the reduction of copper catalysts. On the other hand, the anode was not modified. Non-modified areas were reacted with different alkyne moieties simply by switching anode and cathode (Figure I-18).

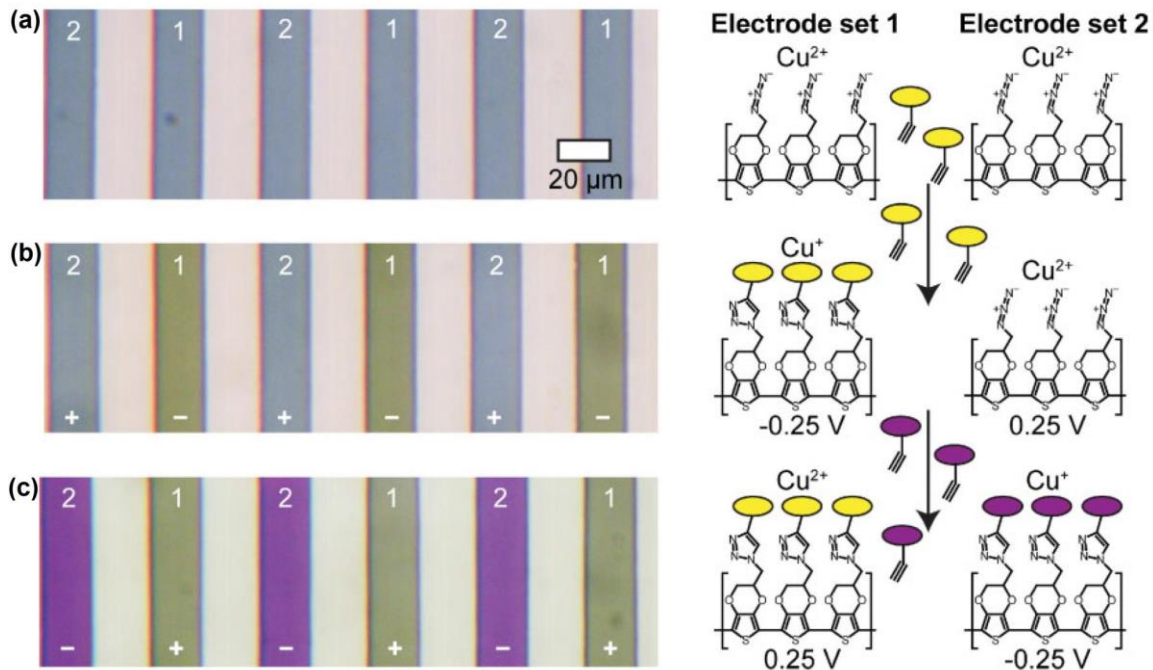


Figure I-18. Functionalization of PEDOT-N₃ electrodes using electrochemically mediated CuAAC. Optical microscopy bright-field image of dried PEDOT-N₃ electrodes after electrochemically mediated CuAAC with alkyne-terminated fluorescein (yellow color) or rhodamine (purple color): (a) without potential (non-modified), (b) cathodic current to electrode *set 1*, and (c) using (b) electrodes and switching current (cathode = *set 2*) in presence of alkyne-terminated rhodamine.^{52a}

Huskens and coworkers prepared gradient functionalized substrates using electrochemically mediated CuAAC.⁵³ The azide modified substrates were placed between the cathode and anode. The area with a higher concentration of Cu^I/L⁺, near the cathode, reacted with fluorescein-alkyne while the farther the substrate was from the cathode the concentration of Cu^I/L⁺ species gradually decreased and showed a gradual decrease in fluorescein intensity. The technique was further used for immobilization of gradient

biomolecule substrates.

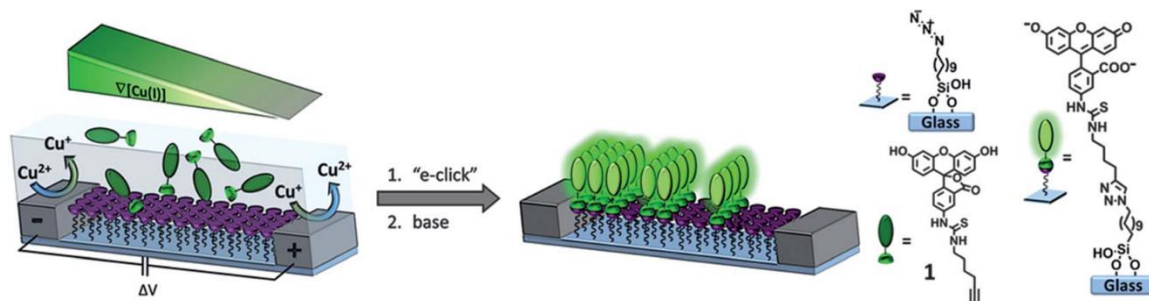


Figure I-19. Gradient surface modification using electrochemically mediated CuAAC.

The concentration of $\text{Cu}^{\text{I}}/\text{L}^+$ was gradually decreased far from cathode.⁵³

Bard and coworkers proposed direct surface patterning by "click chemistry" using scanning electrochemical microscopy (SECM).⁵⁴ Surfaces with an azido functionalized self-assembled monolayer were prepared and a click reaction was carried out with acetylene-functionalized fluorophores. The tip of a gold electrode SECM was used for local reduction of deactivators to activators, and CuAAC occurred only between the tip and substrate, Figure I-20. This approach has the potential to be used in the preparation of protein arrays.

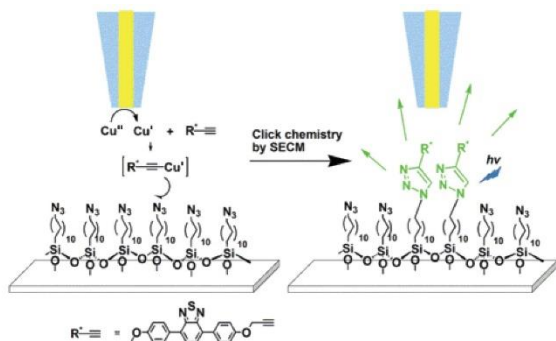


Figure I-20. Locally reduction of deactivators to activators at a gold microelectrode and functionalization of a glass substrate through “click chemistry”.^{54a}

Similarly, a cobalt phthalocyanine functionalized electrode was prepared by “click electrochemistry (CEC)” and used as a pesticide sensor, Figure I-21.⁵⁵ In this study, a glassy carbon electrode (GCE) was selected for electropolymerization with azide functionalized aniline (PANI-N₃). The PANI-N₃ modified electrode was further decorated with terminal-alkynyl (TA) substituted cobalt phthalocyanine (CoPc-TA) under cathodic current. The applied current reduced Cu^{II} to Cu^I and the click reaction (CEC) between PANI-N₃ and CoPc-TA occurred. The modified electrode detected a wider concentration range of pesticides.

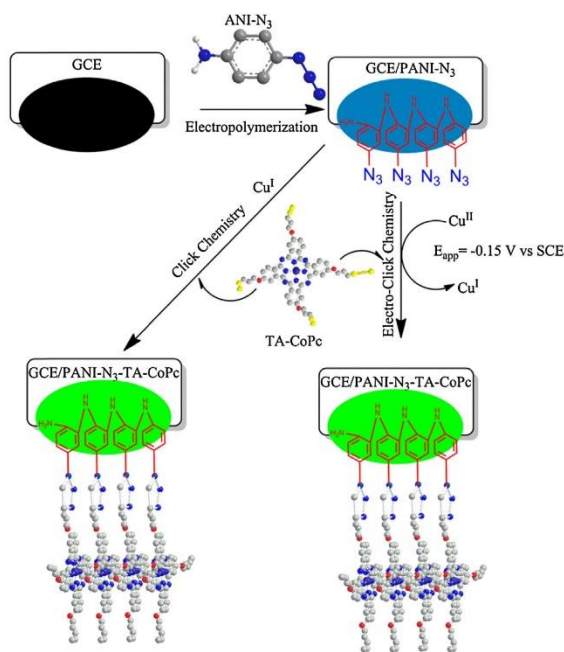


Figure I-21. Electrode modification *via* “click chemistry” and CEC to use of electrochemical pesticide sensors.⁵⁵

Nishizawa and coworkers reported micro-patterning of a flexible electrode PEDOT agarose hydrogel.⁵⁶ The preparation of the PEDOT/agarose electrode is illustrated in Figure I-22. A melted agarose solution was poured over a glass plate fitted with a Pt microelectrode. After gelation of the agarose, electropolymerization was conducted for the synthesis of PEDOT. The PEDOT/agarose electrodes maintained conductivity and flexibility.

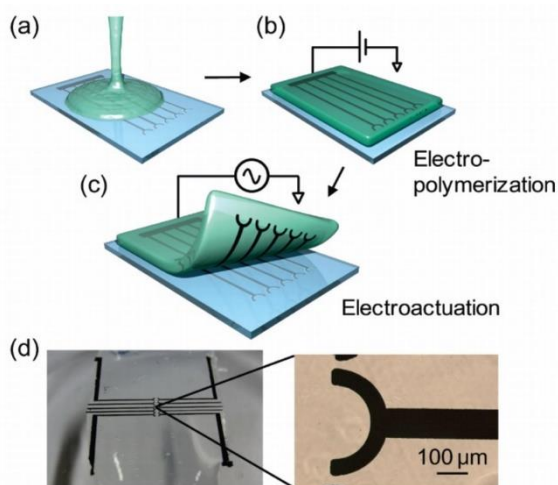


Figure I-22. Schematic illustration of the fabrication of a conducting polymer/hydrogel electrode. (a) A melted agarose solution was poured onto a Pt microelectrode substrate. (b) Electropolymerization of the PEDOT into the gel (c) repeat electrochemically actuation for nondestructively peeling. (d) Photograph of the PEDOT microelectrode array on the gel sheet.⁵⁶

The technique can be further utilized for preparation of conductive and flexible electrodes, Figure I-23, with either natural hydrogels (collagen or glucomannan) or synthetic polymer hydrogels (PAAm or PHEMA).⁵⁷ Since the produced hydrogel/electrodes displayed a high level of oxygen and nutrient permeability, the

electrodes could be used for *in vivo* and *in vitro* biosensors, such as a transdermal iontophoresis patch.

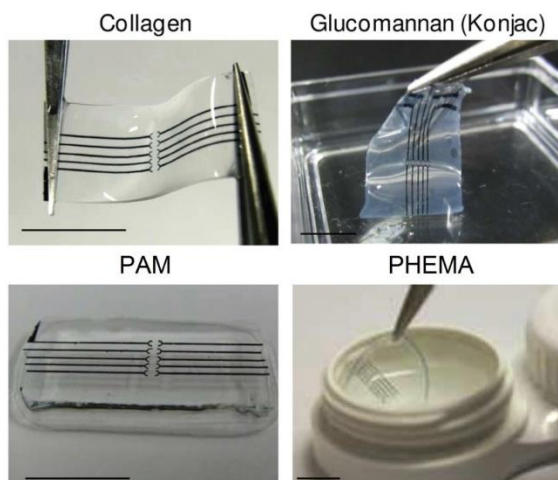


Figure I-23. Photographs of the conductive and flexible electrodes with various hydrogels (collagen, glucomannan, PAAm, and commercially available contact lens (PHEMA)). Scale bar: 5 mm.⁵⁷

I. 6. Summary

Electrochemically mediated polymerization methods have been shown to be useful in the synthesis of new types of polymeric materials. Nonetheless, it was necessary to fully understand the mechanisms, apparatus, advantages and limitations of these techniques described in the literature, which was the focus of this Chapter, prior to further development of the methods. Since kinetic issues were already extensively covered in the existing literature, they received less attention in my own research while more focus was given to the issues regarding procedures for polymer preparation and applications.

Electrochemically mediated ATRP had unique advantages in controlled radical

polymerization, such as precisely controlled the ratio of the concentration of activator to deactivator and recycling transition metal catalysts. Several parameters, such as applied current or potential, and total charge passed, can be controlled in an *e*ATRP, enabling the selection of a desired concentration of the redox-active catalytic species.

This Chapter aimed to provide an overview of *e*ATRP and other electrochemically mediated polymerization and reaction techniques with redox-sensitive initiators; including copper-catalyzed azide-alkyne cycloaddition (click chemistry), electrochemical micropatterning, and RAFT polymerization. The expansion of research in this area over the last decade indicates that electrochemically controlled methods have become an essential tool for the design and synthesis of advanced, high quality, novel polymer materials.

I. 7. Thesis goal

The goal of this thesis was to investigate in detail the mechanistic features of *e*ATRP under various conditions and explore the synthesis of polymers with complex polymer architecture using *e*ATRP. Advantages of *e*ATRP include the ability to control for R_p by E_{app} , provide on-off polymerization, and a simple procedure for removal of transition metals by a deposition process. However, one of the limitations associated with *e*ATRP was its complex reaction setup. The complexity of reaction setup stage could be a substantial obstacle to wide application of *e*ATRP in both academia and industry. This limitation indicated there was a significant need for its simplification. Another objective was to expand the range of monomers that could be polymerized in an *e*ATRP, including polymerization of acrylamides that are typically water soluble monomers that are used for

biomedical applications. There are some limitations associated with polymerization of acrylamides by ATRP. The monomers or polymers can form a complex with ATRP catalysts and tend to lose chain-end functionalities by solvolysis. Aqueous *e*ATRP was used to overcome such limitations.

In order to expand the utility of aqueous phase polymerizations, an environmentally friendly *e*ATRP miniemulsion polymerization was developed. Two catalysts were prepared for the miniemulsion polymerization, one for the oil and one for the water phase, providing communication between both catalysts by electrolysis and electron transfer reactions. Electrochemically mediated RAFT polymerization was examined in presence of conventional radical initiators and RAFT agents.

Research results of fundamental aspects of *e*ATRP studied during my doctoral program are discussed in greater detail throughout Chapters II – VI.

The preparation of polymers with complex polymer architecture (*i.e.*, star polymers) was the main focus of materials development in my thesis. In general, two techniques are predominately used for star synthesis: arm-first and core-first methods. Major advantages of the arm-first method are the ability to incorporate multiple arms, prepare mikto-arm star polymers, and functionalize both the star core and periphery of the arms. However, the challenge of this arm first method is the difficult purification of the product, which consists of a mixture of macroinitiators and star molecules with similar physical properties. This limitation could be overcome if conditions were developed that led to a high level of macroinitiator conversion. *e*ATRP can prevent initial star-star coupling reactions by controlling the initial R_p and then the concentration of activator can be increased to drive

the reaction to high conversion. The star polymers are potentially used for biomedical applications such as cell harvesting surface from temperature responsive surface. Indeed an easier procedure for surface modification was demonstrated by introducing UV crosslinkable groups into star polymers that were deposited on surfaces then crosslinked. The star polymer modified surfaces were then examined for cell-to-polymer interaction study and could potentially be used as smart surfaces for cell harvesting. The results of this research are described in Chapters VII – IX.

I. 8. References

1. (a) Wang, J. S.; Matyjaszewski, K., *J Am Chem Soc* **1995**, *117* (20), 5614-5615; (b) Matyjaszewski, K.; Xia, J. H., *Chem Rev* **2001**, *101* (9), 2921-2990; (c) Tsarevsky, N. V.; Matyjaszewski, K., *Chemical Reviews (Washington, DC, United States)* **2007**, *107* (6), 2270-2299; (d) Matyjaszewski, K.; Tsarevsky, N. V., *Nature Chemistry* **2009**, *1* (4), 276-288; (e) Matyjaszewski, K., *Macromolecules* **2012**, *45* (10), 4015-4039; (f) Matyjaszewski, K.; Tsarevsky, N. V., *J. Am. Chem. Soc.* **2014**.
2. (a) Patten, T. E.; Matyjaszewski, K., *Adv Mater* **1998**, *10* (12), 901-+; (b) Coessens, V.; Pintauer, T.; Matyjaszewski, K., *Prog. Polym. Sci.* **2001**, *26* (3), 337-377; (c) Braunecker, W. A.; Matyjaszewski, K., *Prog Polym Sci* **2007**, *32* (1), 93-146; (d) Lee, H.-i.; Pietrasik, J.; Sheiko, S. S.; Matyjaszewski, K., *Prog. Polym. Sci.* **2010**, *35* (1-2), 24-44.
3. (a) Qiu, J.; Matyjaszewski, K., *Macromolecules* **1997**, *30* (19), 5643-5648; (b) Matyjaszewski, K.; Patten, T. E.; Xia, J. H., *J Am Chem Soc* **1997**, *119* (4), 674-680; (c) Teodorescu, M.; Matyjaszewski, K., *Macromolecules* **1999**, *32* (15), 4826-4831; (d) Percec, V.; Popov, A. V.; Ramirez-Castillo, E.; Monteiro, M.; Barboiu, B.; Weichold, O.; Asandei, A. D.; Mitchell, C. M., *J Am Chem Soc* **2002**, *124* (18), 4940-4941; (e) Wever, D. A. Z.; Raffa, P.; Picchioni, F.; Broekhuis, A. A., *Macromolecules* **2012**, *45* (10), 4040-4045.
4. Matyjaszewski, K.; Tsarevsky, N. V., *J Am Chem Soc* **2014**, *136* (18), 6513-6533.
5. (a) Matyjaszewski, K.; Jakubowski, W.; Min, K.; Tang, W.; Huang, J. Y.; Braunecker, W. A.; Tsarevsky, N. V., *P Natl Acad Sci USA* **2006**, *103* (42), 15309-15314; (b) Matyjaszewski, K.; Dong, H.; Jakubowski, W.; Pietrasik, J.; Kusumo, A., *Langmuir* **2007**, *23* (8), 4528-4531; (c) Dong, H.; Matyjaszewski, K., *Macromolecules* **2008**, *41* (19), 6868-6870; (d) Jakubowski, W.; Kirci-Denizli, B.; Gil, R. R.; Matyjaszewski, K., *Macromol. Chem. Phys.* **2008**, *209* (1), 32-39; (e) Kwak, Y.; Matyjaszewski, K., *Polym Int* **2009**, *58* (3), 242-247; (f) Kwak, Y.; Magenau, A. J. D.; Matyjaszewski, K., *Macromolecules* **2011**, *44* (4), 811-819; (g) Simakova, A.; Averick, S. E.; Konkolewicz, D.; Matyjaszewski, K., *Macromolecules* **2012**, *45* (16), 6371-6379.
6. (a) Mueller, L.; Jakubowski, W.; Tang, W.; Matyjaszewski, K., *Macromolecules* **2007**, *40* (18), 6464-6472; (b) Plichta, A.; Li, W. W.; Matyjaszewski, K., *Macromolecules* **2009**,

- 42 (7), 2330-2332; (c) Zhang, L.; Miao, J.; Cheng, Z.; Zhu, X., *Macromolecular Rapid Communications* **2010**, *31* (3), 275-280; (d) Zhu, G.; Zhang, L.; Zhang, Z.; Zhu, J.; Tu, Y.; Cheng, Z.; Zhu, X., *Macromolecules* **2011**, *44* (9), 3233-3239; (e) D'hooge, D. R.; Konkolewicz, D.; Reyniers, M. F.; Marin, G. B.; Matyjaszewski, K., *Macromol Theor Simul* **2012**, *21* (1), 52-69.
7. (a) Matyjaszewski, K.; Tsarevsky, N. V.; Braunecker, W. A.; Dong, H.; Huang, J.; Jakubowski, W.; Kwak, Y.; Nicolay, R.; Tang, W.; Yoon, J. A., *Macromolecules* **2007**, *40* (22), 7795-7806; (b) Wang, Y.; Matyjaszewski, K., *Abstr Pap Am Chem S* **2011**, 242; (c) Konkolewicz, D.; Wang, Y.; Zhong, M. J.; Krys, P.; Isse, A. A.; Gennaro, A.; Matyjaszewski, K., *Macromolecules* **2013**, *46* (22), 8749-8772; (d) Gois, J. R.; Konkolewicz, D.; Popov, A. V.; Guliasvili, T.; Matyjaszewski, K.; Serra, A. C.; Coelho, J. F. J., *Polym Chem-Uk* **2014**, *5* (16), 4617-4626; (e) Konkolewicz, D.; Krys, P.; Gois, J. R.; Mendonca, P. V.; Zhong, M. J.; Wang, Y.; Gennaro, A.; Isse, A. A.; Fantin, M.; Matyjaszewski, K., *Macromolecules* **2014**, *47* (2), 560-570; (f) Konkolewicz, D.; Wang, Y.; Krys, P.; Zhong, M. J.; Isse, A. A.; Gennaro, A.; Matyjaszewski, K., *Polym Chem-Uk* **2014**, *5* (15), 4396-4417.
8. (a) Erel, I.; Cianga, I.; Serhatli, E.; Yagci, Y., *European Polymer Journal* **2002**, *38* (7), 1409-1415; (b) Ishizu, K.; Kakinuma, H., *J Polym Sci Pol Chem* **2005**, *43* (1), 63-70; (c) Ishizu, K.; Murakami, T.; Takano, S., *Journal of Colloid and Interface Science* **2008**, 322 (1), 59-64; (d) Tasdelen, M. A.; Uygun, M.; Yagci, Y., *Macromol. Chem. Phys.* **2011**, *212* (18), 2036-2042; (e) Konkolewicz, D.; Schroder, K.; Buback, J.; Bernhard, S.; Matyjaszewski, K., *Acs Macro Lett* **2012**, *1* (10), 1219-1223; (f) Tasdelen, M. A.; Ciftci, M.; Yagci, Y., *Macromolecular Chemistry and Physics* **2012**, *213* (13), 1391-1396; (g) Yan, J.; Li, B.; Zhou, F.; Liu, W., *Acs Macro Lett* **2013**, *2* (7), 592-596; (h) Taskin, O. S.; Yilmaz, G.; Tasdelen, M. A.; Yagci, Y., *Polym Int* **2014**, *63* (5), 902-907; (i) Dadashi-Silab, S.; Tasdelen, M. A.; Asiri, A. M.; Khan, S. B.; Yagci, Y., *Macromolecular Rapid Communications* **2014**, *35* (4), 454-459; (j) Ribelli, T. G.; Konkolewicz, D.; Pan, X. C.; Matyjaszewski, K., *Macromolecules* **2014**, *47* (18), 6316-6321; (k) Zhang, T.; Chen, T.; Amin, I.; Jordan, R., *Polym Chem-Uk* **2014**, *5* (16), 4790-4796; (l) Ribelli, T. G.; Konkolewicz, D.; Bernhard, S.; Matyjaszewski, K., *J Am Chem Soc* **2014**, *136* (38), 13303-13312.
9. Qiu, J.; Matyjaszewski, K.; Thouin, L.; Amatore, C., *Macromolecular Chemistry and Physics* **2000**, *201* (14), 1625-1631.
10. Magenau, A. J. D.; Strandwitz, N. C.; Gennaro, A.; Matyjaszewski, K., *Science* **2011**, *332* (6025), 81-84.
11. Magenau, A. J. D.; Bortolamei, N.; Frick, E.; Park, S.; Gennaro, A.; Matyjaszewski, K., *Macromolecules* **2013**, *46* (11), 4346-4353.
12. Bortolamei, N.; Isse, A. A.; Magenau, A. J. D.; Gennaro, A.; Matyjaszewski, K., *Angew. Chem. Int. Ed.* **2011**, *50* (48), 11391-11394.
13. (a) Kamigaito, M.; Ando, T.; Sawamoto, M., *Chem. Rev.* **2001**, *101* (12), 3689-3746; (b) Ouchi, M.; Terashima, T.; Sawamoto, M., *Chem Rev* **2009**, *109* (11), 4963-5050; (c) di Lena, F.; Matyjaszewski, K., *Prog. Polym. Sci.* **2010**, *35* (8), 959-1021.
14. Matyjaszewski, K., *Isr. J. Chem.* **2012**, *52* (3-4), 206-220.
15. Horn, M.; Matyjaszewski, K., *Macromolecules* **2013**, *46* (9), 3350-3357.
16. Fischer, H., *Chem Rev* **2001**, *101* (12), 3581-3610.

17. (a) Honigfort, M. E.; Brittain, W. J.; Bosanac, T.; Wilcox, C. S., *Macromolecules* **2002**, 35 (13), 4849-4851; (b) Hong, S. C.; Matyjaszewski, K., *Macromolecules* **2002**, 35 (20), 7592-7605; (c) Sarbu, T.; Pintauer, T.; McKenzie, B.; Matyjaszewski, K., *Journal of Polymer Science Part A: Polymer Chemistry* **2002**, 40 (18), 3153-3160; (d) Yang, J.; Ding, S.; Radosz, M.; Shen, Y., *Macromolecules* **2004**, 37 (5), 1728-1734; (e) Barré, G.; Taton, D.; Lastécouères, D.; Vincent, J.-M., *J Am Chem Soc* **2004**, 126 (25), 7764-7765; (f) Faucher, S.; Okrutny, P.; Zhu, S., *Macromolecules* **2006**, 39 (1), 3-5; (g) Munirasu, S.; Deshpande, A.; Baskaran, D., *Macromolecular Rapid Communications* **2008**, 29 (18), 1538-1543.
18. (a) Jakubowski, W.; Min, K.; Matyjaszewski, K., *Macromolecules* **2006**, 39 (1), 39-45; (b) Jakubowski, W.; Matyjaszewski, K., *Angewandte Chemie International Edition* **2006**, 45 (27), 4482-4486.
19. (a) Chen, H.; Yang, L.; Liang, Y.; Hao, Z.; Lu, Z., *J Polym Sci Pol Chem* **2009**, 47 (12), 3202-3207; (b) Nicolay, R.; Kwak, Y.; Matyjaszewski, K., *Angew Chem Int Edit* **2010**, 49 (3), 541-544.
20. Abreu, C. M. R.; Serra, A. C.; Popov, A. V.; Matyjaszewski, K.; Guliashvili, T.; Coelho, J. F. J., *Polym Chem-Uk* **2013**, 4 (23), 5629-5636.
21. Wang, G.; Zhu, X.; Wu, J.; Zhu, J.; Chen, X.; Cheng, Z., *Journal of Applied Polymer Science* **2007**, 106 (2), 1234-1242.
22. (a) Li, B.; Yu, B.; Huck, W. T. S.; Zhou, F.; Liu, W., *Angew. Chem.* **2012**, 124 (21), 5182-5185; (b) Li, B.; Yu, B.; Huck, W. T. S.; Liu, W.; Zhou, F., *J. Am. Chem. Soc.* **2013**, 135 (5), 1708-1710; (c) Park, S.; Chmielarz, P.; Gennaro, A.; Matyjaszewski, K., *Angewandte Chemie International Edition* **2015**, 54 (8), 2388 –2392; (d) Chmielarz, P.; Park, S.; Simakova, A.; Matyjaszewski, K., *Polymer* **2015**, 60, 302-307.
23. (a) Min, K.; Gao, H.; Matyjaszewski, K., *Macromolecules* **2007**, 40 (6), 1789-1791; (b) Abreu, C. M. R.; Mendonca, P. V.; Serra, A. C.; Popov, A. V.; Matyjaszewski, K.; Guliashvili, T.; Coelho, J. F. J., *ACS Macro Lett.* **2012**, 1, 1308–1311; (c) Woodruff, S. R.; Davis, B. J.; Tsarevsky, N. V., *Macromolecular Rapid Communications* **2014**, 35 (2), 186-192.
24. (a) Matyjaszewski, K.; Coca, S.; Gaynor, S. G.; Wei, M.; Woodworth, B. E., *Macromolecules* **1997**, 30 (23), 7348-7350; (b) Zhang, Y.; Wang, Y.; Matyjaszewski, K., *Macromolecules* **2011**, 44 (4), 683-685.
25. Mueller, L.; Matyjaszewski, K., *Macromol React Eng* **2010**, 4 (3-4), 180-185.
26. Konkolewicz, D.; Wang, Y.; Krys, P.; Zhong, M.; Isse, A. A.; Gennaro, A.; Matyjaszewski, K., *Polym Chem-Uk* **2014**, 5 (15), 4396-4417.
27. Fantin, M.; Isse, A. A.; Gennaro, A.; Matyjaszewski, K., *Macromolecules* **2015**, 48 (19), 6862-6875.
28. Tang, W.; Matyjaszewski, K., *Macromolecules* **2006**, 39 (15), 4953-4959.
29. De Paoli, P.; Isse, A. A.; Bortolamei, N.; Gennaro, A., *Chem. Commun.* **2011**, 47 (12), 3580-3582.
30. (a) Bortolamei, N.; Isse, A. A.; Di Marco, V. B.; Gennaro, A.; Matyjaszewski, K., *Macromolecules* **2010**, 43 (22), 9257-9267; (b) Isse, A. A.; Gennaro, A.; Lin, C. Y.; Hodgson, J. L.; Coote, M. L.; Guliashvili, T., *J Am Chem Soc* **2011**, 133 (16), 6254-6264.
31. (a) Bell, C. A.; Bernhardt, P. V.; Monteiro, M. J., *J Am Chem Soc* **2011**, 133 (31), 11944-11947; (b) Zerk, T. J.; Bernhardt, P. V., *Inorg Chem* **2014**, 53 (21), 11351-11353.

32. (a) Isse, A. A.; Bortolamei, N.; De Paoli, P.; Gennaro, A., *Electrochimica Acta* **2013**, *110*, 655-662; (b) Lorandi, F.; Fantin, M.; Isse, A. A.; Gennaro, A., *Polymer* **2015**, *72*, 238-245.
33. Konkolewicz, D.; Kryś, P.; Góis, J. R.; Mendonça, P. V.; Zhong, M.; Wang, Y.; Gennaro, A.; Isse, A. A.; Fantin, M.; Matyjaszewski, K., *Macromolecules* **2014**, *47* (2), 560-570.
34. Soerensen, N.; Barth, J.; Buback, M.; Morick, J.; Schroeder, H.; Matyjaszewski, K., *Macromolecules* **2012**, *45* (9), 3797-3801.
35. Nave, P. M., **1969**.
36. (a) Saraç, A. S.; Erbil, C.; Soydan, A. B., *Journal of Applied Polymer Science* **1992**, *44* (5), 877-881; (b) Sarac, A. S., *Prog Polym Sci* **1999**, *24* (8), 1149-1204; (c) Saraç, A. S.; Soydan, A. B.; Coka, V., *Journal of Applied Polymer Science* **1996**, *62* (1), 111-116; (d) Jenkins, D. W.; Hudson, S. M., *Chem Rev* **2001**, *101* (11), 3245-3274.
37. Cosnier, S.; Karyakin, A., *Electropolymerization: concepts, materials and applications*. John Wiley & Sons: 2011.
38. (a) Reuber, J.; Reinhardt, H.; Johannsmann, D., *Langmuir* **2006**, *22* (7), 3362-3367; (b) Bünsow, J.; Mänz, M.; Vana, P.; Johannsmann, D., *Macromol. Chem. Phys.* **2010**, *211* (7), 761-767.
39. Bonometti, V.; Labbe, E.; Buriez, O.; Mussini, P.; Amatore, C., *J Electroanal Chem* **2009**, *633* (1), 99-105.
40. Inzelt, G.; Lewenstam, A.; Scholz, F.; Baucke, F. G., *Handbook of reference electrodes*. Springer: 2013.
41. (a) Li, B.; Yu, B.; Zhou, F., *Macromolecular Rapid Communications* **2013**, *34* (3), 246-250; (b) Chmielarz, P.; Kryś, P.; Park, S.; Matyjaszewski, K., *Polymer* **2015**, *in press*.
42. Park, S.; Cho, H. Y.; Wegner, K. B.; Burdyska, J.; Magenau, A. J. D.; Paik, H. J.; Jurga, S.; Matyjaszewski, K., *Macromolecules* **2013**, *46* (15), 5856-5860.
43. (a) Hadjichristidis, N.; Pitsikalis, M.; Pispas, S.; Iatrou, H., *Chem. Rev.* **2001**, *101* (12), 3747-3792; (b) Vamvakaki, M.; Hadjiyannakou, S. C.; Loizidou, E.; Patrikios, C. S.; Armes, S. P.; Billingham, N. C., *Chemistry of Materials* **2001**, *13* (12), 4738-4744; (c) Gao, H.; Matyjaszewski, K., *Prog Polym Sci* **2009**, *34* (4), 317-350; (d) Blencowe, A.; Tan, J. F.; Goh, T. K.; Qiao, G. G., *Polymer* **2009**, *50* (1), 5-32; (e) Gregory, A.; Stenzel, M. H., *Progress in Polymer Science* **2012**, *37* (1), 38-105.
44. (a) Hosseiny, S. S.; van Rijn, P., *Polymers* **2013**, *5* (4), 1229-1240; (b) Jin, G.-P.; Fu, Y.; Bao, X.-C.; Feng, X.-S.; Wang, Y.; Liu, W.-H., *Journal of Applied Electrochemistry* **2014**, *44* (5), 621-629; (c) Shida, N.; Koizumi, Y.; Nishiyama, H.; Tomita, I.; Inagi, S., *Angewandte Chemie International Edition* **2015**, *54* (13), 3922-3926; (d) Hu, Y.; Yang, G.; Liang, B.; Fang, L.; Ma, G.; Zhu, Q.; Chen, S.; Ye, X., *Acta Biomater.* **2015**, *13* (0), 142-149.
45. (a) Mavré, F.; Anand, R. K.; Laws, D. R.; Chow, K.-F.; Chang, B.-Y.; Crooks, J. A.; Crooks, R. M., *Anal Chem* **2010**, *82* (21), 8766-8774; (b) Ramakrishnan, S.; Shannon, C., *Langmuir* **2010**, *26* (7), 4602-4606; (c) Ishiguro, Y.; Inagi, S.; Fuchigami, T., *Langmuir* **2011**, *27* (11), 7158-7162; (d) Fosdick, S. E.; Knust, K. N.; Scida, K.; Crooks, R. M., *Angew. Chem. Int. Ed.* **2013**, *52* (40), 10438-10456; (e) Loget, G.; Zigah, D.; Bouffier, L.; Sojic, N.; Kuhn, A., *Accounts of Chemical Research* **2013**, *46* (11), 2513-2523.

46. Sun, Y.; Du, H.; Lan, Y.; Wang, W.; Liang, Y.; Feng, C.; Yang, M., *Biosensors Bioelectron.* **2016**, *77*, 894-900.
47. Sun, Y.; Du, H.; Deng, Y.; Lan, Y.; Feng, C., *J. Solid State Electrochem.* **2015**, *20* (1), 105-113.
48. Plamper, F., *Colloid. Polym. Sci.* **2014**, *292* (4), 777-783.
49. (a) Patton, D. L.; Taranekekar, P.; Fulghum, T.; Advincula, R., *Macromolecules* **2008**, *41* (18), 6703-6713; (b) Wessling, B., *Polymers* **2010**, *2* (4), 786-798; (c) Friebe, C.; Hager, M. D.; Winter, A.; Schubert, U. S., *Adv Mater* **2012**, *24* (3), 332-345; (d) Li, M.; Zhang, J.; Nie, H.-J.; Liao, M.; Sang, L.; Qiao, W.; Wang, Z. Y.; Ma, Y.; Zhong, Y.-W.; Ariga, K., *Chemical Communications* **2013**, *49* (61), 6879-6881; (e) Bardini, L.; Ceccato, M.; Hinge, M.; Pedersen, S. U.; Daasbjerg, K.; Marcaccio, M.; Paolucci, F., *Langmuir* **2013**, *29* (11), 3791-3796; (f) Isse, A. A.; Visonà, G.; Ghelfi, F.; Roncaglia, F.; Gennaro, A., *Adv. Synth. Catal.* **2015**, *357* (4), 782-792.
50. Hazimeh, H.; Piogé, S.; Pantoustier, N.; Combellas, C.; Podvorica, F. I.; Kanoufi, F., *Chemistry of Materials* **2013**, *25* (4), 605-612.
51. Bünsow, J.; Johannsmann, D., *Macromolecular Rapid Communications* **2009**, *30* (9-10), 858-863.
52. Hong, V.; Udit, A. K.; Evans, R. A.; Finn, M. G., *ChemBioChem* **2008**, *9* (9), 1481-1486.
53. (a) Hansen, T. S.; Dagaard, A. E.; Hvilsted, S.; Larsen, N. B., *Adv Mater* **2009**, *21* (44), 4483-4486; (b) Hansen, T. S.; Lind, J. U.; Dagaard, A. E.; Hvilsted, S.; Andresen, T. L.; Larsen, N. B., *Langmuir* **2010**, *26* (20), 16171-16177.
54. Nicosia, C.; Krabbenborg, S. O.; Chen, P.; Huskens, J., *Journal of Materials Chemistry B* **2013**, *1* (40), 5417-5428.
55. (a) Ku, S.-Y.; Wong, K.-T.; Bard, A. J., *J. Am. Chem. Soc.* **2008**, *130* (8), 2392-2393; (b) Amemiya, S.; Bard, A. J.; Fan, F.-R. F.; Mirkin, M. V.; Unwin, P. R., *Annual Review of Analytical Chemistry* **2008**, *1* (1), 95-131; (c) Ye, H.; Lee, J.; Jang, J. S.; Bard, A. J., *The Journal of Physical Chemistry C* **2010**, *114* (31), 13322-13328.
56. İpek, Y.; Dinçer, H.; Koca, A., *Sensors Actuators B: Chem.* **2014**, *193* (0), 830-837.
57. Sekine, S.; Ido, Y.; Miyake, T.; Nagamine, K.; Nishizawa, M., *J Am Chem Soc* **2010**, *132* (38), 13174-13175.
58. Ido, Y.; Takahashi, D.; Sasaki, M.; Nagamine, K.; Miyake, T.; Jasinski, P.; Nishizawa, M., *ACS Macro Letters* **2012**, *1* (3), 400-403.
59. Moad, G.; Chong, Y. K.; Postma, A.; Rizzardo, E.; Thang, S. H., *Polymer* **2005**, *46* (19), 8458-8468.
60. (a) Hawker, C. J.; Bosman, A. W.; Harth, E., *Chem. Rev. (Washington, D. C.)* **2001**, *101* (Copyright (C) 2012 American Chemical Society (ACS). All Rights Reserved.), 3661-3688; (b) Nicolas, J.; Guillaneuf, Y.; Lefay, C.; Bertin, D.; Gigmes, D.; Charleux, B., *Progress in Polymer Science* **2013**, *38* (1), 63-235.
61. (a) Poli, R., *Angew. Chem. Int. Ed.* **2006**, *45* (31), 5058-5070; (b) Allan, L. E. N.; Perry, M. R.; Shaver, M. P., *Prog. Polym. Sci.* **2012**, *37* (1), 127-156.
62. (a) Matyjaszewski, K.; Xia, J., *Chemical Reviews* **2001**, *101* (9), 2921-2990; (b) Tsarevsky, N. V.; Matyjaszewski, K., *Chem. Rev.* **2007**, *107* (6), 2270-2299; (c) Siegwart, D. J.; Oh, J. K.; Matyjaszewski, K., *Prog. Polym. Sci.* **2012**, *37* (1), 18-37; (d) Matyjaszewski, K.; Tsarevsky, N. V., *Nat Chem* **2009**, *1* (4), 276-288; (e) Matyjaszewski,

- K.; Spanswick, J., 3.12 - Copper-Mediated Atom Transfer Radical Polymerization. In *Polymer Science: A Comprehensive Reference*, Editors-in-Chief: Krzysztof, M.; Martin, M., Eds. Elsevier: Amsterdam, 2012; pp 377-428.
63. di Lena, F.; Matyjaszewski, K., *Prog. Polym. Sci.* **2010**, *35* (8), 959-1021.
64. (a) Tang, W.; Kwak, Y.; Braunecker, W.; Tsarevsky, N. V.; Coote, M. L.; Matyjaszewski, K., *Journal of American Chemical Society* **2008**, *130* (32), 10702-10713; (b) Magenau, A. J. D.; Kwak, Y.; Schröder, K.; Matyjaszewski, K., *ACS Macro Letters* **2012**, *1* (4), 508-512.
65. (a) Seeliger, F.; Matyjaszewski, K., *Macromolecules* **2009**, *42* (16), 6050-6055; (b) Braunecker, W. A.; Tsarevsky, N. V.; Gennaro, A.; Matyjaszewski, K., *Macromolecules* **2009**, *42* (17), 6348-6360; (c) Morick, J.; Buback, M.; Matyjaszewski, K., *Macromol. Chem. Phys.* **2012**, *213* (21), 2287-2292.
66. (a) Jakubowski, W.; Matyjaszewski, K., *Angew. Chem. Int. Ed.* **2006**, *118* (27), 4594-4598; (b) Matyjaszewski, K.; Jakubowski, W.; Min, K.; Tang, W.; Huang, J.; Braunecker, W. A.; Tsarevsky, N. V., *Proceedings of the National Academy of Sciences* **2006**, *103* (42), 15309-15314.
67. (a) Matyjaszewski, K.; Coca, S.; Gaynor, S. G.; Wei, M.; Woodworth, B. E., *Macromolecules* **1997**, *30* (23), 7348-7350; (b) Percec, V.; Guliashevili, T.; Ladislav, J. S.; Wistrand, A.; Stjern Dahl, A.; Sienkowska, M. J.; Monteiro, M. J.; Sahoo, S., *J. Am. Chem. Soc.* **2006**, *128* (43), 14156-14165; (c) Matyjaszewski, K.; Tsarevsky, N. V.; Braunecker, W. A.; Dong, H.; Huang, J.; Jakubowski, W.; Kwak, Y.; Nicolay, R.; Tang, W.; Yoon, J. A., *Macromolecules* **2007**, *40* (22), 7795-7806; (d) Magenau, A. J. D.; Kwak, Y.; Matyjaszewski, K., *Macromolecules* **2010**, *43* (23), 9682-9689; (e) Zhang, Y.; Wang, Y.; Peng, C.-h.; Zhong, M.; Zhu, W.; Konkolewicz, D.; Matyjaszewski, K., *Macromolecules* **2011**.
68. (a) Jakubowski, W.; Min, K.; Matyjaszewski, K., *Macromolecules* **2005**, *39* (1), 39-45; (b) Matyjaszewski, K.; Dong, H.; Jakubowski, W.; Pietrasik, J.; Kusumo, A., *Langmuir* **2007**, *23* (8), 4528-4531; (c) Li, B.; Yu, B.; Huck, W. T. S.; Zhou, F.; Liu, W. M., *Angew. Chem.-Int. Edit.* **2012**, *51* (21), 5092-5095.
69. Pietrasik, J.; Dong, H.; Matyjaszewski, K., *Macromolecules* **2006**, *39* (19), 6384-6390.
70. (a) Rzaev, J.; Penelle, J., *Angew. Chem. Int. Ed.* **2004**, *43* (13), 1691-1694; (b) Kwiatkowski, P.; Jurczak, J.; Pietrasik, J.; Jakubowski, W.; Mueller, L.; Matyjaszewski, K., *Macromolecules* **2008**, *41* (4), 1067-1069.
71. (a) Kwak, Y.; Matyjaszewski, K., *Macromolecules* **2010**, *43* (12), 5180-5183; (b) Mehmet Atilla, T.; Mustafa, Ç.; Mustafa, U.; Yusuf, Y., Possibilities for Photoinduced Controlled Radical Polymerizations. In *Progress in Controlled Radical Polymerization: Mechanisms and Techniques*, American Chemical Society: 2012; Vol. 1100, pp 59-72; (c) Fors, B. P.; Hawker, C. J., *Angewandte Chemie International Edition* **2012**, *51* (35), 8850-8853; (d) Konkolewicz, D.; Schröder, K.; Buback, J.; Bernhard, S.; Matyjaszewski, K., *ACS Macro Letters* **2012**, *1* (10), 1219-1223.
72. Bortolamei, N.; Isse, A. A.; Magenau, A. J. D.; Gennaro, A.; Matyjaszewski, K., *Angewandte Chemie International Edition* **2011**, *50*, 11391-11394.
73. Kim, B. Y.; Ratcliff, E. L.; Armstrong, N. R.; Kowalewski, T.; Pyun, J., *Langmuir* **2009**, *26* (3), 2083-2092.

74. (a) Hansen, T. S.; Lind, J. U.; Daugaard, A. E.; Hvilsted, S.; Andresen, T. L.; Larsen, N. B., *Langmuir* **2010**, *26* (20), 16171-16177; (b) Bonometti, V.; Labbé, E.; Buriez, O.; Mussini, P.; Amatore, C., *J. Electroanal. Chem.* **2009**, *633* (1), 99-105.
75. (a) Hardy, C. G.; Ren, L. X.; Tamboue, T. C.; Tang, C. B., *J Polym Sci Pol Chem* **2011**, *49* (6), 1409-1420; (b) Kraft, A.; Grimsdale, A. C.; Holmes, A. B., *Angew. Chem. Int. Ed.* **1998**, *37* (4), 402-428.
76. (a) Tria, M. C. R.; Advincula, R. C., *Macromol. Rapid Commun.* **2011**, *32* (13), 966-971; (b) Nunige, S.; Cornut, R.; Hazimeh, H.; Hauquier, F.; Lefrou, C.; Combellas, C.; Kanoufi, F., *Angew. Chem.-Int. Edit.* **2012**, *51* (21), 5208-5212.
77. (a) Broderick, E. M.; Guo, N.; Vogel, C. S.; Xu, C. L.; Sutter, J.; Miller, J. T.; Meyer, K.; Mehrkhodavandi, P.; Diaconescu, P. L., *J. Am. Chem. Soc.* **2011**, *133* (24), 9278-9281; (b) Broderick, E. M.; Guo, N.; Wu, T. P.; Vogel, C. S.; Xu, C. L.; Sutter, J.; Miller, J. T.; Meyer, K.; Cantat, T.; Diaconescu, P. L., *Chem. Commun.* **2011**, *47* (35), 9897-9899; (c) Gregson, C. K. A.; Gibson, V. C.; Long, N. J.; Marshall, E. L.; Oxford, P. J.; White, A. J. P., *Journal of American Chemical Society* **2006**, *128* (23), 7410-7411.
78. Isse, A. A.; Sandona, G.; Durante, C.; Gennaro, A., *Electrochim. Acta* **2009**, *54* (12), 3235-3243.
79. Isse, A. A.; Gennaro, A., *J. Phys. Chem. A* **2004**, *108* (19), 4180-4186.
80. (a) Bard, A. J.; Faulkner, L. R., *Electrochemical methods : fundamentals and applications*. 2nd ed.; Wiley: New York, 2001; (b) Testa, A. C.; Reinmuth, W. H., *Analytical Chemistry* **1961**, *33* (10), 1320-1324.
81. Chan, N.; Cunningham, M. F.; Hutchinson, R. A., *Macromol. Chem. Phys.* **2008**, *209* (17), 1797-1805.
82. Wang, Y.; Zhong, M.; Zhang, Y.; Magenau, A. J. D.; Matyjaszewski, K., *Macromolecules* **2012**, *45* (21), 8929-8932.

Section II.

Investigation of Electrochemically Mediated Atom Transfer Radical Polymerization

Chapter II

Investigation of Electrochemically Mediated Atom Transfer Radical*

II. 1. Preface

Atom transfer radical polymerization (ATRP) is one of the most broadly utilized reversible deactivation radical polymerization (RDRP) techniques that can produce well-defined polymers with predetermined molecular weight. Although ATRP has many advantages in polymer synthetic chemistry, one disadvantage was that it required a high concentration of transition metal catalysts – typically a copper/ligand complex. At the end of 2010, former group member, Dr. Andrew Magenau, developed an electrochemically mediated ATRP process, which utilized ppm levels of transition metal catalysts and electrochemical reduction of added deactivators to activators to initiate the polymerization. Dr. Magenau taught me the basics of electrochemistry and the *e*ATRP reaction and from then on I started to investigate detailed mechanistic features of reactions participating in an *e*ATRP under various conditions.

This Chapter summarizes of *e*ATRP and serves as a basis for the discussions in the following chapters on developing a simplified *e*ATRP reaction (*se*ATRP, Chapter III), polymerization of water-soluble monomers through *e*ATRP in aqueous media by controlling [activator]/[deactivator] ratio, aqueous *e*ATRP (Chapter IV), development of a

*Work in this chapter was published and partially reformatted based on the following manuscript: Magenau, Andrew J. D.; Bortolamei, Nicola; Frick, Elena; **Park, Sangwoo**; Gennaro, Armando; Matyjaszewski, Krzysztof *Macromolecules* **2013**, *46*, 4346

mini-emulsion *e*ATRP (Chapter V), a *e*RAFT system (Chapter VI), and use of *e*ATRP by precisely controlling R_p by applied potential (or current) to obtain a high-yield of well-defined star polymer (Chapter VII). My role in this project was to measure cyclic voltammetry (CV) of copper catalysts, determine applied potentials, from half-wave potential ($E_{1/2}$) to overpotential (η), examine polymerizations carried out with different catalysts concentrations, and evaluate the effects of stirring on the polymerization.

I also conducted several traditional electrochemical analyses for ATRP reaction, which included catalysts characterization based on redox potentials, designing new ligands, and prediction of their activities (*e.g.*, CV analysis). Ligands decorated with electron donating groups enhanced their activity more than the non-modified ligands. In general, a catalyst with 59 mV more negative $E_{1/2}$ shows an order of magnitude enhancement of ATRP equilibrium constant (K_{ATRP}). Former group member, Dr. Kristin Schroeder, systematically investigated the modification of tris(2-pyridylmethyl)amine (TPMA) with electron donating groups at pyridine rings, namely TPMA*1, TPMA*2, and TPMA*3, corresponding to one, two, and three modified pyridine rings (with one methoxy and two methyl groups per each pyridine unit), respectively. Among them, TPMA*3 (with a total number of nine electron donating groups) showed extremely high K_{ATRP} values: it was 1000 times more active than TPMA. These results motivated new catalysts development, for example, active hydrophobic ligands for (mini)emulsion polymerization. Two hydrophobic ligands, bis(2-pyridylmethyl)-octadecylamine (BPMODA) and *N',N''*-dioctadecyl-*N',N''*-bis(2-pyridylmethyl)ethane-1,2-diamine (DOD-BPED) were modified with electron donating groups to form bis[2-(4-methoxy-3,5-

dimethyl)pyridylmethyl]octadecylamine (BPMODA*) and *N',N''*-dioctadecyl-*N',N''*-bis[2-(4-methoxy-3,5-dimethyl)pyridylmethyl] ethane-1,2-diamine (DOD-BPED*) by former group members, Dr. Andrea Elsen and Dr. Joanna Burdyńska. Both of the modified ligands showed more negative reduction potentials than those of original ligands, indicating higher K_{ATRP} . High K_{ATRP} values indicated that the ligands stabilize stronger Cu^{II} (deactivator) rather than Cu^{I} (activator). These catalysts allowed miniemulsion polymerizations with low catalysts loading and resulted in well-defined polymers (Appendices I and II). For the studies included in Appendices I and II, my role was to measure CVs of the newly developed catalysts and compared their activities to the non-modified catalysts. Similarly, iron (Fe) based catalysts were also characterized by using an electrochemical technique; Fe with *N*-heterocyclic carbene (NHC) and bioinspired catalysts, hemin based catalysts, were synthesized by former group member, Seiji Okada, and current group member, Dr. Antonina Simakova, respectively (Appendices III and IV). Electrochemical analysis would elucidate their redox behavior under the selected solution conditions. Both the Fe based catalysts showed reversible redox behavior under polymerization conditions and resulted in well-defined polymers. My role in the projects in Appendices (III and IV) was to conduct CV analysis of the catalysts and predict their activities.

The electrochemical techniques were further used for evaluating real activation step of ATRP reaction in the presence of Cu^0 . There were proposed two models of the reaction – single electron transfer living radical polymerization (SET-LRP) and supplemental activator and reducing agent atom transfer radical polymerization (SARA ATRP). According to the former, as the main activator, Cu^0 activates ATRP initiator to form radical

and deactivators (Cu^{II}). It also claims that Cu^{I} quickly disproportionates and its contribution to activation of alkyl halides is negligible. On the other hand, the latter model is based on the fact that Cu^{I} is the major activator. In this model, Cu^0 acts as a reducing agent for converting Cu^{II} to Cu^{I} and a supplemental activator. To verify the real activation processes, former group members, Dr. Chi-How Peng, Dr. Mingjiang Zhong, Dr. Yu Wang, and Dr. Dominik Konkolewicz, and the current group member, Pawel Krys, and I worked together. I conducted CV analysis, ATRP reaction under solely Cu^0 condition by applying Cu^0 deposition potential, and polymerization with macroinitiators under the same conditions (Appendix V).

I would like to acknowledge my co-worker, Dr. Nicola Bortolamei, for his invaluable discussions on electrochemistry and the *e*ATRP reaction. My appreciation also goes to the aforementioned former and current members of my group.

II. 2. Introduction

Controlled/living radical polymerization (CRP) provides macromolecules of uniform size, predetermined molecular weight, and with retained chain-end functionality.^{2c} Radical polymerization processes of this category are amenable to a vast array of monomer classes (*e.g.*, styrenes, (meth)acrylates, (meth)acrylamides, or vinyl esters), reagents, functional groups, reaction conditions, and allow specific and defined placement of various functionalities. Owing to these characteristics, CRP processes provide exquisite control of macromolecules by granting access to more complex compositions (*i.e.*, block, gradient, statistical copolymers) and complex polymeric architectures, exemplified by star, cyclic, brush, hybrid (*i.e.*, bioconjugate, inorganic/organic), and network-type structures. Furthermore, the versatility of these systems permits them to be performed in disparate polymerization media, ranging from homogeneous organic and aqueous systems to heterogeneous emulsions and suspension systems. Of the existing CRP techniques, the most powerful and commonly employed systems include reversible addition fragmentation chain transfer (RAFT),^{42e, 58} nitroxide mediated polymerization (NMP),⁵⁹ organometallic mediated radical polymerization (OMRP),⁶⁰ and atom transfer radical polymerization (ATRP).^{1e, 14a, 61}

ATRP functions through a catalytic process mediated by redox-active transition metal complexes (Mt/L: Mt = Cu, Ru, Fe, Mo, Os, *etc.*, L = ligand),⁶² forming a dynamic equilibrium between dormant species (alkyl halide initiator: R-X and polymer: P_n-X) and active propagating radicals (P_n•).^{61a} This equilibrium essentially mediates the polymerization, providing a constant [P_n•], and ensures concurrent growth of all polymer

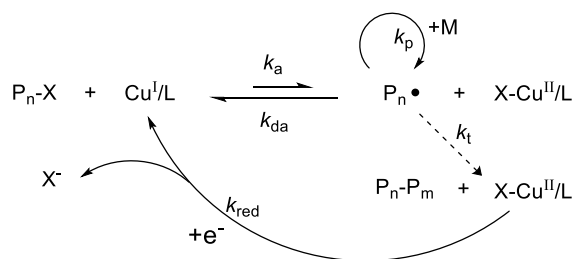
chains. In the dormant state, a lower oxidation state catalyst ($\text{Cu}^{\text{I}}/\text{L}$)²⁹ reduces $\text{P}_n\text{-X}$ to intermittently generate P_n^\bullet and its corresponding higher oxidation state catalyst ($\text{X-Cu}^{\text{II}}/\text{L}$). In the active state, P_n^\bullet can temporarily propagate with monomer (M), terminate, or be deactivated with $\text{X-Cu}^{\text{II}}/\text{L}$ at rates proportional to their respective rate coefficients (k_p , k_t , and k_{da} , respectively) and involved reagent concentrations. The ATRP equilibrium (K_{ATRP}), formally defined as the ratio of activation (k_a) and deactivation (k_{da}) rate coefficients, spans values over *ca.* 10^8 , which can be tuned by the employed reagent structures (*i.e.*, alkyl halide and catalyst)⁶²⁻⁶³ and reaction conditions (*i.e.*, temperature, pressure and solvent).⁶⁴ These various system parameters can be used to optimize and tune the polymerization rate (R_p) and polymer dispersity (M_w/M_n) as dictated by eqs. ((II-1) and ((II-2), where p and DP represent monomer conversion and the degree of polymerization, respectively.

$$R_p = k_p [\text{P}_n^\bullet] [\text{M}] = \left(\frac{k_p k_a [\text{R-X}]_0 [\text{Cu}^{\text{I}}/\text{L}]}{k_{da} [\text{X-Cu}^{\text{II}}/\text{L}]} \right) [\text{M}] \quad (\text{II-1})$$

$$\frac{M_w}{M_n} = 1 + \frac{1}{DP} + \left(\frac{k_p ([\text{R-X}]_0)}{k_{da} [\text{X-Cu}^{\text{II}}/\text{L}]} \right) \left(\frac{2}{p} - 1 \right) \quad (\text{II-2})$$

During the past decade, ATRP has become more universal in application because of several key advancements and its fusion with many externally applied stimuli. One significant improvement was the advent of activators regenerated by electron transfer (ARGET),⁶⁵ and related processes,⁶⁶ which achieved part-per-million (ppm) catalyst loadings, tolerance to O_2 ,⁶⁷ and diminished side reactions,⁶⁸ while maintaining all the traditional attributes of ATRP/CRP. In ARGET type systems, the activator complex is continuously (re)generated by a reducing agent (*e.g.*, Sn^{II} , ascorbic acid, free radical initiator, cathodic current, or light) from otherwise accumulated $\text{X-Cu}^{\text{II}}/\text{L}$ originating from

unavoidable radical termination events. In addition to these advancements, the ATRP process can be manipulated by a variety of stimuli including, but not limited to, pressure,⁶⁹ light,^{8d, 70} and electrical current.^{10, 67c, 71} Applied stimuli provide additional features and control to the ATRP process by enabling the synthesis of high molecular weight polymers,^{69b} local/temporal catalyst activation, and “on-demand” catalyst manipulation.^{10, 70c} Electrochemically mediated ATRP (*e*ATRP), the newest member of the ATRP family, utilizes both the concept/advantages of ARGET ATRP *via* an electrochemical stimulus (Scheme II-1) to provide enhanced levels of polymerization control.



Scheme II-1. Electrochemically Mediated ATRP (*e*ATRP).

Electrochemical methods and reagents are emerging as an ever more powerful tool in polymer science in regard to catalyst characterization,^{9, 63a, 72} catalyst (re)generation,⁷³ redox responsive materials,^{72, 74} and surface chemistries.^{67c, 73a, 75} In ATRP alone, electrochemistry has been critical as a characterization method to determine equilibrium,^{63a} ligand binding,^{30a} and activation rate coefficients.^{29, 31a} In other polymerization systems, catalyst activity was manipulated by utilization of redox sensitive catalysts in the polymerization of lactide.⁷⁶ From a materials perspective, redox-sensitive polymer materials have been developed including well-defined ferrocene containing (meth)acrylate

polymers^{74a} and electro-patterned surfaces brushes.^{67c} In regard to catalyst generation and electro-polymer synthesis, *e*ATRP was recently developed as a tool to effectively synthesize well-defined polymers by mediating ATRP through passage of current. Enhanced levels of polymerization control were realized *via* electrochemical means by generating the active catalyst *in situ* through electrolysis. Control of the polymerization rate and ability to intermittently switch a polymerization between “on” and “off” states were demonstrated.¹⁰ The utility of *e*ATRP was further extended to aqueous/buffered media, typically challenging in ATRP, to produce well-defined polymers by tuning relative catalyst concentrations *via* the applied potential (E_{app}).⁷¹ Most recently, the *e*ATRP process has been extended to surface initiated polymerizations providing controlled and tailorable growth of polymer brushes under ambient conditions, while enabling multiple surface functionalizations by recycling/reusing the reaction medium.^{67c}

To promote widespread application of *e*ATRP, this chapter serves to provide an in-depth investigation and extension of our first report,¹⁰ disseminating practical insight into fundamental polymerization parameters, simplified reaction setups, and an extension of this process as an efficient purification and catalyst recycling tool. Variable electrochemical methods were explored, and polymerization parameters were investigated, including the applied potential, catalyst type and loading, galvanostatic conditions, and electrodeposition/stripping experiments.

II. 3. Results and discussion

Characterization and Control Studies. All experimentation presented in this work

was conducted in a two compartment electrochemical cell equipped with a platinum disk and platinum mesh working electrode, platinum plate counter electrode, and Ag/AgI/I⁻ reference electrode⁷⁷ maintained under an inert N₂ atmosphere. Prior to each polymerization, cyclic voltammetry (CV) was used to verify the existence of the redox active catalyst and to identify appropriate potentials to manipulate its oxidation state. Figure II-1 represents a summary of two CVs and one linear sweep voltammogram (LSV) conducted in a polymerization mixture prior to electrolysis/polymerization. The polymerization medium was composed of a solution of monomer, *n*-butyl acrylate (BA), in solvent, dimethylformamide (DMF), containing a supporting electrolyte, tetrabutylammonium perchlorate (TBAClO₄). Initial *e*ATRP experiments utilized a catalytic system of Cu^{II}/tris(2-pyridylmethyl)amine (Br-Cu^{II}/TPMA) and later involving different ligands to including tris[2-(dimethylamino)ethyl] amine (Me₆TREN) and *N,N,N',N'',N'''*-pentamethyldiethylenetriamine (PMDETA). In all cases, equimolar concentrations of copper(II) and bromide were utilized by adding copper(II) trifluoromethanesulfonate (Cu^{II}OTf₂) and tetrabutylammonium bromide (TBABr), respectively. For clarity, the [TBABr] and formal charges have been omitted from figures and captions. Specific formulation details are supplied in the figure footnotes and experimental section. As expected, a typical copper redox couple of Br-Cu^{II}/TPMA was observed having quasi-reversible behavior with a half-wave potential ($E_{1/2}$) value of 0.322 V vs. Ag/AgI/I⁻. For further reference, CVs were recorded against the saturated calomel electrode (SCE) which gave an $E_{1/2}$ of -0.166 V vs. SCE. In each case, the anodic and cathodic peaks were separated by *ca.* 80 mV under fully compensated conditions (Figure II-1, dashed black line). All following discussions and figures will report applied potential

values as overpotential (η) values, formally defined as the difference between the applied potential (E_{app}) and $E_{1/2}$, unless otherwise stated in the following discussion ($\eta = E_{\text{app}} - E_{1/2}$).

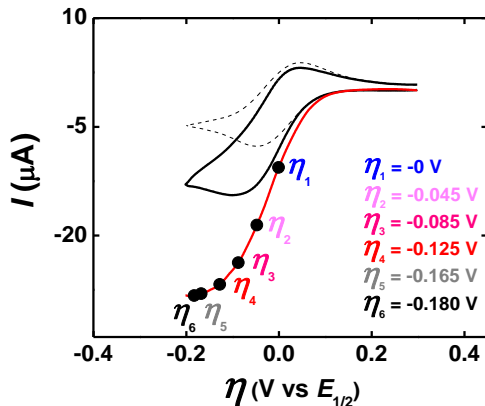
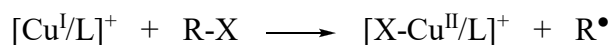
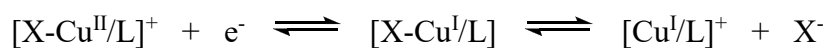


Figure II-1. CV of 1.17 mM Br-Cu^{II}/TPMA in 56% (v/v) BA/DMF ([BA]₀ = 3.9 M) containing 0.2 M TBAClO₄ recorded at a scan rate (ν) of 50 mV/s in the absence (dashed black) and presence (solid black) of 12.9 mM EBiB. LSV (solid red) using an identical formulation to those in CV containing EBiB under convection. Hollow black dots correspond to applied potential values (E_{app}), expressed as overpotential (η) values, used in subsequent *e*ATRP experiments. $E_{1/2}$ values of 0.322 and -0.166 V were determined using Ag/AgI/I⁻ and SCE, respectively.

Once the $E_{1/2}$ value was determined, an alkyl halide initiator (ethyl α -bromoisobutyrate, EBiB) was injected into the working solution, causing a change in the CV shape (Figure II-1, solid black line). Similar to previous literature accounts,^{10, 71} an increase in the cathodic current and decrease in the anodic current were observed, verifying the presence of an additional homogenous chemical reaction.⁷⁸ In the presence of R-X, a catalytic electrochemical-chemical (EC') reaction⁷⁹ occurred where the electrochemically generated

Cu^I/L reacted with R-X regenerating Br-Cu^{II}/L and depleting Cu^I/L near the electrode surface (Scheme II-2.). LSV was next conducted to estimate potential values where limiting current/mass transport conditions existed under convection (*i.e.*, stirring, solid red line). Three regions were observed: (1) the onset of Br-Cu^{II}/L reduction near 0.075 V, (2) an increase in cathodic current with potential, and (3) a limiting current region at diffusion controlled conditions near *ca.* -0.117 V. This LSV indicates a point where no further reduction rate enhancement is possible even after application of increasingly more negative potentials, providing insight into the potential range to study for our later E_{app} (*i.e.*, η) analysis.



(L = ligand, X = halogen, and R-X = alkyl halide)

Scheme II-2. Catalytic Electrochemical-chemical Reaction. [*formal charges have been omitted in this Chapter]

Before conducting *e*ATRP, control bulk electrolysis reactions were carried out in the absence of R-X (at both $\eta = 0$ and -165 mV) to evaluate the electrochemical contribution of Br-Cu^{II}/L and to confirm the absence of any polymerization. In the limiting current regime, a η value of -165 mV was applied to ensure near-quantitative conversion of Br-Cu^{II}/L to Cu^I/L in the vicinity of the electrode and reaction mixture. Under these conditions, the current efficiency (CE) and maximum apparent reduction rate coefficient (k_{red}) can be estimated for Br-Cu^{II}/L. A cathodic current resulted initially of *ca.* -3 mA which absolute

value decreased in an exponential fashion to a nominal and constant value of *ca.* -70 μA (Figure II-2A, black trace). Assuming complete conversion of $\text{Br-Cu}^{\text{II}}/\text{L}$, the theoretical total charge passed (Q_{th}) should equal 2.61 C based upon a single electron reduction and a system containing 2.7×10^{-5} mol of $\text{Br-Cu}^{\text{II}}/\text{L}$. After performing the electrolysis, the charge passed (Q_{exp}) was determined to be 2.85 C after 4500 s, which is slightly larger than the Q_{th} equal to 2.61 C. This corresponds to a CE of *ca.* 92%, implying a small fraction of charge is lost to other reduction processes or due to the presence of O_2 . However, if the charge passed due to the nominal current is subtracted from the total charge passed, a new Q_{exp} value of 2.53 C can be obtained, which is nearly identical to Q_{th} . Furthermore, in the absence of R-X, there is no homogeneous contribution and loss of $\text{Cu}^{\text{I}}/\text{L}$, and therefore, the system can be treated as a first-order homogeneous chemical reaction. When the applied potential is in the limiting current regime, a linear relationship existed, corresponding to a maximum $\text{Br-Cu}^{\text{II}}/\text{L}$ k_{red} of $1.0 \times 10^{-3} \text{ s}^{-1}$, whereas at $\eta = 0 \text{ V}$ the apparent reduction rate coefficient was found to be $4.4 \times 10^{-4} \text{ s}^{-1}$ (Figure II-2B). This maximum k_{red} value was found to be in close proximity to the k_{red} obtained in an identical polymerization system containing R-X (Figure II-2B). Because of this similarity, k_{red} values in *e*ATRP may be estimated under these specific conditions to be between 1.0×10^{-3} and $4.4 \times 10^{-4} \text{ s}^{-1}$. As a side note, each control electrolysis experiment proceeded without polymerization, as confirmed by gel permeation chromatography (GPC) and nuclear magnetic resonance (NMR).

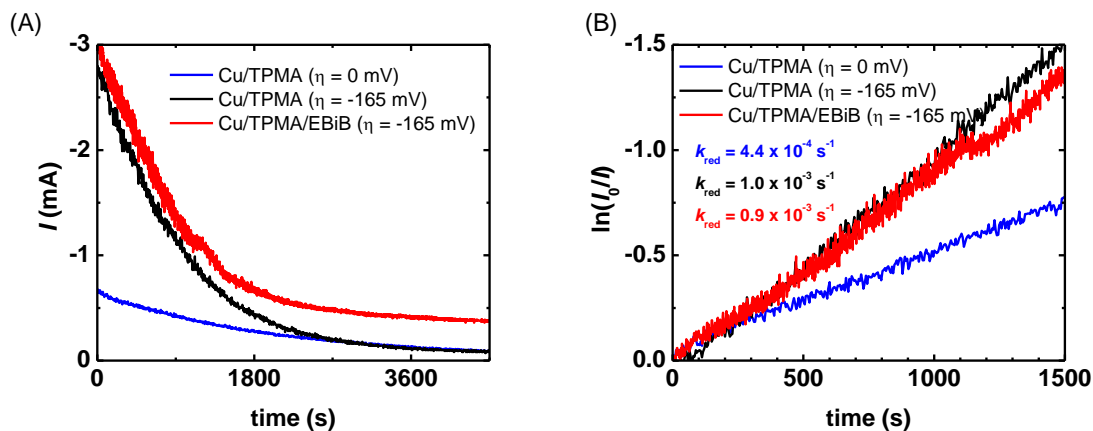


Figure II-2. Electrolysis of Cu^{II} /TPMA at E_{app} of $\eta = 0$ (blue) and -165 mV in the absence (black) or presence of EBiB (red). (A) Current as a function of time, and (B) first order plot of current versus time. Determined k_{red} values are reported in Figure II-2B.

Influence of Applied Potential/Overpotential. After establishment of the system behavior without alkyl halide, a series of polymerizations were carried out with R-X to examine the influence of η on the polymerization behavior. It is well-known that electrode potentials strongly affect the kinetics of reactions occurring on its surface, and in *e*ATRP they would dictate the relative $[\text{Cu}^{\text{I}}/\text{L}]$ and $[\text{Br-Cu}^{\text{II}}/\text{L}]$ within the polymerization mixture. It should be stressed that electrochemical systems like *e*ATRP are heterogeneous in nature and may have different catalyst concentrations in areas near the electrode surface compared to the working solution. Initial scouting experiments revealed that stirring was required during *e*ATRP; otherwise, under stagnant conditions, passivation of the working electrode occurred along with a slow R_p and polymers with large dispersity values ($M_w/M_n \geq 2.0$), as shown in Figure II-3. Our previous reports¹⁰ demonstrated that *e*ATRP was capable of modulating the rate of polymerization; however, the limits of this behavior have yet to be established.

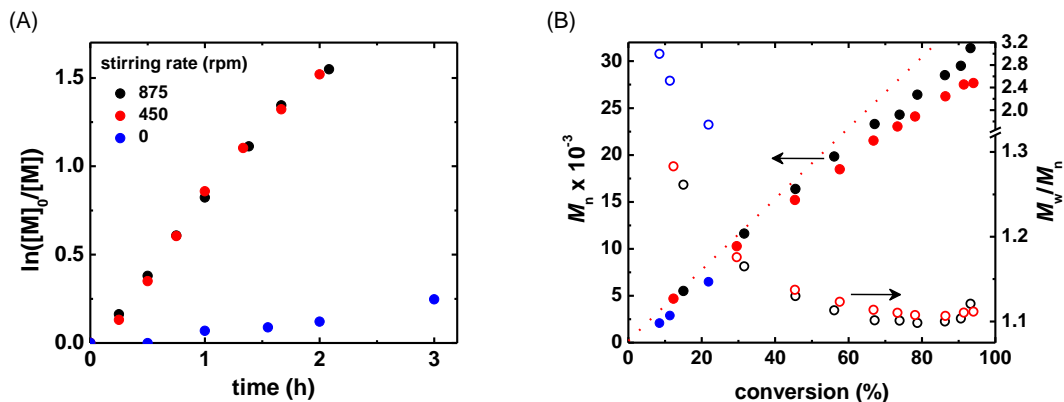


Figure II-3. (A) First order kinetic plot versus time as a function of stirring rate and (B) M_n and M_w/M_n versus monomer conversion for *e*ATRP of BA in DMF as a function of stirring rate. Reaction condition: $[BA]_0/[EBiB]_0/[Br-Cu^{II}/TPMA]_0 = 300/1/0.03$, $[BA]_0 = 3.9$ M, $[TBAClO_4]_0 = 0.2$ M, $T = 45$ °C. The E_{app} of $\eta = -125$ mV at each stir rate.

Figure II-4 summarizes the results of five polymerizations conducted at a broad range of η values spanning over 180 mV beginning from the $E_{1/2}$ at $\eta_1 = 0$ V to $\eta_6 = -0.180$ V. Figure II-4A is a first-order kinetic plot of the resulting five polymerizations, each conducted with identical formulations but with increasingly more negative applied potentials (Figure II-1 for η values). For each polymerization, linear first-order kinetic behavior was observed until *ca.* 80% monomer conversion. Increasingly more negative η values provided larger apparent rate coefficients (k_{app}). A k_{app} of 0.37 and 1.58 h⁻¹ resulted when using η of 0 and -0.165 V, respectively, providing a 4-fold enhancement in the R_p . This increase in k_{app} was synonymous in magnitude with the 4-fold enhancement of k_{red} , when applying the same η values, confirming a correlation exists between the polymerization rate and reduction rate (*i.e.*, current). However, a limiting region existed between $\eta = -0.125$ and -0.165 V, where minimal change in the k_{app} was observed even

with application of progressively more negative potentials ($\eta_4 - \eta_5$) due to mass transport limitations. One additional polymerization was conducted at $\eta_6 = -0.180$ V, confirming the k_{app} limit of 1.58 h^{-1} found for $\eta_5 = -0.165$ V. A semilogarithmic plot of the observed k_{app} versus η values (Figure II-4D) is supplied, illustrating the potential “dependent” and “independent” regimes of the η on the k_{app} .

The resulting number-average molecular weight (M_n) and M_w/M_n values are provided in Figure II-4B. Controlled polymerization behavior was confirmed in all cases by the linear increase of M_n with conversion, while producing a monomodal population of polymers with relatively low M_w/M_n values, approaching *ca.* 1.10. Slightly lower M_w/M_n values were observed for systems operating at more positive potential values owing to a larger $[\text{Br-Cu}^{\text{II}}/\text{L}]$.

During each polymerization, the resulting current was recorded as shown in Figure II-4C. In the early stages of polymerization, high current values were observed representing the original generation of $\text{Cu}^{\text{I}}/\text{L}$ from a purely $\text{Br-Cu}^{\text{II}}/\text{L}$ system to initiate polymerization. Here the concentrations of $\text{Cu}^{\text{I}}/\text{L}$ and $\text{Br-Cu}^{\text{II}}/\text{L}$ are dynamic. After this stage, the current becomes fairly constant resembling the point where equilibrium is reached and a constant concentration of $\text{Br-Cu}^{\text{II}}/\text{L}$ and $\text{Cu}^{\text{I}}/\text{L}$ exist. More negative η values produced larger initial currents, indicative of a faster rate of reduction, and larger stationary current values. In essence, faster rates of reduction provide a higher $[\text{Cu}^{\text{I}}/\text{L}]$ and, therefore, faster polymerizations originating from a higher $[\text{P}_n^\bullet]$. The magnitude of stationary current values, after *ca.* 1 h, reflect the relative $\text{Cu}^{\text{I}}/\text{L}$ regeneration rates and hence terminate rates; *i.e.*, a more negative η equals a higher R_p and stationary current, resulting in more termination.

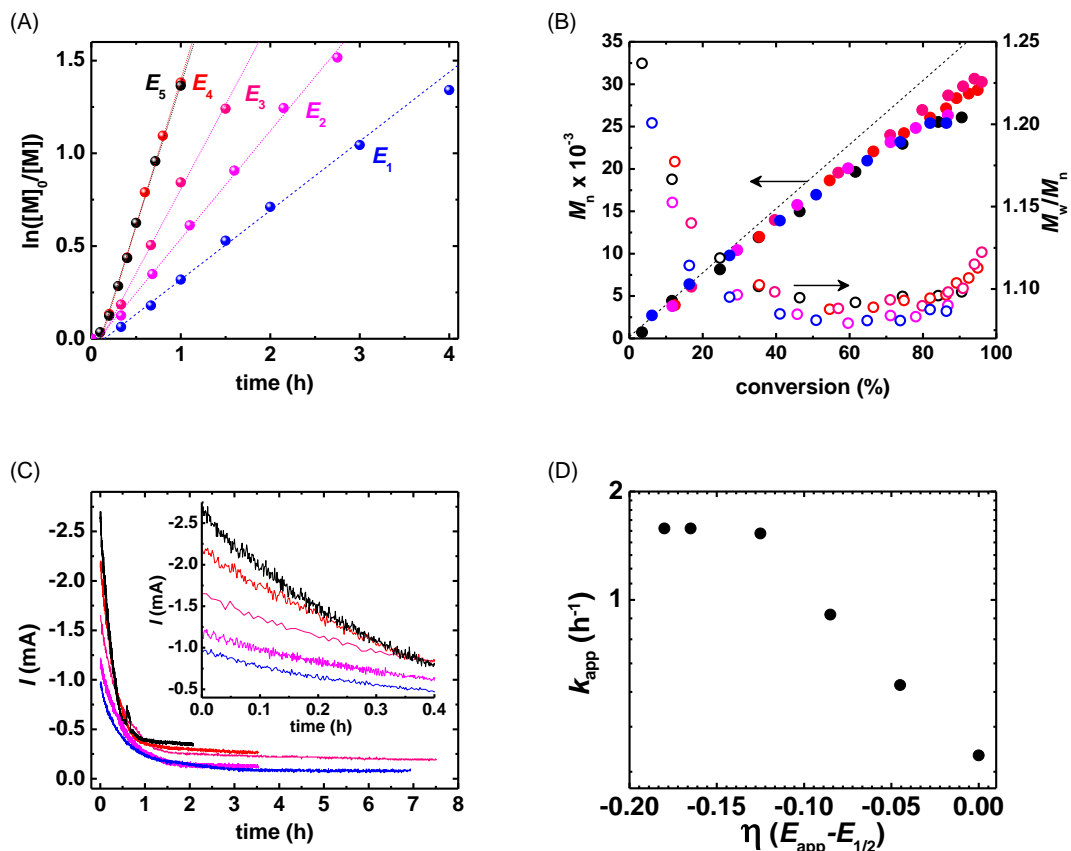


Figure II-4. Kinetics of e ATRP as a function of E_{app} at a η ranging from 0 to -0.180 V. (A) First-order plot of monomer conversion versus time, (B) M_n and M_w/M_n versus conversion, and (C) current versus time, (D) Semi-logarithmic plot of apparent polymerization rate coefficient (k_{app}) versus the overpotential ($\eta = 0, -45, -85, -125, -165$, and -180 mV). Reaction conditions: $[BA]_0/[EBiB]_0/[Br-Cu^{II}/TPMA]_0 = 300/1/0.09$, $[TBAClO_4]_0 = 0.2$ M, $[BA]_0 = 3.9$ M in DMF, $T = 44$ °C, $V_{tot} = 23$ mL, and stirring rate (f) = 875 rpm. For clarity $\eta_6 = -0.180$ V was omitted from (A), (B), and (C).

Influence of $[Br-Cu^{II}/L]_0$. The next series of polymerizations were designed to probe the influence of the concentration of electroactive species within e ATRP. Three polymerizations were conducted using $[Br-Cu^{II}/L]_0$ ranging from 300 to 50 ppm catalyst

loadings, as shown in Figure II-5. In these experiments, identical E_{app} values at $\eta_4 = -0.125$ V were employed.

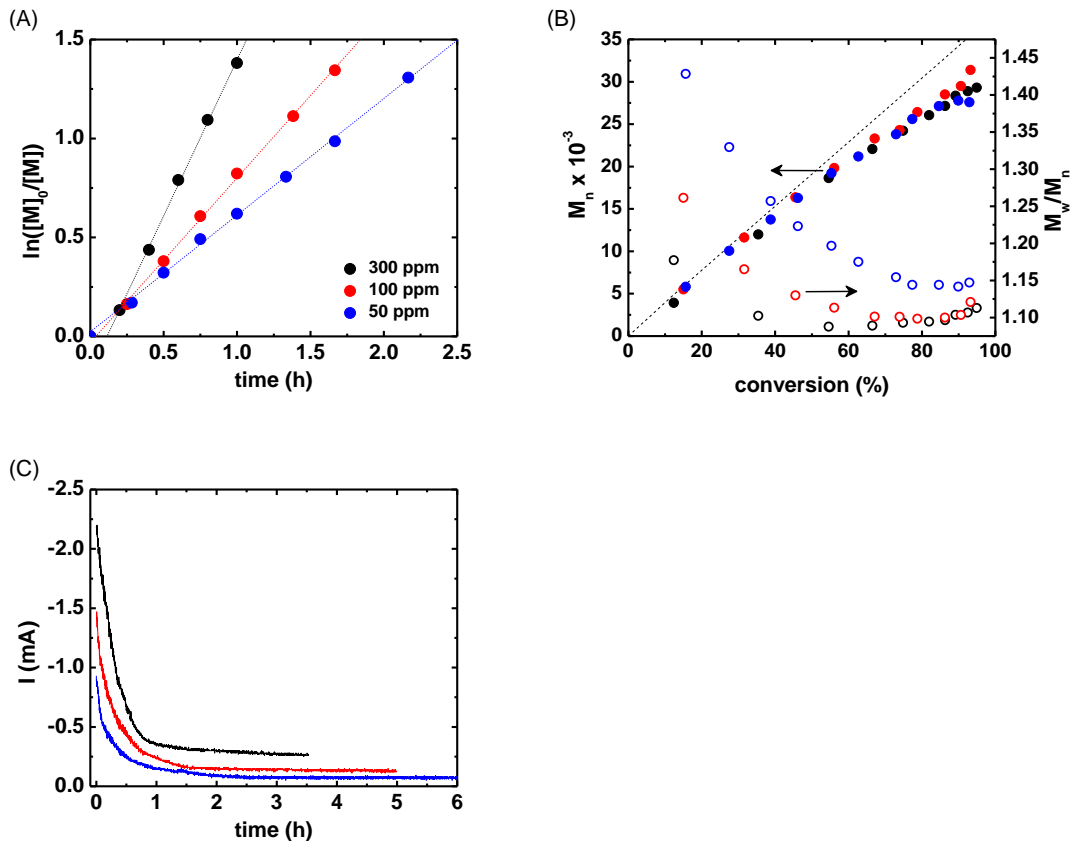


Figure II-5. *e*ATRP as a function of $[\text{Br-Cu}^{\text{II}}/\text{L}]_0$ with a $\eta_4 = -0.125$ V. (A) First-order kinetic plot of monomer consumption, (B) M_n and M_w/M_n versus conversion, and (C) current versus time. Reaction conditions: $[\text{BA}]_0/[\text{EBiB}]_0/[\text{Br-Cu}^{\text{II}}/\text{TPMA}]_0 = 300/1/\text{X}$, $[\text{TBAClO}_4]_0 = 0.2$ M, $[\text{BA}]_0 = 3.9$ M in DMF, $T = 44$ °C, $V_{\text{tot}} = 23$ mL, and $f = 875$ rpm. X = 0.9, 0.3, and 0.15 corresponding to 300, 100, and 50 ppm, respectively.

Figure II-5 shows three polymerizations displaying first-order kinetic behavior as a function of the $[\text{Br-Cu}^{\text{II}}/\text{L}]_0$. As the $[\text{Br-Cu}^{\text{II}}/\text{L}]_0$ increases, the rate of polymerization increases with a near square root dependence, similar to other literature accounts which

display larger rates with higher catalyst loadings.^{66d, 80} A larger R_p reflects a higher $[P_n^\bullet]$, a result of faster reduction rates generating more Cu^I/L . Figure II-5B illustrates, in all cases, a linear increase in M_n with respect to conversion and a profound decreases in the relative M_w/M_n values with larger $[Br-Cu^{II}/L]_0$. This observation is supported by eq. (II-2, where larger $[Br-Cu^{II}/L]$ should produce polymers with lower M_w/M_n values from an increased rate of deactivation and fewer monomer additions within each activation-deactivation cycle. The current profiles (Figure II-5C) further support the relative concentration of $Br-Cu^{II}/L$ in the system, inferred *via* the Cottrell equation,^{79a} where the largest current values were obtained with the largest concentration of electroactive species. Furthermore, the steady state current values (at time > 2 h) imply larger Cu^I/L regeneration rates with larger $[Br-Cu^{II}/L]$.⁸¹

Influence of Ligand Structure. The next series of polymerizations were designed to probe the influence of different catalytic systems within *e*ATRP at 100 ppm catalyst and to demonstrate the ability to gain CRP behavior in otherwise uncontrolled conditions. Three different ligands were selected, to including Me_6TREN , $TPMA$, and $PMDETA$, and electrolysis experiments were performed at relatively equal η values of -0.125 V. CVs pertaining to each complex are supplied in Figure II-6 against $Ag/AgI/I^-$, conducted in the absence and presence of $EBiB$. Consistent with previous reports, the $E_{1/2}$ values became gradually more negative, signifying larger K_{ATRP} values, moving from $PMDETA$ to $TPMA$ to Me_6TREN .^{63a} Furthermore, increased catalytic behavior, *i.e.*, a larger cathodic current, was realized with progressive more active ligands ($PMDETA < TPMA < Me_6TREN$) when in the presence of $EBiB$.

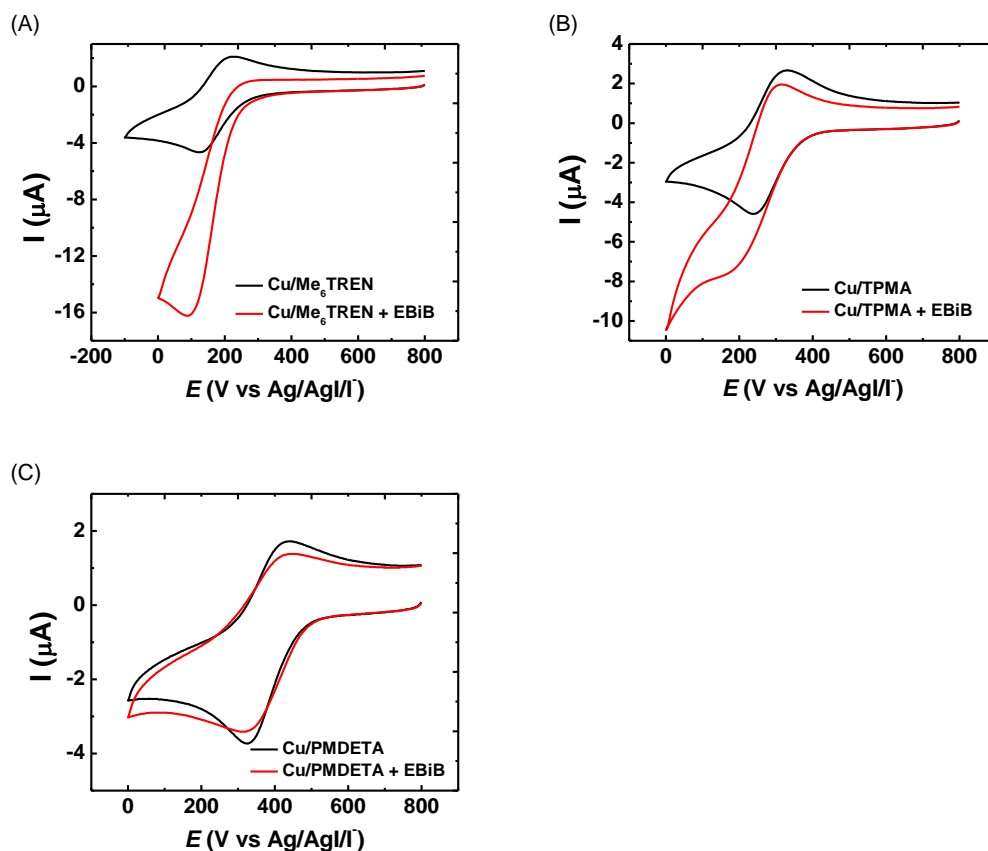


Figure II-6. Cyclic voltammetry of (A) Me₆TREN, (B) TPMA, and (C) PMDETA in the absence (black line) and presence (red line) of EBiB. Experimental condition: $[\text{BA}]_0/[\text{EBiB}]_0/[\text{Br-Cu}^{\text{II}}/\text{L}]_0 = 300/1/0.09$, $[\text{BA}]_0 = 3.9$ M in DMF, $[\text{TBAClO}_4]_0 = 0.2$ M, $T = 44$ °C, $\text{L} = \text{Me}_6\text{TREN}$, TPMA, or PMDETA.

As shown in Figure II-7A, the R_p is heavily dependent on the ligand selection. Progressively more active ligands provide faster rates of polymerization from larger K_{ATRP} values. Furthermore, as shown in Figure II-7B, more active ligands (*i.e.*, Me₆TREN and TPMA) provided lower M_w/M_n values at identical $[\text{Br-Cu}^{\text{II}}/\text{L}]_0$, whereas PMDETA (blue symbols) had M_w/M_n values of *ca.* 2.2. Similar to ARGET ATRP, more active catalysts are capable of maintaining sufficient rates of deactivation, minimizing relative M_w/M_n

values.^{65a} Further to this point, the high activity catalysts were capable of achieving conversion values $\geq 80\%$, whereby PMDETA was limited to 50%. When employing lower activity catalysts (*i.e.*, with PMDETA), *e*ATRP provides two parameters to reduce the M_w/M_n by using a larger $[\text{Br-Cu}^{\text{II}}/\text{L}]_0$ and/or a more positive η value, each essentially increasing the effective $[\text{Br-Cu}^{\text{II}}/\text{L}]$ in the reaction medium. After increasing the catalyst loading to 300 ppm and using a more positive η_4 of -0.125 V, the M_w/M_n value could be decreased to *ca.* 1.3, while concomitantly providing higher conversion values (magenta squares). The current profiles, shown in Figure II-7C, reveal that more active catalysts result in larger initial and stationary current values.

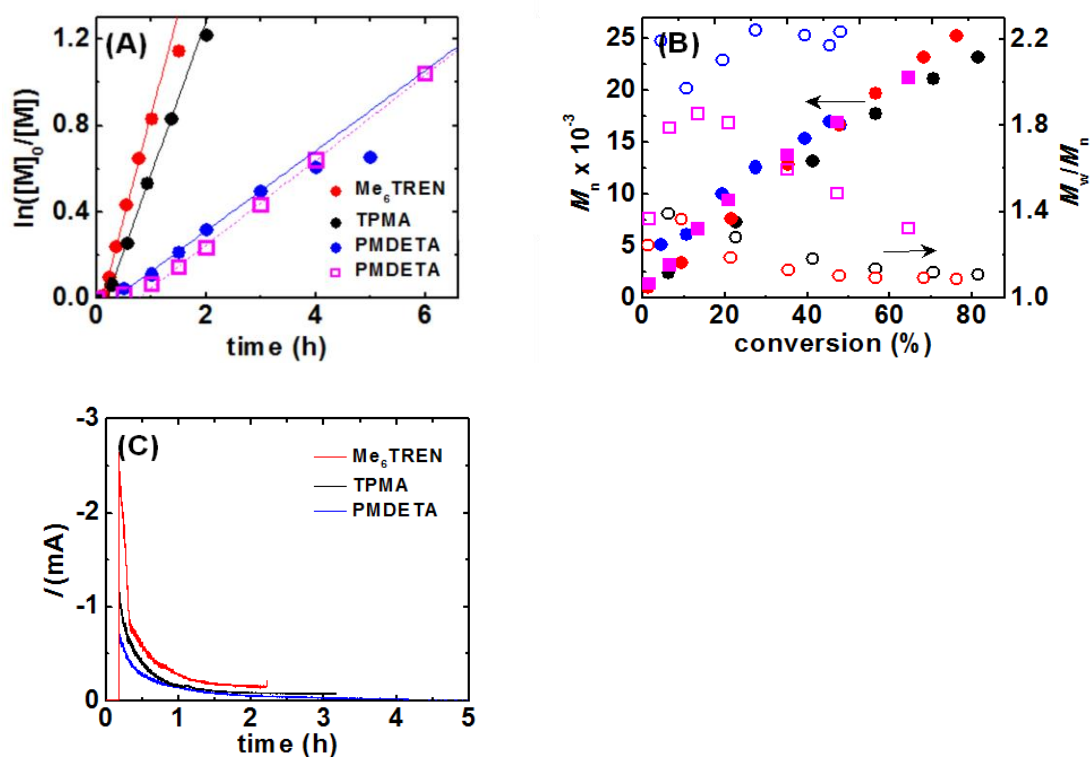


Figure II-7. *e*ATRP as a function of ligand (L = Me₆TREN, TPMA, and PMDETA) with a $\eta = -0.180$ V and 100 ppm catalyst. Note: the second instance of PMDETA (magenta

squares) was conducted instead with a $\eta = -0.125$ V and 300 ppm catalyst. (A) First-order kinetic plot of monomer conversion versus time, (B) M_n and M_w/M_n versus conversion, and (C) current versus time. Reaction conditions: $[BA]_0/[EBiB]_0/[Br-Cu^{II}/L]_0 = 300/1/0.03$, $[TBAClO_4]_0 = 0.2$ M, $[BA]_0 = 3.9$ M in DMF, $T = 44$ °C, $V_{tot} = 23$ mL, and $f = 875$ rpm.

Galvanostatic *e*ATRP. In an effort to improve the feasibility of *e*ATRP, for both academic and industrial research, a galvanostatic *e*ATRP was investigated. When using galvanostatic conditions, *i.e.*, a constant current instead of a constant potential, the reference electrode can be eliminated, and therefore, *e*ATRP can be conducted using a two-electrode system. In order to carry out a galvanostatic *e*ATRP, appropriate current values must be selected which can be rationalized from previously conducted potentiostatic experiments. Polymerization conditions were selected to be identical to those utilized in our applied potential studies (Figure II-4, η_4), except by employing a constant current. For convenience, our selected current values (thick red line) were superimposed over the current profile of a previously conducted potentiostatic polymerization (black line), as shown in Figure II-8A. The selected current values were determined by integration of this current profile, the area designated by red hashes, to determine the Q passed during the course of a potentiostatic *e*ATRP. The selected current values resembled those of the potentiostatic polymerization, whereby an initial high current value (*i.e.*, $I_{app} = -1$ mA for 2800 s) and consecutive low current value (*i.e.*, $I_{app} = -0.3$ mA for 9800 s) were employed. This two-stage current program was hypothesized to rapidly convert the vast majority of $Br-Cu^{II}/L$ to Cu^I/L , initiating *e*ATRP, and next providing compensation for any (re)generated $Br-Cu^{II}/L$ incurred from termination.

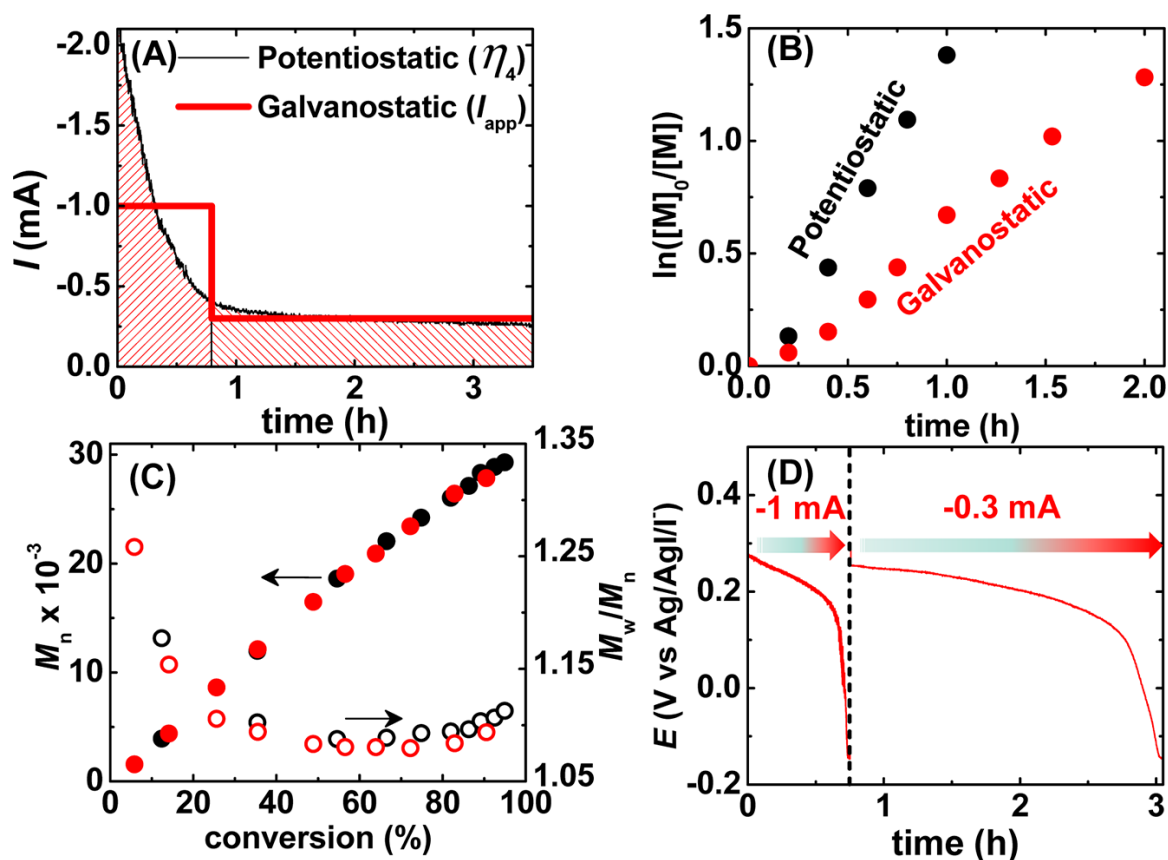


Figure II-8. Galvanostatic versus potentiostatic eATRP. (A) Current versus time for a potentiostatic polymerization (black) using an E_{app} at a $\eta_4 = -0.125$ V and galvanostatic polymerization (red) using an I_{app} of -1 mA ($t = 2800$ s) and -0.3 mA ($t = 9800$ s). Red hashes represent integrated area to calculate Q for current determination. (B) First-order kinetic plot of a potentiostatic and galvanostatic eATRP. (C) M_n and M_w/M_n versus conversion for potentiostatic (black) and galvanostatic (red) eATRP. (D) Monitored applied potential versus time during a galvanostatic eATRP. Reaction conditions: $[BA]_0/[EBiB]_0/[Br-Cu^{II}/TPMA]_0 = 300/1/0.09$, $[TBAClO_4]_0 = 0.2$ M, $[BA]_0 = 3.9$ M in DMF, $T = 44$ °C, $V_{tot} = 23$ mL, and $f = 875$ rpm.

Figure II-8B provides a comparison of the polymerization kinetics in both

potentiostatic and galvanostatic mode. The galvanostatic polymerization proceeded at a slower rate. A lower R_p was expected as a lower stationary current (-1 mA) was imparted in comparison to values as high as -2 mA in potentiostatic mode. Regardless, the resulting polymers from both techniques confirmed controlled polymerizations took place providing polymers with low M_w/M_n values (Figure II-8C). Although a reference electrode was not necessary, the potential at the working electrode was monitored using an Ag/AgI/I⁻ reference electrode to gain insight into the behavior of a galvanostatic *e*ATRP (Figure II-8D). The working electrode potential was observed to be maintained at approximately the $E_{1/2}$ of (Cu^{I/II}/TPMA) or at slightly more negative values. However, at later portions of each current stage, the observed potential progressively became more negative to satisfy the current requirements and/or from an increased solution resistivity due to higher solution viscosities. If the applied current values were maintained for longer durations, more negative potentials would have resulted, leading to substantial copper deposition on the working electrode.

Catalyst Recycling: Deposition and Stripping. One distinct advantage of an electrochemical process is the diversity of techniques which can be conducted. Owing to this diversity, electrochemical deposition and stripping techniques were employed to recycle the copper catalyst (*i.e.*, solely the metal center) for two separate and sequential polymerizations. To begin, a polymerization was conducted using previously established conditions with TPMA and 300 ppm of copper, as reported in Figure II-4 at a $\eta_6 = -0.180$ V. As expected a controlled polymerization occurred resulting in well-defined polymers with narrow M_w/M_n values (Figure II-9A, black dots). The CV prior to polymerization and

the first-order kinetic plot are shown in Figure II-9E (black traces).

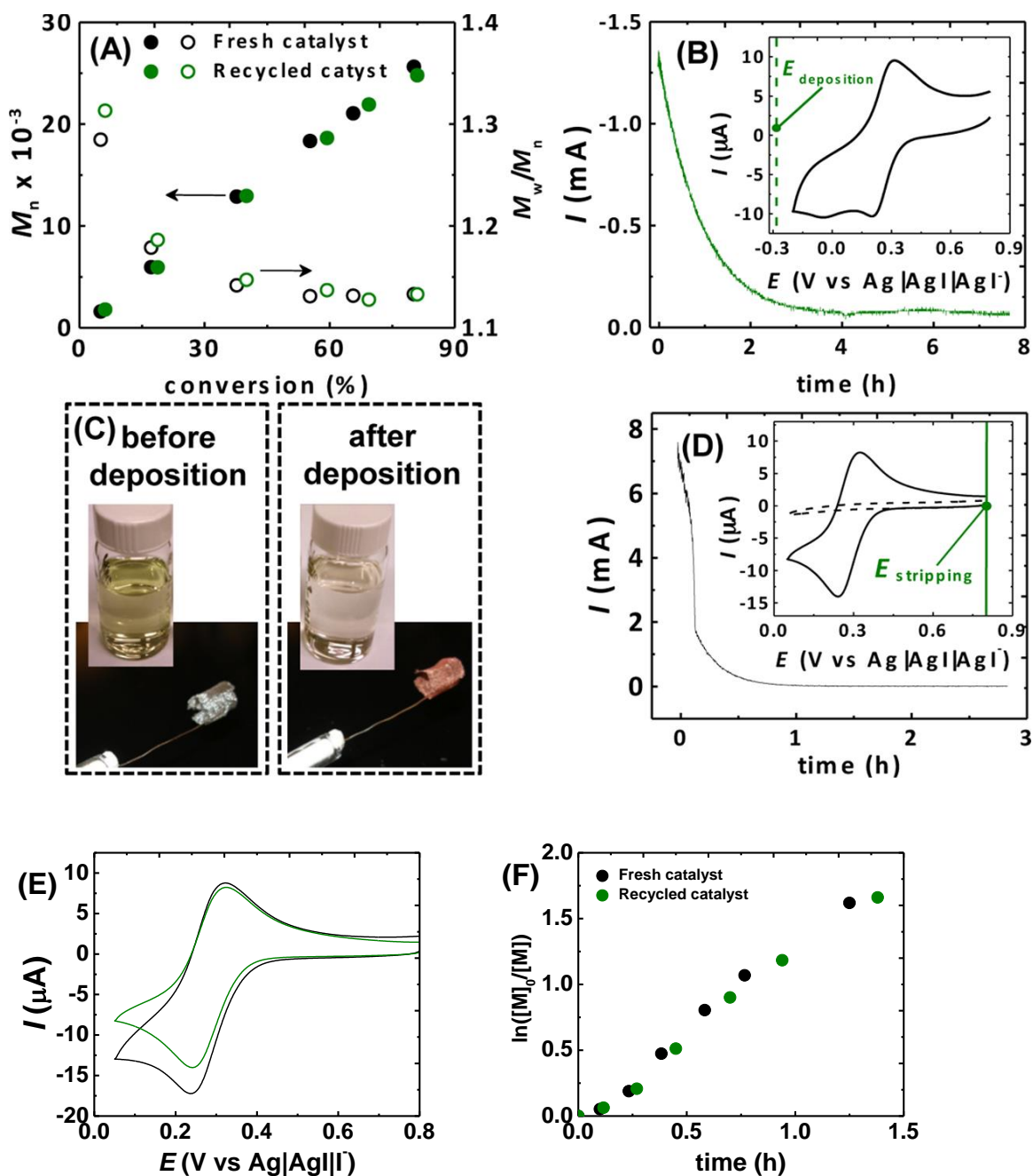


Figure II-9. Recycling of copper via electrodeposition and stripping for sequential eATRP polymerizations. (A) M_n and M_w/M_n versus conversion for fresh (black) and recycled (green) catalyst. (B) Current versus time plot during copper deposition with an E_{app} at -

0.283 V vs. Ag/AgI/I⁻ (inset: CV after first polymerization conducted with $\nu = 250$ mV/s and $T = 65$ °C). (C) Images of crude polymerization mixture and Pt working electrode, before and after deposition. (D) Current versus time during copper stripping with an E_{app} at 0.800 V vs. Ag/AgI/I⁻ (inset: CV before (dashed line) and after (solid line) copper stripping). (E) Cyclic voltammograms of Cu^{II}/TPMA prior to the first (black) and second (green) polymerization at $\nu = 100$ mV/s and $T = 44$ °C. (F) First order kinetic versus time plot of two sequential polymerizations with fresh (black) and recycled (green) copper catalyst. Reaction conditions: [BA]₀/[EBiB]₀/[Br-Cu^{II}/TPMA]₀ = 300/1/0.09, [TBAClO₄]₀ = 0.2 M, [BA]₀ = 3.9 M in DMF, $T = 44$ °C, $V_{tot} = 23$ mL, $\eta_6 = -0.180$ V, and $f = 875$ rpm.

After the first *e*ATRP was completed, the temperature of the reactor was increased to 65 °C and an E_{app} (deposition) of -0.283 V vs. Ag/AgI/I⁻ was utilized. This potential value is approximately 570 mV more negative than the Cu^{I/II}/L couple and nearly 300 mV more negative than that of the Cu⁰ deposition peak, located at *ca.* -45 mV vs. Ag/AgI/I⁻ (Figure II-9B, inset). These conditions were selected based upon optimization experiments for electrodeposition of copper onto the working electrode. When conducting preliminary CV analysis as a function of temperature, the cathodic peak associated with conversion of Cu^I to Cu⁰ shifted to more positive values by nearly 430 mV vs. Ag/AgI/I⁻ upon increasing the reaction temperature from 25 to 60 °C (Figure II-10A). These results confirmed that higher temperatures favored the formation of Cu⁰ on the working electrode. With this in mind, copper deposition was performed at a higher reaction temperature of 65 °C. After application of E_{app} (deposition), the resulting current profile (green line), given in Figure II-9B, decreased, indicating depletion of any soluble copper species in the reaction medium.

The copper deposition process required nearly 4 h to reach nominal current values of *ca.* - 70 μA and was allowed to proceed for a total of 8 h. GPC was conducted before ($M_n = 25100$ and $M_w/M_n = 1.08$) and after deposition ($M_n = 28300$ and $M_w/M_n = 1.11$), confirming a minimal change in the resulting polymer which was accompanied by an increase of monomer conversion from 80 to 94%. A UV-Vis calibration curve was generated to determine the concentration of copper before and after deposition (Figure II-10B). The initial and resulting copper concentrations were found to be 1.18 and 0.05 mM, respectively, indicating over 95% of the Cu was removed from the reaction mixture. Visual confirmation of the copper deposition can be seen in Figure II-9C, both in the working solution (*i.e.*, clear green to clear light yellow solution) and on the working electrode (platinum to metallic copper in appearance).

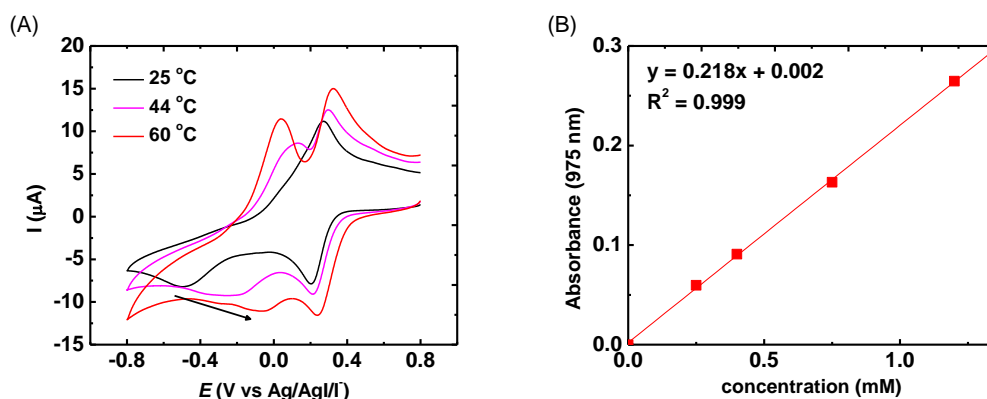


Figure II-10. (A) CV of Cu^{II} /TPMA after polymerization at 25, 44, and 60 $^{\circ}\text{C}$, and (B) a UV-Vis calibration curve of Cu/TPMA absorbance versus concentration.

After collecting essentially all the copper as metallic copper on the working electrode, this copper-coated electrode was directly submerged into another fresh polymerization mixture containing all reagents except for Cu^{II} . Prior to stripping, a CV was recorded

(Figure II-9D, inset (dashed line)), revealing the absence of any cathodic or anodic current responses. Afterward, a positive potential was applied at 0.800 V vs. Ag/AgI/I⁻, resulting in a large anodic current (Figure II-9D) of *ca.* 7-8 mA. The stripping procedure was relatively fast, oxidizing all Cu⁰ to Cu^{II} in less than 1 h, accompanied by a visual color change of the reaction medium to a clear green solution. Confirmation of our stripping procedure was accomplished by CV ((Figure II-9D, inset (solid black line)) by the appearance of the characteristic Cu^{I/II}/TPMA redox couple. Furthermore, UV-Vis measurements and calculations based upon the Q confirmed a [Br-Cu^{II}/L] of 1.07 mM and 1.02 mM, respectively, falling in close proximity to a theoretical [Br-Cu^{II}/L] of 1.05 mM. Once the stripping procedure was completed, an identical polymerization was conducted to that of the first polymerization. The results of this second polymerization are shown in Figure II-9A (green dots), illustrating nearly identical polymers can be obtained by utilizing the recycled copper catalyst.

II. 4. Summary

This work serves as an extension of our initial study of electrochemically mediated atom transfer radical polymerization by providing systematic studies and evaluations of critical polymerization parameters from both an electrochemical and a polymerization standpoint. Polymerization rates were found to be correlated with η , whereby more negative potentials provide faster rates of polymerization and larger current values, until the system becomes mass transport limited. Higher [Br-Cu^{II}/L]₀ yield faster rates of polymerization and larger current values, while simultaneously providing polymers with lower M_w/M_n values. More active catalyst systems resulted in faster rates of polymerization,

larger current values, and lower M_w/M_n values. Control with less active catalyst complexes (*i.e.*, with PMDETA ligand) could be gained upon using more positive potentials and higher $[\text{Br-Cu}^{\text{II}}/\text{L}]_0$. Furthermore, the versatility of *e*ATRP was successfully demonstrated using various electrochemical methods: (a) galvanostatic conditions for simplified reaction setups and (b) copper deposition and stripping procedures for catalyst recycling/purification.

II. 5. Experimental section

Materials. All chemicals were purchased from commercial sources, *e.g.*, Aldrich, TCI, Acros and used as received unless stated otherwise. Tris(2-pyridylmethyl) amine (TPMA) was purchased from ATRP Solutions. *n*-Butyl acrylate (BA) was passed through a column filled with basic alumina to remove inhibitor prior to use.

Measurements. Gel permeation chromatography (GPC): GPC was used to determine number average molecular weight (M_n) and M_w/M_n values. GPC was conducted with a Waters 515 HPLC Pump and Waters 2414 Refractive Index Detector using PSS columns (Styrogel 10^2 , 10^3 , 10^5 Å) in tetrahydrofuran (THF) as an eluent at a flow rate of 1 mL/min at 35 °C. The column system was calibrated with 12 linear polystyrene (PSty, $M_n = 376\sim 2,570,000$). **Nuclear magnetic resonance (NMR):** Conversion of monomer was determined by ^1H NMR spectroscopy. Monomer conversion was measured using ^1H NMR spectroscopy with a Bruker Avance 300 MHz or 500 MHz spectrometer at room temperature. All spectra were recorded in CDCl_3 relative to tetramethylsilane. **Cyclic voltammetry (CV):** All CVs were conducted at 44 °C, unless otherwise stated, with a PARC 263A potentiostat. Stock solutions of copper(II) trifluoromethanesulfonate

(CuOTf₂), ligand, and tetrabutylammonium bromide (TBABr) were prepared in dry solvent containing supporting electrolyte prior to measurement. Measurements were carried out under a N₂ atmosphere using a platinum disk and platinum mesh working and counter electrode, respectively. Potentials were measured versus either an Ag/AgI/I⁻ or SCE reference electrode (Gamry).

Methods. *e*ATRP: An example *e*ATRP is provided with the following formulation: [BA]₀/[EBiB]₀/[TPMA]₀/[Cu^{II}OTf₂]₀/[TBABr]₀ = 300/1/0.03/0.03/0.03, [BA]₀ = 3.9 M in DMF, [TBAClO₄]₀ = 0.2 M, and *T* = 44 °C. Controlled potential electrolysis experiments were carried out with a PARC 263A potentiostat in a thermostatic three-electrode cell using both platinum (Pt) disk (3 mm diameter, Gamry) and Pt gauze (100 mesh, geometrical area ~2.5 cm², Alfa Aesar) working electrodes. The surface area of the Pt gauze working electrode was calculated to be *ca.* 5.19 cm² using a geometric area to surface area conversion factor of 13.4 cm²/in². An Ag/AgI/I⁻ and Pt mesh were used as the reference and counter electrodes during electrolysis, respectively. The electrolysis experiments were carried out in a divided cell, using a glass frit and a salt bridge made of methylcellulose gel saturated with tetrabutylammonium tetrafluoroborate (TBABF₄) to separate the cathodic and anodic compartments. During electrolysis, the cathodic compartment was maintained under vigorous magnetic stirring and an N₂ atmosphere. Prior to each experiment, the working Pt disk electrode was polished with a 0.25 μm diamond paste and sonicated in ethanol. The Pt gauze was activated in 0.1 M H₂SO₄ with cyclic anodic/cathodic steps of 6 seconds with a current density of ~30 mA/cm², for a total time of 30 min. The electrochemical cell was first charged with supporting electrolyte (1.603 g TBAClO₄) and

then put under a slow N₂ flow. After 15 minutes of purging, previously deoxygenated reagents were added including 13 mL of BA, 10 mL of DMF, 0.18 mL of a 0.05 M solution of Cu^{II}/TPMA/TBABr (equimolar), and 45 µL of neat EBiB were added to the electrochemical cell. Samples were withdrawn periodically for ¹H NMR and GPC analysis for conversion, and molecular weight and distribution determination, respectively.

II. 6. References

1. Braunecker, W. A.; Matyjaszewski, K., *Progress in Polymer Science* **2007**, 32 (1), 93-146.
2. (a) Moad, G.; Chong, Y. K.; Postma, A.; Rizzardo, E.; Thang, S. H., *Polymer* **2005**, 46 (19), 8458-8468; (b) Gregory, A.; Stenzel, M. H., *Progress in Polymer Science* **2012**, 37 (1), 38-105.
3. (a) Hawker, C. J.; Bosman, A. W.; Harth, E., *Chem. Rev. (Washington, D. C.)* **2001**, 101 (Copyright (C) 2012 American Chemical Society (ACS). All Rights Reserved.), 3661-3688; (b) Nicolas, J.; Guillaneuf, Y.; Lefay, C.; Bertin, D.; Gigmes, D.; Charleux, B., *Progress in Polymer Science* **2013**, 38 (1), 63-235.
4. (a) Poli, R., *Angew. Chem. Int. Ed.* **2006**, 45 (31), 5058-5070; (b) Allan, L. E. N.; Perry, M. R.; Shaver, M. P., *Prog. Polym. Sci.* **2012**, 37 (1), 127-156.
5. (a) Matyjaszewski, K.; Xia, J., *Chemical Reviews* **2001**, 101 (9), 2921-2990; (b) Kamigaito, M.; Ando, T.; Sawamoto, M., *Chem. Rev.* **2001**, 101 (12), 3689-3746; (c) Tsarevsky, N. V.; Matyjaszewski, K., *Chem. Rev.* **2007**, 107 (6), 2270-2299; (d) Matyjaszewski, K., *Macromolecules* **2012**, 45 (10), 4015-4039; (e) Siegwart, D. J.; Oh, J. K.; Matyjaszewski, K., *Prog. Polym. Sci.* **2012**, 37 (1), 18-37; (f) Matyjaszewski, K.; Tsarevsky, N. V., *Nat Chem* **2009**, 1 (4), 276-288; (g) Matyjaszewski, K.; Spanswick, J., 3.12 - Copper-Mediated Atom Transfer Radical Polymerization. In *Polymer Science: A Comprehensive Reference*, Editors-in-Chief: Krzysztof, M.; Martin, M., Eds. Elsevier: Amsterdam, 2012; pp 377-428.
6. di Lena, F.; Matyjaszewski, K., *Prog. Polym. Sci.* **2010**, 35 (8), 959-1021.
7. De Paoli, P.; Isse, A. A.; Bortolamei, N.; Gennaro, A., *Chem. Commun.* **2011**, 47 (12), 3580-3582.
8. (a) Tang, W.; Kwak, Y.; Braunecker, W.; Tsarevsky, N. V.; Coote, M. L.; Matyjaszewski, K., *Journal of American Chemical Society* **2008**, 130 (32), 10702-10713; (b) Magenau, A. J. D.; Kwak, Y.; Schröder, K.; Matyjaszewski, K., *ACS Macro Letters* **2012**, 1 (4), 508-512.
9. (a) Seeliger, F.; Matyjaszewski, K., *Macromolecules* **2009**, 42 (16), 6050-6055; (b) Braunecker, W. A.; Tsarevsky, N. V.; Gennaro, A.; Matyjaszewski, K., *Macromolecules* **2009**, 42 (17), 6348-6360; (c) Morick, J.; Buback, M.; Matyjaszewski, K., *Macromol. Chem. Phys.* **2012**, 213 (21), 2287-2292.

10. (a) Jakubowski, W.; Matyjaszewski, K., *Angew. Chem. Int. Ed.* **2006**, *118* (27), 4594-4598; (b) Matyjaszewski, K.; Jakubowski, W.; Min, K.; Tang, W.; Huang, J.; Braunecker, W. A.; Tsarevsky, N. V., *Proceedings of the National Academy of Sciences* **2006**, *103* (42), 15309-15314.
11. (a) Matyjaszewski, K.; Coca, S.; Gaynor, S. G.; Wei, M.; Woodworth, B. E., *Macromolecules* **1997**, *30* (23), 7348-7350; (b) Percec, V.; Guliashvili, T.; Ladislaw, J. S.; Wistrand, A.; Stjerndahl, A.; Sienkowska, M. J.; Monteiro, M. J.; Sahoo, S., *J. Am. Chem. Soc.* **2006**, *128* (43), 14156-14165; (c) Matyjaszewski, K.; Tsarevsky, N. V.; Braunecker, W. A.; Dong, H.; Huang, J.; Jakubowski, W.; Kwak, Y.; Nicolay, R.; Tang, W.; Yoon, J. A., *Macromolecules* **2007**, *40* (22), 7795-7806; (d) Magenau, A. J. D.; Kwak, Y.; Matyjaszewski, K., *Macromolecules* **2010**, *43* (23), 9682-9689; (e) Zhang, Y.; Wang, Y.; Peng, C.-h.; Zhong, M.; Zhu, W.; Konkolewicz, D.; Matyjaszewski, K., *Macromolecules* **2011**.
12. (a) Jakubowski, W.; Min, K.; Matyjaszewski, K., *Macromolecules* **2005**, *39* (1), 39-45; (b) Matyjaszewski, K.; Dong, H.; Jakubowski, W.; Pietrasik, J.; Kusumo, A., *Langmuir* **2007**, *23* (8), 4528-4531; (c) Li, B.; Yu, B.; Huck, W. T. S.; Zhou, F.; Liu, W. M., *Angew. Chem.-Int. Edit.* **2012**, *51* (21), 5092-5095.
13. Pietrasik, J.; Dong, H.; Matyjaszewski, K., *Macromolecules* **2006**, *39* (19), 6384-6390.
14. (a) Rzaev, J.; Penelle, J., *Angew. Chem. Int. Ed.* **2004**, *43* (13), 1691-1694; (b) Kwiatkowski, P.; Jurczak, J.; Pietrasik, J.; Jakubowski, W.; Mueller, L.; Matyjaszewski, K., *Macromolecules* **2008**, *41* (4), 1067-1069.
15. (a) Kwak, Y.; Matyjaszewski, K., *Macromolecules* **2010**, *43* (12), 5180-5183; (b) Tasdelen, M. A.; Uygun, M.; Yagci, Y., *Macromol. Chem. Phys.* **2011**, *212* (18), 2036-2042; (c) Mehmet Atilla, T.; Mustafa, Ç.; Mustafa, U.; Yusuf, Y., Possibilities for Photoinduced Controlled Radical Polymerizations. In *Progress in Controlled Radical Polymerization: Mechanisms and Techniques*, American Chemical Society: 2012; Vol. 1100, pp 59-72; (d) Fors, B. P.; Hawker, C. J., *Angewandte Chemie International Edition* **2012**, *51* (35), 8850-8853; (e) Konkolewicz, D.; Schröder, K.; Buback, J.; Bernhard, S.; Matyjaszewski, K., *ACS Macro Letters* **2012**, *1* (10), 1219-1223.
16. (a) Magenau, A. J. D.; Strandwitz, N. C.; Gennaro, A.; Matyjaszewski, K., *Science* **2011**, *332* (6025), 81-84; (b) Bortolamei, N.; Isse, A. A.; Magenau, A. J. D.; Gennaro, A.; Matyjaszewski, K., *Angewandte Chemie International Edition* **2011**, *50*, 11391-11394.
17. (a) Qiu, J.; Matyjaszewski, K.; Thouin, L.; Amatore, C., *Macromol. Chem. Phys.* **2000**, *201* (14), 1625-1631; (b) Kim, B. Y.; Ratcliff, E. L.; Armstrong, N. R.; Kowalewski, T.; Pyun, J., *Langmuir* **2009**, *26* (3), 2083-2092.
18. (a) Hansen, T. S.; Lind, J. U.; Dagaard, A. E.; Hvilsted, S.; Andresen, T. L.; Larsen, N. B., *Langmuir* **2010**, *26* (20), 16171-16177; (b) Bonometti, V.; Labbé, E.; Buriez, O.; Mussini, P.; Amatore, C., *J. Electroanal. Chem.* **2009**, *633* (1), 99-105.
19. (a) Hardy, C. G.; Ren, L. X.; Tamboue, T. C.; Tang, C. B., *J Polym Sci Pol Chem* **2011**, *49* (6), 1409-1420; (b) Kraft, A.; Grimsdale, A. C.; Holmes, A. B., *Angew. Chem. Int. Ed.* **1998**, *37* (4), 402-428.
20. (a) Tria, M. C. R.; Advincula, R. C., *Macromol. Rapid Commun.* **2011**, *32* (13), 966-971; (b) Nunige, S.; Cornut, R.; Hazimeh, H.; Hauquier, F.; Lefrou, C.; Combella, C.; Kanoufi, F., *Angew. Chem.-Int. Edit.* **2012**, *51* (21), 5208-5212.

21. Bortolamei, N.; Isse, A. A.; Di Marco, V. B.; Gennaro, A.; Matyjaszewski, K., *Macromolecules* **2010**, *43* (22), 9257-9267.
22. Bell, C. A.; Bernhardt, P. V.; Monteiro, M. J., *J. Am. Chem. Soc.* **2011**, *133* (31), 11944-11947.
23. (a) Broderick, E. M.; Guo, N.; Vogel, C. S.; Xu, C. L.; Sutter, J.; Miller, J. T.; Meyer, K.; Mehrkhodavandi, P.; Diaconescu, P. L., *J. Am. Chem. Soc.* **2011**, *133* (24), 9278-9281; (b) Broderick, E. M.; Guo, N.; Wu, T. P.; Vogel, C. S.; Xu, C. L.; Sutter, J.; Miller, J. T.; Meyer, K.; Cantat, T.; Diaconescu, P. L., *Chem. Commun.* **2011**, *47* (35), 9897-9899; (c) Gregson, C. K. A.; Gibson, V. C.; Long, N. J.; Marshall, E. L.; Oxford, P. J.; White, A. J. P., *Journal of American Chemical Society* **2006**, *128* (23), 7410-7411.
24. Isse, A. A.; Sandona, G.; Durante, C.; Gennaro, A., *Electrochim. Acta* **2009**, *54* (12), 3235-3243.
25. Isse, A. A.; Gennaro, A., *J. Phys. Chem. A* **2004**, *108* (19), 4180-4186.
26. (a) Bard, A. J.; Faulkner, L. R., *Electrochemical methods : fundamentals and applications*. 2nd ed.; Wiley: New York, 2001; (b) Testa, A. C.; Reinmuth, W. H., *Analytical Chemistry* **1961**, *33* (10), 1320-1324.
27. Chan, N.; Cunningham, M. F.; Hutchinson, R. A., *Macromol. Chem. Phys.* **2008**, *209* (17), 1797-1805.
28. Wang, Y.; Zhong, M.; Zhang, Y.; Magenau, A. J. D.; Matyjaszewski, K., *Macromolecules* **2012**, *45* (21), 8929-8932.

Chapter III

Simplified Electrochemically Mediated Atom Transfer Radical Polymerization using Sacrificial Counter Electrode*

III. 1. Preface

The *e*ATRP procedure has many advantages, such as controlling rate of polymerization (R_p) by applied potential, current, or total passed charge, polymerization with a low catalysts loading system, and well-controlled polymerizations in aqueous media. Surface-initiated *e*ATRP with a tilted working electrode can be used to produce brushes with a gradient thickness because the polymerization can be governed by diffusion control of electro-active compounds (*i.e.*, $\text{Cu}^{\text{I/L}}$) from the working electrode. However, the reaction setup could be a substantial obstacle to the wide application of *e*ATRP in academia and industry. Therefore, there is a significant need for simplifying the *e*ATRP reaction setup to enable its wider application.

The idea behind this project was to use a counter electrode that could be directly immersed in the reaction media without separating gel/membrane. The counter electrode could undergo self-destruction to prevent halide oxidation and, when the proper potential or current is applied, it could act as sacrificial electrode. Aluminum showed well-matched properties among several metal species that were tested. A further simplification of the reaction setup was achieved under galvanostatic conditions, which required only two

*Work in this chapter was published and partially reformatted from the following manuscript: **Park, Sangwoo**; Chmielarz, Paweł; Gennaro, Armando; Matyjaszewski, Krzysztof *Angew. Chem. Int. Ed. Engl.* **2015**, *54*, 2388

electrodes; a working and a counter electrode.

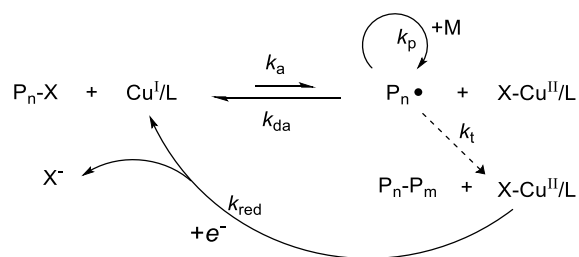
In this project, the polymerization of *n*-butyl acrylate (BA) under different applied potentials, polymerization under galvanostatic conditions, and synthesis of high molecular weight polymers were studied and compared with control experiments by conventional *e*ATRP.

Search for a proper stable metal species for sacrificial counter electrodes showed an interesting behavior that silver (Ag) could reduce $\text{Cu}^{\text{II}}/\text{L}$ to $\text{Cu}^{\text{I}}/\text{L}$. The details of the project are included in Appendix VI. In brief, polymerization occurred in the presence of monomers, initiators, and $\text{Cu}^{\text{II}}/\text{L}$, and well-defined polymers such PBA with $M_w/M_n > 1.2$ were obtained. The detailed mechanism was studied with my former group members, Dr. Valerie Williams and Dr. Paweł Chmielarz, and a current group member, Thomas Ribelli. The polymerization results showed that Ag is a good candidate for a transition metal as a reducing agent for ATRP catalysts, enabling polymerization with low catalysts loading conditions, ease of purification, and ability to be recycled.

I appreciate the contribution of Dr. Paweł Chmielarz to the project, particularly the study of chain extension reactions, and many invaluable discussions. I would also like to thank Prof. Armando Gennaro for his helpful exchange of views.

III. 2. Introduction

There has been interest recently in controlling polymerization by external stimuli, such as chemical, microwave, light, or electrical current.^{10, 27, 70a, 82} Reactions can be potentially stopped and restarted by changing the stimulus.^{70c, 82c, 83} The recently developed electrochemically mediated atom transfer radical polymerization (*e*ATRP) is an example of such a procedure and has been used for the preparation of polymers with pre-determined molecular weight and uniform structure under potentiostatic or galvanostatic conditions.^{1e, 10, 84} In an *e*ATRP, activators, typically a copper(I)/ligand ($\text{Cu}^{\text{I}}/\text{L}$) complex, can be generated near the working electrode surfaces by the reduction of oxidatively stable deactivators ($\text{X-Cu}^{\text{II}}/\text{L}$) under applied potential (E_{app}). The activator ($\text{Cu}^{\text{I}}/\text{L}$) is then homogeneously distributed throughout the reaction mixture by vigorous stirring and reaction of the activator with initiators (for example, alkyl halide, R-X) forms the radical species (R^\bullet) and the oxidized catalyst ($\text{X-Cu}^{\text{II}}/\text{L}$).⁸⁴ Subsequently, the radical species propagate to form polymeric chains by reacting with monomers (M) or are reverted back to the dormant species ($\text{P}_n\text{-X}$) by reaction with the formed $\text{X-Cu}^{\text{II}}/\text{L}$ deactivator complex. By repeating such sequential reactions, well-defined polymers can be obtained with uniform structures (Scheme III-1).



Scheme III-1. Mechanism of *e*ATRP.

*e*ATRP can be carried out with low levels of catalysts, down to ppm of monomer concentration, and can be stopped and restarted by switching the applied potential, *e*ATRP has been successfully used for the synthesis of materials with well-defined polymeric architectures.^{1f, 12, 23a, 23b, 43a, 47, 84-85} However, there are some limitations associated with *e*ATRP, especially in the reaction setup stage. Typically, *e*ATRP polymerizations can be achieved by utilizing a three electrode system, allowing application of a potentiostatic process, that is, at constant applied potential. This requires the presence of a working electrode (WE), a counter electrode (CE), and a reference electrode (RE). In general, a platinum (Pt) mesh electrode is selected as a WE, which provides a high surface area for effectively converting Cu^{II} into Cu^I. The RE is separated from the reaction solution by a supporting electrolyte saturated methylated cellulose (Tylose) gel, such as Ag/AgI/I⁻, and the applied potential is determined by the WE and RE. The CE is generally a Pt mesh electrode that is also separated from the reaction mixture, in a similar manner to the RE, to avoid undesired side reactions, for example oxidation of Cu^I and contamination of the working solution by oxidation products.¹⁰ When an *e*ATRP was attempted with a directly immersed CE (Pt meshed), the results showed no polymerization (Figure III-1 red dots). This could be due to Cu^I/L oxidation, leading to the formation of a naked Cu^{II} deactivator. Therefore, separation of the CE from the polymerization mixture is necessary in a conventional *e*ATRP. Herein, a significant simplification of the procedures used for an *e*ATRP was investigated, by using a sacrificial counter electrode, (*se*ATRP) which does not require any separation and can be directly inserted into the reaction mixture. There are two potential advantages of using *se*ATRP. The first one is the use of an undivided cell, which allows for a simpler, lower cost process, and most of all, the minimization of the

ohmic drop, bringing a beneficial energy saving. The second advantage is the possibility of a galvanostatic process using two electrode system and a current generator, which is simpler than a potentiostat. Both advantages should benefit commercial and academic efforts in the area of *e*ATRP.

III. 3. Results and Discussion

In the ideal case of *se*ATRP, the sacrificial counter electrode should not react with the Cu/L catalysts either in the presence or absence of an applied electric current. Instead, the electrode can only be self-consumed ($M_t \rightarrow M_t^n + ne^-$) under an applied current, which also prevents undesired side reactions, in particular formation of naked deactivators. Copper and aluminum metal wires ($l = 10$ cm and $d = 1$ mm) were prepared and, first of all, tested for their inertness under polymerization conditions, that is, by immersing in the solution mixed with monomer, initiator, and CuBr₂/TPMA. The Cu wire acted as both a supplemental activator and a reducing agent (SARA),^{1f, 27, 33, 86} the reaction showed more than 74% monomer conversion in 2 h. On the other hand, Al wire showed no reduction of Cu^{II}/L to Cu^I/L even though Al has a negative standard potential ($E^0 = -1.66$ V vs. SHE in water). This is likely because the surface of the Al wire is passivated by forming stable oxidized layers to prevent reduction of Cu^{II}/L to Cu^I/L. Therefore the Al wire seemed to fit the requirements of a sacrificial electrode.

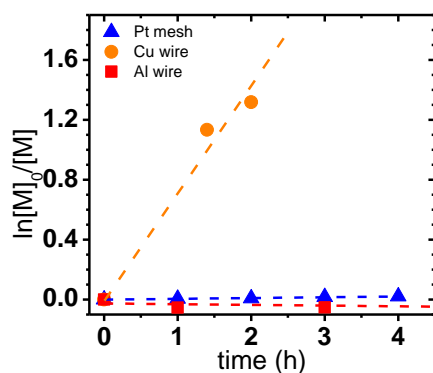
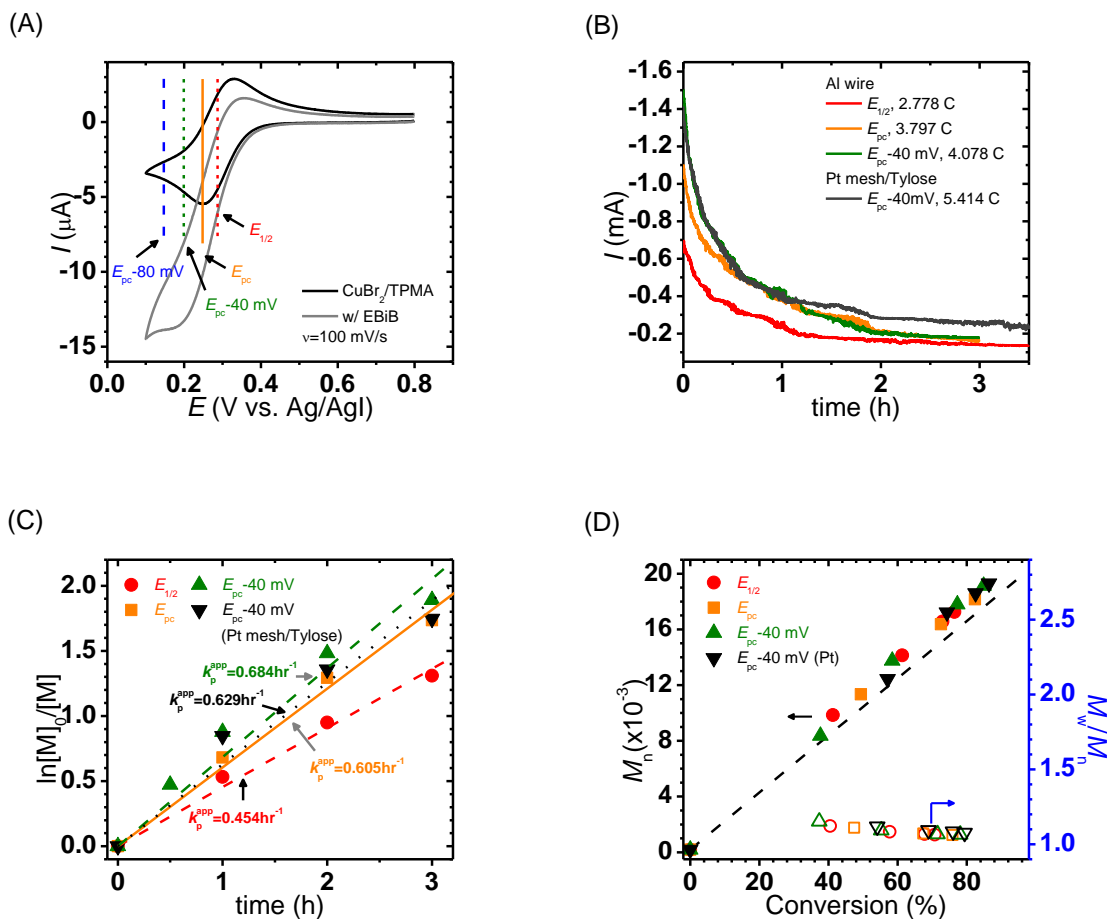


Figure III-1. ATRP with 10 cm metal wires ($d = 1$ mm). Pt mesh = *e*ATRP carried out with a Pt mesh cathode and a directly immersed Pt mesh counter electrode).

A series of *n*-butyl acrylate (BA) polymerizations was carried out under potentiostatic conditions with a Pt mesh WE, an Al CE, and Ag/AgI/I⁻ RE. Control over the rate of polymerization (R_p) was evaluated by applying different constant potentials (E_{app}). Four E_{app} values were selected: $E_{1/2}$, E_{pc} , $E_{pc} - 40$ mV, and $E_{pc} - 80$ mV (Figure III-2). Faster R_p was observed when more negative potentials were applied. The fastest apparent propagation rate constant (k_p^{app}) was observed to be 0.684 hr^{-1} ($E_{app} = E_{pc} - 40$ mV). This value was 1.5 times faster than when $E_{app} = E_{1/2}$. The k_p^{app} values of *se*ATRP and conventional *e*ATRP with $E_{app} = E_{pc} - 40$ mV are well-matched (Table III-1 entries 3 and 4) and identical cathodic current drops were observed (Figure III-2B). All of the BA polymerizations by *se*ATRP showed good evolution of molecular weight (MW), close to theoretical values, and maintained narrow molecular weight distributions (M_w/M_n , MWDs). After the polymerization was completed, a scanning electron microscope (SEM) was used for the examination of the surfaces of the Al wires. Pristine Al wires showed clear surfaces,

however, the surfaces of Al wires showed porous morphologies after the application of current during a *se*ATRP (Figure III-3). The pores on the surface of the wires could be formed by oxidation of aluminum (to Al^{3+}) and reaction with residual water molecules to form Al_2O_3 .⁸⁷ The overall weight loss of the wire was less than 1 mg, in agreement with chronoamperometry (Table III-2). According to ICP-MS analysis, the residual amount of Al and Cu in isolated polymers was 5.2 and 16 ppm, respectively. These values are smaller than the initial amount of oxidized aluminum and Cu, indicating partial removal of residual metals during polymer purification.



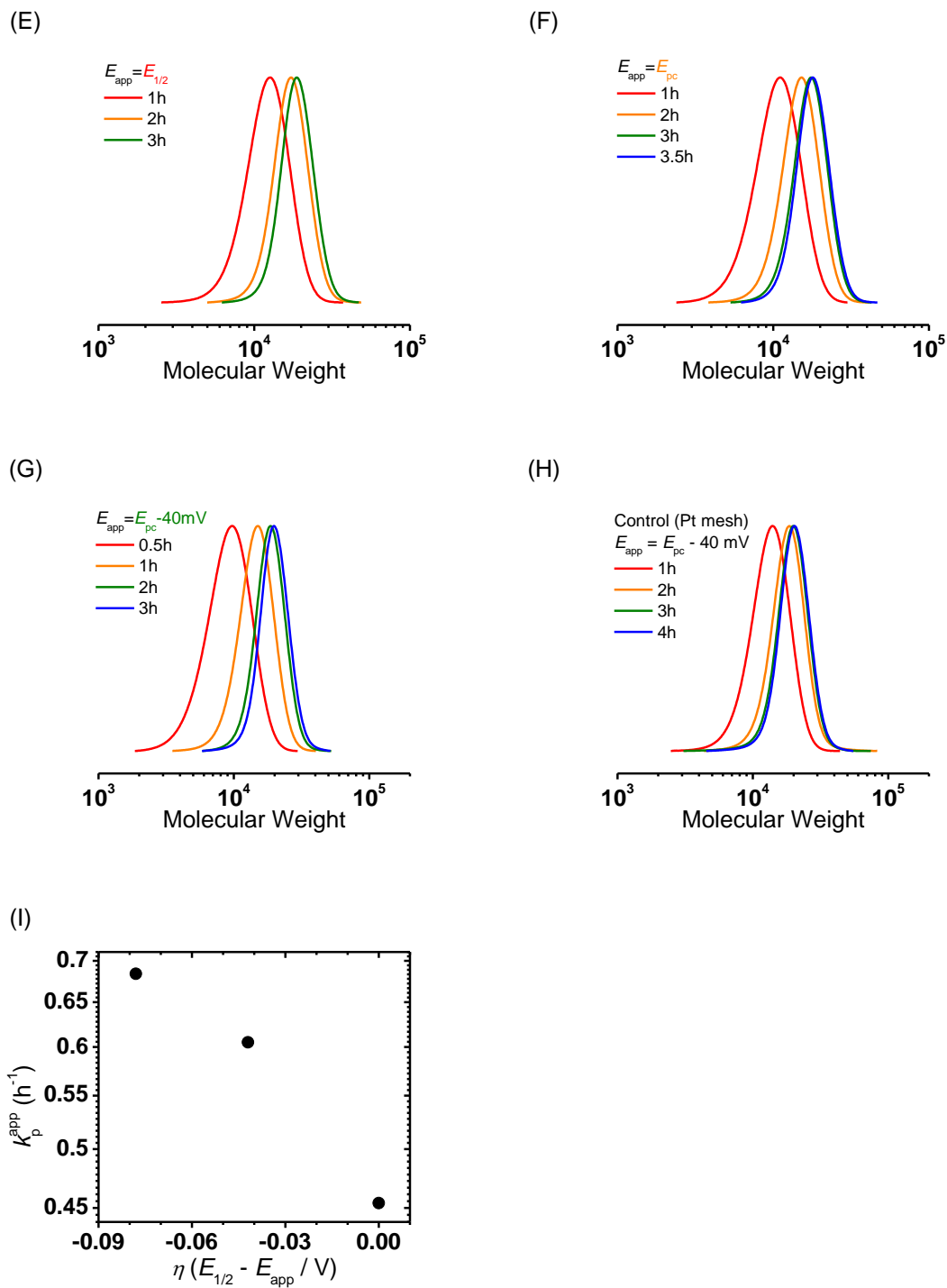
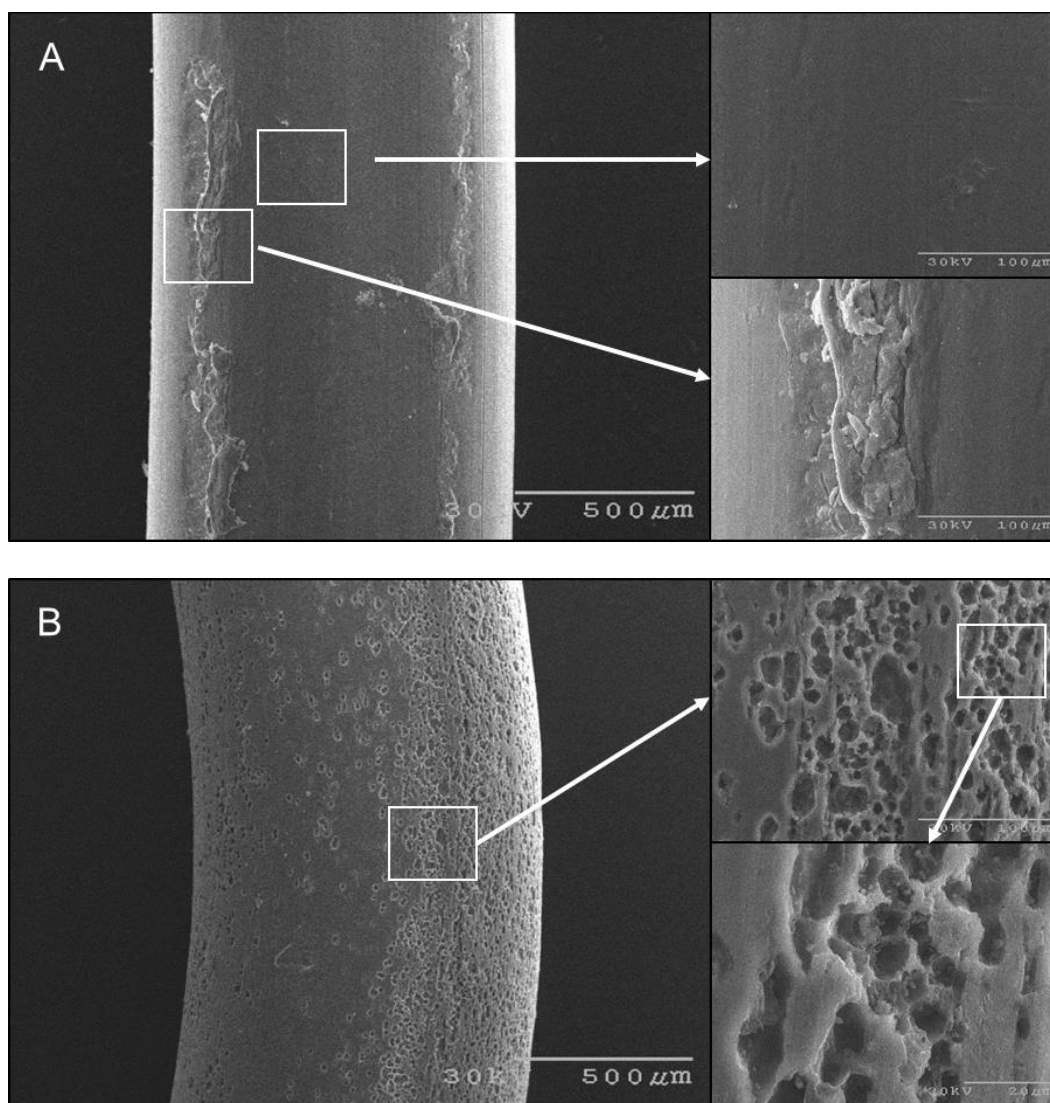


Figure III-2. *se*ATRP of BA with different E_{app} s; reaction condition: $[\text{BA}]/[\text{EBiB}]/[\text{CuBr}_2/\text{TPMA}] = 160/1/0.02$, $[\text{BA}] = 3.49\text{ M}$ in DMF (50% solution

polymerization), $[\text{TBAClO}_4] = 0.2 \text{ M}$, $T = 50 \text{ }^\circ\text{C}$, WE = Pt mesh, CE = Al wire, RE = Ag/AgI/I⁻; (A) CV of CuBr₂/TPMA with and without initiator (dot lines indicate E_{app}); (B) Chronopotentiometry of the BA polymerizations, the reported charges correspond to the total charge passed after 3 h; (C) first-order kinetic plot with different E_{app} s; and (D) M_n and M_w/M_n versus conversion of BA polymerizations by *se*ATRP; (E)-(H) GPC traces of BA polymerization under different E_{app} s; (I) Normalized applied potential $\eta = E_{\text{app}} - E_{1/2}$.



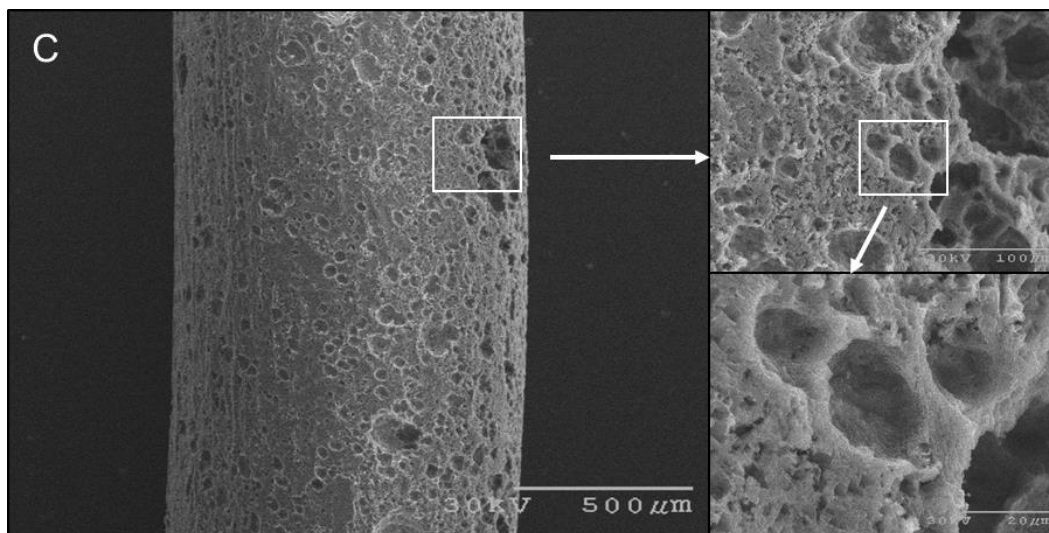


Figure III-3. Surface morphologies of Al wires by SEM; (A) pristine, (B) used for *seATRP* 1 time, and (C) used for *seATRP* 10 times.

Table III-1. Summary of *seATRP* of BA.^a

Entry	[M]/[I]/[CuBr ₂ /TPMA]	E_{app}^b	Conv.	$M_{n,GPC}$	$M_{n,theoretical}$	M_w/M_n^d	k_p^{app}
			(%) ^c	(g/mol) ^d	(g/mol)		(h ⁻¹)
1	160/1/0.02	$E_{1/2}$	76	17250	15800	1.06	0.454
2	160/1/0.02	E_{pc}	82	18150	17000	1.06	0.605
3	160/1/0.02	$E_{pc}-40$ mV	85	19100	17600	1.07	0.684
4 ^e	160/1/0.02	$E_{pc}-40$ mV	86	19300	17800	1.08	0.629
5	1000/1/0.1	$E_{pc}-80$ mV	92	96700	118100	1.17	0.352
6	100/1/0.005	$E_{pc}-80$ mV	23	3400	3100	1.36	0.511
7	400/1/0.04	$E_{pc}-80$ mV	72	34800	40500	1.29	0.674
8	200/1/0.02	$E_{pc}-80$ mV	77	19200	19900	1.07	0.795
9	200/1/0.02	Galvanostatic Conditions ^f	78	18560	20100	1.07	0.788

^aPolymerization conditions: WE = Pt mesh, CE = Al wire ($l = 10$ cm, $d = 1$ mm), RE = Ag/AgI/Γ, supporting electrolyte = tetrabutylammonium perchlorate (TBAClO₄, 0.2 M), $T =$

= 50 °C; ^b*E*_{apps} were selected based on CV analysis without initiator (*v* = 100 mV/s); ^cFinal conversion, determined by ¹H NMR; ^dMWs and MWDs were determined by THF GPC with PMMA standards; ^eUsing conventional *e*ATRP, CE = Pt mesh (separated from reaction mixture by supporting electrolyte saturated Tylose gel); ^f*I*_{apps} = -1.03, -0.53, -0.40, and -0.28 mA for 30 min each steps.

Table III-2. Weight loss of Al wires after *se*ATRP.

Entry	[M]/[I]/[CuBr ₂ /TPMA]	<i>E</i> _{app} ^a	Time (h)		Final conversion (%)	Weight loss (mg)
1	160/1/0.018 ^b	<i>E</i> _{pc} – 40 mV	4	4	84	0.4
2	100/1/0.005 ^b	<i>E</i> _{pc} – 80 mV	0.5	80	52	0.6
3	400/1/0.04 ^c	<i>E</i> _{pc} – 80 mV	4	80	91	< 0.1

^aCV was recorded with scan rate = 100 mV/s; ^bM = BA, I = EBiB; ^cM = *t*BA, I = PBA₅₂-Br; General polymerization conditions: *T* = 50 °C, [TBAClO₄] = 0.2 M, working electrode = Pt mesh (for CV, Pt disk), counter electrode = Al wire, reference electrode = Ag/AgI/I⁻.

The level of preservation of chain-end functionality was investigated by synthesis of high molecular weight of PBA and by chain extension experiments. Synthesis of high MW PBA was examined by targeting a DP of 1000 (that is, [M]/[I] = 1000, Figure III-4). A linear first-order kinetic plot was observed during the polymerization and the MWs of PBA matched well with the theoretical values below 60% monomer conversion. Above 60% monomer conversion the observed MWs showed a slight decrease from the theoretical

values, presumably resulting either from transfer reactions or termination reactions (coupling and disproportionation). Although the MWs were slightly different from the ideal values, the final monomer conversion reached 90% after 10 h and MWD's were lower than 1.2. Chain end functionality was also evaluated by chain extension of a macroinitiator formed by *se*ATRP to form a block copolymer. A PBA with low DP was prepared by *se*ATRP ($M_n=3430$ and $M_w/M_n=1.36$, Figure III-5A and B). The PBA₂₇-Br macroinitiator was then used in a chain extension copolymerization with *tert*-butyl acrylate (*t*BA) as the second monomer. Linear first-order kinetics was observed and GPC traces indicated good incorporation of the second monomer, as essentially a clean peak shift was observed (Figure III-5).

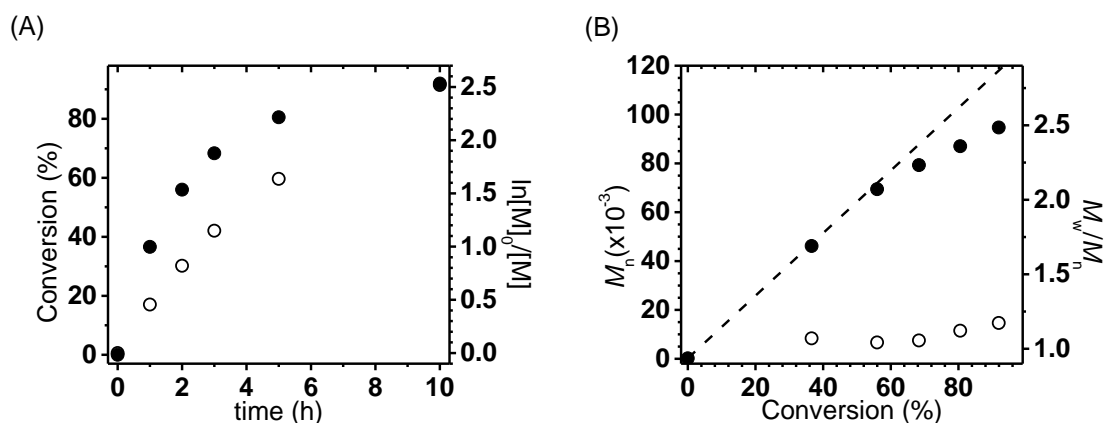


Figure III-4. High MW of PBA by *se*ATRP; (A) Conversion of monomers versus reaction time and (B) MW evolution and MWD results by GPC with PMMA standards.

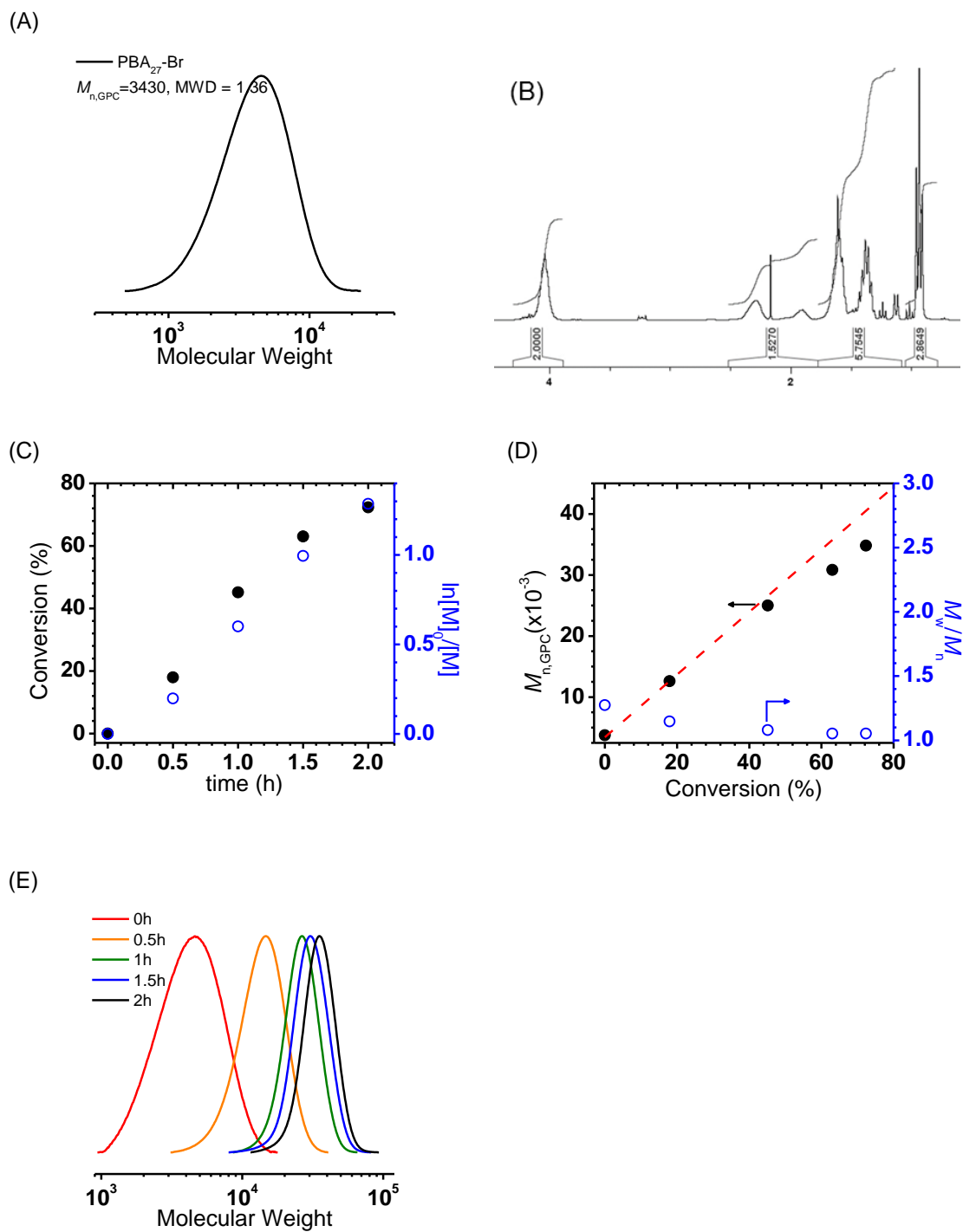
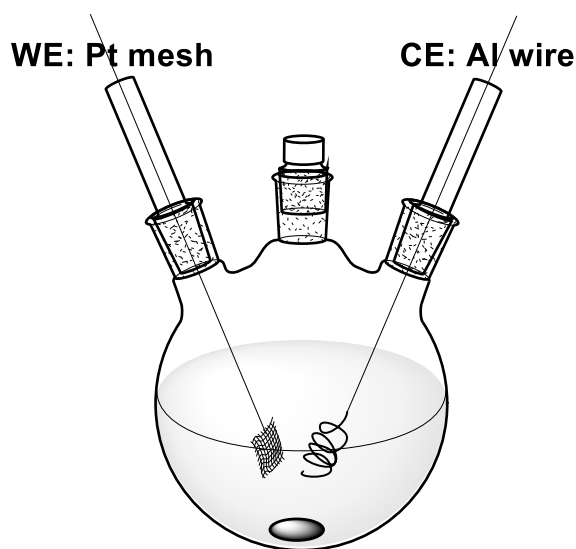


Figure III-5. Chain extension by *se*ATRP; (A) GPC trace of PBA with low DP by *se*ATRP; (B) ^1H NMR spectra of purified sample (in CDCl_3); (C) Conversion of monomers versus

reaction time; (D) MW evolution and MWD results from GPC with PMMA standards; (E) GPC results of block copolymerization.

Polymerization under galvanostatic conditions (constant applied current) was carried out for the purpose of further simplifying the reaction setup, since galvanostatic conditions only require two electrodes: a Pt mesh working cathode and an Al wire counter/sacrificial anode (Scheme III-2). The applied currents (I_{app} s) were determined by the polymerizations carried out under potentiostatic conditions. In general, two characteristic cathodic current responses are observed during the polymerization under potentiostatic conditions: an initial fast current decay followed by a nearly constant current (Figure III-6A). The first response is mainly attributed to the reduction of initially used $X-Cu^{II}/L$ to Cu^I/L and reaction of $R-X$ to form the propagating radical R^\bullet and $X-Cu^{II}/L$. Once the equilibrium is established between $R-X$, Cu^I/L , R^\bullet , and $X-Cu^{II}/L$, an essentially constant current flow was observed owing to the maintenance of a constant concentration of Cu^I/L . On the basis of the chronoamperometry (CA) results, the total passed charge was calculated by integration of the CA area, that is, $Q(C) = A \times s$. Thus, two constant I_{app} s were used for the polymerization under galvanostatic conditions; $I_{app,1} = (-) 0.713$ mA (for 0 to 1.2 h) and $I_{app,2} = (-) 0.297$ mA (for 1.2 to 4 h), where negative values indicate cathodic current. The R_p showed a slight decrease from values observed under potentiostatic conditions when the second current was constantly applied ($I_{app,2}$, Figure III-6C). The values observed for *se*ATRP under galvanostatic conditions showed similar MW evolution and MWD values as compared to polymerizations conducted under potentiostatic conditions. Slow copper deposition on the WE surfaces was observed when applying $I_{app,2}$ ((-) 0.297 mA). The Cu deposition arises

from further reduction of $\text{Cu}^{\text{I}}/\text{L}$ to Cu^0 , since under galvanostatic conditions the applied potentials cannot be exactly controlled. After the polymerization, the residual concentration of $\text{Cu}^{\text{II}}/\text{L}$ in the solution reached 0.1 mM ($\lambda_{\text{max}, \text{Cu}^{\text{II}}/\text{TPMA}} = 975 \text{ nm}$, 20 ppm to monomer molar concentration), that is, overall 80% of Cu^{II} had been removed from the reaction medium (Figure III-6E). To improve controllability, and avoid undesirable Cu deposition, a multi-step current procedure was developed and applied to the reaction mixture. The applied currents were determined from potentiostatic conditions: -1.03, -0.53, -0.40, and -0.28 mA for $I_{\text{app},1}$ to $I_{\text{app},4}$, respectively (30 min for each step). Identical first-order kinetic plots were observed, and GPC analysis indicated similar MW evolution and narrow MWD (Figure III-7). As expected copper deposition on the WE surfaces was not observed in this case.



Scheme III-2. Galvanostatic condition of *se*ATRP.

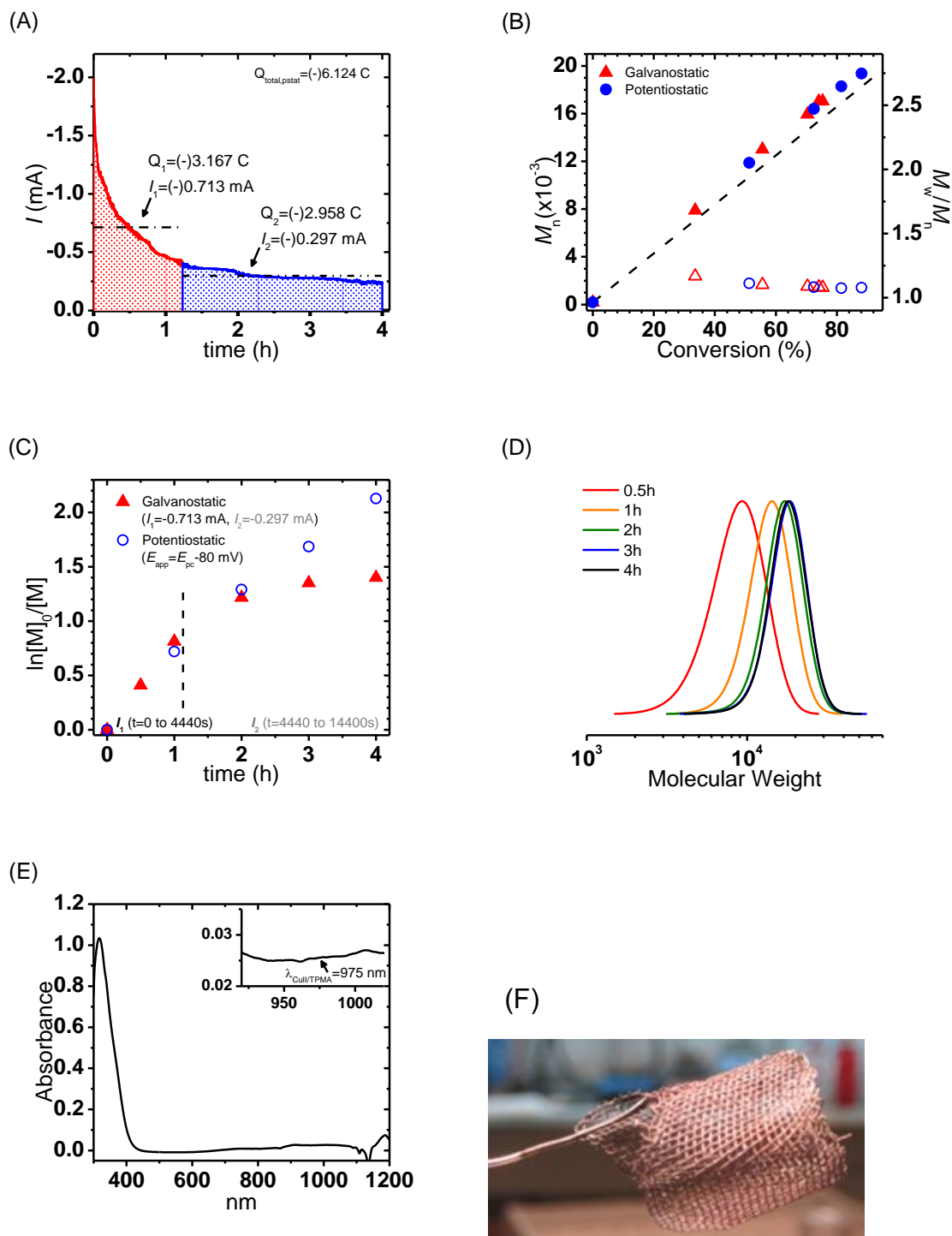


Figure III-6. Galvanostatic *se*ATRP; (A) chronoamperometry results from potentiostatic condition (exponentially drop) and applied current (dot line); (B) MW and MWD results

from GPC with PMMA standards; (C) monomer conversion versus time; (D) GPC traces of BA polymerization; (E) UV-vis spectra of post-polymerization solution; (F) copper deposited on Pt mesh WE.

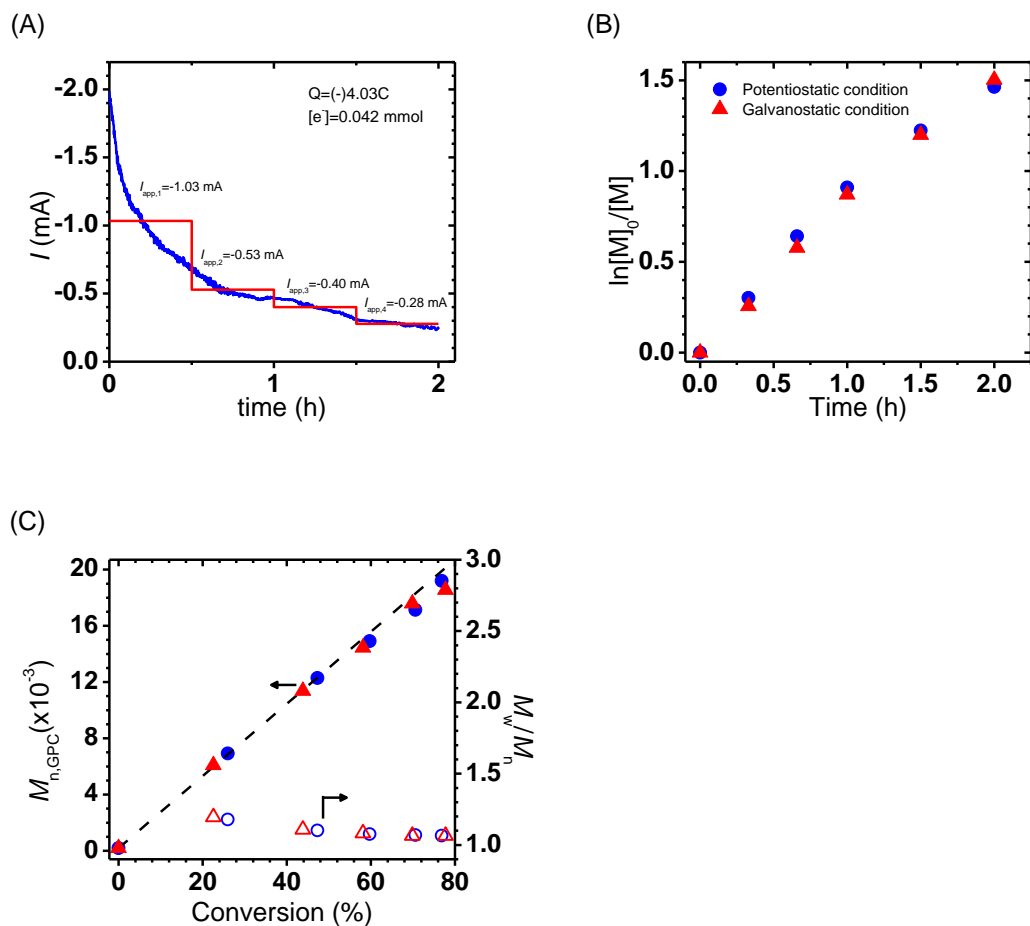


Figure III-7. Multi-step chronoamperometry for galvanostatic *seATRP*; (A) chronoamperometry results from potentiostatic conditions (exponential drop) and applied current (dot line), (B) first-order kinetic plots by potentiostatic and galvanostatic conditions, and (C) MW and MWD results from GPC with PMMA standards.

III. 4. Summary

A simplified electrochemically mediated atom transfer radical polymerization was achieved by using a sacrificial counter electrode (*se*ATRP). The direct immersion of an Al wire counter electrode in the reaction medium can avoid additional preparation setup steps, and the polymerization results indicated good control of reaction kinetics, providing polymers with molecular weight evolution close to theoretical values and generating polymers with narrow molecular-weight distribution. The rate of the polymerizations (R_p) was controlled by applying different potentials (E_{app}), with faster R_p observed using more negative E_{app} . Synthesis of high MW polymers and chain extension reactions indicate good conservation of chain-end functionalities. The *se*ATRP procedure can be further simplified by using only two electrodes and applying a constant current under galvanostatic conditions. The use of a multi-step current procedure showed identical results to polymerizations carried out under potentiostatic conditions, namely linear first-order kinetics and a uniform growth of polymers.

III. 5. Experimental section

Materials. Tetrabutylammonium perchlorate (TBAClO₄, > 98%), copper(II) bromide (CuBr₂, 99%), methylated cellulose (Tylose, MH=300), and ethyl α -bromoisobutyrate (EBiB, 98%) were purchased from Aldrich. *N,N*-dimethylformamide (DMF) was purchased from Acros. Metal wires (platinum, aluminum, and copper) and platinum gauge were purchased from Alfa Aesar. Tris(2-pyridylmethyl)amine (TPMA) was prepared according to a published procedure,⁸⁸ *n*-butyl acrylate (BA, > 99% from Aldrich) and *tert*-butyl acrylate (*t*BA, > 99% from Aldrich) were passed through a column filled with basic alumina prior to use to remove any inhibitor.

Reaction cell configuration for an electrochemical reaction. Electrochemical experiments were carried out under N₂ atmosphere using a Pt disk (for cyclic voltammetry, CV, $A = 0.071 \text{ cm}^2$) and Pt mesh (for chronoamperometry (CA) and chronopotentiometry (CP)) working electrodes. The Pt mesh counter electrode was prepared using a glass frit and a salt bridge made of Tylose gel saturated with TBAClO₄ to separate the cathodic from anodic compartments. The Al sacrificial anode was a wire ($l = 10 \text{ cm}$, $d = 1 \text{ mm}$). The Al wire was washed with acetone and THF, followed by directly immersing the wire in the reaction mixture. All potentials were measured with respect to a Ag/AgI/I⁻ reference electrode (Gamry Ref 600) with scan rate $\nu = 100 \text{ mV/s}$. During the *e*ATRP and *se*ATRP procedures, a condenser was connected to the reaction cell and maintained at -10 °C using a circulating chiller (NESLAB Inc., RTE-111).

Measurements. ¹H NMR (300 MHz) spectra were measured on a Bruker Advance 300 spectrometer using CDCl₃ as solvent. Molecular weights and distributions were determined by GPC (Polymer Standards Services (PSS) columns (guard, 10⁵, 10³, and 10² Å), with THF eluent at 35 °C, flow rate 1.00 mL/min, and with a differential refractive index (RI) detector (Waters, 2410)). The apparent molecular weights and molecular weight distribution (M_w/M_n) were determined by calibration based on linear poly(methyl methacrylate) standards using WinGPC 8.0 software from PSS. All CVs and CAs were recorded by a Gamry Ref 600 potentiostat. Samples for inductively coupled plasma–mass spectrometry (ICP-MS) were prepared by digesting the samples in 2 mL of aqua regia. The concentrations of aluminum (Al) and copper (Cu) in purified polymers were determined using Thermo-Finnigan Element XR ICP-MS. The instrument was calibrated for each

element. The samples were analyzed immediately after the initial calibration, and the elemental results were within the calibration range.

Sacrificial electrode test. TBAClO₄ (2.05 g, 6 mmol) was placed in a seven-neck electrolysis cell maintained at 50 °C under a slow N₂ purge. Then, 15 mL of N₂ purged BA (105 mmol), 0.23 mL of CuBr₂/TPMA stock solution (0.05 M in DMF), and DMF (15 mL) were added to the reaction cell. A metal wire (Cu or Al wires, $l = 10$ cm, $d = 1$ mm) was washed with acetone and THF several times before it was dried in air. The metal wire was immersed in the reaction solution and 96 μ L of EBiB (0.65 mmol) was injected into the flask to initiate the polymerization. Samples were withdrawn periodically to follow the monomer conversion, using ¹H NMR, and to determine the average molecular weight (M_n) and molecular weight distribution (M_w/M_n) by gel permeation chromatography (GPC) measurements (with PMMA standard curve).

General polymerization procedure under potentiostatic conditions. TBAClO₄ (2.05 g, 6 mmol) was placed in a seven-neck electrolysis cell maintained at 50 °C under a slow N₂ purge. Then, 15 mL of N₂ purged BA (105 mmol), 0.23 mL of a N₂ purged CuBr₂/TPMA stock solution (0.05 M in DMF), and DMF (15 mL) were added to the reaction cell. The CV was recorded with a Pt disk working electrode (WE), a Pt mesh counter electrode (CE), and a Ag/AgI/I⁻ reference electrode (RE) for determining the applied potential ($E_{app} = E_{1/2}$, E_{pc} , $E_{pc} - 40$, or $E_{pc} - 80$ mV). 96 μ L of EBiB (0.65 mmol) was injected into the reaction solution and the CV was recorded to confirm electro-catalysts (EC'') reaction. Then the Pt mesh WE, Al wire CE, were prepared and immersed in the polymerization solution and the proper potential was applied using the chronoamperometry

(CA) method. Samples were withdrawn periodically to follow the monomer conversion, using ^1H NMR, and the number average molecular weight (M_n) and molecular weight distribution (M_w/M_n) were determined by gel permeation chromatography (GPC) measurements (with PMMA standard curve).

Chain extension of a PBA-Br macroinitiator with *t*BA. A low DP PBA macroinitiator was prepared by *se*ATRP. Polymerization conditions: $[\text{BA}]/[\text{EBiB}]/[\text{CuBr}_2/\text{TPMA}] = 100/1/0.005$, $[\text{BA}] = 3.49 \text{ M}$ in DMF, $[\text{TBAClO}_4] = 0.2 \text{ M}$, $T = 50^\circ\text{C}$, WE = Pt mesh, CE = Al wire, and RE = Ag/AgI/I $^-$. The polymerization was stopped after 30 min, and the product was purified by dialysis against THF three times using a molecular cut-off of membrane = 2000. The macroinitiator was recovered from the dialyzed solution by rotary evaporation and further dried under vacuum for 1 day. The chain extension with *t*BA was carried out under the following reaction conditions: $[\text{tBA}]/[\text{PBA-Br}]/[\text{CuBr}_2/\text{TPMA}] = 400/1/0.04$, $[\text{tBA}] = 3.41 \text{ M}$ in DMF, $[\text{TBAClO}_4] = 0.2 \text{ M}$, $T = 50^\circ\text{C}$, WE = Pt mesh, CE = Al wire, and RE = Ag/AgI/I $^-$. Samples were withdrawn periodically to follow monomer conversion, using ^1H NMR. The number average molecular weight (M_n) and molecular weight distribution (M_w/M_n) of the samples were determined by gel permeation chromatography (GPC) measurements (with PMMA standard curve).

General polymerization procedure under galvanostatic conditions. Double step galvanostatic conditions: the first polymerization was carried out under potentiostatic conditions and the passed charge, (Q) value, was determined by utilizing the Gamry Echem Analysis program and proper applied current values were calculated based on $I = Q/s$ for

each step. An identical reaction mixture was prepared and polymerization was carried out under applied current, $I_{app,1} = (-) 0.713$ mA and $I_{app,2} = (-) 0.297$ mA. Samples were withdrawn periodically to follow the monomer conversion, using ^1H NMR. The number average molecular weight (M_n) and molecular weight distribution (M_w/M_n) were determined by gel permeation chromatography (GPC) measurements (with PMMA standard curve). Multi-step galvanostatic conditions: Actual conditions were similar to the previous potentiostatic conditions used for determining the correct applied current. The passed charge (Q) value was determined and applied current values were calculated based on $I = Q/s$ for each step. An identical reaction mixture was prepared and polymerization was carried out utilizing multiple applied currents ($I_{app,1} = (-) 1.03$ mA, $I_{app,2} = (-) 0.53$ mA, $I_{app,3} = (-) 0.40$ mA, $I_{app,4} = (-) 0.28$ mA). Samples were withdrawn periodically to follow monomer conversion, using ^1H NMR, and the number average molecular weight (M_n) and molecular weight distribution (M_w/M_n) were determined by gel permeation chromatography (GPC) measurements (with PMMA standard curve).

ICP-MS analysis of Al and Cu in purified polymers. Theoretical amount of Al^{3+} in the reaction mixture calculated from chronoamperometry, (CA), that is, $[\text{Al}^{3+}] = Q/F/3$, corresponds to the maximal concentration of Al in solution (conv. = 77%) should be 12.5 ppm (wt), **Table III-1**, entry 8. The Cu concentration, calculated from the initial catalyst loading, was 78 ppm (wt). According to ICP-MS analysis, the residual amount of Al and Cu in isolated polymers was 5.2 and 16 ppm, respectively. These values are smaller than the initial amount of oxidized aluminum and Cu, indicating partial removal of residual metals during polymer purification by passing through alumina column and/or

precipitation in methanol/water mixtures.

III. 6. References

1. (a) Cheng, Z. P.; Zhu, X. L.; Chen, M.; Chen, J. Y.; Zhang, L. F., *Polymer* **2003**, *44* (8), 2243-2247; (b) Gregson, C. K. A.; Gibson, V. C.; Long, N. J.; Marshall, E. L.; Oxford, P. J.; White, A. J. P., *J Am Chem Soc* **2006**, *128* (23), 7410-7411; (c) Yamago, S.; Ukai, Y.; Matsumoto, A.; Nakamura, Y., *J Am Chem Soc* **2009**, *131* (6), 2100-2101; (d) Kwak, Y.; Matyjaszewski, K., *Macromolecules* **2010**, *43* (12), 5180-5183; (e) Magenau, A. J. D.; Strandwitz, N. C.; Gennaro, A.; Matyjaszewski, K., *Science* **2011**, *332* (6025), 81-84; (f) Leibfarth, F. A.; Mattson, K. M.; Fors, B. P.; Collins, H. A.; Hawker, C. J., *Angew. Chem. Int. Ed.* **2013**, *52* (1), 199-210; (g) Konkolewicz, D.; Wang, Y.; Krys, P.; Zhong, M.; Isse, A. A.; Gennaro, A.; Matyjaszewski, K., *Polymer Chemistry* **2014**, *5* (15), 4396-4417; (h) Ribelli, T. G.; Konkolewicz, D.; Bernhard, S.; Matyjaszewski, K., *J. Am. Chem. Soc.* **2014**, *136* (Copyright (C) 2014 American Chemical Society (ACS). All Rights Reserved.), 13303-13312; (i) Anastasaki, A.; Nikolaou, V.; Pappas, G. S.; Zhang, Q.; Wan, C.; Wilson, P.; Davis, T. P.; Whittaker, M. R.; Haddleton, D. M., *Chemical Science* **2014**, *5* (9), 3536-3542.
2. (a) Fors, B. P.; Hawker, C. J., *Angewandte Chemie International Edition* **2012**, *51* (35), 8850-8853; (b) Yamago, S.; Nakamura, Y., *Polymer* **2013**, *54* (3), 981-994.
3. (a) Magenau, A. J. D.; Bortolamei, N.; Frick, E.; Park, S.; Gennaro, A.; Matyjaszewski, K., *Macromolecules* **2013**; (b) Matyjaszewski, K., *Macromolecules* **2012**, *45* (10), 4015-4039.
4. (a) Bortolamei, N.; Isse, A. A.; Magenau, A. J. D.; Gennaro, A.; Matyjaszewski, K., *Angew. Chem. Int. Ed.* **2011**, *50* (48), 11391-11394; (b) Li, B.; Yu, B.; Huck, W. T. S.; Zhou, F.; Liu, W., *Angew. Chem.* **2012**, *124* (21), 5182-5185; (c) Park, S.; Cho, H. Y.; Wegner, K. B.; Burdyska, J.; Magenau, A. J. D.; Paik, H.-j.; Jurga, S.; Matyjaszewski, K., *Macromolecules* **2013**; (d) Li, B.; Yu, B.; Huck, W. T. S.; Liu, W.; Zhou, F., *J. Am. Chem. Soc.* **2013**, *135* (5), 1708-1710; (e) Hosseiny, S. S.; van Rijn, P., *Polymers* **2013**, *5* (4), 1229-1240; (f) Matyjaszewski, K.; Tsarevsky, N. V., *J. Am. Chem. Soc.* **2014**; (g) Plamper, F., *Colloid. Polym. Sci.* **2014**, *292* (4), 777-783.
5. (a) Matyjaszewski, K.; Tsarevsky, N. V.; Braunecker, W. A.; Dong, H.; Huang, J.; Jakubowski, W.; Kwak, Y.; Nicolay, R.; Tang, W.; Yoon, J. A., *Macromolecules (Washington, DC, United States)* **2007**, *40* (22), 7795-7806; (b) Zhang, Y.; Wang, Y.; Peng, C.-h.; Zhong, M.; Zhu, W.; Konkolewicz, D.; Matyjaszewski, K., *Macromolecules* **2011**, *45* (1), 78-86; (c) Konkolewicz, D.; Wang, Y.; Zhong, M.; Krys, P.; Isse, A. A.; Gennaro, A.; Matyjaszewski, K., *Macromolecules* **2013**, *46* (22), 8749-8772; (d) Konkolewicz, D.; Krys, P.; Gois, J. R.; Mendonca, P. V.; Zhong, M.; Wang, Y.; Gennaro, A.; Isse, A. A.; Fantin, M.; Matyjaszewski, K., *Macromolecules* **2014**, *47* (2), 560-570; (e) Konkolewicz, D.; Krys, P.; Góis, J. R.; Mendonça, P. V.; Zhong, M.; Wang, Y.; Gennaro, A.; Isse, A. A.; Fantin, M.; Matyjaszewski, K., *Macromolecules* **2014**, *47* (2), 560-570; (f) Zhong, M.; Wang, Y.; Krys, P.; Konkolewicz, D.; Matyjaszewski, K., *Macromolecules* **2013**, *46* (10), 3816-3827; (g) Peng, C.-H.; Zhong, M.; Wang, Y.; Kwak, Y.; Zhang, Y.; Zhu, W.; Tonge,

- M.; Buback, J.; Park, S.; Krys, P.; Konkolewicz, D.; Gennaro, A.; Matyjaszewski, K., *Macromolecules* **2013**, *46* (10), 3803-3815; (h) Wang, Y.; Zhong, M.; Zhu, W.; Peng, C.-H.; Zhang, Y.; Konkolewicz, D.; Bortolamei, N.; Isse, A. A.; Gennaro, A.; Matyjaszewski, K., *Macromolecules* **2013**, *46* (10), 3793-3802; (i) Mendonca, P. V.; Konkolewicz, D.; Averick, S. E.; Serra, A. C.; Popov, A. V.; Guliashvili, T.; Matyjaszewski, K.; Coelho, J. F. J., *Polymer Chemistry* **2014**, *5* (19), 5829-5836.
6. (a) Thompson, G. E., *Thin Solid Films* **1997**, *297* (1-2), 192-201; (b) Su, Z.; Hahner, G.; Zhou, W., *J. Mater. Chem.* **2008**, *18* (47), 5787-5795.
7. Xia, J.; Matyjaszewski, K., *Macromolecules* **1999**, *32* (8), 2434-2437.

Chapter IV

Electrochemically Mediated ATRP of Acrylamides in Water*

IV. 1. Preface

ATRP in aqueous media has been highlighted because of its environmentally friendly reaction conditions and potential utility for the preparation of materials for biomedical applications. However, several challenges exist in aqueous ATRP such as high activation rate, dissociation of halides from the $X\text{-Cu}^{\text{II}}/\text{L}$ deactivators, decrease in stability of Cu/ligand complexes, disproportionation of $\text{Cu}^{\text{I}}/\text{L}$, and hydrolysis of carbon–halogen bonds, which could eventually result in uncontrolled polymerization reactions. Former group members Dr. Saadyah Averick, Dr. Dominik Konkolewicz, and Dr. Andrew Magenau, and current colleague Dr. Antonina Simakova and I improved the status of aqueous ATRP by focusing on overcoming these limitations by adjusting $[\text{Cu}^{\text{I}}]/[\text{Cu}^{\text{II}}]$ ratio through control of the dosing rate of the reducing agent, which decreased K_{ATRP} value and suppressed termination reaction by forming and maintaining a low radical concentration. It was also determined that the addition of an excess of salt with a suitable counterion, for example NaBr, shifted the equilibrium from dissociated species to (re)formation of $X\text{-Cu}^{\text{II}}/\text{L}$ ($X^- + \text{Cu}^{\text{II}}/\text{L}_{\text{naked}} \rightarrow X\text{-Cu}^{\text{II}}/\text{L}$). In the presence of salts with halide anions, the level of disproportionation of $\text{Cu}^{\text{I}}/\text{L}$ was negligible.

By developing, and adhering to the optimal conditions for an aqueous ATRP, former

*Work in this chapter was published and partially reformatted based on the following manuscript: Chmielarz, Paweł; **Park, Sangwoo**; Simakova, Antonina; Matyjaszewski, Krzysztof *Polymer* **2015**, 60, 302

group members, Dr. Nicola Bortolamei and Dr. Andrew Magenau, successfully polymerized water soluble monomers (*e.g.*, oligo(ethylene oxide) monomethyl ether methacrylate) using aqueous *e*ATRP. The major focus of this Chapter is to extend the use of aqueous ATRP to a broader range of water-soluble monomers, specifically acrylamides. Polymerization of acrylamides by ATRP is accompanied by several additional challenges, including relatively low values of ATRP equilibrium constant and potential side reactions, such as ligand displacement from the copper catalyst by the formed polymer and loss of chain-end halide by nucleophilic substitution.

To overcome such challenges and achieve good control over acrylamide polymerization, former group member, Dr. Paweł Chmielarz, and I systemically investigated the primary polymerization parameters that included temperature, monomer concentration, and catalyst composition. Further studies were carried out under optimal conditions and we were able to successfully synthesize polyacrylamide with different target DPs, and chain extended the formed macroinitiators with *N*-isopropyl acrylamide. My role in this project was to design polymerization conditions and analyze the results carried out under various reaction conditions.

I would like to acknowledge Dr. Paweł Chmielarz for his contribution to the project, and Dr. Antonina Simakova for her helpful discussions.

IV. 2. Introduction

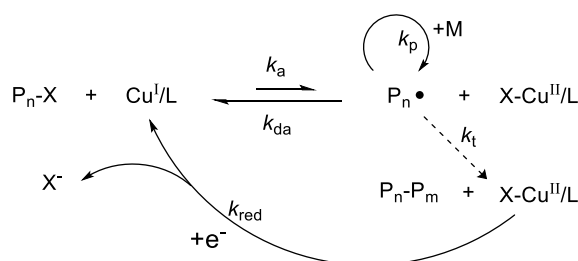
Atom transfer radical polymerization (ATRP) is among the most successful reversible deactivation radical polymerization (RDRP) methods, allowing effective control over (co)polymer molecular weight (MW), synthesis of (co)polymers with narrow molecular weight distribution (MWD), site selected functionalities, controlled architectures, and well-defined compositions.^{1a, 1c-e, 2b-d, 14c, 15, 89} The list of monomers successfully polymerized by ATRP includes various styrenes, (meth)acrylates, (meth)acrylamides, acrylonitrile and other monomers.^{1e, 3a, 3c, 3e, 90} During the past few years, water-soluble poly(meth)acrylates^{5g, 86d, 91} and polyacrylamides⁹² were successfully prepared with relatively narrow MWD and targeted degrees of polymerization (DP). Polyacrylamide (PAAm) and its derivatives are especially interesting, because they are widely used in cosmetics, biomedical applications, including drug delivery, wastewater treatment, and oil recovery, due to the high water solubility of these polymers.^{3e, 92f, 93}

However, successful ATRP of acrylamide and its derivatives may present some challenges related to relatively low values of ATRP equilibrium constant and side reactions, including ligand displacement from the copper catalyst by the formed polymer and loss of chain-end halogen by nucleophilic substitution.^{1e} The best control for the ATRP of (meth)acrylamides were obtained using one of the most active catalytic systems (Cu^{I} /tris(2-(dimethylamino)ethyl)amine (Me_6TREN)) due to its intrinsically high values of the equilibrium constant, K_{ATRP} .^{2b, 94} Also, polymerization in water was successful due to higher K_{ATRP} and relative stability of Cu^{I} /L complexes.^{92i, 92n, 95} However, since in water Cu^{II} /L bond can easily dissociate, either high concentration of catalysts are needed or use

of salts with halide anions is required.^{86d, 96} The concurrent nucleophilic substitution (solvolysis) of alkyl halides in water can be suppressed at lower temperatures. Thus, aqueous systems at relatively low temperature and high concentration of Cu catalysts seem to be most effective.^{92i, 92n, 95}

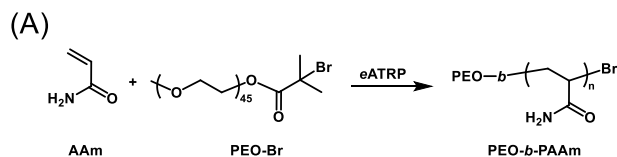
The advent of new low concentration catalyst ATRP systems, proceeding at parts per million (ppm) concentrations of catalyst, such as activators regenerated by electron transfer (ARGET) ATRP^{5a, 5c, 5e, 20b, 97} initiators for continuous activator regeneration (ICAR) ATRP,^{5a, 6a, 6b, 8e} supplemental activator and reducing agent (SARA) ATRP,^{7a, 7c, 7f, 21, 98} photoinduced ATRP (photoATRP),^{5g, 8d, 8f, 8k} and electrochemically mediated ATRP (*e*ATRP)^{10-11, 13b, 67c, 96b} provide well-controlled polymerizations of various monomers using highly active copper catalysts and more environmentally benign and industrially scalable reaction conditions.^{1e} Among low ppm ATRP methods, *e*ATRP stands out due to the possibility of recycling/reusing the transition metal (*e.g.*, copper),^{11, 99} control over the polymerization rate and the ability to intermittently switch a polymerization between “on” and “off” states. During an *e*ATRP, the ratio of the concentration of activator to deactivator is precisely controlled by electrochemical potential.¹¹ Several parameters, such as applied current (*I*), potential (*E*), and total passed charge (*Q*), can be controlled in an *e*ATRP to allow selection of the desired concentration of the redox-active catalytic species.^{20b} A targeted amount of the catalyst complex (X-Cu^{II}/L) can be electrochemically reduced to the activator species (Cu^I/L) at the electrode surface.^{96b} The reduced activator then diffuses through the reaction mixture under vigorous stirring, and reacts with initiators (*i.e.*, alkyl halide, P-X) to form radical species (P_n•) and the oxidized catalyst deactivator (X-Cu^{II}/L).

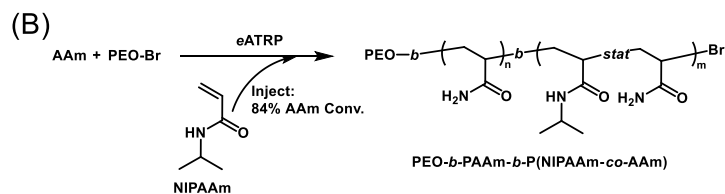
Consequently, the radical species propagate to form polymeric chains by reacting with monomer (M), or are converted back to a dormant species (P_n-X) (Scheme IV-1). *e*ATRP can precisely control the ratio of activator to deactivator by changing the applied electrical stimuli, which allows for fast and controlled polymerizations and the synthesis of polymers with complex architectures.^{11, 13b, 96b}



Scheme IV-1. Mechanism of *e*ATRP.

This chapter is focused on aqueous *e*ATRP of acrylamide and also reports the preparation of diblock poly(ethylene oxide)-*block*-poly(acrylamide) (PEO-*b*-PAAm) (Scheme IV-2A) and triblock poly(ethylene oxide)-*block*-poly(acrylamide)-*block*-poly(*N*-isopropylacrylamide-*stat*-acrylamide) (PEO-*b*-PAAm-*b*-P(NIPAAm-*stat*-AAm)) copolymers (Scheme IV-2B) by *e*ATRP.





Scheme IV-2. (A) Synthesis of PEO-*b*-PAAm diblock copolymers *via eATRP*; (B) Synthesis of PEO-*b*-PAAm-*b*-P(NIPAAm-*stat*-AAm) pseudo-triblock copolymers *via eATRP*.

IV. 3. Results and Discussion

A well-controlled ATRP of acrylamide and its derivatives in aqueous media is challenging due to a potential deactivation of the catalyst, slow activation, and loss of halide chain end functionality.^{92e, 92i, 95-96} The objective of this study was to investigate and optimize polymerization conditions for acrylamide using poly(ethylene oxide) macroinitiators (PEO MI, $M_n = 2000$, $M_w/M_n = 1.16$) resulting in diblock copolymers poly(ethylene oxide)-*block*-poly(acrylamide). *eATRP* was used under potentiostatic conditions (applied constant potential) with a conventional three electrode system – a platinum (Pt) mesh working electrode, a Pt mesh counter electrode (separation from the reaction media using methylated cellulose gel), and a Ag/AgI/I⁻ reference electrode. Various polymerization parameters were examined, including temperature, monomer concentration, ligand structure, and a monomer/initiator molar ratio (DP) to determine the best reaction conditions. Table IV-1 summarizes results of the block copolymers synthesis with unsubstituted acrylamide.

Table IV-1. Summary of PEO-*b*-PAAm Synthesis by *e*ATRP.

entry	time (h)	[AAm]/ [PEO MI]/ [CuBr ₂ /2L]	[PEO MI] (mM)	Ligand	k_p^{app} (h ⁻¹) ^a	conv (%) ^a	$M_{n,theo}$ ($\times 10^{-3}$) ^b	M_n^{app} ($\times 10^{-3}$) ^a	M_w/M_n^c
1	24	200/1/0.1	6.4	TPMA	0.068	44	8.3	14.2	1.53
2	30	200/1/0.1	6.4	TPMA	0.094	93	15.3	16.1	1.84
3	30	200/1/0.1	14.1	TPMA	0.036	66	11.4	11.9	1.55
4	10	100/1/0.05	12.8	TPMA	0.059	44	5.2	5.8	1.15
5	10	100/1/0.05	12.8	TPMA*2	0.191	86	8.1	8.3	1.38
6	10	200/1/0.1	6.4	TPMA*2	0.185	82	13.7	14.4	1.10
7	10	400/1/0.2	3.2	TPMA*2	0.164	73	22.9	24.7	1.20
8	10	1000/1/0.5	1.3	TPMA*2	0.157	53	39.8	42.2	1.19
9	1	100/1/0.05	12.8	Me ₆ TREN	2.598	87	8.2	9.0	1.09
10	1	200/1/0.1	6.4	Me ₆ TREN	2.135	86	14.2	15.8	1.16
11	2	400/1/0.2	3.2	Me ₆ TREN	1.514	96	29.2	35.5	1.17
12	1	1000/1/0.5	1.3	Me ₆ TREN	1.240	71	52.1	53.4	1.16

General reaction condition: $T = 0\text{ }^{\circ}\text{C}$ (except entry 1 = $22\text{ }^{\circ}\text{C}$); $V_{tot} = 33\text{ mL}$ (in H₂O/DMF = 9/1 by v/v); $E_{app} = E_{pc} - 120\text{ mV}$ (vs. Ag/AgI/I⁻); [AAm] = 1.3 M (except entry 3 = 2.8 M); [CuBr₂/2L] = 0.64 mM (except entry 3 = 1.41 mM); Supporting electrolyte concentration (tetraethylammonium bromide, TEABr) = 0.1 M; Working electrode = Pt mesh; Counter electrode = Pt mesh (separated from the reaction solution by the supporting electrolyte saturated Tylose gel (MH = 300)); Reference electrode = Ag/AgI/I⁻; ^aMonomer

conversion, apparent M_n and k_p were determined by NMR; $^bM_{n,theo} = ([M]_0/[MI]_0) \times$ conversion $\times M_{monomer} + M_{PEOMI}$; c MWD was determined by aqueous GPC with PEO standard curves.

Effect of Temperature and Monomer Concentration. The effect of reaction temperature on the diblock copolymer formation was evaluated by comparing room (22 °C) and low (0 °C) temperatures (Table IV-1, entries 1–2, Figure IV-1). When the polymerization was carried out at room temperature (22 °C), the monomer conversion reached 44% and no further monomer consumption was observed. The MW evolution with conversion correlated closely with the theoretical MW at the initial stage of the reaction but deviated at higher conversion (initiation efficiency 58%, Table 1, entry 1, Figure 1A–B). In contrast, in the polymerization conducted at 0 °C, monomer conversion reached 93% and evolution of experimental MW with conversion followed the theoretical prediction. Contributions of side reactions are lower at lower temperature (*e.g.*, $T = 0$ °C). The side reactions may include loss of chain-end functionality by solvolysis of C-Br bond, competitive complexation of Cu(I) by polymer chains, or reduced initiation efficiency.

The effect of AAm (monomer, M) concentration on the diblock copolymer formation was investigated (Table IV-1, entries 2–3, Figure IV-1). Polymerizations were performed at two different $[M]_0 = 1.3$ and 2.8 M. Polymerization at $[AAm]_0 = 2.8$ M (Table IV-1, entry 3) showed livingness of the polymerization before solution viscosity notably increased. However, the apparent propagation rate constant (k_p^{app}) was 0.036 h^{-1} , 2.6 times slower than the polymerization at $[M]_0 = 1.3$ M ($k_p^{app} = 0.094\text{ h}^{-1}$) in kinetic plot and reached only 66% monomer conversion at 30 h. The higher $[M]_0$ reduced medium polarity

(and K_{ATRP}) and decreased monomer solubility in the reaction media (insoluble at 60 wt% monomers).^{89d} Thus, better control over polymerization was achieved under more dilute conditions (84 wt% in H₂O, Table IV-1, entry 2).

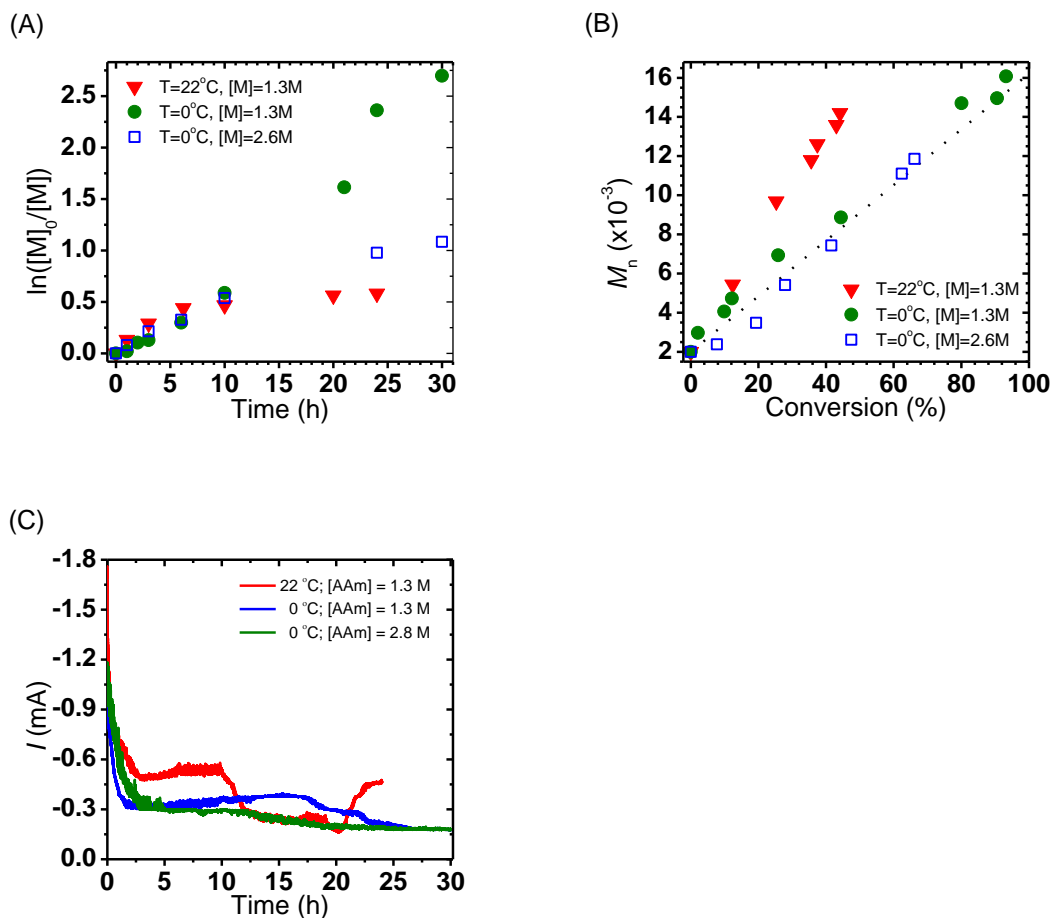


Figure IV-1. Kinetics of eATRP of acrylamide as a function of polymerization temperature and monomer concentration. (A) First-order kinetic plot of monomer conversion versus time, (B) M_n versus monomer conversion, (C) CA results of acrylamides polymerization. General reaction conditions: $[A\text{Am}]/[\text{PEO MI}]/[\text{CuBr}_2/2\text{TPMA}] = 200/1/0.1$, $[\text{TEABr}]_0 = 0.1\text{ M}$, $E_{\text{app}} = E_{\text{pc}} - 120\text{ mV}$ (vs. Ag/AgI/I).

Influence of Ligand Structure. The next series of experiments explored different catalytic systems for *e*ATRP of acrylamide at 500 ppm catalyst loading. Three different ligands were selected tris(2-pyridylmethyl)amine (TPMA), bis(4-methoxy-3,5-dimethylpyridin-2-ylmethyl)-pyridin-2-ylmethyl-amine (TPMA*2), and Me₆TREN, and *e*ATRP was performed at $E_{app} = E_{pc} - 120$ mV. As shown in Figure IV-2A, the rate of polymerization is strongly dependent on ligand and complex structure. More reducing complexes provide faster polymerization due to larger K_{ATRP} values (Table IV-1, entries 4–5, 9). Furthermore, all of these ligands provided lower M_w/M_n values (<1.5, Figure IV-2B) at identical $[Br-Cu^{II}/L]_0$ (Figure IV-3A-C). These results show that active catalysts, in the presence of ammonium bromide, are capable of maintaining sufficient rates of deactivation, thereby reducing M_w/M_n values.⁹⁷ Only the most active catalysts with TPMA*2 and Me₆TREN ligands were capable of achieving high conversion values ($\geq 80\%$), whereby with TPMA conversion was limited to 44%. When employing a lower activity catalysts (*i.e.*, with TPMA), the M_w/M_n can be reduced by either using a higher $[Br-Cu^{II}/L]_0$ and/or a more positive E_{app} value, each essentially increasing the effective $[Br-Cu^{II}/L]$ in the reaction medium.¹¹ $E_{1/2}$ values for each complex are shown in the Figure IV-4 against Ag/AgI/I⁻, conducted in the absence and presence of a PEO MI. The $E_{1/2}$ values gradually became more negative, signifying larger K_{ATRP} values, on moving from TPMA to TPMA*2 to Me₆TREN, these values are different from those reported in MeCN solution (TPMA < Me₆TREN ~ TPMA*2, Table IV-1, Figure IV-4).^{11, 100} Furthermore, increased electrocatalytic (*EC'*) behavior was observed in CV measurements. Decreased anodic response was obtained with more active ligands (TPMA < TPMA*2 < Me₆TREN) in the presence of PEO MI (Figure IV-4). The results indicate more active catalysts can

react faster with alkyl halide and form radical species and $X\text{-Cu}^{\text{II}}/\text{L}$ which subsequently requires less current (I) to oxidize residual $\text{Cu}^{\text{I}}/\text{L}$ species. Briefly, a polymerization with $\text{Cu}/\text{Me}_6\text{TREN}$ catalysts were 8-14 times faster (compare k_p^{app} ; Table IV-1, entries 9-12 vs. 5-8) than with Cu/TPMA^*2 and 44 times faster than with Cu/TPMA (compare k_p^{app} ; Table IV-1, entry 9 vs. 4). Those tendencies are nicely matched with faster R_p and narrower MWDs when using more active catalysts.

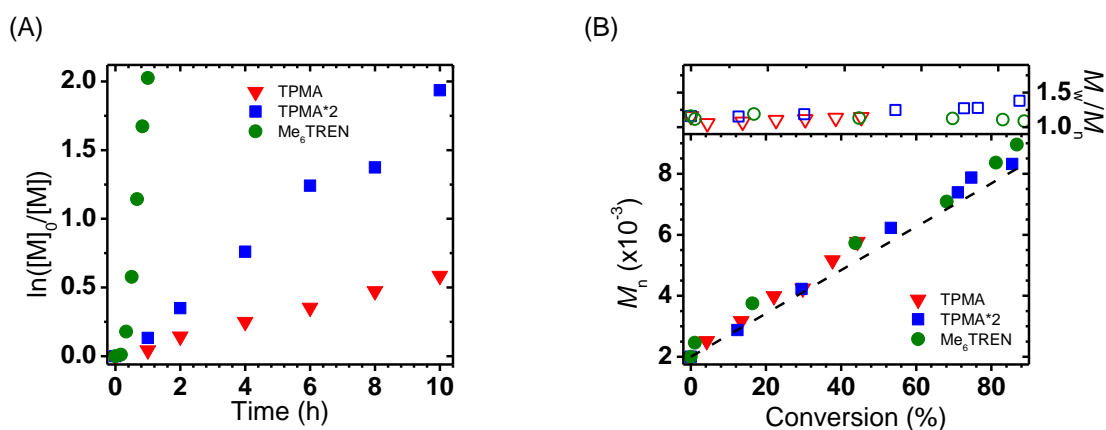
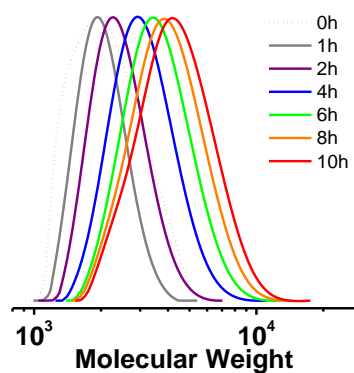
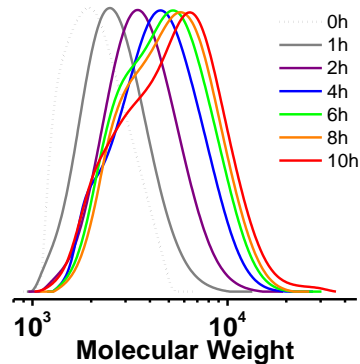


Figure IV-2. eATRP of acrylamide as a function of ligand (L = TPMA, TPMA*2, and Me₆TREN). (A) First-order kinetic plot of monomer conversion versus time, and (B) M_n and M_w/M_n versus monomer conversion. Reaction conditions: $[\text{AAm}]/[\text{PEO MI}]/[\text{CuBr}_2/2\text{L}] = 100/1/0.05$, $[\text{AAm}] = 1.3 \text{ M}$, $[\text{CuBr}_2/2\text{L}] = 0.64 \text{ mM}$, $T = 0 \text{ }^\circ\text{C}$, $[\text{TEABr}]_0 = 0.1 \text{ M}$, $E_{\text{app}} = E_{\text{pc}} - 120 \text{ mV}$ (vs. $\text{Ag}/\text{AgI}/\text{I}^-$).

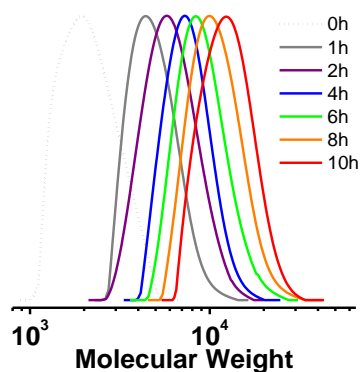
(A) Entry 4 (TPMA; DP=100)



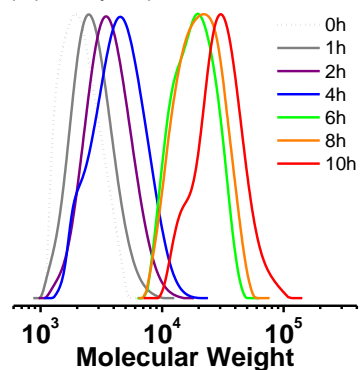
(B) Entry 5 (TPMA*2; DP=100)



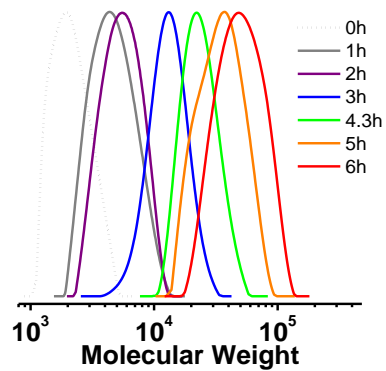
(C) Entry 6 (TPMA*2; DP=200)



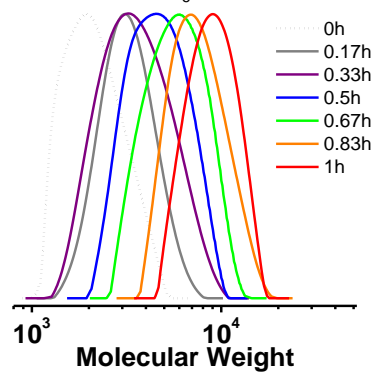
(D) Entry 7 (TPMA*2; DP=400)



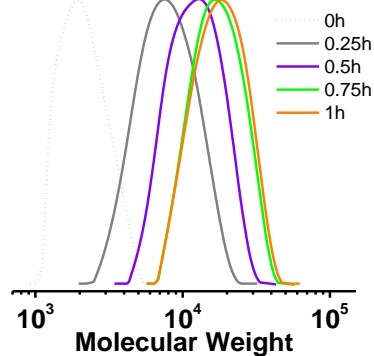
(E) Entry 8 (TPMA*2; DP=1000)



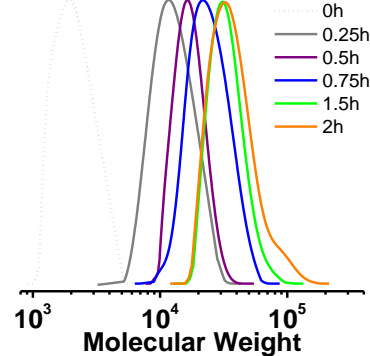
(F) Entry 9 (Me_6TREN ; DP=100)



(G) Entry 10 (Me₆TREN; DP=200)



(H) Entry 11 (Me₆TREN; DP=400)



(I) Entry 12 (Me₆TREN; DP=1000)

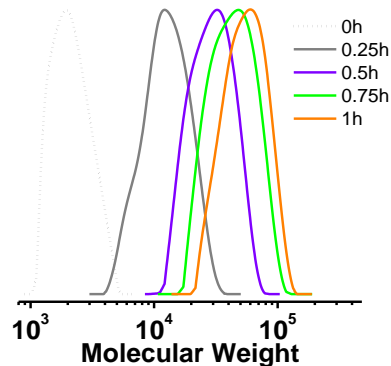
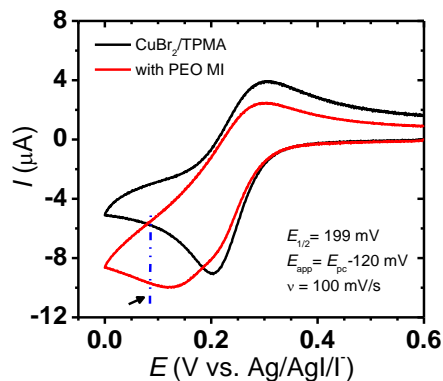
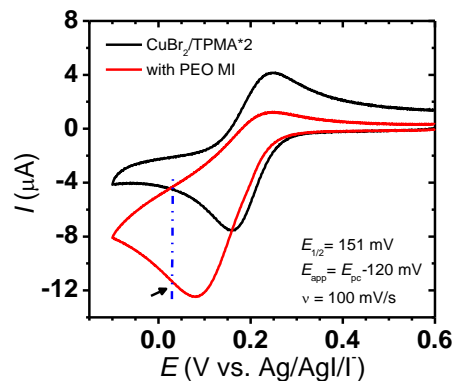


Figure IV-3. GPC traces during the *e*ATRP of acrylamides as a function of ligand (A, B and F, DP = 100) and as a function of DP (for TPMA*2: B-E; for Me₆TREN: F-I).

(A)



(B)



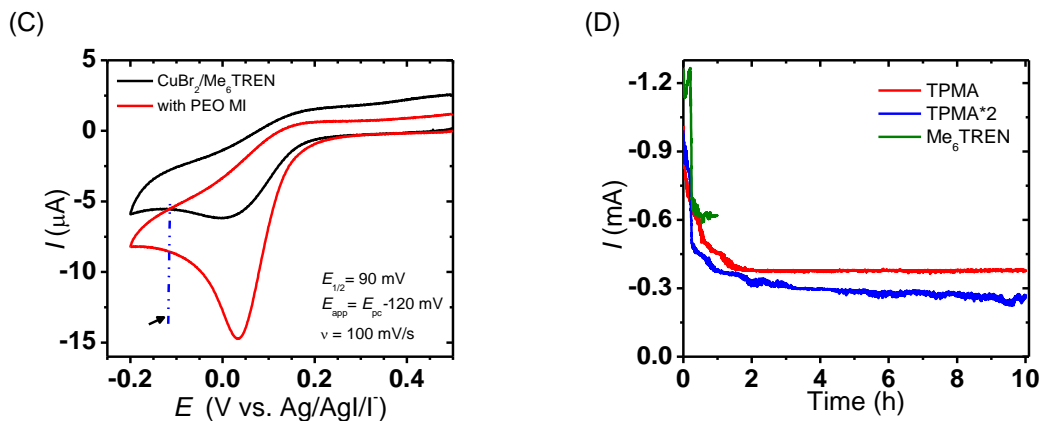
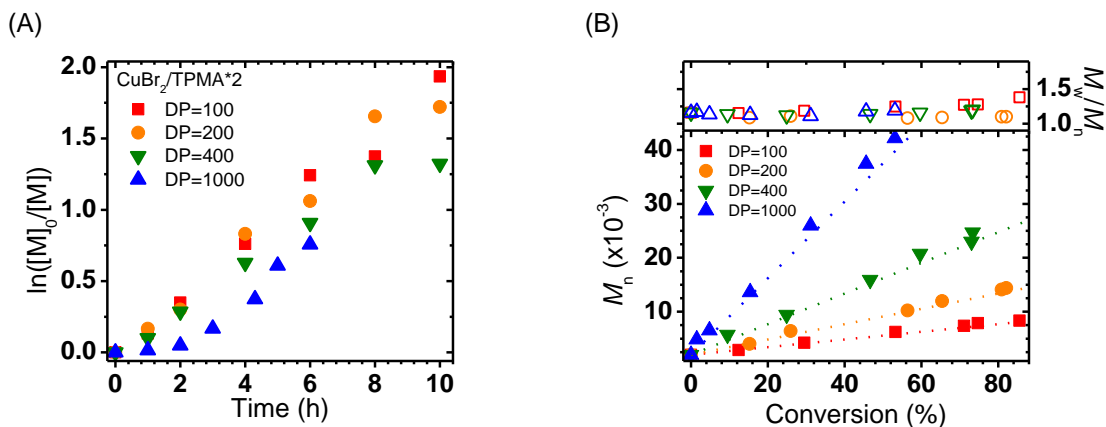


Figure IV-4. Cyclic voltammetry results of (A) TPMA, (B) TPMA*2, and (C) Me₆TREN in the absence (black) and presence of PEO MI (red). Arrows indicate applied potential. (D) Current profile versus time. Reaction conditions: [AAm]/[PEO MI]/[CuBr₂/2L] = 100/1/0.05, [AAm] = 1.3 M, [CuBr₂/2L] = 0.64 mM, $T = 0\text{ }^{\circ}\text{C}$, [TEABr]₀ = 0.1 M, $E_{\text{app}} = E_{\text{pc}} - 120\text{ mV}$ (vs. Ag/AgI/I⁻).

Effect of Degree of Polymerization ($[M]_0/[MI]_0$). The effect of initial molar ratio of AAm (M) to PEO MI (MI) on the diblock copolymer formation was investigated in the presence of TPMA*2 (Table IV-1, entries 5–8, Figure IV-5, and Figure IV-3B-E) and Me₆TREN (Table IV-1, entries 9–12, Figure IV-6, and Figure IV-3F-I) as ligands. Polymerizations were performed at four different ratios of $[M]_0/[MI]_0 = 100, 200, 400$, and 1000. To investigate the effect of DP, k_p^{app} (initial time periods) was measured and compared to initiator concentration. The rate of polymerization (R_p) is defined as $R_p = k_p[M][P\cdot] = k_p[M]K_{\text{ATRP}} \frac{[PX][Cu^I L]}{[X-Cu^{II} L]}$, *i.e.*, first order in respect to R-X concentration. Indeed, k_p^{app} approximately increased linearly with [PEO MI] (Figure IV-5D and Figure IV-6D).

High MW copolymers were obtained by targeting higher DPs. MW evolutions were well-matched with the theoretical values (Figure IV-5B and Figure IV-6B) and maintained narrow MWD. Slightly higher R_p and monomer conversion of $> 80\%$ were obtained for polymerizations at higher concentration of MI (e.g., $[M]_0/[MI]_0=100$), the presence of higher concentrations of MI could suppress fraction of terminated chains and reduce MWD.^{13b} Under optimal polymerization condition ($\text{CuBr}_2/\text{Me}_6\text{TREN}$ and $T = 0\text{ }^\circ\text{C}$), all of PAAm blocks had narrow MWD. The MWD of second block can be determined using the following equation: $Y_{\text{PEO-PAAm}} = w_{\text{PEO}}^2 Y_{\text{PEO}} + w_{\text{PAAm}}^2 Y_{\text{PAAm}}$, where w is weight fraction of each block and $Y = D - 1$.¹⁰¹ The weight fraction of PAAm was 0.76 (Table IV-1, entry 9) based on monomer consumption. According to the equation, the calculated MWD of PAAm block was 1.14 (the broadest MWD was 1.21 (Table IV-1, entry 10)), indicating that well-defined polymers were synthesized by *e*ATRP under optimal condition.



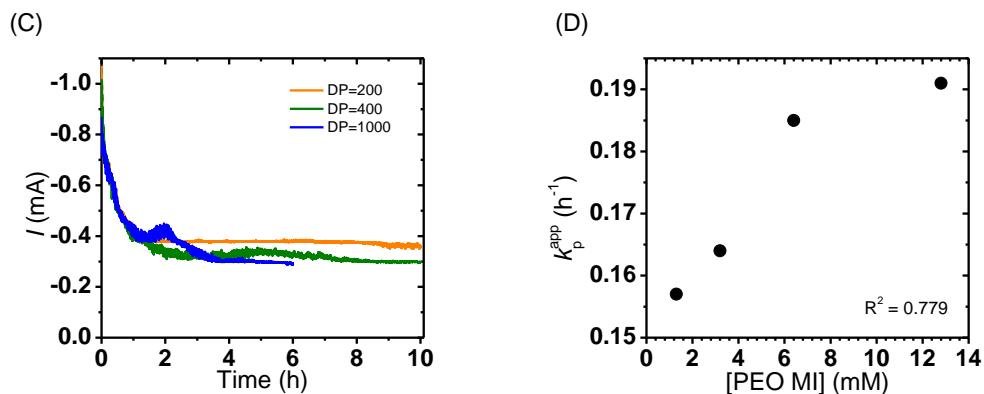
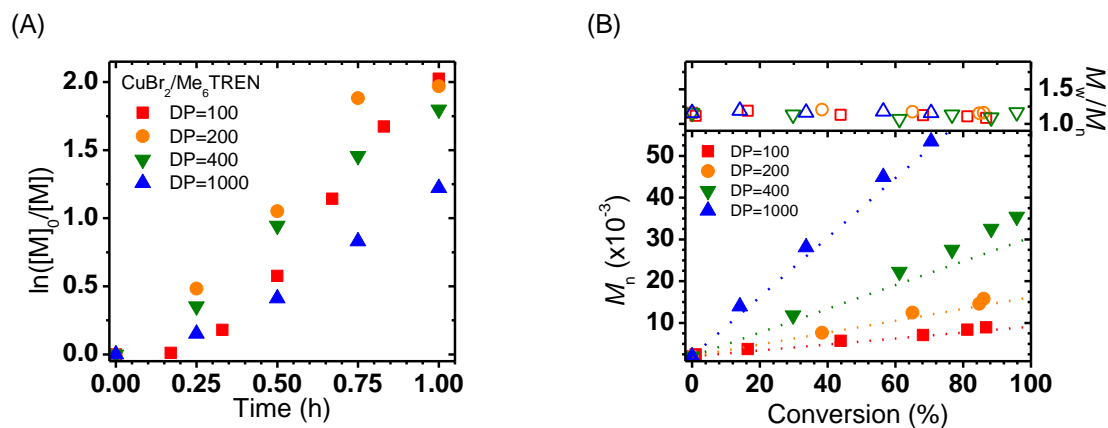


Figure IV-5. *e*ATRP of acrylamide as a function of targeted DP (100, 200, 400, and 1000).

(A) First-order kinetic plot of monomer conversion versus time, (B) M_n and M_w/M_n versus monomer conversion, (C) Current profile versus time during the *e*ATRP, and (D) The apparent propagation rate constant (k_p^{app}) versus the PEO MI concentration. Reaction conditions: [AAM] = 1.3 M, [CuBr₂/2TPMA*2] = 0.64 mM, $T = 0^\circ\text{C}$, [TEABr]₀ = 0.1 M, $E_{\text{app}} = E_{\text{pc}} - 120 \text{ mV}$ (vs. Ag/AgI/T).



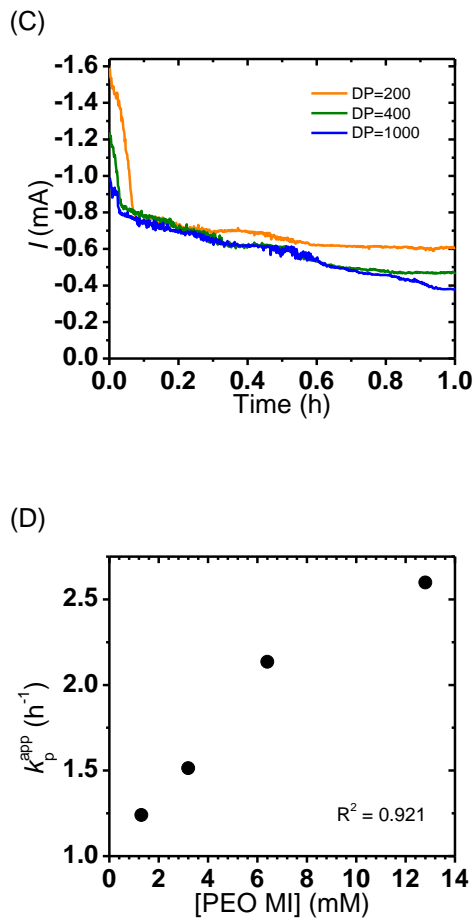
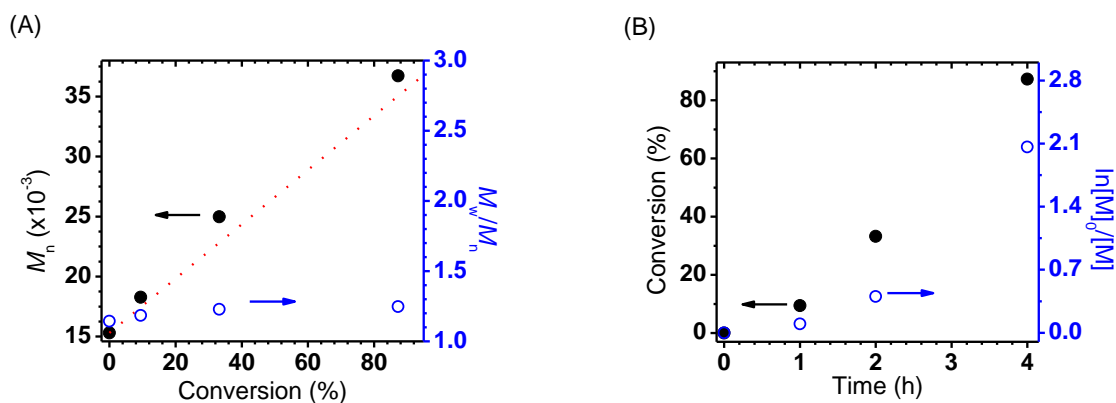


Figure IV-6. *e*ATRP of acrylamide as a function of targeted DP (100, 200, 400, and 1000).

(A) First-order kinetic plot of monomer conversion versus time, (B) M_n and M_w/M_n versus monomer conversion, (C) Current profile versus time during the *e*ATRP, (D) The apparent propagation rate constant (k_p^{app}) versus the PEO MI concentration. Reaction conditions: [AAM] = 1.3 M, [CuBr₂/2Me₆TREN] = 0.64 mM, $T = 0$ °C, [TEABr]₀ = 0.1 M, $E_{\text{app}} = E_{\text{pc}} - 120$ mV (vs. Ag/AgI/I⁻).

***In situ* Chain Extension Experiments.** The PEO-*b*-PAAM-Br macroinitiator was prepared and *in situ* chain extension was carried out with NIPAAm. The reactivity ratio of

AAM/NIPAAm was close to 1 ($r_{\text{AAM}} \sim 1$, $r_{\text{NIPAAm}} \sim 1$, and $r_{\text{AAM}} \times r_{\text{NIPAAm}} \sim 1$) and statistical copolymers were expected to be obtained from *in situ* NIPAAm chain extension.¹⁰² In the first step, conversion of AAm reached 84% after 1 h, yielding the PEO-*b*-PAAm₁₈₇-Br macroinitiator ($M_{\text{n,NMR}} = 15300$ [$M_{\text{n,theory}} = 14000$], $M_{\text{w}}/M_{\text{n}} = 1.14$), then NIPAAm was added into the reaction without purification of the macroinitiator. The conversion of the second block reached 87% after 4 h. The second block was a statistical copolymer with *ca.* 15% AAm content. The chain extended block copolymer, PEO-*b*-PAAm₁₈₇-*b*-P(NIPAAm₁₈₉-*stat*-AAm₁₃), had a $M_{\text{n,NMR}}$ of 36700 and a $M_{\text{w}}/M_{\text{n}}$ of 1.25 ($M_{\text{n,theory}} = 35100$). Linear first-order kinetics was observed and GPC traces indicated successful incorporation of the second monomer, as a clean shift in the MW peak toward higher MW was observed (Figure IV-7). The MW evolution with conversion closely followed theoretical MW indicating high initiation efficiency (Figure IV-7A). This result confirms that the halogen end groups are preserved during the *e*ATRP of AAm.



(C)

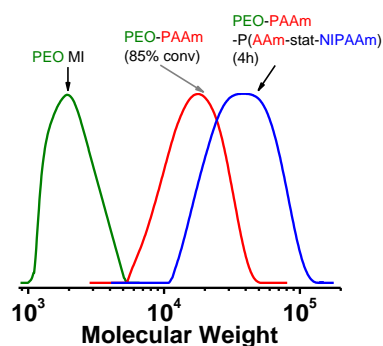


Figure IV-7. *In situ* chain extension by *e*ATRP; (A) M_n and M_w/M_n versus monomer conversion, (B) First-order kinetic plot of monomer conversion versus time, and (C) GPC results of block copolymerization. Reaction conditions: $[NIPAAm]/[PEO-b-PAAm-Br]/[CuBr_2/2Me_6TREN] = 200/1/0.1$, $[NIPAAm] = 1.1$ M, $[CuBr_2/2Me_6TREN] = 0.55$ mM, $[TEABr]_0 = 0.1$ M, $E_{app} = E_{pc} - 120$ mV (vs. Ag/AgI/I⁻).

IV. 4. Summary

Electrochemically mediated atom transfer radical polymerization (*e*ATRP) of acrylamide was investigated under a variety of conditions, including temperature, monomer concentration, ligand structure, and monomer to macroinitiator molar ratio (targeted DP). They were correlated with polymerization rates, polymer properties, and applied currents during the *e*ATRP to optimize reaction conditions (in terms of R_p , controlled MWs and narrow MWDs); Reactions with Me₆TREN as the ligand were faster than with TPMA or TPMA*2. Low monomer content (84% water) and low temperature (0 °C) provide for the best control over *e*ATRP of acrylamide. In addition, an *in situ* chain extension with NIPAAm confirmed the preservation of terminal halogen end group during

the *e*ATRP of AAm. *e*ATRP provides a powerful tool for the synthesis of functional water-soluble polyacrylamides with controlled chain length and narrow molecular weight distributions.

IV. 5. Experimental Section

Materials. Monohydroxy poly(ethylene glycol) methyl ether (HO-PEO, $M_n = 2000$), triethylamine (TEA), tetraethylammonium bromide (TEABr, 99%), tetrabutylammonium hexafluorophosphate (TBAPF₆), copper(II) bromide (CuBr₂, 99.9%), methylated cellulose (Tylose, MH=300), and 2-bromoisobutyryl bromide (BriBBr, 98%) were purchased from Aldrich. Platinum (Pt) wires and Pt gauge mesh were purchased from Alfa Aesar. Tris(2-pyridylmethyl)amine (TPMA) was prepared according to a previously published procedure.¹⁰³ Bis(4-methoxy-3,5-dimethyl-pyridin-2-ylmethyl)-pyridin-2-ylmethyl-amine (TPMA*2) was prepared according to a previously published procedure.¹⁰⁰ Tris(2-(dimethylamino)ethyl)amine (Me₆TREN) was synthesized according to literature procedures and stored under nitrogen prior to use.¹⁰³⁻¹⁰⁴ Acrylamide (AAm, ~99%) was purchased from Fluka. *N*-Isopropylacrylamide (NIPAAm, >99%) was purchased from Aldrich and was purified by recrystallization from hexane to remove the inhibitor. *N,N*-dimethylformamide (DMF) was purchased from Acros.

Synthesis of Poly(ethylene oxide) Macroinitiator (PEO MI). PEO MI was prepared (by reacting monohydroxy PEO methyl ether (HO-PEO, $M_n = 2000$, $M_w/M_n = 1.16$ (by aqueous GPC)) with BriBBr in the presence of triethylamine) and characterized by ¹H NMR showing over 99.7% of the functionalization efficiency, according to a previously

published procedure.^{13b} A 20 g (10 mmol) sample of HO-PEO was dissolved in a mixture of methylene chloride (30 mL) and 5.5 mL of TEA (20 mmol), and the reaction flask was placed in an ice bath. Then, 4.9 mL of BriBBBr (20 mmol) was slowly added to the reaction mixture, and the solution was stirred for 24 h at room temperature. The product was purified by washing the solution with pure water three times and the organic layer was collected. The final product was collected after precipitation by addition to diethyl ether. The resulting white powder was dried overnight under vacuum.

Preparation of CuBr₂/L Solution. Stock solutions of CuBr₂ (0.06 g, 0.25 mmol) and appropriate ligand (TPMA – 0.30 g, TPMA*2 – 0.20 g or Me₆TREN – 0.11 g; 0.5 mmol) were dissolved in dry DMF (total volume = 5 mL). The prepared CuBr₂/L solutions (50 mM) were used as catalysts for *e*ATRP.

Cell Configuration for Electrochemical Reaction. Electrolysis experiments were carried out under N₂ atmosphere using a Pt disk (for cyclic voltammetry (CV), *A*=0.071 cm²) and Pt mesh (for chronoamperometry (CA)) working electrodes. The Pt mesh counter electrode was prepared using a glass frit and a salt bridge made of Tylose gel saturated with TBAPF₆ to separate the cathodic and anodic compartments. All of potentials were measured versus an Ag/AgI/I⁻ reference electrode (Gamry Ref 600). During *e*ATRP procedure the temperature of 0 °C was maintained using a circulating chiller (NESLAB Inc., RTE-111).

PEO-*b*-PAAm Block Copolymer Synthesis by *e*ATRP. TEABr (0.69 g, 3 mmol) and AAm (3.00 g, 42 mmol) were placed in a seven neck electrolysis cell maintained at 0 °C

(or 22 °C) under a slow N₂ purge. Then, 27.58 mL of nitrogen purged distilled and 0.42 mL of CuBr₂/L stock solution (0.05 M in DMF) were added. The CV was recorded with Pt disk working electrode (WE), Pt mesh counter electrode (CE), and Ag/AgI/I⁻ reference electrode (RE) for determining applied potential ($E_{app} = E_{pc} - 120$ mV). A solution of 0.42 g of PEO MI (0.21 mmol) in 2 mL of DMF was injected to the reaction solution and CV was measured to confirm an increased cathodic response. Then the Pt mesh WE, Pt mesh CE, and Ag/AgI/I⁻ RE were prepared and immersed in the polymerization solution and the selected potential was applied using chronoamperometry (CA) method with vigorous stirring (1100 rpm) during the polymerization. Samples were withdrawn periodically to follow the monomer conversion and apparent number average molecular weight (M_n) by ¹H NMR, and to determine molecular weight distribution (M_w/M_n) by gel permeation chromatography (GPC) measurements with PEO standard curve.

***In situ* Chain Extension of NIPAAm from Growing PEO-*b*-PAAm.** For the *in situ* chain extension experiment, PEO-*b*-PAAm-Br macroinitiator was polymerized using the *e*ATRP method as described above. Polymerization conditions: [AAm]/[PEO MI]/[CuBr₂/2Me₆TREN] = 200/1/0.1, [AAm] = 1.3 M, [CuBr₂/2Me₆TREN]₀ = 0.64 mM, [TEABr]₀ = 0.1 M, $E_{app} = E_{pc} - 120$ mV (vs. Ag/AgI/I⁻), $T = 0$ °C, WE = Pt mesh, CE = Pt mesh, separated from the reaction solution by the supporting electrolyte saturated Tylose gel (MH 300), and RE = Ag/AgI/I⁻. The polymerization was stopped after 1 h of reaction, and an aliquot was taken for analysis (¹H NMR and GPC). Then, a NIPAAm, TEABr and fresh batch of CuBr₂/L was added under nitrogen, and the reaction was started by the application of an appropriate E_{app} . The chain extension with NIPAAm was carried out

under the following reaction conditions: $[\text{NIPAAm}]/[\text{PEO-PAAm-Br}]/[\text{CuBr}_2/2\text{Me}_6\text{TREN}] = 200/1/0.1$, $[\text{NIPAAm}] = 1.1 \text{ M}$, $[\text{CuBr}_2/2\text{Me}_6\text{TREN}] = 0.55 \text{ mM}$, $[\text{TEABr}]_0 = 0.1 \text{ M}$, $E_{\text{app}} = E_{\text{pc}} - 120 \text{ mV}$ (vs. $\text{Ag}/\text{AgI}/\text{I}^-$), $T = 0 \text{ }^\circ\text{C}$, WE = Pt mesh, CE = Pt mesh (separated from the reaction solution by the supporting electrolyte saturated Tylose gel (MH 300)), and RE = $\text{Ag}/\text{AgI}/\text{I}^-$. The polymerization was continued for 4 h. Samples were withdrawn periodically to follow the monomer conversion and apparent number average molecular weight (M_n) using ^1H NMR, and to determine molecular weight distribution (M_w/M_n) by aqueous gel permeation chromatography (GPC) measurements vs. a PEO standards.

Measurements. Monomer conversion was measured using ^1H NMR spectroscopy in D_2O , in a Bruker Avance 300 MHz spectrometer at $27 \text{ }^\circ\text{C}$. Molecular weights and distributions were determined by aqueous GPC (Waters Ultrahydrogel columns – guard, UH250 and 1000), with phosphine buffered saline as eluent at $30 \text{ }^\circ\text{C}$, flow rate 1.00 mL/min , and a differential refractive index (RI) detector (Waters, 2410). The apparent molecular weights and dispersity (M_w/M_n) were determined with a calibration based on PEO standards using WinGPC 8.0 software from PSS. All CVs and CAs were recorded by a Gamry Ref 600 potentiostat.

IV. 6. References

1. (a) Kato, M.; Kamigaito, M.; Sawamoto, M.; Higashimura, T., *Macromolecules* **1995**, 28 (5), 1721-1723; (b) Wang, J. S.; Matyjaszewski, K., *J Am Chem Soc* **1995**, 117 (20), 5614-5615; (c) Matyjaszewski, K.; Xia, J. H., *Chem Rev* **2001**, 101 (9), 2921-2990; (d) Braunecker, W. A.; Matyjaszewski, K., *Progress in Polymer Science* **2007**, 32 (1), 93-146; (e) Tsarevsky, N. V.; Matyjaszewski, K., *Chemical Reviews (Washington, DC, United States)* **2007**, 107 (6), 2270-2299; (f) Matyjaszewski, K.; Tsarevsky, N. V., *Nature Chemistry* **2009**, 1 (4), 276-288; (g) di Lena, F.; Matyjaszewski, K., *Prog. Polym. Sci.* **2010**, 35 (8), 959-1021; (h) Lee, H.-i.; Pietrasik, J.; Sheiko, S. S.; Matyjaszewski, K., *Prog.*

Polym. Sci. **2010**, 35 (1-2), 24-44; (i) Matyjaszewski, K., *Macromolecules* **2012**, 45 (10), 4015-4039; (j) Matyjaszewski, K., *Isr. J. Chem.* **2012**, 52 (3-4), 206-220; (k) Siegwart, D. J.; Oh, J. K.; Matyjaszewski, K., *Prog. Polym. Sci.* **2012**, 37 (1), 18-37; (l) Krol, P.; Chmielarz, P., *Prog Org Coat* **2014**, 77 (5), 913-948; (m) Matyjaszewski, K.; Tsarevsky, N. V., *J. Am. Chem. Soc.* **2014**, 136 (Copyright (C) 2014 American Chemical Society (ACS). All Rights Reserved.), 6513-6533.

2. (a) Wang, J.-S.; Matyjaszewski, K., *Macromolecules* **1995**, 28 (23), 7901-10; (b) Qiu, J.; Matyjaszewski, K., *Macromolecules* **1997**, 30 (19), 5643-5648; (c) Matyjaszewski, K.; Jo, S. M.; Paik, H.-j.; Gaynor, S. G., *Macromolecules* **1997**, 30 (20), 6398-6400; (d) Matyjaszewski, K.; Jo, S. M.; Paik, H.-j.; Shipp, D. A., *Macromolecules* **1999**, 32 (20), 6431-6438; (e) Teodorescu, M.; Matyjaszewski, K., *Macromolecules* **1999**, 32 (15), 4826-4831; (f) Kowalewski, T.; Tsarevsky, N. V.; Matyjaszewski, K., *J Am Chem Soc* **2002**, 124 (36), 10632-10633; (g) Wever, D. A. Z.; Raffa, P.; Picchioni, F.; Broekhuis, A. A., *Macromolecules* **2012**, 45 (10), 4040-4045; (h) Krol, P.; Chmielarz, P., *Express Polym Lett* **2013**, 7 (3), 249-260.

3. (a) Longenecker, R.; Mu, T.; Hanna, M.; Burke, N. A. D.; Stover, H. D. H., *Macromolecules (Washington, DC, United States)* **2011**, 44 (22), 8962-8971; (b) Simakova, A.; Averick, S. E.; Konkolewicz, D.; Matyjaszewski, K., *Macromolecules* **2012**, 45 (16), 6371-6379; (c) Averick, S.; Simakova, A.; Park, S.; Konkolewicz, D.; Magenau, A. J. D.; Mehl, R. A.; Matyjaszewski, K., *Acs Macro Lett* **2012**, 1 (1), 6-10; (d) Hu, J.; Zhang, G.; Ge, Z.; Liu, S., *Prog. Polym. Sci.* **2014**, 39 (6), 1096-1143; (e) Vancoillie, G.; Frank, D.; Hoogenboom, R., *Prog. Polym. Sci.* **2014**, 39 (6), 1074-1095; (f) Ran, J.; Wu, L.; Zhang, Z.; Xu, T., *Prog. Polym. Sci.* **2014**, 39 (1), 124-144; (g) Mendonca, P. V.; Averick, S. E.; Konkolewicz, D.; Serra, A. C.; Popov, A. V.; Guliashvili, T.; Matyjaszewski, K.; Coelho, J. F. J., *Macromolecules (Washington, DC, United States)* **2014**, 47 (Copyright (C) 2014 American Chemical Society (ACS). All Rights Reserved.), 4615-4621; (h) Gois, J. R.; Konkolewicz, D.; Popov, A. V.; Guliashvili, T.; Matyjaszewski, K.; Serra, A. C.; Coelho, J. F. J., *Polym. Chem.* **2014**, 5 (Copyright (C) 2014 American Chemical Society (ACS). All Rights Reserved.), 4617-4626; (i) Mendonca, P. V.; Konkolewicz, D.; Averick, S. E.; Serra, A. C.; Popov, A. V.; Guliashvili, T.; Matyjaszewski, K.; Coelho, J. F. J., *Polym Chem-Uk* **2014**, 5 (19), 5829-5836; (j) Konkolewicz, D.; Krys, P.; Gois, J. R.; Mendonca, P. V.; Zhong, M.; Wang, Y.; Gennaro, A.; Isse, A. A.; Fantin, M.; Matyjaszewski, K., *Macromolecules* **2014**, 47 (2), 560-570.

4. (a) Konak, C.; Ganchev, B.; Teodorescu, M.; Matyjaszewski, K.; Kopeckova, P.; Kopecek, J., *Polymer* **2002**, 43 (13), 3735-3741; (b) Neugebauer, D.; Matyjaszewski, K., *Macromolecules* **2003**, 36 (8), 2598-2603; (c) Xia, Y.; Yin, X.; Burke, N. A. D.; Stover, H. D. H., *Macromolecules* **2005**, 38 (14), 5937-5943; (d) Xia, Y.; Burke, N. A. D.; Stover, H. D. H., *Macromolecules* **2006**, 39 (6), 2275-2283; (e) Jiang, J. G.; Lu, X. Y.; Lu, Y., *J Polym Sci Pol Chem* **2007**, 45 (17), 3956-3965; (f) Tan, Y.; Yang, Q. B.; Sheng, D. K.; Su, X. F.; Xu, K.; Song, C. L.; Wang, P. X., *E-Polymers* **2008**; (g) Siegwart, D. J.; Bencherif, S. A.; Srinivasan, A.; Hollinger, J. O.; Matyjaszewski, K., *J. Biomed. Mater. Res., Part A* **2008**, 87A (2), 345-358; (h) Ye, J. D.; Narain, R., *J Phys Chem B* **2009**, 113 (3), 676-681; (i) Millard, P.-E.; Mougin, N. C.; Boeker, A.; Mueller, A. H. E., *ACS Symposium Series* **2009**, 1023 (Controlled/Living Radical Polymerization: Progress in ATRP), 127-137; (j) Pan, P.; Fujita, M.; Ooi, W.-Y.; Sudesh, K.; Takarada, T.; Goto, A.; Maeda, M., *Langmuir*

2012, 28 (40), 14347-14356; (k) Otsuka, I.; Travelet, C.; Halila, S.; Fort, S.; Pignot-Paintrand, I.; Narumi, A.; Borsali, R., *Biomacromolecules* **2012**, 13 (5), 1458-1465; (l) Yamashita, K.; Yamamoto, K.; Kadokawa, J.-i., *Polymer* **2013**, 54 (7), 1775-1778; (m) Bruns, N.; Lorcher, S.; Makyla, K.; Pollard, J.; Renggli, K.; Spulber, M., *Chimia* **2013**, 67 (11), 777-781; (n) Anastasaki, A.; Haddleton, A. J.; Zhang, Q.; Simula, A.; Droesbeke, M.; Wilson, P.; Haddleton, D. M., *Macromol Rapid Comm* **2014**, 35 (10), 965-970.

5. (a) Shalaby, S. W.; McCormick, C. L.; Butler, G. B., *ACS Symposium Series* **1991**, 467, R9-R9; (b) Qiu, Y.; Park, K., *Adv Drug Deliver Rev* **2001**, 53 (3), 321-339; (c) Murdan, S., *J Control Release* **2003**, 92 (1-2), 1-17; (d) Schmaljohann, D., *Adv Drug Deliver Rev* **2006**, 58 (15), 1655-1670; (e) Wever, D. A. Z.; Picchioni, F.; Broekhuis, A. A., *Progress in Polymer Science* **2011**, 36 (11), 1558-1628.

6. (a) Xia, J.; Gaynor, S. G.; Matyjaszewski, K., *Macromolecules* **1998**, 31 (17), 5958-5959; (b) Tang, W.; Matyjaszewski, K., *Macromolecules* **2006**, 39 (15), 4953-4959; (c) Tang, W.; Kwak, Y.; Braunecker, W.; Tsarevsky, N. V.; Coote, M. L.; Matyjaszewski, K., *J. Am. Chem. Soc.* **2008**, 130 (32), 10702-10713; (d) Lin, C.-Y.; Marque, S. R. A.; Matyjaszewski, K.; Coote, M. L., *Macromolecules* **2011**, 44 (19), 7568-7583.

7. Zhang, Q.; Wilson, P.; Li, Z. D.; McHale, R.; Godfrey, J.; Anastasaki, A.; Waldron, C.; Haddleton, D. M., *J Am Chem Soc* **2013**, 135 (19), 7355-7363.

8. (a) Tsarevsky, N. V.; Pintauer, T.; Matyjaszewski, K., *Macromolecules* **2004**, 37 (26), 9768-9778; (b) Bortolamei, N.; Isse, A. A.; Magenau, A. J. D.; Gennaro, A.; Matyjaszewski, K., *Angew Chem Int Edit* **2011**, 50 (48), 11391-11394.

9. (a) Matyjaszewski, K.; Jakubowski, W.; Min, K.; Tang, W.; Huang, J. Y.; Braunecker, W. A.; Tsarevsky, N. V., *P Natl Acad Sci USA* **2006**, 103 (42), 15309-15314; (b) Jakubowski, W.; Matyjaszewski, K., *Angew Chem Int Edit* **2006**, 45 (27), 4482-4486; (c) Dong, H.; Matyjaszewski, K., *Macromolecules* **2008**, 41 (19), 6868-6870; (d) Kwak, Y.; Matyjaszewski, K., *Polym Int* **2009**, 58 (3), 242-247; (e) Nicolay, R.; Kwak, Y.; Matyjaszewski, K., *Angew Chem Int Edit* **2010**, 49 (3), 541-544.

10. (a) Mueller, L.; Jakubowski, W.; Tang, W.; Matyjaszewski, K., *Macromolecules* **2007**, 40 (18), 6464-6472; (b) Plichta, A.; Li, W. W.; Matyjaszewski, K., *Macromolecules* **2009**, 42 (7), 2330-2332; (c) Konkolewicz, D.; Magenau, A. J. D.; Averick, S. E.; Simakova, A.; He, H. K.; Matyjaszewski, K., *Macromolecules* **2012**, 45 (11), 4461-4468.

11. (a) Matyjaszewski, K.; Tsarevsky, N. V.; Braunecker, W. A.; Dong, H.; Huang, J.; Jakubowski, W.; Kwak, Y.; Nicolay, R.; Tang, W.; Yoon, J. A., *Macromolecules* **2007**, 40 (22), 7795-7806; (b) Konkolewicz, D.; Wang, Y.; Zhong, M. J.; Krys, P.; Isse, A. A.; Gennaro, A.; Matyjaszewski, K., *Macromolecules* **2013**, 46 (22), 8749-8772; (c) Abreu, C. M. R.; Serra, A. C.; Popov, A. V.; Matyjaszewski, K.; Guliashvili, T.; Coelho, J. F. J., *Polym Chem-Uk* **2013**, 4 (23), 5629-5636; (d) Konkolewicz, D.; Wang, Y.; Krys, P.; Zhong, M. J.; Isse, A. A.; Gennaro, A.; Matyjaszewski, K., *Polym Chem-Uk* **2014**, 5 (15), 4396-4417; (e) Gois, J. R.; Rocha, N.; Popov, A. V.; Guliashvili, T.; Matyjaszewski, K.; Serra, A. C.; Coelho, J. F. J., *Polym Chem-Uk* **2014**, 5 (12), 3919-3928.

12. (a) Tasdelen, M. A.; Uygur, M.; Yagci, Y., *Macromol. Chem. Phys.* **2011**, 212 (18), 2036-2042; (b) Tasdelen, M. A.; Ciftci, M.; Yagci, Y., *Macromol. Chem. Phys.* **2012**, 213 (13), 1391-1396; (c) Zhang, T.; Chen, T.; Amin, I.; Jordan, R., *Polym Chem-Uk* **2014**, 5 (16), 4790-4796.

13. (a) Magenau, A. J. D.; Strandwitz, N. C.; Gennaro, A.; Matyjaszewski, K., *Science* **2011**, 332 (6025), 81-84; (b) Li, B.; Yu, B.; Huck, W. T. S.; Zhou, F.; Liu, W. M., *Angew. Chem.-Int. Edit.* **2012**, 51 (21), 5092-5095; (c) Magenau, A. J. D.; Bortolamei, N.; Frick, E.; Park, S.; Gennaro, A.; Matyjaszewski, K., *Macromolecules* **2013**, 46 (11), 4346-4353; (d) Park, S.; Cho, H. Y.; Wegner, K. B.; Burdynska, J.; Magenau, A. J. D.; Paik, H. J.; Jurga, S.; Matyjaszewski, K., *Macromolecules* **2013**, 46 (15), 5856-5860.
14. (a) Shen, Y.; Tang, H.; Ding, S., *Prog. Polym. Sci.* **2004**, 29 (10), 1053-1078; (b) Ding, S.; Xing, Y.; Radosz, M.; Shen, Y., *Macromolecules* **2006**, 39 (19), 6399-6405.
15. Schroder, K.; Mathers, R. T.; Buback, J.; Konkolewicz, D.; Magenau, A. J. D.; Matyjaszewski, K., *Acs Macro Lett* **2012**, 1 (8), 1037-1040.
16. Fukuda, T.; Goto, A., *Macromol Rapid Comm* **1997**, 18 (8), 683-688.
17. Mumick, P. S.; McCormick, C. L., *Polymer Engineering & Science* **1994**, 34 (18), 1419-1428.
18. Xia, J. H.; Matyjaszewski, K., *Macromolecules* **1999**, 32 (8), 2434-2437.
19. Queffelec, J.; Gaynor, S. G.; Matyjaszewski, K., *Macromolecules* **2000**, 33 (23), 8629-8639.

Chapter V

Miniemulsion Polymerization of n-Butyl Acrylate by Electrochemically Mediated Atom Transfer Radical Polymerization*

V. 1. Preface

Electrochemically mediated atom transfer radical polymerization (*e*ATRP) of *n*-butyl acrylate (BA) in a miniemulsion was realized by exploiting conditions that allowed for electrochemical communication between the aqueous and organic phase catalysts. The polymerization was conducted in the dispersed media utilizing a combination of hydrophilic copper complexes formed with *N,N*-bis(2-pyridylmethyl)-2-hydroxyethylamine (BPMEA), 2,2'-bipyridine (bpy), and tris(2-pyridylmethyl)amine (TPMA) ligands and hydrophobic complexes with bis(2-pyridylmethyl)octadecylamine (BPMODA) and bis[2-(4-methoxy-3,5-dimethyl) pyridylmethyl]octadecylamine (BPMODA*) ligands were selected for the aqueous and organic phase, respectively. The redox potentials of the copper complexes, obtained by cyclic voltammetry, guided the selection of proper combination of catalysts. When a catalyst with appropriate negative redox potential was used in the continuous phase, *i.e.*, aqueous phase, reduction of the organic phase catalyst occurred through an interfacial communication between the two phases, which was established through an efficient electron transfer at the liquid/liquid

*Work in this Chapter will be submitted for publication.

interface. Several parameters were investigated to produce well-defined PBAs, including applied potential, catalysts combination, and various target degrees of polymerization (DP). The water-soluble catalyst Cu/BPMEA, used in combination with Cu/BPMODA* in the organic phase, provided the best control over the BA miniemulsion *e*ATRP. My role in this project was synthesizing organic or aqueous phase ligands, optimizing polymerization conditions, and analyzing the obtained results.

I would like to acknowledge Yi Wang and Dr. Marco Fantin for their contribution to the project and helpful discussions.

V. 2. Introduction

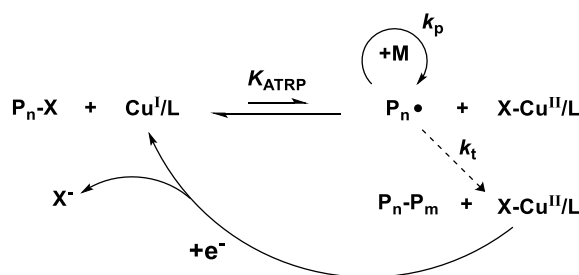
Copper-based atom transfer radical polymerization (ATRP) is a well-known reversible deactivation radical polymerization (RDRP) technique, used for the synthesis of well-defined polymers with a predetermined molecular weight (MW) and narrow molecular weight distribution (MWD or M_w/M_n).^{1a, 1b, 1e, 1f, 2b, 2c, 14a, 15} ATRP is a powerful polymerization tool that allows a control over polymer compositions (*e.g.*, block and gradient copolymers), topology (*e.g.*, stars and polymeric bottlebrushes), and site specific functionalities (*e.g.*, α -, ω -, or both, periphery or core functional stars, and side group functional brushes).^{2b, 42d, 61e, 105} In addition, a wide range of monomers are polymerized by ATRP, including (meth)acrylates, styrenes and acrylamides.^{1f, 3a, 3c, 3e}

Generally in an ATRP, a copper catalyst ($\text{Cu}^{\text{I}}/\text{L}$) activates an alkyl halide initiator (R-X), to form a radical (R^\bullet) and a deactivator complex ($\text{X-Cu}^{\text{II}}/\text{L}$). The R^\bullet (or polymeric radical, P_n^\bullet) propagates by addition of a few monomer units, before being quickly deactivated by the $\text{X-Cu}^{\text{II}}/\text{L}$ complex to (re)form a dormant polymeric species ($\text{P}_n\text{-X}$) and the original activator complex ($\text{Cu}^{\text{I}}/\text{L}$). The initial ATRP procedure required > 10000 parts per million (ppm) of Cu based catalysts, compared to monomer molar concentration. Therefore, extensive purification of the products was necessary for many applications.^{15, 18a-e, 18g, 106} Currently, several catalyst (re)generation methods allow performing ATRP reactions with a low ppm level of catalysts: these techniques include activators regenerated by electron transfer (ARGET) ATRP,^{5a, 5b, 5d-g, 20b, 80, 107} initiators for continuous activator regeneration (ICAR) ATRP,^{6, 65b, 108} supplemental activator and reducing agent (SARA) ATRP,^{7a, 7c-f, 21, 109} photoinduced ATRP (photoATRP)^{8a, 8c-f, 8h, 8j-l, 22}, and electrochemically

mediated ATRP (*e*ATRP).^{10-13, 23b, 110} In an *e*ATRP, the reduction of the stable X-Cu^{II}/L complex to Cu^I/L occurs by means of a cathodic current flowing from a working electrode (Scheme V-1). The rate and control of the polymerization (R_p) can be tuned by modulating the electrochemical parameters applied to the system, such as current intensity, applied potential (E_{app}), or total electric charge injected into the system.¹¹ The rate of polymerization (R_p , eq. (V-1))^{1f} can be easily enhanced until mass-transfer limit is encountered by quantitatively reducing the Cu^{II}/L catalyst to Cu^I/L; “on-off” polymerization can be obtained by simply stopping E_{app} between negative and positive values (*i.e.* by reduction and (re)oxidation of the complex). The rate of an ATRP is defined by the following equation,

$$R_p = k_p K_{ATRP} \frac{[R-X][Cu^I/L]}{[X-Cu^{II}/L]} [M] \quad (V-1)$$

where k_p is the monomer propagation rate constant and K_{ATRP} is the ATRP equilibrium constant.



Scheme V-1. Mechanism of electrochemically mediated atom transfer radical polymerization (*e*ATRP).

ATRP can polymerize various monomers under homogeneous conditions in a wide

range of solvents, from organic to aqueous environments.^{1f} In addition ATRP was carried out in a wide array of heterogeneous conditions, *i.e.*, microemulsions,¹¹¹ miniemulsions,¹¹² and emulsions¹¹³ and well-defined latexes were obtained in each case. The advantages of heterogeneous aqueous systems are efficient heat dissipation during polymerization, low viscosity, and elimination of volatile organic solvents.¹¹⁴ Among the heterogeneous polymerization systems, miniemulsion polymerization allows for formation of stable particles that do not suffer from Ostwald ripening.¹¹⁵ In a miniemulsion ATRP, polymeric chains and hydrophobic catalysts are confined within a dispersed organic phase.¹¹⁵⁻¹¹⁶ Therefore in an *e*ATRP polymer chains and catalyst complex are confined in individual organic phase droplets and are separated from the electrode by an aqueous continuous phase which means deactivators cannot be reduced at the electrode surface exposed to water. A dual catalytic system was evaluated in order to overcome this challenge. The generation of the proper balance between hydrophilic/hydrophobic properties and redox potentials provided access to controlled *e*ATRP and well-defined polymers.

Hydrophobic copper ligands, such as bis(2-pyridylmethyl)octadecylamine (BPMODA), were specifically designed for oil-in-water emulsions. The presence of the octadecyl (C₁₈) hydrocarbon chain in BPMODA provides sufficient hydrophobicity to efficiently confine the copper complex to the organic phase. However, the activity of Cu^I/BPMODA is low and relatively high catalysts loadings are required to maintain a suitable *R_p*.¹¹⁷ Polydentate ligands such as tris[2-(dimethylamino)ethyl]amine (Me₆TREN) or tris(2-pyridylmethyl)amine (TPMA) can enhance catalytic activity.^{88, 118} Indeed those two systems are 10³ to 10⁵ times more active than the conventionally used Cu/bpy complex.^{1a,}

^{94b, 114, 119} Nevertheless, copper complexes with Me₆TREN and TPMA are not sufficiently hydrophobic to be confined in the organic phase and requires specially designed oil-soluble ligands. It was previously reported that the miniemulsion polymerization using a BPMODA modified with 6 electron donor groups, bis[2-(4-methoxy-3,5-dimethyl)pyridylmethyl]octadecylamine (BPMODA*) allowed low ppm catalysts loading miniemulsion ATRP because of higher K_{ATRP} than non-modified BPMODA.¹¹⁷ Heterogeneous polymerization showed a linear evolution of molecular weight with conversion and narrow molecular-weight distribution using only 250 ppm Cu complex. Herein, Cu/BPMODA* was selected as ligand for an organic phase catalyst; an hydrophilic ligand, *N,N*-bis(2-pyridylmethyl)-2-hydroxyethylamine (BPMEA), was synthesized to be used as the aqueous phase copper ligand. The communication between continuous phase catalysts (aqueous phase) and organic phase catalyst (BA droplets) was investigated for the *e*ATRP of well-defined polymer latexes.

V. 3. Results and discussion

Conventional *e*ATRP with CuBr₂/BPMODA*. A conventional *e*ATRP in homogenous solution was carried out to examine the catalytic activity of CuBr₂/BPMODA* and the effect of hexadecane (HD) on the polymerization (Figure V-1). Reaction conditions were adjusted to mimic the organic phase of an emulsion polymerization: [BA]/[EBiB]/[CuBr₂]/[BPMODA*] = 283/1/0.3/0.3, with 5 wt% HD at 60 °C under $E_{\text{app}} = E_{\text{pc}} - 80$ mV. After a 0.5 h of induction with negligible monomer conversion, a linear first-order kinetic plot was observed. MW increased linearly with monomer conversion and MWD was narrow (final $M_w/M_n = 1.16$). GPC traces of the

growing PBA chains showed a clean peak shift from low MW to higher MW, without any shoulders, confirming that a well-controlled homogenous *e*ATRP in an organic solvent could be carried out in the presence of HD. An organic phase with similar composition was used during the emulsion *e*ATRP.

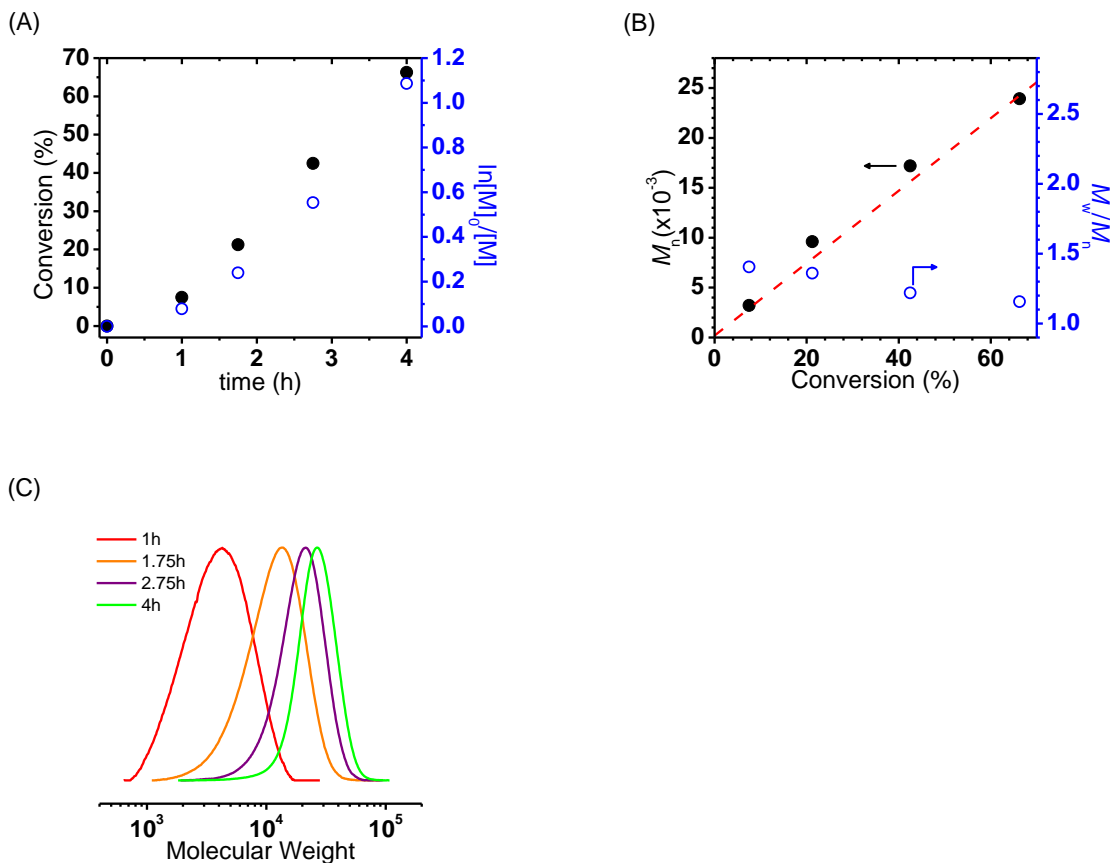


Figure V-1. Conventional *e*ATRP of BA with $\text{CuBr}_2/\text{BPMDA}^*$. (A) Monomer conversion vs. time, (B) MW and MWD vs. monomer conversion, and (C) GPC traces. Reaction condition: $[\text{BA}]/[\text{EBiB}]/[\text{CuBr}_2]/[\text{BPMDA}^*] = 283/1/0.3/0.3$; $[\text{BA}]_0 = 4.19 \text{ M}$ (in DMF); 5 wt% of HD (vs. wt of BA); $[\text{TBAClO}_4] = 0.2 \text{ M}$; $E_{\text{app}} = E_{\text{pc}} - 80 \text{ mV}$.

Partition Experiments. The hydrophobicity of $\text{CuBr}_2/\text{BPMEA}$ was verified by

partition experiments. The distribution of the catalyst between the organic (BA) and the aqueous phase was determined by UV-Vis spectrometry. A calibration curve was obtained by preparing CuBr₂/BPMEA solutions of different concentration, 0.1 to 20 mM in water, Figure V-2. Based on the calibration curve, residual [Cu/BPMEA]_{aq}/[Cu/BPMEA]₀ ratios were calculated, Table V-1 and Figure V-3. The results indicated that CuBr₂/BPMEA complex strongly preferred to reside in the aqueous phase. Conversely, according to previous reports,¹¹⁷ CuBr₂/BPMODA and CuBr₂/BPMODA* have a high preference for organic phase, 66 and 90% for BPMODA and BPMODA*, respectively (*T* = RT and [Cu/L] = 2.5 mM). Therefore, CuBr₂/BPMEA was used as the aqueous phase catalyst and CuBr₂/BPMODA* as the organic phase catalyst. These results suggest that each complex is well confined in its own phase and that the communication between the two catalysts mostly occurs at the oil/water interface.

Table V-1. Partition experiments of CuBr₂/BPMEA catalysts with aqueous/BA solution.

	[Cu/BPMEA] ₀			
	2.5 mM		5 mM	
	RT	60 °C	RT	60 °C
[Cu/BPMEA] _{aq} /[Cu/BPMEA] ₀ (15 vol% BA) ^a	0.54	0.88	0.73	0.98
[Cu/BPMEA] _{aq} /[Cu/BPMEA] ₀ (30 vol% BA) ^b	0.53	0.96	0.74	0.99

Cu = CuBr₂; Ratios of [Cu/BPMEA]_{aq}/[Cu/BPMEA]₀ was determined by calibration curve

prepared by the known amount of CuBr₂/BPMEA in water (Figure V-2 and Figure V-3);

^a13.5 wt% of BA; ^b27.8 wt% of BA.

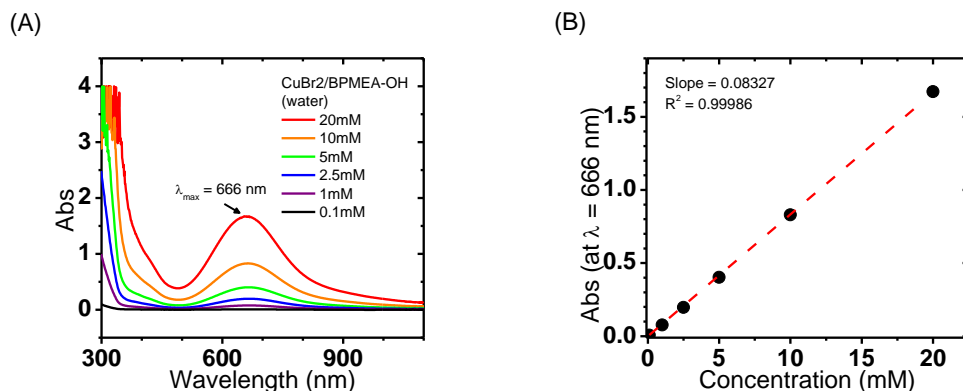


Figure V-2. (A) UV-Vis spectra of CuBr₂/BPMEA at different concentrations (0.1 to 20 mM). (B) Calibration curve (absorbance vs. concentration) obtained from the UV-Vis spectra ($R^2 = 0.99986$).

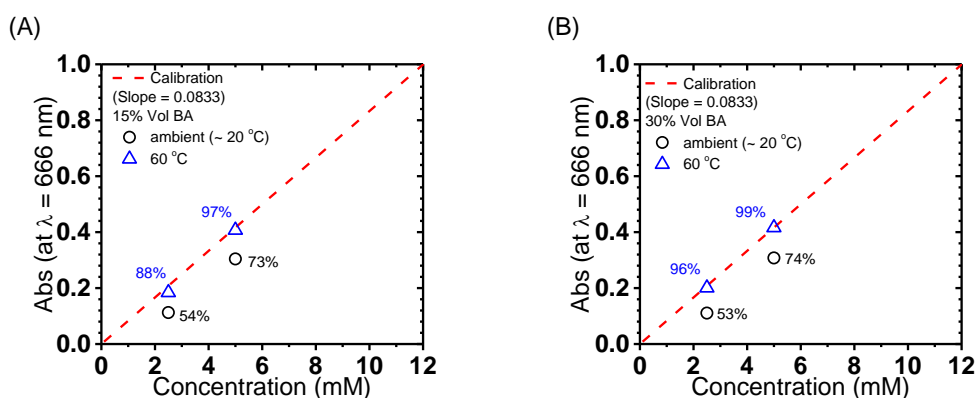
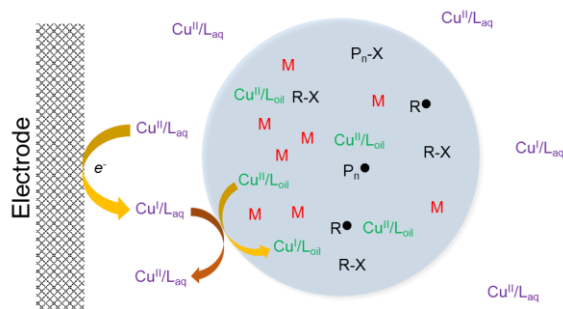


Figure V-3. Partition experiments of CuBr₂/BPMEA in (A) 50/50 and (B) 70/30 water/BA mixtures (by v/v). T = ambient (~ 20 °C) or 60 °C. Calibration curve was obtained from Figure V-2.

Polymerization Mechanism and CV analysis of catalysts. The proposed mechanism for miniemulsion polymerization is illustrated in Scheme V-2. The catalyst in the continuous phase (aqueous) is reduced to the active Cu^I/L_{aq} complex at the working

electrode. Then, electron transfer (ET) occurs at the oil/water interface: $\text{Cu}^{\text{I}}/\text{L}_{\text{aq}} + \text{Cu}^{\text{II}}/\text{L}_{\text{oil}} \rightarrow \text{Cu}^{\text{II}}/\text{L}_{\text{aq}} + \text{Cu}^{\text{I}}/\text{L}_{\text{oil}}$. Since all compounds required for the polymerization are in the oil droplets, the reduced $\text{Cu}^{\text{I}}/\text{L}_{\text{oil}}$ could activate R-X and initiate the polymerization in the organic phase. CV analysis confirmed that the aqueous phase catalyst is a stronger reducing agent than is the organic phase catalyst, which is a necessary condition for an efficient ET between the two phases.¹²⁰

Half-wave potentials, evaluated as the half-sum of cathodic and anodic peaks ($E_{1/2} = (E_{\text{pc}} + E_{\text{pa}})/2$) are listed in Table V-2. Typically, the $E_{1/2}$ of the aqueous phase catalyst is more negative than $E_{1/2}$ of the organic phase catalyst,^{28, 96a} indicating that the complexes are stronger reducing agents in water than they are in organic solvents.^{64b, 119} A possible catalyst combination for miniemulsion polymerization by *e*ATRP is $\text{CuBr}_2/\text{BPMEA}$ in the aqueous phase and $\text{CuBr}_2/\text{BPMODA}^*$ in the organic phase, which showed a difference in the half-wave potential, or $E_{1/2}$ mismatch, of -0.135 V ($E_{1/2}$ mismatch = $\Delta E_{1/2} = E_{1/2, \text{water}} - E_{1/2, \text{oil}} = -0.267 \text{ V} + 0.132 \text{ V} = -0.135 \text{ V}$). Hence, based on CV analysis, $\text{CuBr}_2/\text{BPMEA}$ is a significantly stronger reducing agent than $\text{CuBr}_2/\text{BPMODA}^*$, and ET from aqueous phase catalysts to organic phase catalysts should occur.



Scheme V-2. Proposed mechanism of miniemulsion polymerization by *e*ATRP.

Table V-2. Results from CV analysis of various CuBr₂/L complexes.

L <i>E</i> _{1/2} (V vs. SCE)	Aqueous Phase			Organic Phase ¹	
	bpy	BPMEA	TPMA	BPMODA	BPMODA*
	-0.093	-0.267	-0.318	-0.040 (-0.070 ²)	-0.132

¹BA/anisole = 50/50 (by v/v) ² BA/anisole = 70/30 (by v/v); Measurement condition: [CuBr₂/L] = 1 mM in water (bpy, BPMEA, and TPMA) or BA/anisole (BPMODA and BPMODA*); WE = Pt disk; CE = Pt mesh; RE = SCE; scan rate = 100 mV/s.

Controlled Polymerization of BA by Miniemulsion *e*ATRP. The composition of both the aqueous phase and organic phase in the miniemulsion polymerization are listed in Table V-3. The miniemulsion was prepared by ultrasonic treatment at 0 °C to prevent undesirable reactions. Tsarevsky and coworkers recently reported an ATRP miniemulsion polymerization with SDS emulsifier.¹²¹ SDS had negative effects on the ATRP: it reacted with the copper complex, decomposing the Cu^{II} deactivator complex. However, the addition of an excess of Br ions prevented complexation between SDS and the deactivator. Therefore, SDS was used in the presence of 0.1 M NaBr to prevent loss of catalyst and to increase solution conductivity. DLS analysis showed that NaBr did not destabilize the particles in the miniemulsion (Figure V-4A).

Table V-3. Composition of organic and aqueous phases in miniemulsion polymerization.

Component	Weight (g)	Comments
Organic phase		
BA	7.15	20 vol% (18 wt%) to total solution
EBiB	0.04 ^a	[BA]/[EBiB] = 283/1
HD	0.39	5.4 wt% to BA
CuBr ₂ /BPMODA* ^b	0.01/0.03	[CuBr ₂]/[BPMODA*] = 1/1
Aqueous phase		
Water	32	Distilled water
SDS	0.33	4.6 wt% to BA
NaBr	0.41	[NaBr] = 0.1 M

CuBr₂/BPMEA^c 0.01/0.01 [CuBr₂/BPMEA] = 1 mM

Polymerization conditions: $T = 60\text{ }^{\circ}\text{C}$; WE = Pt mesh; CE = Pt mesh (separated from reaction mixtures by supporting electrolyte saturated methylated cellulose gel); RE = Ag/AgI/I⁻; ^aamount of EBiB was various based on target degree of polymerization (DP); ^bBPMODA was used for controlled experiments; ^cbpy was used for controlled experiments.

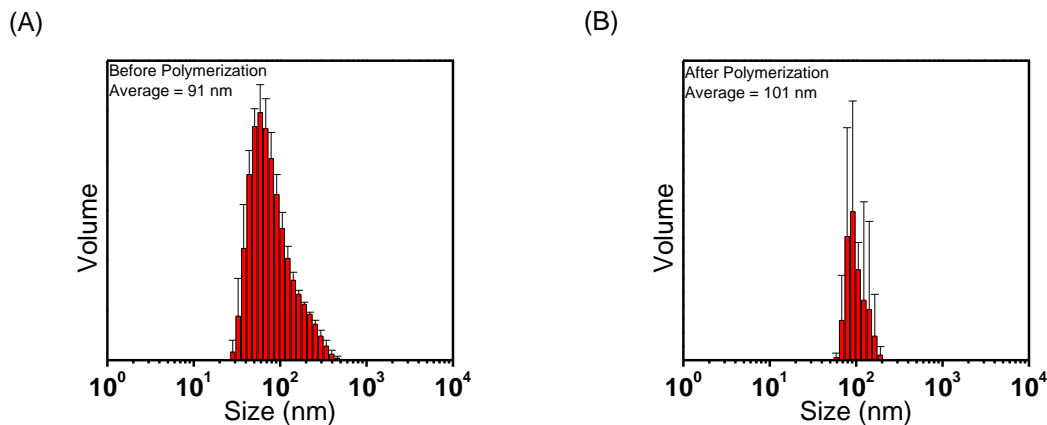


Figure V-4. Particle sizes of miniemulsion polymerization. (A) Before polymerization and (B) after polymerization (Figure V-5 entry 4).

The experiments listed in Table V-4 were conducted to elucidate the effect of the applied current and the role of the catalyst in each phase. Polymerization did not occur in the absence of organic phase catalyst (CuBr₂/BPMODA*, entry 1) or in the absence of aqueous phase catalyst (CuBr₂/BPMEA, entry 2). In the reaction without aqueous phase catalysts, the same value of E_{app} was used as in Table V-4, entry 1, because no redox peak was observed by CV analysis. As expected, no polymerization was observed without applied current (entry 3), confirming that the active Cu^I catalyst must be produced at the working electrode in order to trigger polymerization. Moreover, the selected Cu complexes should be well-confined in the respective phases ensuring that the electron transfer reaction

predominantly occurs at the interface between aqueous phase and oil droplets. The apparently low measurement of monomer conversion ($< 7\%$) could be due to monomer evaporation under mild N_2 flow conditions. These results clearly indicate that a redox catalyst is required in both phases.

Table V-4. Control polymerization of BA by miniemulsion *e*ATRP.

Entry	[M]/[R-X] ^a	L _{oil}	L _{aq}	E_{app} ^b	Conv. (%) ^c	$M_{n,GPC}^d/M_{n,th}$	M_w/M_n^d
1	283/1	-	BPMEA	E_{pc}	7	n/a	n/a
2	283/1	BPMODA*	-	E_{pc} ^e	6	n/a	n/a
3	283/1	BPMODA*	BPMEA	-	3	n/a	n/a

General conditions: 20 vol% BA, 5.4 wt% HD, 4.6 wt% SDS, 1.4 mM organic phase catalysts, and 1 mM aqueous phase catalysts; WE = Pt mesh (estimated surface area = 3.6 cm²); CE = Pt mesh (separated from reaction mixture); RE = Ag/AgI/I⁻; V_{tot} = 40 mL; [NaBr] = 0.1 M; T = 60 °C; ^a[M]/[CuBr₂] = 1000/1; ^bscan rate (v) = 100 mV/s; ^cdetermined by gravimetric analysis (total reaction time = 24 h); ^ddetermined by THF GPC with PSty standards; ^e E_{app} was the same as in the polymerization in entry 2.

Effect of Different Catalysts Combinations for Miniemulsion Polymerization.

Different combinations of copper complexes were examined in order to investigate the roles of different catalysts in the oil and water phases, (Figure V-5 and Table V-5). To compare the polymerization results conditions where $E_{app} = E_{pc}$ was selected for each investigated system. The first combination investigated, CuBr₂/BPMODA_{oil} (in organic phase) and CuBr₂/BPMEA_{aq} (in aqueous phase), showed a larger $E_{1/2}$ mismatch ($\Delta E = -0.227$ V, Table V-2). In this case, electron transfer from aqueous to organic phase was predicted to be faster, due to the ease of reduction of CuBr₂/BPMODA, which was indeed demonstrated by the occurrence of a fast polymerization, conversion = 94%, $k_p^{app} = 0.108$

h⁻¹, Table V-5, entry 1. However, K_{ATRP} of CuBr₂/BPMODA was 2 orders of magnitude lower than that of CuBr₂/BPMODA*.¹¹⁷ According to eq. (V-1), this indicated that a very high [Cu^I/BPMODA]/[Br-Cu^{II}/BPMODA] ratio was established in the oil droplets to maintain a high rate of polymerization.^{28, 94b} This resulted in formation of a low a concentration of deactivators in the oil phase, due to an excessive reduction of Br-Cu^{II}/BPMODA_{oil} by Cu^I/BPMEA_{aq}, and consequently in a poorly controlled reaction, with a broader MWD ($M_w/M_n = 1.50$). In addition, GPC traces showed a poor growth of the polymers (Figure V-5C). This observation was further corroborated by the behavior of the catalyst combination CuBr₂/BPMODA_{oil} and CuBr₂/TPMA_{aq}, which has the largest $\Delta E_{1/2} = -0.279$ V. In MeCN, CuBr₂/TPMA is an excellent reducing agent, *ca.* 150 times more active than *N,N*-Bis(2-pyridinylmethyl)-1-propanamine (BPMPA), which has a structure similar to that of BPMODA.¹¹⁹ In the miniemulsion polymerization, the mismatch is amplified because CuBr₂/TPMA is a better reducing agent in aqueous media than it is in MeCN.^{12, 64b, 96a} The large reactivity mismatch promoted the complete reduction of the organic phase catalyst to Cu^IBr/BPMODA_{oil}, which led to an uncontrolled ATRP. The obtained polymers had a very broad MWD ($M_w/M_n = 2.53$) and monomer conversion stopped at only 17% because of the loss of chain-end functionalities caused by termination reactions resulting from depletion of Cu^{II} deactivators in the organic phase.

Conversely, the combination CuBr₂/BPMODA*_{oil} and CuBr₂/bpy_{aq} which have a smaller mismatch between redox potentials ($\Delta E_{1/2} = 0.039$ V). CuBr₂/bpy_{aq} is a slightly weaker reducing agent than is CuBr₂/BPMODA*_{oil} (Table V-2), which alludes to a low efficiency of the ET from aqueous to organic phase. As a result, with the BPMODA*_{oil}-

bpy_{aq} combination, monomer conversion was modest (57%) and k_p^{app} was 0.037 h⁻¹. The optimal combination of catalysts that afforded well-controlled polymers, BPMODA*_{oil}-BPMEA_{aq}, had an adequate mismatch between half-wave potentials of the complexes; $\Delta E_{1/2} = E_{1/2,\text{aq}} - E_{1/2,\text{oil}} = -0.135$ V. Apparent propagation rate constant was higher than that of BPMODA*_{oil}-bpy_{aq} combination ($k_p^{\text{app}} = 0.048$ h⁻¹), and resulted in formation of well-defined polymers. GPC traces showed a clean peak shift from low to high molecular weight range (Figure V-5F). Thus, further investigation of eATRP miniemulsion mainly focused on utilization of the BPMODA*-BPMEA catalysts combination.

Table V-5. Summary of catalysts combination for miniemulsion polymerization.

Entry	[M]/[R-X] ^a	L _{oil}	L _{aq}	E_{app} ^b	Conv. (%) ^c	$M_{n,\text{GPC}}^{\text{d}}/M_{n,\text{th}}$	M_w/M_n^{d}
1	283/1	BPMODA	BPMEA	E_{pc}	94	31600/34300	1.50
2	283/1	BPMODA	TPMA	E_{pc}	17	8200/6400	2.53
3	283/1	BPMODA*	bpy	E_{pc}	57	20900/20900	1.26
4	283/1	BPMODA*	BPMEA	E_{pc}	68	27400/24900	1.19

General conditions: 20 vol% BA, 5.4 wt% HD, 4.6 wt% SDS, 1.4 mM organic phase catalysts, and 1 mM aqueous phase catalysts; WE = Pt mesh (estimated surface area = 3.6 cm²); CE = Pt mesh (separated from reaction mixture); RE = Ag/AgI/I⁻; $V_{\text{tot}} = 40$ mL; [NaBr] = 0.1 M; $T = 60$ °C; ^a[M]/[CuBr₂] = 1000/1; ^bscan rate (v) = 100 mV/s; ^cdetermined by gravimetric analysis (total reaction time = 24 h); ^ddetermined by THF GPC with PSty standards.

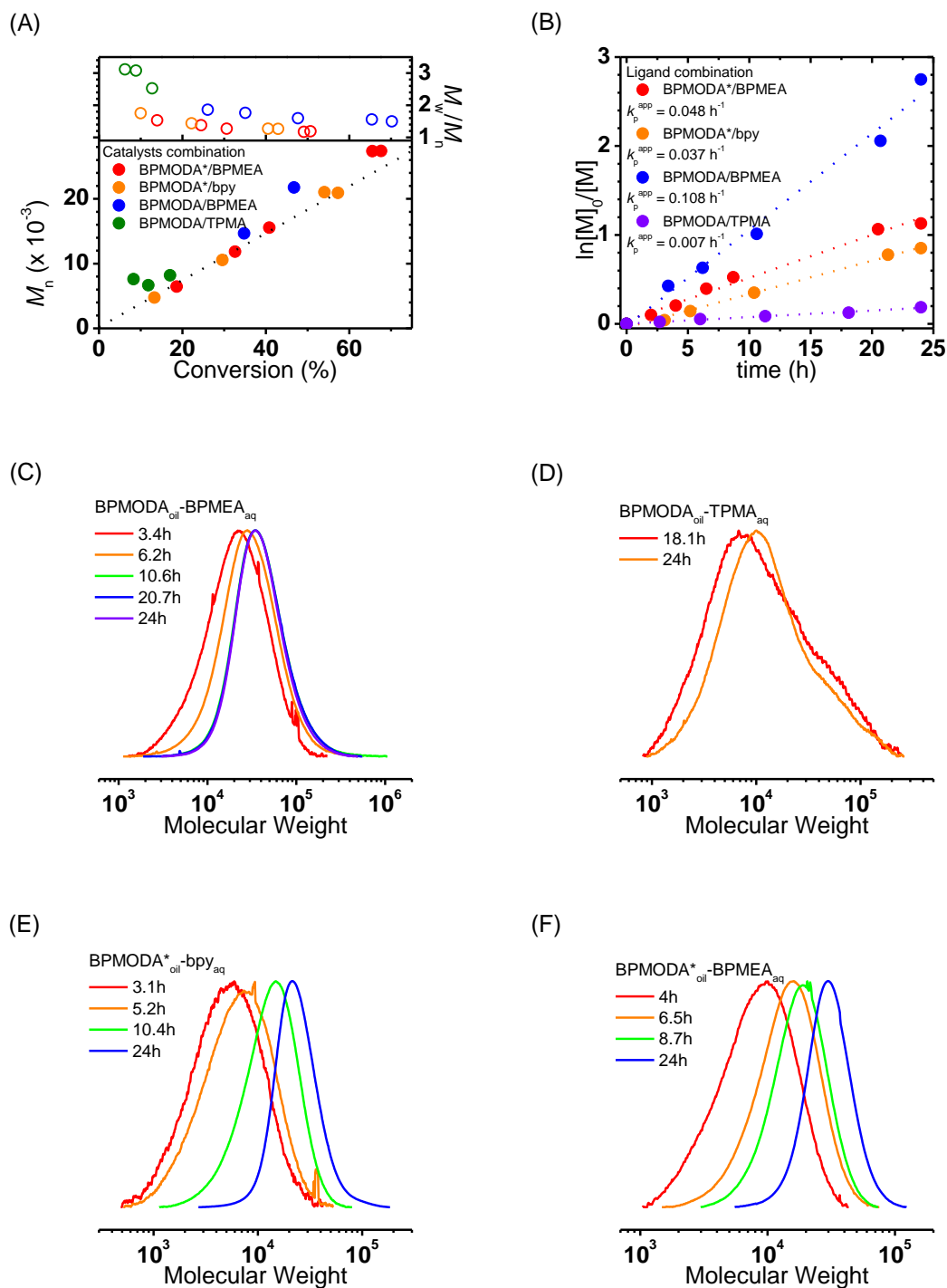


Figure V-5. Miniemulsion *e*ATRP with different catalysts combination. (A) MW and MWD evolution vs. monomer conversion. GPC traces obtained during *e*ATRP with

different catalysts combination and (B) kinetic plots of miniemulsion *e*ATRP. (C-F) GPC traces of the polymerization with catalysts of (C) BPMODA_{oil}-BPMEA_{aq}, (D) BPMODA_{oil}-TPMA_{aq}, (E) BPMODA*_{oil}-bpy_{aq}, and (F) BPMODA*_{oil}-BPMEA_{aq} (Table V-5).

Effects of E_{app} and Targeting Different DPs in Miniemulsion Polymerization. A series of miniemulsion polymerizations were carried out at different E_{app} s (entry 4 in Table V-5 and entries 1-2 in Table V-6). E_{app} s were selected based on the reversible CV recorded in the miniemulsion polymerization solution (Figure V-6A). For each of the three E_{app} s, M_n increased linearly with monomer conversion and matched well with the theoretical values ($M_{n,th}$) and narrow molecular-weight distributions were obtained, indicating a uniform growth of polymer chains. As expected, more reducing conditions resulted in an increased reaction rate; the apparent rate of polymerization (k_p^{app}) gradually increased with decreasing E_{app} ($k_p^{app} = 0.035, 0.036, \text{ and } 0.041 \text{ h}^{-1}$ for $E_{1/2}$, E_{pc} , and $E_{pc} - 80 \text{ mV}$, respectively). In addition, the most reducing condition, $E_{app} = E_{pc} - 80 \text{ mV}$, led to the highest monomer conversion after 24 h (71%). DLS analysis showed that the miniemulsion particles were stable during the polymerization (Figure V-4B): and particle size was very similar before and after conducting the polymerization, 91 and 101 nm, respectively.

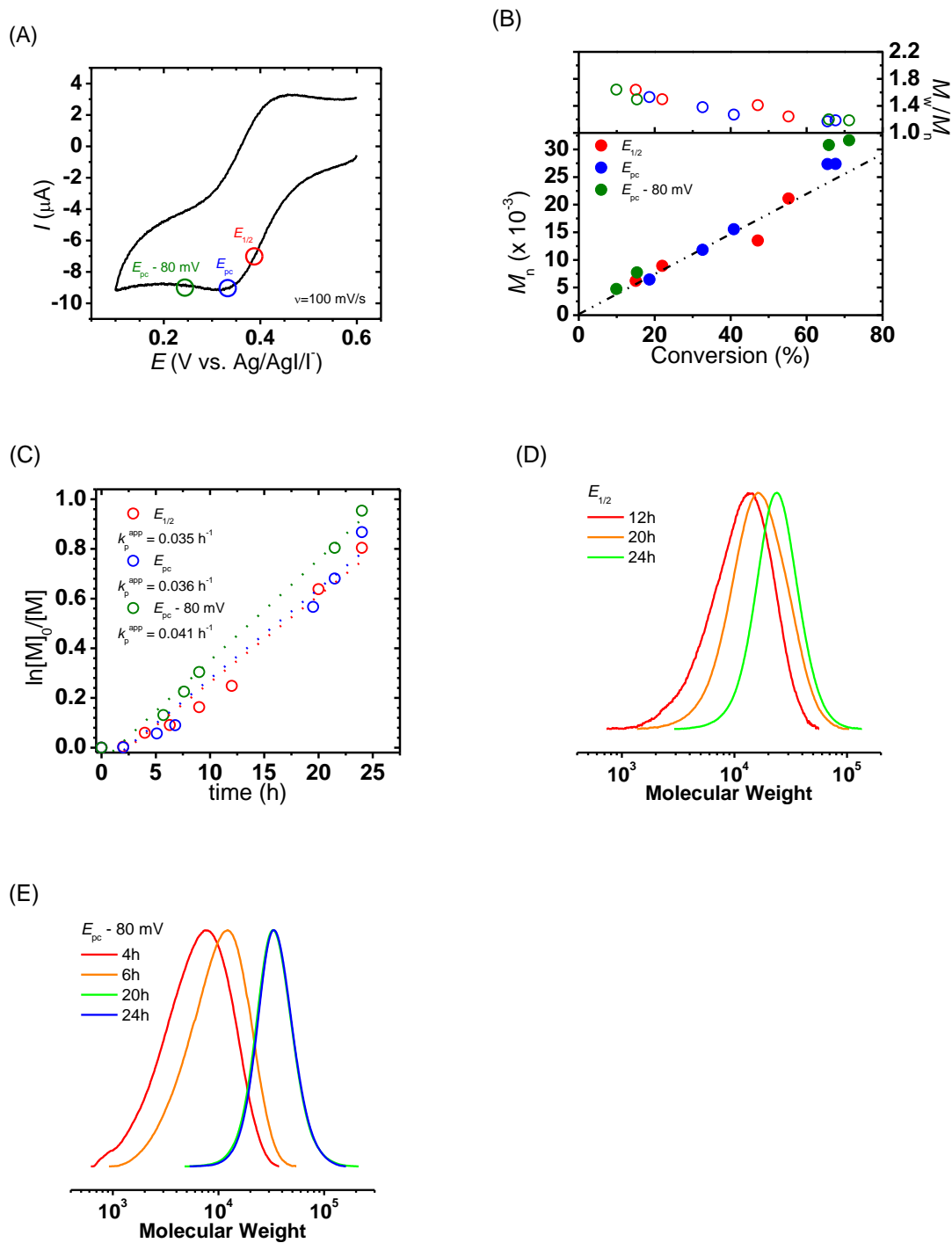


Figure V-6. Effects of E_{app} s on miniemulsion polymerization. (A) CV of polymerization mixture, (B) MW evolution and MWD vs. conversion, (C) kinetic plots of the

polymerizations, (D-E) GPC trace with various E_{app} s: (D) $E_{1/2}$ and (E) $E_{pc} - 80$ mV.

Table V-6. Polymerization with different E_{app} s and targeting DPs.

Entry	[M]/[R-X] ^a	L _{oil}	L _{aq}	E_{app} ^b	Conv. (%) ^c	$M_{n,GPC}^d/M_{n,th}$	M_w/M_n^d
1	283/1	BPMODA*	BPMEA	$E_{1/2}$	55	21100/20100	1.24
2	283/1	BPMODA*	BPMEA	$E_{pc} - 80$ mV	71	31700/25900	1.19
3	150/1	BPMODA*	BPMEA	E_{pc}	53	4400/4000	1.77
4	500/1	BPMODA*	BPMEA	E_{pc}	28	21200/18100	1.26

General conditions: 20 vol% BA, 5.4 wt% HD, 4.6 wt% SDS, 1.4 mM organic phase catalysts, and 1 mM aqueous phase catalysts; WE = Pt mesh (estimated surface area = 3.6 cm²); CE = Pt mesh (separated from reaction mixture); RE = Ag/AgI/I; $V_{tot} = 40$ mL; [NaBr] = 0.1 M; $T = 60$ °C; ^a[M]/[CuBr₂] = 1000/1; ^bscan rate (v) = 100 mV/s; ^cdetermined by gravimetric analysis (total reaction time = 24 h); ^ddetermined by THF GPC with PSty standards.

Polymerizations with different targeted DP were further carried out at $E_{app} = E_{pc}$ by varying amount of initiator, entry 4 in Table V-5 and entries 3-4 in Table V-6. All polymerizations showed linear first-order kinetics, linear increase in MW vs. monomer conversion, M_n matching the theoretical values, and narrow MWDs (Figure V-7). The rate of polymerization (eq. (V-1)) is affected by the concentration of initiator, and accordingly the lowest target DP ([M]/[R-X] = 150) showed the highest k_p^{app} (Figure V-7B). GPC traces of each polymerization showed a clear peak shift from low to high molar mass (Figure V-5F and Figure V-7C-D).

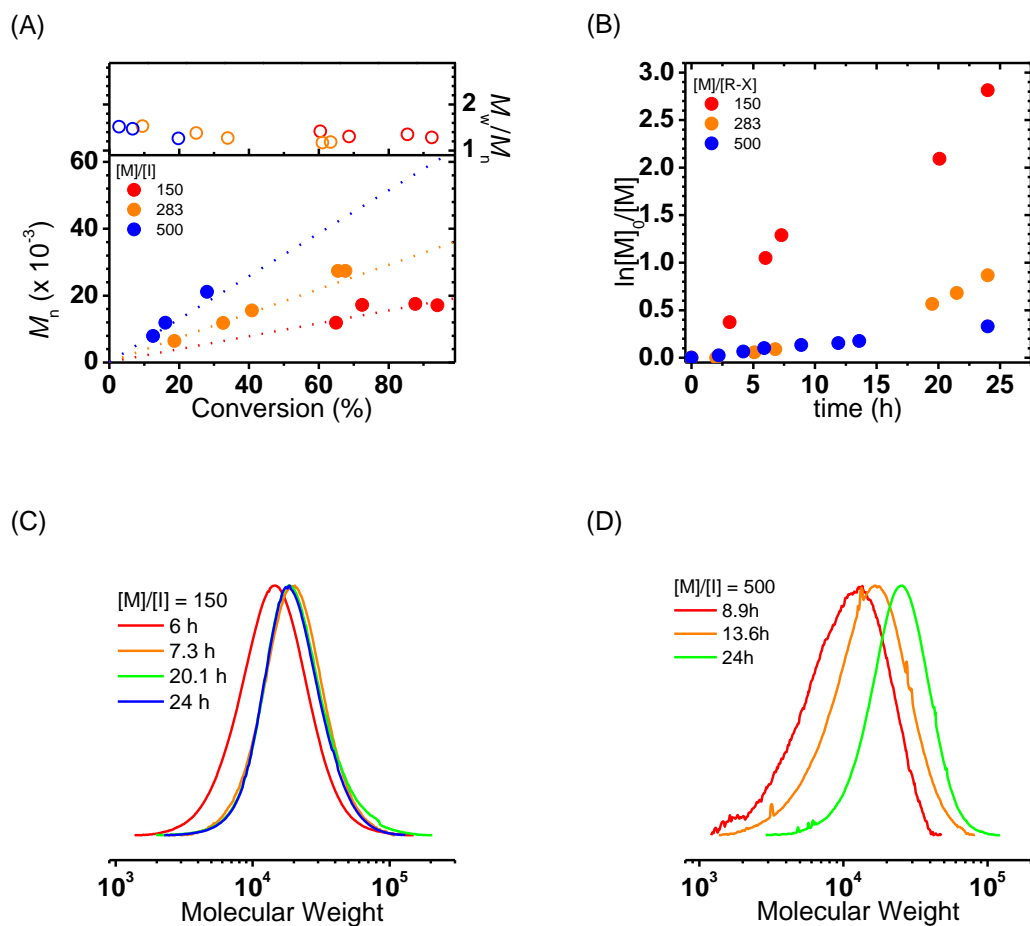


Figure V-7. Polymerization under different target DP. (A) MW and MWD vs. monomer conversion, (B) kinetics plot of miniemulsion eATRP with different target DP: $[M]/[R-X]$ = 150 (red), 283 (orange), and 500 (blue), and GPC traces for target DP = (C) 150 and (D) 500.

V. 4. Summary

Well-controlled eATRP miniemulsion polymerization was achieved using a selected combination of Cu/BPMEA and Cu/BPMODA* catalyst complexes. The effect of different parameters on the heterogeneous polymerization was investigated by varying E_{app} ,

catalysts combination, and target DP. Two catalysts, each one of them confined in either the aqueous or the organic phase, were required. Reduction of the aqueous phase catalyst occurred at the electrode/water interface while the reduction of the organic phase catalyst occurred at the water/oil interface with the hydrophilic catalyst acting as an aqueous shuttle between electrode and Cu catalysts confined within organic droplets. The correct selection of the two catalysts controlled the electron transfer at the water/oil interface to generate an appropriate ratio of $[Cu^I/Cu^{II}]_{oil}$ in the dispersed phase to control the polymerization. The selection of an inappropriate combination catalysts resulted in either a low rate of polymerization or a loss of control during the polymerization. Under the optimal reaction conditions, polymers with predetermined DP were obtained and application of a more negative E_{app} increased R_p .

V. 5. Experimental section

Materials. Tetrabutylammonium perchlorate (TBAClO₄, > 98%), tetrabutylammonium hexafluorophosphate (TBAPF₆, 98%), tetraethylammonium bromide (TEABr, 98%), copper(II) bromide (CuBr₂, 99%), methylated cellulose (Tylose, MH = 300), 2-chloromethyl-4-methoxy-3,5-dimethylpyridine hydrochloride (98%), dichloromethane (DCM, > 99.5%), 2,2'-bipyridyl (bpy, 99%), 2-(chloromethyl)pyridine hydrochloride, octadecylamine (99%), sodium dodecyl sulfate (SDS, 99%), hexadecane (HD, 99%) and ethyl α -bromoisobutyrate (EBiB, 98%) were purchased from Sigma-Aldrich. *N,N*-dimethylformamide (DMF) and sodium bromide (NaBr, 99%) were purchased from Acros. Metal wires (platinum and copper) and platinum gauge were purchased from Alfa Aesar. Tributylhexadecylphosphonium bromide (97%) was

purchased from Fluka. Magnesium sulfate anhydrous (MgSO_4 , 98.9%) and sodium hydroxide (NaOH , 99%) were purchased from Fisher. Sodium chloride (NaCl , 99%) was purchased from EMD chemicals. Tris(2-pyridylmethyl)amine (TPMA) was prepared according to a published procedure,⁸⁸ *n*-butyl acrylate (BA, 99%, Aldrich) and was passed through a column filled with basic alumina prior to use to remove polymerization inhibitors.

Synthesis of *N,N*-bis(2-pyridylmethyl)-2-hydroxyethylamine (BPMEA). BPMEA was synthesized by a modified literature procedure.¹²² 2-Picolyl chloride hydrochloride (5.0 g, 3.1×10^{-2} mol) was dissolved in 20 mL of distilled water. Ethanolamine (0.9 mL, 2.1×10^{-2} mol) was slowly injected into the solution. The mixture was stirred and heated to 60 °C. A solution of 2.4 g NaOH in 10 mL of water was added slowly to the previous mixture. The dark brown solution was stirred for 5 h and cooled to room temperature. The product was extracted with DCM and concentrated. The obtained dark oil was passed through basic alumina with DCM. The solution was concentrated to obtain the desired product.

Synthesis of bis(2-pyridylmethyl)octadecylamine (BPMODA). BPMODA was synthesized by a modified literature procedure.⁸⁸ 2-(Chloromethyl)pyridine hydrochloride (8.4 g, 51.2 mmol) and octadecylamine (6.57 g, 24.39 mmol) were dissolved in 30 mL of DCM. The NaOH solution was added to the mixture to maintain pH at 8-9 for a week. The organic layer was collected, washed with distilled water three times, and then condensed. The desired product was separated by column chromatography with hexanes/ethyl acetate (4/1, v/v) as eluent. The final product was analyzed by ^1H NMR.

Synthesis of bis[2-(4-methoxy-3,5-dimethyl)pyridylmethyl]octadecylamine

(BPMODA*). BPMODA* was synthesized by a modified literature procedure.¹¹⁷ 2-Chloromethyl-4-methoxy-3,5-dimethyl pyridine hydrochloride (15 g, 67.5 mmol) and of octadecylamine (8.67 g, 32.2 mmol) were dissolved in 100 mL of THF. Then, 55 mL of 5 M NaOH_{aq} were added to the mixture. The biphasic system was heated at 60 °C for 5 days. The organic layer was collected and washed with brine until pH *ca.* 9. Then, the organic layer was collected, dried over MgSO₄ and concentrated. The desired product was separated by column chromatography with hexanes/ethyl acetate (4/1, v/v) as eluent. The final product was analyzed by ¹H NMR.

Partition experiment of CuBr₂/BPMEA. Aqueous solutions of CuBr₂/BPMEA (1/2 by mole) were prepared at various concentrations, *i.e.*, 0.1, 1, 2.5, 5, 10, and 20 mM. Catalyst absorbance was recorded by UV-Vis spectroscopy (maximum wavelength, λ_{max} , was 666 nm). A linear calibration was obtained from the correlation between absorbance and catalyst concentration curves. Solutions of CuBr₂/BPMEA in water were prepared at two concentrations (2.5 and 5 mM) and then mixed with BA to obtain 15/85 and 30/70 water/BA ratios (by v/v). The mixtures were vigorously stirred using a Vortex Mixer at either RT or 60 °C. The aqueous phase was collected and absorbance at 666 nm was recorded by UV-Vis spectrometer.

Cyclic voltammetry (CV) analysis of catalysts. CV was performed on 1 mM CuBr₂/L catalyst solutions (L = bpy or BPMEA for aqueous phase catalyst; BPMODA or BPMODA* for organic phase catalysts; CuBr₂/L mole ratio = 1/2). In aqueous phase, 0.1 M of TEABr (0.63 g, 3 mmol) was used as a supporting electrolyte in a total volume of 30 mL. Organic phase catalysts were prepared in BA/anisole solution (1/1, by v/v) with 0.1

M TBAPF₆ as a supporting electrolyte. CV spectra were recorded at a Pt disk working electrode (WE) with a Pt mesh counter electrode (CE) and a saturated calomel (SCE) reference electrode (RE). Scan rate (v) was 100 mV/s.

Conventional *e*ATRP with CuBr₂/BPMODA* catalysts. TBAClO₄ (2.05 g, 6 mmol), CuBr₂ (28 mg, 1.26×10^{-1} mmol), and BPMODA* (71 mg, 1.26×10^{-1} mmol) were placed in a seven-neck electrolysis cell maintained at 60 °C under a slow N₂ purge. Then, 18 mL of N₂ purged BA (126 mmol) and DMF (12 mL) were added to the reaction. To evaluate the impact of hexadecane (HD) on the polymerization, the same amount of HD used in the miniemulsion polymerization was added to this conventional homogenous reaction (1.04 mL, 3.55 mmol). A CV was recorded at 100 mV/s with this electrode setup: Pt disk WE; a Pt mesh CE separated from polymerization mixture by a glass frit filled with Tylose gel (saturated in TBAClO₄); a Ag/AgI/0.1 M TBAI (Ag/AgI/I⁻) in DMF reference electrode. Appropriate applied potential was selected from the CV results ($E_{app} = E_{pc} - 80$ mV, where E_{pc} = cathodic peak potential). EBiB (65 μ L, 4.44×10^{-1} mmol) was injected into the reaction solution and a second CV was recorded to confirm the electrochemical catalytic (*EC'*) process. The Pt mesh electrode was then used as the WE for the polymerization using the chronoamperometry (CA) method. Samples were withdrawn periodically to follow monomer conversion by ¹H NMR. Number-average molecular weight (M_n) and molecular weight distribution (M_w/M_n) were determined by gel permeation chromatography (GPC).

Miniemulsion polymerization by *e*ATRP. A stock solution of BA (50 mL, 348.76 mmol), CuBr₂ (78 mg, 0.35 mmol), and BPMODA* (198 mg, 0.35 mmol) was prepared. HD (0.50 mL, 1.71 mmol), EBiB (29 μ L, 1.97×10^{-1} mmol, to target degree of

polymerization (DP) = 283) were added to 8 mL of the BA containing stock solution (the amount of EBiB was adjusted for different targeted DPs). SDS (329 mg, 1.14 mmol), NaBr (411 mg, 4 mmol), CuBr₂ (9 mg, 0.04 mmol), and BPMEA (10 mg, 0.04 mmol) were dissolved in 32 mL of distilled water. The organic and aqueous solutions were mixed (total volume \approx 40 mL), placed in an ice bath, and dispersed by a probe sonicator, amplitude = 70% for 15 min; (application and rest time of 1 s each). Nitrogen was bubbled through the miniemulsion solution for 30 min, prior to recording a CV at 100 mV/s with a Pt disk WE, and the same CE and RE described above. The CV allowed for accurate selection of the applied potential ($E_{app} = E_{1/2}$, E_{pc} , or $E_{pc} - 80$ mV, where $E_{1/2}$ is the half-sum of the cathodic and anodic peak potential). A Pt mesh WE was used for CA under proper E_{app} . Samples were withdrawn periodically to follow the monomer conversion by gravimetric analysis, while M_n and M_w/M_n were determined by GPC.

Apparatus and characterization. Ultrasound treatment was carried out using Ultrasonics W-385 sonicator. UV-Vis spectra were recorded by Agilent 8453 with a glass cuvette (length = 1 cm). ¹H NMR (300 MHz) spectra were measured on a Bruker Advance 300 spectrometer using CDCl₃ as a solvent. M_n and M_n/M_w were determined by GPC equipped with Polymer Standards Services (PSS) columns (guard, 10⁵, 10³, and 10² Å) and a differential refractive index detector (Waters, 2410), with THF as eluent at a flow rate 1.00 mL/min ($T = 35$ °C). GPC traces were processed by WinGPC 8.0 software (PSS) using a calibration based on linear polystyrene (PSty) standards. CVs and CAs were recorded by a Gamry Ref 600 potentiostat. During the *e*ATRP, a condenser was connected to the reaction cell and maintained at -10 °C using a circulating chiller (NESLAB Inc.,

RTE-111). Particle size and size distribution were determined by using a Zetasizer Nano from Malvern Instruments, Ltd.

V. 6. References

1. (a) Wang, J. S.; Matyjaszewski, K., *J Am Chem Soc* **1995**, *117* (20), 5614-5615; (b) Coessens, V.; Pintauer, T.; Matyjaszewski, K., *Prog. Polym. Sci.* **2001**, *26* (3), 337-377; (c) Matyjaszewski, K.; Xia, J. H., *Chem Rev* **2001**, *101* (9), 2921-2990; (d) Braunecker, W. A.; Matyjaszewski, K., *Prog Polym Sci* **2007**, *32* (1), 93-146; (e) Matyjaszewski, K., *Macromolecules* **2012**, *45* (10), 4015-4039; (f) Matyjaszewski, K., *Isr. J. Chem.* **2012**, *52* (3-4), 206-220; (g) Matyjaszewski, K.; Tsarevsky, N. V., *J. Am. Chem. Soc.* **2014**; (h) Kamigaito, M.; Ando, T.; Sawamoto, M., *Chem. Rev.* **2001**, *101* (12), 3689-3746.
2. (a) Davis, K. A.; Matyjaszewski, K., Statistical, Gradient, Block, and Graft Copolymers by Controlled/Living Radical Polymerizations. In *Advances in Polymer Science*, Springer Berlin / Heidelberg: 2002; Vol. 159; (b) Matyjaszewski, K.; Spanswick, J., 3.12 - Copper-Mediated Atom Transfer Radical Polymerization. In *Polymer Science: A Comprehensive Reference*, Editors-in-Chief: Krzysztof, M.; Martin, M., Eds. Elsevier: Amsterdam, 2012; pp 377-428; (c) Matyjaszewski, K., *Science* **2011**, *333*, 1104-1105; (d) Gao, H.; Matyjaszewski, K., *Prog. Polym. Sci.* **2009**, *34*, 317-350; (e) Blencowe, A.; Tan, J. F.; Goh, T. K.; Qiao, G. G., *Polymer* **2009**, *50* (1), 5-32.
3. (a) Qiu, J.; Matyjaszewski, K., *Macromolecules* **1997**, *30* (19), 5643-5648; (b) Teodorescu, M.; Matyjaszewski, K., *Macromolecules* **1999**, *32* (15), 4826-4831; (c) Wever, D. A. Z.; Raffa, P.; Picchioni, F.; Broekhuis, A. A., *Macromolecules* **2012**, *45* (10), 4040-4045.
4. (a) Honigfort, M. E.; Brittain, W. J.; Bosanac, T.; Wilcox, C. S., *Macromolecules* **2002**, *35* (13), 4849-4851; (b) Hong, S. C.; Matyjaszewski, K., *Macromolecules* **2002**, *35* (20), 7592-7605; (c) Sarbu, T.; Pintauer, T.; McKenzie, B.; Matyjaszewski, K., *Journal of Polymer Science Part A: Polymer Chemistry* **2002**, *40* (18), 3153-3160; (d) Yang, J.; Ding, S.; Radosz, M.; Shen, Y., *Macromolecules* **2004**, *37* (5), 1728-1734; (e) Barré, G.; Taton, D.; Lastécouères, D.; Vincent, J.-M., *J Am Chem Soc* **2004**, *126* (25), 7764-7765; (f) Duquesne, E.; Labruyère, C.; Habimana, J.; Degée, P.; Dubois, P., *Journal of Polymer Science Part A: Polymer Chemistry* **2006**, *44* (2), 744-756; (g) Munirasu, S.; Deshpande, A.; Baskaran, D., *Macromolecular Rapid Communications* **2008**, *29* (18), 1538-1543.
5. (a) Matyjaszewski, K.; Jakubowski, W.; Min, K.; Tang, W.; Huang, J. Y.; Braunecker, W. A.; Tsarevsky, N. V., *P Natl Acad Sci USA* **2006**, *103* (42), 15309-15314; (b) Matyjaszewski, K.; Dong, H.; Jakubowski, W.; Pietrasik, J.; Kusumo, A., *Langmuir* **2007**, *23* (8), 4528-4531; (c) Stoffelbach, F.; Griffete, N.; Bui, C.; Charleux, B., *Chemical Communications* **2008**, (39), 4807-4809; (d) Chan, N.; Cunningham, M. F.; Hutchinson, R. A., *Macromol. Chem. Phys.* **2008**, *209* (17), 1797-1805; (e) Jakubowski, W.; Kirci-Denizli, B.; Gil, R. R.; Matyjaszewski, K., *Macromol. Chem. Phys.* **2008**, *209* (1), 32-39; (f) Kwak, Y.; Matyjaszewski, K., *Polym Int* **2009**, *58* (3), 242-247; (g) Nicolay, R.; Kwak, Y.; Matyjaszewski, K., *Angew Chem Int Edit* **2010**, *49* (3), 541-544; (h) Kwak, Y.; Magenau, A. J. D.; Matyjaszewski, K., *Macromolecules* **2011**, *44* (4), 811-819; (i)

- Simakova, A.; Averick, S. E.; Konkolewicz, D.; Matyjaszewski, K., *Macromolecules* **2012**, *45* (16), 6371-6379.
6. (a) Mueller, L.; Jakubowski, W.; Tang, W.; Matyjaszewski, K., *Macromolecules* **2007**, *40* (18), 6464-6472; (b) Plichta, A.; Li, W. W.; Matyjaszewski, K., *Macromolecules* **2009**, *42* (7), 2330-2332; (c) Zhang, L.; Miao, J.; Cheng, Z.; Zhu, X., *Macromolecular Rapid Communications* **2010**, *31* (3), 275-280; (d) Zhu, G.; Zhang, L.; Zhang, Z.; Zhu, J.; Tu, Y.; Cheng, Z.; Zhu, X., *Macromolecules* **2011**, *44* (9), 3233-3239; (e) D'hooge, D. R.; Konkolewicz, D.; Reyniers, M. F.; Marin, G. B.; Matyjaszewski, K., *Macromol Theor Simul* **2012**, *21* (1), 52-69; (f) Konkolewicz, D.; Magenau, A. J. D.; Averick, S. E.; Simakova, A.; He, H.; Matyjaszewski, K., *Macromolecules* **2012**, *45* (11), 4461-4468; (g) Matyjaszewski, K.; Jakubowski, W.; Min, K.; Tang, W.; Huang, J.; Braunecker, W. A.; Tsarevsky, N. V., *Proceedings of the National Academy of Sciences* **2006**, *103* (42), 15309-15314; (h) Mohammad Rabea, A.; Zhu, S., *Industrial & Engineering Chemistry Research* **2014**, *53* (9), 3472-3477.
7. (a) Matyjaszewski, K.; Tsarevsky, N. V.; Braunecker, W. A.; Dong, H.; Huang, J.; Jakubowski, W.; Kwak, Y.; Nicolay, R.; Tang, W.; Yoon, J. A., *Macromolecules* **2007**, *40* (22), 7795-7806; (b) Konkolewicz, D.; Wang, Y.; Zhong, M. J.; Krys, P.; Isse, A. A.; Gennaro, A.; Matyjaszewski, K., *Macromolecules* **2013**, *46* (22), 8749-8772; (c) Abreu, C. M. R.; Serra, A. C.; Popov, A. V.; Matyjaszewski, K.; Guliashvili, T.; Coelho, J. F. J., *Polym Chem-Uk* **2013**, *4* (23), 5629-5636; (d) Gois, J. R.; Konkolewicz, D.; Popov, A. V.; Guliashvili, T.; Matyjaszewski, K.; Serra, A. C.; Coelho, J. F. J., *Polym Chem-Uk* **2014**, *5* (16), 4617-4626; (e) Konkolewicz, D.; Krys, P.; Gois, J. R.; Mendonca, P. V.; Zhong, M. J.; Wang, Y.; Gennaro, A.; Isse, A. A.; Fantin, M.; Matyjaszewski, K., *Macromolecules* **2014**, *47* (2), 560-570; (f) Konkolewicz, D.; Wang, Y.; Krys, P.; Zhong, M. J.; Isse, A. A.; Gennaro, A.; Matyjaszewski, K., *Polym Chem-Uk* **2014**, *5* (15), 4396-4417; (g) Rosen, B. M.; Percec, V., *Chem. Rev.* **2009**, *109* (11), 5069-5119.
8. (a) Erel, I.; Cianga, I.; Serhatli, E.; Yagci, Y., *European Polymer Journal* **2002**, *38* (7), 1409-1415; (b) Wang, G.; Zhu, X.; Wu, J.; Zhu, J.; Chen, X.; Cheng, Z., *Journal of Applied Polymer Science* **2007**, *106* (2), 1234-1242; (c) Ishizu, K.; Murakami, T.; Takano, S., *Journal of Colloid and Interface Science* **2008**, *322* (1), 59-64; (d) Tasdelen, M. A.; Uygun, M.; Yagci, Y., *Macromol. Chem. Phys.* **2011**, *212* (18), 2036-2042; (e) Konkolewicz, D.; Schroder, K.; Buback, J.; Bernhard, S.; Matyjaszewski, K., *Acs Macro Lett* **2012**, *1* (10), 1219-1223; (f) Tasdelen, M. A.; Ciftci, M.; Yagci, Y., *Macromolecular Chemistry and Physics* **2012**, *213* (13), 1391-1396; (g) Taskin, O. S.; Yilmaz, G.; Tasdelen, M. A.; Yagci, Y., *Polym Int* **2014**, *63* (5), 902-907; (h) Ribelli, T. G.; Konkolewicz, D.; Pan, X. C.; Matyjaszewski, K., *Macromolecules* **2014**, *47* (18), 6316-6321; (i) Zhang, T.; Chen, T.; Amin, I.; Jordan, R., *Polym Chem-Uk* **2014**, *5* (16), 4790-4796; (j) Ribelli, T. G.; Konkolewicz, D.; Bernhard, S.; Matyjaszewski, K., *J Am Chem Soc* **2014**, *136* (38), 13303-13312.
9. (a) Magenau, A. J. D.; Strandwitz, N. C.; Gennaro, A.; Matyjaszewski, K., *Science* **2011**, *332* (6025), 81-84; (b) Bortolamei, N.; Isse, A. A.; Magenau, A. J. D.; Gennaro, A.; Matyjaszewski, K., *Angew. Chem. Int. Ed.* **2011**, *50* (48), 11391-11394; (c) Magenau, A. J. D.; Bortolamei, N.; Frick, E.; Park, S.; Gennaro, A.; Matyjaszewski, K., *Macromolecules* **2013**, *46* (11), 4346-4353; (d) Park, S.; Cho, H. Y.; Wegner, K. B.; Burdyska, J.; Magenau, A. J. D.; Paik, H.-j.; Jurga, S.; Matyjaszewski, K., *Macromolecules* **2013**, *46* (15), 5856-

5860; (e) Chmielarz, P.; Park, S.; Simakova, A.; Matyjaszewski, K., *Polymer* **2015**, *60* (0), 302-307; (f) Chmielarz, P.; Park, S.; Sobkowiak, A.; Matyjaszewski, K., *Polymer* **2016**, *88*, 36-42; (g) Park, S.; Chmielarz, P.; Gennaro, A.; Matyjaszewski, K., *Angew. Chem.* **2015**, *127* (8), 2418-2422; (h) Yan, J.; Li, B.; Yu, B.; Huck, W. T.; Liu, W.; Zhou, F., *Angew. Chem. Int. Ed.* **2013**, *52* (35), 9125-9129; (i) Li, B.; Yu, B.; Huck, W. T. S.; Liu, W.; Zhou, F., *J. Am. Chem. Soc.* **2013**, *135* (5), 1708-1710; (j) Li, B.; Yu, B.; Huck, W. T. S.; Zhou, F.; Liu, W., *Angew. Chem. Int. Ed.* **2012**, *51* (21), 5092-5095; (k) Inagi, S.; Fuchigami, T., *Macromol. Rapid Commun.* **2014**, *35* (9), 854-867.

10. (a) Min, K.; Matyjaszewski, K., *Macromolecules* **2005**, *38* (20), 8131-8134; (b) Kagawa, Y.; Kawasaki, M.; Zetterlund, P. B.; Minami, H.; Okubo, M., *Macromolecular Rapid Communications* **2007**, *28* (24), 2354-2360.

11. (a) Min, K.; Gao, H. F.; Matyjaszewski, K., *J. Am. Chem. Soc.* **2005**, *127* (11), 3825-3830; (b) Min, K.; Jakubowski, W.; Matyjaszewski, K., *Macromolecular Rapid Communications* **2006**, *27* (8), 594-598; (c) Bombalski, L.; Min, K.; Dong, H. C.; Tang, C. B.; Matyjaszewski, K., *Macromolecules* **2007**, *40* (21), 7429-7432.

12. (a) Qiu, J.; Gaynor, S. G.; Matyjaszewski, K., *Macromolecules* **1999**, *32* (9), 2872-2875; (b) Jousset, S.; Qiu, J.; Matyjaszewski, K., *Macromolecules* **2001**, *34* (19), 6641-6648; (c) Eslami, H.; Zhu, S. P., *Polymer* **2005**, *46* (15), 5484-5493; (d) Eslami, H.; Zhu, S. P., *Journal of Polymer Science Part a-Polymer Chemistry* **2006**, *44* (6), 1914-1925; (e) Min, K.; Gao, H.; Yoon, J. A.; Wu, W.; Kowalewski, T.; Matyjaszewski, K., *Macromolecules* **2009**, *42* (5), 1597-1603.

13. (a) Cunningham, M. F., *Prog. Polym. Sci.* **2008**, *33* (4), 365-398; (b) Min, K.; Matyjaszewski, K., *Central European Journal of Chemistry* **2009**, *7* (4), 657-674; (c) Qiu, J.; Charleux, B.; Matyjaszewski, K., *Prog Polym Sci* **2001**, *26* (10), 2083-2134; (d) Zetterlund, P. B.; Kagawa, Y.; Okubo, M., *Chem. Rev.* **2008**, *108* (9), 3747-3794; (e) Asua, J. M., *Prog. Polym. Sci.* **2014**, *39* (10), 1797-1826.

14. Asua, J. M., *Prog. Polym. Sci.* **2002**, *27* (7), 1283-1346.

15. (a) Antonietti, M.; Landfester, K., *Prog. Polym. Sci.* **2002**, *27* (4), 689-757; (b) Schork, F. J.; Poehlein, G. W.; Wang, S.; Reimers, J.; Rodrigues, J.; Samer, C., *Colloids Surf. Physicochem. Eng. Aspects* **1999**, *153* (1-3), 39-45.

16. Elsen, A. M.; Burdynska, J.; Park, S.; Matyjaszewski, K., *Macromolecules* **2012**, *45* (18), 7356-7363.

17. (a) Xia, J.; Matyjaszewski, K., *Macromolecules* **1999**, *32* (8), 2434-2437; (b) Xia, J.; Gaynor, S. G.; Matyjaszewski, K., *Macromolecules* **1998**, *31* (17), 5958-5959.

18. (a) Tang, W.; Kwak, Y.; Braunecker, W.; Tsarevsky, N. V.; Coote, M. L.; Matyjaszewski, K., *J. Am. Chem. Soc.* **2008**, *130* (32), 10702-10713; (b) Tang, W.; Matyjaszewski, K., *Macromolecules* **2006**, *39* (15), 4953-4959.

19. Schmickler, W.; Santos, E., *Interfacial electrochemistry*. Springer Science & Business Media: 2010.

20. (a) Tsarevsky, N. V.; Pintauer, T.; Matyjaszewski, K., *Macromolecules* **2004**, *37* (26), 9768-9778; (b) Fantin, M.; Isse, A. A.; Gennaro, A.; Matyjaszewski, K., *Macromolecules* **2015**, *48* (19), 6862-6875.

21. Braunecker, W. A.; Tsarevsky, N. V.; Gennaro, A.; Matyjaszewski, K., *Macromolecules* **2009**, *42* (17), 6348-6360.

22. Teo, V. L.; Davis, B. J.; Tsarevsky, N. V.; Zetterlund, P. B., *Macromolecules* **2014**, 47 (18), 6230-6237.
23. Kickelbick, G.; Paik, H.-j.; Matyjaszewski, K., *Macromolecules* **1999**, 32 (9), 2941-2947.

Chapter VI

Electrochemically Mediated Reversible Addition- Fragmentation Chain Transfer Polymerization of Methyl Methacrylate*

VI. 1. Preface

The results of an investigation of electrochemically mediated reversible addition-fragmentation chain transfer (RAFT) polymerization of methyl methacrylate (MMA) are reported in the chapter. The two approaches that were the main focus of this study were a concurrent electrochemically mediated atom transfer radical polymerization (*e*ATRP)/RAFT and a pure *e*RAFT polymerization. In the concurrent *e*ATRP/RAFT polymerization, the added chain transfer agents (CTAs) were activated by electrochemically reduced Cu^I/ligand catalysts, resulting in controlled radical polymerization that followed either an ATRP or the RAFT mechanism. Four parameters were exploited to achieve the optimal polymerization conditions, including different (pseudo)halides, ligands, catalysts concentrations, and applied potentials (E_{app} s). The best conditions for *e*ATRP/RAFT of MMA were attained by utilizing high loadings of the CuBr/bpy catalyst system. However the high concentration of transition metal catalysts residues in the final products would have adverse effects on the application of the products

*Work in this Chapter will be submitted for publication.

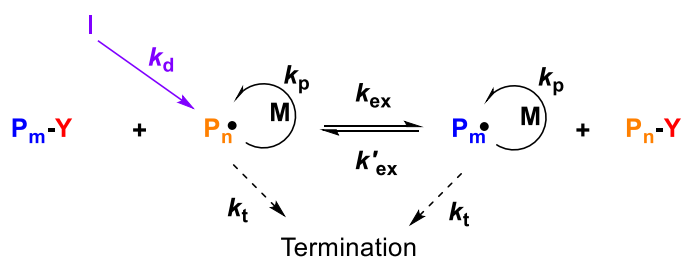
as advanced materials. Therefore, a metal-free system was highly desired. The second approach, a pure *e*RAFT procedure, eliminated employment of a transition metal catalyst. In the latter system, the radical species could be introduced by electrolysis a conventional radical source, *e.g.*, benzoyl peroxide (BPO) or other free radical generating chemical compound (*i.e.*, aryl diazonium compounds). Two radical sources, BPO and 4-bromobenzyl diazonium, were selected and electrolyzed for the initiation of *e*RAFT polymerization. Several parameters were investigated to achieve good control for an *e*RAFT polymerization of MMA, including radical sources, species of working electrodes, and applied potentials. Under the optimized conditions, well-defined PMMAs were synthesized at the targeted degree of polymerization. My role in this project was to optimize polymerization conditions and analyze the results, resulting in a major contribution to the project.

I would like to acknowledge Yi Wang and Dr. Marco Fantin for their contributions to the project and helpful discussions.

VI. 2. Introduction

Reversible addition-fragmentation chain transfer (RAFT) polymerization has been highlighted as a robust and powerful tool for the synthesis of well-defined (co)polymers with predicted molecular weights (MWs) and narrow molecular weight distributions (MWDs). A wide range of vinyl monomers, *i.e.*, (meth)acrylate, styrene, acrylamide, and vinyl acetate were successfully polymerized by RAFT.¹²³ In addition, copolymers with complex architecture, *e.g.*, star, hyper branched, and polymeric bottle brushes, were synthesized.^{58, 124}

Typically, RAFT requires a conventional radical source, *e.g.*, 2,2'-azobis(2-methylpropionitrile) (AIBN) to form radical species (R^\bullet) that subsequently react with monomers (M) or chain transfer agents (CTA) initiating exchange reactions (k_{ex}) between propagating chains. Multiple exchange reactions result in uniform growth of the polymeric chains and well-defined polymers can be obtained (Scheme VI-1). Since termination reactions could occur during the polymerization, a continuous supply of radicals by thermal degradation may be required to compensate for the chain termination reaction.^{123a, 125}



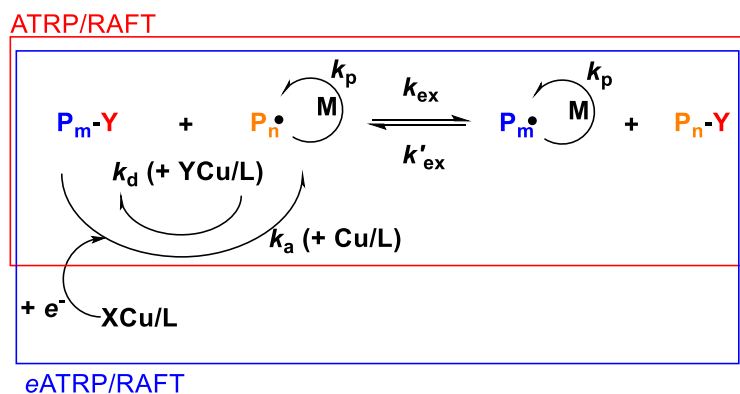
Scheme VI-1. General mechanism for RAFT polymerization.

One major disadvantage of RAFT polymerization is the undesired decomposition of chain-end functionalities, such as hydrolysis, aminolysis, and thermal degradation.^{123a} Indeed thermolysis, one of the chain-end degradation reactions, would be unavoidable due to the thermal-induced decomposition of conventional radical sources during the polymerization. The production of polymers lacking chain-end functionalities would be limited the use of products for advanced materials, *e.g.*, materials requiring well-defined polymeric architecture. Several techniques were developed to avoid or minimize the loss of chain-end functionalities, such as room temperature RAFT,¹²⁶ photo-induced RAFT,¹²⁷ and concurrent atom transfer radical polymerization (ATRP)/RAFT.¹²⁸ Such alternative techniques could prevent the loss of chain-end functionalities and allow for preparation of well-defined polymers.

Electrochemically mediated controlled polymerization, especially in ATRP, showed unique advantages that not only involved on-off polymerization but also the ability to control the rate of polymerization (R_p) by applied electric potential, current, or total passed charges.^{10-12, 129} Furthermore, high yield of polymers with complex polymeric architecture, *e.g.*, star polymers, were successfully achieved by controlling R_p and minimizing initial termination reactions.^{13b} In this chapter, concurrent ATRP/RAFT polymerization under electrochemically control is examined to further expand the concept of electrochemically mediated control radical polymerization to RAFT polymerization. Radical sources were introduced to the reaction mixture by electrolysis, and well-defined poly(methyl methacrylates (PMMA) were synthesized. Several reaction conditions were investigated, including radical sources, electrodes, and total reaction volume.

VI. 3. Results and Discussion

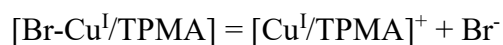
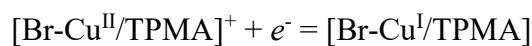
Concurrent *e*ATRP/RAFT Polymerization with 1-Cyano-1-methylethyldiethyl Dithiocarbamate (MANDC). MANDC showed poor chain transfer efficiency for the polymerization of methyl methacrylate (MMA) polymerization.^{123a} However, when the polymerization was carried out in the presence of an ATRP catalysts ($\text{Cu}^{\text{I}}/\text{L}$) the DC groups acted as pseudo-halogen (Scheme VI-2, red box) and the overall reaction followed an ATRP mechanism.¹³⁰ When this observation was combined with electrochemistry the highly oxidized $\text{X-Cu}^{\text{II}}/\text{L}$ could be reduced to $\text{Cu}^{\text{I}}/\text{L}$ and subsequently react with CTAs in a concurrent ATRP/RAFT reaction, Scheme VI-2, blue box. Various MMA polymerizations with MANDC/ Cu/L were examined in order to elucidate the proposed mechanism.

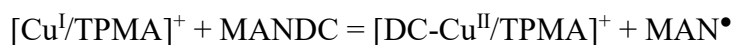


Scheme VI-2. Concurrent ATRP/RAFT polymerization (red box) and electrochemically mediated ATRP/RAFT polymerization (blue box).

Table VI-1 lists the results of concurrent *e*ATRP/RAFT polymerization of MMA in the presence of different copper (II) species (Br and DC), ligands, applied potentials (E_{appS}),

and solvents that were examined to optimize the polymerization conditions. To determine the effect of E_{app} s the reaction was carried out under two similar conditions, Table VI-1, entry 1 and 2, Figure VI-1, and Figure VI-2 by chronoamperometry (CA) applying a constant potential. In CV measurements, cathodic and anodic peaks of CuBr₂/TPMA were shifted, indicating activation of MANDC by electrochemical catalytic (EC') behavior. A slightly faster polymerization was observed at a more negative E_{app} (apparent propagation rate constant, $k_p^{app} = 0.10$ vs. 0.07 h^{-1}). Both polymerizations showed a higher $M_{n, GPC}$ than $M_{n, th}$ in the initial time periods and M_w/M_n values were generally broad > 1.4 . Such uncontrolled results could be mainly due to the change of catalysts species during the polymerization, *i.e.*, CuBr/TPMA \rightarrow CuDC/TPMA (Scheme VI-3). Indeed after the polymerization, CV results (Figure VI-1F) showed a newly formed CuDC/TPMA redox peak (reversible, $E_{1/2} = 0 \text{ V}$ vs. Ag/AgI/I⁻. *cf.* $E_{1/2}$ of CuBr₂/TPMA = 0.31 V) and bromide oxidation¹³¹ (irreversible, $E_{pa} = 1.02$ and 1.16 V). When polymerization was carried out under the selected E_{app} s for CuBr₂/TPMA, the potentials then generated a more Cu^{II} dominant condition, mostly deactivation, when the reactions proceeded. When the polymerization was carried out in the presence of a less polar solvent, *i.e.*, anisole, Table VI-1, entry 2 vs. 3, and Figure VI-3, a similar apparent polymerization rate was observed and CuDC/TPMA formation was observed.





Scheme VI-3. CuDC₂/TPMA formation.

Table VI-1. Summary of MMA polymerization by concurrent *e*ATRP/RAFT

Entry	[M]/ [MANDC]	CuX ₂	L	[Cu/L] (ppm)	<i>E</i> _{app}	Conv (%) ^a	<i>M</i> _{n, GPC} (× 10 ³) ^b	<i>M</i> _{n, th} (× 10 ⁻³) ^c	<i>M</i> _w / <i>M</i> _n ^b
1	400	CuBr ₂	TPMA	100	0.24 ^d	62	25.5	25.0	1.46
2	400	CuBr ₂	TPMA	100	0.25 ^e	64	26.5	25.8	1.42
3 ^g	400	CuBr ₂	TPMA	100	0.32 ^e	53	22.6	21.4	1.60
4	400	CuDC ₂	TPMA	100	-0.01 ^e	36	23.1	14.6	1.51
5	185	CuBr ₂	bpy	2700	-0.25 ^f	81	12.5	15.2	1.34

General polymerization condition: [MMA] = 4.67 M in DMF; *T* = 80 °C; WE = Pt mesh; CE = Pt mesh (separated by supporting electrolyte saturated methylated cellulose); RE = Ag/AgI/I⁻; ^adetermined by ¹H NMR after 24 h; ^bdetermined by THF GPC with PMMA calibration; ^ccalculated by [M]/[CTA] × Conv + *MW*_{CTA}; ^d*E*_{pc, CuBr₂/TPMA}; ^e*E*_{1/2 CuX₂/TPMA}; ^f*E*_{1/2 CuBr₂/bpy} – 500 mV; ^gin anisole.

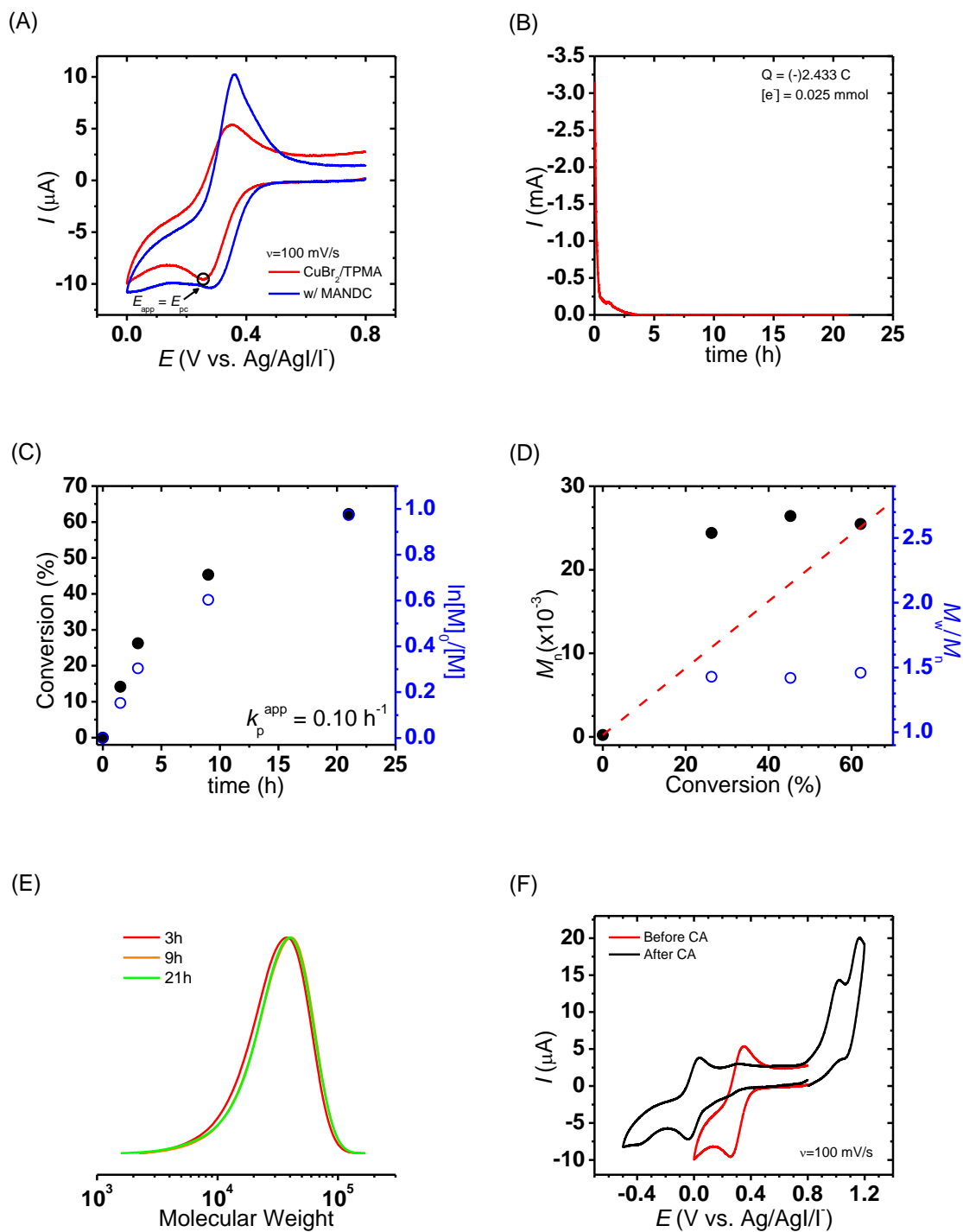
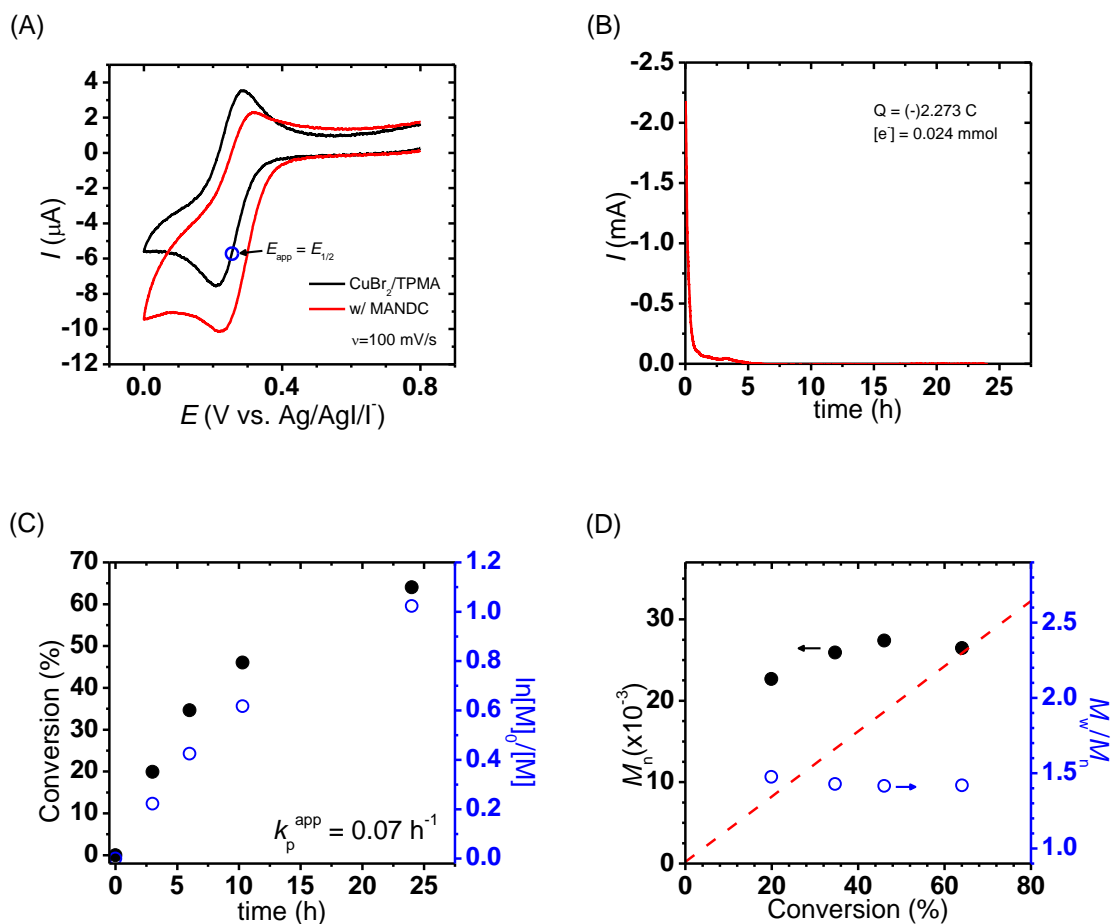


Figure VI-1. Polymerization of MMA by concurrent *e*ATRP/RAFT under $E_{app} = E_{pc}$

(Table VI-1, entry 1). (A) CV spectra of CuBr₂/TPMA without or with MANDC (red and

blue, respectively); (B) CA curve for MMA polymerization; (C) monomer consumption vs. reaction time; (D) MW and MWD vs. monomer conversion; (E) GPC trace of the polymerization; (F) CV spectra of before and after polymerization.



(F)

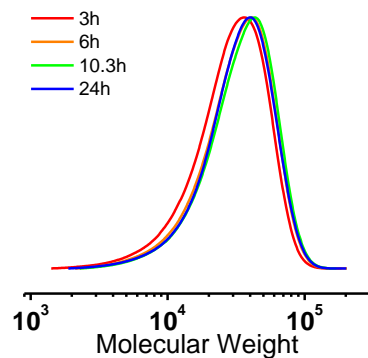
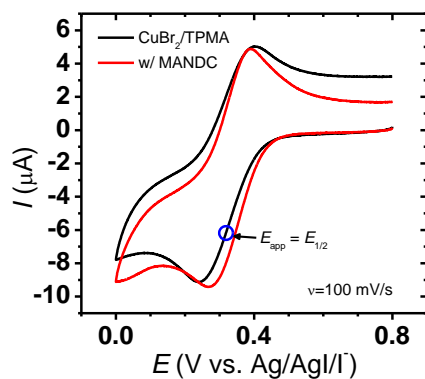
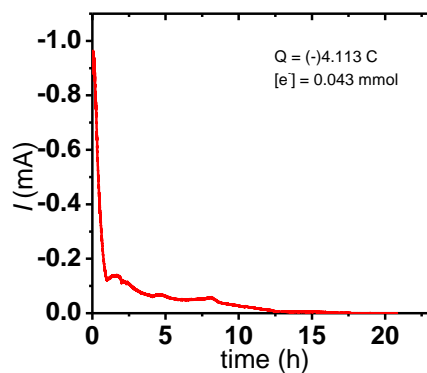


Figure VI-2. Polymerization of MMA by concurrent *e*ATRP/RAFT under $E_{\text{app}} = E_{1/2}$ (Table VI-1, entry 2). (A) CV spectra of $\text{CuBr}_2/\text{TPMA}$ without or with MANDC (black and red, respectively); (B) CA curve for MMA polymerization; (C) monomer consumption vs. reaction time; (D) MW and MWD vs. monomer conversion; (E) GPC trace of the polymerization.

(A)



(B)



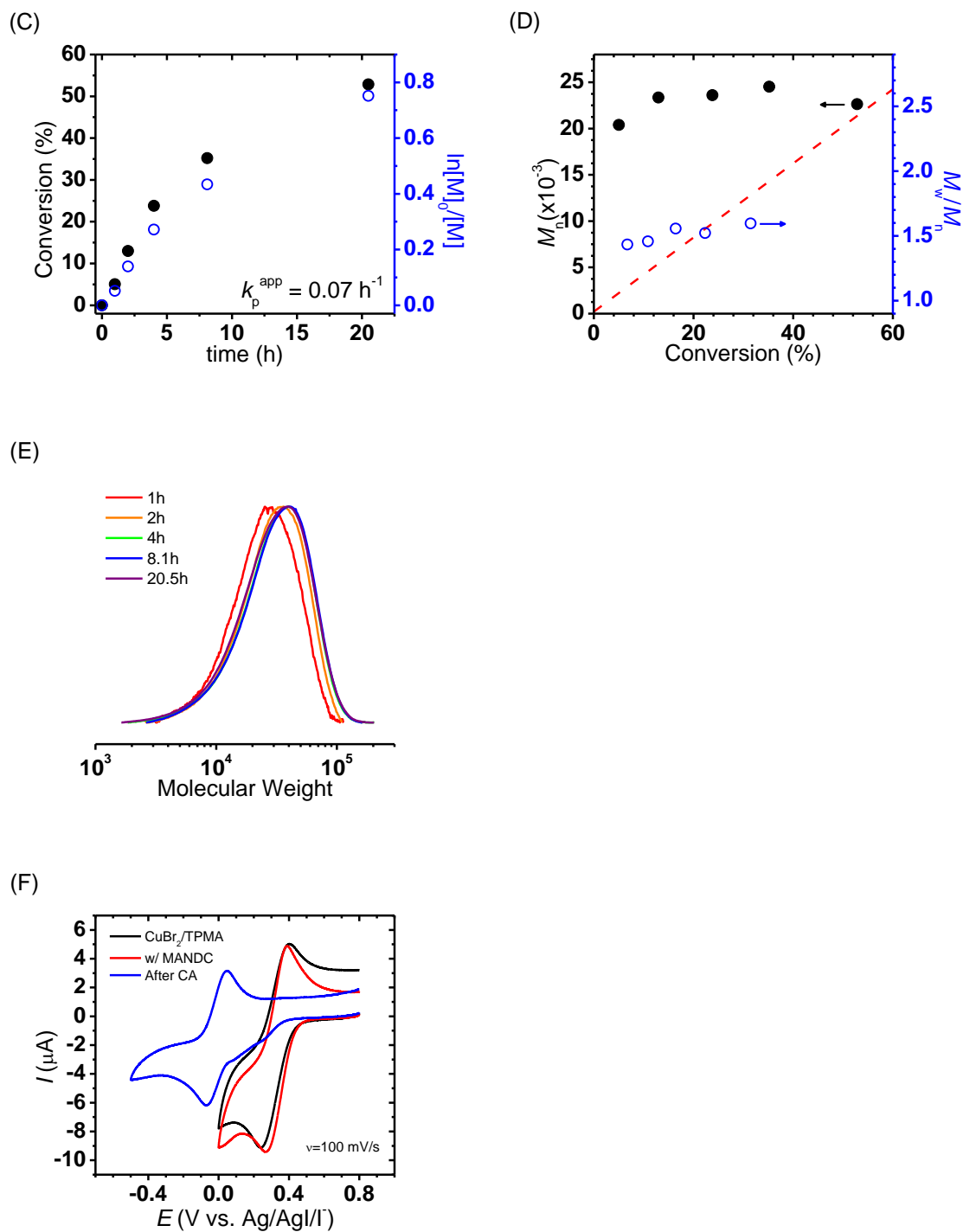


Figure VI-3. Polymerization of MMA by concurrent *e*ATRP/RAFT under $E_{\text{app}} = E_{1/2}$ in anisole (Table VI-1, entry 3) (A) CV spectra of CuBr₂/TPMA without or with MANDC

(black and red, respectively); (B) CA curve for MMA polymerization; (C) monomer consumption vs. reaction time; (D) MW and MWD vs. monomer conversion; (E) GPC trace of the polymerization. (F) CV spectra of before and after polymerization.

During the polymerization, the CuBr/L complex formed a CuDC/L complex and to avoid undesired changes in the ratio of $[Cu^I/L]/[Cu^{II}/L]$ during the polymerization, due to catalysts changes, a CuDC₂/TPMA was selected as catalysts (Table VI-1, entry 4) under $E_{app} = E_{1/2, CuDC/TPMA}$. The results showed an even lower R_p and conversion than identical reaction conditions with CuBr₂/TPMA (Table VI-1, entry 2 vs. 4). Typically, activation of alkyl pseudohalogen is very sensitive to the selection of catalyst combinations,¹³⁰ probably CuDC/TPMA combination was mismatched with MANDC.

When polymerizations were conducted with CuX/TPMA catalysts, polymers with a higher MW and broad MWD were observed. In order to achieve a higher monomer conversion (> 80%) with a uniform polymeric structure, different catalysts were examined *i.e.*, CuBr₂/bpy. Based on previous researches on the concurrent ATRP/RAFT of MMA,¹³⁰ CuBr/bpy was considered to be a good candidate for MMA polymerization in the presence of MANDC. In addition, higher concentrations of the copper catalysts were expected to improve deactivation steps during the polymerization. MMA polymerizations with a high CuBr₂/bpy concentration (*ca.* 2700 ppm) were used for the concurrent *e*ATRP/RAFT (Table VI-1, entry 5, and Figure VI-5). E_{app} was selected as $E_{1/2, CuBr_2/bpy} - 500$ mV, the E_{app} value was under Cu^I dominant conditions for both CuBr/bpy and CuDC/bpy. Under this particular condition, 81% monomer conversion was observed and a relatively narrow

MWD was obtained ($M_w/M_n = 1.34$). Even though polymerization was successfully carried out, the system required a high concentration of catalyst. Therefore, purification would be required from the synthesized products.

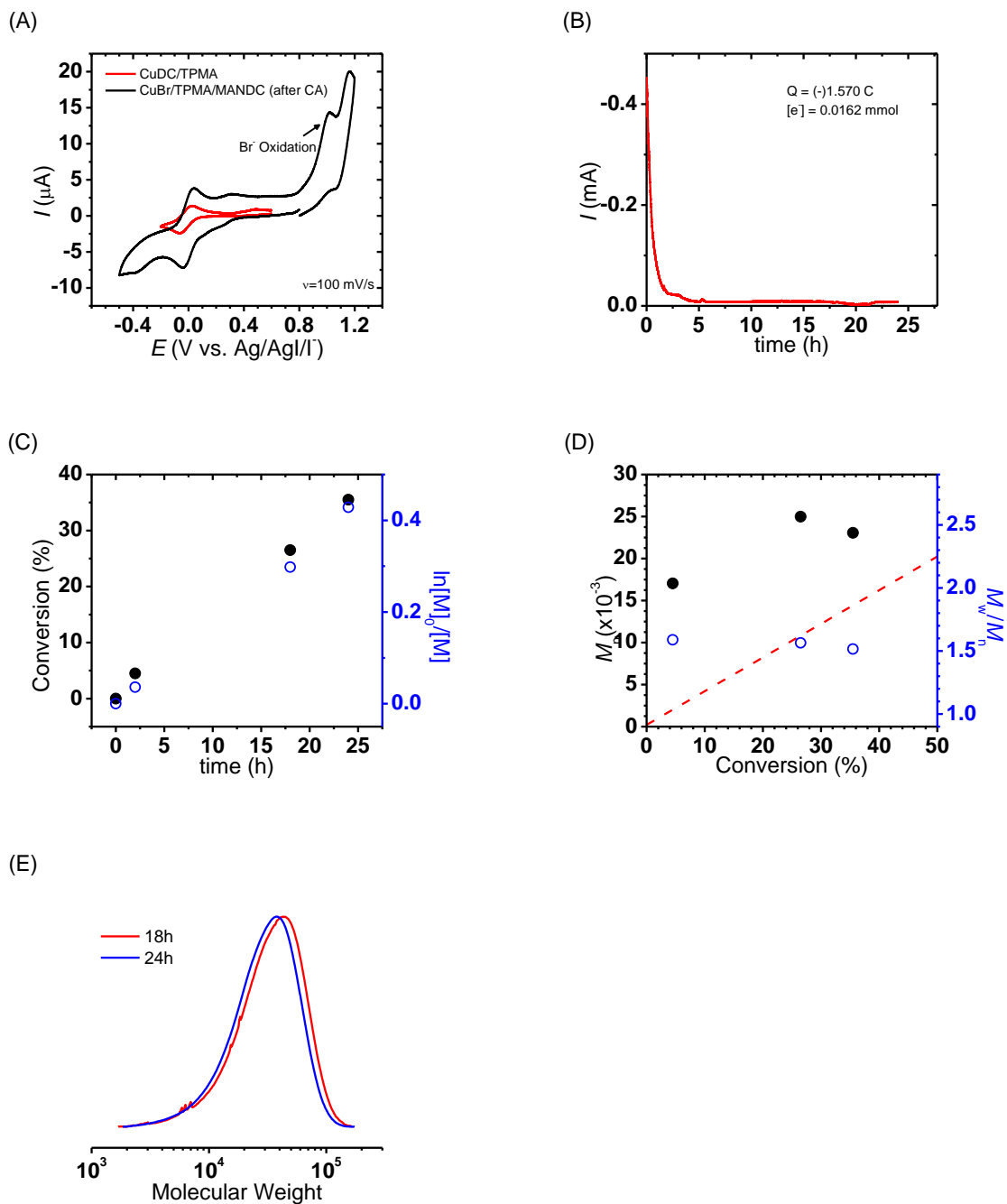


Figure VI-4. Polymerization of MMA by concurrent *e*ATRP/RAFT with CuDC₂/TPMA (Table VI-1, entry 4) (A) comparing CV spectra of CuDC₂/TPMA (red) and after polymerization with CuBr₂/TPMA/MANDC (black); (B) CA curve for MMA polymerization; (C) monomer consumption vs. reaction time; (D) MW and MWD vs. monomer conversion; (E) GPC trace of the polymerization.

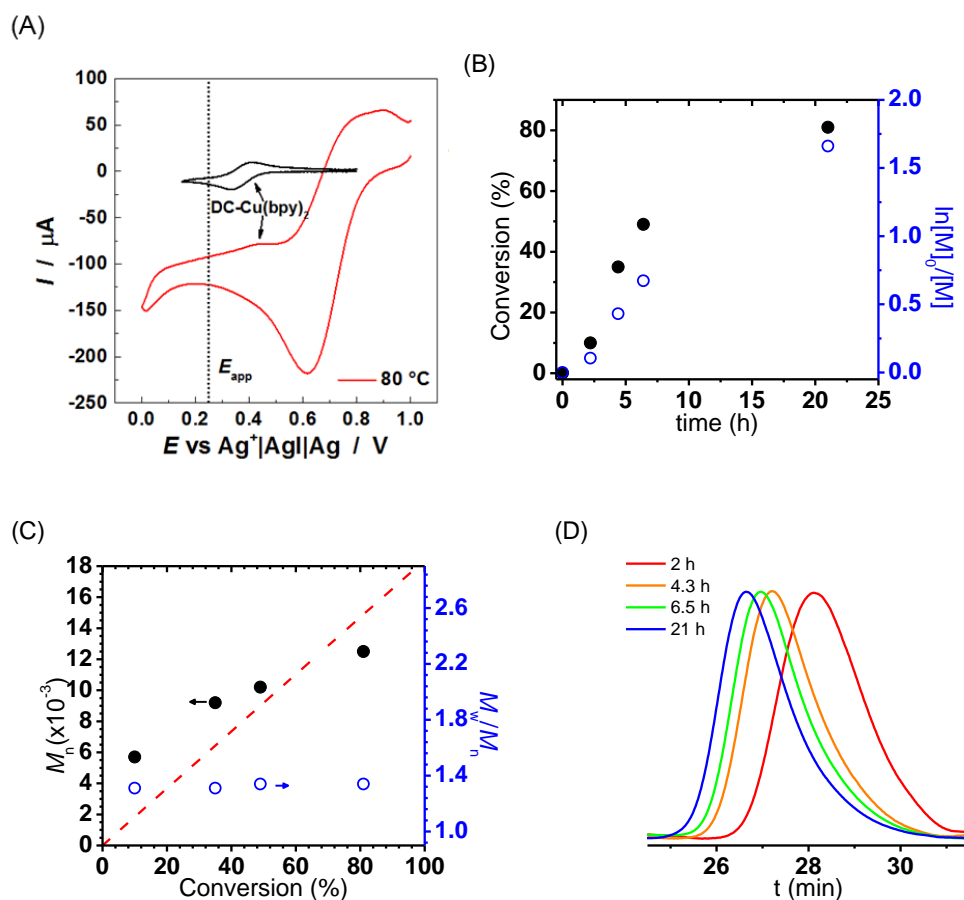
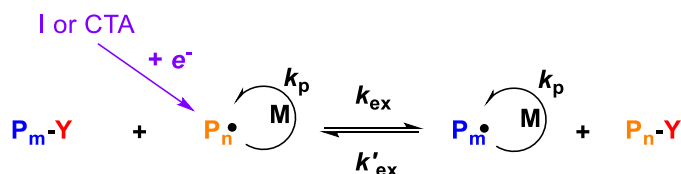


Figure VI-5. Polymerization of MMA by concurrent *e*ATRP/RAFT with CuBr₂/bpy catalysts (Table VI-1, entry 5) (A) CV spectra of CuBr/bpy (red) and CuDC/bpy (black); (B) monomer consumption vs. reaction time; (C) MW and MWD vs. monomer conversion;

(D) GPC eluogram of the polymerization.

From Concurrent *e*ATRP/RAFT to *e*RAFT. The optimal conditions for concurrent *e*ATRP/RAFT of MMA was use of MANDC as transfer agent with high concentration of CuBr₂/bpy. The resulting polymers containing a high concentration of transition metal catalysts which would be a challenge for potential applications requiring advanced materials. Thus, additional purification steps would be required. On the other hand, RAFT polymerization typically employed only organic compounds, such as CTAs, radical sources (*e.g.*, AIBN), and monomers. In the conventional RAFT process, polymerization is initiated by thermal dissociation of radical sources and heating does not significantly affect the final products. However, synthesis of temperature responsive polymers in certain solvents would be a challenge. For example, aqueous RAFT polymerization of *N*-isopropylacrylamide (NIPAAm) showed two different R_p s because of the synthesized PNIPAAm aggregated at the elaborated temperatures, *i.e.*, > 32 °C.¹³² As a result, obtaining polymers with uniform structure and predetermined MW was difficult to achieve. Additionally, temperature dependent chain-end degradation was observed from RAFT polymerization of *N*-arylmethacrylamides with trithiocarbonate.¹³³ Therefore, development of a RAFT polymerization at ambient temperature is highly demanded because the process would eliminate or minimize such disadvantages. Several techniques were investigated for ambient temperature polymerization, such as light (or photo) induced RAFT,^{83, 127a, 127b, 134} activation of CTA by reducing agents,¹³⁵ and redox initiation system.^{126b, 136} Herein, electrochemically mediated RAFT polymerization at ambient temperature was investigated. The advantage of *e*RAFT is that it is a relatively simpler

procedure than concurrent *e*ATRP/RAFT, and free from residual transition metal catalysts. Scheme VI-4 shows the proposed mechanism of *e*RAFT polymerization. Radical sources can be introduced directly from electrolysis of CTA or organic compounds, and propagation takes place in the presence of monomers. Exchange reactions were included to prepare uniform and well-defined polymers.



Scheme VI-4. Proposed mechanism of *e*RAFT. Radical species are introduced from a direct electrolysis of conventional initiator or CTA.

Electrochemically Generation of Radicals and MMA Polymerization. Direct electrolysis of 4-cyano-4-(phenylcarbonothioylthio)pentanoic acid (CPPA), benzoyl peroxide (BPO), and 4-bromobenzenediazonium tetrafluoroborate (BBDA) was carried out in the presence of MMA. Electrolysis of CPPA chain transfer agent in the presence of MMA showed no polymerization (Table VI-2, entry 1, Figure VI-6). Therefore detailed electrochemical studies were carried out with 1 mM of pure CPPA solution. The peak current is proportional to the concentration of electroactive compounds ($i_p = 268600n^{3/2}AD^{1/2}Cv^{1/2}$ at $T = 25^\circ\text{C}$, where i_p = potential at maximum peak current, n = number of electrons, A = electrode surface area, D = diffusion coefficient, C = concentration of electroactive compound, and v = scan rate), the electrolysis of the CTA showed a decreased change of cathodic peak intensity (Figure VI-7). Based on the CV and

CA results, two electrons were transferred for electrolysis of CTA, which formed an anionic species and RAFT process could not be initiated.

Table VI-2. Summary of direct electrolysis for free radical polymerization.

Entry	[M]/[R]	R	E_{app}	t (h)	Conv. (%) ^a	Q (C)	k_p^{app}	$M_{n, GPC}$ ($\times 10^{-3}$) ^b	$M_{n, th}$ ($\times 10^{-3}$) ^b	M_w/M_n^b
1	500/1	CPPA	$E_{pc, CPPA} - 80$ mV	16	-	17.942	-	-	-	-
2	4670/1	BPO	$E_{pc, BPO} - 80$ mV	20	37.6	1.025	0.023	71.1	175.8	1.78
3	500/1	BBDA	$E_{pc, BBDA} - 80$ mV	22	8.4	0.003	0.009 ^c	41.2	4.2	1.41

General reaction condition: [MMA] = 4.67 M in DMF; $T = RT$ (~ 22 °C); WE = Pt mesh; CE = Pt mesh (separated by supporting electrolyte saturated methylated cellulose); RE = Ag/AgI/I⁻; $V_{tot} = 30$ mL; [TBAPF₆] = 0.1 M; ^adetermined by ¹H NMR; ^bdetermined by THF GPC with PMMA calibration; ^cinitial time period.

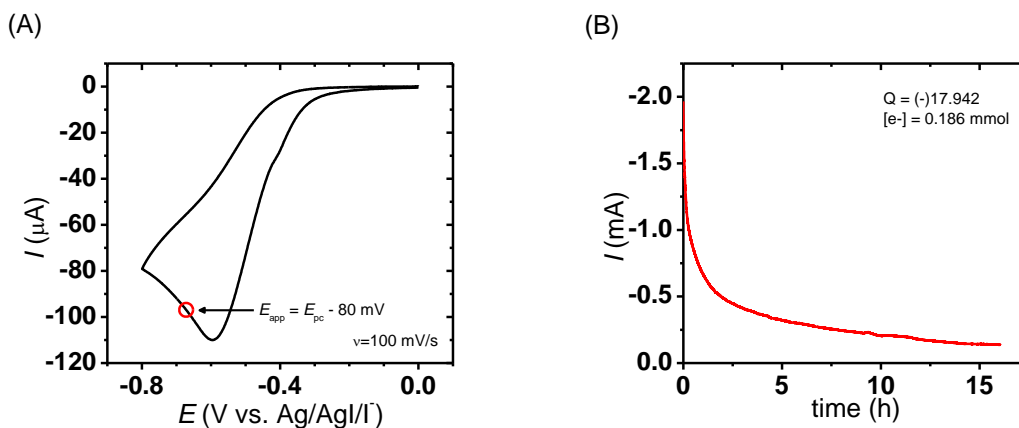


Figure VI-6. Electrolysis of CPPA in the presence of MMA. (A) CV analysis of CPPA

($E_{\text{app}} = E_{\text{pc,CPPA}} - 80 \text{ mV}$) and (B) CA result of electrolysis.

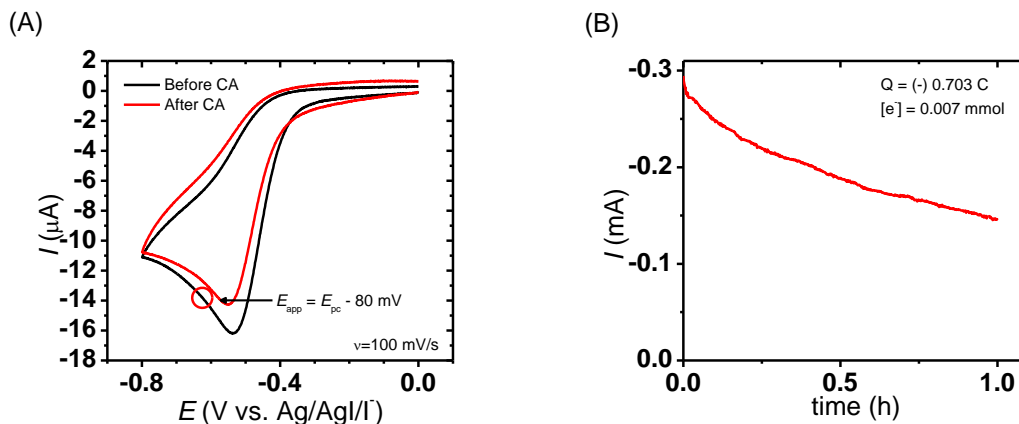


Figure VI-7. Electrolysis of 1 mM of CPPA in DMF. (A) CV of CPPA ($E_{\text{app}} = E_{\text{pc,CPPA}} - 80 \text{ mV}$) and (B) CA result of electrolysis.

On the other hand, free radical polymerization was successfully carried out by electrolysis of BPO (Figure VI-8). 20 h electrolysis of BPO in the presence of MMA generated a PMMA with broad MWD. Another candidate for electrogenerated source of radicals was an aryl diazonium salt. An aryl diazonium can be electrolyzed and form a benzyl radical. The highly active benzyl radicals can be used for radical polymerization.¹³⁷ Indeed, surface initiated ATRP was carried out with benzyl diazonium salt modified electrode.¹³⁸ The polymerization of MMA with BBDA was successfully conducted by a free radical polymerization process (Figure VI-9). The final product showed $M_n = 41200$ and $M_w/M_n = 1.41$.

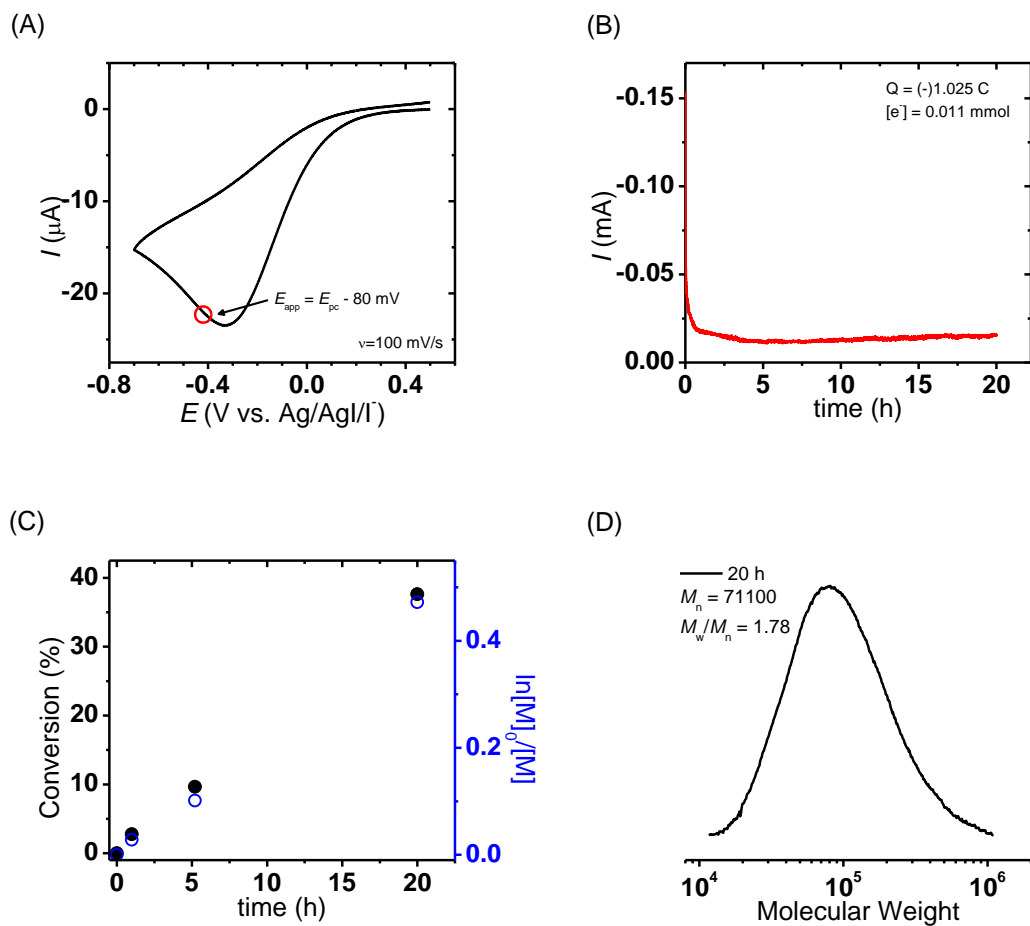


Figure VI-8. Electrolysis of BPO in the presence of MMA. (A) CV analysis of BPO ($E_{app} = E_{pc,BPO} - 80$ mV), (B) CA result of electrolysis, (C) monomer consumption vs. reaction time, and (D) GPC trace of final sample.

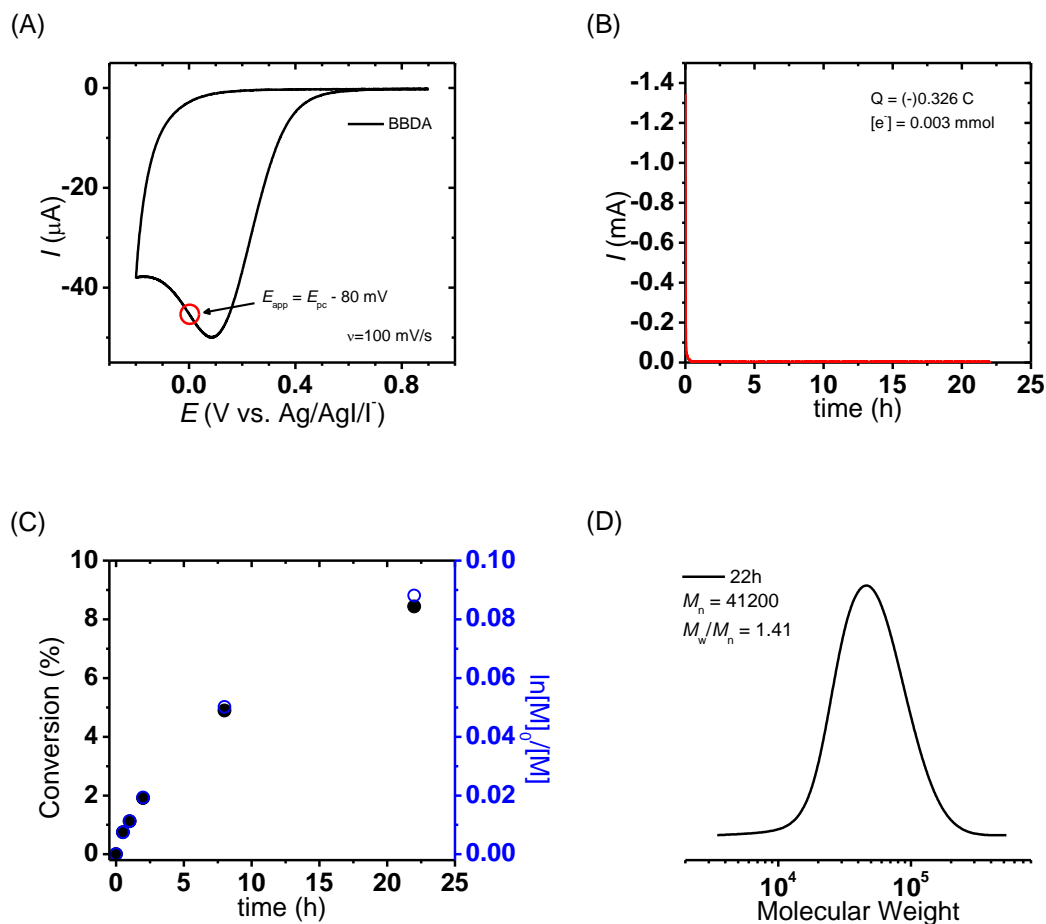


Figure VI-9. Electrolysis of BBDA in the presence of MMA. (A) CV analysis of BBDA ($E_{app} = E_{pc, BBDA} - 80$ mV), (B) CA result of electrolysis, (C) monomer consumption vs. reaction time, and (D) GPC trace of final sample.

eRAFT Polymerization of MMA. Two radical sources were selected (BPO and BBDA) and examined for eRAFT of MMA. Polymerization of MMA with BPO/CPPA was carried out (Table VI-3, entry 1-3). When very negative E_{app} s ($E_{app} = E_{pc, BPO} - 170$ mV, Table VI-3, entry 1) were selected, no polymerization was observed. This was because the E_{pc} s of BPO and CPPA were close (Figure VI-10A) and the selected E_{app} could electrolyze

both compounds. On the other hand mild electrolysis conditions ($E_{\text{app}} = E_{\text{pc,BPO}} + 320 \text{ mV}$, Table VI-3, entry 3) could not successfully decompose BPO and no polymerization took place. When E_{app} of $E_{\text{pc,BPO}} - 50 \text{ mV}$ was selected, polymerization was observed (Figure VI-10). Linear first-order kinetics were observed and MW increased with monomer conversion with a narrow MWD. Therefore the BPO/CPPA combination showed a disadvantage in the difficulty of selection of an appropriate E_{app} s, which called for a use of different radical source, *i.e.*, BBDA, for further development of *e*RAFT polymerization.

Table VI-3. Summary of eRAFT polymerization of MMA.

Entry	[M]/[CPPA]/[R] []	R	WE	A (cm ²) ^a	E_{app}	E (V. Ag/AgI/I ⁻)	t (h)	Conv (%) ^b	Q (C)	k_p^{app} (h ⁻¹)	$M_{n,GPC}$ ($\times 10^{-3}$) ^c	$M_{n,th}$ ($\times 10^{-3}$)	M_w/M_n^c
1	500/1/1	BPO	Pt	4	$E_{pc,BPO} - 170$ mV ^d	-0.62	20	< 5	22.02	-	-	-	-
2	500/1/1	BPO	Pt	4	$E_{pc,BPO} - 50$ mV ^d	-0.30	20	24	26.36	0.013	7.2	12.4	1.17
3	500/1/1	BPO	Pt	4	$E_{pc,BPO} + 320$ mV ^d	-0.20	20	-	12.12	-	-	-	-
4	500/1/1+9 ^e	BBDA	Pt	4	E_{pc}	0.23	44	40	0.53	0.004 ^f	19.8	20.3	1.20
5	500/1/10	BBDA	Pt	4	E_{pc}	0.23	24	40	0.33	0.023	12.6	20.1	1.14
6	500/1/10	BBDA	Cu	8	E_{pc}	0.10	24	13	1.03	0.006	6.1	6.7	1.35
7	500/1/10	BBDA	Gr	> 4	E_{pc}	-0.03	24	18	14.11	0.008	9.8	9.3	1.42
8	500/1/10	BBDA	CF	4	E_{pc}	-0.05	24	34	12.68	0.018	13.9	17.4	1.24
9	500/1/10	BBDA	Pt	4	$E_{pc} - 120$ mV	0.14	24	29	0.53	0.014	12.6	14.9	1.20
10 ^g	500/1/10	BBDA	Pt	4	n/a ^g	n/a ^g	24	26	1.04	0.013	10.6	13.5	1.27
11	200/1/4	BBDA	Pt	4	E_{pc}	0.23	48	60	0.34	0.019	9.1	12.2	1.14
12	1000/1/20	BBDA	Pt	4	E_{pc}	0.39	24	22	4.29	0.010			

General condition: in MMA/DMF = 1/1 (v/v), CE = Pt mesh (separated by supporting electrolyte saturated methylated cellulose), RE = Ag/AgI/I⁻; $T = RT$; $V_{tot} = 30$ mL; [TBAPF₆] = 0.1 M; ^aestimated geometric electrode area; ^bdetermined by ¹H NMR; ^cTHF GPC with PMMA standards; ^ddetermined by CV of pure BPO (Figure VI-10A); ^eadded 9 equilibrium of BBDA after 1 day; ^f $k_p^{app} = 0.017$ (after adding BBDA); ^gapplied constant currents ($I = -12$ μ A).

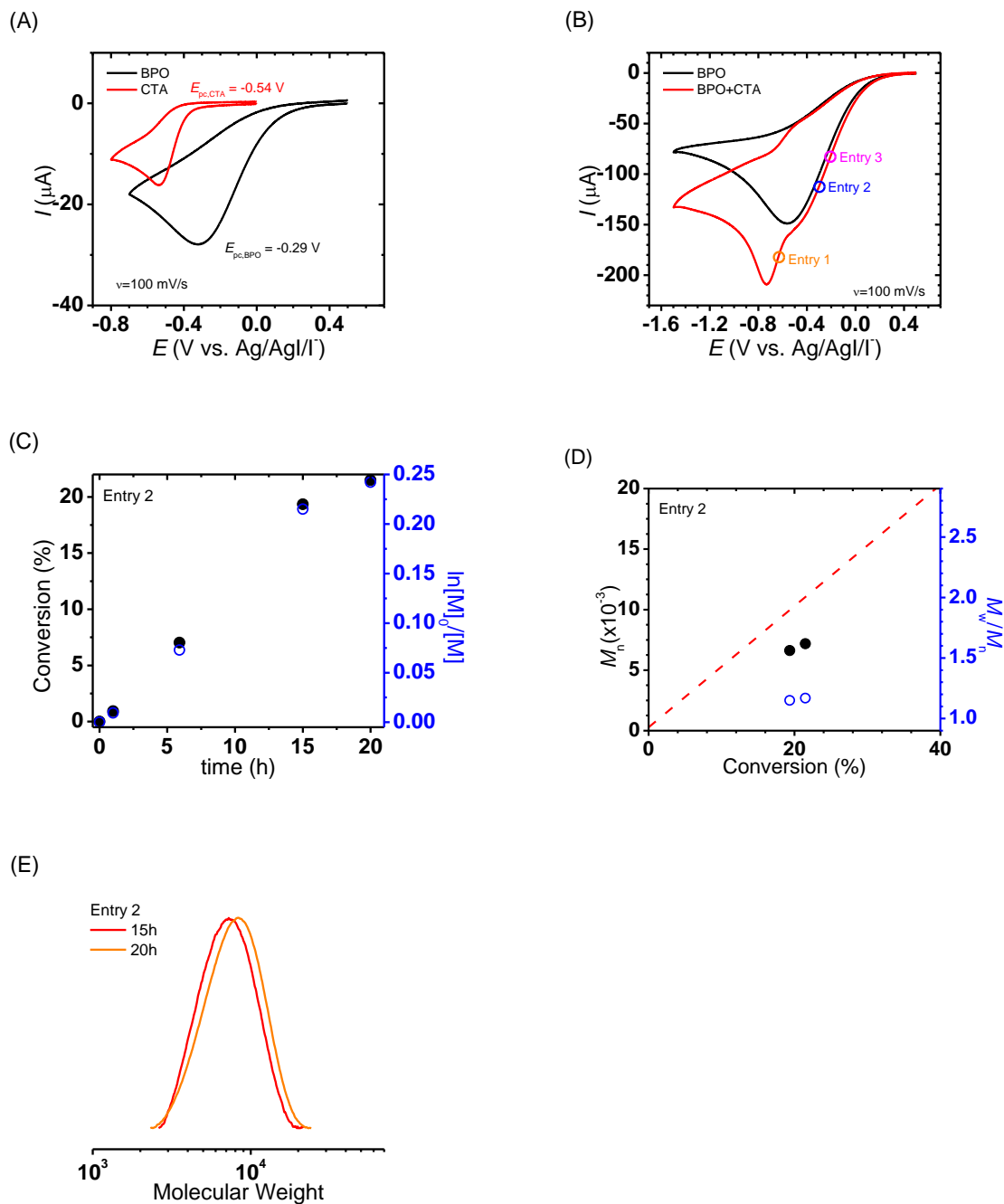


Figure VI-10. eRAFT of MMA with CPPA/BPO combination. (A) CV of pure BPO and CTA (1 mM concentration in pure DMF at RT), (B) CV of BPO and BPO/CPPA in polymerization mixture, (C) monomer consumption vs. reaction time (Table VI-3, entry 2),

(D) MW and MWD vs. conversion (Table VI-3, entry 2), and (E) GPC traces of PMMA.

The main advantage of *e*RAFT with BBDA/CPPA is the simplified selection of an appropriate E_{app} s. Typically, aryl diazonium salts show a mild reduction potential in the range of -0.10 to 0.37 V (vs. SCE, $E_{\text{pc, BBDA}} = 0.11$ V vs. Ag/AgI/I).¹³⁷ Such a positive cathodic peak potential of diazonium salts prevents any undesired decomposition of CPPA ($E_{\text{pc, CPPA}} = -0.54$ V vs. Ag/AgI/I) upon electrolysis of the diazonium compounds. Free radical polymerization of MMA was successfully achieved by electrolysis of BBDA (Table VI-2, entry 3, and Figure VI-8), indicating BBDA can be used as the radical source. Various reaction parameters were investigated for *e*RAFT polymerization (Table VI-3, entry 4-11). Initial polymerization was conducted with $[\text{MMA}]/[\text{CPPA}]/[\text{BBDA}] = 500/1/1$ (Figure VI-11). Slow $k_{\text{p}}^{\text{app}} (= 0.004 \text{ h}^{-1})$ was observed over 20 h. R_{p} was enhanced by adding of 9 eq. of BBDA and the $k_{\text{p}}^{\text{app}}$ was increased to 0.017 h^{-1} . When polymerization was carried out with $[\text{MMA}]/[\text{CPPA}]/[\text{BBDA}] = 500/1/10$, similar monomer conversion was reached as entry 4 in Table VI-3 and similar $k_{\text{p}}^{\text{app}}$ was observed (0.023 h^{-1}). MWs increased linearly with increasing monomer conversion, and polymers maintained a narrow MWD. However, passivation at the surface of working electrode was observed during the electrolysis (Figure VI-11A and Figure VI-12A, nearly symmetric CV and no redox response after 1st CV cycle). This is presumably because thiol groups of CTA can be coordinate to the Pt surfaces.^{124, 139} Therefore a different working electrode (WE) was examined to improve *e*RAFT polymerization.

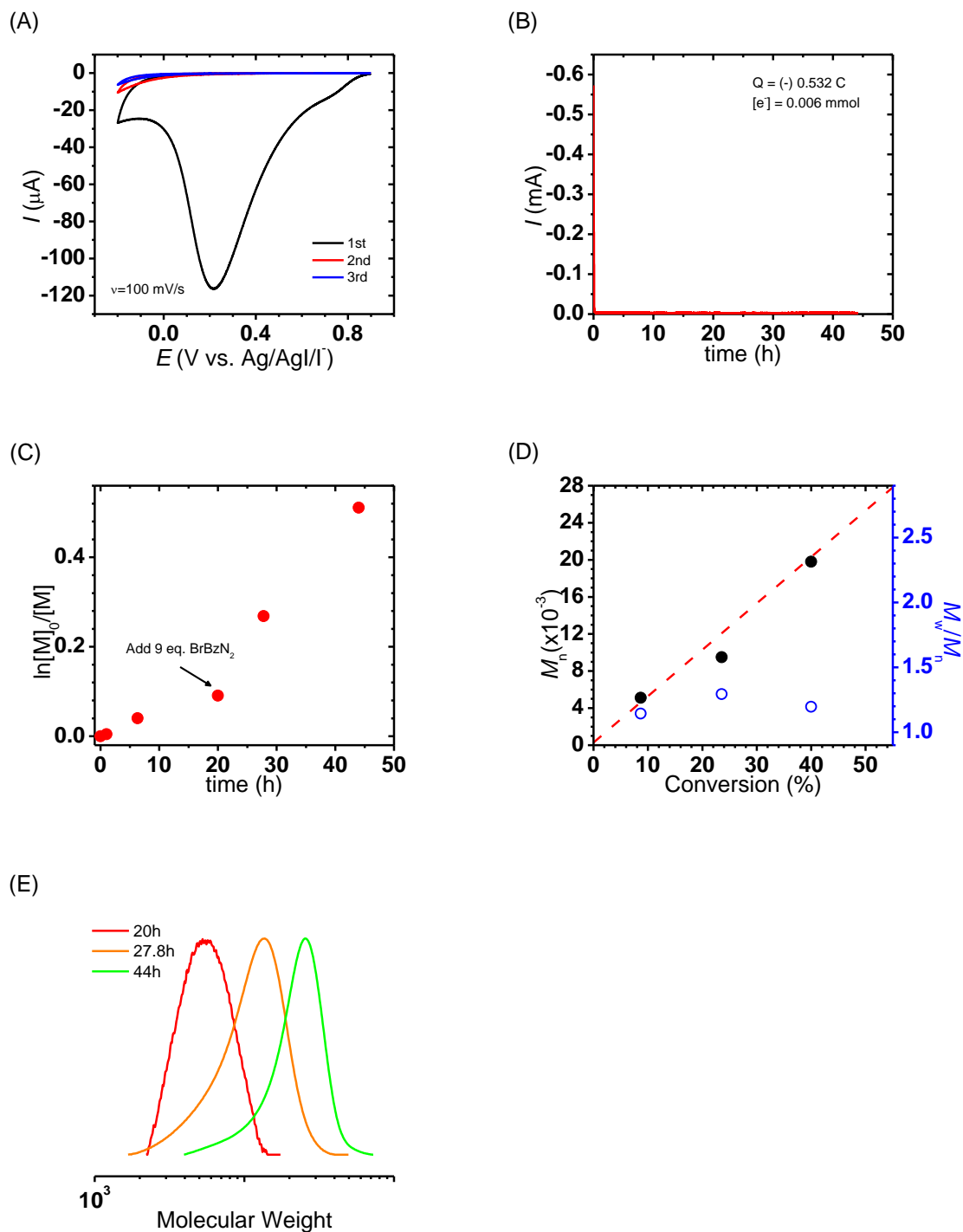


Figure VI-11. eRAFT polymerization of MMA with BBDA/CPPA combination. (A) CV of BBDA/CPPA with 3 consecutive cycles, (B) CA result of the polymerization, (C)

monomer consumption vs. reaction time (9 eq. of BBDA was additionally introduced at 20 h), (D) MW and MWD vs. conversion, and (E) MW evolutions by THF GPC.

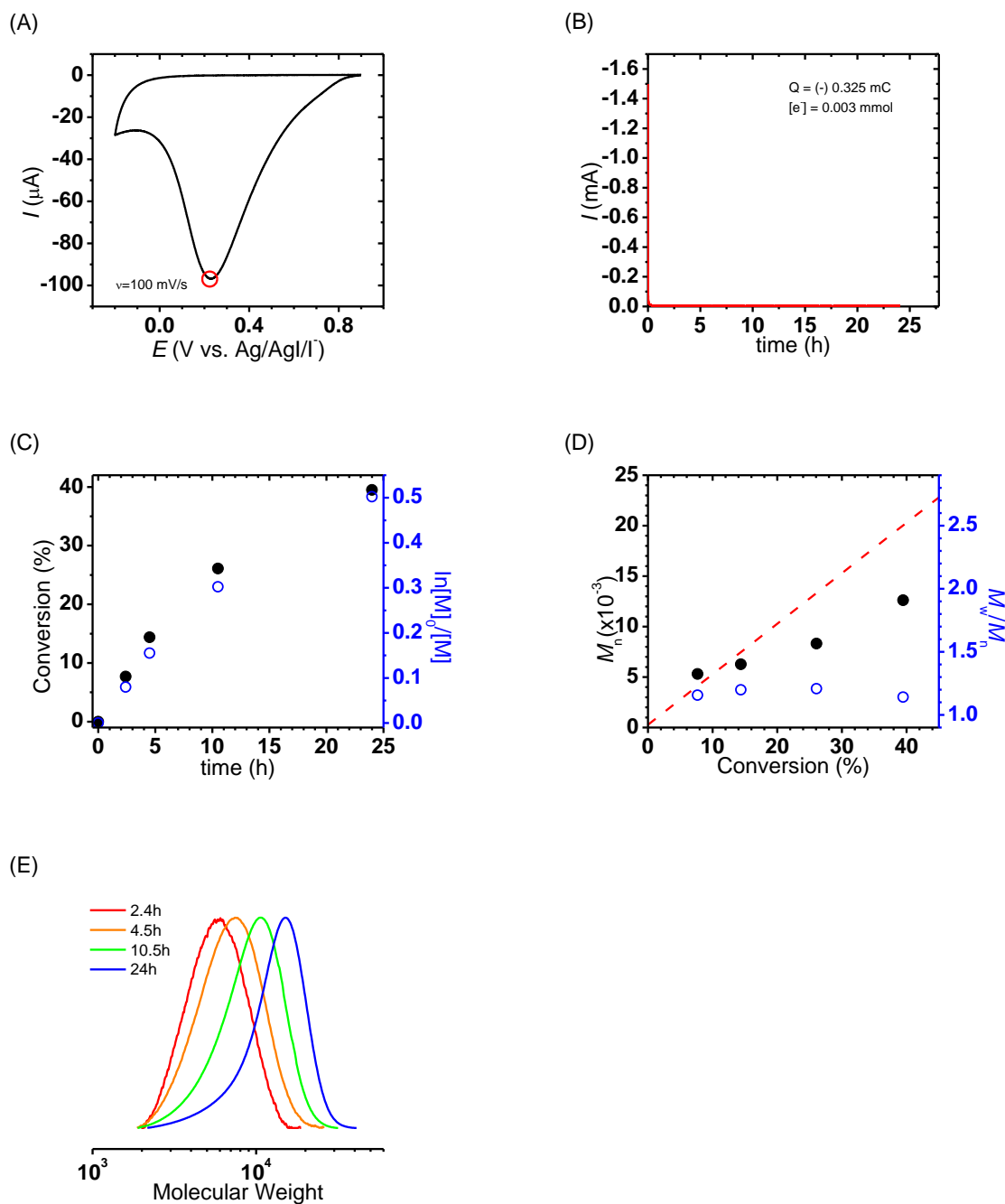
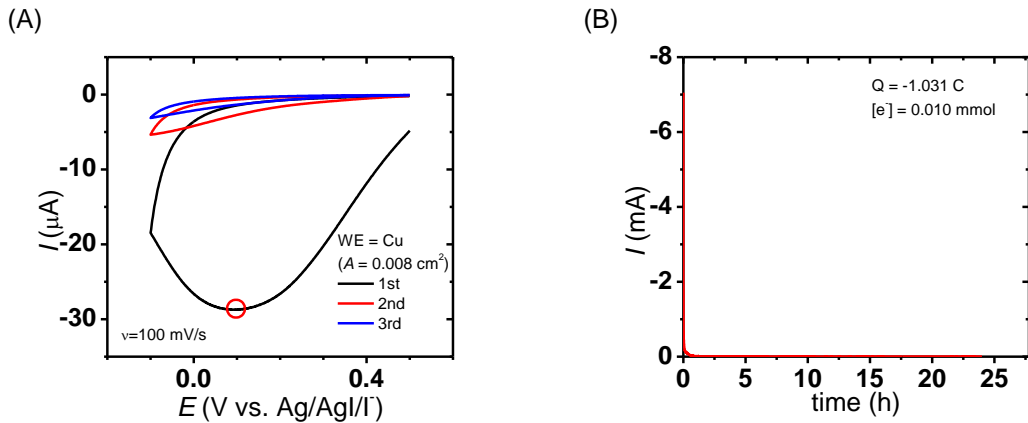


Figure VI-12. eRAFT polymerization of MMA with $[CPPA]/[BBDA] = 10/1$. (A) CV of

BBDA/CPPA, (B) CA result of the polymerization, (C) monomer consumption vs. reaction time, (D) MW and MWD vs. conversion, and (E) MW evolutions by THF GPC.

Different WE for *e*RAFT. Four WEs were selected for examination in an *e*RAFT polymerization (Table VI-3, entry 5-8) – Pt, copper wire (Cu), graphite rod (Gr), and carbon felt (CF). The first WE examined was Cu wire. Cu oxidation ($\text{Cu}^{2+} + 2e^- \rightarrow \text{Cu}^0$) potential was 0.34 V (vs. SHE, $E_{\text{pa,observed}} = 0.68$ V vs. Ag/AgI/I⁻), which was more positive than the previous *e*RAFT conditions. Thus, oxidation of Cu was negligible during the *e*RAFT process. CV was recorded by house-made Cu microelectrode ($A = 0.008 \text{ cm}^2$) and the results showed passivation of WE surface (Figure VI-13B). After 1 day reaction, *ca.* 13% conversion was calculated (Figure VI-13), indicating that Pt WE is a better choice for *e*RAFT polymerization than a Cu electrode.



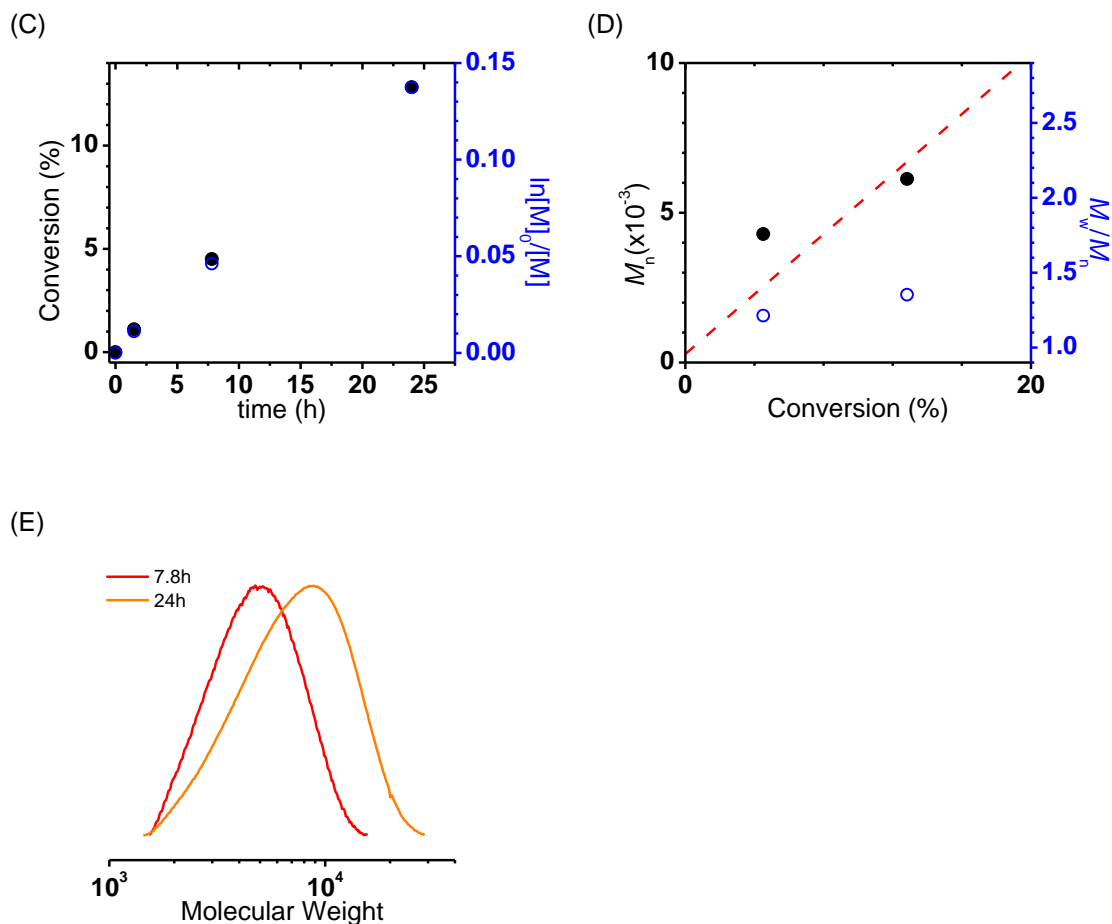
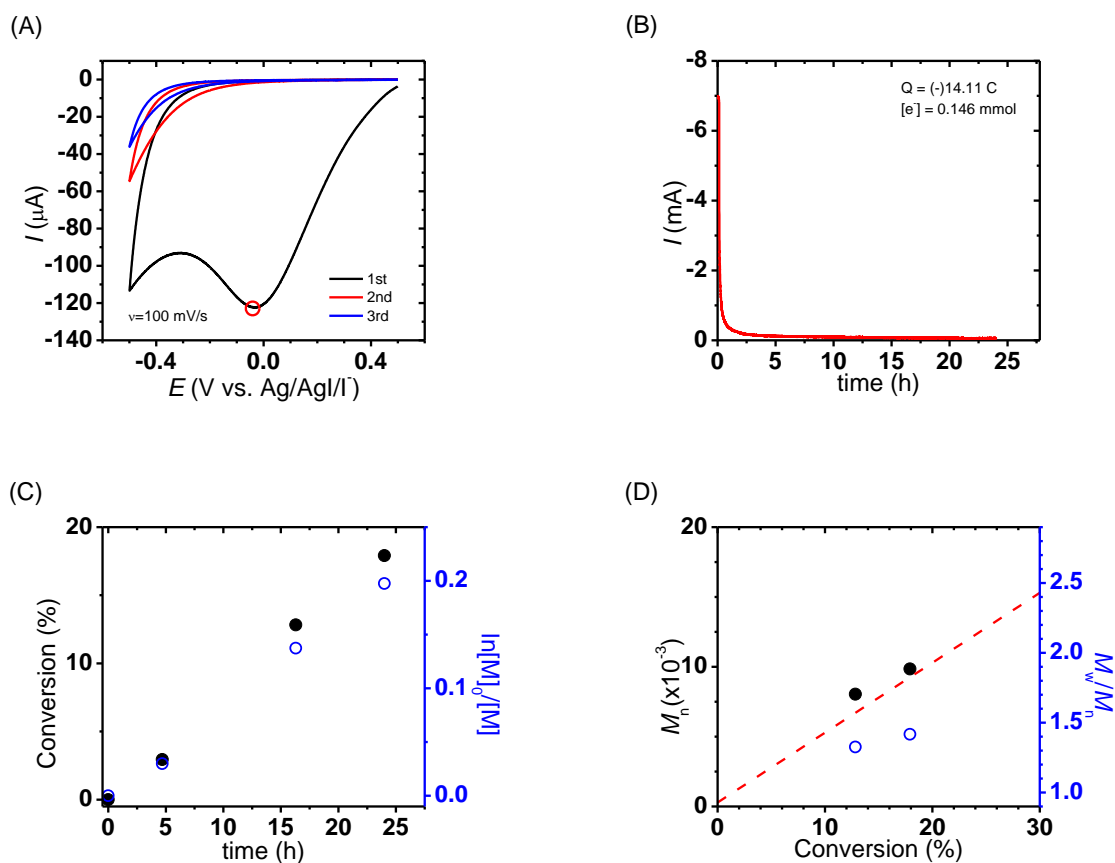


Figure VI-13. eRAFT polymerization of MMA with Cu WE. (A) CV of BBDA/CPPA with 3 consecutive cycles (by Cu microelectrode, $A = 0.008 \text{ cm}^2$), (B) CA result of the polymerization, (C) monomer consumption vs. reaction time, (D) MW and MWD vs. conversion, and (E) MW evolutions by THF GPC.

Two carbon electrodes were then examined: Gr and CF. All CVs were recorded by glassy carbon (GC) disk electrode ($A = 0.071 \text{ cm}^2$) under these particular conditions. The occurrence of passivation was also confirmed using carbon-based electrode (Figure VI-14A and Figure VI-15A). Linear first-order kinetic was observed by Gr WE and MWs

were well-matched with theoretical values while maintaining narrow MWDs (Figure VI-15). However, monomer conversion only reached 18% in 24 h. To achieve a higher monomer conversion, a CF WE was used because CF has a porous structure that should allow for an effective electrolysis of BBDA. Similarly, linear first-order kinetics was obtained and a slightly higher monomer conversion was achieved (34%). Compared to Pt WE, significant improvements were not observed when carbon-based electrodes were used. Further studies were carried out using Pt WE.



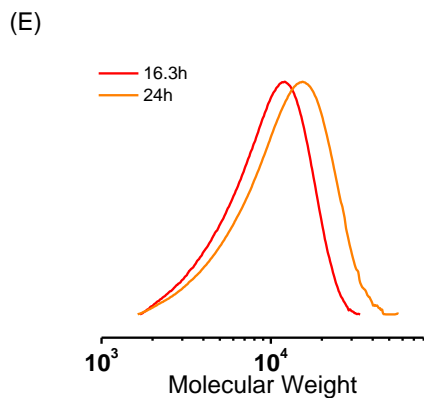
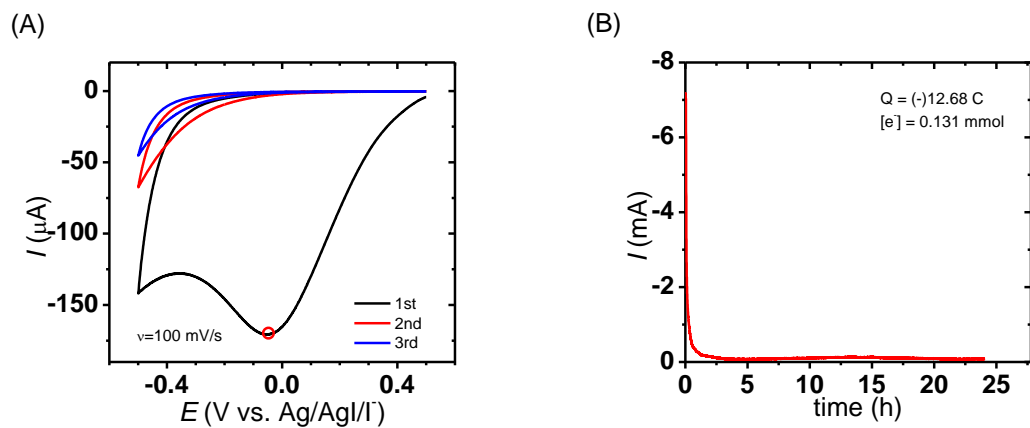


Figure VI-14. *e*RAFT polymerization of MMA with Gr WE. (A) CV of BBDA/CPPA with 3 consecutive cycles (by GC electrode, $A = 0.071 \text{ cm}^2$), (B) CA result of the polymerization, (C) monomer consumption vs. reaction time, (D) MW and MWD vs. conversion, and (E) MW evolutions by THF GPC.



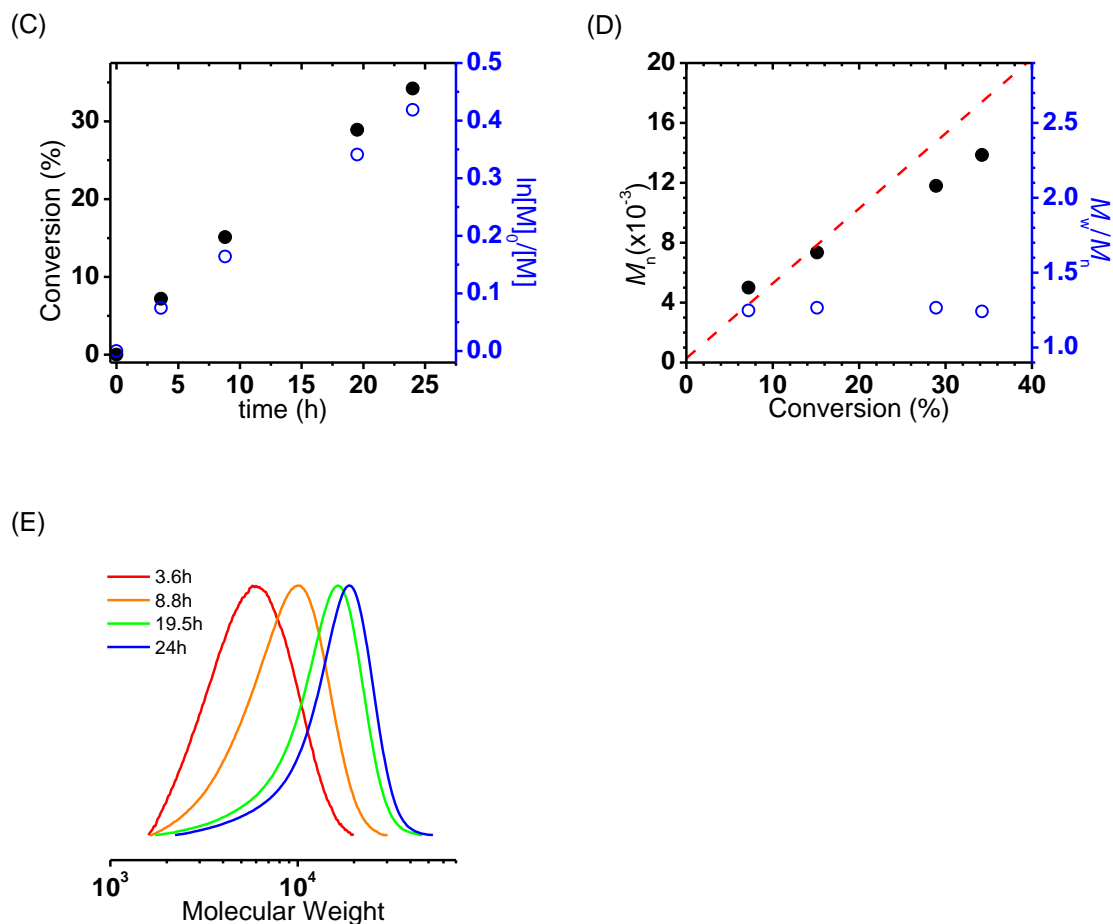
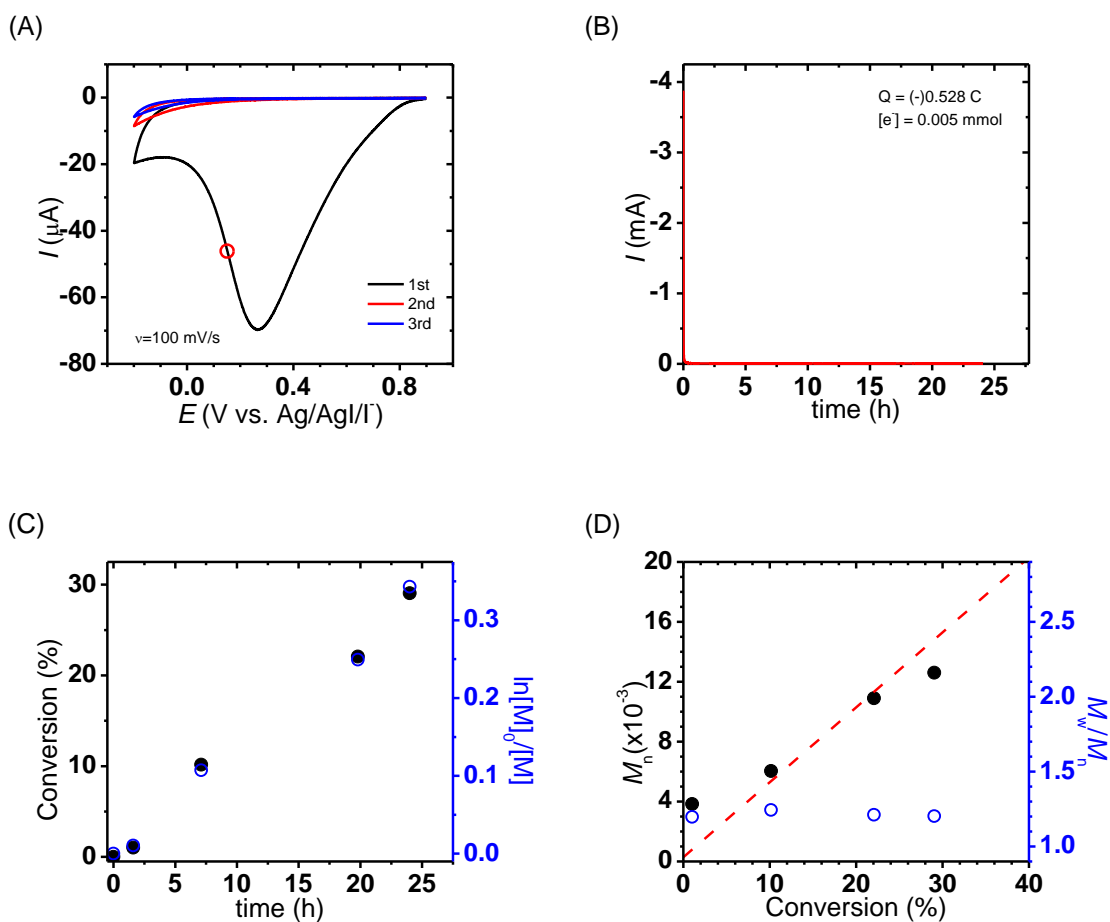


Figure VI-15. *e*RAFT polymerization of MMA with CF WE. (A) CV of BBDA/CPPA in 3 consecutive cycles (by GC electrode, $A = 0.071 \text{ cm}^2$), (B) CA result of the polymerization, (C) monomer consumption vs. reaction time, (D) MW and MWD vs. conversion, and (E) MW evolutions by THF GPC.

Effect of E_{app} s and Development of Galvanostatic Conditions for *e*RAFT. Two different approaches were examined to accelerate the rate of polymerization: application of a more negative potential and application of a constant current (Galvanostatic condition). When a more negative potential ($E_{\text{app}} = E_{\text{pc}} - 120 \text{ mV}$, Table VI-3, entry 9) was applied,

k_p^{app} was 0.014 h^{-1} , which was lower than polymerization under E_{pc} (0.023 h^{-1} , Table VI-3, entry 5). This is probably because a faster reduction of BBDA introduced higher concentration of radicals than that under E_{pc} conditions. The higher radical concentration resulted in higher amount of CTA intermediates, quickly passivating the working electrode surfaces and leading to a poor reduction of BBDA.



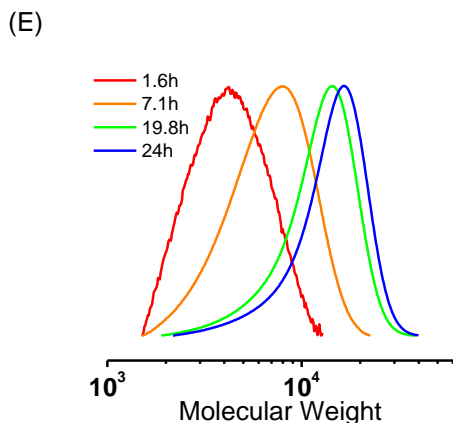


Figure VI-16. *e*RAFT polymerization of MMA under $E_{\text{app}} = E_{\text{pc}} - 120$ mV. (A) CV of BBDA/CPPA with 3 consecutive cycles, (B) CA result of the polymerization, (C) monomer consumption vs. reaction time, (D) MW and MWD vs. conversion, and (E) MW evolutions by THF GPC.

Galvanostatic condition for *e*RAFT were examined for optimizing reaction conditions. Based on the polymerization under potentiostatic condition, stable current values were found at (-) 3 – 4 μA . To enhance R_p , a 3 times higher constant current (= (-) 12 μA) was applied to the polymerization solution. An identical reaction mixture to that employed for polymerization under potentiostatic condition (Table VI-3, entry 5) was prepared and a constant current was applied (Table VI-3, entry 10). Although linear first-order kinetic and good MW evolutions were observed (Figure VI-17), monomer conversion after 24 h was only 26%, which was not a significant improvement compared to the previous cases. Based on these results, the optimal conditions for *e*RAFT was obtained using Pt WE under $E_{\text{app}} = E_{\text{pc}}$.

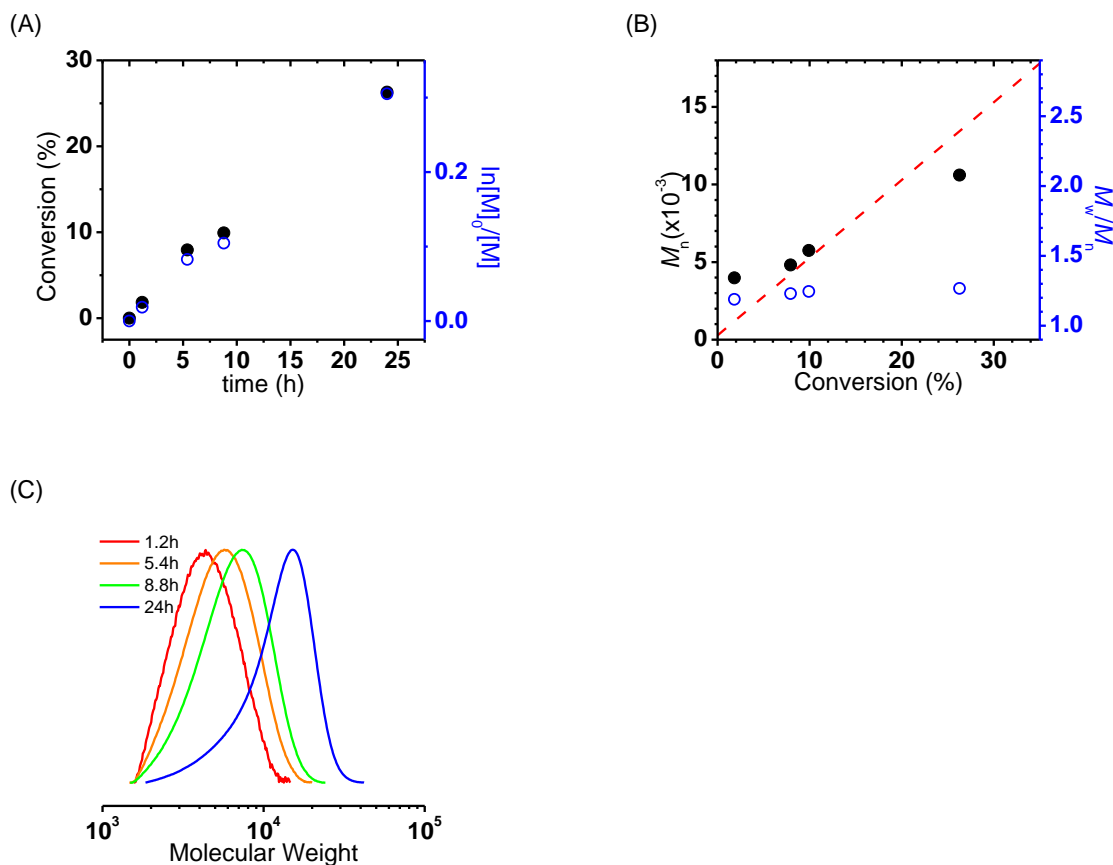


Figure VI-17. eRAFT polymerization of MMA under Galvanostatic condition ($I = -12 \mu\text{A}$).

(A) monomer consumption vs. reaction time, (B) MW and MWD vs. conversion, and (C) MW evolutions by THF GPC.

Polymerization of MMA with Different Target DP. Different $[\text{MMA}]/[\text{CPPA}]$ ratios were examined to control target MW, *i.e.*, $[\text{M}]/[\text{CTA}] = 200, 500, \text{ and } 1000$ (Table VI-3, entry 5, 10, and 11). In all cases, a constant concentration of BBDA was used ($= 0.09 \text{ M}$ in DMF). Under the optimal conditions for eRAFT, well-defined polymers were obtained and MW matched well with the theoretical values (Figure VI-18).

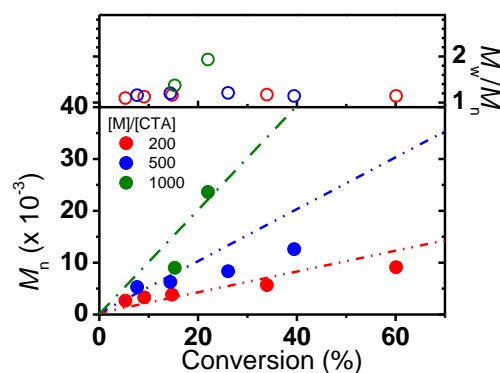


Figure VI-18. *e*RAFT polymerization of MMA with different target DP. [MMA]/[CPPA] = 200, 500, and 1000 (red, blue, and green, respectively).

VI. 4. Summary

In this chapter, conditions for a concurrent *e*ATRP/RAFT polymerization and an *e*RAFT polymerization were investigated. In the concurrent *e*ATRP/RAFT procedure dithiocarbonates were activated by electrochemically reduced $\text{Cu}^{\text{I}}/\text{L}$ and a controlled polymerization was initiated. The optimal conditions for *e*ATRP/RAFT of MMA were achieved by utilization of a high concentration of CuBr/bpy catalysts (*ca.* 2700 ppm to [M]) with a very negative potential ($E_{\text{app}} = E_{1/2\text{CuBr2/bpy}} - 500 \text{ mV}$). Such a high concentration of transition metal catalysts would have adverse effects on potential applications of the resulting polymers. The development of *e*RAFT overcame such limitations by utilizing only organic compounds. Radical sources were introduced by electrolysis and synthesis of well-defined PMMA was achieved with target DP.

VI. 5. Experimental Section

Materials. 4-Cyano-4-(phenylcarbonothioylthio)pentanoic acid (CPPA), copper (II) bromide (CuBr_2), tetrabutylammonium hexafluorophosphate (TBAPF_6), 4-bromobenzenediazonium tetrafluoroborate (BBDA), tetraethylthiuram disulfide (TETDF), and graphite rod were purchased from Aldrich at the highest purity available and used without further purification unless stated. Copper (II) diethyldithiocarbamate (CuDC_2) was purchased from TCI. All solvents were purchased from commercial sources, *e.g.*, Aldrich, TCI, Acros and used as received unless stated otherwise. Platinum (Pt) wires, Pt gauge mesh, carbon felt, copper (Cu) wire were purchased from Alfa Aesar. Methyl methacrylate (MMA, Aldrich) was passed through a column filled with basic alumina to remove inhibitor prior to use. Benzoyl peroxide (BPO, Aldrich) was dissolved in acetone and precipitated against water, and the white powders were dried under vacuum for 1 day. Tris(2-pyridylmethyl)amine (TPMA) was prepared according to a previously published procedure.¹⁰³ 1-Cyano-1-methylethyldiethyldithiocarbamate (MANDC) was prepared according to a previously published procedure.¹³⁰

Preparation of CuX_2 /TPMA Solution. Stock solutions of CuX_2 (0.25 mmol, where X = Br or DC) and 0.3 g of TPMA were dissolved in dry DMF (total volume = 5 mL). The prepared CuX_2 /TPMA solutions (50 mM) were used as catalysts for *e*ATRP/RAFT.

Cell Configuration for Electrochemical Reaction. Typically, cyclic voltammetry (CV) spectra were recorded by a Pt disk ($A=0.071 \text{ cm}^2$) against saturated-calomel electrode or Ag/AgI/I⁻ reference electrode. Electrolysis experiments were carried out under N_2

atmosphere using a Pt mesh, Cu wire, copper felt, or graphite rod (chronoamperometry (CA)) working electrodes. The Pt mesh counter electrode was prepared using a glass frit and a salt bridge made of Tylose gel saturated with TBAPF₆ to separate the cathodic and anodic compartments. All CVs and CAs were conducted with a Gamry ref 600 potentiostat.

General Procedures for *e*ATRP/RAFT Polymerization. TBAPF₆ (2.05 g, 6 mmol) was placed in a seven neck electrolysis cell maintained at 80 °C under a slow N₂ purge. Nitrogen pre-purged MMA (15 mL, 0.14 mol) and DMF (15 mL) were added to the electrochemical cell. 0.28 mL of a copper/TPMA stock solution was injected to the reaction mixture, and CV was recorded with Pt disk working electrode (WE), Pt mesh counter electrode (CE), and Ag/AgI/I⁻ reference electrode (RE) for determining applied potential. Electrolysis of catalysts was carried out using CA method with vigorous stirring (1100 rpm). Samples were withdrawn periodically to follow the monomer conversion and apparent number average molecular weight (M_n) by ¹H NMR, and to determine molecular weight distribution (M_w/M_n) by gel permeation chromatography with PMMA standard curve.

General Procedures for *e*RAFT Polymerization. TBAPF₆ (2.05 g, 6 mmol), chain transfer agent (*e.g.*, 0.28 mmol for [M]/[CTA] = 500/1), and BBDA (2.80 mmol) were placed in a seven neck electrolysis cell maintained at room temperature ($T = 22$ °C) under a slow N₂ purge. Nitrogen pre-purged MMA (15 mL, 0.14 mol) and DMF (15 mL) were added to the electrochemical cell. CV was recorded with Pt disk WE, Pt mesh CE, and Ag/AgI/I⁻ or SCE RE for determining applied potential. Electrolysis of catalysts was

carried out using CA method with vigorous stirring (1100 rpm). Samples were withdrawn periodically to follow the monomer conversion and apparent number average molecular weight (M_n) by ^1H NMR, and to determine molecular weight distribution (M_w/M_n) by gel permeation chromatography with PMMA standard curve.

Measurements. Monomer conversion was measured using ^1H NMR spectroscopy in CDCl_3 , in a Bruker Avance 300 MHz spectrometer. GPC was used to determine number average molecular weight (M_n) and M_w/M_n values. GPC was conducted with a Waters 515 HPLC Pump and Waters 2414 Refractive Index Detector using PSS columns (Styrogel 10^2 , 10^3 , 10^5 Å) in tetrahydrofuran (THF) as an eluent at a flow rate of 1 mL/min at 35 °C.

VI. 6. References

1. (a) Moad, G.; Rizzardo, E.; Thang, S. H., *Aust. J. Chem.* **2009**, *62* (11), 1402-1472; (b) Chiefari, J.; Chong, Y. K.; Ercole, F.; Krstina, J.; Jeffery, J.; Le, T. P. T.; Mayadunne, R. T. A.; Meijs, G. F.; Moad, C. L.; Moad, G.; Rizzardo, E.; Thang, S. H., *Macromolecules* **1998**, *31* (16), 5559-5562.
2. (a) Rossner, C.; Vana, P., *Angew. Chem. Int. Ed.* **2014**, *53* (46), 12639-12642; (b) Moad, G.; Chong, Y. K.; Postma, A.; Rizzardo, E.; Thang, S. H., *Polymer* **2005**, *46* (19), 8458-8468.
3. Fischer, H., *Chem. Rev.* **2001**, *101* (12), 3581-3610.
4. (a) Convertine, A. J.; Ayres, N.; Scales, C. W.; Lowe, A. B.; McCormick, C. L., *Biomacromolecules* **2004**, *5* (4), 1177-1180; (b) Zheng, H.; Bai, W.; Hu, K.; Bai, R.; Pan, C., *J. Polym. Sci., Part A: Polym. Chem.* **2008**, *46* (7), 2575-2580.
5. (a) Muthukrishnan, S.; Pan, E. H.; Stenzel, M. H.; Barner-Kowollik, C.; Davis, T. P.; Lewis, D.; Barner, L., *Macromolecules* **2007**, *40* (9), 2978-2980; (b) Xu, J.; Shanmugam, S.; Duong, H. T.; Boyer, C., *Polymer Chemistry* **2015**, *6* (31), 5615-5624; (c) Xu, J.; Jung, K.; Boyer, C., *Macromolecules* **2014**, *47* (13), 4217-4229; (d) Shanmugam, S.; Xu, J.; Boyer, C., *Macromolecules* **2014**, *47* (15), 4930-4942.
6. (a) Kwak, Y.; Nicolay, R.; Matyjaszewski, K., *Aust. J. Chem.* **2009**, *62* (11), 1384-1401; (b) Zhang, W.; Wang, C.; Li, D.; Song, Q.; Cheng, Z.; Zhu, X., *Macromolecular Symposia* **2008**, *261* (1), 23-31; (c) Kwak, Y.; Nicolay, R.; Matyjaszewski, K., *Macromolecules* **2008**, *41* (18), 6602-6604; (d) Kwak, R. N. Y.; Matyjaszewski, K., *Macromolecules* **2008**, *41* (13), 4585-4596; (e) Zhang, W.; Zhu, X.; Cheng, Z.; Zhu, J., *J. Appl. Polym. Sci.* **2007**, *106* (1), 230-237.

7. (a) Park, S.; Chmielarz, P.; Gennaro, A.; Matyjaszewski, K., *Angew. Chem. Int. Ed. Engl.* **2015**, *54* (8), 2388-92; (b) Magenau, A. J. D.; Bortolamei, N.; Frick, E.; Park, S.; Gennaro, A.; Matyjaszewski, K., *Macromolecules* **2013**, *46* (11), 4346-4353; (c) Magenau, A. J. D.; Strandwitz, N. C.; Gennaro, A.; Matyjaszewski, K., *Science* **2011**, *332* (6025), 81-84; (d) Bortolamei, N.; Isse, A. A.; Magenau, A. J. D.; Gennaro, A.; Matyjaszewski, K., *Angew. Chem. Int. Ed.* **2011**, *50* (48), 11391-11394.
8. Park, S.; Cho, H. Y.; Wegner, K. B.; Burdynska, J.; Magenau, A. J. D.; Paik, H. J.; Jurga, S.; Matyjaszewski, K., *Macromolecules* **2013**, *46* (15), 5856-5860.
9. Kwak, Y.; Matyjaszewski, K., *Macromolecules* **2008**, *41* (18), 6627-6635.
10. Allen, G. D.; Buzzeo, M. C.; Villagrán, C.; Hardacre, C.; Compton, R. G., *J. Electroanal. Chem.* **2005**, *575* (2), 311-320.
11. Wang, X.; Li, S.; Su, Y.; Huo, F.; Zhang, W., *J. Polym. Sci., Part A: Polym. Chem.* **2013**, *51* (10), 2188-2198.
12. Abel, B. A.; McCormick, C. L., *Macromolecules* **2016**.
13. (a) Yamago, S.; Nakamura, Y., *Polymer* **2013**, *54* (3), 981-994; (b) Shanmugam, S.; Boyer, C., *J. Am. Chem. Soc.* **2015**.
14. (a) Zhang, Z.; Wang, W.; Xia, H.; Zhu, J.; Zhang, W.; Zhu, X., *Macromolecules* **2009**, *42* (19), 7360-7366; (b) Maximiano, P.; Mendonça, P. V.; Costa, J. R. C.; Haworth, N. L.; Serra, A. C.; Guliashvili, T.; Coote, M. L.; Coelho, J. F. J., *Macromolecules* **2016**, *49* (5), 1597-1604.
15. (a) Martin, L.; Gody, G.; Perrier, S., *Polymer Chemistry* **2015**, *6* (27), 4875-4886; (b) Luo, J.; Li, M.; Xin, M.; Sun, W., *Macromol. Chem. Phys.* **2015**, *216* (15), 1646-1652.
16. Allongue, P.; Delamar, M.; Desbat, B.; Fagebaume, O.; Hitmi, R.; Pinson, J.; Savéant, J.-M., *J. Am. Chem. Soc.* **1997**, *119* (1), 201-207.
17. Hazimeh, H.; Piogé, S.; Pantoustier, N. g.; Combellas, C.; Podvorica, F. I.; Kanoufi, F. d. r., *Chem. Mater.* **2013**, *25* (4), 605-612.
18. (a) Polsky, R.; Gill, R.; Kaganovsky, L.; Willner, I., *Anal. Chem.* **2006**, *78* (7), 2268-2271; (b) Petrovykh, D. Y.; Kimura-Suda, H.; Opdahl, A.; Richter, L. J.; Tarlov, M. J.; Whitman, L. J., *Langmuir* **2006**, *22* (6), 2578-2587.
19. Xia, J. H.; Matyjaszewski, K., *Macromolecules* **1999**, *32* (8), 2434-2437.

Section III.

Synthesis of Complex Polymeric Architectures

Chapter VII

Star Synthesis Using Macroinitiators *via* Electrochemically Mediated Atom Transfer Radical Polymerization *

VII. 1. Preface

*e*ATRP provides several advantages, including the ability to directly control the rate of polymerization by adjusting $[\text{Cu}^{\text{I}}]/[\text{Cu}^{\text{II}}]$ ratio by applied potentials and conduct the polymerization under low catalysts loading conditions. This Chapter mainly focuses on the extension of *e*ATRP from preparation of linear homopolymers and block copolymers to copolymers with more complex polymer architecture, *e.g.*, star polymers.

Well-defined star polymers can be synthesized through several controlled radical polymerization (CRP) techniques, including stable free radical polymerization (SFRP), reversible addition-fragmentation transfer polymerization (RAFT), and atom transfer radical polymerization (ATRP). Among these techniques, ATRP provides many advantages including application to a broad range of monomers in multiple solvents under mild reaction conditions. Two methods are generally selected and utilized for synthesis star polymers by ATRP, the core-first or the arm-first method. In the case of the core-first method, initiators containing multiple initiating groups are selected, or prepared, and polymer chains are grown from the multi-functional initiator, the core of the targeted star. The advantages of this method include ease of purification and preparation of stars with a

*Work in this chapter was published and partially reformatted based on the following manuscript: **Park, Sangwoo**; Cho, Hong Yul; Wegner, Katarzyna Barbara; Burdyska, Joanna; Magenau, Andrew J. D.; Paik, Hyun-jong; Jurga, Stefan; Matyjaszewski, Krzysztof *Macromolecules* **2013**, 46 (15), 5856

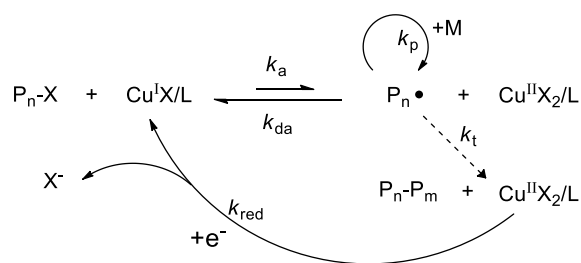
pre-determined number of arms. However, the process has a limitation related to the synthesis of mikto arm star polymers. On the other hand, the arm-first method utilizes pre-synthesized macroinitiators, or macromonomers, and is carried out simply by a chain extension of the pre-formed arms with crosslinkers. During the synthesis of star polymers, the incorporated macroinitiators can form the arms of the stars, whereas crosslinker forms the core of the stars. Advantages of this method are the ability to form stars with a higher number of arms than does the core-first method, and the ease in which the procedure can be employed for synthesis of mikto arm star polymers, and the ability to prepare peripheral or core functionalized star polymers. Nonetheless, purification of arm first stars can be challenging because of similar physical properties of macroinitiators and star molecules. To overcome this limitation, former group member, Dr. Joanna Burdynska, systemically studied star synthesis using activator (re)generation electro transfer (ARGET) ATRP and succeeded in achieving a high yield of a well-defined star copolymer. A small amount of reducing agent was introduced at the beginning of the polymerization to form and maintain a low $[\text{Cu}^{\text{I}}]/[\text{Cu}^{\text{II}}]$ ratio that prevented initial fast star-star coupling reactions. In the later stages of the reaction, since growing star molecules with larger cores were less susceptible to the coupling reaction, a higher amount of reducing agents was used to generate a high $[\text{Cu}^{\text{I}}]/[\text{Cu}^{\text{II}}]$ ratio and a faster rate of polymerization was achieved resulting in high star yields. The technique developed for ARGET ATRP was extended and applied to *e*ATRP star synthesis.

In this project, I designed reactions and analyzed the products of the star synthesis. Based on the discussions with former group members, Dr. Hong Yul Cho and Dr. Joanna Burdynska, multi-step applied potentials were used to successfully achieve a high star yield.

Well defined stars synthesized by the core-first method *via* *e*ATRP and *se*ATRP are discussed in Appendix VII. A functionalized beta-cyclodextrin (β -CD-Br) ATRP initiator was prepared and chain extended with *n*-butyl acrylate (BA). The polymerization results indicated preparation of well-defined star polymers as the reactions progressed, while maintaining narrow molecular weight distribution and molecular weight increasing with increasing monomer conversion. Further chain extension experiments with tert-butyl acrylate (*t*BA) confirmed preservation of high chain end functionalities. My role in the study, included in Appendix VII, was synthesizing functional initiators and analyzing the progress of the polymerizations. I would like to acknowledge former group members, Dr. Hong Yul Cho, Dr. Joanna Burdyska, Dr. Andrew Magenau, Dr. Katarzyna Wegner, and Dr. Paweł Chmielarz for their efforts and contributions to this project.

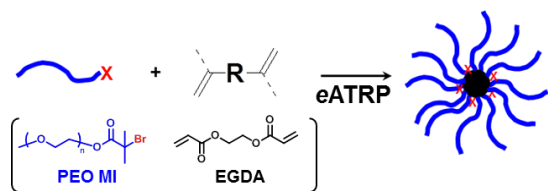
VII. 2. Introduction

The recently developed electrochemically mediated atom transfer radical polymerization (*e*ATRP) provides a new tool for conducting a controlled/living radical polymerization.¹⁴⁰ *e*ATRP can regenerate the activator species in a way similar to other activator (re)generated ATRP system,^{66d, 66e, 141} and provides a unique procedure for controlling the ratio of activator to deactivator.^{11, 140, 142} In this method, the electrochemical potential is applied to reduce a copper (II) ligand complex ($\text{Cu}^{\text{II}}/\text{L}$, L = ligand) and form active $\text{Cu}^{\text{I}}/\text{L}$ species near the working electrode surface. With a vigorous stirring, the reduced $\text{Cu}^{\text{I}}/\text{L}$ could efficiently diffuse to the bulk solution and the remaining $\text{Cu}^{\text{II}}/\text{L}$ (from bulk solution) could diffuse to the electrode and be reduced to $\text{Cu}^{\text{I}}/\text{L}$. Generated catalyst complex subsequently reacts with an alkyl halide (initiator: R-X, polymer: $\text{P}_n\text{-X}$) to produce propagating radicals (P_n^\bullet) and form well-defined polymers (Scheme VII-1). A particular advantage of *e*ATRP is a possibility of the control over the $\text{Cu}^{\text{I}}/\text{Cu}^{\text{II}}$ ratio, and thus over the polymerization rate (R_p), simply governed by the applied potential (E_{app}). More negative E_{app} can accelerate R_p before mass transport limitation is reached.¹¹ For example, polymerizations of *n*-butyl acrylate (BA) were carried out with various applied potentials. The results showed 4 times enhanced R_p when applying potential from half-wave potential ($E_{1/2}$) to $E_{1/2} - 165$ mV. Furthermore, a cessation or rejuvenation of the polymerization (“on-demand” polymerization) was achieved by modulating applied potentials – switching E_{app} s simply by the chronoamperometry method (from 99% $\text{Cu}^{\text{II}}/\text{L}$ to 50% $\text{Cu}^{\text{II}}/\text{L}$).¹⁴⁰



Scheme VII-1. Mechanism of *e*ATRP.

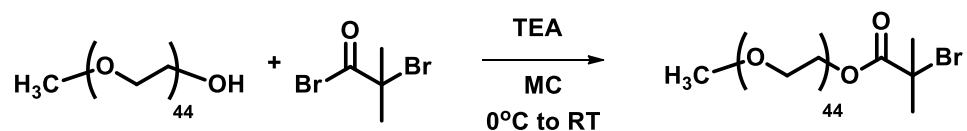
*e*ATRP can polymerize various monomers under selected reaction conditions, for example, BA, methyl acrylate, or oligo(ethylene oxide) monomethyl ether methacrylate with selected E_{app} , Cu concentrations, ligands, solvents and other parameters.^{11, 140} *e*ATRP could have potential advantages for synthesis of complex polymeric architectures, for example star polymers. Star polymers, consisting of multiple arms linked to a central core, combine interesting properties of a branched architecture, globular shape, and chemically crosslinked structure.^{42, 60b, 61a-d, 143} One approach to prepare star polymers *via* normal ATRP is the macroinitiator (MI) method, in which the chain-end functionalized linear MIs can react with divinyl- or multi vinyl- compounds (crosslinkers), to form a dense core (from crosslinker) and stretched arms (MI).^{42c, 144} The MI method can provide star polymers with various chemical composition, stimuli-responsiveness, and site specific functionalities.^{143b, 145} Here, we report the first example of poly(ethylene oxide) (PEO) based star synthesis by *e*ATRP (Scheme VII-2).



Scheme VII-2. Synthesis of PEO star polymers *via* macroinitiator method.

VII. 3. Results and Discussion

The PEO MIs were prepared by reacting monohydroxy PEO methyl ether (HO-PEO, $M_n = 2000$) with 2-bromoisobutyryl bromide in the presence of triethylamine (TEA) base (Scheme VII-3). Chain-end functionalities were characterized by ^1H NMR showing over 95% of the functionalization efficiency (Figure VII-1, equation (VII-1)). The repeating unit of ethylene oxide (EO) groups can be calculated by equation (VII-2). The chain extension with poly(*n*-butyl acrylate) (PBA) was carried out *via* eATRP and was used to further confirm the chain-end functionality of MI. According to GPC analysis, the MI peaks were completely shifted during the formation of the block copolymers (PEO-*b*-PBA), indicating nearly quantitative MI consumption, and thus very high chain-end functionality (> 99%, Figure VII-2).



Scheme VII-3. Synthesis of PEO MI. Reaction conditions: [HO-PEO]/[BriBBR]/[TEA]=1/2/2, $V_{\text{tot}}=500$ mL, $[\text{HO-PEO}]_0=0.04\text{M}$ in dichloromethane.

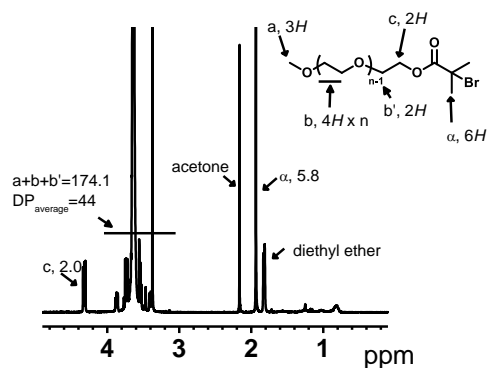
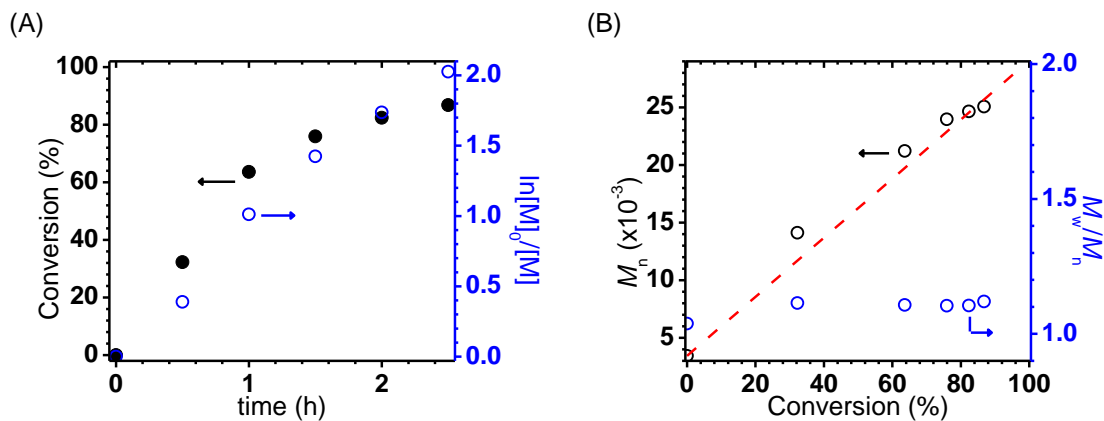


Figure VII-1. ^1H NMR spectrum of PEO MI ($\text{DP}_{\text{average}} = 44$).

$$f = \frac{I_{1.93, \text{observed}}}{I_{1.93, \text{theoretical}}} = \frac{5.8}{6} \quad (\text{VII-1})$$

$$A_a + A_b + A_{b'} = 174.1 = 44(n - 1) + 2 + 3 \quad (\text{VII-2})$$

where, $I_{1.93}$ is the integration values of the peak at $\delta = 1.93$ ppm corresponding to the $(\text{Br})\text{C}-(\text{CH}_3)_2$ (Figure VII-1, α proton), and A_a , A_b , and $A_{b'}$ = observed peak areas (4 to 3.4 ppm), n = number of repeating EO units.



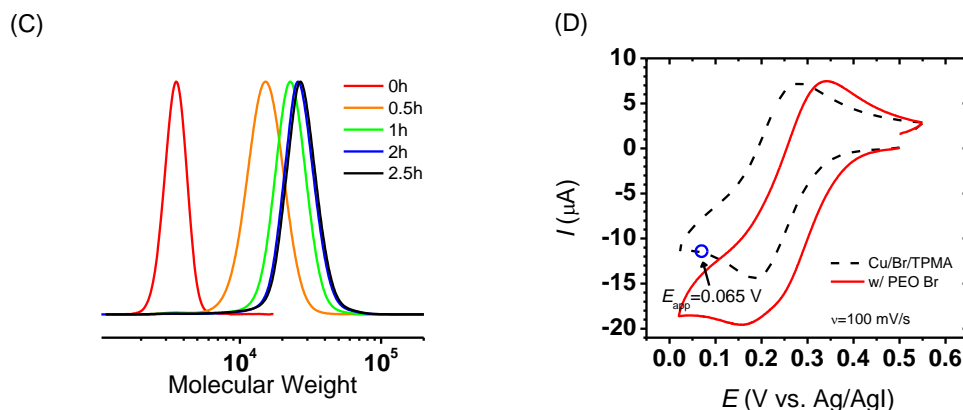
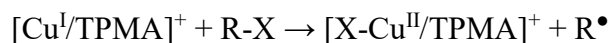
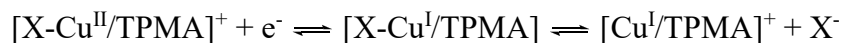


Figure VII-2. Chain extension of PEO with BA; (A) Conversion and first-order kinetic plot versus time; (B) Number average molecular weights and molecular weight distributions versus the monomer conversion; (C) GPC traces for the molecular weight evolution; (D) CV of CuBr₂/TPMA (black, dot) and addition of initiator (red), blue circle indicates E_{app} .

The star synthesis was carried out using the PEO MIs and ethylene glycol diacrylate (EGDA). The cyclic voltammetry measurement confirmed the reduction of Cu^{II} to Cu^I with TPMA ligand. Figure VII-3 shows CV spectra of CuBr₂/TPMA catalyst complex (red) and the CV in the presence of catalysts and PEO MI (blue). The CV of CuBr₂/TPMA provides the half-wave potential ($E_{1/2}$) = 0.252 V (versus Ag/AgI/I, in DMF at 60 °C). When the PEO MI was added to the mixture, an increased cathodic current was observed, due to electrochemical-catalytic (EC'') reaction (Scheme VII-4): (1) X-Cu^{II}/L was reduced to Cu^I/L by cathodic current, and then (2) the PEO MI reacted with Cu^I/L to reform X-Cu^{II}/L and activated radical chain (P_n^\bullet). Therefore, the cathodic current increased to compensate for the spontaneously (re)formed X-Cu^{II}/L during the cathodic scan. A range of applied

potentials between 0.340 and 0.065 V (vs. Ag/AgI/I⁻) was chosen for the star formation polymerizations to provide different R_p .



(X = halogen, and R-X = alkyl halide (PEO MI))

Scheme VII-4. Catalytic electrochemical-chemical reaction. [*formal charges have been omitted in this chapter]

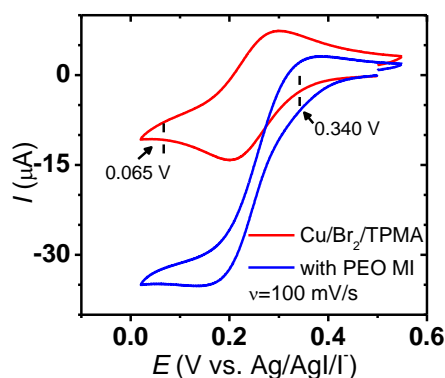


Figure VII-3. CV of CuBr₂/TPMA alone (red) and in the presence of PEO MI (blue).

Variation of MI Concentrations. The objective of the study was to achieve high star yields *via* eATRP and therefore various polymerization parameters were examined, including MI concentration, MI to crosslinker (X) molar ratio, and E_{app} . Table VII-1 summarized results of the star synthesis under different reaction conditions. Initially, the effect of MI concentration on the star formation was evaluated by three MI concentrations,

i.e., [PEO MI] = 100, 25, and 12.5 mM. The polymerizations with high MI concentration (100 mM, Entry 1) provided only < 1% of star yield (Figure VII-4). In contrast, favorable results were observed (> 80% star yield) using lower concentrations of MI (25 mM, Entries 2-4), and a further improvement was observed (> 95%) using 12.5 mM of MI (Entries 5-6). The polymerization with high MI concentrations might lead to increased radical termination reactions between growing polymeric chains, which in consequence would lead to poor arm conversions and broadening of molecular weight distributions.¹⁴⁶ On the other hand, the dilution of MI could suppress fast termination between growing polymeric chains, and favor their intramolecular cyclization, subsequently providing higher star yields.

Table VII-1. Summary of Star Synthesis by *e*ATRP.

Entry	[EGDA]/[MI]	[PEOMI] (mM)	Star (%) ¹	yield	E_{app} (V vs. Ag/AgI/T)	$M_{n,app}$ ²	M_w/M_n ²
1	2.5	100	< 1		0.065	n/a ³	n/a ³
2	2.5	25	87		0.065	15500	1.19
3	5	25	90		0.189	23300	1.25
4	10	25	94		0.189	44800	1.43
5	10	12.5	95		0.189	46200	1.28
6	10	12.5	97		0.340 - 0.189	45600	1.32
7	15	12.5	Gelled		0.189	n/a ³	n/a ³

¹Star yield was determined by MI conversion by area of GPC eluogram; ²Apparent M_n was determined by THF GPC with PMMA standards; ³Not available; General reaction condition: V_{tot} = 20 mL (in DMF); T = 60 °C; [Cu/Br₂/TPMA] = 0.5 mM (except Entry 1 = 0.75 mM); Supporting electrolyte concentration (tetrabutylammonium perchlorate, TBAClO₄) = 0.2 M; Working electrode = Pt mesh; Counter electrode = Pt mesh (separated from the reaction solution by the supporting electrolyte saturated Tylose gel (MW = 300));

Reference electrode = Ag/AgI/I⁻.

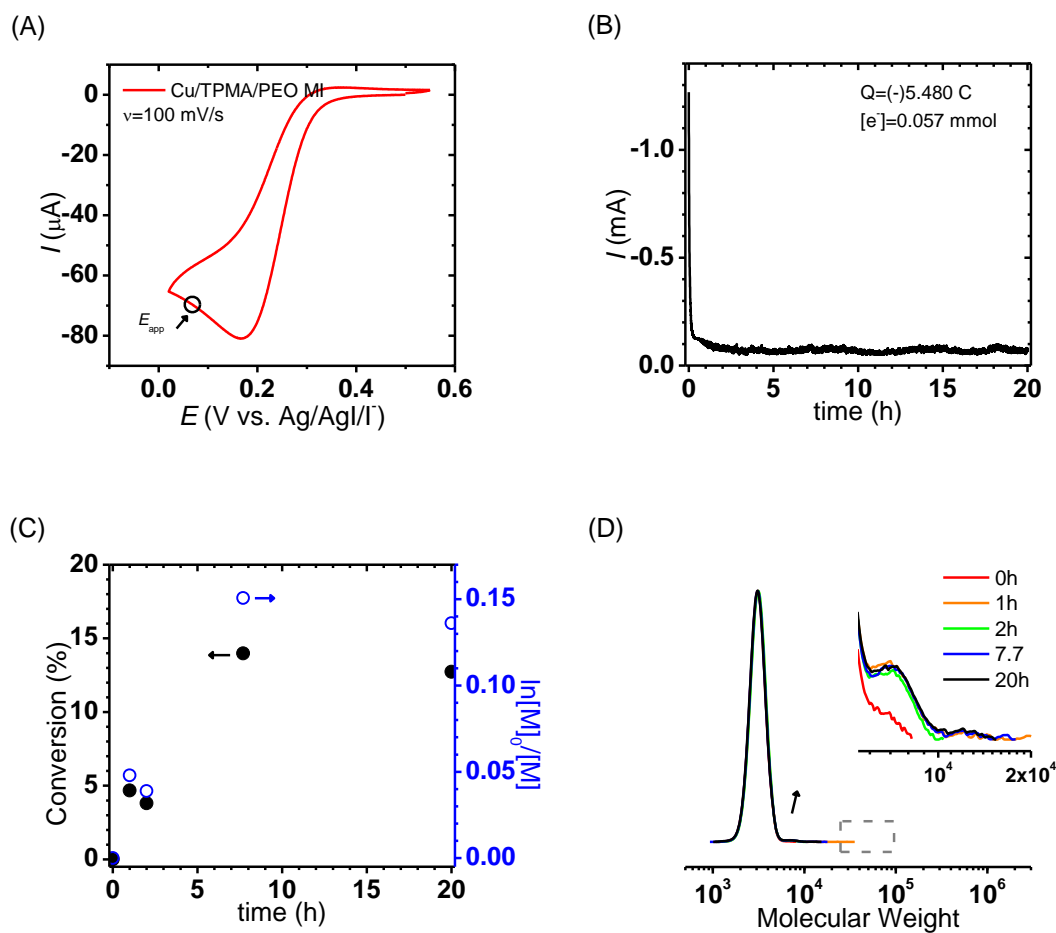


Figure VII-4. PEO star synthesis (Table VII-1, entry 1); (A) CV (black circle: applied potential); (B) CA results, total passed charge = 5.48 C; (C) crosslinker conversion and log plot; (D) GPC traces.

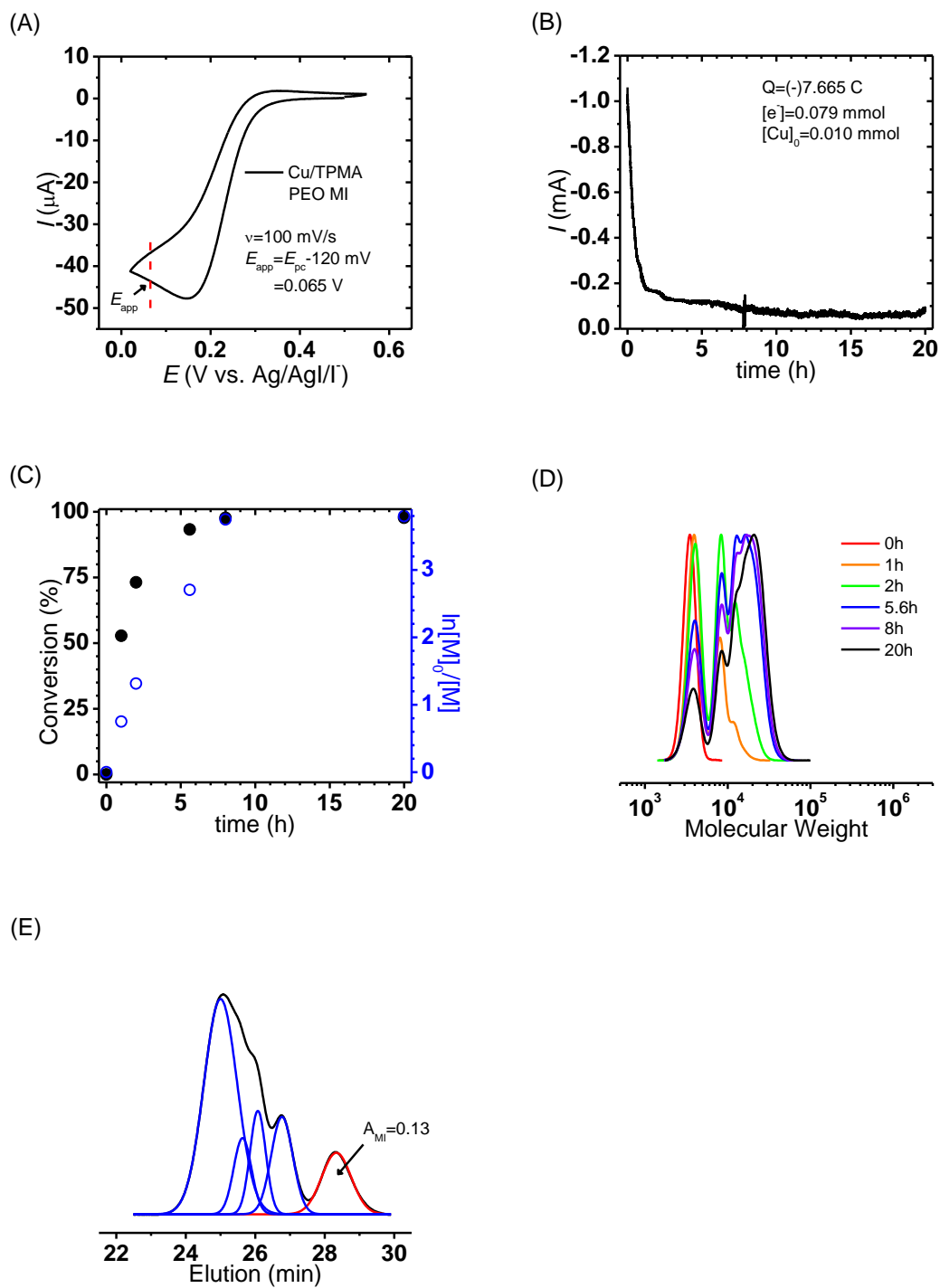


Figure VII-5. PEO star synthesis (Table VII-1, entry 2); (A) CV (red line: applied potential); (B) CA results, total passed charge = 7.67 C; (C) crosslinker conversion and log

plot; (D) GPC traces; (E) eluograms of star polymers (20 h).

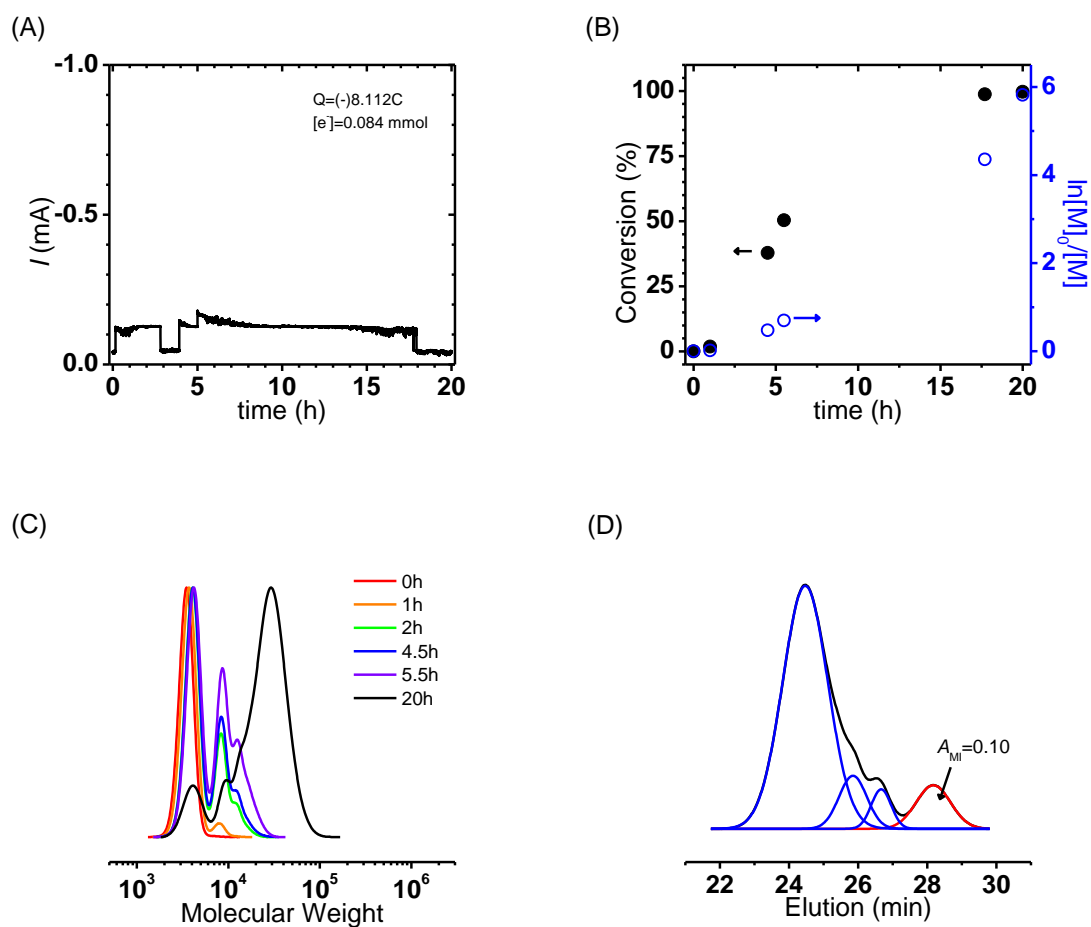


Figure VII-6. PEO star synthesis (Table VII-1, entry 3); (A) CA results, total passed charge=8.11 C; (B) crosslinker conversion and log plot; (C) GPC traces; (D) eluograms of star polymers (20 h).

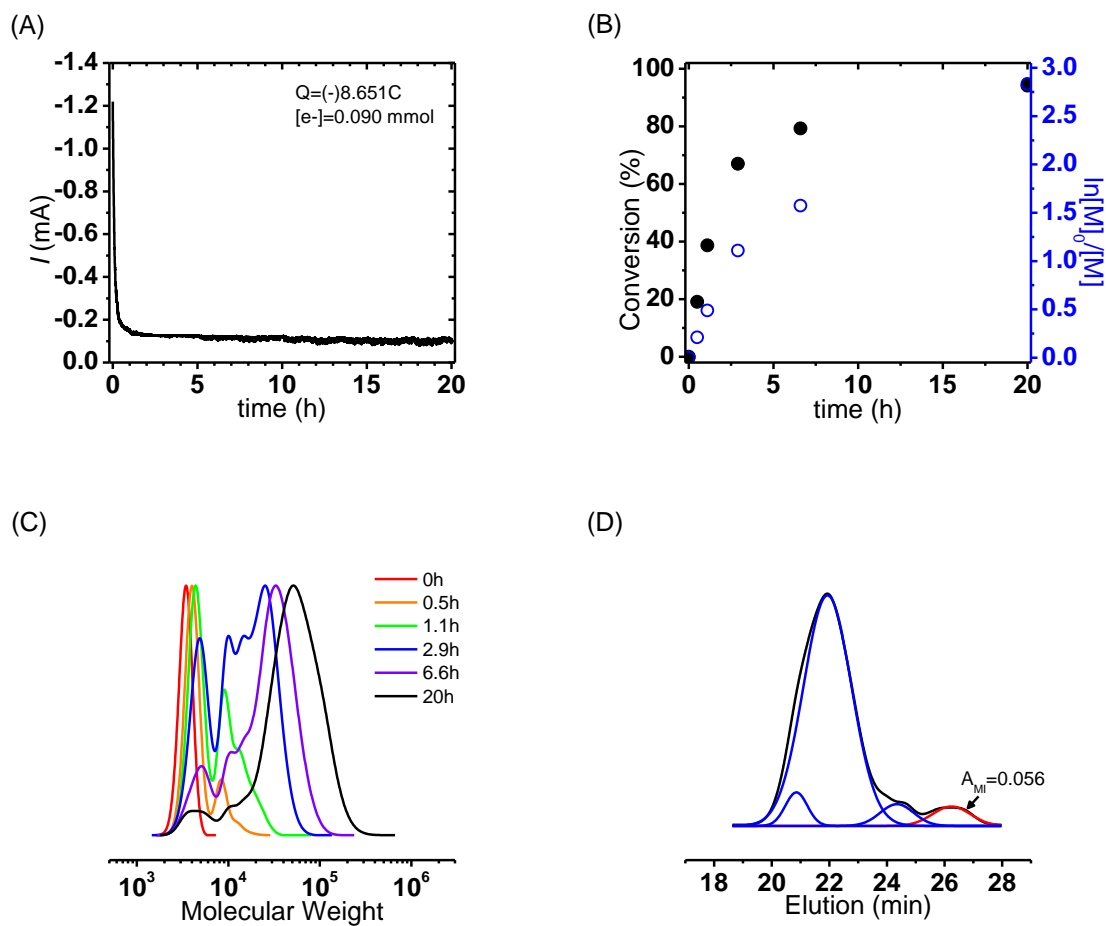


Figure VII-7. PEO star synthesis (Table VII-1, entry 4); (A) CA results, total passed charge=8.65 C; (B) crosslinker conversion and log plot; (C) GPC traces; (D) eluograms of star polymers (20 h).

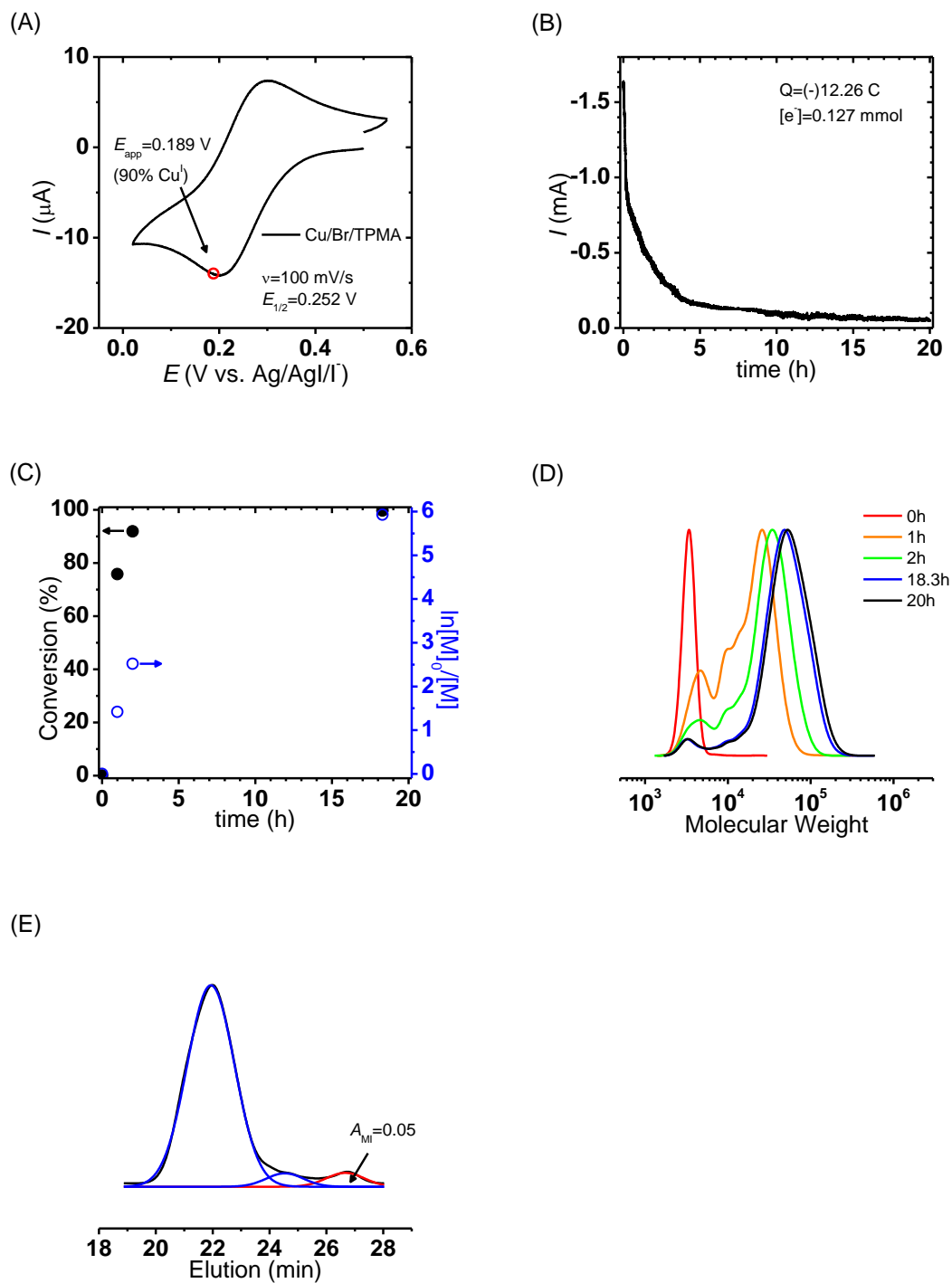
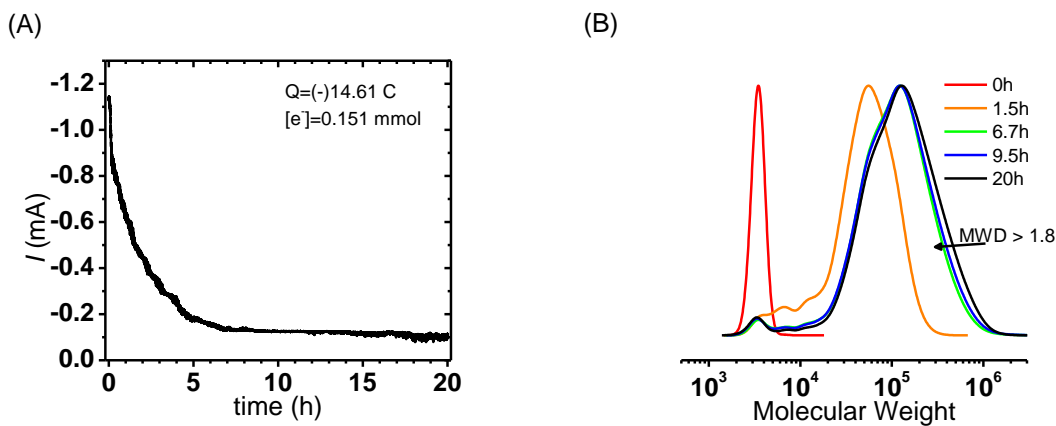


Figure VII-8. PEO star synthesis (Table VII-1, entry 5); (A) CV (red circle: applied potential); (B) CA results, total passed charge = 12.26 C; (C) crosslinker conversion and

log plot; (D) GPC traces; (E) eluograms of star polymers (20 h).

Variation of $[X]/[MI]$. The effect of EGDA (X) to PEO MI (MI) ratio on the star yields was investigated. Polymerizations were performed with four different ratios of $[X]/[MI] = 2.5, 5, 10,$ and 15 . The star polymerization with 2.5 equimolar (eq.) of X (Entry 2, $[MI] = 25$ mM) showed 87% star yield (Figure VII-5), however higher star yields were observed using higher molar ratios of $[X]/[MI]$; 90% and 95% star yields were observed using 5 eq. of X (Entry 3) and 10 eq. of X (Entries 4-6), respectively. According to these results, increased amounts of crosslinker can provide a more expanded, less congested core, and as a consequently, higher number of MI can be incorporated to the star molecules.¹⁴⁷ However, polymerization with the highest ratio of $[X]/[MI]$ (15 eq. of X) resulted in gelation by star-star coupling reactions from the expanded star core (Entry 7, Figure VII-9).¹⁴⁸



(C)

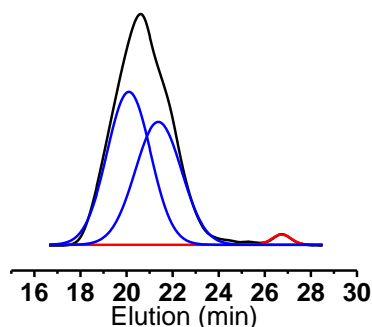
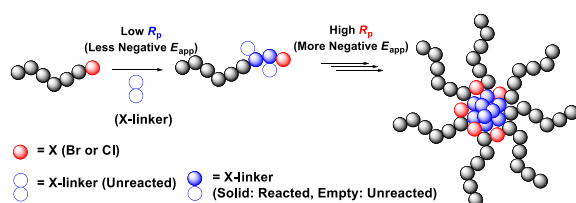


Figure VII-9. PEO Star polymerization (Table 1, entry 7); (A) CA results, total passed charge = 14.61 C; (B) GPC trace; (C) eluograms of star polymers (20 h).

Effect of E_{app} . Different E_{app} values were used to control of R_p by applying chronoamperometry over a range of 0.340 to 0.065 V (versus Ag/AgI/I⁻, 5% to > 99% of Cu^I, respectively by Nernst equation). More negative applied potential (E_{app}) leads to higher [Cu^I]/[Cu^{II}] ratio near working electrode surface. When combined with a vigorous stirring (900 rpm), such ratio might be adjusted throughout the solution, thus allowing R_p to be controlled by E_{app} .¹¹ When the polymerization was carried out at $E_{app} = 0.065$ V, the polymerization showed fast consumption of X as well as fast star formation (Figure VII-5). Similar results were observed in Entry 5; > 90% X consumption was observed in ~ 1 h, forming high molecular weight star polymers (Figure VII-8D). To minimize the loss of chain-end functionalities due to the fast reaction, the rate of polymerization was gradually increased using multi-step chronoamperometry (Entry 6). By applying a more positive potential ($E_{app,1} = 0.336$ V vs. Ag/AgI/I⁻) during the early stages of the reaction, the E_{app} can generate low radical concentrations, thus suppressing the premature termination as well

as star-star coupling reactions (k_p^{app} was 0.36 h^{-1} when $E_{\text{app}} = 0.336 \text{ V}$ (vs. Ag/AgI/T, entry 6, early stage), the observed value was 3.5 times less than $E_{\text{app}} = 0.189 \text{ V}$ (vs. Ag/AgI/T, $k_p^{\text{app}} = 1.26 \text{ h}^{-1}$, entry 5, early stage)). Then, the radical concentration was gradually elevated by applying increasingly more negative potentials (Figure VII-10, 0.336 to 0.189 V vs. Ag/AgI/T) and allowing for a faster polymerization. At this point the steric hindrance generated by arms of pre-stars would reduce star-star coupling reactions, while still allowing for incorporation of linear MIs (Scheme VII-5).¹⁴⁹ GPC-MALLS analysis indicated the star synthesis with multi-step chronoamperometry (Entry 6) provided higher molecular weights ($M_{n,\text{MALLS}} = 118.5 \times 10^3$) than polymerization with a single step E_{app} ($M_{n,\text{MALLS}} = 106.9 \times 10^3$, Entry 5). In addition, slightly higher star yield was observed in GPC eluogram (Figure VII-10E), because the polymerization with multi-step chronoamperometry (Entry 6) was less effected by star-star coupling reaction.



Scheme VII-5. Synthesis of PEO Star Polymers using Multi-step E_{app} .

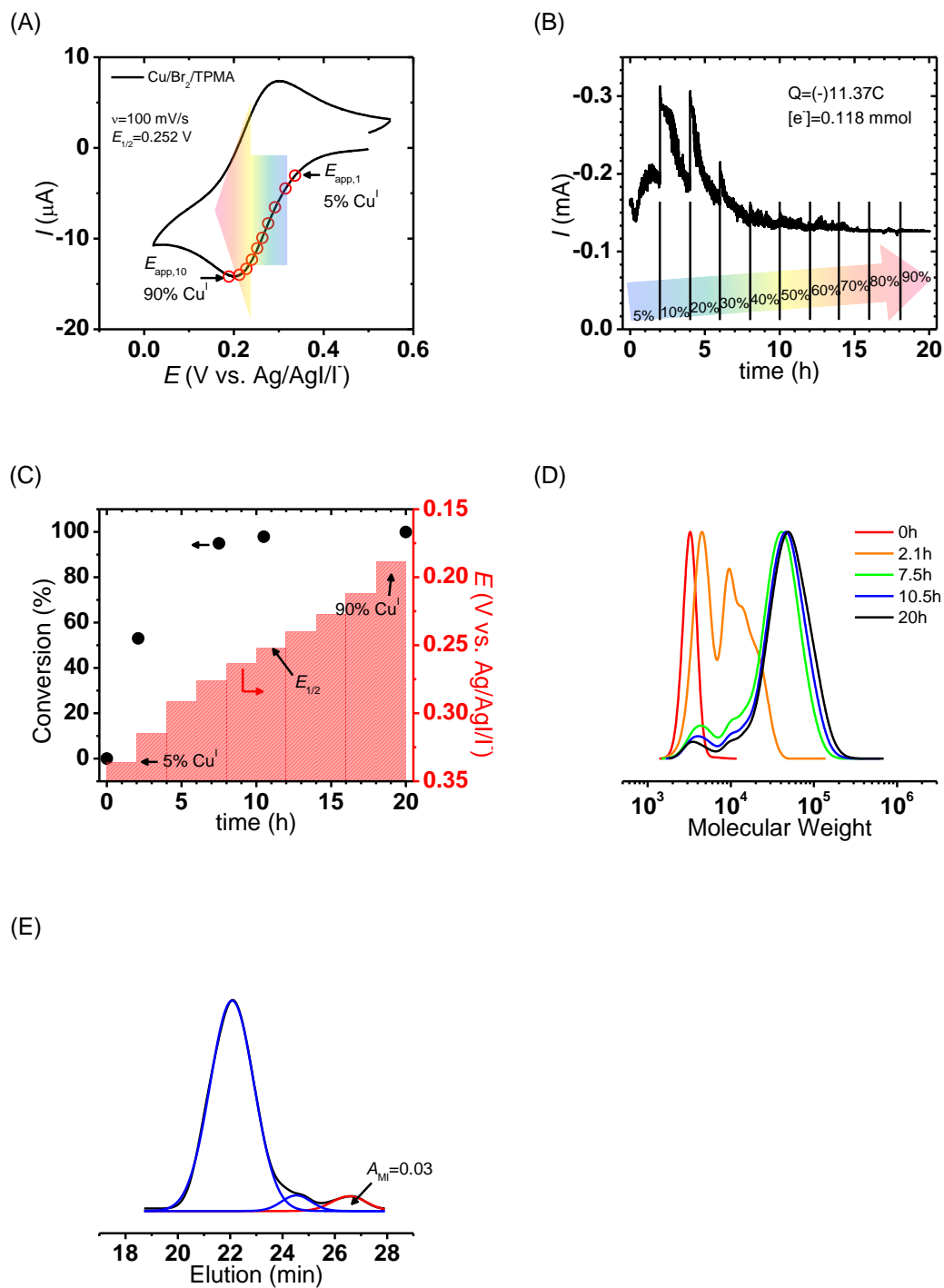


Figure VII-10. PEO star synthesis (Table VII-1, entry 6); (A) CV (E_{app} s from 0.340 to 0.189 V); (B) CA results, total passed charge = 11.37 C; (C) crosslinker conversion and

E_{app} versus time; (D) GPC traces; (E) GPC eluograms of star polymers (20 h).

VII. 4. Summary

The synthesis of star polymers *via* arm-first method was examined under various *e*ATRP conditions, achieving high star yields (up to 95%). Dilution of the [MI] (from 100 to 12.5 mM) and increased amounts of crosslinker improved the star yield ($[X]/[MI]=10$, > 95%). Additionally, multi-step chronoamperometry technique allowed for gradual increase of R_p , thus reducing star-star coupling and providing higher molecular weight stars with higher yield.

VII. 5. Experimental Section

Materials. Mono-hydroxy poly(ethylene glycol) methyl ether (HO-PEO, $M_n = 2000$), triethylamine (TEA), tetrabutylammonium perchlorate (TBAClO₄, > 98%), tetraethylammonium bromide (TEABr), 2-bromoisobutyl bromide (BriBBBr, 98%), copper(II) trifluoromethanesulfonate (CuOTf₂) were purchased from Aldrich. Ethylene glycol diacrylate (EGDA, 90% from Fluka), *n*-butyl acrylate (BA, > 99% from Aldrich) were purified by passing through a column filled with basic alumina to remove the inhibitor then stored at -5 °C until use. Tris(2-pyridylmethyl)amine (TPMA) was prepared according to a previously published procedure.⁸⁸

Synthesis of poly(ethylene oxide) macroinitiator (PEO MI). 20 g (10 mmol) of HO-PEO was dissolved in methylene chloride (30 mL) with 5.5 mL of TEA (20 mmol), and the reaction flask was placed in an ice bath. Then, 4.9 mL of BriBBBr (20 mmol) was slowly

added to the reaction mixture and the solution was stirred for 24 h at room temperature. The final product was purified by washing with pure water three times and the organic layer was collected. The final product was collected by precipitation against diethyl ether. The resulting white powder was dried overnight under vacuum.

Preparation of Cu/Br₂/TPMA solution. Stock solutions of CuOTf₂ (0.18 g, 0.5 mmol), TPMA (0.15 g, 0.5 mmol), and TEABr (0.21 g, 1 mmol) were dissolved in dry DMSO (total volume = 10 mL). The prepared Cu/Br₂/TPMA solution (50 mM) was used as catalysts for *e*ATRP.

Reaction cell configuration for *e*ATRP. Electrolysis experiments were carried out under N₂ atmosphere using a platinum (Pt) disk (for cyclic voltammetry, CV) and Pt mesh (for chronoamperometry, CA) working electrodes. The Pt mesh counter electrode was prepared using a glass frit and a salt bridge made of methylcellulose gel saturated with TBAClO₄ to separate the cathodic and anodic compartments. Potentials were measured versus an Ag/AgI/I⁻ reference electrode (Gamry Ref 600). To avoid solution evaporation during *e*ATRP procedure a condenser was connected to the reaction cell and cooled to -10 °C using a circulating chiller (NESLAB Inc., RTE-111).

Block copolymer synthesis by chain extension of PEO MI (PEO-*b*-PBA) by *e*ATRP. PEO MI (1.0 g, 0.50 mmol) and TBAClO₄ (1.37 g, 4 mmol) were added to a seven neck electrolysis cell maintained at 50 °C under a slow N₂ purge. Then, N₂ purged BA (14.3 mL, 100 mM), Cu/Br₂/TPMA solution (0.3 mL), and DMF (20 mL) were added to the reaction cell. The solution was subjected to an applied potential of (0.065 V vs.

Ag/AgI/I⁻) using potentiostatic instrument with vigorous stirring (900 rpm) during the polymerization. Samples were withdrawn periodically to follow the monomer conversion, using gas chromatography (GC), and to determine number average molecular weight (M_n) and molecular weight distribution (M_w/M_n) by gel permeation chromatography (GPC) measurements (with PMMA standard curve).

Star polymer synthesis. The following conditions provide an example of *e*ATRP for star polymer synthesis: PEO MI (500 mg, 2.5×10^{-1} mmol) and TBAClO₄ (1.37 g, 4 mmol) were added to a seven neck electrolysis cell maintained at 50 °C under a N₂ purge. Then, N₂ purged EGDA (450 µL, 2.5 mM), Cu/Br₂/TPMA solution (0.2 mL), and DMF (20 mL) were added to the reaction cell. The solution was subjected to an applied potential (0.340 to 0.189 V vs. Ag/AgI/I⁻) using potentiostatic instrument with vigorously stirring (900 rpm) during polymerization. Samples were withdrawn periodically for gas chromatography (GC) analysis for conversion of EGDA, and GPC measurement for molecular weight and distribution determination of the star polymers (with PMMA standard curve). The final star polymers were purified by dialysis, molecular weight cut-off = 1000, under methanol for measuring absolute molecular weight by GPC with multi angle laser light scattering detector (MALLS).

Measurements. ¹H NMR (300 MHz) spectra were taken on a Bruker Avance 300 spectrometer using CDCl₃ as a solvent. GC analysis was carried out using a Shimadzu GC 17A equipped with a FID detector and a Unichrom Scientific 30 m column (520-6330). Molecular weights and distributions were determined by GPC (Polymer Standards Services (PSS) columns (guard, 10⁵, 10³, and 10² Å), with THF eluent at 35 °C, flow rate 1.00

mL/min, and differential refractive index (RI) detector (Waters, 2410)). The apparent molecular weights and dispersity (M_w/M_n) were determined with a calibration based on linear poly(methyl methacrylate) standards using WinGPC 8.0 software from PSS. Absolute molecular weights were determined using ASTRA software from Wyatt Technology by GPC-MALLS containing RI detector (Wyatt Technology, Optilab REX), viscometer detector (Wyatt Technology, ViscoStar), and a multi-angle laser light scattering (MALLS) detector (Wyatt Technology, DAWN EOS) with the light wavelength at 690 nm. All CVs and CAs were conducted with a Gamry Ref 600 potentiostat.

VII. 6. References

1. Bortolamei, N.; Isse, A. A.; Magenau, A. J. D.; Gennaro, A.; Matyjaszewski, K., *Angew. Chem. Int. Ed.* **2011**, *50* (48), 11391-11394.
2. (a) Matyjaszewski, K.; Jakubowski, W.; Min, K.; Tang, W.; Huang, J.; Braunecker, W. A.; Tsarevsky, N. V., *Proc. Natl. Acad. Sci. USA* **2006**, *103* (42), 15309-15314; (b) Jakubowski, W.; Matyjaszewski, K., *Angewandte Chemie, International Edition* **2006**, *118* (27), 4594-4598; (c) Magenau, A. J. D.; Kwak, Y.; Matyjaszewski, K., *Macromolecules* **2010**, *43* (23), 9682-9689; (d) Zhang, Y.; Wang, Y.; Peng, C.-h.; Zhong, M.; Zhu, W.; Konkolewicz, D.; Matyjaszewski, K., *Macromolecules* **2011**.
3. (a) Li, B.; Yu, B.; Huck, W. T. S.; Zhou, F.; Liu, W., *Angewandte Chemie, International Edition* **2012**, *51* (21), 5092-5095; (b) Li, B.; Yu, B.; Huck, W. T. S.; Liu, W.; Zhou, F., *J. Am. Chem. Soc.* **2013**, *135* (5), 1708-1710; (c) Magenau, A. J. D.; Bortolamei, N.; Frick, E.; Park, S.; Gennaro, A.; Matyjaszewski, K., *Macromolecules* **2013**, *46* (11), 4346-4353.
4. (a) Hadjichristidis, N.; Pitsikalis, M.; Pispas, S.; Iatrou, H., *Chem. Rev.* **2001**, *101* (12), 3747-3792; (b) Vamvakaki, M.; Hadjiyannakou, S. C.; Loizidou, E.; Patrickios, C. S.; Armes, S. P.; Billingham, N. C., *Chemistry of Materials* **2001**, *13* (12), 4738-4744; (c) Stenzel, M. H.; Davis, T. P., *J. Polym. Sci., Part A Polym. Chem.* **2002**, *40* (24), 4498-4512; (d) Gao, H.; Matyjaszewski, K., *Progress in Polymer Science* **2009**, *34* (4), 317-350; (e) Blencowe, A.; Tan, J. F.; Goh, T. K.; Qiao, G. G., *Polymer* **2009**, *50* (1), 5-32; (f) Matyjaszewski, K.; Xia, J., *Chemical Reviews* **2001**, *101* (9), 2921-2990; (g) Tsarevsky, N. V.; Matyjaszewski, K., *Chem. Rev.* **2007**, *107* (6), 2270-2299; (h) Allan, L. E. N.; Perry, M. R.; Shaver, M. P., *Prog. Polym. Sci.* **2012**, *37* (1), 127-156; (i) Gregory, A.; Stenzel, M. H., *Progress in Polymer Science* **2012**, *37* (1), 38-105; (j) Siegwart, D. J.; Oh, J. K.; Matyjaszewski, K., *Prog. Polym. Sci.* **2012**, *37* (1), 18-37; (k) Higashihara, T.; Hayashi, M.; Hirao, A., *Progress in Polymer Science* **2011**, *36* (3), 323-375; (l) Tasdelen, M. A.;

- Kahveci, M. U.; Yagci, Y., *Progress in Polymer Science* **2011**, 36 (4), 455-567; (m) Beija, M.; Marty, J.-D.; Destarac, M., *Progress in Polymer Science* **2011**, 36 (7), 845-886; (n) Matyjaszewski, K.; Tsarevsky, N. V., *Nat Chem* **2009**, 1 (4), 276-288.
5. (a) Gao, H.; Matyjaszewski, K., *J. Am. Chem. Soc.* **2007**, 129 (38), 11828-11834; (b) Zhu, W.; Zhong, M.; Li, W.; Dong, H.; Matyjaszewski, K., *Macromolecules* **2011**, 44 (7), 1920-1926.
6. (a) Hadjichristidis, N., *J. Polym. Sci., Part A Polym. Chem.* **1999**, 37 (7), 857-871; (b) Fukukawa, K.-i.; Rossin, R.; Hagooly, A.; Pressly, E. D.; Hunt, J. N.; Messmore, B. W.; Wooley, K. L.; Welch, M. J.; Hawker, C. J., *Biomacromolecules* **2008**, 9 (4), 1329-1339; (c) Park, S.; Cho, H. Y.; Yoon, J. A.; Kwak, Y.; Srinivasan, A.; Hollinger, J. O.; Paik, H.-j.; Matyjaszewski, K., *Biomacromolecules* **2010**, 11 (10), 2647-2652; (d) Cho, H. Y.; Gao, H.; Srinivasan, A.; Hong, J.; Bencherif, S. A.; Siegwart, D. J.; Paik, H.-j.; Hollinger, J. O.; Matyjaszewski, K., *Biomacromolecules* **2010**, 2199-2203; (e) Cho, H. Y.; Srinivasan, A.; Hong, J.; Hsu, E.; Liu, S.; Shrivats, A.; Kwak, D.; Bohaty, A. K.; Paik, H.-j.; Hollinger, J. O.; Matyjaszewski, K., *Biomacromolecules* **2011**, 12 (10), 3478-3486; (f) Ferreira, J.; Syrett, J.; Whittaker, M.; Haddleton, D.; Davis, T. P.; Boyer, C., *Polym. Chem.* **2011**, 2 (8), 1671-1677; (g) Park, S.; Zhong, M.; Lee, T.; Paik, H.-j.; Matyjaszewski, K., *ACS Applied Materials & Interfaces* **2012**, 4 (11), 5949-5955; (h) Zhang, Z.; Hao, X.; Gurr, P. A.; Blencowe, A.; Hughes, T. C.; Qiao, G. G., *Aust. J. Chem.* **2012**, 65 (8), 1186-1190.
7. (a) Gao, H.; Ohno, S.; Matyjaszewski, K., *J. Am. Chem. Soc.* **2006**, 128 (47), 15111-15113; (b) Gao, H.; Matyjaszewski, K., *Macromolecules* **2007**, 40 (3), 399-401; (c) Gao, H.; Matyjaszewski, K., *Macromolecules* **2008**, 41 (12), 4250-4257.
8. Gao, H.; Matyjaszewski, K., *Macromolecules* **2006**, 39 (9), 3154-3160.
9. Gao, H.; Min, K.; Matyjaszewski, K., *Macromolecules* **2007**, 40 (22), 7763-7770.
10. Burdyńska, J.; Cho, H. Y.; Mueller, L.; Matyjaszewski, K., *Macromolecules* **2010**, 43 (22), 9227-9229.
11. Xia, J.; Matyjaszewski, K., *Macromolecules* **1999**, 32 (8), 2434-2437.

Chapter VIII

Modification of the Surface of Silicon Wafers with Temperature Responsive Crosslinkable Poly((Oligo Ethylene Oxide) Methacrylate) Based Star Polymers*

VIII. 1. Preface

This Chapter focuses on utilization of star polymers as a surface modifier. The advantages of preparation of star polymers by the arm-first method were discussed in Chapter VII. Star polymers with UV crosslinkable groups (benzophenone moieties) at the periphery of the star molecules were synthesized and utilized for modification of the surface of silicon wafers. Oilgo(ethylene oxide) monomethyl ether methacrylates (OEOMAs) were selected as the repeating units of star arms in order to introduce thermoresponsive properties, due to their lower critical solution temperature (LCST) behavior and biocompatibility. Moreover, their LCST can be tuned by copolymerization of OEOMAs of different molecular weights. One of interesting observations from this study was the high stability of crosslinked star polymer film on the silicon wafer substrate. Typically, ethylene oxide (EO) units can weakly bond to -Si-O-H; however, the presence of multiple EO groups present on the star molecules showed strong binding affinity to the wafer surface due to multiple hydrogen bonding. A more detailed study of the mechanisms was conducted by my former group member, Dr. Patricia Golas in conjunction with Prof.

*Work in this chapter was published and partially reformatted based on the following manuscript: **Sangwoo Park**; Mingjiang Zhong; Taeheon Lee; Hyun-jong Paik; Krzysztof Matyjaszewski *ACS Appl Mater Interfaces* **2012**, 4, 5949

Robert Tilton.

The synthesized thermoresponsive OEOMA based star polymers surfaces can be further utilized as cell harvesting surfaces, as addressed in Chapter IX.

My main contributions in this research topic included the synthesis of star polymers, surface modification and analyzing LCST behavior of the polymers. I appreciate the contribution of my former group member, Dr. Mingjiang Zhong, for his AFM analysis. I also would like to thank my previous group member, Taeheon Lee, for his efforts on synthesis of functional initiators, and Prof. Hyun-jong Paik for invaluable discussions.

VIII. 2. Introduction

The modification of surfaces by the deposition of polymeric materials is an attractive procedure because of easy modification of the chemical/physical properties of the targeted surfaces. Examples include surfaces for cell cultivation or immobilization of bioactive compounds on surfaces for biomedical applications, preparation of high efficiency antifouling/antibacterial surfaces, and desalination filter membranes, etc.¹⁵⁰ Typically, two polymer modification techniques have been exploited for the preparation of polymer modified surfaces: grafting from and grafting onto. The grafting from technique can introduce dense grafting of well-defined polymer chains on the surfaces of substrates.^{67b, 151} However, the grafting from method requires several preparation steps: immobilization of initiating groups on the target surface, and inert conditions during polymerization. Nevertheless, in some cases, a high graft density and the formation of high molecular weight polymeric chains can be achieved. The grafting onto technique can modify the target surfaces by utilizing coupling reactions between reactive polymer chain-ends and functional surfaces.¹⁵² However, it is difficult to accomplish high grafting density when employing the grafting onto method. To overcome the limitations of both procedures, the development of a simple technique providing a uniform robust polymer film for surface modification is required. One of the feasible ways to overcome the limitations should be to use star shape polymers with multiple group binding to the surfaces. For instance, Sofia *et al.* used linear and star shape poly(ethylene oxide) (PEO) for silicon (Si) wafer surface modifications, and compared their graft densities.¹⁵³ The results from star shape PEO modified surfaces showed a higher grafting density than linear PEO, because of effective

overlap at the surfaces by spreading polymer chains (arms of star polymers). Kim *et al.* recently reported a high efficiency of antifouling membranes prepared by using star polymers.¹⁵⁴

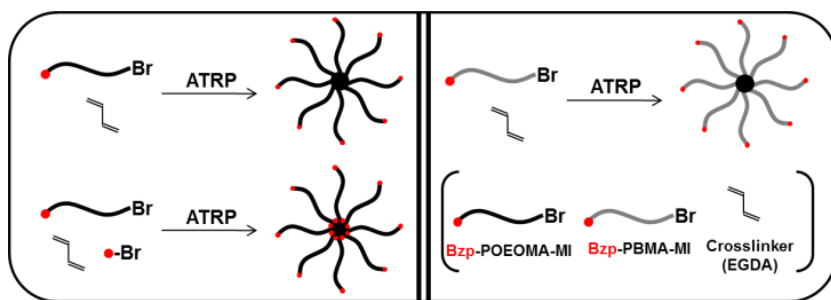
A recent development in the atom transfer radical polymerization (ATRP) technique provides a convenient procedure for the synthesis of functional polymers with complex architectures.^{1e, 2b, 2d, 15, 42c, 61c, 61d, 155} Star shape polymers possess an architecture with multiple linear arms linked to a central core and combine interesting properties of a branched architecture, globular shape, and chemically crosslinked structure.^{42c, 42d, 156} One approach to star macromolecules is the synthesis of α -functionalized linear macroinitiators (MIs) by ATRP and subsequent chain extension with divinyl or multivinyl compounds to form the crosslinked core of a star polymer.¹⁵⁷ This approach can provide star polymers with various chemical composition, stimuli-responsiveness, and site specific functionalities.^{42c, 42d}

Recently, PEO based polymeric materials have been successfully used because of their physical adhesion to metal-oxo surfaces. For example, Soler-Illia and Sanchez¹⁵⁸ reported the interaction between PEO based surfactants and transition metal alkoxides and discussed the mechanism for interactions between the PEO surfactants and transition metal surface, while Voronin *et al.*¹⁵⁹ reported interactions between PEO and fumed silica. However, in most cases, the degree of coordination is too weak to sustain long term adsorption between the PEO based materials and metallic substrates. This Chapter discusses the results of a systematic study that provides a simple and robust procedure for the preparation of thermally responsive, stable polymer films on the surfaces of Si wafers by star polymers.

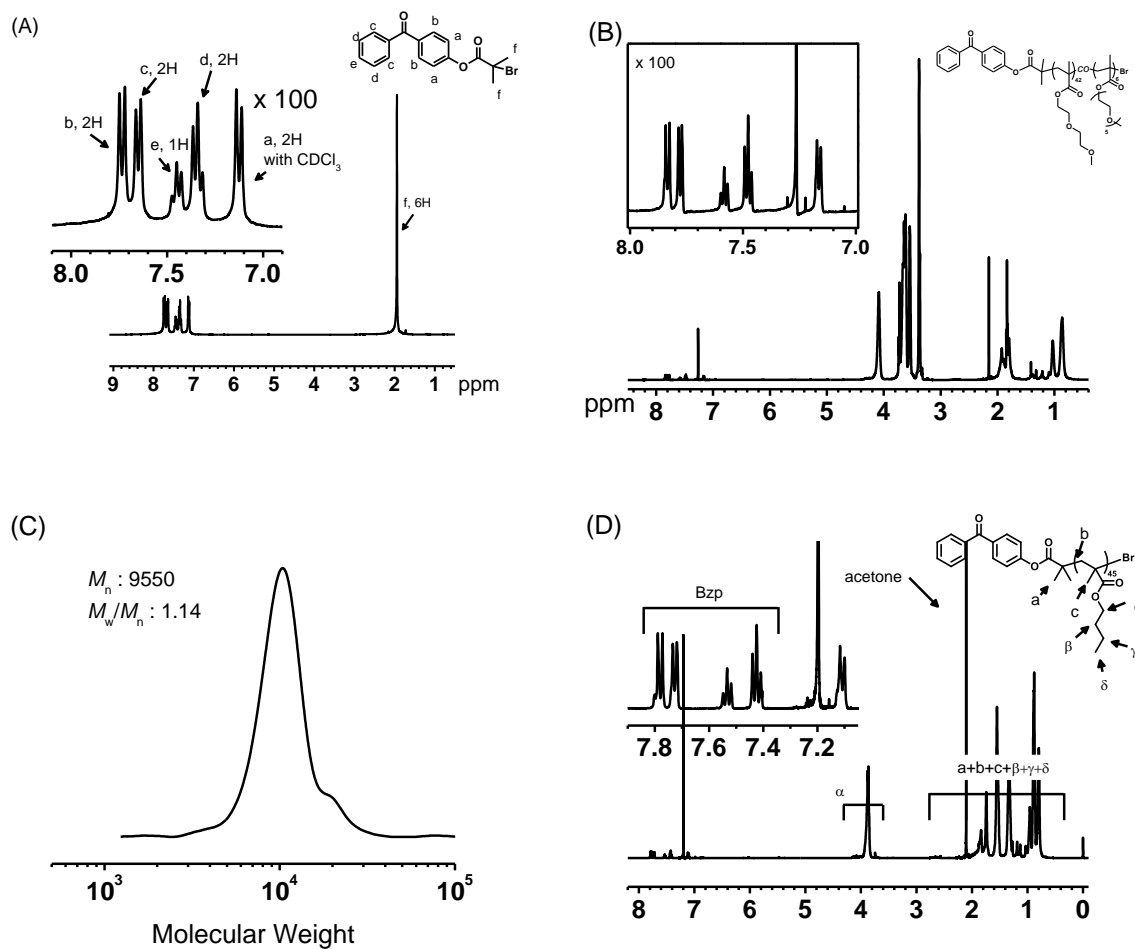
Linear and star polymers, with variable composition and functionalities based on oligo(ethylene oxide) methyl ether methacrylate (OEOMA), a derivative of PEO, and *n*-butyl methacrylate (BMA) as comonomers were prepared. The introduction of UV reactive groups, benzophenone (Bzp), into the polymers, at the α -chain-end for linear polymers and within the core and/or at the periphery of the star polymers, provided the ability for crosslinking polymer films, deposited on the surfaces of a silicon wafer and provides a simple procedure for stable surface modification.

VIII. 3. Results and Discussion

Preparation of UV crosslinkable polymers. The benzophenone initiator (Bzp-ini) was prepared by the reaction between 4-hydroxybenzophenone and 2-bromoisobutyryl bromide under basic conditions. The purity of the final product was measured by ^1H NMR (Figure VIII-1A). Macroinitiators containing α -Bzp, Bzp-POEOMA (MI) and Bzp-PBMA (MI), Figure VIII-1B-E, were synthesized by ATRP and successfully purified by fractional precipitation. Subsequently each of the MIs was chain extended with a crosslinker, (EGDA), to prepare Bzp-POEOMA and Bzp-PBMA star polymers, respectively. The Bzp-dual functionalized POEOMA star polymers (core and periphery) were prepared by the addition of a fraction of low molecular weight Bzp-ini to the MI prior to the star core forming polymerization (Scheme VIII-1).



Scheme VIII-1. Preparation of benzophenone functionalized POEOMA and PBMA linear and star polymers.



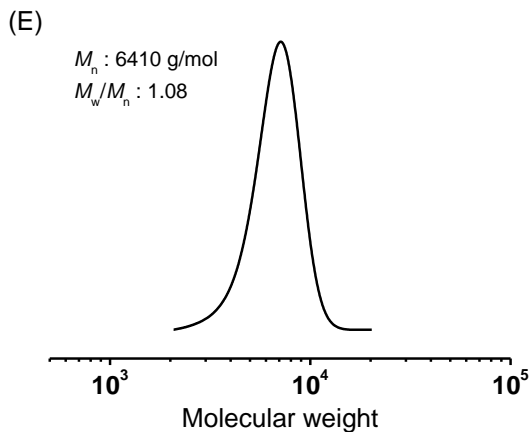


Figure VIII-1. (A) ^1H NMR spectrum of Bzp-initiator; 300 MHz ^1H NMR spectrum and GPC trace of (B-C) Bzp-POEOMA MI, and (D-E) Bzp-PBMA MI. The MW of each polymer was determined by PMMA standards.

Each of the polymerizations was monitored by THF GPC (Figure VIII-2). The Bzp-POEOMA and Bzp-dual functionalized POEOMA star polymers were successfully purified by fractional-precipitation against an excess THF/ethyl ether (10/90, by v/v) mixture (Figure VIII-2A and B) while the Bzp-PBMA star polymers were precipitated against a THF/methanol (10/90, by v/v) mixture to remove any unreacted MIs. The final products were dried overnight under vacuum. THF GPC curves show that purified products were successfully isolated. The absolute molecular weights were determined by GPC-MALLS. Table VIII-1 lists the MWs of the linear and star polymers and the number of arms in the stars. The chemical structure of each star polymer was determined by ^1H NMR (Figure VIII-2D) and benzophenone functionalities in the star polymers were confirmed by the presence of signals at $\delta = 8\text{--}7$ ppm.

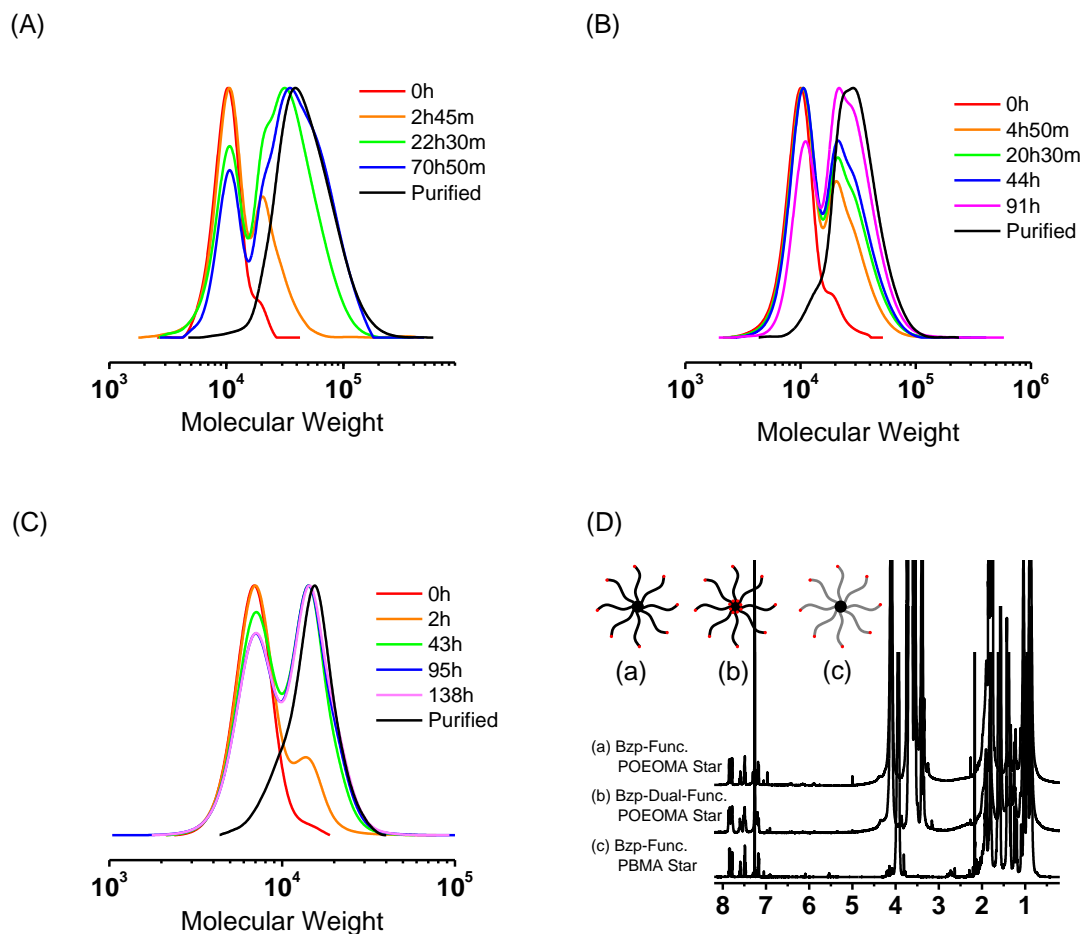


Figure VIII-2. GPC traces of (A) Bzp-POEOMA star, (B) Bzp-dual functional POEOMA star and (C) Bzp-PBMA star polymers; (D) 300 MHz ^1H NMR spectra of (a) Bzp-POEOMA star, (b) Bzp-dual functionalized POEOMA star, and (c) Bzp-PBMA star polymers.

Table VIII-1. Summary of the Bzp functionalized polymers.

Entry	Polymer	MW(M_n)	MWD (M_w/M_n)	dn/dc ^c	# of Arms ^d
1	Bzp-POEOMA MI	9,550 ^a	1.14		
2	Bzp-PBMA MI	6,410 ^a	1.08		

3	Bzp-POEOMA star	109,500 ^b	1.50	0.077	11
4	Bzp-dual POEOMA star	109,800 ^b	1.53	0.102	11
5	Bzp-PBMA star	51,780 ^b	1.21	0.074	8

^a MWs were determined by THF GPC with PMMA standard; ^b MWs of star polymers were determined by GPC-MALLS; ^c dn/dc values were obtained from 100% mass recovery by using ASTRA program; ^d number of arm was calculated by MW_{star} (entry 3-5) divided by MW_{MI} (entry 1 and 2).

Modification of the surface of Si wafers with linear and star polymers. Table VIII-2 provides a summary of polymer film thicknesses and stabilities before/after the multiple washing procedures with THF, MeOH, water, and acetone. Polymer solutions (0.3% by wt/v) were prepared and the solutions were spin-coated onto silicon wafers and then dried for 10 min. Ellipsometric analysis revealed the successful formation of polymer films after spin-coating of the polymers onto the silicon wafer. The polymers deposited on the silica surfaces were exposed to UV light ($\lambda = 365$ nm) to trigger Bzp crosslinking reactions, and then the surfaces were washed several times with solvents to remove residual/unreacted components. After washing, the surfaces were dried for 5 h under vacuum, and ellipsometric analysis was carried out to measure the thicknesses of the polymer films. The ellipsometric results showed that the polymer films prepared by the deposition of linear polymers and the BMA star polymer (Table VIII-2, entries 1,2, and 5) were vulnerable to solvent exposure and indeed were unstable, as a result, the polymers were easily removed from the surface. In contrast, different results were observed from Bzp containing POEOMA based star polymers. Both of the surfaces modified with Bzp functionalized

POEMA (Table VIII-2, entry 3 and 4) showed that the polymer films adhered to the Si wafer surfaces and were resistant to solvent washing. Figure VIII-3 shows images of the two surfaces modified with POEOMA based star polymers after washing. The surface modified with the Bzp-dual functionalized POEOMA star (Table VIII-2, entry 4) showed higher stability when compared to the partially stable surface modified with the Bzp periphery functionalized POEOMA star (Table VIII-2, entry 3). The polymer film from entry 3 showed a bumpy surface (Figure VIII-3A), while that from entry 4 (Table VIII-2) showed formation of a smooth surface (Figure VIII-3B). The results could be attributed to better chelating effects and/or the effect of multiple hydrogen bonds between the densely crosslinked multiple arm structure of the Bzp-dual functionalized POEOMA and the surface SiO₂/Si-OH layers. Interaction of PEO with the Si/SiO₂ wafer surfaces was previously reported.¹⁵⁸⁻¹⁶⁰ The PEO moieties of the star polymers can interact with Si/SiO₂ in a similar way, also *via* hydrogen bonding with surface silanol groups. Because the POEOMA star polymers contain multiple PEO moieties (from the star arms), a large number of the ether oxygen atoms could effectively cover the Si/SiO₂ wafer surface. Among two POEOMA star polymers, Bzp-dual-functionalized star polymers can introduce additional cross-linking points to the polymer films and, therefore, a denser POEOMA network should enhance adhesion.

Table VIII-2. Thicknesses and stabilities of the polymer modified surfaces.

Entry	Polymer	Thickness (nm) ^a		Stability
		(before	(after	

		washing)	washing)	
1	Bzp-POEOMA MI	28.8 ± 1.3	ND	ND
2	Bzp-PBMA MI	27.7 ± 1.2	ND	ND
3	Bzp-POEOMA star	32.3 ± 0.8	33.5 ± 2.8	Partially stable
4	Bzp-dual POEOMA star	30.5 ± 1.1	31.2 ± 1.5	Stable
5	Bzp-PBMA star	28.8 ± 0.9	ND	ND

^a The average thicknesses of polymer film were determined by ellipsometry with 5 times measurements with standard deviations; ND: not detected.

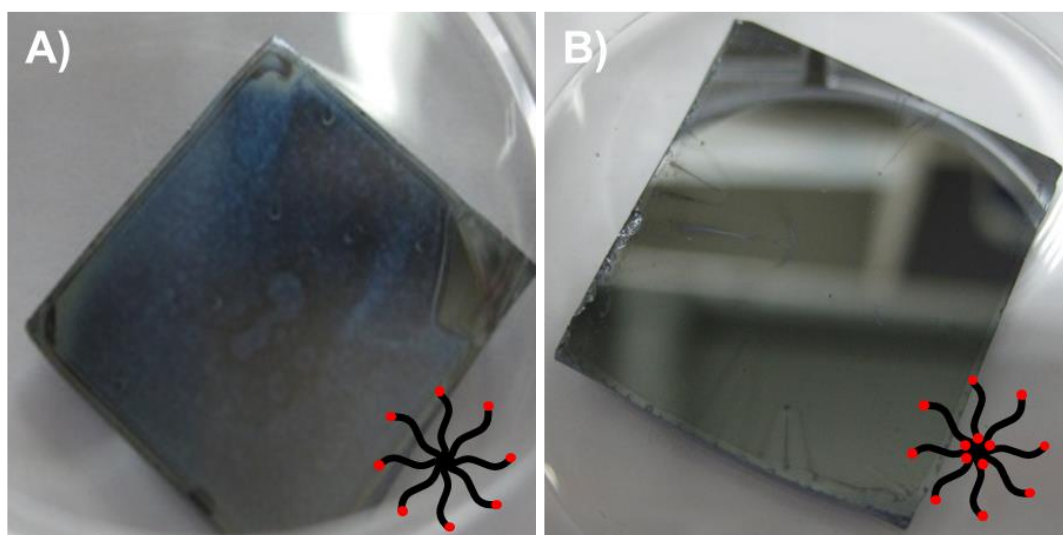


Figure VIII-3. Photograph of star polymers modified surfaces; (A) Bzp-POEOMA star polymers and (B) Bzp-dual functionalized POEOMA star polymers.

Temperature responsive polymer surfaces. The Bzp-dual functionalized POEOMA star polymers (Table VIII-2, entry 4) were evaluated as materials for the preparation of temperature responsive polymer surfaces and then utilized to prepare UV triggered

patternable surfaces. Because the star polymers contained photocrosslinkable moieties (Bzp), the surface modification was simply conducted by exposing the deposited film to UV light ($\lambda = 365$ nm). The thicknesses of the crosslinked polymer films were measured and, because the solutions were of relatively low concentrations (0.3 to 1.0 %, wt/v), they increased linearly with increasing polymer solution concentration (Figure VIII-4).

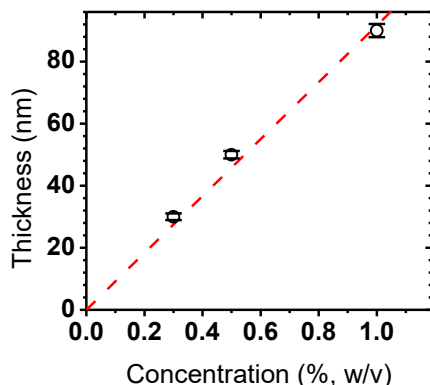


Figure VIII-4. Variation in polymer film thicknesses when using different concentrations of polymer solution. The average values were determined by averaging 5 ellipsometry measurements with standard deviations.

The POEOMA based star polymers have LCST behavior and the critical temperature (T_c) was approximately 27 °C (Figure VIII-5). The star polymers were deposited onto the silicon wafer surfaces, crosslinked and then the temperature responsiveness of the modified surfaces was measured. Contact angle measurements were carried out to determine the thermal response behavior. Table VIII-3 lists film thicknesses and contact angle results for the POEOMA based star modified surfaces. Two different temperatures were chosen to measure the surface contact angle, 20 and 37 °C, one below and one above T_c of the star

polymers, respectively. Below T_c (20 °C), the contact angle of the modified surfaces was around 50°, and above T_c (37 °C) it was approximately 72° clearly showing that the hydrophilicity of the modified surfaces can be controlled by changing of the temperature of the environment.

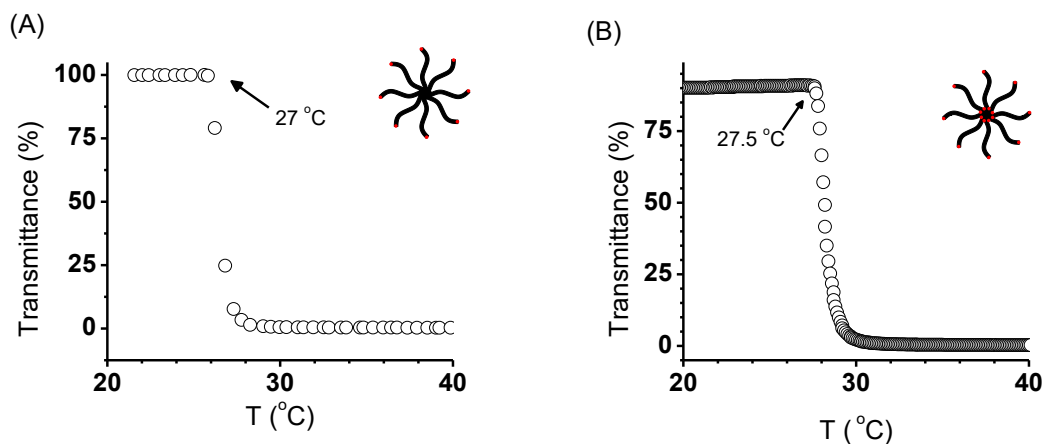


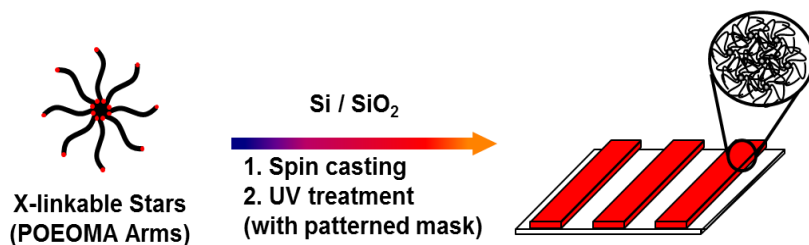
Figure VIII-5. Temperature response behavior of (A) Bzp-POEOMA star and (B) Bzp-dual functionalized POEOMA star. Concentration of solutions were 1 mg/mL and heating rates were 1 °C/min.

Table VIII-3. Summaries of contact angle measurements and film thicknesses.

Entry	Solution Concentration ^a (%)	Contact Angle ^b (°)		Thickness ^c (nm)
		20 °C	37 °C	
1	0.3	50.0 ± 1.2	71.5 ± 1.4	31 ± 1.1
2	0.5	49.5 ± 0.7	72.1 ± 0.6	52 ± 1.2
3	1.0	56.3 ± 5.1	73.9 ± 1.2	89 ± 2.1

^a Bzp-dual functionalized POEOMA star polymers were dissolved in CHCl_3 (% wt/v); ^b Contact angles were determined by sessile drop method with 5 times measurements; ^c Thicknesses were determined by ellipsometry with 5 times measurements

Surface patterning using the Bzp-dual functionalized POEOMA star polymers. The Bzp-dual functionalized star polymers were utilized to prepare patterned surfaces (Scheme VIII-2). A solution of the star polymer (0.3%, by wt/v in CHCl_3) was deposited on the surface of a silicon wafer by spin-coating and then the film was exposed to UV light ($\lambda = 365 \text{ nm}$) for 10 min using a stripe patterned mask, 100 μm width with 4 mm, length for optical microscopic analysis and AFM measurements. After UV irradiation, the surface was gently washed several times with acetone, methanol, THF, and dried. Figure VIII-6 shows the optical microscopic images of the patterned surfaces. Well defined film patterns were successfully formed, and the shape and size of each pattern was well-matched to the photomask. AFM measurements were used for determination of the polymer film height profiles (Figure VIII-7). The results showed that the polymer film thickness was $\sim 30 \text{ nm}$ with $\pm 10 \text{ nm}$ roughness. The film thickness was well-matched by non-patterned star polymer modified surfaces.



Scheme VIII-2. Surface patterning by Bzp-dual functionalized POEOMA star polymers.

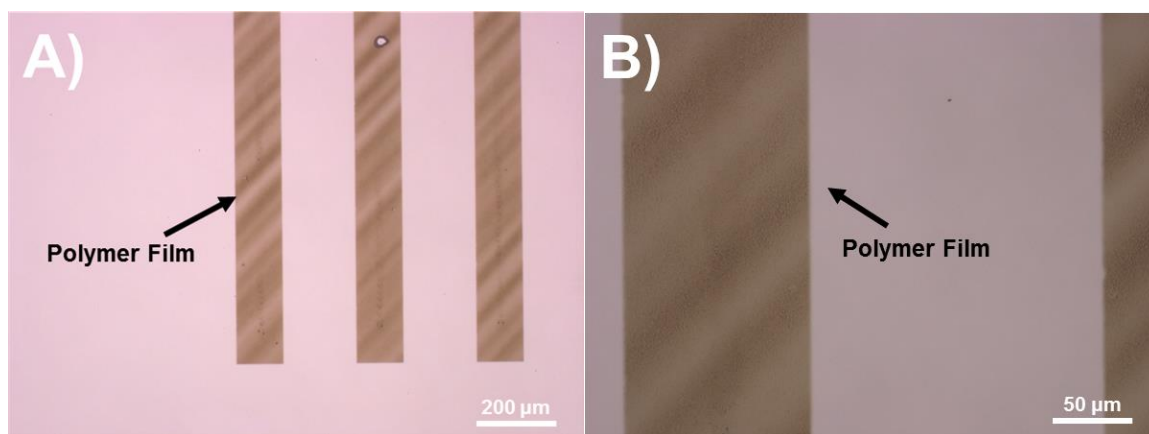
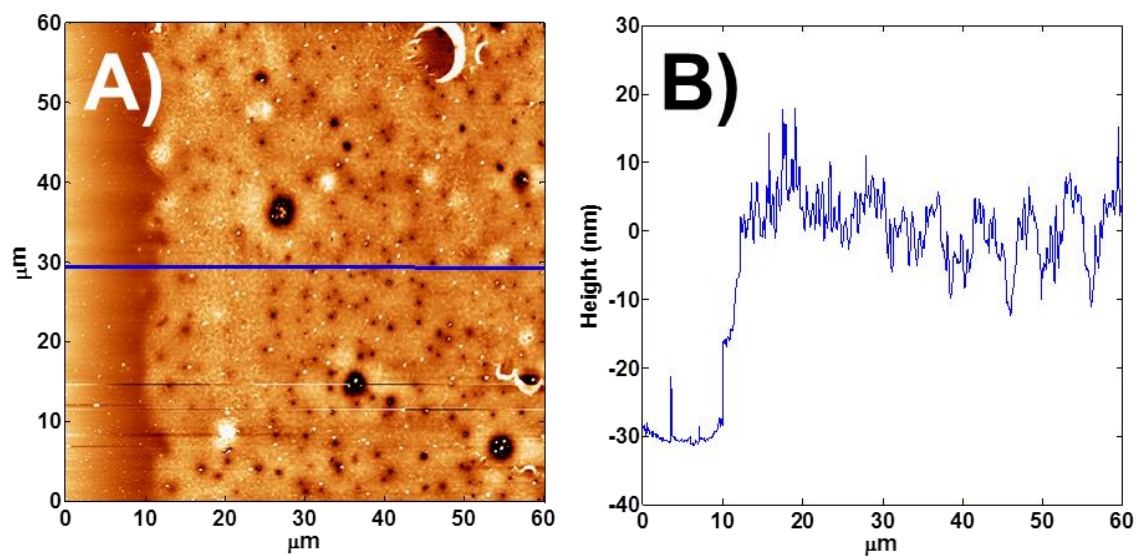


Figure VIII-6. Optical microscopic images of polymer patterned surfaces; (A) Scale bars correspond to 200 μm (magnification 5x), (B) 50 μm (magnification 20x).



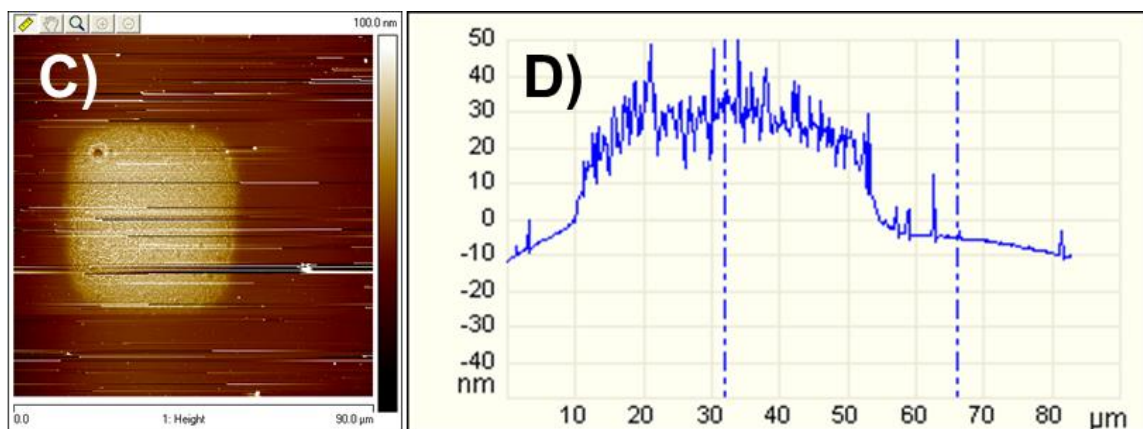


Figure VIII-7. AFM analysis of stripe patterned surface (100 μm width) – (A) height image and (B) height profile (blue line); AFM analysis for 50 μm square patterned surface – (C) Height image, (D) height profile.

VIII. 4. Summary

The well-defined POEOMA and PBMA polymers, both linear and star shape, containing photocrosslinkable benzophenone groups were successfully prepared by ATRP. POEOMA star polymers with benzophenone functional groups on the periphery and within the core (dual functionalization) formed films with good stability after deposition of a polymer solution onto the surface of silicon wafers and UV triggered crosslinking. The POEOMA star polymers have LCST at ~ 27 °C, and temperature responsive behavior of the deposited films could be observed for the modified surfaces by changing the temperature of the environment. Furthermore, patterned polymer surfaces were easily prepared by simple UV irradiation with a photomask.

VIII. 5. Experimental Section

Materials. 2-(2-Methoxyethoxy)ethyl methacrylate (MEO₂MA, 95%), oligo(ethylene oxide) methacrylate with 4 (to 5) ethylene oxide unit (OEOMA₃₀₀, $M_n = 300$), n-butyl methacrylate (BMA, 99%), and ethylene glycol diacrylate (EGDA, 90%) were purchased from Aldrich and purified by passing through a column filled with basic alumina to remove the inhibitor then stored at -5 °C. CuBr (99%, Aldrich) and CuCl (90%, Aldrich) were purified using literature procedures.¹⁶¹ All other reagents, 4-hydroxybenzophenone, 2-bromoisobutyryl bromide, 4,4'-dinonyl-2,2'-bipyridine (dNbpy), 2,2'-bipyridine (bpy), copper(II) bromide (CuBr₂), *N,N,N',N'',N'''*-pentamethyldiethylenetriamine (PMDETA), triethylamine (TEA) and solvents were purchased at the highest purity from Aldrich and used without further purification. Silicon wafer was purchased from MEMC Electronic Materials, Inc.

Synthesis of benzophenone initiator (Bzp-ini). Benzophenonyl 2-bromoisobutyrate (Bzp-ini) was prepared according to a previously published procedure.¹⁶² Briefly, 10 g (50 mmol) of 4-hydroxy benzophenone was dissolved in methylene chloride (30 mL) with 7.6 mL of TEA (55 mmol), and the reaction flask was placed in an ice bath. Then 6.8 mL of 2-bromoisobutyryl bromide (55 mmol) was slowly added to the reaction mixture and the solution stirred for 12 h. The desired product was separated by extraction with pure water three times, and the organic layer was collected and dried overnight.

Synthesis of Bzp-POEOMA and Bzp-PBMA linear polymers. Similar procedures were used for the preparation of both macroinitiators (Bzp-POEOMA MI and Bzp-PBMA MI). Briefly, Bzp-ini (209 mg, 6.38×10^{-1} mmol), CuBr (37 mg, 2.55×10^{-1} mmol), CuBr₂ (13 mg, 6.38×10^{-2} mmol), and dNbpy (246 mg, 6.38×10^{-1} mmol) were added to a 25 mL

Schlenk flask and vacuumed dried. The flask was backfilled with nitrogen. MEO₂MA (10 mL, 54.19 mmol), OEOMA₃₀₀ (2.7 mL, 9.56 mmol) and anisole (12.7 mL) were then added to the flask and the mixture was stirred at 60 °C. The reaction was stopped after 2 h and the solution was passed through neutral alumina to remove the copper complex. The product was precipitated by addition of excess hexane and dried under vacuum overnight. GPC analysis showed $M_n = 9,550$ and $M_w/M_n = 1.14$ (PMMA standards). The Bzp-PBMA MI was prepared using the same molar ratio of reagents and the M_n and M_w/M_n of final products were measured by GPC ($M_n = 6,410$ and $M_w/M_n = 1.08$ (PMMA standards)).

Synthesis of Bzp-POEOMA and Bzp-PBMA star polymers. The Bzp-POEOMA and Bzp-PBMA star polymers were synthesized using the macroinitiator (MI) method (Scheme VIII-1). In a typical experiment, a 15 mL Schlenk flask was charged with EGDA (98 μ L, 5% (w/w to MI), 6.28×10^{-1} mmol), Bzp-POEOMA MI (2 g, 2.09×10^{-1} mmol, $M_n = 9,550$, $M_w/M_n = 1.14$), PMDETA (7 μ L, 4.19×10^{-2} mmol) and 5 mL of anisole. The flask was degassed and subjected to three freeze-thaw cycles, and during the final cycle, the flask was filled with nitrogen and CuCl (10 mg, 4.19×10^{-2} mmol) was quickly added to the frozen mixture. The flask was sealed with a glass stopper then evacuated and back-filled with nitrogen three times before it was immersed in an oil bath at 60 °C. Samples were taken at timed intervals to measure molecular weight evolution by GPC. The Bzp-PBMA star polymer was prepared with the same molar ratio of reagents.

Modification of silicon wafers with the polymers. Polymers were deposited onto the surface of silicon wafers by spin-casting solutions of the star macromolecules in chloroform at a velocity of 1,000 rpm. UV irradiation ($\lambda = 365$ nm, for 10 min) was used

to covalently crosslinking star polymers and tether them to the silicon wafer surface. The surface was washed 3 times with methanol, 3 times with THF, and 3 times with water to remove any unstable and/or unreacted residue species.

Measurements. ^1H NMR (300 MHz) spectra were taken on a Bruker Avance 300 spectrometer using CDCl_3 as a solvent. The LCST of the macroinitiator solutions in water were measured on a Varian Cary 5000 UV-vis spectroscopy with a temperature control circulator. Transmittance of polymer solutions in pure DI water was monitored at 600 nm as a function of temperature (cell path length: 10 mm; heating rate: 1 $^\circ\text{C}/\text{min}$). Molecular weights were determined by gel permeation chromatography (GPC; Polymer Standards Services (PSS) columns (guard, 10^5 , 10^3 , and 10^2 Å), with THF eluent at 35 $^\circ\text{C}$, flow rate 1.00 mL/min, and differential refractive index (RI) detector (Waters, 2410)). The apparent molecular weights and dispersity (M_w/M_n) were determined with a calibration based on linear poly(methyl methacrylate) standards using WinGPC 7.0 software from PSS. The contact angle measurements of the polymer modified surfaces were measured at two different temperatures (20 $^\circ\text{C}$ and 37 $^\circ\text{C}$) with a contact angle measuring system VCA optima (AST products, Inc.) including a microscopy heating plate TC 324 heating controller (Warner instrument). DI water was gently placed on the sample surfaces using an auto-syringe. Each sample was measured five times and the results were averaged with standard deviations. Optical microscopic images were obtained by Olympus STM6-F10-2 microscope machine with Olympus LG-PS2 light source. Tapping mode AFM experiments were carried out using a Dimension V scanning probe microscope with a NanoScope V controller (Veeco). The measurements were performed in air using commercial Si

cantilevers with a nominal spring constant and resonance frequency of 42 N/m and 330 kHz, respectively. Set-point values (A/A_0) were maintained 0.7-0.85, where A and A_0 refer to the "tapping" and "free" cantilever amplitude, respectively.

VIII. 6. References

1. (a) Goddard, J. M.; Hotchkiss, J. H., *Prog. Polym. Sci.* **2007**, 32 (7), 698-725; (b) Huang, J.; Murata, H.; Koepsel, R. R.; Russell, A. J.; Matyjaszewski, K., *Biomacromolecules* **2007**, 8 (5), 1396-1399; (c) Murata, H.; Koepsel, R. R.; Matyjaszewski, K.; Russell, A. J., *Biomaterials* **2007**, 28 (32), 4870-4879; (d) Huang, J.; Koepsel, R. R.; Murata, H.; Wu, W.; Lee, S. B.; Kowalewski, T.; Russell, A. J.; Matyjaszewski, K., *Langmuir* **2008**, 24 (13), 6785-6795; (e) Kurt, P.; Gamble, L. J.; Wynne, K. J., *Langmuir* **2008**, 24 (11), 5816-5824; (f) Uhlmann, P.; Merlitz, H.; Sommer, J.-U.; Stamm, M., *Macromol. Rapid Commun.* **2009**, 30 (9-10), 732-740; (g) Dong, H.; Ye, P.; Zhong, M.; Pietrasik, J.; Drumright, R.; Matyjaszewski, K., *Langmuir* **2010**, 26 (19), 15567-15573; (h) Nandivada, H.; Ross, A. M.; Lahann, J., *Prog. Polym. Sci.* **2010**, 35 (1-2), 141-154; (i) Brun-Graeppi, A. K. A. S.; Richard, C.; Bessodes, M.; Scherman, D.; Merten, O.-W., *Prog. Polym. Sci.* **2010**, 35 (11), 1311-1324; (j) Vasconcellos, F. C.; Swiston, A. J.; Beppu, M. M.; Cohen, R. E.; Rubner, M. F., *Biomacromolecules* **2010**, 11 (9), 2407-2414; (k) Stuart, M. A. C.; Huck, W. T. S.; Genzer, J.; Muller, M.; Ober, C.; Stamm, M.; Sukhorukov, G. B.; Szleifer, I.; Tsukruk, V. V.; Urban, M.; Winnik, F.; Zauscher, S.; Luzinov, I.; Minko, S., *Nat Mater* **2010**, 9 (2), 101-113; (l) Motornov, M.; Roiter, Y.; Tokarev, I.; Minko, S., *Prog. Polym. Sci.* **2010**, 35 (1-2), 174-211; (m) Liu, F.; Urban, M. W., *Progress in Polymer Science* **2010**, 35 (1-2), 3-23; (n) Chen, T.; Ferris, R.; Zhang, J.; Ducker, R.; Zauscher, S., *Progress in Polymer Science* **2010**, 35 (1-2), 94-112; (o) Lee, K. P.; Arnot, T. C.; Mattia, D., *J. Membr. Sci.* **2011**, 370 (1-2), 1-22; (p) Yang, W. J.; Cai, T.; Neoh, K.-G.; Kang, E.-T.; Dickinson, G. H.; Teo, S. L.-M.; Rittschof, D., *Langmuir* **2011**, 27 (11), 7065-7076; (q) Ye, P.; Dong, H.; Zhong, M.; Matyjaszewski, K., *Macromolecules* **2011**, 44 (7), 2253-2260; (r) Haraguchi, Y.; Shimizu, T.; Yamato, M.; Okano, T., *RSC Advances* **2012**, 2 (6), 2184-2190; (s) Razi, F.; Sawada, I.; Ohmukai, Y.; Maruyama, T.; Matsuyama, H., *J. Membr. Sci.* **2012**, 401-402 (0), 292-299; (t) Muñoz-Bonilla, A.; Fernández-García, M., *Prog. Polym. Sci.* **2012**, 37 (2), 281-339.
2. (a) Ejaz, M.; Yamamoto, S.; Ohno, K.; Tsujii, Y.; Fukuda, T., *Macromolecules* **1998**, 31 (17), 5934-5936; (b) Matyjaszewski, K.; Miller, P. J.; Shukla, N.; Immaraporn, B.; Gelman, A.; Luokala, B. B.; Siclovan, T. M.; Kickelbick, G.; Vallant, T.; Hoffmann, H.; Pakula, T., *Macromolecules* **1999**, 32 (26), 8716-8724; (c) Yoshikawa, C.; Goto, A.; Tsujii, Y.; Fukuda, T.; Yamamoto, K.; Kishida, A., *Macromolecules* **2005**, 38 (11), 4604-4610; (d) Matyjaszewski, K.; Dong, H.; Jakubowski, W.; Pietrasik, J.; Kusumo, A., *Langmuir* **2007**, 23 (8), 4528-4531; (e) Barbey, R.; Lavanant, L.; Paripovic, D.; Schüwer, N.; Sugnaux, C.; Tugulu, S.; Klok, H.-A., *Chem. Rev.* **2009**, 109 (11), 5437-5527; (f) Olivier, A.; Meyer, F.; Raquez, J.-M.; Damman, P.; Dubois, P., *Prog. Polym. Sci.* **2012**, 37 (1),

- 157-181; (g) Kikuchi, M.; Terayama, Y.; Ishikawa, T.; Hoshino, T.; Kobayashi, M.; Ogawa, H.; Masunaga, H.; Koike, J.-i.; Horigome, M.; Ishihara, K.; Takahara, A., *Polym J* **2012**, *44* (1), 121-130.
3. (a) Gao, H.; Matyjaszewski, K., *J. Am. Chem. Soc.* **2007**, *129* (20), 6633-6639; (b) Binder, W. H.; Sachsenhofer, R., *Macromol. Rapid Commun.* **2008**, *29* (12-13), 952-981; (c) Hoyle, C. E.; Lowe, A. B.; Bowman, C. N., *Chem. Soc. Rev.* **2010**, *39* (4), 1355-1387; (d) Tillet, G.; Boutevin, B.; Ameduri, B., *Prog. Polym. Sci.* **2010**, *36* (2), 191-217; (e) Galvin, C. J.; Genzer, J., *Prog. Polym. Sci.* **2012**, *37* (7), 871-906.
4. Sofia, S. J.; Premnath, V.; Merrill, E. W., *Macromolecules* **1998**, *31* (15), 5059-5070.
5. Kim, D.-G.; Kang, H.; Han, S.; Lee, J.-C., *J. Mater. Chem.* **2012**, *22* (17), 8654-8661.
6. (a) Coessens, V.; Pintauer, T.; Matyjaszewski, K., *Prog. Polym. Sci.* **2001**, *26* (3), 337-377; (b) Matyjaszewski, K.; Tsarevsky, N. V., *Nat Chem* **2009**, *1* (4), 276-288; (c) Gao, H.; Matyjaszewski, K., *Progress in Polymer Science* **2009**, *34* (4), 317-350; (d) Lee, H.-i.; Pietrasik, J.; Sheiko, S. S.; Matyjaszewski, K., *Prog. Polym. Sci.* **2010**, *35* (1-2), 24-44; (e) Siegwart, D. J.; Oh, J. K.; Matyjaszewski, K., *Prog. Polym. Sci.* **2012**, *37* (1), 18-37; (f) Matyjaszewski, K., *Macromolecules* **2012**, *45* (10), 4015-4039; (g) Matyjaszewski, K., *Israel Journal of Chemistry* **2012**, *52* (3-4), 206-220; (h) Kubisa, P.; Vairon, J., In *Polymer Science: A Comprehensive Reference*; Matyjaszewski, K.; Möller, M., Eds. Elsevier BV: Amsterdam: 2012.
7. (a) Hadjichristidis, N., *J. Polym. Sci., Part A: Polym. Chem.* **1999**, *37* (7), 857-871; (b) Blencowe, A.; Tan, J. F.; Goh, T. K.; Qiao, G. G., *Polymer* **2009**, *50* (1), 5-32; (c) Higashihara, T.; Hayashi, M.; Hirao, A., *Prog. Polym. Sci.* **2011**, *36* (3), 323-375; (d) Ferreira, J.; Syrett, J.; Whittaker, M.; Haddleton, D.; Davis, T. P.; Boyer, C., *Polymer Chemistry* **2011**, *2* (8), 1671-1677.
8. (a) Xia, J.; Zhang, X.; Matyjaszewski, K., *Macromolecules* **1999**, *32* (13), 4482-4484; (b) Gao, H.; Matyjaszewski, K., *J. Am. Chem. Soc.* **2007**, *129* (38), 11828-11834.
9. Soler-Illia, G. J. d. A. A.; Sanchez, C., *New J. Chem.* **2000**, *24* (7), 493-499.
10. Voronin, E. F.; Gun'ko, V. M.; Guzenko, N. V.; Pakhlov, E. M.; Nosach, L. V.; Leboda, R.; Skubiszewska-Zieba, J.; Malysheva, M. L.; Borysenko, M. V.; Chuiko, A. A., *J. Colloid Interface Sci.* **2004**, *279* (2), 326-340.
11. (a) Yang, P.; Zhao, D.; Margolese, D. I.; Chmelka, B. F.; Stucky, G. D., *Nature* **1998**, *396* (6707), 152-155; (b) Madathingal, R. R.; Wunder, S. L., *Macromolecules* **2011**, *44* (8), 2873-2882.
12. Acar, M. H.; Matyjaszewski, K., *Macromol. Chem. Phys.* **1999**, *200* (5), 1094-1100.
13. Park, S.; Cho, H. Y.; Yoon, J. A.; Kwak, Y.; Srinivasan, A.; Hollinger, J. O.; Paik, H. J.; Matyjaszewski, K., *Biomacromolecules* **2010**, *11* (10), 2647-52.

Chapter IX

Photo-cross-linkable Thermoresponsive Star Polymers

Designed for Control of Cell-Surface Interactions*

IX. 1. Preface

This Chapter discusses the use of UV crosslinkable oligo(ethylene oxide) monomethyl ether methacrylate (OEOMA) based star polymers for the formation of a cell harvesting surface. In Chapter 8, the preparation of functional OEOMA based star polymers was highlighted and their post-fabrication use for modification of silicon wafer surfaces. The star polymers provided successful photo-patterning on silicon wafers and generated a stable polymeric film after UV irradiation.

This Chapter describes the synthesis of OEOMA based star polymers and their use for post-synthesis modification of commercially available polystyrene substrates, thereby allowing a study of the interaction between cells and polymer modified surfaces. The modified surface could potentially be used for cell sheet engineering.

In general, cell sheet engineering enables the preparation and removal of non-damaged singular proliferated cell sheets from temperature responsive surfaces and direct transplantation to damaged tissues. One of the conventional cell harvesting techniques is enzyme treatment. However, once the cultivated cells are treated with an enzyme, extracellular matrices (ECMs) and cell-to-cell junction proteins are digested, which make

*Work in this chapter was published and partially reformatted based on the following manuscript: **Park, Sangwoo**; Cho, Hong Yul; Yoon, Jeong Ae; Kwak, Yungwan; Srinivasan, Abiraman; Hollinger, Jeffrey O.; Paik, Hyun-jong; Matyjaszewski, Krzysztof *Biomacromolecules* **2010**, *11* (10), 2647

it difficult to obtain a cohesive non-damaged singular cell matrix. Currently, cell sheet engineering focuses on utilizing one of the inherent properties of cells: cells adhere to hydrophobic surfaces and detach themselves from hydrophilic surfaces. The application of this specific characteristic in cell sheet engineering utilizes temperature responsive substrates, such as poly(*N*-isopropylacrylamide) modified surfaces for preparation of cell sheets. The fully cultivated cells are detached from the substrate simply by changing the temperature to one below the critical solution temperature (LCST) to convert a hydrophobic surface to a hydrophilic surface.

The goal of this project was to synthesize a surface formed by post-fabrication modifiable star polymers with LCST behavior, and examine cell attachment/detachment under biocompatible temperature changes for potential biomedical applications. OEOMA based star polymers were synthesized and characterized then used for the preparation of thermoresponsive surfaces. Dr. Yungwan Kwak helped me with the optimization of polymerization conditions and Dr. Jeong Ae Yoon provided advice on the spin coating parameters that were examined in order to obtain uniformly modified polymer surfaces. In addition, Dr. Yoon analyzed individual star polymers and polymer modified surfaces by AFM. Biological analyses were conducted in collaboration with Dr. Abiraman Srinivasan.

Polymers with another complex polymeric architecture, polymeric bottlebrushes, were examined in a study of cell migration behavior on soft moduli controllable surfaces, as discussed in Appendix VIII. In brief, poly(*n*-butyl acrylate) based polymer bottlebrushes were prepared and functionalized with reversibly photo-crosslinkable groups, *e.g.*, coumarin. The crosslinked polymer brushes showed supersoft elastic behavior and its moduli could be changed by UV irradiation; ([2+2] cyclization (photo-dimerization) was

induced by irradiation > 300 nm; and retrocyclization (photo-scission) < 300 nm). Surfaces covered by the polymer brushes showed good cell adhesion on stiffer surfaces, whereas after conversion to softer surfaces the cells showed a globular shape, indicative of detachment. My role in this project was to collect data and analyze the physical properties of the polymers.

I appreciate valuable discussions with my former M.Sc. advisor Prof. Hyun-jong Paik and my coworkers for their efforts.

IX. 2. Introduction

Star polymers, containing multiple linear arms connected at a central branched core, have interesting properties because of their branched architecture, globular shape and chemically crosslinked arms.^{42d, 156a, 163} A recent development in controlled/living radical polymerization techniques provided a convenient procedure for the synthesis of star polymers *via* arm-first methods.^{42c, 164} For example, α -functionalized linear polymers (macroinitiators, MI) were synthesized by atom transfer radical polymerization (ATRP) and were subsequently crosslinked with divinyl or multivinyl compounds to form star polymers.¹⁵⁷ This way, star polymers with various chemical structures of core, arms and arm end-functionality were prepared. The bio-related properties such as enhanced cell interactions of star polymers containing poly(ethylene oxide) arms, could be affected by introducing RGD (Arg-Gly-Asp) moieties.¹⁶⁵ Another interesting aspect would be introduction of additional functionality *via* stimuli responsiveness.^{150n, 166} For example, thermoresponsive polymers undergo large physicochemical changes in response to small temperature changes.^{150h, 167} In particular, the lower critical solution temperature (LCST) behavior of water-soluble thermoresponsive polymers has been widely used in various applications including intelligent bioactive surfaces and drug delivery.^{150h, 167b}

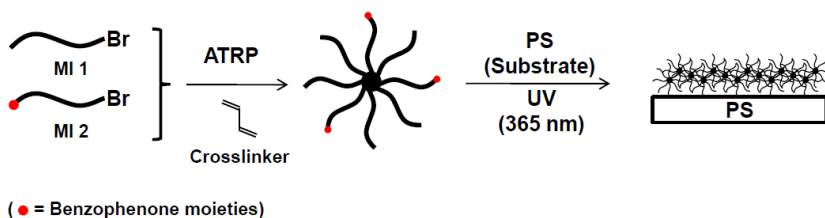
Recently, several studies have been focused on thermally responsive polymers for bio-related applications.¹⁶⁸ For example, Okano *et al.* highlighted the facile cell sheet engineering for reconstruction of damaged tissue based on thermoresponsive surfaces containing poly(*N*-isopropyl acrylamide) (PNIPAAm).¹⁶⁹ Traditional cell-based therapies employ an injection of a single cell suspension that is expected to remain around the

damaged host tissue to promote wound healing. However, in most cases, the injected cells are not retained there, resulting in poor localization, size, and shape of the injected cells. Okano used the sharp physicochemical thermal transition of PNIPAAm to successfully develop a smart surface, which enabled reversible cell adhesion to, and detachment from, the solid substrate by controlling its hydrophobicity by small temperature changes.^{168d}

Polymers containing poly(ethylene oxide) (PEO) derivatives have been successfully used in many biomedical applications such as bioseparation, biosensors, bio-assays and cell engineering.^{168a, 168e, 168g, 170} Surfaces coated with PEO or oligo(ethylene oxide) are generally biocompatible materials. The value of LCST of oligo(ethylene oxide) (meth)acrylate copolymers, with a different number of ethylene oxide unit, can be precisely adjusted by varying the comonomer composition.^{168f, 171} In this Chapter, the synthesis of photo-attachable, photo-crosslinkable and thermoresponsive star polymers, based on benzophenone-P(MEO₂MA-*co*-OEOMA₃₀₀)_n-PEGDMA was described and potentially used for cell-sheet engineering. The photosensitive benzophenone units are located at the periphery of the star structures and upon UV irradiation can be used for either crosslinking or attachment to surfaces.¹⁷² A commercially available, tissue culture polystyrene substrates were modified with the star polymers containing peripheral benzophenone groups under UV irradiation ($\lambda = 365$ nm). Crosslinkable star polymers allowed simple surface modification process with better precisely control crosslinking density, distance between crosslinking points. The substrates modified with star polymers were evaluated for hydrophilicity/hydrophobicity and cell-surface interaction in response to variation in temperature.

IX. 3. Results and Discussion

Benzophenonyl 2-bromoisobutyrate initiators (Bzp-ini) for ATRP were successfully synthesized by the reaction of 4-hydroxybenzophenone and 2-bromoisobutyryl bromide under basic condition (90% yield). The structure of Bzp-ini was confirmed by ^1H NMR spectroscopy, where all of the characteristic peaks were identified, as described in the experimental section.



Scheme IX-1. Synthetic pathway to benzophenone-P(MEO₂MA-*co*-OEOMA₃₀₀)_n-PEGDMA star polymers and preparation of modified surface using UV irradiation.

Two thermoresponsive macroinitiators (MI and Bzp-MI) were synthesized by copolymerization of two PEO analogue monomers (MEO₂MA and OEOMA₃₀₀) with either EBiB for MI or Bzp-ini for Bzp-MI synthesis (Scheme IX-1). In order to suppress termination by radical-radical coupling or disproportionation reaction and to produce well-controlled polymers, addition of deactivator (CuBr₂) and bipyridine-based ligand were employed.^{2c, 61a, 61b, 61d, 173} The well-defined macroinitiators (MI and Bzp-MI) were obtained as characterized by ^1H NMR and GPC. The presence of benzophenone moiety at the chain-end of Bzp-MI polymers was verified by ^1H NMR spectroscopy (7.90-7.25 ppm, Figure IX-1A-b). The apparent (relative to linear polystyrene standards) molecular weight (MW)

and molecular weight distribution (MWD) of MIs were measured by GPC with THF as eluent. The MWs of MI were $M_n = 9,750$ and $8,650$ and MWDs were 1.28 and 1.15 for the MI and Bzp-MI, respectively.

Table IX-1. Characterization of Prepared Macroinitiators and Star Polymers.

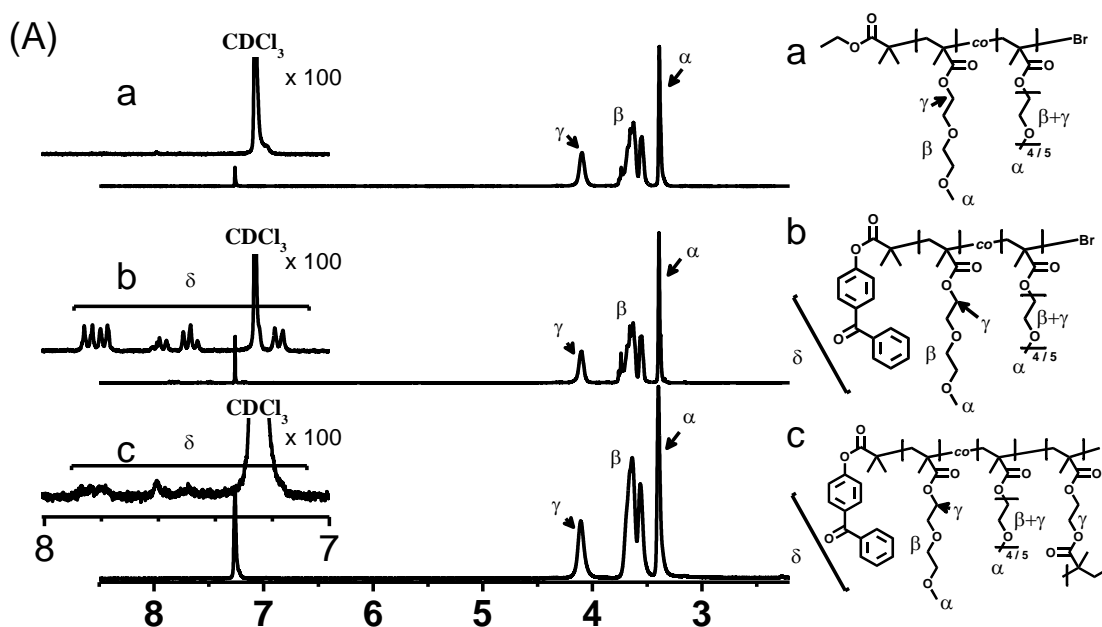
entry	M_n	M_w/M_n	LCST ^g (°C)
MI ^a	9,750 ^d	1.28	37
Bzp-MI ^b	8,650 ^e	1.15	36
Star Polymers ^c	98,200 ^f	1.23	27

Experimental conditions: ^a $[MEO_2MA]/[OEOMA_{300}]/[EBiB]/[CuBr]/[CuBr_2]/[dNbpy] = 85/15/1/0.4/0.1/1$, $[MEO_2MA]_0 = 4.26$ M in anisole at 60 °C; ^b $[MEO_2MA]/[OEOMA_{300}]/[Bzp-ini]/[CuBr]/[CuBr_2]/[dNbpy] = 85/15/1/0.4/0.1/1$, $[MEO_2MA]_0 = 4.26$ M in anisole at 60 °C; ^c $[MI]/[Bzp-MI]/[EGDMA]/[CuCl]/[dNbpy] = 3/1/12/4/8$, $[MI]_0 = 0.052$ M in anisole at 60 °C; ^{d,e}relative values measurement by GPC in THF with RI detector (linear polystyrene standard). The mol% of $OEOMA_{300}$ calculated by ¹H NMR (14.7 and 15.8% respectively); ^fThe absolute molecular weight determined by GPC-MALLS in THF, $N_{arm} \approx 10$; ^gdetermined by UV-vis spectroscopy.

Random copolymers of MEO_2MA and $OEOMA_{300}$ exhibit LCST between 26 and 67 °C in water, depending on the wt% of each monomers.^{168f, 171, 174} The predicted LCST of the prepared MIs should be around 35 °C, based on the co-monomer composition (15 mol% (23 wt%) $OEOMA_{300}$ relative to MEO_2MA), a convenient temperature for cell-study. Comonomer compositions in the MIs were determined by measuring the peak area ratios

of $\text{CH}_3\text{-O-}$ to $\text{-CH}_2\text{CH}_2\text{O-}$ groups in the side chains of the resulting copolymers (Figure IX-1A). The incorporated mol% of OEOMA₃₀₀ in the MI and Bzp-MI closely matched the feed ratio of OEOMA₃₀₀, indicating an ideal radical copolymerization.

The cloud points were determined by spectrophotometric detection of the changes in transmittance ($\lambda = 600 \text{ nm}$) of aqueous solutions of MIs heated at a constant rate ($1 \text{ }^\circ\text{C/min}$, Table IX-1).^{168f} The LCST values of MIs were $37 \text{ }^\circ\text{C}$ and $36 \text{ }^\circ\text{C}$ for the MI and Bzp-MI, respectively, which are close to the predicted value ($35 \text{ }^\circ\text{C}$, calculated for a random copolymers containing 15 mol% (23 wt%) of OEOMA₃₀₀). The Bzp-MI exhibited somewhat lower LCST than the non-functionalized MI, presumably due to incorporation of the hydrophobic benzophenone group in the Bzp-MI (Table IX-1).



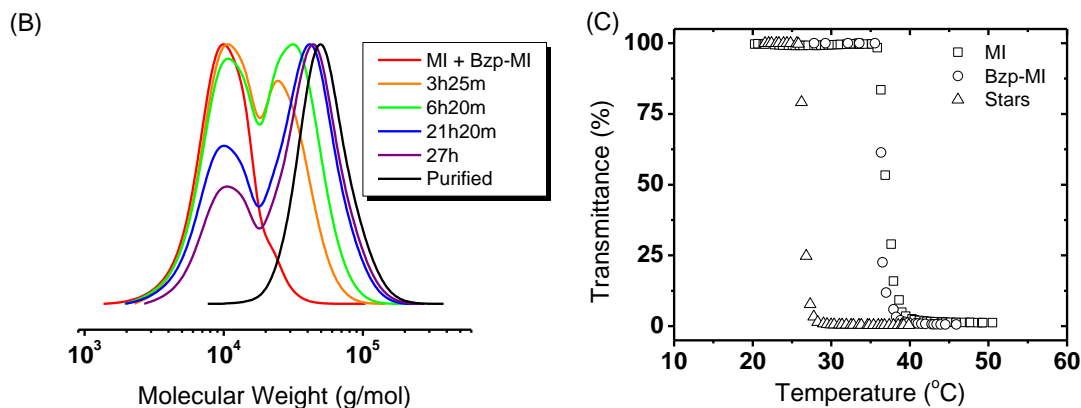


Figure IX-1. (A) ^1H NMR spectra of (a) MI, (b) Bzp-MI, and (c) Star Polymers in CDCl_3 . (B) Evolution of GPC traces during synthesis of benzophenone-P(MEO₂MA-*co*-OEOMA₃₀₀)_n-PEGDMA star polymers. (C) Plots of transmittance as a function of temperature measured for aqueous solutions (1 mg/mL) of MI, Bzp-MI, and star polymers (cloud points: 37, 36 and 27 °C, respectively).

Figure IX-1B shows the evolution of MWD measured by GPC during the synthesis of the star polymers. Chain extension of the MI and Bzp-MI with a divinyl compound (EGDMA) resulted in crosslinking of pendant vinyl groups to form stars that contain multiple arms and a central core. 3/1 mole ratio between [MI] and [Bzp-MI] was used to avoid potential cytotoxicity and enable sufficient crosslinking density by presence of ~ 0.5 mol% Bzp-groups in the star polymers during the surface modification.¹⁷⁵ After polymerization, the products were separated by precipitation in a THF/ethyl ether (= 10/90, by v/v) mixture. The absolute MWs ($M_{n,\text{MALLS}}$) of the purified products, measured by multiangle laser light scattering ($M_{n,\text{MALLS}}$), was 98,200 and the distribution was narrow ($M_w/M_n = 1.23$). The average arm number per star polymer, calculated as a ratio of $M_{n,\text{MALLS}}$

of star polymers to the average $M_{n,RI}$ of the linear MIs (without considering contribution of the core), was *ca.* 10. Figure IX-1A-c shows ^1H NMR spectrum of purified star polymers. The signal of aromatic protons in the 7.90-7.25 ppm region confirms the presence of the benzophenone group in the star polymers. The diameter and shape of the star polymers were characterized using DLS and AFM (Figure IX-2). DLS analysis showed that the hydrodynamic radius of the star polymers was *ca.* 15 nm in water at 15 °C, *i.e.*, below LCST. Image analysis by AFM confirmed that the individual star polymers under high dilution concentration had 15 to 20 nm diameters with a globular shape, as deposited on a mica substrate. The LCST of the star polymers was lower (27 °C) than those of MI and Bzp-MI, presumably due to the incorporation of the hydrophobic EGDMA into the core of the stars. In general, LCST of thermoresponsive copolymers (*e.g.*, PNIPAAm) decreases as the fraction of hydrophobic monomers in the copolymer increases.^{92c, 176}

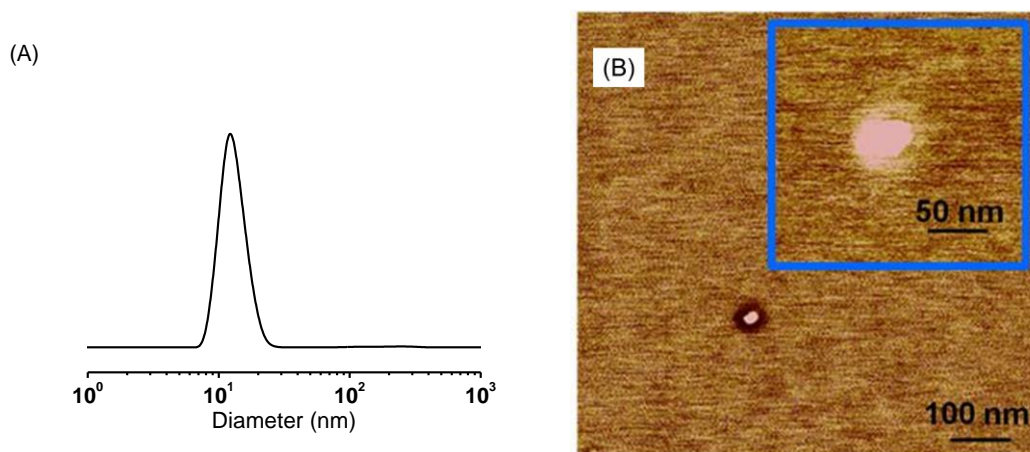


Figure IX-2. (A) DLS analysis of benzophenone-(P(MEO₂MA-*co*-OEOMA₃₀₀))_n-PEGDMA star polymers in cold water: average particle size *ca.* 15 nm (by volume distribution), (B) AFM image of the individual star polymer on the mica substrate.

For surface modification, methanol solutions of the star polymers (0.2, 0.3 and 0.4% (by wt/v)) were spin-cast on a polystyrene surface, which were exposed to UV irradiation ($\lambda = 365$ nm) for 10 min. Absorption of UV light at a wavelength of about 365 nm by the benzophenone units located at the star periphery triggered the formation of a biradical triplet excited state. The *O*-centered radicals could abstract hydrogen atoms from the polystyrene chains at the surface and the *C*-centered radicals could form new C-C bonds.¹⁷² The efficiency of attachment of stars to polystyrene surface was evaluated by ATR-IR (Figure IX-3). When the unmodified polystyrene surfaces were examined by attenuated total reflection infrared (ATR-IR) spectroscopy, a band from C-H bending and overtone bands from monosubstituted aromatic rings of polystyrene were observed in the region close to C=O stretching (Figure IX-3A-a). After the star polymers were coated onto the surface, the carbonyl (C=O) stretching band from the star polymers appeared at 1729 cm⁻¹. It partially overlapped with one of the bands from the monosubstituted aromatic rings (1745 cm⁻¹, Figure IX-3A-b). Without UV exposure, the deposited star polymers on polystyrene surface were completely removed by washing with methanol, as confirmed by IR analysis (Figure IX-3A-c). On the other hand, after UV irradiation for 10 min, more than 90% of the star polymers remained on polystyrene surface even after thorough methanol washing (Figure IX-3A-d), indicating the successful attachment of star polymers onto the surface *via* covalent bonds. In addition, AFM image revealed the uniform surface coverage of star polymers, and ATR-IR spectra showed increasing of specific peak intensity from star polymers with increasing of star polymer concentration (Figure IX-3B-C and Figure IX-4). The contact angle measurement was used for verifying the hydrophilicity change. The results showed the rather slight broadening of LCST than

individual star polymers' behavior (Figure IX-5). This observation might be affected by connection of star polymer film with several anchoring groups; densely crosslinked cores and UV-crosslinkable Bzp-groups. During photo-induced crosslinking, the anchoring groups in the star polymers were multi-connected, and thus the mobility of arms in the star polymers was significantly reduced.¹⁷⁷

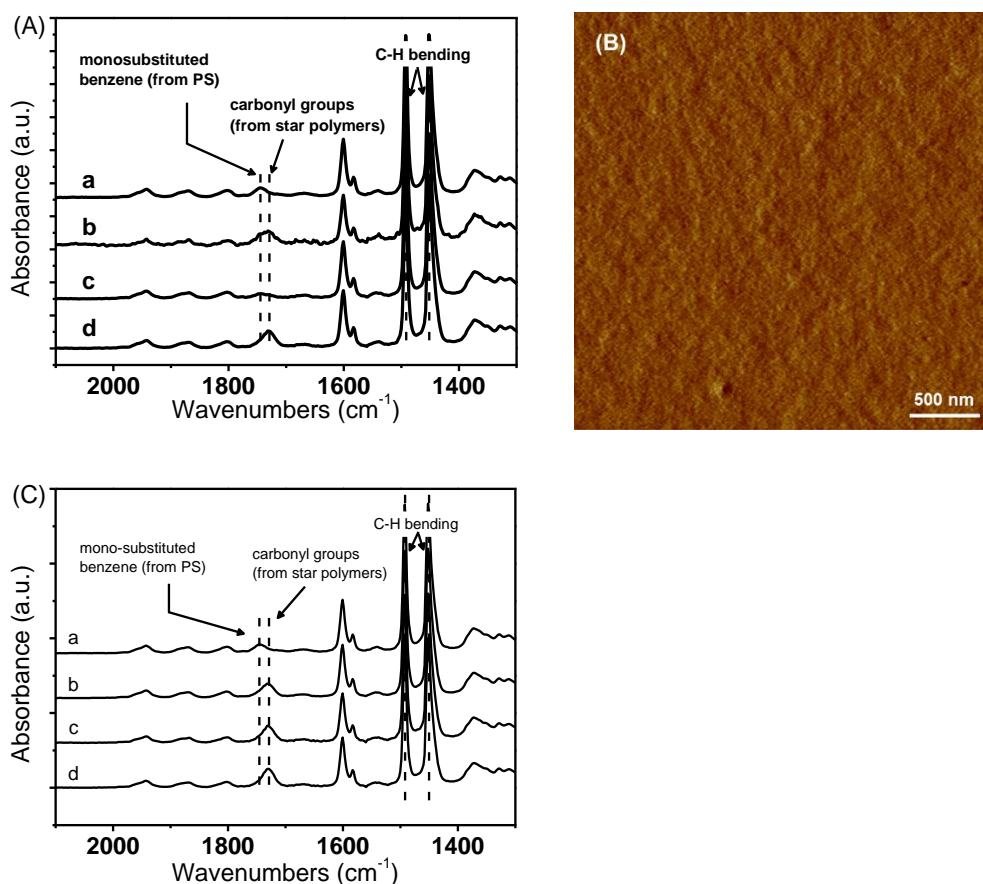


Figure IX-3. (A) ATR-IR spectra of (a) untreated PS surface, (b) PS surface coated with star polymers before UV irradiation, (c) PS surface coated with star polymers *without* UV irradiation and washed with methanol, and (d) PS surface coated with star polymers *with* UV irradiation and washed with methanol. Star polymer solution concentration: 0.2% (by

wt/v, in methanol); (B) AFM image of thin (*ca.* 30nm) films of star polymers coated on the silicon wafer. (C) ATR-IR spectra of modified surfaces; unmodified polystyrene (a), star polymer modified surfaces (b-d, 0.2-0.4% (wt/v), respectively each).

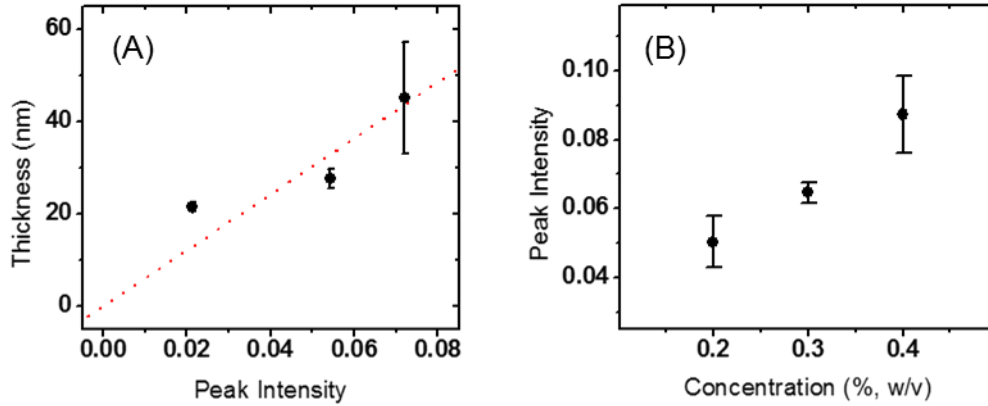


Figure IX-4. (A) Calibration curve from a known amount of star polymers deposited films, (B) relative peak intensity values from variable thickness stars modified PS surfaces. The thickness of films: 0.2% - 31 nm, 0.3% - 39 nm and 0.4% - 53 nm. Calibration curve was made based on a known amount of star polymer casted both Si wafer and PS surfaces. The equation for calibration was as follows; (i) Relative peak intensity (by ATR-IR): $A_{\text{standard}} = A_{\text{sample}} - A_{\text{control}}$, where A = area of peak, $A_{\text{sample}} = A_{[1750-1700]} / A_{[1500-1400]}$, and $A_{\text{control}} = A_{[1750-1700]} / A_{[1500-1400]}$; Peak area from star polymers was ignored ($1500 \sim 1400 \text{ cm}^{-1}$), (ii) Film thickness (by ellipsometry): The film thicknesses of star polymers were determined by ellipsometry and each measurement was repeated more than 5 times.

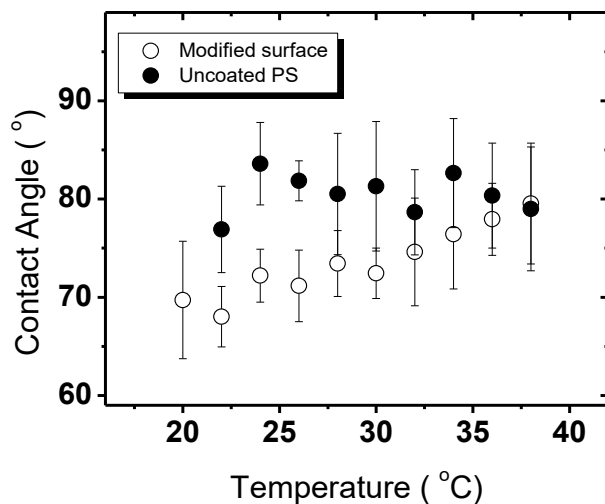


Figure IX-5. Temperature-dependent contact angle changes (20 to 38 °C) for star polymers modified PS surface (●: Uncoated PS, ○: Star Polymers modified PS) by sessile drop methods (data from five separate experiments with standard deviations).

The surfaces modified with the thermoresponsive star polymers were evaluated for cell attachment/shrinkage. The live/dead cell assay was carried out for verifying cytotoxicity of purified MIs and star polymers, and the materials were revealed as nontoxic by the assays (Figure IX-6). Cell-surface interaction was studied using NIH 3T3 (mouse fibroblast cell line), cultured in DMEM with 10% (v/v) FBS, 1% (v/v) p/s solution (complete DMEM). The modified surfaces were ethanol sterilized before cell seeding. Subsequently, 5×10^4 cells were seeded onto the modified surfaces. After 2 days incubation at 37 °C, the cells spread very well onto the modified surface (Figure IX-7). Upon adding cold DMEM media ($T = 4$ °C) to the culture plate, the cells gradually shrank. The ratio of attached/shrank cells on both control and modified surfaces were calculated after counting the number of “attached” and “shrank” cells when above LCST and immediately after

adding cold media. In control experiment on unmodified surface, the cells were seen attached to the unmodified substrate, irrespective of the temperature change (before: 3.0 ± 0.5 , after: 3.4 ± 0.4). However, in the case of the modified surface, the ratio decreased dramatically by the addition of cold media (before: 4.5 ± 0.9 , after: 0.4 ± 0.1). This could be attributed to the surface property change from hydrophobic to hydrophilic by LCST behavior of star polymers. The results presented in Figure IX-7 were obtained with uniform film of star polymers with a thickness of 31 nm. Cells attach well on the hydrophobic surfaces but weakly on the hydrophilic (or less hydrophobic) surfaces. In comparison, control experiment revealed that cells which are located onto the unmodified substrate were not influenced under temperature change. In addition, for thicker polymeric films (39 and 53 nm), the cells attached less efficiently (Figure IX-8). This observation is in agreement with previous work by Okano group. Above critical polymer film thickness, the polymer chains could be stretched away from the substrate surface relatively, resulting in enhanced chain mobility.¹⁷⁸ Therefore, as the films became thicker, the arms tended to be more hydrophilic (or less hydrophobic) at 37 °C, cells were not easily attached onto the surface due to the enhanced interaction with water molecules.

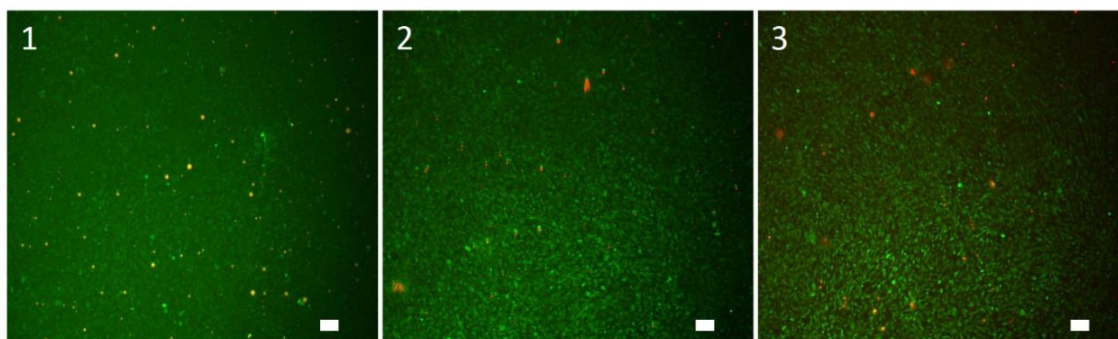
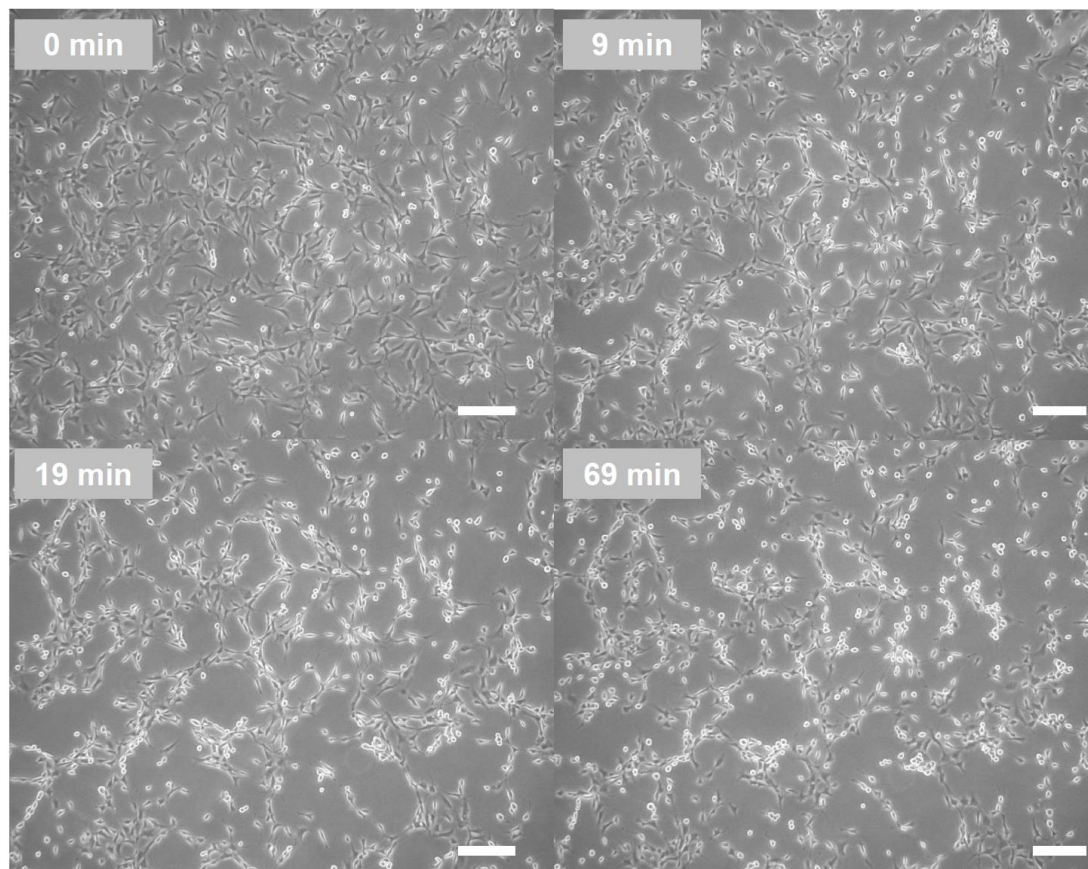


Figure IX-6. *In-vitro* cell viability assay of MC3T3-E1.4 cells mixed in suspension with

(1) Bzp-MI, (2) star polymers, and (3) cells only (control experiment). The live cells fluoresce green and the dead cells fluoresce red. Scale bars correspond to 100 μm (magnification: 10x).



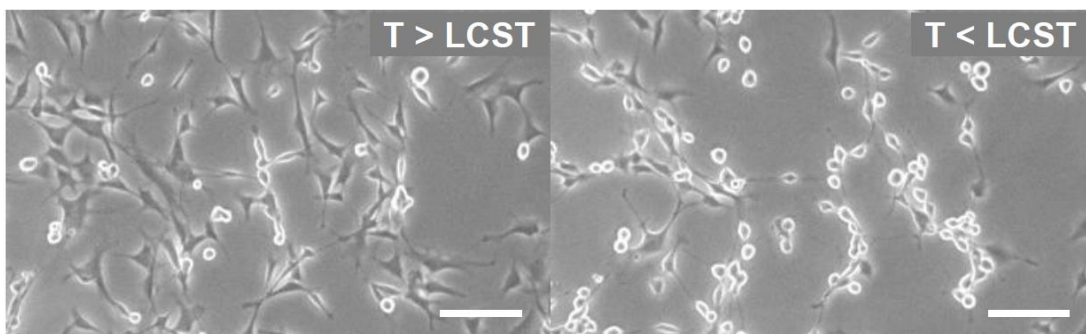


Figure IX-7. (top) Phase contrast microscopic images of NIH 3T3 (mouse fibroblast cell) on PS modified with star polymers: after 48 h of incubation at 37 °C and cooling the sample by adding cold media (4 °C). (bottom) high magnification of 0 and 69 min. This estimated thickness of star polymer film was 30.5 nm. Scale bars correspond to 200 μm , respectively each.

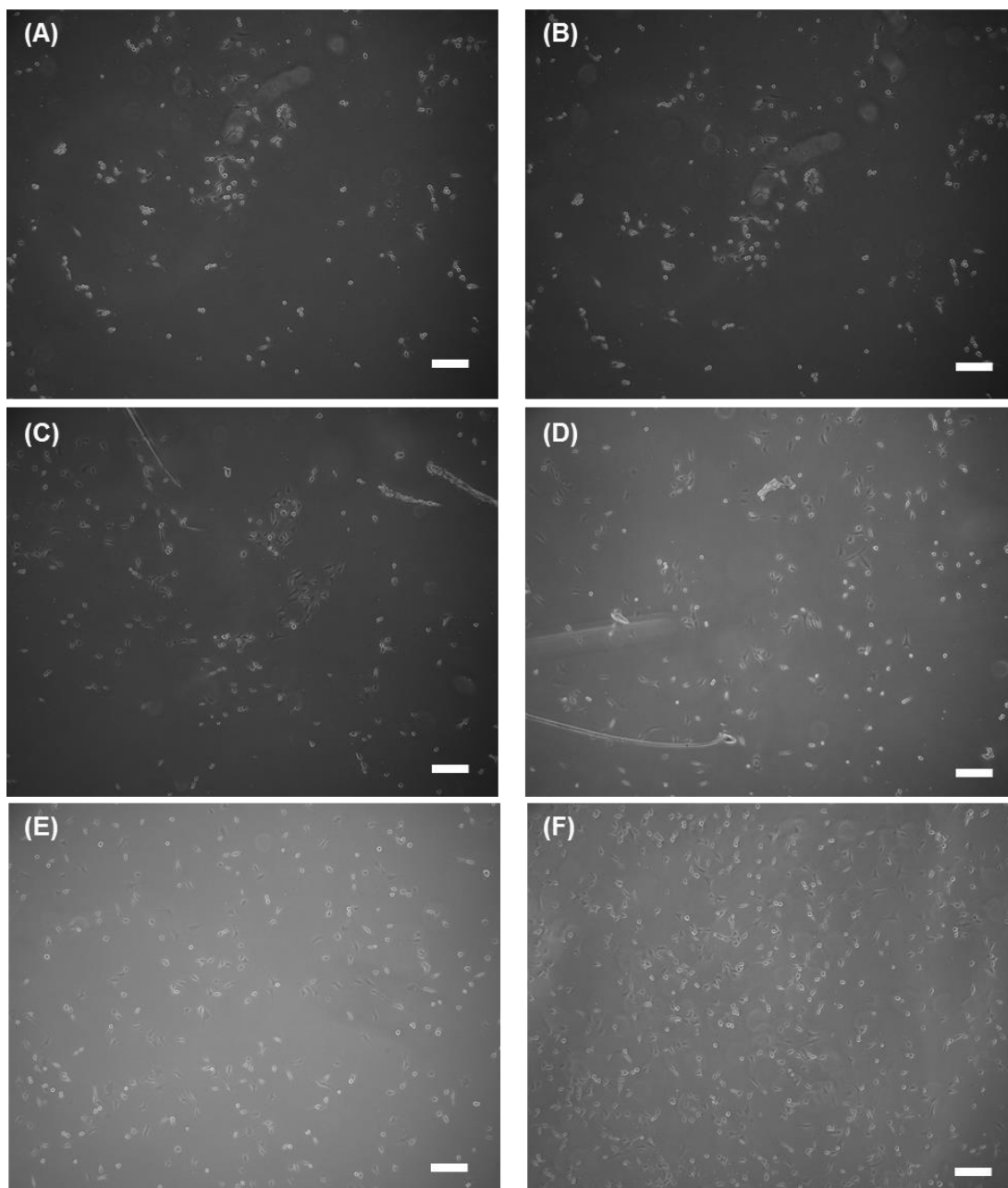


Figure IX-8. Phase contrast microscopic images of NIH 3T3 on PS modified with star polymers and unmodified PS: (a, b) after 48 h of incubation at 37 °C and 70 min after cooling the sample by adding cold media (4 °C) from stars modified surface (0.3% star solution was used), (c, d) after 48 h of incubation at 37 °C and 70 min after cooling the

sample by adding cold media (4 °C) from stars modified surface (0.4% star solution was used), and (e, f) after 48 h of incubation at 37 °C and 70 min after cooling the sample by adding cold media (4 °C) from unmodified surface. Scale bars correspond to 200 μ m (magnification 5x). This estimated thickness of star polymer films were 39 nm (a, b) and 53 nm (c, d).

IX. 4. Summary

Two different thermoresponsive macroinitiators were prepared by ATRP. One macroinitiator, containing benzophenone functionality, was prepared by initiating an ATRP with a benzophenonyl-2-bromoisobutyrate; the other with ethyl 2-bromoisobutyrate. The LCST of both MIs were \sim 36 °C, similar to the values predicted based on content of OEOMA₃₀₀. Star polymers were prepared by crosslinking a mixture of MIs with EGDMA. The LCST of the star polymers (27 °C) was lower than LCST of the MI, due to incorporation of a hydrophobic EGDMA core. The presence of benzophenone and PEO moieties and EGDMA in the stars was verified by ¹H NMR spectra. A flat polystyrene substrate was modified with the star polymers by simple UV irradiation of the deposited polymer film. The film thickness was controlled by solution concentration and was determined by calibration curve from a known amount of polymers deposited film. Contact angle measurement confirmed that the modified surfaces displayed predictable changes in wettability depending on temperature. NIH 3T3 cells attached well to the polymeric surface at 37 °C and shrank from the surface after decreasing the temperature below LCST (4 °C). The star modified substrate provides surfaces suitable for cell adhesion above LCST, but only below a critical film thickness (\sim 30 nm).

IX. 5. Experimental Section

Materials. Monomers, 2-(2-methoxyethoxy)ethyl methacrylate (MEO₂MA), oligo(ethylene oxide) methacrylate with ~ 4 EO unit (OEOMA₃₀₀, $M_n = 300$) and ethylene glycol dimethacrylate (EGDMA) were purchased from Aldrich and purified by passing twice through a column filled with basic alumina to remove the inhibitors. CuBr (98%, Acros) and CuCl (97%, Aldrich) were purified using a literature procedure.¹⁷⁹ All other reagents, 4-hydroxy benzophenone, 2-bromoisobutyryl bromide, 4,4'-dinonyl-2,2'-bipyridine (dNbpy), copper(II) bromide (CuBr₂), ethyl 2-bromoisobutyrate (EBiB), triethylamine (TEA) and solvents were purchased at the highest purity from Aldrich and used without further purification. Polystyrene tissue culture grade petri dishes were obtained from Fisher Scientific and were cut into small pieces (1 × 1 cm), followed by washing in sterile phosphate buffer solution (PBS) to remove the debris and organic residues from the surface and were sterilized with 70% ethanol. NIH 3T3 (mouse fibroblast cell) cells and MC3T3-E1.4 (mouse calvarial pre-osteoblast like cells, embryonic day 1, subclone 4) were obtained from American Type Culture Collection (ATCC) and cultured in Dulbecco's Modified Eagle Medium (DMEM) or alpha MEM, purchased from GIBCO, supplemented with 10% fetal bovine serum (FBS) and 1% penicillin/streptomycin (p/s).

Synthesis of a Benzophenonyl 2-Bromoisobutyrate (Bzp-ini). Benzophenonyl 2-bromoisobutyrate (Bzp-ini) was prepared according to a previously published procedure.^{150b} Briefly, a clean and dry 250 mL flask was charged with 4-hydroxy benzophenone (10 g, 5.04×10^{-2} mol), TEA (7.6 mL, 5.45×10^{-2} mol) and methylene chloride (30 mL). The flask was placed in an ice bath and 2-bromoisobutyryl bromide (6.8

mL, 5.45×10^{-2} mol) was added dropwise. The reaction mixture was stirred for 12 h at room temperature and was washed successively with 300 mL of saturated NaHCO_3 and 300 mL of deionized (DI) water. The organic layer was dried overnight with anhydrous Na_2SO_4 . The solvent was evaporated under reduced pressure to yield the desired compound. Its structure was confirmed by ^1H NMR spectroscopy (δ , CDCl_3 as solvent): 7.90-7.25 ppm (m, 9H, *Ar*-(C=O)-*Ar*-), 2.09 ppm (s, 6H, -OCOC(*CH*₃)₂Br).

Synthesis of P(MEO₂MA-*co*-OEOMA₃₀₀) Macroinitiator (MI). A clean and dry 25 mL Schlenk flask was charged with MEO₂MA (10 mL, 54.2 mmol), OEOMA₃₀₀ (1.7 mL, 6.02 mmol), dNbpy (246 mg, 6.38×10^{-1} mmol) and anisole (11.7 mL). The flask was degassed by three freeze-pump-thaw cycles. During the final cycle, the flask was filled with nitrogen and then CuBr (37 mg, 2.55×10^{-1} mmol) and CuBr₂ (13 mg, 6.38×10^{-2} mmol) were quickly added to the frozen mixture. The flask was sealed with a glass stopper then evacuated and back-filled with nitrogen three times before it was immersed in an oil bath at 60 °C. EBiB (104 μL , 6.38×10^{-1} mmol) was purged with N_2 for 10 minutes and then injected into the reaction flask, through the side arm of the Schlenk flask. The reaction was stopped after 2 h and the reaction mixture was passed through neutral alumina to remove the copper complex. The product was precipitated from excess hexane and dried under vacuum overnight. GPC analysis showed $M_n = 9,750$ and $M_w/M_n = 1.28$ (polystyrene standards).

Synthesis of Benzophenone-P(MEO₂MA-*co*-OEOMA₃₀₀) Macroinitiator (Bzp-MI). A clean and dry 25 mL Schlenk flask was charged with MEO₂MA (10 mL, 54.2 mmol), OEOMA₃₀₀ (1.7 mL, 6.02 mmol), dNbpy (246 mg, 6.38×10^{-1} mmol) and anisole

(9.7 mL). The flask was degassed by three freeze-pump-thaw cycles. During the final cycle, the flask was filled with nitrogen and CuBr (37 mg, 2.55×10^{-1} mmol) and CuBr₂ (13 mg, 6.38×10^{-2} mmol) were quickly added to the frozen mixture. The flask was sealed with a glass stopper then evacuated and back-filled with nitrogen three times before it was immersed in an oil bath at 60 °C. The Bzp-ini (209 mg, 6.38×10^{-1} mmol) was dissolved in anisole (2 mL) and purged with N₂ before injection into the reaction flask through the side arm of the Schlenk flask. The reaction was stopped after 2 h and the solution was passed through neutral alumina to remove the copper complex. The product was precipitated by addition to excess hexane and dried under vacuum overnight. GPC analysis showed $M_n = 8,650$ and $M_w/M_n = 1.15$ (polystyrene standards).

Synthesis of Benzophenone-(P(MEO₂MA-*co*-OEOMA₃₀₀))_n-PEGDMA Star Polymer. A clean and dry 15 mL Schlenk flask was charged with ethylene glycol dimethacrylate (EGDMA, 39 μ L, 8.12% (by w/w to MI), 2.08×10^{-1} mmol), MI (507 mg, 5.19×10^{-2} mmol, $M_n = 9,750$, $M_w/M_n = 1.28$), Bzp-MI (150 mg, 1.73×10^{-2} mmol, $M_n = 8,650$, $M_w/M_n = 1.15$), and 3 mL of anisole. The flask was purged with N₂ for 30 minutes to remove oxygen, and then CuCl (7 mg, 6.92×10^{-2} mmol) was quickly added to the frozen mixture. The flask was sealed with a glass stopper then evacuated and back-filled with nitrogen three times before it was immersed in an oil bath at 60 °C. A solution of dNbpy (57 mg, 1.39×10^{-1} mmol) in anisole (1 mL) was purged with N₂ before injection into the reaction flask through the side arm of the Schlenk flask. At time intervals, samples were withdrawn *via* a syringe fitted with a stainless needle, diluted with tetrahydrofuran (THF) then were passed through a neutral alumina column to remove catalyst residues. The

samples were used to evaluate progress of polymerization. The final product was precipitated by addition to excess THF/ethyl ether and dried under vacuum overnight. The absolute molecular weight of products were measured by GPC-MALLS ($M_{n,MALLS} = 98,200$ and $M_w/M_n = 1.23$, The dn/dc value was calculated using ASTRA program with the precisely measured amount of injected star polymers. The calculated value was 0.077).

Surface Modification. The star polymers were deposited onto polystyrene surface by spin-casting solutions of varying concentrations ($2 \sim 4$ mg/mL) in methanol at a velocity of 1,000 rpm. UV irradiation ($\lambda = 365$ nm, for 10 min) was used to covalently tether them to the polystyrene surface. The surface was washed with methanol 3 times to remove untethered star polymers.

Live/Dead cell assay. Benzophenone-(P(MEO₂MA-*co*-OEOMA₃₀₀))_n-PEGDMA star polymers were tested for cell viability and cytotoxicity using the Live/Dead cytotoxicity staining kit (Invitrogen). Briefly, 5×10^4 MC3T3-E1.4 cells were seeded onto the coated and uncoated polystyrene surface and cultured in a 24-well tissue culture polystyrene plate containing α -MEM media supplemented with 10% (v/v) FBS and 1% (v/v) p/s, at 37 °C and 5% CO₂. After 24 hrs, the cell culture media was aspirated and washed with PBS-Tween. Thereafter, 0.5 mL of live/dead stain was added (calcein 1:2000 and ethidium homodimer 1:500, diluted in PBS) to the cells and incubated at 37 °C for 30 minutes in the dark and images were captured using a Zeiss Axiovert 200 fluorescence microscope.

Cell Attachment-shrinkage Assays. The NIH 3T3 (mouse fibroblast cell) cells were cultured in DMEM containing 10% (v/v) FBS, 1% (v/v) p/s solution (complete DMEM) at

37 °C and 5% CO₂. The modified polymeric surface pieces were placed in a 12 well tissue culture polystyrene plate, seeded with 5×10^4 NIH 3T3 fibroblast cells and were allowed to adhere overnight. Cell attachment and spreading on the surface modified polymeric materials was confirmed using phase contrast microscopy (Zeiss Axiovert 200 microscope). The temperature dependent behavior of the surfaces was tested by switching the temperature from 37 °C to 20 °C, and was investigated after 2 days of in vitro cell culture. Briefly, the cells were exposed to room temperature and fresh cold DMEM cell culture media was added to make the coated polymeric surface hydrophilic; the cell attachment was determined using phase contrast microscopy. The images were taken every 5 min for up to 70 min.

Measurements. ¹H NMR (300 MHz) spectra were recorded on a Bruker Avance 300 spectrometer using CDCl₃ as a solvent. The LCST of the macroinitiator solutions in water were measured on a Varian Cary 5000 UV-vis spectroscopy with temperature control circulator. Transmittance of polymer solutions in pure DI water was monitored at 600 nm as a function of temperature (cell path length: 10 mm; heating/cooling cycle rate: 1 °C/min). Molecular weights were determined by gel permeation chromatography (GPC; Polymer Standards Services (PSS) columns (guard, 10⁵, 10³, and 10² Å), with THF eluent at 35 °C, flow rate 1.00 mL/min, and differential refractive index (RI) detector (Waters, 2410)). The apparent molecular weights and molecular weight distribution (M_w/M_n) were determined with a calibration based on linear polystyrene standards using WinGPC 6.0 software from PSS. The particle size of the star polymers was measured by dynamic light scattering (DLS) on a high performance particle sizer, Model HP5001 from Malvern Instruments, Ltd. ATR-

IR spectra of the polymer modified surfaces were obtained using a Magna-IR 560 Spectrometer from Thermo-Nicolet. The peak intensity was determined by OMNIC 7.2 software from Thermo Electronic Corporation. The thickness of the star polymer layers on the polystyrene were estimated based on the calibration curves obtained from surfaces casted with known amount of star polymers. The contact angles of uncoated and modified polystyrene surfaces were measured at different temperatures, ranging from 20 °C to 37 °C, with a contact angle measuring system VCA optima (AST products, Inc.) including a microscopy heating plate TC 324 Heater Controller (Warner instrument corporation). DI water was gently placed on the sample surfaces using an auto-syringe. Each sample was measured five times and the results were averaged with standard deviations. Cell attachment/shrinkage, morphology and spreading were examined using phase-contrast microscopy (Zeiss Axiovert 200). Tapping mode Atomic force microscopy (AFM) experiments were carried out using a Dimension V scanning probe microscope with a NanoScope V controller (Veeco). The measurements were performed in air using commercial Si cantilevers with a nominal spring constant and resonance frequency of 42 N/m and 330 kHz, respectively. Set-point values (A/A_0) were maintained 0.7 to 0.85, where A and A_0 refer to the "tapping" and "free" cantilever amplitude, respectively.

IX. 6. References

1. (a) Hadjichristidis, N., *J. Polym. Sci., Part A: Polym. Chem.* **1999**, *37* (7), 857-871; (b) Taton, D.; Gnanou, Y.; Matmour, R.; Angot, S.; Hou, S.; Francis, R.; Lepoittevin, B.; Moinard, D.; Babin, J., *Polym. Int.* **2006**, *55* (10), 1138-1145; (c) Blencowe, A.; Tan, J. F.; Goh, T. K.; Qiao, G. G., *Polymer* **2009**, *50* (1), 5-32; (d) Lapienis, G., *Prog. Polym. Sci.* **2009**, *34* (9), 852-892.

2. (a) Connal, L. A.; Vestberg, R.; Hawker, C. J.; Qiao, G. G., *Macromolecules* **2007**, *40* (22), 7855-7863; (b) Gao, H.; Matyjaszewski, K., *Progress in Polymer Science* **2009**, *34* (4), 317-350.
3. (a) Xia, J.; Zhang, X.; Matyjaszewski, K., *Macromolecules* **1999**, *32* (13), 4482-4484; (b) Gao, H.; Matyjaszewski, K., *J. Am. Chem. Soc.* **2007**, *129* (38), 11828-11834.
4. (a) Tugulu, S.; Silacci, P.; Stergiopoulos, N.; Klok, H.-A., *Biomaterials* **2007**, *28* (16), 2536-2546; (b) Bencherif, S. A.; Gao, H.; Srinivasan, A.; Siegwart, D. J.; Hollinger, J. O.; Washburn, N. R.; Matyjaszewski, K., *Biomacromolecules* **2009**, *10* (7), 1795-1803.
5. (a) Ternat, C.; Ouali, L.; Sommer, H.; Fieber, W.; Velazco, M. I.; Plummer, C. J. G.; Kreutzer, G.; Klok, H.-A.; Manson, J.-A. E.; Herrmann, A., *Macromolecules* **2008**, *41* (19), 7079-7089; (b) Giguère, G.; Zhu, X. X., *Biomacromolecules* **2009**, *11* (1), 201-206; (c) Urban, M. W., *Progress in Polymer Science* **2009**, *34* (8), 679-687; (d) Chen, T.; Ferris, R.; Zhang, J.; Ducker, R.; Zauscher, S., *Progress in Polymer Science* **2010**, *35* (1-2), 94-112; (e) Lee, H.-i.; Pietrasik, J.; Sheiko, S. S.; Matyjaszewski, K., *Progress in Polymer Science* **2010**, *35* (1-2), 24-44; (f) Sheiko, S. S.; Sumerlin, B. S.; Matyjaszewski, K., *Progress in Polymer Science* **2008**, *33* (7), 759-785; (g) Oh, J. K.; Drumright, R.; Siegwart, D. J.; Matyjaszewski, K., *Prog. Polym. Sci.* **2008**, *33* (4), 448-477; (h) Nuttelman, C. R.; Rice, M. A.; Rydholm, A. E.; Salinas, C. N.; Shah, D. N.; Anseth, K. S., *Progress in Polymer Science* **2008**, *33* (2), 167-179; (i) Bajpai, A. K.; Shukla, S. K.; Bhanu, S.; Kankane, S., *Prog. Polym. Sci.* **2008**, *33* (11), 1088-1118; (j) Wu, D. Y.; Meure, S.; Solomon, D., *Prog. Polym. Sci.* **2008**, *33* (5), 479-522.
6. (a) Kaneko, Y.; Nakamura, S.; Sakai, K.; Kikuchi, A.; Aoyagi, T.; Sakurai, Y.; Okano, T., *Polym. Gels Networks* **1999**, *6* (5), 333-345; (b) Wei, H.; Cheng, S.-X.; Zhang, X.-Z.; Zhuo, R.-X., *Prog. Polym. Sci.* **2009**, *34* (9), 893-910; (c) Fechner, N.; Badi, N.; Schade, K.; Pfeifer, S.; Lutz, J.-F., *Macromolecules* **2009**, *42* (1), 33-36; (d) Nandivada, H.; Ross, A. M.; Lahann, J., *Prog. Polym. Sci.* **2010**, *35* (1-2), 141-154; (e) Elloumi-Hannachi, I.; Yamato, M.; Okano, T., *J. Intern. Med.* **2010**, *267* (1), 54-70.
7. (a) Nath, N.; Chilkoti, A., *Adv. Mater.* **2002**, *14* (17), 1243-1247; (b) Alarcón, C. d. I. H.; Pennadam, S.; Alexander, C., *Chem. Soc. Rev.* **2005**, *34* (3), 276 - 285; (c) Lutz, J.-F.; Andrieu, J.; Uezguen, S.; Rudolph, C.; Agarwal, S., *Macromolecules* **2007**, *40* (24), 8540-8543; (d) Matsuda, N.; Shimizu, T.; Yamato, M.; Okano, T., *Adv. Mater.* **2007**, *19* (20), 3089-3099; (e) Kumar, A.; Srivastava, A.; Galaev, I. Y.; Mattiasson, B., *Prog. Polym. Sci.* **2007**, *32* (10), 1205-1237; (f) Lutz, J.-F., *J. Polym. Sci., Part A: Polym. Chem.* **2008**, *46* (11), 3459-3470; (g) Tan, I.; Zarafshani, Z.; Lutz, J.-F.; Titirici, M.-M., *ACS Appl. Mater. Interfaces* **2009**, *1* (9), 1869-1872.
8. (a) Yang, J.; Yamato, M.; Kohno, C.; Nishimoto, A.; Sekine, H.; Fukai, F.; Okano, T., *Biomaterials* **2005**, *26* (33), 6415-6422; (b) Yamato, M.; Akiyama, Y.; Kobayashi, J.; Yang, J.; Kikuchi, A.; Okano, T., *Prog. Polym. Sci.* **2007**, *32* (8-9), 1123-1133.
9. (a) Groll, J.; Fiedler, J.; Engelhard, E.; Ameringer, T.; Tugulu, S.; Klok, H.-A.; Brenner, R. E.; Moeller, M., *J. Biomed. Mater. Res. A* **2005**, *74A* (4), 607-617; (b) Yao, Y.; Ma, Y.-Z.; Qin, M.; Ma, X.-J.; Wang, C.; Feng, X.-Z., *Colloids Surf., B* **2008**, *66* (2), 233-239; (c) Wischerhoff, E.; Uhlig, K.; Lankenau, A.; Boerner, H. G.; Laschewsky, A.; Duschl, C.; Lutz, J.-F., *Angew. Chem. Int. Ed.* **2008**, *47* (30), 5666-5668.
10. (a) Lutz, J.-F.; Hoth, A., *Macromolecules* **2006**, *39* (2), 893-896; (b) Dong, H.; Matyjaszewski, K., *Macromolecules* **2010**, *43* (10), 4623-4628.

11. (a) Prucker, O.; Naumann, C. A.; Ruehe, J.; Knoll, W.; Frank, C. W., *J. Am. Chem. Soc.* **1999**, *121* (38), 8766-8770; (b) Taton, K. S.; Guire, P. E., *Colloids and Surfaces, B: Biointerfaces* **2002**, *24* (2), 123-132; (c) Dankbar, D. M.; Gauglitz, G., *Anal. Bioanal. Chem.* **2006**, *386* (7-8), 1967-1974.
12. (a) Matyjaszewski, K., *J. Macromol. Sci., Pure Appl. Chem.* **1997**, *A34* (10), 1785-1801; (b) Wang, J.-L.; Grimaud, T.; Matyjaszewski, K., *Macromolecules* **1997**, *30* (21), 6507-6512; (c) Braunecker, W. A.; Matyjaszewski, K., *Progress in Polymer Science* **2007**, *32* (1), 93-146; (d) Matyjaszewski, K.; Xia, J., *Chemical Reviews* **2001**, *101* (9), 2921-2990; (e) Tsarevsky, N. V.; Matyjaszewski, K., *Chem. Rev.* **2007**, *107* (6), 2270-2299; (f) Wang, J.-S.; Matyjaszewski, K., *Macromolecules* **1995**, *28* (23), 7901-7910; (g) Matyjaszewski, K.; Tsarevsky, N. V., *Nat Chem* **2009**, *1* (4), 276-288.
13. (a) Han, S.; Hagiwara, M.; Ishizone, T., *Macromolecules* **2003**, *36* (22), 8312-8319; (b) Lutz, J.-F.; Akdemir, O.; Hoth, A., *J. Am. Chem. Soc.* **2006**, *128* (40), 13046-13047.
14. Nakagawa, Y.; Suzuki, T.; Tayama, S., *Toxicology* **2000**, *156* (1), 27-36.
15. (a) Gil, E. S.; Hudson, S. M., *Prog. Polym. Sci.* **2004**, *29* (12), 1173-1222; (b) Xia, Y.; Yin, X.; Burke, N. A. D.; Stoeber, H. D. H., *Macromolecules* **2005**, *38* (14), 5937-5943.
16. (a) Zhulina, E. B.; Borisov, O. V.; Pryamitsyn, V. A.; Birshtein, T. M., *Macromolecules* **1991**, *24* (1), 140-149; (b) Plummer, R.; Hill, D. J. T.; Whittaker, A. K., *Macromolecules* **2006**, *39* (24), 8379-8388.
17. Akiyama, Y.; Kikuchi, A.; Yamato, M.; Okano, T., *Langmuir* **2004**, *20* (13), 5506-5511.
18. (a) Shinoda, H.; Matyjaszewski, K., *Macromolecules* **2001**, *34* (18), 6243-6248; (b) Ziegler, M. J.; Matyjaszewski, K., *Macromolecules* **2001**, *34* (3), 415-424; (c) Davis, K. A.; Charleux, B.; Matyjaszewski, K., *Journal of Polymer Science Part A: Polymer Chemistry* **2000**, *38* (12), 2274-2283.
19. Huang, J.; Murata, H.; Koepsel, R. R.; Russell, A. J.; Matyjaszewski, K., *Biomacromolecules* **2007**, *8* (5), 1396-1399.

Section VI.

Summary and Outlook

Chapter X

Summary and Outlook

The goal of this dissertation was to carry out fundamental studies on electrochemically mediated atom transfer radical polymerization (*e*ATRP) and the synthesis of polymers with complex polymeric architectures. In the first section, recent progress on electrochemically controlled chemical reactions and polymerizations were discussed, including copper-catalyzed azide-alkyne cycloaddition (click chemistry), electrochemical micro-patterning, and RAFT polymerization. The expansion of research in this area over the last decade indicates that electrochemically controlled procedures have become an essential tool for the design and synthesis of advanced, high quality, novel polymeric materials. Therefore, there was a need for an in-depth study of the fundamentals of *e*ATRP, which is addressed in Section II.

Section II encompasses five Chapters (II – VI) and six appendices (I – VI) that focus on fundamental studies of *e*ATRP. Chapter II explored the critical reaction parameters of an *e*ATRP, *i.e.*, applied potentials (E_{app}), catalysts type and loading, polymerization under galvanostatic conditions, and recycling the transition metal catalysts. Even though *e*ATRP showed many advantages for a control polymerization, the complexity of the reaction setup could be a substantial obstacle to the wide application of *e*ATRP in academia and industry. Chapter III addressed procedures for development of a simplified *e*ATRP (*se*ATRP) setup by using sacrificial counter electrode to solve the complexity of the initial *e*ATRP. *se*ATRP used a sacrificial aluminum anode as a substitute for the conventional counter electrode and eliminated the additional separation apparatus, such as electrolyte saturated

polysaccharide gels or membranes. A further simplified *e*ATRP system was achieved by polymerization under galvanostatic conditions. In this particular development only a platinum cathode and an aluminum anode were required for polymerizations. Chapter IV expanded *e*ATRP from organic media to an aqueous environment. Several challenges existed in aqueous ATRP including high activation rate, dissociation of halides from the X-Cu^{II}/L deactivators, decrease in stability of Cu/ligand complexes, disproportionation of Cu^I/L, and hydrolysis of carbon–halogen bonds, which could eventually result in uncontrolled polymerization reactions. Improvement in aqueous ATRP was achieved by developing conditions for continuously adjusting the activator/deactivator ratio, which decreased K_{ATRP} value and suppressed termination reactions by forming and maintaining a low radical concentration in the reaction medium. It was also determined that the addition of an excess of salt with a suitable counterion shifted the equilibrium from dissociated species to (re)formation of deactivators. Conditions for the successful *e*ATRP of water soluble monomers were developed, however, several additional challenges were still encountered in the polymerization of acrylamides, including relatively low values of ATRP equilibrium constant and potential side reactions. The primary polymerization parameters; such as reaction temperature, monomer concentration, and catalyst composition were systemically investigated in order to overcome such challenges and achieve a good control over acrylamide polymerization. Under the optimized conditions, successful polymerization of acrylamides was achieved. The *e*ATRP under aqueous media was further explored by expanding *e*ATRP to aqueous disperse media, *i.e.*, miniemulsion polymerization. Chapter V described miniemulsion polymerization which required development of communication between aqueous and organic phase catalysts. The

catalysts in the continuous phase, *i.e.*, aqueous phase catalysts, were reduced electrochemically but required electron transfer to organic phase catalysts to initiate the ATRP reaction in confined organic phase droplets in order to prepare well-defined polymers. The last Chapter (VI) in this section examined electrochemically mediated reversible addition-fragmentation chain transfer (RAFT) polymerization. Two approaches were evaluated: concurrent electrochemically controlled ATRP/RAFT and a pure *e*RAFT system. In the former approach, chain transfer agents (CTAs) were activated by electrochemically reduced Cu^I/ligand catalysts, resulting in a controlled polymerization that followed either the ATRP or RAFT mechanism. Optimal conditions for *e*ATRP/RAFT required the presence of a large amount of transition metal catalysts (*i.e.*, CuBr/bpy) therefore, conditions for a more environmentally benign reaction (*e*RAFT) to be conducted were developed. Electrolysis of an aryl diazonium salt produced radical sources and a successful *e*RAFT of MMA was accomplished.

Section II encompasses three projects (Chapters VII-IX) that centered on developing conditions for the synthesis of star polymers in high yields and utilization of functional star polymers in applications requiring advanced materials. Chapter VII mainly discussed controlled R_p for synthesis of high yielded star polymers by *e*ATRP. The rate of polymerization (R_p) was fine-tuned under selected E_{app} s with the aim of achieving *e*ATRP of macroinitiators/macromonomers. During the initial periods of star synthesis, a low R_p was employed by applying positive E_{app} s, to prevent premature intermolecular termination. Later, R_p was increased by simply switching to a more negative E_{app} , which subsequently resulted in a fast crosslinking reaction that occurred between pre-star molecules consisting

of a small number of crosslinking sites and a high yield of stars. Chapter VIII and Chapter IX detail the synthesis of functional star polymers for surface modification and examination of one potential application, a cell harvesting system. Star polymers composed of multiple arms showed a superior surface coverage compared to linear polymers, and incorporation of additional crosslinkable groups, were expected to allow successful formation of a stable surface. This idea was confirmed in Chapter VIII through synthesis of star polymers with light-induced crosslinkable groups that showed a uniform surface coverage and modification. The study was further extended to research on temperature responsive surfaces for potential application in a cell harvesting system (Chapter IX). Star polymers with thermoresponsive arms and photo-crosslinkable moieties were prepared and modified commercially available polystyrene surfaces. The modified surfaces revealed a temperature responsive behavior – at the lower temperature the surfaces displayed hydrophilic properties and in the opposite case converted to hydrophobic surfaces. The interactions between cells and the polymer modified surfaces were explored and confirmed possible applications in cell sheet engineering.

The results of my research might be contributed to the wide spread use of *e*ATRP in academia as well as evaluation in industry and have provided guidelines for rapid determination of optimal polymerization conditions. Based on the studies in this this dissertation on copper catalyzed *e*ATRP, future studies may extend the focus of research to polymerization with other inexpensive and non/less toxic transition metal catalyzed systems, *e.g.*, iron *e*ATRP. In addition, further investigations on synthesis of copolymers with other complex polymeric architectures may open opportunities to study relevant topics

such as optimal preparation of polymeric bottle brushes. By electrochemically controlling R_p , undesired intra/intermolecular crosslinking reaction may be suppressed, leading to the synthesis of well-defined polymeric bottle brushes. Polymerization of ionic liquids may be used in the development of polymeric electrolytes for batteries. Such polymeric architectures may be applied in biomedical engineering such as scaffold for tissue (re)generation by development of well-defined network polymers and electrochemically active nanocarriers for target drug delivery/sensors.

Appendices

Appendix I

Active Ligands for Low PPM Miniemulsion Atom Transfer

Radical Polymerizations^{*}

A-I. 1. Introduction

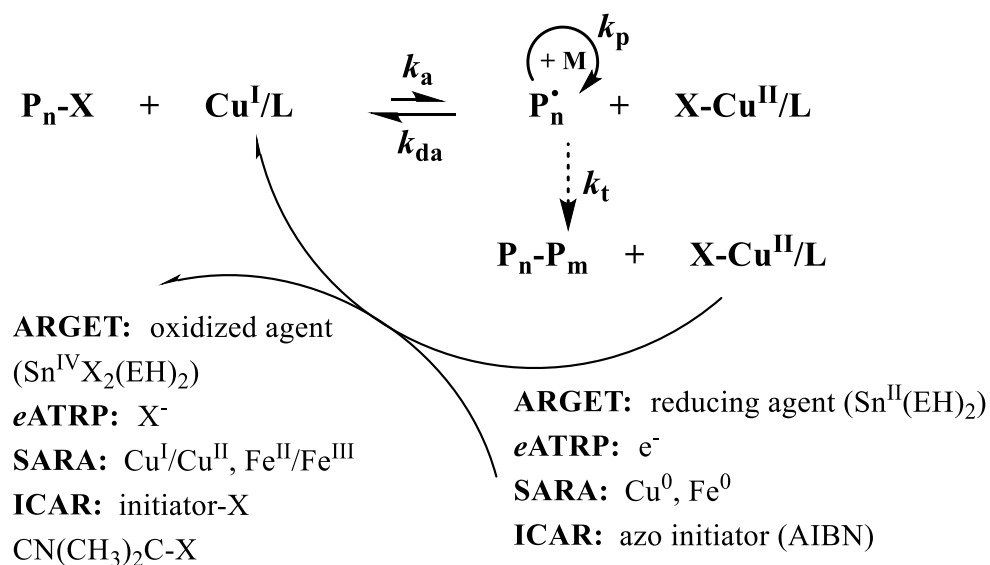
Atom transfer radical polymerization (ATRP)^{1a, 180} is a robust and powerful method of polymerization as it is able to not only control the composition (e.g., statistical, block, and gradient), and topology (e.g., stars and brushes), but also can polymerize monomers with a range of functionalities (e.g., (meth)acrylates, styrenics, and acrylamides) with predetermined molecular weights and narrow molecular weight distributions (M_w/M_n).^{2b, 61e, 105, 181} Furthermore, ATRP has proven to be successful in homogeneous (*i.e.*, organic and aqueous) and heterogeneous¹⁸² (e.g., microemulsion,¹¹¹ miniemulsion,¹¹² and emulsions¹¹³) media.

Control in ATRP relies on the dynamic equilibrium between propagating (P_n^\bullet) and dormant species (P_n-X , $X = Cl$ or Br). The alkyl halide is reversibly activated by lower oxidation state catalyst complexes (Cu^I/L , $L = \text{Ligand}$) to form the macroradical species, P_n^\bullet , and deactivated by the high oxidation state catalyst complex ($X-Cu^{II}/L$). The equilibrium constant of ATRP, K_{ATRP} , is then defined as the ratio of activation (k_a) and deactivation (k_{da}) rate constants, which determines concentration of radicals present in the polymerization. As the equilibrium of ATRP favors the deactivated state, the number of

^{*}Work in this appendix was published and partially reformatted based on the following manuscript: Elsen, Andrea M.; Burdyńska, Joanna; **Park, Sangwoo**; Matyjaszewski, Krzysztof *Macromolecules* **2012**, 45, 7356

active radicals (P_n^\bullet) available for propagation (k_p) and termination (k_t) is well controlled.

Several advances have been made to homogenous ATRP, making it more environmentally friendly and industrially viable.¹⁸³ The addition of an appropriate reducing agent, such as tin(II) 2-ethylhexanoate, glucose, ascorbic acid or hydrazine in activators regenerated by electron transfer (ARGET) ATRP,¹⁸⁴ application of a potential as in electrochemically mediated ATRP (*e*ATRP),¹⁸⁵ addition of copper wire as in supplemental activators and reducing agent (SARA) ATRP,¹⁸⁶ or addition of thermal initiators as in initiators for continuous activator regeneration (ICAR) ATRP¹⁸⁴ are all proven methods of well-controlled ATRP with ppm levels of catalyst. In each case, reduction of $[X-Cu^{II}/L]$ species, accumulated during irreversible termination, restores the activator, $[Cu^I/L]$ (Scheme A-I-1).



Scheme A-I-1. Low ppm catalyst ATRP mechanisms.

Utilizing such systems decreases the catalyst concentrations up to 1000 times in

comparison to normal ATRP. As the rate of polymerization decreases with decreasing catalyst concentrations, the rate of activation (k_a) must be significantly enhanced to maintain the rate of polymerization comparable to normal ATRP. Enhancing k_a can be achieved by using the complex of Cu^{I} with branched multidentate ligands. The most common branched tetradentate ligands are tris[2-(dimethylamino)ethyl]amine (Me_6TREN)¹⁸⁷ and tris(2-pyridylmethyl)amine (TPMA).¹⁸⁸ Copper catalyst complexes with these ligands in normal ATRP display 10^3 - 10^5 times higher activity than the originally used Cu^{I} /2,2'-bipyridine complex.^{1a, 173c}

In addition to the aforementioned advances, ATRP has been successfully extended to aqueous dispersed media (*e.g.*, microemulsion,¹¹¹ miniemulsion,¹¹² and emulsions¹¹³), all of which resulted in well-defined polymer latexes. Polymerizations utilizing aqueous conditions are also under consideration for industrial processes as they are recognized to be a mild, environmentally benign technique. Water as a polymerization medium not only eliminates the necessity of using volatile organic solvents but also ensures greater heat dissipation during polymerization. Moreover, low viscosity of the dispersed aqueous solutions allows for obtaining high weight fractions of the polymer, which is not accessible in bulk or organic solvent polymerizations.^{114a}

However, such heterogeneous polymerizations require careful design, as there are multiple components involved. A surfactant which generates a stable dispersion but does not interfere with the polymerization, a reducing agent which quickly and efficiently reduces $\text{X-Cu}^{\text{II}}/\text{L}$, and a hydrophobic catalyst which remains in the oil phase are all necessary ingredients for a successful ATRP in aqueous dispersed media.^{182d} The most

commonly utilized ligand in emulsion based ATRP is bis(2-pyridylmethyl)octadecylamine (BPMODA).¹⁸⁹ While this ligand is successful under normal ATRP conditions in dispersed media, it is unable to perform well at low catalyst concentrations due to a relatively low K_{ATRP} value. Conversely, highly active ligands such as CuBr₂/TPMA and CuBr₂/Me₆TREN complexes, which have thrived in low catalyst homogeneous ATRP, show much higher affinity toward water than the organic phase and, therefore, are less useful in aqueous dispersed media.

While remarkable headway has been made within homogenous ATRP polymerizations, including low ppm catalyst systems,¹⁸⁴ the synthesis of highly active ligands,¹⁹⁰ and development of new metal complexes¹⁹¹ etc., less progress has been made for low catalyst heterogeneous ATRPs. To date, there are very few reports of successful ARGET ATRP in aqueous dispersed media;¹⁹² the majority of these systems utilize activators generated by electron transfer (AGET) ATRP as the higher oxidation state catalyst may be used for the polymerization set up, but requires > 1000 ppm of total catalyst.

This Appendix outlines the design, synthesis, and characterization of a new ligand, (bis[2-(4-methoxy-3,5-dimethyl)pyridylmethyl]octadecylamine) (BPMODA*), for ARGET ATRP in aqueous dispersed media. Addition of electron donating groups (EDGs)^{190, 193} to the structure of BPMODA resulted in a ligand with a K_{ATRP} value *ca.* 10⁻⁵, two order of magnitude higher. Homogeneous polymerizations under normal ATRP conditions revealed the newly synthesized ligand to have a higher rate of polymerization without loss of control as compared to BPMODA. Partition experiments of the ligands indicate the hydrophobicity of BPMODA has not been compromised by the EDGs, as the

majority of the ligand remains in the organic phase. Heterogeneous polymerizations conducted over a range of catalyst concentrations (250 - 2000 ppm) with BPMODA* consistently resulted in polymerizations with increased control throughout the polymerizations, particularly at lower monomer conversions.

A-I. 2. Results and Discussion

Ligand Design and Characterization. As BPMODA has proven itself to be an excellent ligand for aqueous dispersed polymerizations, the logical process for generating a highly active, yet hydrophobic ligand, was to alter the structure of BPMODA to increase activity. Previous studies on 2,2'-bipyridine and TPMA ligands demonstrated that increasing the electron donating properties of ligand substituents resulted in rate enhancements of the polymerizations.^{190, 193} The addition of methoxy- and two methyl groups on each pyridinyl ring, for a total of six electron donating groups, was expected to increase the activity of BPMODA without greatly affecting the hydrophobicity of the ligand. The synthesis of BPMODA* was straightforward and based on that of BPMODA, as reported in the literature: the coupling of 2-chloromethyl-4-methoxy-3,5-dimethylpyridine hydrochloride with the primary amine, octadecylamine.

It has been reported that half-wave potential ($E_{1/2}$) values are correlated to K_{ATRP} , which provides insight into the activity of catalysts complex.¹⁹⁴ Cyclic voltammetry (CV) was used to determine the $E_{1/2}$ values of BPMODA and BPMODA*, -0.098 and -0.204 V (vs. SCE), respectively. From this correlation, it can be concluded that the supplemental electron donating substituents present on BPMODA* should increase the K_{ATRP} value 10⁻

⁷, for BPMODA, to *ca.* 10^{-5} . The two orders of magnitude increase in K_{ATRP} value causes BPMODA* to have a similar activity to TPMA. To test the suggested increase in catalytic activity of BPMODA*, several polymerizations were conducted under homogeneous, normal ATRP conditions.

Homogeneous Polymerizations. Normal ATRP was conducted at three different ratios of $\text{Cu}^{\text{I}}/\text{L}$ to $\text{X-Cu}^{\text{II}}/\text{L}$ (80/20, 95/5, and 99/1) for BPMODA and BPMODA*. All polymerizations were carried out in 20% anisole at 60 °C with a targeted DP = 200; conditions and results are summarized in Table A-I-1. Regardless of the ligand used, a well-controlled polymerization was obtained. Every polymerization demonstrated both linear first-order kinetics, indicating a constant amount of radicals, and linear growth of number average molecular weights (M_n) with monomer conversion (Figure A-I-2). Experimental M_n values ($M_{n,\text{GPC}}$) strongly correlated with theoretical values while M_w/M_n decreased with monomer conversion, whose final values were below 1.15. The singular distinction between the polymerizations with each ligand is the rate of polymerization (R_p). From the first-order kinetic plots it is evident that the rate of polymerization is much faster when BPMODA* is used as the ligand. It is important to note the increase in R_p does not come with any loss in control over the polymerization. This data supports the conclusion of the CV: BPMODA* does have a higher K_{ATRP} value compared to BPMODA due to the addition of six electron donating groups. However, higher K_{ATRP} values did not originate in decreased values of k_{da} as evidenced by narrow molecular weight distributions.

Figure A-I-2 also demonstrates the effects of catalyst concentration on the polymerizations with BPMODA*. Those polymerizations conducted with higher

percentages of deactivator ($\text{Br-Cu}^{\text{II}}/\text{L}$) present at the beginning of the reaction showed the slowest R_p . As the percentage of initial deactivator was decreased (5 and 1%) a corresponding increase in the rate of polymerization was seen. The lack of deactivator present during the initial stages of these polymerizations did result in larger M_w/M_n values at early monomer conversions, however, the final M_w/M_n values were nearly identical (1.08-1.09).

Table A-I-1. Normal ATRP of *n*-BA with BPMODA and BPMODA*.

Entry ^{a,b}	CuBr	CuBr ₂	t (h)	Conv. ^c	$M_{n,\text{GPC}}$	$M_{n,\text{th}}$	M_w/M_n
1	0.80	0.20	48	0.56	14 500	14 400	1.04
2*	0.80	0.20	24	0.88	17 900	22 600	1.08
3	0.95	0.05	49	0.62	15400	15 800	1.09
4*	0.95	0.05	7.5	0.82	19 300	20 900	1.08
5	0.99	0.01	48	0.63	12 800	16 000	1.13
6*	0.99	0.01	6	0.84	18 400	21 400	1.09

^aAll polymerizations were conducted in 20% (v/v) anisole at 60 °C with $[\text{BA}]/[\text{EBiB}]/[\text{Ligand}] = 200/1/1$. ^bEntries labeled with (*) utilized BPMODA*, all other entries utilized BPMODA. ^cDetermined by ¹H NMR.

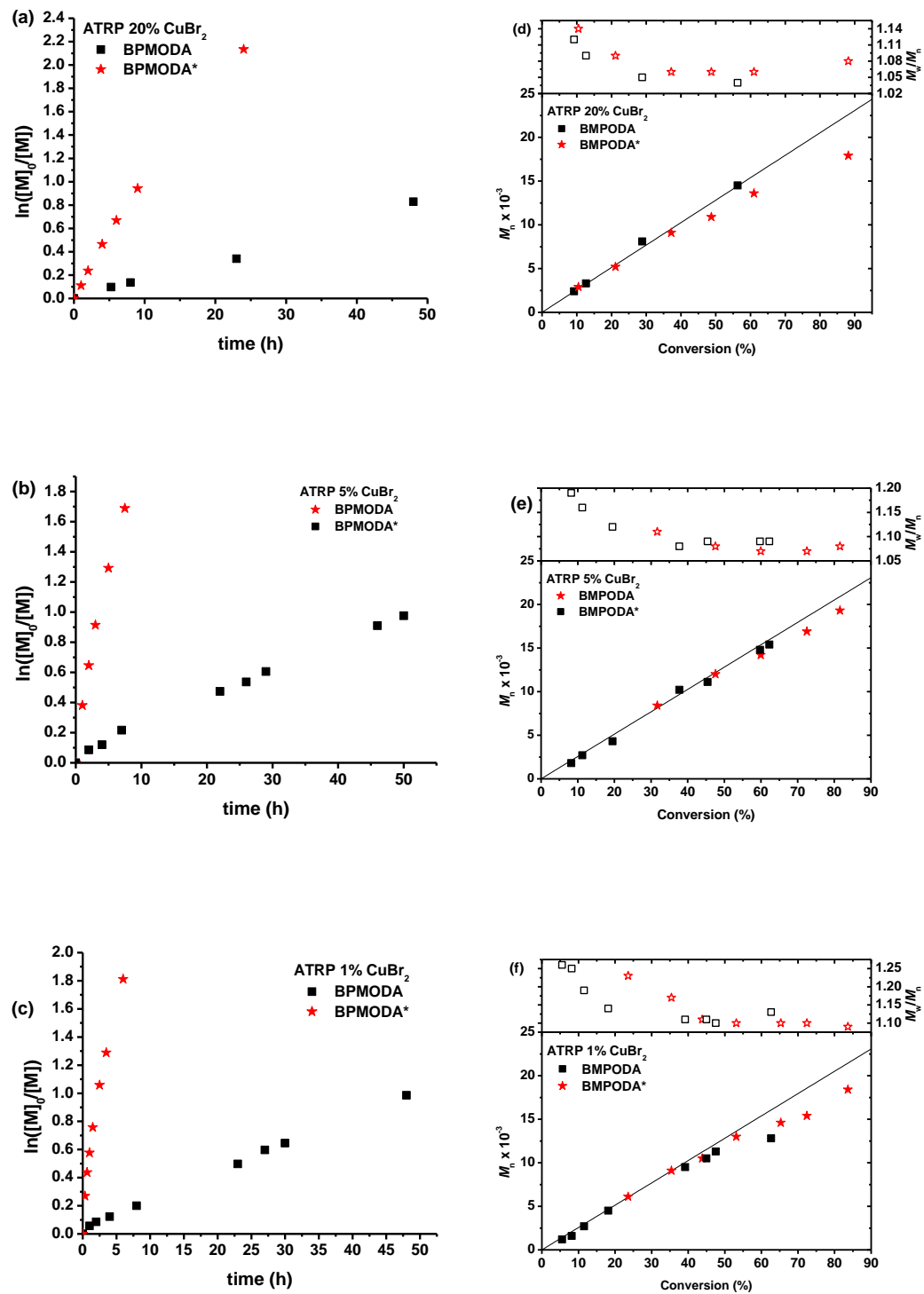


Figure A-I-1. First order kinetic plots (a-c) and evolution of M_n and M_w/M_n with

conversion (d-f) for the normal ATRP of BA at = 80/20; 99/5; and 99/1 for BPMODA and BPMODA*. All polymerizations were conducted with $[BA]/[EBiB]/[CuBr]/[CuBr_2]/[Ligand] = 200/1/X/Y/1$ ($X = 0.80, 0.95, 0.99$ and $Y = 0.20, 0.05, 0.01$) in 20% (v/v) anisole at 60 °C.

Both ligands were then tested under SARA ATRP conditions, which require significantly less catalyst (50 ppm), in contrast to normal ATRP (5000 ppm), along with Cu^0 wire as a reducing agent. It was expected that BPMODA, a ligand with a low K_{ATRP} value, would result in a poorly controlled polymerization, while BPMODA*, with a K_{ATRP} value similar to that of TPMA, would afford a well-controlled ATRP. To test this hypothesis, a third polymerization was carried out under SARA ATRP conditions which employed TPMA.

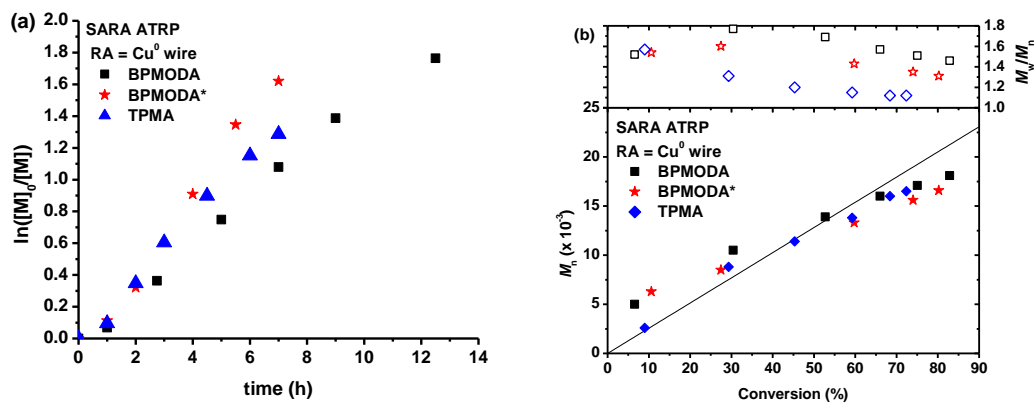


Figure A-I-2. First-order kinetic plots (a) and evolution of M_n and M_w/M_n with monomer conversion (b) for the SARA ATRP of BA with BPMODA, BPMODA*, or TPMA. All polymerizations were conducted with $[BA]/[EBiB]/[CuBr_2]/[Ligand]/[Cu^0 \text{ wire}] = 200/1/0.01/0.03/1 \text{ cm}$ in 20% (v/v) anisole at 60 °C.

Figure A-I-2 shows the linear first order kinetics by each of the three ligands tested. BPMODA* and TPMA had very similar R_p , while BPMODA was the slowest. The difference in R_p under SARA ATRP conditions was not as dramatic as was seen in normal ATRP, which is attributed to the presence of the reducing agent. The rate of polymerization is dependent on the rate at which Cu^0 wire reduces $\text{Br-Cu}^{\text{II}}/\text{L}$ to $\text{Cu}^{\text{I}}/\text{L}$ and the least reducing catalyst should be more quickly converted to its lower oxidation state. While the $M_{n,\text{GPC}}$ values increased linearly with monomer conversion for each ligand, it is evident that TPMA afforded the most well-controlled polymerization. When TPMA was utilized, there was the strongest correlation between $M_{n,\text{GPC}}$ and $M_{n,\text{th}}$, along with the lowest M_w/M_n values. Although BPMODA* did not afford as much control as TPMA, it did offer a more controlled polymerization than BPMODA. Both ligands demonstrated M_w/M_n values which decreased with monomer conversion, however, the values were broader than those given by TPMA. Nevertheless, BPMODA* offered more control than BPMODA.

Partition Experiments. Before starting polymerization under miniemulsion type conditions, the partition coefficient for each complex was determined at various catalyst concentrations. UV-Vis was used to determine the absorbance of both the organic and aqueous layers, from which the concentration of the catalyst and respective partition coefficient ($\lambda = [\text{Cu}]_{\text{org}}/[\text{Cu}]_{\text{aq}}$) was determined (Table A-I-2). At each concentration tested, a higher percentage catalyst, for both ligands, was transferred to the aqueous phase when stirred at 80 °C. The electron donating groups present on BPMODA* do not appear to have an effect on the partition coefficient as similar amounts of catalyst remained in the organic phase.

Table A-I-2. Partitioning of CuBr₂/BPMODA and CuBr₂/BPMODA* in BA/Water (w/w)
= 30/100.

30/100		[CuBr ₂ /L] Initial Conc.			
(w/w)		2.5 mM		1 mM	
(org:Aq)		Reg	Star	Reg	Star
λ	r.t.	1.96	9.04	2.93	4.20
λ	80 °C	0.26	2.23	1.33	0.48
[Cu] _{org} /[Cu] _{int}	r.t.	66.2	90.0	74.5	80.8
[Cu] _{org} /[Cu] _{int}	80 °C	20.9	69.0	57.2	32.4

Heterogeneous Polymerizations. Polymerizations were carried out under miniemulsion conditions with both BPMODA and BPMODA*. To start, ligand and copper were dissolved in monomer to form the catalyst by stirring at 60 °C for 30 – 60 min. The solubility of BPMODA* in monomer was significantly better as compared to BPMODA. To form the catalyst in BA with BPMODA, it was required to stir at 60 °C for 1 h and the final solution was very cloudy. On the other hand, BPMODA* required only 30 min to fully form the catalyst in BA and the final solution was translucent, as seen in Figure A-I-3. This increased solubility of BPMODA* in monomer is advantageous not only for ease of polymerization setup but also for consistency of results as it is much easier to see if the catalyst is fully dissolved with BPMODA*.

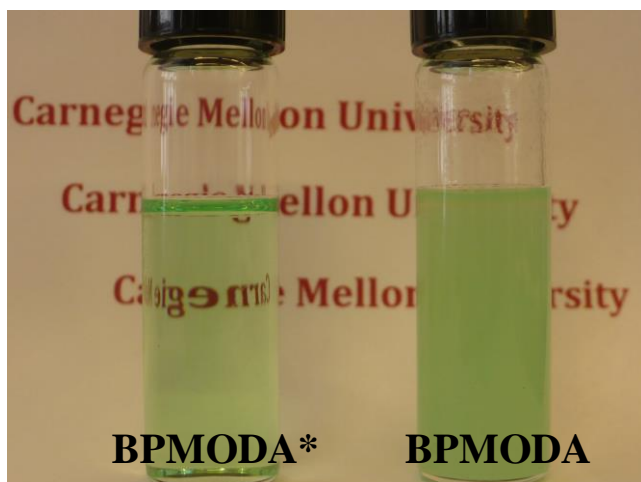


Figure A-I-3. 500 ppm catalyst solutions in BA with BPMODA* and BPMODA.

Though AGET ATRP (catalyst ~ 2000 ppm) with BPMODA in miniemulsion is common and well-studied, it was important to compare the newly synthesized ligand under identical conditions, after which the catalyst concentration was systematically lowered until ARGET ATRP conditions were reached; Table A-I-3 and Figure A-I-4 summarize these results. Linear first order kinetics were observed for both ligands when 2000 ppm of catalyst was utilized (Figure A-I-4a). Both polymerizations exhibited $M_{n, \text{GPC}}$ values which strongly correlated the $M_{n, \text{th}}$ values as well as low M_w/M_n values. However, the molecular weight distribution at early monomer conversion is the distinguishing mark between the ligands. While both ligands offer M_w/M_n values which decrease with monomer conversion, BPMODA* affords polymers with significantly lower M_w/M_n values at the beginning states of the polymerization. For example, BPMODA showed a $M_w/M_n = 2.69$ at 20% monomer conversion, while BPMODA* showed a $M_w/M_n = 1.54$ at 16% monomer conversion. As AGET ATRP operates under similar mechanistic conditions to SARA ATRP, the rates of polymerizations for the ligands were similar due to the presence of the reducing agent,

ascorbic acid. As the concentration of catalyst was lowered, similar trends were seen. At both 1000 and 500 ppm of catalyst, BPMODA* resulted in polymerizations with lower M_w/M_n values at all monomer conversions.

Table A-I-3. A(R)GET ATRP of BA in miniemulsion with BPMODA and BPMODA*.^a

Entry ^b	CuBr ₂ (ppm)	Ligand	AA	Conv. ^c	$M_{n,th}$	$M_{n,GPC}$	M_w/M_n^d	M_w/M_n^e
1	0.4 (2000)	0.4	0.2	0.55	14 100	15 300	2.69	1.23
2*	0.4 (2000)	0.4	0.2	0.54	13 800	13 500	1.54	1.15
3	0.2 (1000)	0.2	0.1	0.87	22 400	18 000	2.49	1.60
4*	0.2 (1000)	0.2	0.1	0.54	14 000	14 000	1.62	1.18
5	0.1 (500)	0.1	0.05	0.87	22 300	18 500	1.61	1.48
6*	0.1 (500)	0.1	0.05	0.84	21 600	18 200	1.45	1.33
7	0.05 (250)	0.05	0.025	0.88	22 000	21 000	2.64 ^f	2.61
8*	0.05 (250)	0.05	0.025	0.93	23 800	18 900	1.66	1.51

^a [BA]/[EBiB] = 200/1, [Brij98]/[Hexadecane] = 2.3/3.6 wt% vs. BA, $T = 80\text{ }^{\circ}\text{C}$; ^b entries labeled with (*) used BPMODA*, all others used BPMODA; ^c determined by gravimetry; ^d monomer conversion < 45% unless otherwise noted; ^e M_w/M_n values of final polymer sample; ^f monomer conversion = 66 %.

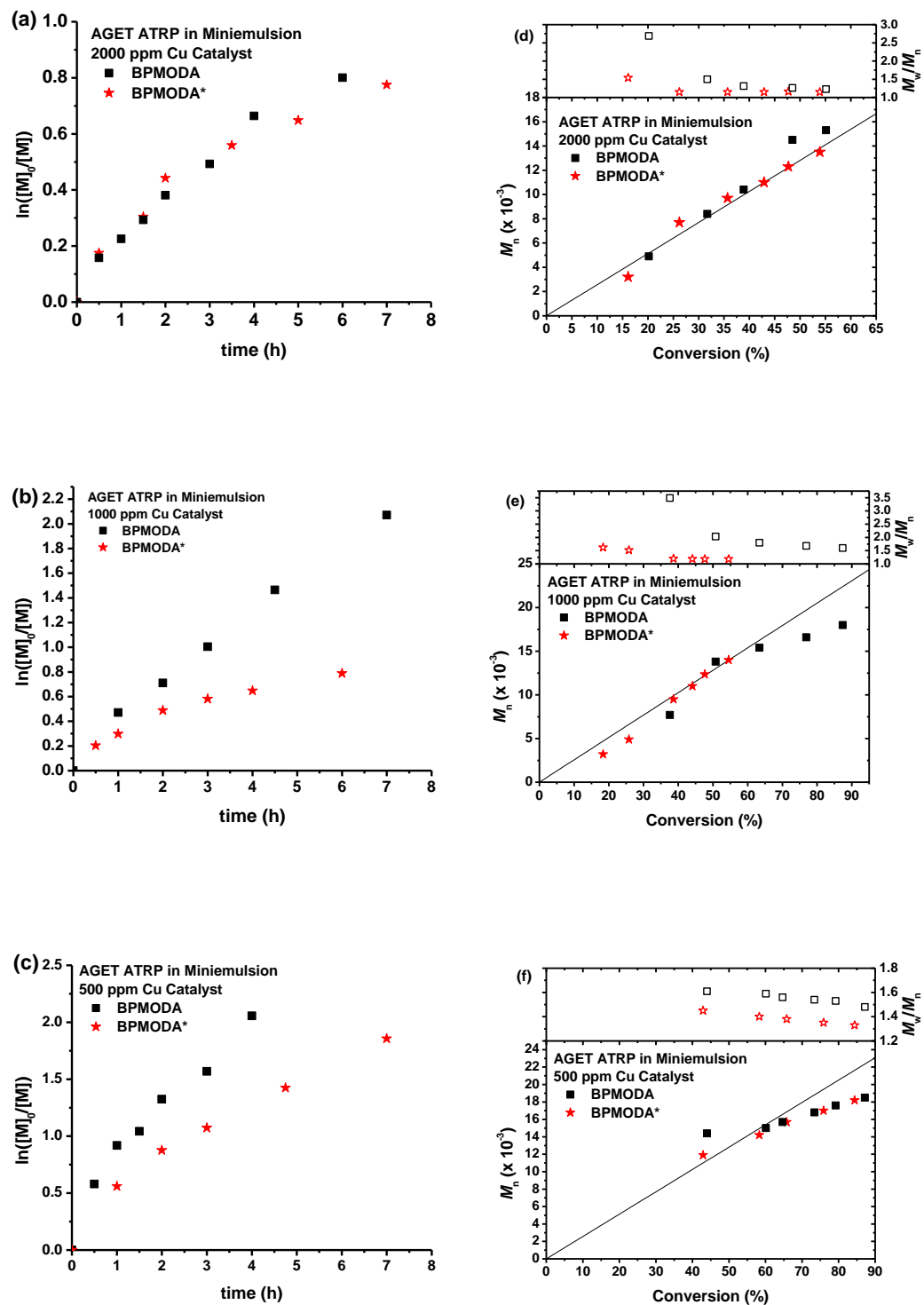


Figure A-I-4. First-order kinetic plots (a-c) and evolution of molecular weights and M_w/M_n

with conversion (d-f) of AGET ATRP of BA with BPMODA and BPMODA* in miniemulsion. ^a [BA]/[EBiB] = 200/1, [Brij98]/[Hexadecane]= 2.3/3.6 wt% vs. BA, *T* = 80 °C.

In an attempt to find the “the maximum activity” for each ligand, the catalyst concentrations were reduced even further. 250 ppm of catalyst resulted in very different polymerizations for each ligands. The first order kinetic plot can be seen in Figure A-I-5, which demonstrates the kinetic plots for BPMODA are not linear at this concentration. The plot levels off, indicating the polymerization has stopped. The number average molecular weight does not grow linearly with monomer conversion and the polymerization stops at 90% conversion. Additionally, the M_w/M_n values are quite large (> 2.5) throughout the polymerization. However, when an identical polymerization was carried out with BPMODA*, a significant increase in control was seen. BPMODA* afforded linear first order kinetics, $M_{n, GPC}$ values which had a reasonable correlation to the theoretical values and $M_w/M_n < 1.5$ throughout the polymerization. While the polymerization with BPMODA* at 250 ppm of catalyst was not ideal, it did offer much more control than BPMODA.

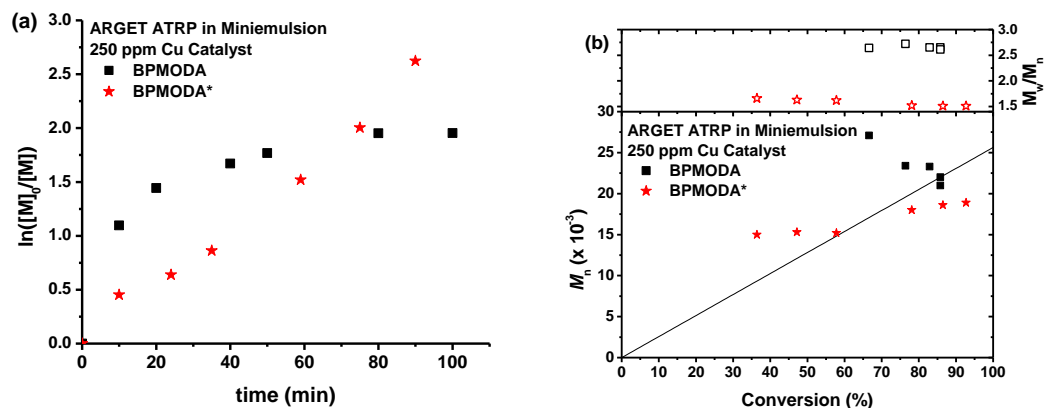


Figure A-I-5. First-order kinetic plot (a-c) and evolution of molecular weight and M_w/M_n with conversion (d-f) of AGET ATRP of BA with BPMODA and BPMODA* in miniemulsion. ^a $[BA]/[EBiB] = 200/1$, $[Brij98]/[Hexadecane] = 2.3/3.6$ wt% vs. BA, $T = 80$ °C.

The previous set of miniemulsion polymerizations maintained the ratio of ascorbic acid and ligand to copper throughout all polymerizations. While this allowed a systematic study of the ligands over a range of catalyst concentrations, it did not allow for the optimal polymerization conditions at low catalyst concentrations. For example, ARGET ATRP utilizes an excess of ligand compared to copper, ensuring the catalyst is formed. To fully realize the potential of BPMODA*, a series of polymerizations were conducted with conditions more suited toward low catalyst concentrations.

A-I. 3. Summary

The design, synthesis, and characterization of BPMODA*, a highly active ligand for ARGET ATRP in aqueous dispersed media were reported. The modification of

traditionally used BPMODA, a ligand with low catalyst activity, was achieved through the addition of electron donating groups, which resulted in a ca. 100 fold increase in the K_{ATRP} value. Homogeneous polymerizations under normal ATRP conditions confirmed the newly synthesized ligand to have a higher R_p without loss of control. Additionally, the hydrophobicity of BPMODA was not been compromised by the supplementary EDGs as demonstrated by partition experiments. Heterogeneous polymerizations conducted over a range of catalyst concentrations (2000 - 250 ppm) with BPMODA* consistently resulted in polymerizations with increased control throughout the polymerizations, particularly at early monomer conversions.

A-I. 4. Experimental Section

Materials. *n*-Butyl acrylate (BA, 99%, Aldrich) was passed through a column filled with basic alumina prior to use. 2-Chloromethyl-4-methoxy-3,5-dimethylpyridine hydrochloride (Py-HCl*, 98%, Aldrich), copper(I) bromide ($\text{Cu}^{\text{I}}\text{Br}$, 99.999%, Aldrich), copper(II) bromide ($\text{Cu}^{\text{II}}\text{Br}_2$, 99.999%, Aldrich), copper(II) trifluoromethanesulfonate ($\text{Cu}^{\text{II}}(\text{OTf})_2$, 98%, Aldrich) copper wire ($d = 0.5$ mm, 99.9%, Alfa Aesar), ethyl α -bromoisobutyrate (EBiB, 98%, Aldrich), hexadecane (99%, Aldrich), L-ascorbic acid (AA, >99%, Aldrich), magnesium sulfate (MgSO_4 , Fisher Scientific), octadecyl amine (95%, Fluka), polyoxyethylene(20) oleyl ether (Brij 98, Aldrich), sodium hydroxide pellets (NaOH , 99.2%, Fisher Scientific), tetrabutylammonium perchlorate (TBAClO_4 , 98%, Aldrich), tetraethylammonium bromide (TBABr , 99% Aldrich), tributylhexadecyl phosphonium bromide ($\text{Bu}_3\text{P}^+\text{Br}^-$, 97%, Fluka), and solvents were purchased from Aldrich and used as received. BPMODA,¹⁸⁸ tris(2-pyridylmethyl)amine (TPMA)¹⁸⁸ and tris(2-

(dimethylamino)ethyl)amine (Me₆TREN)¹⁸⁷ were synthesized according to previously published procedures.

Characterization. Molecular weight and molecular weight distributions of the formed polymers were measured by gel permeation chromatography (GPC) using Polymer Standards Services (PSS) columns (guard, 10⁵, 10³, and 10² Å), with THF eluent at 35 °C, flow rate 1.00 mL/min, and differential refractive index (RI) detector (Waters, 2410). Diethyl ether was used as the internal standard to correct for any fluctuation of the THF flow rate. The number-average molecular weights (M_n) and molecular weight distribution (M_w/M_n) were determined with a calibration based on linear polystyrene standards using WinGPC 6.0 software from PSS. Absorbance of catalyst solutions was measured by UV-Vis (Agilent, 8453). ¹H NMR spectra were recorded in CDCl₃ as a solvent using Bruker 300 MHz spectrometer.

BPMODA* Synthesis. Octadecyl amine (17 g, 64 mmol), Py-HCl* (30 g, 135 mmol, 2.1 eq.) Bu₃P⁺Br⁻ (1.6 g, 3.2 mmol, 0.05 eq.), and a stir bar were added to a 500 mL round bottom flask. The solids were dissolved in THF (200 mL), followed by 5 N NaOH_{aq} (110 mL). The biphasic mixture was refluxed at 60 °C for 5 d. After separation of the organic phase from the aqueous, it was washed with brine until the pH ~ 9. The organic layer was dried with MgSO₄ and the solvent was removed *via* rotary evaporator. The resulting solid was characterized via ¹H NMR (300 MHz, CDCl₃). δ : 0.85 (*t*, 3H, CH₂Me), 1.00-1.22 (*m*, 30H, (CH₂)₁₅Me), 1.40 (*m*, 2H, CH₂CH₂(CH₂)₁₅Me), 2.04 (*s*, 6H, 5-Py-CH₃), 2.18 (*s*, 6H, 3-Py-CH₃), 2.42 (*m*, 2H, CH₂CH₂(CH₂)₁₅Me), 3.63 (*s*, 4H, 2-Py-CH₂), 3.67 (*s*, 6H, 4-Py-OCH₃), 8.11 (*s*, 2H, 5-PyH).

Electrochemical Analysis. All of the voltammograms were recorded at 25 °C with a Gamry Reference 600 potentiostat. A 40 mL of MeCN containing 0.05 M TBAClO₄ supporting electrolyte was prepared using previously dried reagents. To this solution was added 0.8 mL of a 0.05 M solution of Cu^{II}(OTf)₂/BPMODA* (or BPMODA)/2TBABr (1.0 mM). Measurements were carried out under a nitrogen atmosphere at a scan rate of 25 mV/s using platinum disk working electrode and platinum mesh counter electrode. Potentials were recorded versus a saturated calomel electrode (Gamry) separated from the working solutions by a porous Vycor tip.

ATRP Polymerization. An example ATRP procedure formulated with 2000 ppm of CuBr₂/BPMODA catalyst and targeted degree of polymerization (DP) equal to 200 is given as follows; see Table A-I-1 for specific reaction conditions. A 10 mL Schlenk flask was charged with BA (5 mL, 35 mmol), EBiB (0.44 mL of 76.9 mg/mL solution in anisole, 0.17 mmol), BPMODA (0.79 mL of 100 mg/mL solution in anisole, 174 mmol), CuBr₂ (0.78 mL of 20 mg/mL solution in acetonitrile, 70 mmol), anisole (1.8 mL) and a stir bar. The reaction mixture was degassed by at least three freeze-pump-thaw cycles and filled with nitrogen again. With positive pressure of N₂, CuBr (19.9 mg, 140 mmol) was added to the 10 mL Schlenk flask. The flask was evacuated and refilled with nitrogen at least 6 times. The Schlenk flask was placed in a 60 °C oil bath. Samples were taken periodically to measure conversion *via* ¹H NMR and number average molecular weights *via* GPC.

SARA ATRP of BA. An example SARA ATRP procedure formulated with 50 ppm of CuBr₂/BPMODA catalyst and targeted DP = 200 is given as follows; A 10 mL Schlenk flask was charged with Cu⁰ wire (1 cm) and a stir bar, after which, the flask was degassed

and backfilled with nitrogen (N_2) six times. A mixture of anisole (1.5 mL), EBiB (0.44 mL of 76.9 mg/mL solution in anisole, 0.17 mmol), BPMODA (0.24 mL of 10 mg/mL solution in anisole, 5.2 μ mol), and $CuBr_2$ (0.39 mL of 1 mg/mL solution in anisole, 1.7 μ mol) was added to a glass vial and purged with nitrogen for 20 min. Previously deoxygenated BA (5 mL, 35 mmol) was added to the vial. Immediately, the reaction mixture was transferred *via* an airtight syringe to the Schlenk flask, which was placed in a thermostated water bath at 60 °C. Samples were taken periodically to measure conversion *via* 1H NMR and number average molecular weights *via* GPC.

Partition Experiments. Calibration curves were generated for $CuBr_2$ /BPMODA* (1/1 ratio) catalyst in monomer (BA) and $CuBr_2$ /Me₆TREN (1/1.5 ratio) catalyst in water. Stock solutions were prepared of varying catalyst concentrations (8, 5, 2.5, 1, and 0.2 mM) whose absorbance was determined using UV-Vis. A linear relationship was obtained correlating absorbance with catalyst concentration. Solutions of $CuBr_2$ /BPMODA and $CuBr_2$ /BPMODA* (1/1 ratio) in BA were prepared at various concentrations (2.5 and 1 mM). The solutions were mixed with deionized water in a 30/100 (w/w) ratio and were stirred at either RT or 80 °C for 1 h. The organic phase was separated from the aqueous phase, after which the absorbance was measured *via* UV-Vis spectrometer at 780 nm. Me₆TREN was added to the aqueous phase at a ratio of $CuBr_2$ /Me₆TREN (1/1.5), assuming 100% of the catalyst was transferred to the aqueous phase, after which the concentration of the catalyst was determined by the absorbance at 800 nm. In the case of BPMODA, only the absorption of the aqueous phase was measured, from which the concentration of catalyst remaining in the organic phase was calculated.

A(R)GET ATRP in Miniemulsion. An example AGET ATRP in miniemulsion procedure formulated with 2000 ppm of CuBr₂/BPMODA catalyst and targeted DP = 200 is given as follows; see Table A-I-3 for specific reaction conditions. CuBr₂ (17 mg, 0.078 mmol) and BPMODA (17.4 mg, 0.078 mmol) were dissolved in BA (5.0 g, 39.1 mmol) in a round bottom flask at 60 °C to form a solution of the copper complex. The solution was then cooled to room temperature prior to dissolving the initiator EBiB (26 µL, 0.195 mmol) and hexadecane (0.14 mL, 0.826 mmol) in the solution. A 5 mM solution of Brij 98 in deionized water (20.2 mL) was added to the organic BA solution and was subjected to sonication in an ice bath (Heat Systems Ultrasonics W-385 sonicator; output control set at 8 and duty cycle at 70% for 1 min). The resulting stable miniemulsion was purged with nitrogen for 30 min. A predeoxygenated aqueous solution of AA (0.7 mL, containing 6.9 mg AA) was injected into the miniemulsion over a period of 3 min to activate the catalyst and start the polymerization. Samples were taken periodically to measure the conversion gravimetrically and to determine the number-average molecular weights by GPC.

A-I. 5. References

1. (a) Wang, J. S.; Matyjaszewski, K., *J. Am. Chem. Soc.* **1995**, *117*, 5614-5615; (b) Matyjaszewski, K.; Xia, J., *Chem. Rev.* **2001**, *101*, 2921-2990; (c) Braunecker, W. A.; Matyjaszewski, K., *Prog. Polym. Sci.* **2007**, *32*, 93-146; (d) Matyjaszewski, K., *Macromolecules* **2012**, *45*, 4015-4039; (e) Kato, M.; Kamigaito, M.; Sawamoto, M.; Higashimura, T., *Macromolecules* **1995**, *28* (5), 1721-1723.
2. (a) Davis, K. A.; Matyjaszewski, K., Statistical, Gradient, Block, and Graft Copolymers by Controlled/Living Radical Polymerizations. In *Advances in Polymer Science*, Springer Berlin / Heidelberg: 2002; Vol. 159; (b) Matyjaszewski, K.; Spanswick, J., 3.12 - Copper-Mediated Atom Transfer Radical Polymerization. In *Polymer Science: A Comprehensive Reference*, Editors-in-Chief: Krzysztof, M.; Martin, M., Eds. Elsevier: Amsterdam, 2012; pp 377-428; (c) Matyjaszewski, K.; Tsarevsky, N. V., *Nat. Chem.* **2009**, *1*, 276-288; (d) Matyjaszewski, K., *Science* **2011**, *333*, 1104-1105; (e) Gao, H.; Matyjaszewski, K., *Prog.*

- Polym. Sci.* **2009**, *34*, 317-350; (f) Coessens, V.; Pintauer, T.; Matyjaszewski, K., *Prog. Polym. Sci.* **2001**, *26* (3), 337-377.
3. (a) Cunningham, M. F., *Prog. Polym. Sci.* **2002**, *27* (6), 1039-1067; (b) Qiu, J.; Charleux, B.; Matyjaszewski, K., *Prog. Polym. Sci.* **2001**, *26* (10), 2083-2134; (c) Min, K.; Gao, H. F.; Matyjaszewski, K., *Journal of the American Chemical Society* **2006**, *128* (32), 10521-10526; (d) Min, K.; Matyjaszewski, K., *Cent. Eur. J. Chem.* **2009**, *7*, 657-674.
 4. (a) Min, K.; Matyjaszewski, K., *Macromolecules* **2005**, *38* (20), 8131-8134; (b) Kagawa, Y.; Kawasaki, M.; Zetterlund, P. B.; Minami, H.; Okubo, M., *Macromolecular Rapid Communications* **2007**, *28* (24), 2354-2360.
 5. (a) Min, K.; Gao, H. F.; Matyjaszewski, K., *J. Am. Chem. Soc.* **2005**, *127* (11), 3825-3830; (b) Min, K.; Jakubowski, W.; Matyjaszewski, K., *Macromolecular Rapid Communications* **2006**, *27* (8), 594-598; (c) Bombalski, L.; Min, K.; Dong, H. C.; Tang, C. B.; Matyjaszewski, K., *Macromolecules* **2007**, *40* (21), 7429-7432.
 6. (a) Qiu, J.; Gaynor, S. G.; Matyjaszewski, K., *Macromolecules* **1999**, *32* (9), 2872-2875; (b) Jousset, S.; Qiu, J.; Matyjaszewski, K., *Macromolecules* **2001**, *34* (19), 6641-6648; (c) Eslami, H.; Zhu, S. P., *Polymer* **2005**, *46* (15), 5484-5493; (d) Eslami, H.; Zhu, S. P., *Journal of Polymer Science Part A-Polymer Chemistry* **2006**, *44* (6), 1914-1925; (e) Min, K.; Gao, H.; Yoon, J. A.; Wu, W.; Kowalewski, T.; Matyjaszewski, K., *Macromolecules* **2009**, *42* (5), 1597-1603.
 7. (a) Tsarevsky, N.; Matyjaszewski, K., *Chem. Rev.* **2007**, *107*, 2270-2299; (b) Pintauer, T.; Matyjaszewski, K., *Chem. Soc. Rev.* **2008**, *37*, 1087-1097.
 8. Matyjaszewski, K.; Jakubowski, W.; Min, K.; Tang, W.; Huang, J.; Braunecker, W. A.; Tsarevsky, N. V., *Proc. Natl. Acad. Sci. U.S.A.* **2006**, *103* (42), 15309-14.
 9. Magenau, A. J. D.; Strandwitz, N. C.; Gennaro, A.; Matyjaszewski, K., *Science* **2011**, *332*, 81-84.
 10. Magenau, A. J. D.; Kwak, Y.; Matyjaszewski, K., *Macromolecules* **2010**, *43* (23), 9682-9689.
 11. Xia, J. H.; Gaynor, S. G.; Matyjaszewski, K., *Macromolecules* **1998**, *31*, 5958-5959.
 12. Xia, J. H.; Matyjaszewski, K., *Macromolecules* **1999**, *32*, 2434-2437.
 13. Wang, J.-S.; Matyjaszewski, K., *Macromolecules* **1995**, *28* (23), 7901-7910.
 14. Cunningham, M. F., *Prog. Polym. Sci.* **2008**, *33* (4), 365-398.
 15. Oh, J. K., *Journal of Polymer Science Part A: Polymer Chemistry* **2008**, *46*, 6983-7001.
 16. Magenau, A. J. D.; Kwak, Y.; Schroeder, K.; Matyjaszewski, K., *ACS Macro Lett.* **2012**, *1*, 508-512.
 17. di Lena, F.; Matyjaszewski, K., *Prog. Polym. Sci.* **2010**, *35*, 959-1021.
 18. (a) Cheng, C.; Shu, J.; Gong, S.; Shen, L.; Qiao, Y.; Changqing, F., *New J. Chem.* **2010**, *34*, 163-170; (b) Stoffelbach, F.; Griffete, N.; Bui, C.; Charleux, B., *Chem. Commun.* **2008**, 4807-4809; (c) Simms, R. W.; Cunningham, M. F., *Macromolecules* **2007**, *40*, 860-866.
 19. Schroeder, K.; Mathers, R. T.; Buback, J.; Konkolewicz, D.; Magenau, A. J. D.; Matyjaszewski, K., *Macro Letters* **2012**, *1*, 1037-1040.
 20. (a) Qiu, J.; Matyjaszewski, K.; Thouin, L.; Amatore, C., *Macromol. Chem. Phys.* **2000**, *201*, 1625-1631; (b) Tang, W.; Kwak, Y.; Braunecker, W.; Tsarevsky, N.; Coote, M. L.; Matyjaszewski, K., *J. Am. Chem. Soc.* **2008**, *130*, 10702-10713; (c) Braunecker, W.; Tsarevsky, N.; Gennaro, A.; Matyjaszewski, K., *Macromolecules* **2009**, *42*, 6348-6360.

Appendix II

ARGET ATRP in Miniemulsion with 50 PPM of Copper

Catalyst*

A-II. 1. Introduction

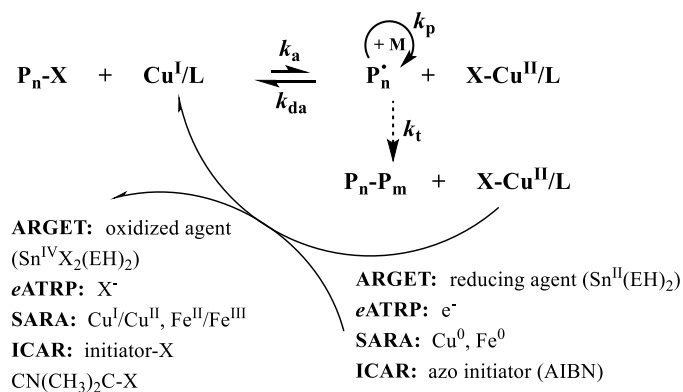
Polymerization in aqueous dispersed media is recognized to be a mild, environmentally benign technique and therefore widely considered for use on an industrial scale. Water as a reaction medium not only affords greater heat dissipation during polymerization, but also eliminates the necessity of using volatile organic solvents.^{114a, 114c, 182d, 195} Atom transfer radical polymerization (ATRP)^{1a, 180} has been successfully extended to aqueous dispersed media including microemulsion,^{111a, 196} miniemulsion,^{112c, 197} and emulsions^{113a-c, 113e, 198}, all of which resulted in well-defined polymers and latexes.

Control in ATRP relies on the dynamic equilibrium between propagating (P_n^\bullet) and dormant species (P_n-X , $X = Cl$ or Br). Through reversible activation of the alkyl halide by the lower oxidation state catalyst complexes (Cu^I/L , $L = \text{Ligand}$) the macroradical species, P_n^\bullet , is formed and then deactivated by the high oxidation state catalyst complex ($X-Cu^{II}/L$). The ratio of activation (k_a) and deactivation (k_{da}) rate constants is defined as the equilibrium constant of ATRP, K_{ATRP} , and determines the number of radicals present in the polymerization. As the equilibrium of ATRP favors the deactivated state, the number of

*Work in this appendix was published and partially reformatted based on the following manuscript: Andrea M. Elsen; Joanna Burdyńska; **Sangwoo Park**; Krzysztof Matyjaszewski *ACS Macro Letters* **2013**, 2, 822

active radicals (P_n^\bullet) available for propagation (k_p) and termination (k_t) is well controlled.

Several advances have been made to homogenous ATRP, which allow for the use of ppm levels of catalyst, affording more environmentally friendly and industrially viable systems.¹⁸³ The addition of a reducing agent, such as tin(II) 2-ethylhexanoate, glucose, ascorbic acid or hydrazine in activators regenerated by electron transfer (ARGET) ATRP,^{184, 199} application of a potential as in electrochemically mediated ATRP (*e*ATRP),¹⁸⁵ light in photochemical process,²⁰⁰ addition of copper wire as in supplemental activators and reducing agent (SARA) ATRP,¹⁸⁶ or addition of thermal initiators as in initiators for continuous activator regeneration (ICAR) ATRP¹⁸⁴ are all proven methods. In each case, the activator, Cu^I/L , is resorted through the reduction of accumulated $X-Cu^{II}/L$ species during irreversible termination (Scheme A-II-1).



Scheme A-II-1. Low ppm catalyst ATRP mechanisms.

The key to successful ARGET ATRP in aqueous dispersed media systems lies with the ligand as it must be both hydrophobic and highly active. Hydrophobicity prevents the catalyst from diffusing to the aqueous phase¹⁹⁶ while high activity, or K_{ATRP} value, affords

well controlled polymerizations at low catalyst concentrations. The most commonly employed ligand in emulsion based ATRP is *N,N'*-bis(2-pyridylmethyl)octadecylamine (BPMODA).²⁰¹ Due to a relatively low K_{ATRP} value, this ligand is successful under normal ATRP conditions in dispersed media, however, it is unable to perform well at low catalyst concentrations as in ARGET ATRP. Conversely, ligands with high K_{ATRP} values such as tris[2-(dimethylamino)-ethyl]amine (Me₆TREN)¹⁸⁷ and tris(2-pyridylmethyl)amine (TPMA),^{1a} which perform well in low catalyst homogeneous ARGET ATRP^{183-184, 199}, show much higher affinity toward water than the oil phase. Therefore, these ligands are not useful in aqueous dispersed media. This Appendix focused on the design, synthesis, and characterization of new hydrophobic and active ATRP catalysts, *N',N''*-dioctadecyl-*N',N''*-bis[2-(4-methoxy-3,5-dimethyl)pyridylmethyl]ethane-1,2-diamine (DOD-BPED*).

A-II. 2. Results and Discussion

A new ligand for ARGET ATRP in miniemulsion, *N,N'*-bis[2-(4-methoxy-3,5-dimethyl)pyridylmethyl]octadecylamine (BPMODA*) was recently reported and addressed on Appendix I²⁰² which resulted in well controlled heterogeneous polymerizations conducted with as low as 250 ppm of CuBr₂/BPMODA* catalyst. The success of this catalyst was attributed to increased ligand activity from the addition of six electron donating groups to the tridentate BPMODA-based structure. It is the goal of this Appendix to expand the previously reported work through the design and synthesis of a new tetradentate ligand for ARGET ATRP in miniemulsion systems: *N',N''*-dioctadecyl-*N',N''*-bis[2-(4-methoxy-3,5-dimethyl)pyridylmethyl]ethane-1,2-diamine (DOD-BPED*) whose structure is given in Figure A-II-1.

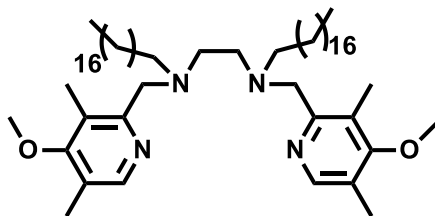


Figure A-II-1. Structure of DOD-BPED*.

When considering the design of the new ligand, hydrophobicity and K_{ATRP} value were increased through the number of aliphatic chains present as well as the denticity of the ligand. The structure of DOD-BPED*, whose detailed synthetic procedure may be found in the Experimental Section, was based on *N,N'*-dimethyl-*N,N'*-bis(2-pyridylmethyl)ethane-1,2-diamine (BPED), a tetradentate ligand known to have a K_{ATRP} value similar to that of TPMA.^{194b} Two octadecyl chains were incorporated into the BPED-based structure affording increased hydrophobicity over BPMODA* which contains only one aliphatic chain. In addition to being tetradentate, as compared to the less active tridentate structure of BPMODA*, six electron donating groups were also included on two pyridine rings to further increase activity.^{190, 194b, 203}

It has been reported that half-wave potentials ($E_{1/2}$ values) measured by cyclic voltammetry (CV) are correlated to K_{ATRP} thereby providing insight into the activity of a catalyst complex.¹⁹⁴ DOD-BPED*, when complexed with CuBr_2 , is insoluble in acetonitrile preventing the measurement of the $E_{1/2}$ and K_{ATRP} values by CV. Utilizing a solvent other than acetonitrile for CV, will provide a trend in $E_{1/2}$ value changes with ligand structure. For example, the $E_{1/2}$ value of BPMODA* is more negative, indicating a more active ligand, than BPMODA due to the presence of electron donating groups (EDGs) on

BPMODA*. When measured in DMF, a similar trend for the BPMODA to BPMODA* structure change was observed: -0.07 and -0.14 V (vs. SCE), respectively. Comparison of the cyclic voltammograms of *N',N''*-dioctadecyl-*N',N''*-bis(2-pyridylmethyl)ethane-1,2-diamine (DOD-BPED) ($E_{1/2} = -0.13$ V) with that of DOD-BPED* ($E_{1/2} = -0.17$ V) resulted in a more negative $E_{1/2}$ values for DOD-BPED* due to the EDGs within the structure. This shift toward a more negative $E_{1/2}$ value indicates a higher K_{ATRP} value for DOD-BPED* than for DOD-BPED.

CuBr₂/DOD-BPED* was first tested as a catalyst under homogeneous ARGET ATRP conditions and compared with CuBr₂/TPMA and CuBr₂/BPMODA. *n*-Butyl methacrylate (BMA) was polymerized at a targeted DP = 200 with 50 ppm of CuBr₂/L catalyst and Sn^{II}(EH)₂ as the reducing agent. Specific reaction conditions and results are summarized in Table A-II-1 and Figure A-II-2. Linear first-order kinetics as well as similar rates of polymerization (R_p) were observed for all ligands. While all polymerizations demonstrated good correlation between experimental ($M_{n,\text{exp}}$) and theoretical ($M_{n,\text{th}}$) molecular weights, the final M_w/M_n values of 1.12, 1.38 and 1.42 for TPMA, DOD-BPED* and BPMODA, respectively, signify the polymerization with BPMODA was the least controlled. ARGET ATRPs conducted with CuBr₂/TPMA are established and known to offer a high degree of control at catalyst concentrations as low as 10 ppm and such was the case in this work. While the polymerization with DOD-BPED* resulted in a larger M_w/M_n value as compared to TPMA, the linear first-order kinetics and good correlation of $M_{n,\text{exp}}$ and $M_{n,\text{th}}$ values are promising results for successful heterogeneous polymerizations with low catalyst concentrations.

Table A-II-1. ARGET ATRP of BMA with TPMA and DOD-BPED*.

Entry ^a	t (h)	Conv. ^b	$M_{n,th}$	$M_{n,GPC}$	M_w/M_n
TPMA	8	0.35	9 800	11 000	1.12
DOD-BPED*	7.5	0.27	7 700	7 600	1.38
BPMODA	7	0.30	8 600	10 500	1.42

^aAll polymerizations were conducted with [BMA]/[EBPA]/[CuBr₂]/[Ligand]/[Sn^{II}(EH)₂] = 200/1/0.01/0.03/0.1, 20% (v/v) anisole, $T=60\text{ }^{\circ}\text{C}$. ^b Determined by ¹H NMR.

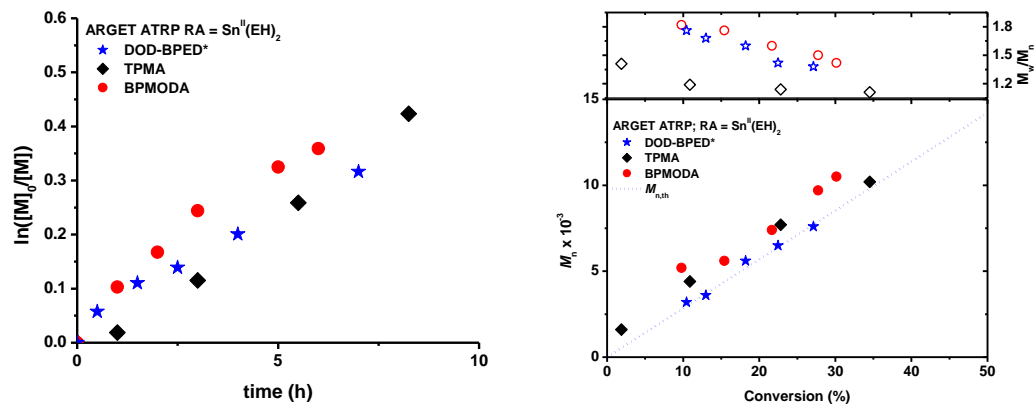


Figure A-II-2. First-order kinetic plots (a) and evolution of M_n and M_w/M_n with monomer conversion (b) for the ARGET ATRP of BMA with DOD-BPED*, TPMA, or BPMODA. All polymerizations were conducted with [BMA]/[EBPA]/[CuBr₂]/[Ligand]/[Sn^{II}(EH)₂] = 200/1/0.01/0.03/0.1, 20% (v/v) anisole, $T=60\text{ }^{\circ}\text{C}$.

Polymerizations under heterogeneous miniemulsion conditions were conducted with CuBr₂/DOD-BPED* catalyst whose concentration was systematically decreased from 250

to 50 ppm at a targeted DP = 2000 as detailed in Table A-II-2 (entries 1-3) and Figure A-II-3a-b. Although lower catalyst concentrations resulted in a decreased rate of polymerization (R_p), linear first-order kinetics was observed for each polymerization. All polymerizations demonstrated linear growth of molecular weight with monomer conversion in addition to good correlation between $M_{n,exp}$ and $M_{n,th}$ values. When 250 or 100 ppm (entries 1 and 2) of CuBr₂/DOD-BPED* catalyst was employed, M_w/M_n values were low (*ca.* 1.23 and 1.24, respectively). Only a slight increase of the final M_w/M_n value (*ca.* 1.33) was observed when a mere 50 ppm (entry 3) of catalyst was utilized.

Table A-II-2. ARGET ATRP of BMA in Miniemulsion with DOD-BPED*^a.

Entry	BMA	EBPA	CuBr ₂ (ppm)	Ligand	AA	Conv ^b	$M_{n,th}$	$M_{n,GPC}$	M_w/M_n
1	2000	1	0.5 (250)	0.5	0.25	0.54	152 800	173 700	1.23
2	2000	1	0.2 (100)	0.2	0.1	0.44	124 700	124 900	1.24
3	2000	1	0.1 (50)	0.1	0.05	0.28	80 600	78 200	1.33
4	5000	1	0.5 (50)	0.5	0.25	0.37	261 300	248 900	1.33
5	10000	1	1 (50)	1	0.5	0.37	527 700	755 500	1.39

^a[Brij 98]/[hexadecane] = 2.3/3.6 wt% vs. BMA, $T = 80\text{ }^{\circ}\text{C}$. ^bDetermined by gravimetry.

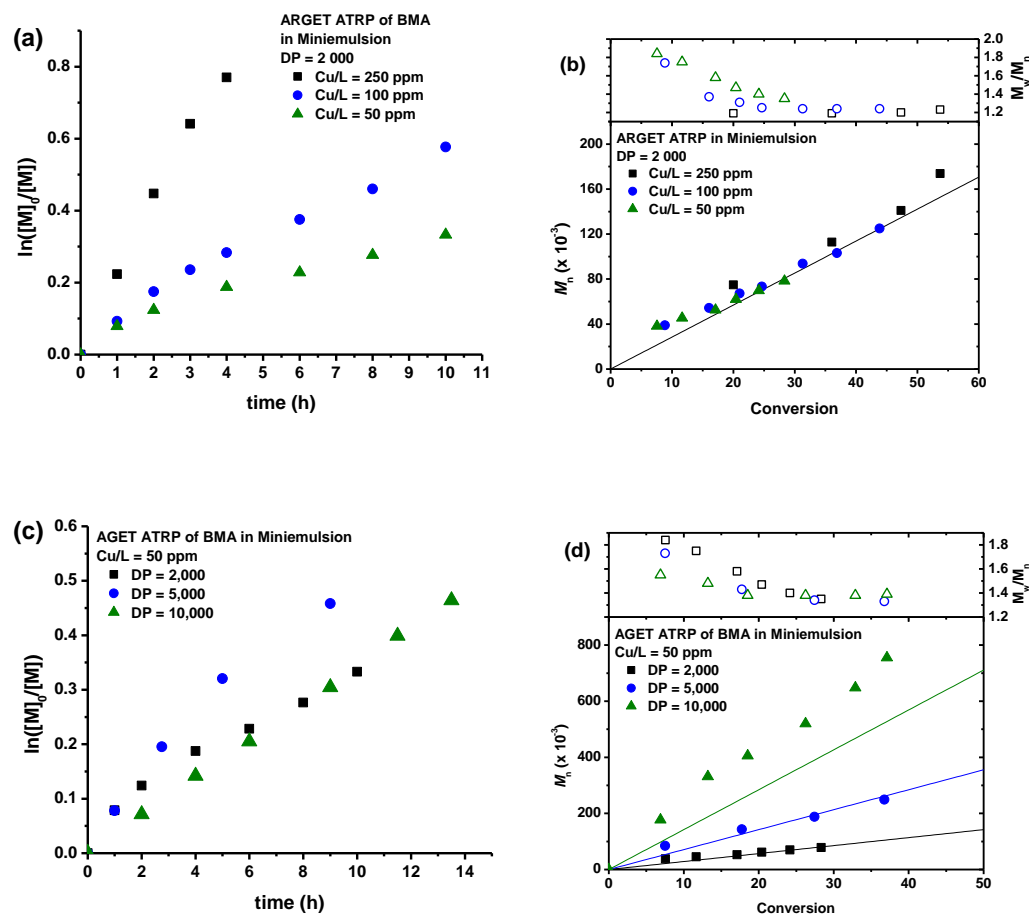


Figure A-II-3. First-order kinetic plots (a, c) and evolution of M_n and M_w/M_n with monomer conversion (b, d) for the ARGET ATRP of BMA DOD-BPED* under miniemulsion conditions. All polymerizations were conducted with [Brij 98]/[hexadecane] = 2.3/3.6 wt% vs. BMA, $T = 80^\circ\text{C}$. Specific reaction conditions in Table A-II-2.

Maintaining the catalyst concentration at 50 ppm, the targeted degree of polymerizations were systematically increased from DP = 2000 to DP = 10000 while keeping monomer conversion below 50% to avoid any particle aggregation. Table A-II-2 (entries 3-5) and Figure A-II-3c-d summarize these results. All polymerizations

demonstrated linear first-order kinetics as well as linear growth of molecular weight with monomer conversion. M_w/M_n values decreased with monomer conversion reaching final M_w/M_n values = 1.35, 1.33, and 1.39 for DP = 2000, 5000, and 10000, respectively. The synthesis of large polymers with low M_w/M_n values may be attributed to the more active ligand, DOD-BPED*, which allows for low catalyst concentrations during the polymerization thereby reducing the $\text{Cu}^{\text{I}}/\text{L}$ induced catalytic radical termination effect.²⁰⁴ However, this may also be due to compartmentalization where radical-radical termination is limited due to the separation of radicals in the miniemulsion system.²⁰⁵ The generation of a polymer with $M_{n,\text{exp}} > 700,000$ and narrow MWD values while utilizing only 50 ppm of catalyst (Table A-II-2, entry 5) is an extraordinary advance of ATRP in aqueous dispersed media.

A-II. 3. Summary

In summary, careful ligand design is an important tool for the improvement and expansion of ATRP success. A series of polymerizations were presented in this work which clearly illustrate the utility of DOD-BPED* for ATRP in miniemulsion. Well controlled polymerizations were achieved with as low as 50 ppm of catalyst. Moreover, while maintaining this level of catalyst concentration, it was shown that DOD-BPED* can successfully polymerize BMA at a targeted DP = 10000. Most significantly, very high molecular weight polymers of $M_{n,\text{exp}} > 700,000$ with low M_w/M_n values were achieved using only 50 ppm of $\text{CuBr}_2/\text{DOD-BPED}^*$ catalyst.

A-II. 4. Experimental Section

Materials. *n*-Butyl methacrylate (BMA, 99%, Aldrich) was passed through a column filled with basic alumina prior to use. 2-Chloromethyl-4-methoxy-3,5-dimethylpyridine hydrochloride (Py-HCl*, 98%, Aldrich), 2-(chloromethyl)pyridine hydrochloride (Py-HCl, 98%, Aldrich), copper(II) bromide ($\text{Cu}^{\text{II}}\text{Br}_2$, 99.999%, Aldrich), copper(II) chloride ($\text{Cu}^{\text{II}}\text{Cl}_2$, 99.999%, Aldrich), *N,N*-dimethylformamide, (DMF, Fisher Scientific, >99%), ethyl- α -bromophenylacetate (EBPA, 97%, Aldrich), *N,N'*-ethylenebis(stearamide) (beads, < 840 μm , Aldrich), hexadecane (99%, Aldrich), L-ascorbic acid (AA, >99%, Aldrich), lithium aluminum hydride (LiAlH_4 , powder, 95%, Aldrich), magnesium sulfate (MgSO_4 , Fisher Scientific), polyoxyethylene(20) oleyl ether (Brij 98, Aldrich), tetrabutylammonium hexafluorophosphate (TBAPF_6 , >98%, Aldrich), tin(II) 2-ethylhexanoate ($\text{Sn}^{\text{II}}(\text{EH})_2$, 95%, Aldrich), tributylhexadecyl phosphonium bromide ($\text{Bu}_3\text{P}^+\text{Br}^-$, 97%, Fluka), and solvents were purchased from Aldrich and used as received. BPMODA,¹⁸⁸ tris(2-pyridylmethyl)amine (TMPA)¹⁸⁸ were synthesized according to previously published procedures.

Characterization. Molecular weight and molecular weight distributions of the formed polymers were measured by gel permeation chromatography (GPC) using Polymer Standards Services (PSS) columns (guard, 10^5 , 10^3 , and 10^2 Å), with THF eluent at 35 °C, flow rate 1.00 mL/min, and differential refractive index (RI) detector (Waters, 2410). Diethyl ether was used as the internal standard to correct for any fluctuation of the THF flow rate. The number-average molecular weights (M_n) and molecular weight distribution (M_w/M_n) were determined with a calibration based on linear polystyrene standards using WinGPC 6.0 software from PSS. Absorbance of catalyst solutions was measured by UV-

Vis (Agilent, 8453). ^1H NMR spectra were recorded in CDCl_3 as a solvent using Bruker 300 MHz spectrometer.

Electrochemical Analysis. All voltammograms of TPMA, BPMODA, BPMODA*, DOD-BPED, and DOD-BPED* were recorded at 25 °C with a Gamry Reference 600 potentiostat. CuBr_2 (22.3 mg, 0.1 mmol), ligand (0.1 mmol), and TBAPF_6 (1.56 g, 4 mmol) were placed in 7 necked reaction flask and nitrogen purged. The N_2 bubbled DMF (20 mL) was injected to the mixture and additional N_2 bubbled for 10 min to keep N_2 atmosphere. Measurements were carried out under a nitrogen atmosphere at a scan rate of 25 mV/s using platinum disk working electrode and platinum mesh counter electrode. Potentials were recorded versus a saturated calomel electrode (SCE, from Gamry) separated from the working solutions by a porous Vycor tip. Half-wave potentials ($E_{1/2}$) were determined by averaging cathodic and anodic peaks.

Synthesis of N,N' -dioctadecylethylenediamine. A dry 500 mL three-neck round bottom flask was charged with N,N' -ethylenebis(stearamide) (3.00 g, 5.1 mmol), lithium aluminum hydride (0.577 g, 15.2 mmol) and then dry THF (150 mL) was added under nitrogen atmosphere. The flask was equipped with a condenser, sealed and placed in an oil bath. The reaction mixture was refluxed under nitrogen atmosphere for 48 hrs. The process was terminated by the slow addition of 1 M HCl_{aq} until the evolution of bubbles ceased. After the quenching, the mixture was extracted with hexanes (4 x 50 mL), and then combined organic phases were washed with 1 M NaOH_{aq} (30 mL), water (30 mL), dried with anhydrous sodium sulfate and concentrated. The product was isolated as white wax and characterized by ^1H NMR analysis (300 MHz, CDCl_3). δ : 0.88 (t, $J=8.8$ Hz, 6H,

CH_2CH_3), 1.18-1.38 (*s*, 60H, $(\text{CH}_2)_{15}\text{CH}_3$), 1.47 (*m*, 4H, $\text{NCH}_2\text{CH}_2(\text{CH}_2)_{15}\text{Me}$), 2.57 (*t*, $J=7.0$ Hz, 4H, $\text{NCH}_2\text{CH}_2(\text{CH}_2)_{15}\text{Me}$), 2.70 (*s*, 4H, $\text{CH}_2\text{NCH}_2\text{CH}_2(\text{CH}_2)_{15}\text{Me}$).

Synthesis of DOD-BPED*. *N,N'*-dioctadecylethylenediamine (1.50 g, 2.65 mmol), 2-chloromethyl-4-methoxy-3,5-dimethylpyridine hydrochloride (1.30 g, 5.44 mmol), and tributylhexadecylphosphonium bromide (0.135 g, 0.266 mmol) were dissolved in THF (30 mL), and then 5 N NaOH_{aq} (4 mL) was added. The biphasic mixture was refluxed at 60 °C for 5 d. After separation of the organic phase from the aqueous, it was washed with brine until the pH \sim 9. The organic layer was dried with MgSO_4 and the solvent was removed *via* rotary evaporator. The resulting solid was characterized via ^1H NMR (300 MHz, CDCl_3). δ : 0.80 (*t*, $J=6.7$ Hz, 6H, CH_2Me), 0.98-1.33 (*m*, 64H, $(\text{CH}_2)_{15}\text{Me}$), 2.14 (*s*, 6H, 5-Py- CH_3), 2.20 (*s*, 6H, 3-Py- CH_3), 2.26 (*t*, $J=7.5$ Hz, 4H, $\text{CH}_2\text{CH}_2(\text{CH}_2)_{15}\text{Me}$), 2.42 (*s*, 4H, $\text{CH}_2\text{NCH}_2(\text{CH}_2)_{16}\text{Me}$), 3.53 (*s*, 4H, 2-Py- CH_2), 3.64 (*s*, 6H, 4-Py- OCH_3), 8.04 (*s*, 2H, 5-PyH).

Synthesis of DOD-BPED. *N,N'*-dioctadecylethylenediamine (0.500 g, 0.885 mmol), 2-(chloromethyl)pyridine hydrochloride (0.298 g, 1.82 mmol), and tributylhexadecylphosphonium bromide (0.045 g, 0.089 mmol) were dissolved in THF (20 mL), and then 5 N NaOH_{aq} (1.5 mL) was added. The reaction was performed and worked up in the same way as DOD-BPED*. The resulting solid was characterized via ^1H NMR (300 MHz, CDCl_3). δ : 0.80 (*t*, $J=6.7$ Hz, 6H, CH_2Me), 0.98-1.33 (*m*, 64H, $(\text{CH}_2)_{15}\text{Me}$), 2.14 (*s*, 6H, 5-Py- CH_3), 2.20 (*s*, 6H, 3-Py- CH_3), 2.26 (*t*, $J=7.5$ Hz, 4H, $\text{CH}_2\text{CH}_2(\text{CH}_2)_{15}\text{Me}$), 2.42 (*s*, 4H, $\text{CH}_2\text{NCH}_2(\text{CH}_2)_{16}\text{Me}$), 3.53 (*s*, 4H, 2-Py- CH_2), 3.64 (*s*, 6H, 4-Py- OCH_3), 8.04 (*s*, 2H, 5-PyH).

ARGET ATRP of BMA. An example ARGET ATRP procedure formulated with 50 ppm of CuBr₂/DOD-BPED& catalyst and targeted DP = 200 is given as follows; see Table A-II-1 for specific reaction conditions. A 10 mL Schlenk flask charged with a stir bar was degassed and backfilled with nitrogen (N₂) six times. A mixture of anisole (1.4 mL), EPBA (28 µL, 0.16 mmol), DOD-BPED* (0.41 mL of 10 mg/mL solution in anisole, 4.7 µmol), and CuCl₂ (0.21 mL of 1 mg/mL solution in anisole, 1.6 µmol) was added to a glass vial and purged with nitrogen for 20 min. Previously deoxygenated BMA (5 mL, 31 mmol) was added to the vial. Immediately, the reaction mixture was transferred *via* an airtight syringe to the Schlenk flask, which was placed in a thermostated water bath at 60 °C. Previous deoxygenated Sn^{II}(EH)₂ (0.64 mL of 10 mg/mL solution in anisole, 15.7 µmol) was added to the Schlenk flask to start the polymerization. Samples were taken periodically to measure conversion *via* ¹H NMR and number average molecular weights *via* GPC.

ARGET ATRP in Miniemulsion. An example ARGET ATRP in miniemulsion procedure formulated with 250 ppm of CuBr₂/DOD-BPED* catalyst and targeted DP = 2000 is given as follows; see Table A-II-2 for specific reaction conditions. CuBr₂ (2.0 mg, 8.8 µmol) and DOD-BPED* (7.6 mg, 8.8 µmol) were dissolved in BMA (5.0 g, 35.2 mmol) in a round bottom flask at 60 °C to form a solution of the copper complex. The solution was then cooled to room temperature prior to dissolving the initiator EPBA (43 µL, 17.6 µmol) and hexadecane (0.14 mL, 63 µmol) in the solution. A 5 mM solution of Brij 98 in deionized water (20 mL) was added to the organic BMA solution and was subjected to sonication in an ice bath (Heat Systems Ultrasonics W-385 sonicator; output control set at 8 and duty cycle at 70% for 1 min). The resulting stable miniemulsion was purged with

nitrogen for 30 min. A predeoxygenated aqueous solution of AA (0.6 mL, containing 0.6 mg AA) was injected into the miniemulsion over a period of 3 min to activate the catalyst and start the polymerization. Samples were taken periodically to measure the conversion gravimetrically and to determine the number-average molecular weights by GPC.

A-II. 5. References

1. (a) Cunningham, M. F., *Prog. Polym. Sci.* **2008**, *33* (4), 365-398; (b) Zetterlund, P. B.; Kagawa, Y.; Okubo, M., *Chem. Rev.* **2008**, *208*, 3747-3794; (c) Min, K.; Matyjaszewski, K., *Cent. Eur. J. Chem.* **2009**, *7*, 657-674; (d) Qiu, J.; Charleux, B.; Matyjaszewski, K., *Progress in Polymer Science* **2001**, *26* (10), 2083-2134.
2. (a) Wang, J. S.; Matyjaszewski, K., *J. Am. Chem. Soc.* **1995**, *117*, 5614-5615; (b) Matyjaszewski, K.; Xia, J., *Chem. Rev.* **2001**, *101*, 2921-2990; (c) Braunecker, W. A.; Matyjaszewski, K., *Prog. Polym. Sci.* **2007**, *32*, 93-146; (d) Matyjaszewski, K., *Macromolecules* **2012**, *45*, 4015-4039; (e) Kato, M.; Kamigaito, M.; Sawamoto, M.; Higashimura, T., *Macromolecules* **1995**, *28* (5), 1721-1723.
3. (a) Min, K.; Matyjaszewski, K., *Macromolecules* **2005**, *38* (20), 8131-8134; (b) Kagawa, Y.; Kawasaki, M.; Zetterlund, P. B.; Minami, H.; Okubo, M., *Macromol. Rapid Commun.* **2007**, *28* (24), 2354-2360.
4. (a) Min, K.; Gao, H. F.; Matyjaszewski, K., *J. Am. Chem. Soc.* **2005**, *127* (11), 3825-3830; (b) Min, K.; Jakubowski, W.; Matyjaszewski, K., *Macromol. Rapid Commun.* **2006**, *27* (8), 594-598; (c) Bombalski, L.; Min, K.; Dong, H. C.; Tang, C. B.; Matyjaszewski, K., *Macromolecules* **2007**, *40* (21), 7429-7432; (d) Min, K.; Yu, S.; Lee, H. I.; Mueller, L.; Sheiko, S. S.; Matyjaszewski, K., *Macromolecules* **2007**, *40* (18), 6557-6563.
5. (a) Qiu, J.; Gaynor, S. G.; Matyjaszewski, K., *Macromolecules* **1999**, *32* (9), 2872-2875; (b) Jousset, S.; Qiu, J.; Matyjaszewski, K., *Macromolecules* **2001**, *34* (19), 6641-6648; (c) Eslami, H.; Zhu, S. P., *Polymer* **2005**, *46* (15), 5484-5493; (d) Eslami, H.; Zhu, S. P., *J. Polym. Sci., Part A: Polym. Chem.* **2006**, *44* (6), 1914-1925; (e) Min, K.; Gao, H.; Yoon, J. A.; Wu, W.; Kowalewski, T.; Matyjaszewski, K., *Macromolecules* **2009**, *42* (5), 1597-1603.
6. (a) Tsarevsky, N.; Matyjaszewski, K., *Chem. Rev.* **2007**, *107*, 2270-2299; (b) Pintauer, T.; Matyjaszewski, K., *Chem. Soc. Rev.* **2008**, *37*, 1087-1097.
7. (a) Matyjaszewski, K.; Jakubowski, W.; Min, K.; Tang, W.; Huang, J.; Braunecker, W. A.; Tsarevsky, N. V., *Proc. Natl. Acad. Sci. U.S.A.* **2006**, *103* (42), 15309-14; (b) Jakubowski, W.; Matyjaszewski, K., *Angew. Chem., Int. Ed.* **2006**, *45* (27), 4482-4486.
8. Magenau, A. J. D.; Strandwitz, N. C.; Gennaro, A.; Matyjaszewski, K., *Science* **2011**, *332*, 81-84.
9. Konkolewicz, D.; Schroeder, K.; Buback, J.; Bernhard, S.; Matyjaszewski, K., *ACS Macro Lett.* **2012**, *1*, 1219-1223.

10. Magenau, A. J. D.; Kwak, Y.; Matyjaszewski, K., *Macromolecules* **2010**, *43* (23), 9682-9689.
11. Oh, J. K., *J. Polym. Sci., Part A: Polym. Chem.* **2008**, *46*, 6983-7001.
12. Xia, J. H.; Gaynor, S. G.; Matyjaszewski, K., *Macromolecules* **1998**, *31*, 5958-5959.
13. Elsen, A. M.; Burdyska, J.; Park, S.; Matyjaszewski, K., *Macromolecules* **2012**, 7356-7363.
14. Tang, W.; Kwak, Y.; Braunecker, W.; Tsarevsky, N.; Coote, M. L.; Matyjaszewski, K., *J. Am. Chem. Soc.* **2008**, *130*, 10702-10713.
15. (a) Schroeder, K.; Mathers, R. T.; Buback, J.; Konkolewicz, D.; Magenau, A. J. D.; Matyjaszewski, K., *ACS Macro Lett.* **2012**, *1*, 1037-1040; (b) Magenau, A. J. D.; Kwak, Y.; Schroeder, K.; Matyjaszewski, K., *ACS Macro Lett.* **2012**, *1*, 508-512.
16. (a) Qiu, J.; Matyjaszewski, K.; Thouin, L.; Amatore, C., *Macromol. Chem. Phys.* **2000**, *201*, 1625-1631; (b) Braunecker, W.; Tsarevsky, N.; Gennaro, A.; Matyjaszewski, K., *Macromolecules* **2009**, *42*, 6348-6360.
17. Wang, Y.; Soerensen, N.; Zhong, M.; Schroeder, H.; Buback, M.; Matyjaszewski, K., *Macromolecules* **2013**, *46*, 683-691.
18. Cunningham, M. F., *Progress in Polymer Science* **2002**, *27* (6), 1039-1067.
19. Xia, J. H.; Matyjaszewski, K., *Macromolecules* **1999**, *32*, 2434-2437.

Appendix III

Initiators for Continuous Activator Regeneration Atom Transfer Radical Polymerization of Methyl Methacrylate and Styrene with *N*-Heterocyclic Carbene as Ligands for Fe-Based Catalysts*

A-III. 1. Introduction

Iron (Fe) based catalysts for atom transfer radical polymerization (ATRP) are attractive due to low toxicity, biocompatibility and are less expensive than more common copper-based catalysts.^{1e, 4, 14a, 14b, 61a, 62, 206} A variety of Fe based catalysts have been prepared and studied for ATRP since the first reports in 1997.^{66a, 207} Several ligands were used to enhance the catalytic activity of the Fe complexes, such as phosphines,^{6d, 208} multidentate amines,^{96a, 208c, 209} imines,²¹⁰ amine-bis(phenolate)s,²¹¹ hemins,²¹² thiocarbamates,²¹³ organic acids,²¹⁴ carbenes,²¹⁵ metallocenes,²¹⁶ and triflates.²¹⁷ In addition, onium salts such as ammonium, phosphonium, imidazolium, and phosphazanium have been used to form complexes with Fe halides.²¹⁸ *N*-hetero cyclic carbenes (NHC) are among the strongest electron donating ligands and form stable organometallic complexes. The electronic and steric properties of NHC can be easily modified, and the ligands have lower toxicity than commercially available P and N based ligands. Therefore, NHCs are frequently used as ligands for organometallic complexes to improve the catalysts activity in various reactions.²¹⁹ Indeed,

*Work in this appendix was published and partially reformatted based on the following manuscript: Okada, Seiji; **Park, Sangwoo**; Matyjaszewski, Krzysztof *ACS Macro Letters* **2014**, 3, 944

Fe NHC complexes have used for C-C bond formation, hydrosilylation, C-H activation, and borylation reactions.²²⁰

Iron trihalides (FeX_3) are stable in air and act as deactivators for Fe catalyzed ATRP. Using activator (re)generate condition, Fe^{III} can be reduced to Fe^{II} (activator) and performs ATRP.^{6d, 218f, 218g, 221} For example, in *initiators for continuous activator regeneration* (ICAR) ATRP, thermally decomposable radical initiators, such as 2,2'-azobis(isobutyronitrile) (AIBN), are used to reduce Fe^{II} from Fe^{III} .^{6d, 65b, 218f, 218g} ICAR ATRP with FeX_3 permits diminishing the catalyst loading condition (up to ppm level), while still resulting in well-defined polymers. Chelating ligands with high electron donating groups typically achieved more active catalysts, therefore the active catalysts can be utilized for ATRP with diminishing catalysts loading system.^{208h, 208i, 210d} Fe NHC, specifically $\text{FeX}_3(\text{NHC})$ complexes can generate such catalysts, due to strong electron donicity of NHC. In this Appendix, newly synthesized Fe NHC compounds were synthesized and utilized for the polymerization of well-defined PMMA.

A-III. 2. Results and Discussion

A series of air stable $\text{FeX}_3(\text{NHC})$ complexes were prepared according to previously reported literature procedures.²²² Complexes of FeX_3 ($\text{X} = \text{Cl}$ or Br , Figure A-III-1) with 1 equivalent (eq.) of either 1,3-bis(2,6-di-*i*-propylphenyl)imidazol-2-ylidene (IDipp) or 1,3-bis(2,6-di-*i*-propylphenyl)imidazolidin-2-ylidene (HIDipp) were prepared: $\text{FeCl}_3(\text{IDipp})$ (**I-Cl**), $\text{FeCl}_3(\text{HIDipp})$ (**H-Cl**), $\text{FeBr}_3(\text{IDipp})$ (**I-Br**) and $\text{FeBr}_3(\text{HIDipp})$ (**H-Br**). The compounds have a high-spin iron(III) center, which is a good agreement on Fe catalyzed

ATRP.^{210d, 210f, 222-223} In addition, the synthesized catalysts are non-hygroscopic (FeX₃ are hygroscopic), ease of handling is other advantage.

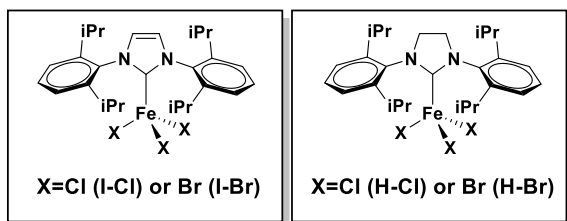


Figure A-III-1. Structures of FeX₃(NHC) catalysts.

The four FeX₃(NHC) complexes were analyzed by electrochemical methods (cyclic voltammetry, or CV). Generally catalysts with more negative $E_{1/2}$ indicated more reducing power, therefore fast polymerizations can be observed when using more reducing catalyst complexes (more negative $E_{1/2}$).^{9, 11, 61a, 63b, 224} The $E_{1/2}$ values for the series of FeX₃(NHC)s were measured and the results showed -0.48 (**I-Cl**), -0.48 (**H-Cl**), -0.36 (**I-Br**) and -0.35 (**H-Br**) V (versus Fe^{0/+}). All of the CV spectra showed a single reversible redox peak ($\Delta E = 0.07$ V, Figure A-III-2). The chloride complexes, **I-Cl** and **H-Cl** showed more negative $E_{1/2}$ values, however the bond dissociation energy of C-Br is less than C-Cl, the catalysts activity has been compensated. Complexes with all of the NHC ligands showed more negative $E_{1/2}$ values than FeCl₃/Cl⁻ or FeBr₃/Br⁻ (-0.41 and -0.21 V vs. Fe^{0/+}, respectively, Figure A-III-2), indicating NHC's are strongly electron donating to FeX₃. Dissociation of FeX₃(NHC) complexes was not observed during CV measurements (singular redox peak).²²⁵ No significant difference was observed between unsaturated and saturated Fe(NHC) complexes.

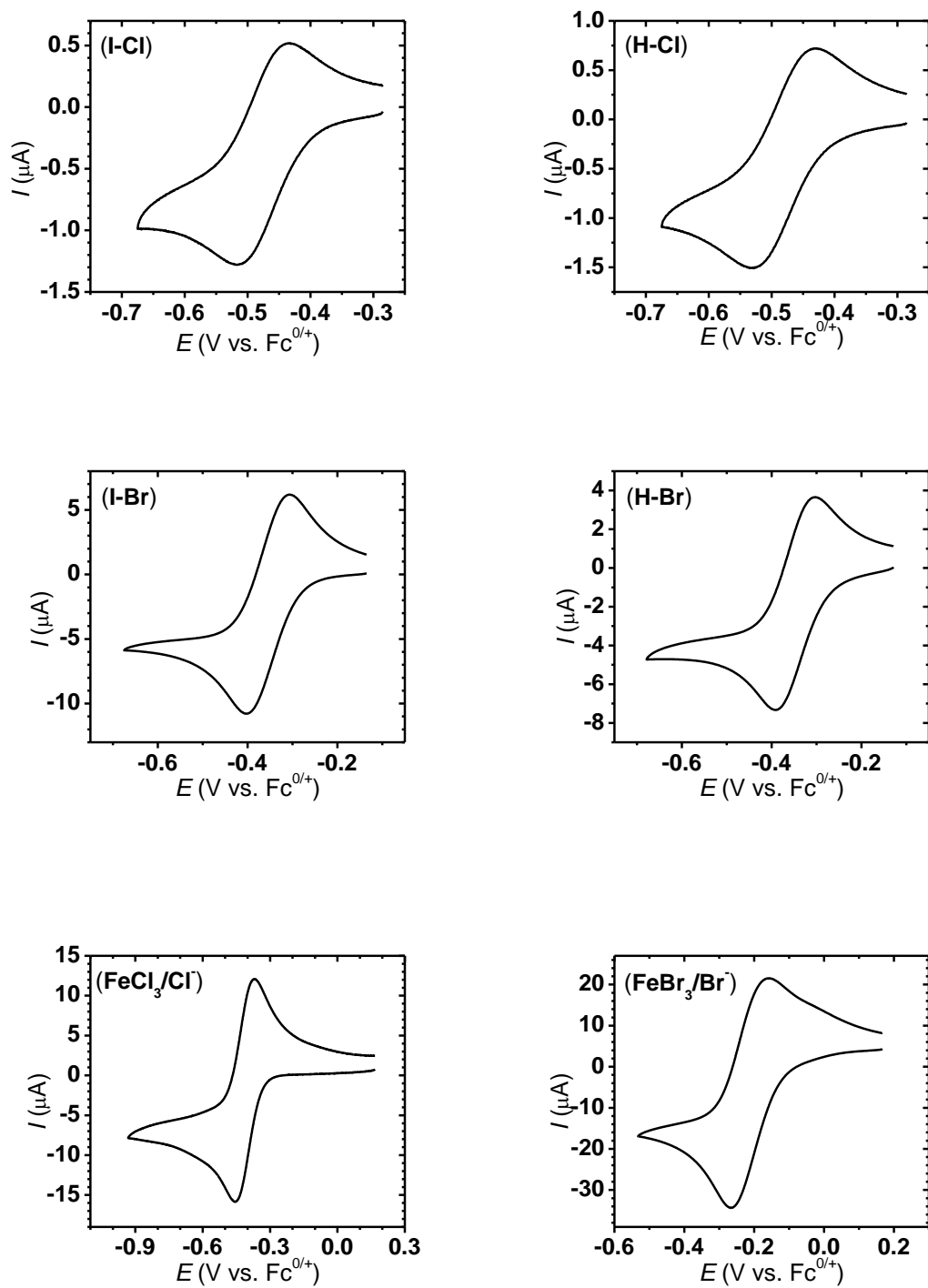


Figure A-III-2. Cyclic voltammograms of I-Cl, H-Cl, I-Br, H-Br, $\text{FeCl}_3/\text{TBACl}$, and $\text{FeBr}_3/\text{TBABr}$; Measurement condition: working electrode = glassy carbon electrode,

counter electrode = platinum meshed electrode, reference electrode = Ag/AgI/I⁻ and externally referred by Fc^{0/+}, supporting electrolyte = 0.2 M Bu₄NPF₆ in CH₂Cl₂. ([Cat.] = 1.0 mM, scan rate 50 mV/s).

ICAR ATRP of methyl methacrylate (MMA) was carried out with 50 ppm of catalyst complexes (Table A-III-1) to investigate their catalytic activities. The polymerizations were conducted in 50% anisole at 60 °C with the ratio of [MMA]/[EBPA]/[Cat.]/[AIBN] = 200/1/0.01/0.2 (where, EBPA: ethyl 2-bromo-2-phenylacetate). Table A-III-1 lists the results of ICAR ATRPs of MMA. Good control and high activity over the polymerization were observed with FeX₃(NHC)s catalysts, on the other hand polymerization with FeX₃/X⁻ showed lower activity and more broad MWD (Table A-III-2). All complexes exhibited the same rate of polymerization (*R_p*), although Cl derivatives have more negative *E*_{1/2} than Br ones. This is because that the bond dissociation energy of C-Br bond on chain end is more labile than that of C-Cl, so that the catalysts can compensate the reducibility and also the rate of polymerization can be determined by decomposition of azo-initiator (AIBN) in ICAR ATRP.^{6a} Slightly decreased *R_p*s were observed when high monomer conversions (> 50% conversion) due to the transfer reaction of the growing polymeric chains and decreasing the amount of the decomposed AIBN (Figure A-III-3B).

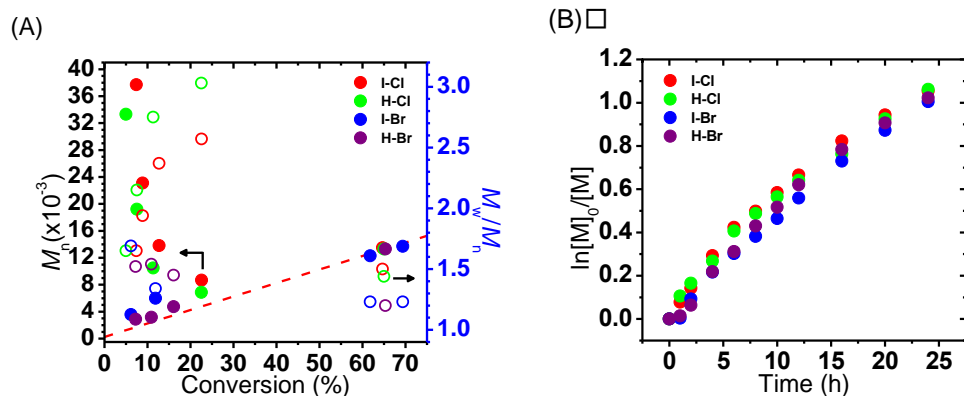


Figure A-III-3. (A) Plot of M_n and M_w/M_n vs. conversion; (B) kinetic plots of $\ln([M]_0/[M])$ vs. time with iron complexes; Reaction condition: $[MMA]/[EBPA]/[Cat.]/[AIBN] = 200/1/0.01/0.2$, $[MMA] = 4.7$ M in 50% (v/v) anisole at 60 °C for 24 h.

Table A-III-1. Summaries of ICAR ATRP of MMA with 50 ppm of catalysts.

Entry	Catalysts	Conv ^c (%)	$M_{n, GPC}^d$	$M_{n, th}$	M_w/M_n^c
1 ^a	I-Cl	65	13,100	13,300	1.45
2 ^a	H-Cl	65	13,000	13,300	1.40
3 ^a	I-Br	63	12,600	12,900	1.23
4 ^a	H-Br	64	12,900	13,000	1.20
5 ^b	I-Cl/TBACl	38	10,900	7,800	1.75
6 ^b	I-Br/TBABr	45	9,200	9,300	1.39

^a $[MMA]/[EBPA]/[Cat.]/[AIBN] = 200/1/0.01/0.2$; $[MMA] = 4.7$ M in 50% (v/v) anisole at 60 °C for 24 h. ^b $[MMA]/[EBPA]/[Cat.]/[TBAX]/[AIBN] = 200/1/0.01/0.02/0.2$; $[MMA] = 4.7$ M in 50% (v/v) anisole at 60 °C for 24 h. ^cConversion measured by GC. ^d M_n and M_w/M_n based on GPC with PMMA standards in THF.

Table A-III-2. ICAR ATRP of MMA using **FeX₃** (X = Cl, Br) with or without additives.

Entry	Catalysts	Conv ^d (%)	$M_{n, \text{GPC}}^e$	$M_{n, \text{th}}$	M_w/M_n^d
1 ^a	FeCl ₃	28	6,100	5,900	2.34
2 ^a	FeBr ₃	28	6,700	5,900	2.06
3 ^b	FeCl ₃ /TBACl	45	9,700	9,300	1.38
4 ^b	FeBr ₃ /TBABr	41	9,000	8,500	1.37
5 ^c	FeCl ₃ /PPh ₃	56	9,800	11,599	1.48
6 ^c	FeBr ₃ /PPh ₃	58	10,300	12,000	1.34

^a[MMA]/[EBPA]/[Cat.]/[AIBN] = 200/1/0.01/0.2; [MMA] = 4.7 M in 50% (v/v) anisole at 60 °C for 24 h. ^b[MMA]/[EBPA]/[Cat.]/[TBAX]/[AIBN] = 200/1/0.01/0.02/0.2; [MMA] = 4.7 M in 50% (v/v) anisole at 60 °C for 24 h. ^c[MMA]/[EBPA]/[Cat.]/[PPh₃]/[AIBN] = 200/1/0.01/0.02/0.2; [MMA] = 4.7 M in 50% (v/v) anisole at 60 °C for 24 h. ^dConversion measured by GC. ^e M_n and M_w/M_n based on GPC with PMMA standards.

ICAR ATRP with **I-Cl** and **H-Cl** resulted in ~ 65% monomer conversions (both cases), the number average molecular weight (M_n) of the final products matched to the theoretical value, but relatively broad molecular weight distributions (M_w/M_n = 1.45 and 1.40, respectively), which probably caused by inefficient activation of **I-Cl** and **H-Cl** (Table A-III-1, entries 1 and 2, and Figure A-III-3A). On the other hands, ICAR ATRP of MMA with Br derivatives (**I-Br** or **H-Br**) showed the similar R_p but better polymerization results were observed compared to Cl derivatives. $M_{n, \text{GPC}}$ values were much closer to the theoretical values (Figure A-III-3B), and more uniform polymers were synthesized (M_w/M_n

= 1.23 and 1.20, respectively, Table A-III-1, entries 3 and 4), under same reaction conditions (conversion = ~ 64%, after 1 day). The best control of MMA polymerization was attained with **H-Br**. FeX_3 with extra halide using tetrabutylammonium halide (TBAX, with X = Cl or Br) and triphenylphosphine (PPh_3) showed less activity and controllability than $\text{Fe}(\text{NHC})_3$ s, presumably due to the strong electron donicity of the carbene ligands and stability of $\text{FeX}_3(\text{NHC})_3$ s (Table A-III-2).

ICAR ATRPs with **I-Cl** and **I-Br** were also carried out in the presence of additional halides anions, *i.e.*, 2 eq. of TBAX. The presence of halide anions could affect catalytic activity of FeX_3 for either ATRP or ATRA due to the formation of FeX_4^- .^{218e, 218f, 225} However, no improvement was observed under ICAR ATRP with **I-Cl** or **I-Br**, due to strong complexation of the $\text{Fe}(\text{NHC})_3$ s. CV measurements (for example, **I-Br**) showed neither additional peaks nor $E_{1/2}$ changes (Figure A-III-4). ICAR ATRP of MMA with **I-Cl** in the presence of 2 eq. X^- showed slower polymerization, conversion 48% was reached after 24 h with higher M_w/M_n (1.75) (Table A-III-1, entries 5 and 6).

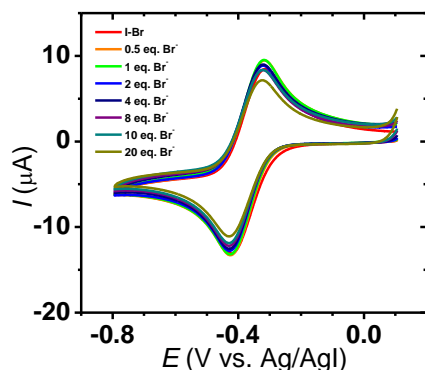


Figure A-III-4. Cyclic voltammograms of **I-Br** with various ratio of TBABr (Br^-);

Measurement condition: working electrode = glassy carbon electrode, counter electrode = platinum meshed electrode, reference electrode = Ag/AgI/I⁻ and externally referred by Fc^{0/+}, supporting electrolyte = 0.2 M Bu₄NPF₆ in CH₂Cl₂. ([Cat.] = 1.0 mM, scan rate 50 mV/s).

ICAR ATRP of styrene (St) were then carried out to determine the catalytic activity of FeX₃(NHC) (Table A-III-3). As shown in Figure A-III-5A, polymerization of St using FeX₃(NHC)s was successful with a linear relationship between M_n and conversion and a narrow molecular weight distribution (Figure A-III-5A). Monomer conversions reached about 53% and 56% after 72h for **I-Cl** and **H-Cl**. According to GPC analysis, molecular weights were $M_n = 9,500$ and $9,600$ and $M_w/M_n = 1.24$ and 1.29 , respectively (Table A-III-3, entries 1 and 2). Similar as MMA polymerization, no significant differences in R_p were observed (radical concentration can be determined by decomposition of AIBN) (Figure A-III-5B). Polymers formed with the Br derivatives (**I-Br** and **H-Br**) showed lower M_w/M_n values of 1.13 and 1.19, for **I-Br** and **H-Br**, respectively (Table A-III-3, entries 3-4) and much better controllability than FeX₃ (Table A-III-3, entries 5-6). Unsaturated NHC showed better controllability than saturated one unlike polymerization of MMA.

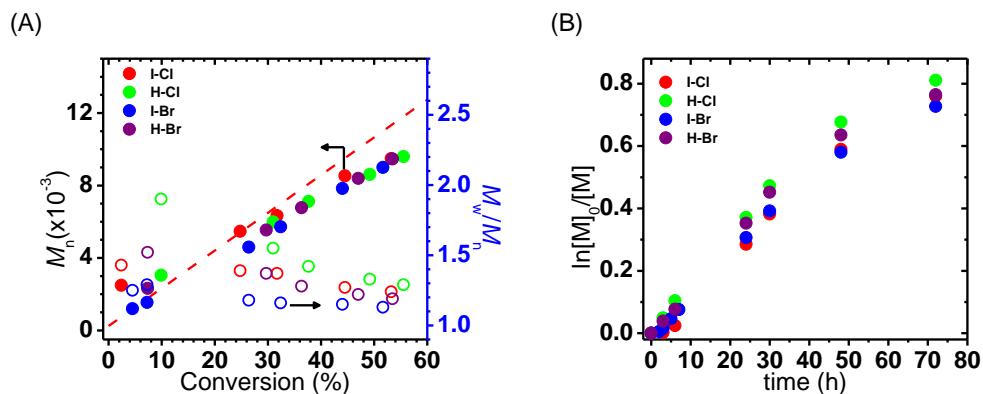


Figure A-III-5. (A) Plot of M_n and M_w/M_n vs. conversion; (B) kinetic plots of $\ln([M]_0/[M])$ vs. time; Reaction conditions: $[\text{Sty}]/[\text{EBPA}]/[\text{Cat.}]/[\text{AIBN}] = 200/1/0.01/0.2$; $[\text{Sty}] = 4.4$ M in 50% (v/v) anisole at 60 °C for 72 h.

Table A-III-3. Summaries of ICAR ATRP of Sty with 50 ppm of catalysts.^a

Entry	Catalysts	Conv, ^b (%)	$M_{n,\text{GPC}}^c$	$M_{n,\text{th}}$	M_w/M_n^b
1	I-Cl	53	9,500	11,300	1.24
2	H-Cl	56	9,600	11,800	1.29
3	I-Br	52	9,000	11,000	1.13
4	H-Br	53	9,500	11,400	1.19
5	FeCl ₃	46	9,600	9,700	2.94
6	FeBr ₃	48	9,800	10,200	2.89

^a $[\text{Sty}]/[\text{EBPA}]/[\text{Cat.}]/[\text{AIBN}] = 200/1/0.01/0.2$; $[\text{Sty}] = 4.4$ M in 50% (v/v) anisole at 60 °C for 72 h. ^bConversion measured by GC. ^c M_n and M_w/M_n based on GPC with PSty standards in THF.

A-III. 3. Summary

In summary, ICAR ATRP of MMA and Sty were successfully carried out with low catalysts loading (50 ppm $\text{FeX}_3(\text{NHC})\text{s}$). The new complexes showed higher activity and better control for ICAR ATRP than FeX_3 , FeX_3/TBAX or $\text{FeX}_3/\text{PPh}_3$, presumably due to the strong electron donicity of the carbene ligands and stability of $\text{FeX}_3(\text{NHC})\text{s}$. Br derivatives exhibited better efficient activation than Cl derivatives, best control can be achieved by using **I-Br** and **H-Br** catalysts.

A-III. 4. Experimental Section

Materials. 1,3-Bis(2,6-di-*i*-propylphenyl)imidazol-2-ylidene (IDipp), 1,3-bis(2,6-di-*i*-propylphenyl)imidazolidin-2-ylidene (HIDipp), methyl methacrylate (MMA), styrene (Sty), ethyl 2-bromo-2-phenyl acetate (EBPA), tetrabutylammonium chloride (TBACl), tetrabutylammonium bromide (TBABr), 2,2'-azobis(isobutyronitrile) (AIBN), THF and anisole were purchased from Sigma Aldrich. Anhydrous FeCl_3 and FeBr_3 were purchased from Alfa Aesar. MMA and Sty were passed through a column of basic alumina to remove any inhibitor before use. AIBN was recrystallized from cold methanol before use. THF was purified with a Grubbs-type column system manufactured by Innovative Technology.

Measurements. Monomer conversion was measured using gas chromatography (GC) (SHIMAZU GC-17A) attached HP-1 column (Agilent). Molecular weight (M_n) and molecular weight distribution (M_w/M_n) were determined by gel permeation chromatography (GPC) using PSS columns in THF as an eluent at a flow rate of 1 mL/min at 35 °C. The GPC system was composed of Waters 515 HPLC Pump and Waters 2414

Refractive Index Detector. Each sample was filtered over neutral alumina prior to analysis. Cyclic voltammetry (CV) was recorded at 25 °C with a Gamry Reference 600 potentiostat using a standard three electrode system consisting of a glassy carbon working electrode, platinum mesh counter electrode, and Ag/AgI/I⁻ reference electrode. CV measurements were carried out under a nitrogen atmosphere at a scan rate of 50 mV/s. Potentials were recorded versus a Ag/AgI/I⁻ reference electrode and externally referenced to ferrocene/ferrocenium (Fc^{0/+}).

General procedures for synthesis of FeX₃(NHC) complexes. Reactions were carried out under a N₂ atmosphere. A flask was charged with anhydrous FeX₃ (X = Cl or Br) (0.70 mmol) and 10 mL of THF then IDipp or HIDipp (0.70 mmol) was added in one portion. The solution was allowed to stir at 25 °C for 1 h. All volatiles were removed *in vacuo*, and the residue was treated with 5 mL of toluene, which resulted in formation of a precipitate. The precipitate was collected by filtration and washed with hexane, and subsequent recrystallization from THF/hexane provided the desired compounds in high purity.

General procedures for polymerization. Stock solutions of the FeX₃(NHC) (or FeX₃, for control) complexes 1% (v/v) were prepared. Monomer (MMA or Sty), EBPA, catalysts, TBAX (if needed), and anisole were added to a 10 mL Schlenk flask equipped with a stir bar. The mixture was degassed *via* three freeze-pump-thaw cycles, and then AIBN was added when the solution was frozen during the final cycle. The flask was sealed and placed in an oil bath at 60 °C. Samples were taken periodically under N₂ atmosphere using a N₂ purged syringe, diluted with THF, passed through a column of neutral alumina to remove the iron catalysts, and analyzed by GC and GPC.

A-III. 5. References

1. (a) Kamigaito, M.; Ando, T.; Sawamoto, M., *Chem. Rev.* **2001**, *101* (12), 3689-3746; (b) Matyjaszewski, K.; Xia, J., *Chemical Reviews* **2001**, *101* (9), 2921-2990; (c) Ouchi, M.; Terashima, T.; Sawamoto, M., *Chemical Reviews* **2009**, *109* (11), 4963-5050; (d) Matyjaszewski, K.; Tsarevsky, N. V., *Nature chemistry* **2009**, *1* (4), 276-288; (e) di Lena, F.; Matyjaszewski, K., *Prog. Polym. Sci.* **2010**, *35* (8), 959-1021; (f) Matyjaszewski, K., *Macromolecules* **2012**, *45* (10), 4015-4039; (g) Matyjaszewski, K.; Tsarevsky, N. V., *Journal of the American Chemical Society* **2014**, *136* (18), 6513-6533.
2. (a) Ando, T.; Kamigaito, M.; Sawamoto, M., *Macromolecules* **1997**, *30* (16), 4507-4510; (b) Matyjaszewski, K.; Coca, S.; Gaynor, S. G.; Wei, M.; Woodworth, B. E., *Macromolecules* **1997**, *30* (23), 7348-7350.
3. (a) Xue, Z.; Lee, B. W.; Noh, S. K.; Lyoo, W. S., *Polymer* **2007**, *48* (16), 4704-4714; (b) Satoh, K.; Aoshima, H.; Kamigaito, M., *J. Polym. Sci., Part A: Polym. Chem.* **2008**, *46* (18), 6358-6363; (c) Uchiike, C.; Ouchi, M.; Ando, T.; Kamigaito, M.; Sawamoto, M., *J. Polym. Sci., Part A: Polym. Chem.* **2008**, *46* (20), 6819-6827; (d) Xue, Z.; Noh, S. K.; Lyoo, W. S., *J. Polym. Sci., Part A: Polym. Chem.* **2008**, *46* (9), 2922-2935; (e) Xue, Z.; Linh, N. T. B.; Noh, S. K.; Lyoo, W. S., *Angew. Chem. Int. Ed.* **2008**, *47* (34), 6426-6429; (f) Xue, Z.; He, D.; Noh, S. K.; Lyoo, W. S., *Macromolecules* **2009**, *42* (8), 2949-2957; (g) He, D.; Xue, Z.; Khan, M. Y.; Noh, S. K.; Lyoo, W. S., *J. Polym. Sci., Part A: Polym. Chem.* **2010**, *48* (1), 144-151; (h) Zhu, G.; Zhang, L.; Zhang, Z.; Zhu, J.; Tu, Y.; Cheng, Z.; Zhu, X., *Macromolecules* **2011**, *44* (9), 3233-3239; (i) Wang, Y.; Kwak, Y.; Matyjaszewski, K., *Macromolecules* **2012**, *45* (15), 5911-5915; (j) Nishizawa, K.; Ouchi, M.; Sawamoto, M., *Macromolecules* **2013**, *46* (9), 3342-3349.
4. (a) Matyjaszewski, K.; Wei, M.; Xia, J.; McDermott, N. E., *Macromolecules* **1997**, *30* (26), 8161-8164; (b) Ibrahim, K.; Yliheikkilä, K.; Abu-Surrah, A.; Löfgren, B.; Lappalainen, K.; Leskelä, M.; Repo, T.; Seppälä, J., *Eur. Polym. J.* **2004**, *40* (6), 1095-1104; (c) Niibayashi, S.; Hayakawa, H.; Jin, R.-H.; Nagashima, H., *Chem. Commun.* **2007**, (18), 1855-1857; (d) Luo, R.; Sen, A., *Macromolecules* **2008**, *41* (12), 4514-4518; (e) Zhang, L.; Cheng, Z.; Lü, Y.; Zhu, X., *Macromol. Rapid Commun.* **2009**, *30* (7), 543-547; (f) Aoshima, H.; Satoh, K.; Umemura, T.; Kamigaito, M., *Polymer Chemistry* **2013**, *4* (12), 3554-3562; (g) Tsarevsky, N. V.; Pintauer, T.; Matyjaszewski, K., *Macromolecules* **2004**, *37* (26), 9768-9778; (h) Wang, G.-X.; Lu, M.; Liu, L.-C.; Wu, H.; Zhong, M., *J. Appl. Polym. Sci.* **2013**, *128* (5), 3077-3083; (i) He, W.; Cheng, L.; Zhang, L.; Liu, Z.; Cheng, Z.; Zhu, X., *Polymer Chemistry* **2014**, *5* (2), 638-645; (j) Nakanishi, S.-i.; Kawamura, M.; Kai, H.; Jin, R.-H.; Sunada, Y.; Nagashima, H., *Chemistry – A European Journal* **2014**, *20* (19), 5802-5814.
5. (a) Gibson, V. C.; O'Reilly, R. K.; Reed, W.; Wass, D. F.; White, A. J. P.; Williams, D. J., *Chem. Commun.* **2002**, (17), 1850-1851; (b) O'Reilly, R. K.; Gibson, V. C.; White, A. J. P.; Williams, D. J., *J. Am. Chem. Soc.* **2003**, *125* (28), 8450-8451; (c) Gibson, V. C.; O'Reilly, R. K.; Wass, D. F.; White, A. J. P.; Williams, D. J., *Macromolecules* **2003**, *36* (8), 2591-2593; (d) Allan, L. E. N.; Shaver, M. P.; White, A. J. P.; Gibson, V. C., *Inorg. Chem.* **2007**, *46* (21), 8963-8970; (e) O'Reilly, R. K.; Shaver, M. P.; Gibson, V. C.; White, A. J. P., *Macromolecules* **2007**, *40* (21), 7441-7452; (f) Shaver, M. P.; Allan, L. E. N.;

- Gibson, V. C., *Organometallics* **2007**, 26 (19), 4725-4730; (g) Ferro, R.; Milione, S.; Erra, L.; Grassi, A., *Inorg. Chem. Commun.* **2008**, 11 (5), 535-538.
6. (a) Allan, L. E. N.; MacDonald, J. P.; Reckling, A. M.; Kozak, C. M.; Shaver, M. P., *Macromolecular Rapid Communications* **2012**, 33 (5), 414-418; (b) Allan, L. E. N.; MacDonald, J. P.; Nichol, G. S.; Shaver, M. P., *Macromolecules* **2014**, 47 (4), 1249-1257.
7. Simakova, A.; Mackenzie, M.; Averick, S. E.; Park, S.; Matyjaszewski, K., *Angew. Chem. Int. Ed.* **2013**, 52 (46), 12148-12151.
8. (a) Qin, S.-H.; Qin, D.-Q.; Qiu, K.-Y., *New J. Chem.* **2001**, 25 (7), 893-895; (b) Qin, D.-Q.; Qin, S.-H.; Qiu, K.-Y., *J. Polym. Sci., Part A: Polym. Chem.* **2001**, 39 (19), 3464-3473; (c) Cao, J.; Zhang, L.; Jiang, X.; Tian, C.; Zhao, X.; Ke, Q.; Pan, X.; Cheng, Z.; Zhu, X., *Macromol. Rapid Commun.* **2013**, 34 (22), 1747-1754.
9. (a) Zhu, S.; Yan, D., *J. Polym. Sci., Part A: Polym. Chem.* **2000**, 38 (23), 4308-4314; (b) Zhu, S.; Yan, D., *Macromolecules* **2000**, 33 (22), 8233-8238; (c) Zong, G.; Chen, H.; Wang, C.; Liu, D.; Hao, Z., *J. Appl. Polym. Sci.* **2010**, 118 (6), 3673-3677.
10. Louie, J.; Grubbs, R. H., *Chem. Commun.* **2000**, (16), 1479-1480.
11. Kotani, Y.; Kamigaito, M.; Sawamoto, M., *Macromolecules* **1999**, 32 (20), 6877-6880.
12. Wang, Y.; Matyjaszewski, K., *Macromolecules* **2010**, 43 (9), 4003-4005.
13. (a) Teodorescu, M.; Gaynor, S. G.; Matyjaszewski, K., *Macromolecules* **2000**, 33 (7), 2335-2339; (b) Sarbu, T.; Matyjaszewski, K., *Macromol. Chem. Phys.* **2001**, 202 (17), 3379-3391; (c) Ishio, M.; Katsube, M.; Ouchi, M.; Sawamoto, M.; Inoue, Y., *Macromolecules* **2008**, 42 (1), 188-193; (d) Bai, L.; Zhang, L.; Zhang, Z.; Tu, Y.; Zhou, N.; Cheng, Z.; Zhu, X., *Macromolecules* **2010**, 43 (22), 9283-9290; (e) Wang, Y.; Matyjaszewski, K., *Macromolecules* **2011**, 44 (6), 1226-1228; (f) Wang, Y.; Zhang, Y.; Parker, B.; Matyjaszewski, K., *Macromolecules* **2011**, 44 (11), 4022-4025; (g) Mukumoto, K.; Wang, Y.; Matyjaszewski, K., *ACS Macro Letters* **2012**, 1 (5), 599-602; (h) Yu, H.; Zhang, Z.; Cheng, Z.; Zhu, J.; Zhou, N.; Zhang, W.; Zhu, X., *J. Polym. Sci., Part A: Polym. Chem.* **2012**, 50 (11), 2182-2187.
14. (a) Herrmann, W. A., *Angew. Chem. Int. Ed.* **2002**, 41 (8), 1290-1309; (b) Díez-González, S.; Marion, N.; Nolan, S. P., *Chem. Rev.* **2009**, 109 (8), 3612-3676.
15. Bézier, D.; Sortais, J.-B.; Darcel, C., *Adv. Synth. Catal.* **2013**, 355 (1), 19-33.
16. (a) Zhang, L.; Cheng, Z.; Shi, S.; Li, Q.; Zhu, X., *Polymer* **2008**, 49 (13-14), 3054-3059; (b) Zhang, L.; Cheng, Z.; Tang, F.; Li, Q.; Zhu, X., *Macromolecular Chemistry and Physics* **2008**, 209 (16), 1705-1713.
17. Matyjaszewski, K.; Jakubowski, W.; Min, K.; Tang, W.; Huang, J.; Braunecker, W. A.; Tsarevsky, N. V., *Proceedings of the National Academy of Sciences* **2006**, 103 (42), 15309-15314.
18. Przyojski, J. A.; Arman, H. D.; Tonzetich, Z. J., *Organometallics* **2012**, 31 (8), 3264-3271.
19. Shaver, M. P.; Allan, L. E. N.; Rzepa, H. S.; Gibson, V. C., *Angewandte Chemie International Edition* **2006**, 45 (8), 1241-1244.
20. (a) Qiu, J.; Matyjaszewski, K.; Thouin, L.; Amatore, C., *Macromolecular Chemistry and Physics* **2000**, 201 (14), 1625-1631; (b) Magenau, A. J. D.; Kwak, Y.; Schröder, K.; Matyjaszewski, K., *ACS Macro Letters* **2012**, 1 (4), 508-512; (c) Schröder, K.; Mathers, R. T.; Buback, J.; Konkolewicz, D.; Magenau, A. J. D.; Matyjaszewski, K., *ACS Macro Letters* **2012**, 1 (8), 1037-1040; (d) Magenau, A. J. D.; Bortolamei, N.; Frick, E.; Park, S.;

- Gennaro, A.; Matyjaszewski, K., *Macromolecules* **2013**, *46* (11), 4346-4353.
21. Eckenhoff, W. T.; Biernesser, A. B.; Pintauer, T., *Inorganica Chimica Acta* **2012**, *382* (0), 84-95.
22. Mueller, L.; Jakubowski, W.; Tang, W.; Matyjaszewski, K., *Macromolecules* **2007**, *40* (18), 6464-6472.

Appendix IV

Bioinspired Fe-Based Catalyst for Atom Transfer Radical Polymerization*

A-IV. 1. Introduction

Atom transfer radical polymerization (ATRP) provides well-defined polymers with predetermined molecular weight and narrow molecular weight distributions and precisely controlled architecture.^{1d, 1e, 180a, 226} Copper based ATRP catalysts are the most efficient for the preparation of a broad range of well-defined polymers.²²⁷ However, the development of new transition metal-based catalysts remains of great interest in order to extend the range of polymers that can be prepared by ATRP.^{14c} Consequently, iron-mediated ATRP has been widely investigated because of its low toxicity and biocompatibility, especially advantageous when targeting biological applications.^{209f, 210b, 218f, 228} Despite these potential benefits of iron-based catalysts, their application in ATRP is quite limited because of their lower activity and selectivity. Therefore, the design and development of new iron-based catalysts comparable in activity to traditional catalysts and able to polymerize a broader range of monomers is critical for progress in this field.

ATRP is typically performed in organic solvents, but performing ATRP in aqueous media provides several advantages. Water is an environmentally benign solvent, enabling direct polymerization of water-soluble monomers, faster reactions, and polymerization in

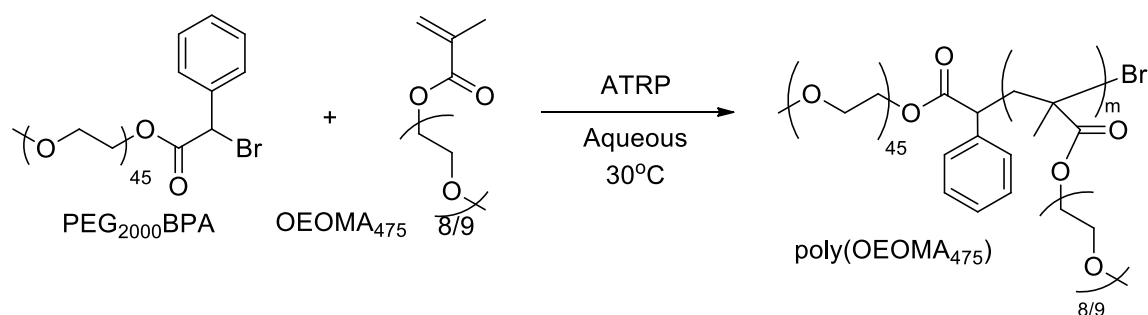
*Work in this chapter has been published and partially reformatted in the following manuscript: Simakova, Antonina, Mackenzie, Matthew, Averick, Saadyah E., **Park, Sangwoo**, Matyjaszewski, Krzysztof *Angew. Chem. Int. Ed. Engl.* **2013**, 52, 12148

the presence of biomolecules.²²⁹ Several methods for well-controlled Cu-based ATRP in water have been developed, but in the majority of reports a limited number of catalytic systems and narrow range of monomers are used.^{5g, 230} Difficulties with control of ATRP in aqueous media are associated with some side reactions including catalyst and chain end instabilities, as well as a large equilibrium constant responsible for significantly increased rates of reaction.²³¹ Our group has recently reported the synthesis of protein-polymer hybrids by ATRP under biologically relevant conditions, which were designed to sustain the structure of a protein during polymerization as well as provide good control.²³² In this system, a protein served as an initiator, but recent publications by Bruns²³³ and di Lena^{233a, 234} shows that certain proteins/enzymes can also serve as catalysts for ATRP. Protein based catalysts, so called ATRPases, with iron heme centers, such as horseradish peroxidase (HRP), catalase or hemoglobin (Hb) act as ATRP catalysts and can produce high molecular weight (MW) polymers with molecular weight distributions (MWDs) close to 1.5, indicative of some limited control. These catalytic systems can potentially expand the range of polymerizable monomers because of different catalyst structure and tolerance to pH variation. However, a major drawback of using proteins for catalysis is their sensitivity to reaction conditions and high molecular weight.²³⁵ Therefore, the development of synthetic analogues that can reproduce or enhance the properties of native catalytic proteins without the need for such stringent conditions and high mass-loading of the catalyst would allow for broader application of these bioinspired catalytic systems.²³⁶

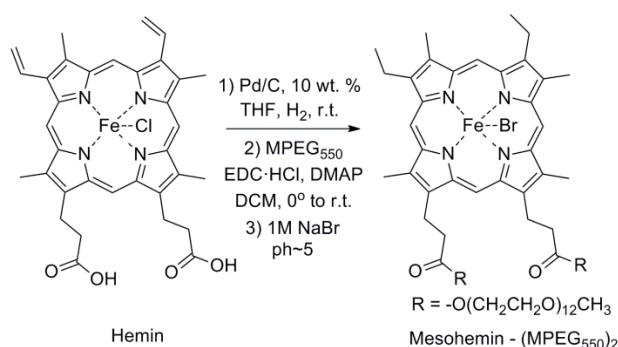
Application of the naturally occurring hematin, the structure of which is similar to the prosthetic group of HRP, Hb, or catalase, for catalysis of radical polymerization reactions

of vinyl monomers showed that it can successfully replace HRP.²³⁷ Indeed, some iron porphyrins can induce an atom transfer process, as in ATRP, and even provide certain level of control indicated by linear increase of molecular weight with conversion and moderate dispersity values ($M_w/M_n < 2$; M_w = weight average molecular weight and M_n = number average molecular weight).²³⁸ Poly(*N*-isopropyl acrylamide) (PNIPAAm) prepared in the presence of alkyl halide initiator and hematin had relatively high M_w/M_n values (1.8-2.1). These results indicate that iron porphyrins can act as catalysts for ATRP, but significant improvements are needed to prepare well-defined materials.

Hemin was chosen for initial testing as an iron based catalyst for ATRP. Hemin is a ferric form of heme with a chloride ligand instead of hydroxyl group as in hematin.²³⁹ Hemin was used to catalyze activators generated by electron transfer (AGET) ATRP of oligo(ethylene oxide) methyl ether methacrylate (OEOMA₄₇₅, average MW 475)²⁴⁰ in aqueous media with ascorbic acid as reducing agent (Scheme A-IV-1). This method allows *in situ* generation of Fe(II) species, thereby preventing the irreversible formation of μ -oxo bisiron(III) complexes that can occur between two iron (II) porphyrins in the presence of oxygen.^{239, 241} However, this catalyst has low halidophilicity,²⁴² low solubility in water, and can itself polymerize because of the presence of vinyl moieties.²⁴³ Therefore, we developed a second generation hemin-inspired catalyst that addressed these issues and provided significantly improved performance in the preparation of well-defined polymers (Scheme A-IV-2).



Scheme A-IV-1. AGET ATRP of OEOMA₄₇₅.



Scheme A-IV-2. Hemin and its modification to mesohemin-(MPEG₅₅₀)₂.

A-IV. 2. Results and Discussion

We first attempted to improve the reported earlier²³⁴ catalase catalytic system, by addition of NaCl, yielding polymers with a higher MW and narrower MWD (Table A-IV-1, entry 1, Figure A-IV-1). Since the ATRPase catalytic systems had limited halidophilicity, an additional halide salt was necessary for faster deactivation and controlled polymerization. This strategy was also applied to the next series of experiments with hemin.

A set of polymerizations was conducted to determine if the prosthetic group, hemin, can be used alone to catalyze ATRP without the entire protein. Initial results demonstrated

that hemin can be reduced *in situ* by ascorbic acid and catalyze ATRP; however the deactivation rate was slow, resulting in rapid but poorly controlled polymerization (Table A-IV-1, entry 2). The polymerization reached a conversion of 60% of the monomer in 1 h and stopped after that time, forming a polymer with high values of $M_w/M_n = 1.65$. Macroinitiator residue in gel permeation chromatography (GPC) traces indicated low initiation efficiency (Figure A-IV-2). To determine if the low halidophilicity of hemin caused the poor control over the polymerization, reactions were conducted in the presence of excess halide salts (Table A-IV-1, entry 3-4). Addition of KBr resulted in more linear kinetic plots and improved the initiation efficiency (Figure A-IV-3 and Figure A-IV-4A). Addition of NaCl led to a slower polymerization and higher M_w/M_n (Figure A-IV-3 and Figure A-IV-4B), indicating that the presence of extra bromide ions shifts the equilibrium towards stable Fe(III)-X species, increasing the deactivation efficiency. Bromide salt enhances both the polymerization rate and the initiation efficiency, compared to chloride salt. Therefore, further polymerizations were conducted in the presence of excess bromide salt to enhance the deactivation and initiation efficiencies.

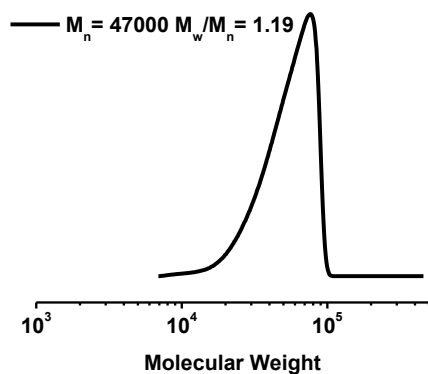


Figure A-IV-1. GPC traces for ATRP reaction catalyzed by catalase. $[\text{OE}(\text{O}A)_{480}]_0 = 0.5$ M; $[\text{OE}(\text{O}A)_{480}]/[\text{PEG}_{2000}\text{iBBr}]/[\text{Asc. A}]/[\text{Catalase}] = 78/1/15/0.007$, 100 mM NaCl, water, 30 °C.

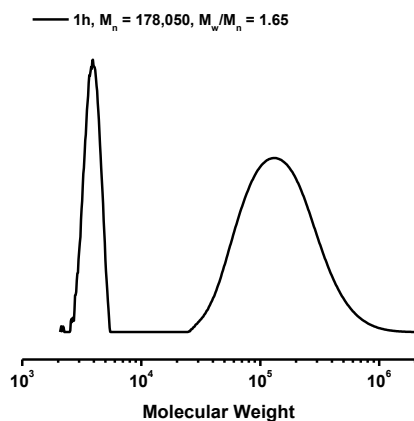


Figure A-IV-2. GPC traces for ATRP reaction catalyzed by hemin. $[\text{OE}(\text{O}A)_{475}]_0 = 0.45$ M; $[\text{OE}(\text{O}A)_{475}]/[\text{I}]/[\text{Asc. A}]/[\text{Hemin}] = 227/1/10/1$, water/DMF (3/1), 30 °C.

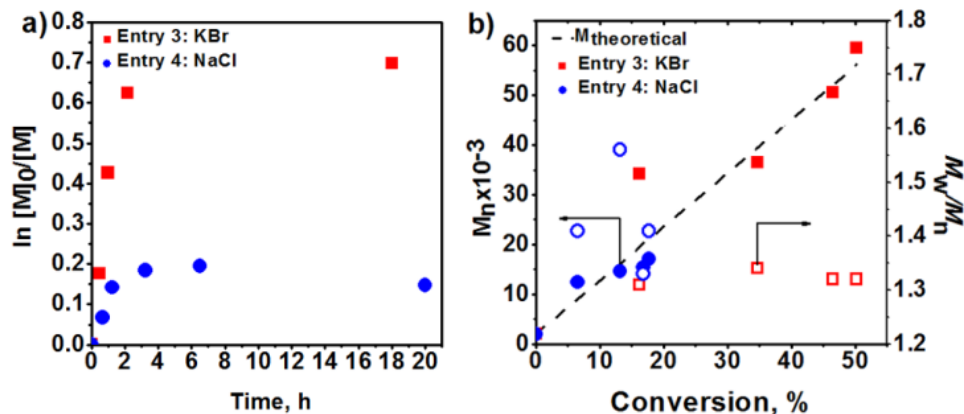


Figure A-IV-3. First-order kinetic plots (a), evolution of M_n and M_w/M_n with conversion (b). $[OEOMA_{475}]_0 = 0.45$ M; $[OEOMA_{475}]/[I]/[Asc. A]/[Hemin] = 227/1/10/1$, 100 mM NaCl/KBr, water, 30 °C.

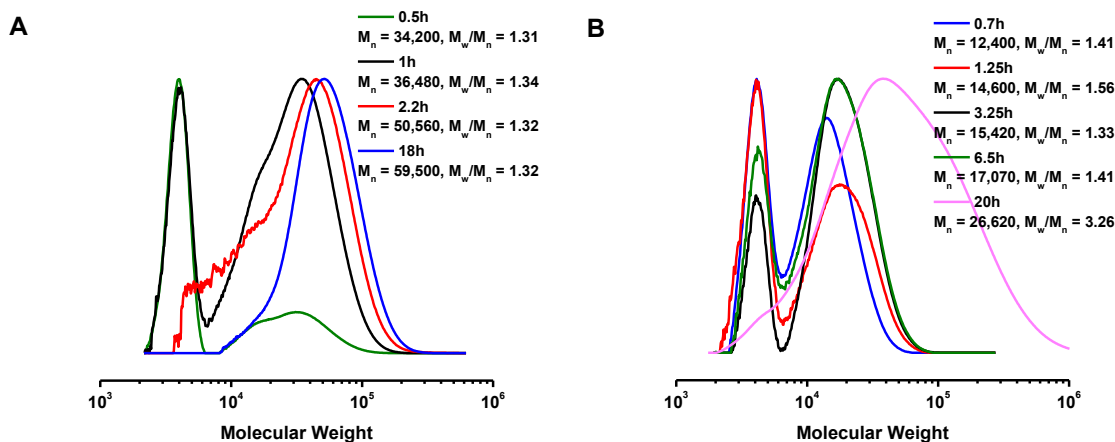


Figure A-IV-4. GPC traces for ATRP reaction catalyzed by hemin in the presence of 100 mM KBr (A) and NaCl (B). $[OEOMA_{475}]_0 = 0.45$ M; $[OEOMA_{475}]/[I]/[Asc. A]/[Hemin] = 227/1/10/1$, 100 mM NaCl/KBr, water, 30 °C.

Table A-IV-1. Experimental conditions and results of ATRP of OEO(M)A₄₇₅.

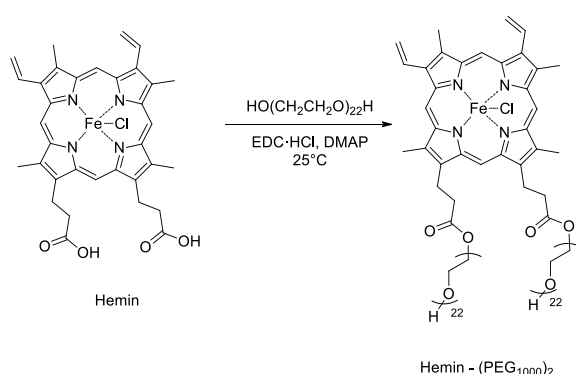
	M/I/RA/Cat	Catalyst	Salt	Solvent	Time/h	Conv./%	$M_{n,th} \times 10^{-3}$ 3a	$M_{n,GPC} \times 10^{-3}$ 3b	M_w/M_n
1	78/1/15/0.007	Catalase	NaCl	H ₂ O	16	49	20	47	1.19
2	227/1/10/1	Hemin	-	H ₂ O	1	60	67	178	1.65
3	227/1/10/1	Hemin	KBr	H ₂ O	18	50	56	60	1.32
4	227/1/10/1	Hemin	NaCl	H ₂ O	20	14	17	27	3.26
5	227/1/10/1	Hemin- (PEG ₁₀₀₀) ₂	KBr	H ₂ O	5	78	86	116	1.32
6	227/1/1/1	Hemin- (PEG ₁₀₀₀) ₂	KBr	H ₂ O	6	47	53	103	1.72
7	227/1/10/1	Mesohemin- (MPEG ₅₅₀) ₂	KBr	H ₂ O	5.5	75	83	101	1.30
8	227/1/5/1	Mesohemin- (MPEG ₅₅₀) ₂	KBr	H ₂ O	6	65	72	86	1.28
9	227/1/1/1	Mesohemin- (MPEG ₅₅₀) ₂	KBr	H ₂ O	6	60	66	63	1.19
10	227/1/1/1	Mesohemin- (MPEG ₅₅₀) ₂	TBABr	Anisole	6	54	61	94	1.22

[I] = 2 mM, except entry 1: [I] = 5 mM; I = PEG₂₀₀₀BPA, except entry 1: I = PEG₂₀₀₀BBr; 30 °C; 20% [M] (v/v); entry 2-4: 20% DMF (v/v), 5-9: 6% DMF (v/v); M = OEOMA₄₇₅, except entry 1: M = OEOMA₄₈₀; entries 2-4: 20% DMF (v/v), entries 5-9: 6% DMF (v/v).

^a $M_{n,th} = ([M]_0/[I]_0) \times \text{conversion} \times M_{\text{monomer}}$; ^buniversal calibration.

Although the initiation efficiency was improved by addition of the extra halide salt, complete consumption of the macroinitiator required more than 1 h, according to the GPC traces (Figure A-IV-4A). The slow initiation led to a MW higher than predicted and a

broader MWD, plausibly because of the limited solubility of the hemin catalyst in the aqueous media. It was reported that hematin with attached poly(ethylene glycol) (PEG) chains can be used in aqueous media without cosolvents or pH adjustments.^{237b} Therefore, to determine if modification of hemin with water-soluble moieties can improve the catalytic performance, the hemin carboxyl groups were esterified with PEG₁₀₀₀ (Scheme A-IV-3).



Scheme A-IV-3. Hemin modification scheme with PEG.

The initial experiments using hemin-(PEG₁₀₀₀)₂ instead of hemin resulted in a well-controlled polymerization (Table A-IV-1, entry 5), as evidenced by linear semilogarithmic kinetic plots up to high conversion, linear increase of the MW with conversion, and a narrow MWD around 1.3 (Figure A-IV-5). Another indication of enhanced control was a significant reduction of the macroinitiator residues in the GPC traces, already after 30 min (Figure A-IV-6). These results suggested that in addition to excess bromide salt, PEG tails improve the performance of the catalysts because of better solubility and stability of the catalyst.^{228e} However, a 10 fold excess of ascorbic acid was required for successful polymerization. With only 1 equivalent, poor control was observed and the MWD

broadened to $M_w/M_n \approx 1.72$ (Table A-IV-1, entry 6). This limited control could be due to a possible copolymerization of hemin through its vinyl bonds (Figure A-IV-5). Indeed, the precipitated polymers had a brown color and UV-Vis analysis revealed spectra typical for metal porphyrins (Figure A-IV-7).²⁴⁴

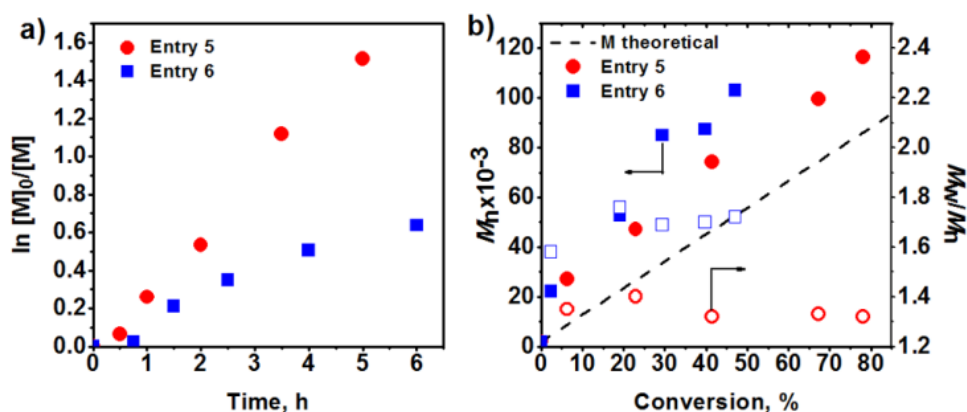


Figure A-IV-5. First-order kinetic plots (a), evolution of M_n and M_w/M_n with conversion (b), GPC traces. $[OEOMA_{475}]_0 = 0.45$ M; $[OEOMA_{475}]/[I]/[Asc. A]/[Hemin-(PEG_{1000})_2] = 227/1/n/1$, $n = 1, 10$, water, 30 °C, 100 mM KBr.

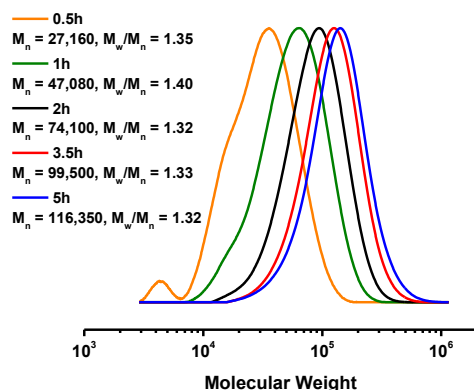


Figure A-IV-6. GPC traces for ATRP reaction catalyzed by hemin-(PEG₁₀₀₀)₂.

$[\text{OEOMA}_{475}]_0 = 0.45 \text{ M}$; $[\text{OEOMA}_{475}]/[\text{I}]/[\text{Asc. A}]/[\text{Hemin}-(\text{PEG}1000)_2] = 227/1/10/1$,
 100 mM KBr, water, 30 °C.

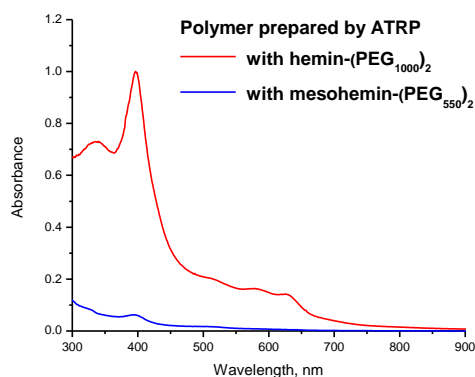
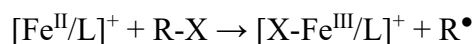
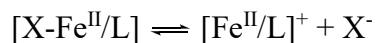
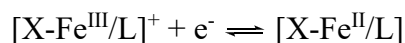


Figure A-IV-7. UV-Vis spectra of the purified polymer after AGET ATRP catalyzed by hemin-PEG and mesohemin-PEG (1 wt. %).

To exclude the possibility of copolymerization of the catalyst, hemin was converted to mesohemin by hydrogenation, and then esterified with methoxy PEG₅₅₀ (Scheme A-IV-2). The resulting modified iron porphyrin preserved its structure, as confirmed by the presence of the characteristic Soret band at 437 nm and Q bands in the visible region of UV-Vis spectra in CHCl₃ (Figure A-IV-8). The structure of the complex was characterized by electrospray ionization mass spectrometry (ESI-MS) with a [mesohemin-(MPEG₅₅₀)₂]⁺ species at m/z ranging from 1266.1 to 1927 with an interval of 44 because of the distribution present in MPEG²⁴⁵ and [mesohemin-(MPEG₅₅₀)₂]²⁺ species at m/z ranging from 584.8 to 1064 with an interval of 22 (Figure A-IV-9). Cyclic voltammetry (CV) analysis of mesohemin-(PEG₅₅₀)₂ showed the presence of two reduced states ($E_{pc} = -0.73$ and -0.94 V versus $\text{Fc}^{0/+}$) (Figure A-IV-10), probably because of iron center interaction with side PEG

groups. However, upon addition of 10 equivalents of NaBr only one cathodic peak ($E_{pc} = -0.89$ V versus $\text{Fc}^{0/+}$) suggested formation of mesohemin-(MPEG₅₅₀)₂Br species. The CV indicated a quasi-reversible reaction. The half-wave potential ($E_{1/2}$) is slightly more negative for mesohemin-(PEG₅₅₀)₂Br than for hemin-Br (-0.78 and -0.75 V vs. $\text{Fc}^{0/+}$, respectively). Upon addition of initiator (ethyl α -bromophenylacetate), the cyclic voltammogram showed an increase of the cathodic current and a decrease of the anodic current, because of a reaction of electrochemically produced Fe(II) species with the alkyl halide, *i.e.*, a regeneration of Fe(III) species (Scheme A-IV-4).



(X = halogen, and R-X = alkyl halide (Initiator), L = hemin or mesohemin-(MPEG₅₅₀)₂)

Scheme A-IV-4. Catalytic Electrochemical-chemical Reaction.

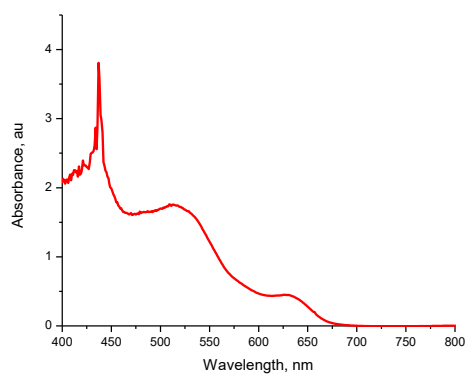


Figure A-IV-8. UV-Vis spectra of mesohemin-(MPEG₅₅₀)₂ in CH₃Cl.

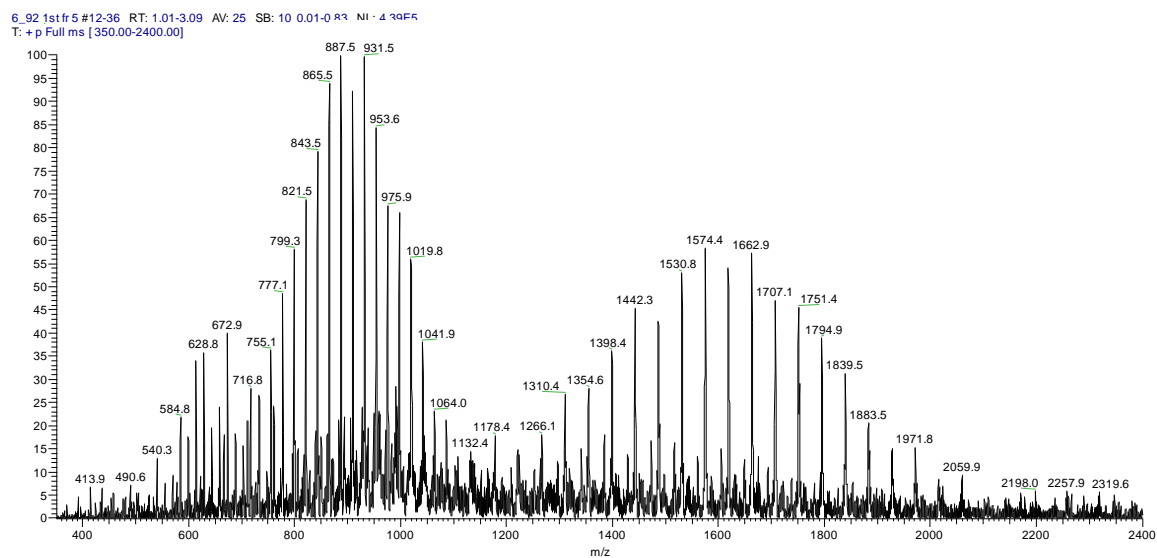


Figure A-IV-9. ESI of mesohemin-(MPEG₅₅₀)₂: 250 μ M in water:methanol = 1:3.

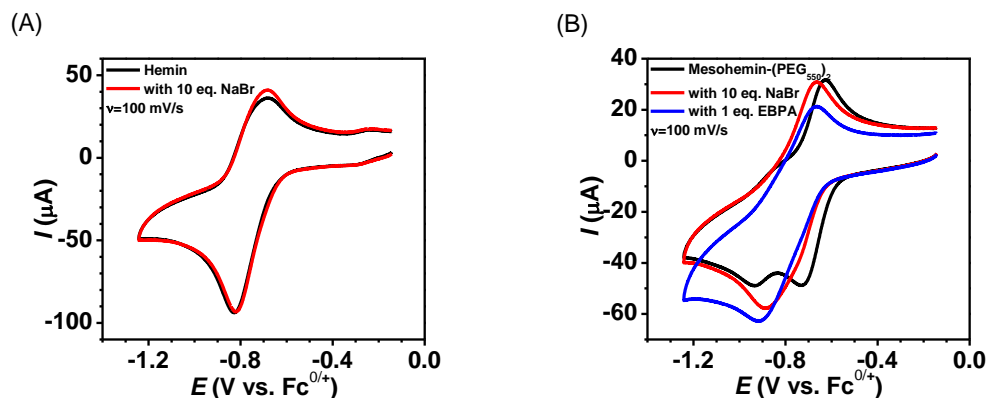


Figure A-IV-10. Cyclic voltammogram of (A) Hemin and (B) Mesohemin-(MPEG₅₅₀)₂, scan rate = 100 mV/s, supporting electrolyte=TBAPF₆ (0.1 M in DMF).

This optimized second-generation catalyst, consisting of hydrogenated hemin (mesohemin) with MPEG₅₅₀ tails, performed significantly better than original hemin or hemin-(PEG₁₀₀₀)₂ (Table A-IV-1, entries 7-10). Polymerizations using mesohemin-(PEG₅₅₀)₂ as a catalyst were fast, providing initially linear first order kinetic plots, linear evolution of MW with conversion and M_w/M_n values close to 1.2 (entry 7). However, after approximately 60% conversion, the rate of polymerization decreased, plausibly because of the excessive amount of ascorbic acid. A decrease of the molar ratio of ascorbic acid to mesohemin-(PEG₅₅₀)₂ from 10/1 to 5/1 to 1/1 resulted in more linear kinetic plots, linear increase of MW with conversion, and a narrower MWD. When the ratio of ascorbic acid to mesohemin-(MPEG₅₅₀)₂ was 1/1, the experimental MW correlated well with theoretical values. Mesohemin cannot copolymerize and become incorporated into the polymer chain. Thus, it shows an enhanced performance because a catalyst incorporated into a polymer chain cannot efficiently participate in atom transfer reactions. Indeed, essentially colorless

polymers were prepared with mesohemin-based catalysts (Figure A-IV-7).

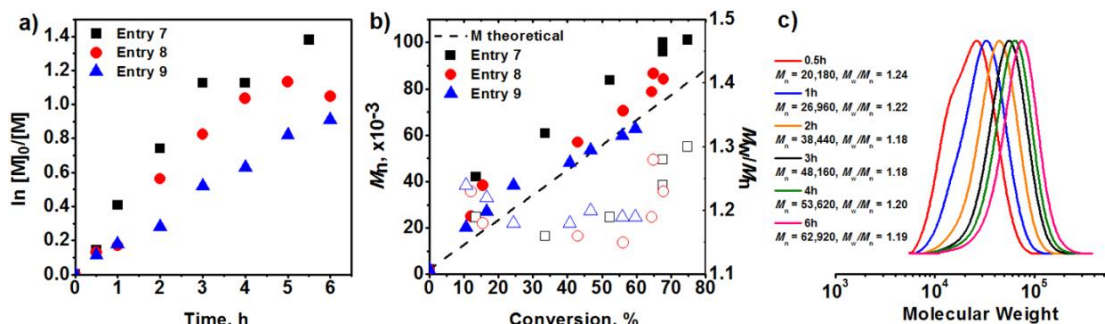


Figure A-IV-11. First-order kinetic plots (a), evolution of MW and MWD with conversion (b), GPC traces with conversion (c). $[OEOMA_{475}]_0 = 0.45$ M; $[OEOMA_{475}]/[I]/[Asc. A]/[Mesohemin-(MPEG_{550})_2] = 227/1/1n/1$, $n = 1, 5, 10$, water, 30 °C, 100 mM KBr.

To show the versatility of the mesohemin based catalyst for ATRP, a polymerization was performed in organic media (Table A-IV-1, entry 10). An AGET ATRP of $OEOMA_{475}$ in anisole was activated by addition of $Sn(EH)_2$ as a reducing agent and displayed close to linear first order kinetic plots and a linear MW evolution with conversion (Figure A-IV-12). A slow initiation was indicated by slight curvature during initial stage of polymerization in the semilogarithmic kinetic plot and experimental MW higher than theoretically predicted. Dispersities stayed low throughout course of polymerization.

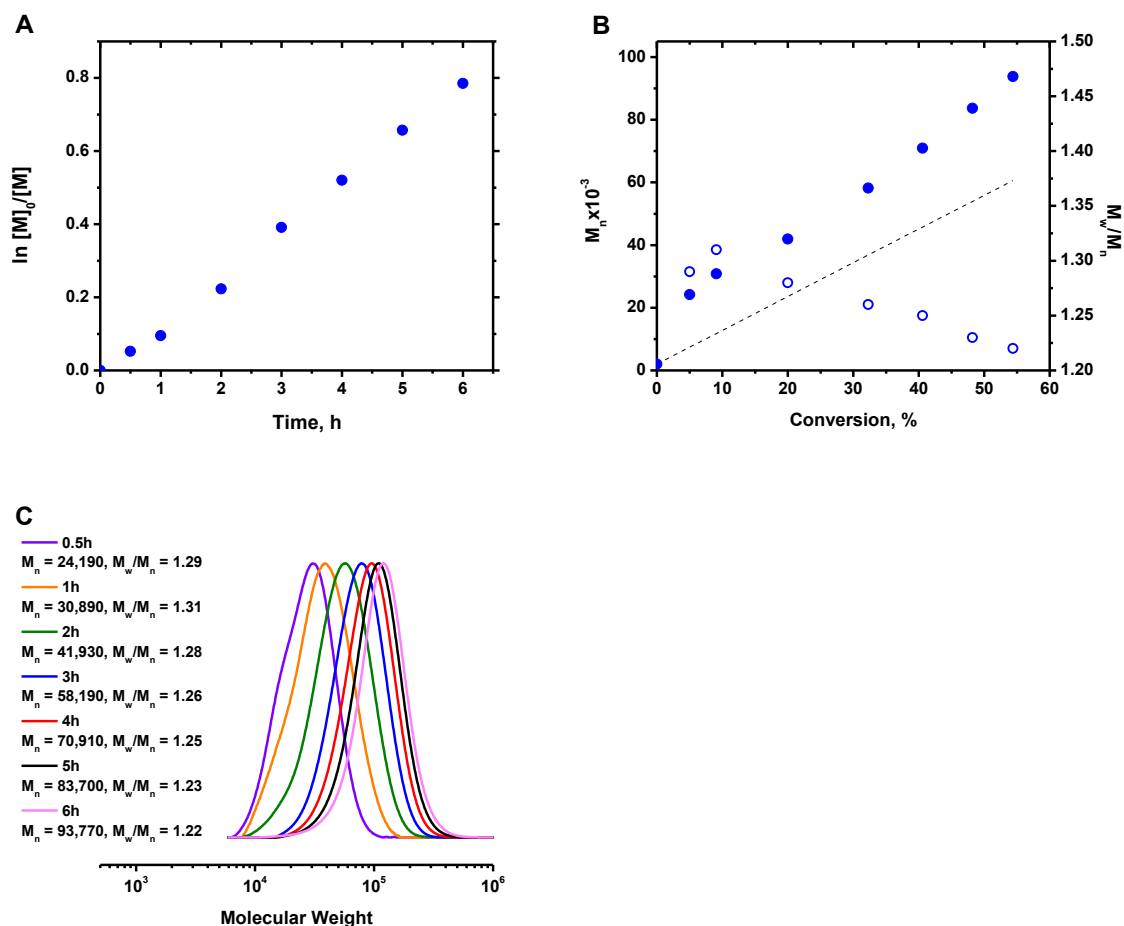


Figure A-IV-12. (A) First-order kinetic plot, (B) evolution of molecular weight and molecular weight distribution with conversion, (C) GPC traces with conversion. $[\text{OEOMA}_{475}]_0 = 0.45 \text{ M}$; $[\text{OEOMA}_{475}]/[\text{I}]/[\text{Sn}(\text{EH})_2]/[\text{Mesohemin}-(\text{MPEG}_{550})_2] = 227/1/1/1$, anisole, 60°C .

A-IV. 3. Summary

A bioinspired iron porphyrin based complex was designed and successfully used as a new ATRP catalyst. Mesohemin-(MPEG₅₅₀)₂, prepared from naturally occurring hemin, performs significantly better than hemin itself or previously-reported hematin. This can be

attributed to its increased solubility because of the PEG tails and hydrogenated vinyl bonds, preventing copolymerization and allowing for faster deactivation in the presence of excess bromide salt. Mesohemin-(MPEG₅₅₀)₂ can be used for ATRP of methacrylates in both organic and aqueous media. This new, environmentally benign ATRP catalyst is very promising and its further modifications are under investigation.

A-IV. 4. Experimental Section

Materials. All chemicals were purchased from commercial sources, *e.g.*, Aldrich, TCI, and used as received if not stated otherwise. Oligo(ethylene oxide) methyl ether methacrylate (OEOMA₄₇₅, 99%, average molecular weight 475, Aldrich) and oligo(ethylene oxide) methyl ether acrylate (OEOMA₄₈₀, 99%, average molecular weight 480, Aldrich) were passed over a column of basic alumina (Fisher Scientific) prior to use to remove inhibitor. Poly(ethylene glycol) bromophenyl acetate (PEG₂₀₀₀BPA), poly(ethylene oxide) isobutyryl bromide (PEO₂₀₀₀iBBBr)²⁴⁶ and mesohemin²⁴⁷ were prepared as previously reported in literature.

Instrumentation. Gel permeation chromatography (GPC): GPC was used to determine number average molecular weight (M_n) and M_w/M_n values. The GPC was conducted with a Waters 515 HPLC Pump and Waters 2414 Refractive Index Detector using PSS columns (SDV 10², 10³, and 10⁵ Å) in tetrahydrofuran (THF) as an eluent at a flow rate of 1 mL/min at 35 °C. The apparent molecular weights (M_n) and polydispersities (M_w/M_n) were determined using linear poly(methyl methacrylate) (M_n = 800 ~ 1,820,000) standards using WinGPC 7.0 software from PSS. The previously reported Mark-Houwink

parameters were used for universal calibration using WinGPC 7.0 software from PSS. Conversion was determined using GPC by following the decrease of monomer peak area relative the increase of polymer peak area as previously reported. **Mass spectroscopy:** Mass spectra were recorded on a mass spectrometer with a Varian Saturn 2100T MS with 3900 GC using an EI source. In each case, characteristic fragments with their relative intensities in percentages are shown. Electrospray mass spectra were measured on a Thermo-Fisher LCQ ESI/APCI Ion Trap containing a quadrupole field ion trap mass spectrometer with electrospray ionization (ESI). **Electrochemical Analysis:** All of the cyclic voltammograms (CV) were recorded at 25 °C with a Gamry Reference 600 potentiostat using a standard three-electrode system consisting of a glassy carbon (GC) working electrode, platinum mesh counter electrode, and Ag/AgI/I⁻ reference electrode. A solution of 0.1 M TBAPF₆ supporting electrolyte in 20 mL of DMF was prepared using previously dried reagents. To prepare 1 mM solutions this mixture were added either to 13 mg hemin or 34 mg of mesohemin-(MPEG₅₅₀)₂. CV measurements were carried out under a nitrogen atmosphere at a scan rate of 100 mV/s. Potentials were recorded versus a Ag/AgI/I⁻ reference electrode and the recorded voltammograms were externally referenced to ferrocene/ferrocenium (Fc^{0/+}).

Hemin-(PEG₁₀₀₀)₂ synthesis. Hemin (200 mg, 0.307 mmol), poly(ethylene glycol) (PEG₁₀₀₀, MW_{avg.}=1000) (1227 mg, 1.227 mmol) and N-(3-dimethylaminopropyl)-N-(ethylcarbodiimide hydrochloride) (EDC·HCl) (259 mg, 1.350 mmol) were mixed in 8 mL of dry dichloromethane (DCM). Mixture was cooled on ice and DMAP (8 mg, 0.067 mmol) was added. Reaction mixture was brought to room temperature and kept 24h. After

completion of reaction the solution was washed with 0.1 M HCl (2x10 ml), and with saturated NaHCO₃ (2x10 ml). After that mixture was dried with MgSO₄ and solvent was removed under reduced pressure. The product was tested without further purification.

Mesohemin-(MPEG₅₅₀)₂ synthesis. Mesohemin (400 mg, 0.610 mmol), poly(ethylene glycol) methyl ether (MPEG₅₅₀, MW_{avg.}=550) (1341 mg, 2.440 mmol) and N-(3-dimethylaminopropyl)-N (ethylcarbodiimide hydrochloride (EDC·HCl) (515 mg, 2.680 mmol) were mixed in 8 mL of dry dichloromethane (DCM). Mixture was cooled on ice and DMAP (16 mg, 0.130 mmol) was added. Reaction mixture was brought to room temperature and kept 24h. After completion of reaction the solution was washed with 0.1 M HCl (2 × 10 mL), and with saturated NaHCO₃ (2 × 10 mL). After that mixture was dried with MgSO₄ and solvent was removed under reduced pressure. The residue was purified by column chromatography on alumina with chloroform/methanol (9/1) mixture. Fractions were collected, solvent was removed, residue was dissolved in 1M HCl in DCM, washed with saturated NaHCO₃, and washed with slightly acidic 1M NaBr. After that the product solution was dried with MgSO₄ and solvent was removed under reduced pressure yielding 418 g of mesohemin-(MPEG₅₅₀)₂ (45 % yield). The final compound was analyzed by ESI-MS and UV-Vis. λ_{max} = 437, 521, and 626 nm. m/z 1266.1-1927 with interval of 44 (M⁺), 584.8-1086 with interval 22 (M²⁺).

General procedure for synthesis of poly(OEOMA₄₇₅) by AGET ATRP. A series of aqueous AGET ATRP reactions were carried out. The following procedure describes a typical polymerization of OEOMA₄₇₅ catalyzed by mesohemin-(MPEG₅₅₀)₂: KBr (60 mg, 0.5 mmol), OEOMA₄₇₅ (1.08 g, 2.27 mmol), mesohemin-(MPEG₅₅₀)₂ (17.9 mg, 0.01 mmol)

were dissolved in H₂O (3.6 mL). The mixture was charged into a 10 mL Schlenk flask and purged with nitrogen for 1h, then placed in an oil bath at 30 °C. An ascorbic acid solution (100 mM) was purged with nitrogen, and then added into reaction mixture (0.1 ml). 33 mM stock solution of PEG2000BPA in DMF was purged with nitrogen, and then added into reaction mixture (0.3 ml). Samples were taken throughout the reaction for GPC analysis.

A-IV. 5. References

1. (a) Matyjaszewski, K.; Spanswick, J., Copper-Mediated Atom Transfer Radical Polymerization. In *Polymer Science: A Comprehensive Reference*, 2012; Vol. Vol. 3, pp 377-428; (b) Matyjaszewski, K., *Macromolecules* **2012**, *45* (10), 4015-4039; (c) Matyjaszewski, K.; Tsarevsky, N. V., *Nature Chemistry* **2009**, *1* (4), 276-288; (d) Matyjaszewski, K.; Xia, J., *Chem. Rev.* **2001**, *101*, 2921-2990.
2. Braunecker, W. a.; Matyjaszewski, K., *Prog. Polym.Sci.* **2007**, *32* (1), 93-146.
3. di Lena, F.; Matyjaszewski, K., *Prog. Polym. Sci.* **2010**, *35* (8), 959-1021.
4. (a) O'Reilly, R. K.; Gibson, V. C.; White, A. J. P.; Williams, D. J., *J. Am. Chem. Soc.* **2003**, *125* (28), 8450-8451; (b) Tsarevsky, N. V.; Matyjaszewski, K., *Chem. Rev.* **2007**, *107* (6), 2270-2299; (c) Wang, Y.; Zhang, Y.; Parker, B.; Matyjaszewski, K., *Macromolecules* **2011**, *44* (11), 4022-4025; (d) He, W.; Zhang, L.; Miao, J.; Cheng, Z.; Zhu, X., *Macromol. Rapid Commun.* **2012**, *33* (12), 1067-73; (e) Mukumoto, K.; Wang, Y.; Matyjaszewski, K., *ACS Macro Lett.* **2012**, *1* (5), 599-602; (f) Schroeder, H.; Yalalov, D.; Buback, M.; Matyjaszewski, K., *Macromolecular Chemistry and Physics* **2012**, *213* (19), 2019-2026; (g) Nishizawa, K.; Ouchi, M.; Sawamoto, M., *Macromolecules* **2013**, *46*, 3342-3349; (h) Eckenhoff, W. T.; Biernesser, A. B.; Pintauer, T., *Inorganica Chimica Acta* **2012**, *382*, 84-95; (i) Aoshima, H.; Satoh, K.; Umemura, T.; Kamigaito, M., *Polymer Chemistry* **2013**, *4* (12), 3554-3562.
5. (a) Wang, X. S.; Armes, S. P., *Macromolecules* **2000**, *33*, 6640-6647; (b) Heredia, K. L.; Bontempo, D.; Ly, T.; Byers, J. T.; Halstenberg, S.; Maynard, H. D., *J. Am. Chem. Soc.* **2005**, *127*, 16955-16960; (c) Gauthier, M. A.; Klok, H.-A., *Chemical Communications* **2008**, (23), 2591-2611; (d) Lutz, J.-F.; Börner, H. G., *Progress in Polymer Science* **2008**, *33* (1), 1-39; (e) Peeler, J. C.; Woodman, B. F.; Averick, S.; Miyake-Stoner, S. J.; Stokes, A. L.; Hess, K. R.; Matyjaszewski, K.; Mehl, R. A., *J. Am. Chem. Soc.* **2010**, *132*, 13575-13577; (f) Finn, M. G.; Pokorski, J. K.; Breitenkamp, K.; Liepold, L. O.; Qazi, S., *J. Am. Chem. Soc.* **2011**, *133*, 9242-9245.
6. (a) Mougin, N. C.; van Rijn, P.; Park, H.; Müller, A. H. E.; Böker, A., *Adv. Func. Mat.* **2011**, *21*, 2470-2476; (b) Konkolewicz, D.; Magenau, A. J. D.; Averick, S. E.; Simakova, A.; He, H.; Matyjaszewski, K., *Macromolecules* **2012**, *45* (11), 4461-4468; (c) Simakova, A.; Averick, S. E.; Konkolewicz, D.; Matyjaszewski, K., *Macromolecules* **2012**, *45* (16),

- 6371-6379; (d) Nguyen, N. H.; Kulis, J.; Sun, H.-J.; Jia, Z.; van Beusekom, B.; Levere, M. E.; Wilson, D. a.; Monteiro, M. J.; Percec, V., *Polym. Chem.* **2013**, *4*, 144-155.
7. (a) Tsarevsky, N. V.; Pintauer, T.; Matyjaszewski, K., *Macromolecules* **2004**, *37*, 9768-9778; (b) Bortolamei, N.; Isse, A. a.; Magenau, A. J. D.; Gennaro, A.; Matyjaszewski, K., *Angew. Chem. Int. Ed.* **2011**, *50*, 1-5; (c) Zhang, Q.; Wilson, P.; Li, Z.; McHale, R.; Godfrey, J.; Anastasaki, A.; Waldron, C.; Haddleton, D. M., *J. Am. Chem. Soc.* **2013**, *135* (19), 7355-7363.
8. Averick, S.; Simakova, A.; Park, S.; Konkolewicz, D.; Magenau, A. J. D.; Mehl, R. A.; Matyjaszewski, K., *ACS Macro Lett.* **2012**, *1* (1), 6-10.
9. (a) Sigg, S. J.; Seidi, F.; Renggli, K.; Silva, T. B.; Kali, G.; Bruns, N., *Macromol. Rapid Commun.* **2011**, *32* (21), 1710-5; (b) Silva, T. B.; Spulber, M.; Kocik, M. K.; Seidi, F.; Charan, H.; Rother, M.; Sigg, S. J.; Renggli, K.; Kali, G.; Bruns, N., *Biomacromolecules* **2013**, *14* (8), 2703-2712.
10. Ng, Y.-H.; di Lena, F.; Chai, C. L. L., *Chem. Comm.* **2011**, *47* (22), 6464-6.
11. Polizzi, K. M.; Bommarius, A. S.; Broering, J. M.; Chaparro-Riggers, J. F., *Curr. Opin. Chem. Biol.* **2007**, *11*, 220-5.
12. (a) Guin, J.; De Sarkar, S.; Grimme, S.; Studer, A., *Angewandte Chemie* **2008**, *120* (45), 8855-8858; (b) Shu, J. Y.; Tan, C.; DeGrado, W. F.; Xu, T., *Biomacromolecules* **2008**, *9* (8), 2111-2117.
13. (a) Akkara, J. A.; Wang, J.; Yang, D.-P.; Gonsalves, K. E., *Macromolecules* **2000**, *33*, 2377-2382; (b) Singh, A.; Roy, S.; Samuelson, L., *J. Macromol. Sci. Pure Appl. Chem.* **2001**, *A38*, 37-41.
14. (a) Islamova, R. M.; Nazarova, S. V.; Koifman, O. I., *Macroheterocycles* **2011**, *4* (2), 97-105; (b) Yamashita, K.; Yamamoto, K.; Kadokawa, J., *Polymer* **2013**, *54* (7), 1775-1778.
15. Morgan, B.; Dolphin, D., Synthesis and structure of biomimetic porphyrins. In *Metal Complexes with Tetrapyrrole Ligand I*, Buchler, J., Ed. Springer Berlin Heidelberg: 1987; Vol. 64, pp 115-203.
16. Lutz, J.-F., *Journal of Polymer Science Part A: Polymer Chemistry* **2008**, *46* (11), 3459-3470.
17. Zhang, L.; Cheng, Z.; Tang, F.; Li, Q.; Zhu, X., *Macromolecular Chemistry and Physics* **2008**, *209*, 1705-1713.
18. Wade, R. S.; Castro, C. E., *J. Am. Chem. Soc.* **1973**, *95*, 226-230.
19. Nishide, H., *J. Polym. Sci., Part A: Polym. Chem.* **1981**, *19*, 1109-1117.
20. Mamardashvili, N. Z.; Golubchikov, O. a., *Russ. Chem. Rev.* **2001**, *70*, 577-606.
21. Varray, S.; Aubagnac, J. L.; Lamaty, F.; Lazaro, R.; Martinez, J.; Enjalbal, C., *Analisis* **2000**, *28*, 263-268.
22. Lee, S. B.; Russell, A. J.; Matyjaszewski, K., *Biomacromolecules* **2003**, *4* (5), 1386-93.
23. Burns, D. H.; Lai, J.-j.; Smith, K. M., *J. Chem. Soc. Perkin Trans I* **1988**, (5), 3119-3131.

Appendix V

Reversible-Deactivation Radical Polymerization in the Presence of Metallic Copper. Activation of Alkyl Halides by Cu⁰*

A-V. 1. Introduction

Atom transfer radical polymerization (ATRP)^{1a, 1d, 1e, 248} is one of the most important reversible-deactivation radical polymerization (RDRP)²⁴⁹ techniques for the synthesis of homopolymers, copolymers, and hybrid materials with well-defined composition, functionalities, and architecture. In ATRP, control over the macromolecular structure is achieved using a transition metal catalyst, most commonly a copper catalyst. In the lower oxidation state, the transition metal catalyst activates alkyl halides, to generate propagating radicals and the transition metal complex in the higher oxidation state which deactivates the propagating radical. ATRP has been used to produce materials with various architectures, however initial catalyst systems usually required over 1000 parts per million (ppm) of the copper catalysts to achieve high conversion. Recently, new ATRP techniques, such as activators regenerated by electron transfer (ARGET) ATRP,^{19a, 250} initiators for continuous activator regeneration (ICAR) ATRP,^{19a} supplemental activator and reducing agent (SARA) ATRP,²⁵¹ electrochemically mediated ATRP (*e*ATRP),^{10, 252} and

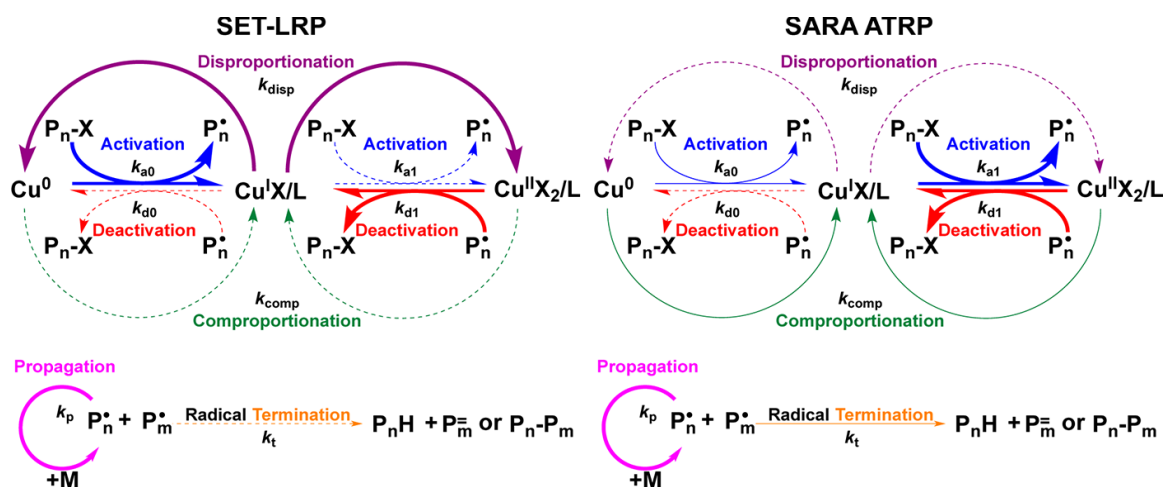
*Work in this appendix was published and partially reformatted based on the following manuscript: Peng, Chi-How; Zhong, Mingjiang; Wang, Yu; Kwak, Yungwan; Zhang, Yaozhong; Zhu, Weipu; Tonge, Matthew; Buback, Johannes; **Park, Sangwoo**; Krys, Pawel; Konkolewicz, Dominik; Gennaro, Armando; Matyjaszewski, Krzysztof *Macromolecules* **2013**, 46, 3803

photochemically mediated ATRP²⁵³ have been developed, which results in controlled polymerizations with low concentrations of catalyst (< 100 ppm). In all cases, the Cu^I activator species are regenerated from the Cu^{II} species that accumulate as a consequence of radical termination. In ICAR ATRP, a conventional free radical initiator is added to regenerate the Cu^I species, while in ARGET ATRP a reducing agent is added to reduce excess Cu^{II} species. A wide variety of reducing agents have been used in ARGET ATRP including organotin complexes,^{19a, 250, 254} sulfites,²⁵⁵ ascorbic acid,²⁵⁰ or glucose.²⁵⁰ In SARA ATRP, zerovalent metals are employed as the reducing agents, and they also act as supplemental activators of alkyl halides.^{251b, 256}

ATRP in the presence of zerovalent metals, which act as reducing agents and direct activators, was initially reported in 1997.^{66a} However, in 2006, an alternative mechanism, single electron transfer-living radical polymerization (SET-LRP),²⁵⁷ was proposed to describe the RDRP of methyl acrylate (MA) in DMSO, in the presence of Cu⁰ metal with a more active ligand, Me₆TREN, although all components (Cu⁰, Me₆TREN, and polar solvents) were previously used in ATRP of acrylates.^{66a, 94a, 258} SET-LRP was proposed to rely on exclusive activation of alkyl halides by Cu⁰ by an outer sphere electron transfer process to form radicals and Cu^IX/L species, followed by instantaneous and complete disproportionation of the Cu^IX/L species to regenerate Cu⁰ and form Cu^{II}X₂/L species, acting as radical deactivator.^{257, 259}

Scheme A-V-1 presents all reactions involved in RDRP in the presence of Cu⁰. The purpose of this scheme is to show that SET-LRP and SARA ATRP include the same reactions but differ dramatically in their very different relative contributions. Scheme A-

V-1 shows how three different Cu species (Cu^0 , Cu^{I} , and Cu^{II}) can interconvert. This can occur spontaneously (comproportionation/disproportionation) or assisted by alkyl halides ($\text{P}_n\text{-X}$) and radicals (P_n^\bullet). Line thickness describes the magnitude (or contributions) of the rates of the different reactions; thick bold lines represent major (dominating) reactions, regular solid lines represent contributing reactions and dashed lines represent minor reactions that could be neglected.



Scheme A-V-1. Schematic illustration of possible reactions between $\text{P}_n\text{-X}$, P_n^\bullet radicals, Cu^0 , $\text{Cu}^{\text{I}}\text{X/L}$, and $\text{Cu}^{\text{II}}\text{X}_2/\text{L}$ species in the RDRP in the presence of Cu^0 . The proposed SET-LRP mechanism is shown as the left panel, and the proposed SARA ATRP mechanism is shown as the right panel. Bold arrows illustrate major (dominating) reactions, regular solid line represent contributing reactions and dash lines represent minor reactions that could be neglected.

The common points of SARA ATRP and SET-LRP include the propagation of radicals with monomer, and participation in termination reactions, although some SET-LRP

systems incorrectly²⁶⁰ claim zero termination, even at complete monomer conversion.²⁶¹ In addition, both SARA ATRP and SET-LRP rely on $\text{Cu}^{\text{II}}\text{X}_2/\text{L}$ species as the dominant deactivator, and negligible deactivation from $\text{Cu}^{\text{I}}\text{X}/\text{L}$ species. The major differences between SET-LRP and SARA ATRP include the relative contribution of activation by Cu^0 and $\text{Cu}^{\text{I}}\text{X}/\text{L}$ species and the position and relative importance of comproportionation/disproportionation reactions. In particular, SET-LRP neglects any activation of alkyl halides by $\text{Cu}^{\text{I}}\text{X}/\text{L}$, whereas $\text{Cu}^{\text{I}}\text{X}/\text{L}$ is the major activator in SARA ATRP. SET-LRP assumes instantaneous and complete disproportionation of $\text{Cu}^{\text{I}}\text{X}/\text{L}$ species, whereas SARA ATRP is based on relatively slow comproportionation which under some condition may dominate (but not necessarily) over disproportionation. Finally, SET-LRP assumes exclusive activation of alkyl halides by Cu^0 *via* outer sphere electron transfer (OSET), whereas in SARA ATRP, Cu^0 acts only as a supplemental activator of alkyl halides via inner sphere electron transfer (ISET), as well as a reducing agent.^{7a, 251b, 251c}

This Appendix is one of a series of studies whose main purpose is to clearly establish the mechanism of RDRP in the presence of Cu^0 by quantitative evaluation of contributions of various participating reactions. This requires not only determination of the relevant rate coefficients but also concentrations of the involved reagents under conditions resembling those present in a real polymerization. Most RDRPs in the presence of Cu^0 have been carried out for MA in DMSO at ambient temperature with Me_6TREN ligand used at concentrations *ca.* 10 mol% vs. alkyl halide as initiator. Since under typical RDRP conditions, 1 to 3% of chains terminate, the 10 mol% of ligand vs. initiator can be translated to *ca.* 20 to 3 fold excess of ligand vs. soluble Cu species; 20-fold if 1% of chains terminate

and predominantly Cu^{II} species are formed and 3-fold if 3% of chains terminate and Cu^I species dominate.

This Appendix investigates the comproportionation/disproportionation reactions²⁶² and showed that comproportionation dominates over disproportionation and both are slow under typical conditions for RDRP in the presence of Cu⁰, *i.e.*, ambient temperature, MA/DMSO mixtures, excess Me₆TREN ligand over soluble Cu species. The same is true for reactions in pure DMSO. Nevertheless, to discriminate between SARA ATRP and SET-LRP, it is necessary to determine the activation rate coefficient of alkyl halides by Cu⁰. The presence of competing reactions involved in the RDRP in the presence of Cu⁰, complicate separation of the activation of alkyl halides by Cu⁰ from the other reactions during polymerization. Recently, Nicolas and coworkers²⁶³ determined the rate of the Cu⁰ activation process in the presence of stable radical, *N-tert-butyl-N*-[1-diethylphosphono-(2,2-dimethylpropyl)], which traps radicals rapidly and shuts down the deactivation reactions. Nicolas *et al.*²⁶³ noted that ethyl 2-bromoisobutyrate (EBiB) reacts relatively slowly with Cu⁰ in the presence of *N,N,N',N'',N''*-pentamethyldiethylenetriamine (PMDETA) as the ligand ($k_{a0} = 6.3 \times 10^{-5} \text{ s}^{-1}$). In this and other papers of this series we use a notation of k^{app} for apparent rate coefficients, since they comprise all Cu species of a specified oxidation state (Cu⁰, Cu^I and Cu^{II}) but without precisely defined association with ligands and halogens. This Appendix reports experiments designed to measure the activation rate coefficient of alkyl halides by Cu⁰ wire (k_{a0}^{app}) both during polymerization and in model reactions without the presence of a stable radical trap. The effects of ligand structure and its concentration, the presence of solvent, and chain length on the value of

k_{a0}^{app} will also be discussed in this appendix.

A-V. 2. Results and Discussion

As highlighted in Scheme A-V-1, RDRP in the presence of Cu^0 is a complex system, with reactions that can occur between three distinct oxidation states of Cu, or between these metallic species and alkyl halides or alkyl radicals. Despite the complexity of the system, the overall polymerization mechanism can be studied by separating the reaction into a series of model reactions and determining the rates of each of the individual reaction steps. Recent studies reported very large values of the activation rate coefficients of alkyl halides by $\text{Cu}^{\text{I}}/\text{Me}_6\text{TREN}$ in model systems in DMSO,²⁶⁴ and other solvents,^{94c, 265} as well as large values of the ATRP equilibrium constants in pure DMSO and acetonitrile and mixtures of solvents with monomer.²⁶⁶ This Appendix reports the activation rate coefficient for Cu^0 and $\text{Cu}^{\text{I}}/\text{Me}_6\text{TREN}$ in model experiments in DMSO and mixtures of monomer and solvents. As shown at the end of the Appendix, the kinetic information gained from model experiments for each reaction step can be combined together to accurately describe this complex system.

In general, the reactions highlighted in Scheme A-V-1 can be written as distinct reactions, as shown in Scheme A-V-2. Scheme A-V-2 also shows the derivation of dimensions for the rate coefficients of the heterogeneous reactions in the presence of Cu^0 . There are six possible reactions that involve interconversion of Cu species in RDRP in the presence of Cu^0 . On the basis of the ATRP equilibrium, activation and deactivation by Cu^{I} and Cu^{II} are bimolecular reactions with rate coefficients k_{a1}^{app} and k_{d1}^{app} , respectively.^{248b}

Although, the speciation of Cu species should be considered for each of the reactions to measure accurate rate coefficients,^{30a} for simplicity, in this series of papers, only the apparent overall rate coefficients of these reactions are considered, using the overall concentrations of Cu^I and Cu^{II} species, which are [Cu^IX/L] and [Cu^{II}X₂/L], respectively. The reactions that involve Cu⁰ are formally termolecular reactions which could include a combination of several elementary steps.



$$R_{\text{a1}} = k_{\text{a1}}^{\text{app}} [\text{R-X}][\text{Cu}^{\text{I}}\text{X/L}] \Rightarrow \{\text{M} \cdot \text{s}^{-1}\} = k_{\text{a1}}^{\text{app}} \{\text{M}^2\} \Rightarrow k_{\text{a1}}^{\text{app}} = \{\text{M}^{-1}\text{s}^{-1}\} \quad (\text{A-V-2})$$



$$R_{\text{d1}} = k_{\text{d1}}^{\text{app}} [\text{R}^\bullet][\text{Cu}^{\text{II}}\text{X}_2/\text{L}] \Rightarrow \{\text{M} \cdot \text{s}^{-1}\} = k_{\text{d1}}^{\text{app}} \{\text{M}^2\} \Rightarrow k_{\text{d1}}^{\text{app}} = \{\text{M}^{-1}\text{s}^{-1}\} \quad (\text{A-V-4})$$



$$R_{\text{comp}} = \frac{S}{V} k_{\text{comp}}^{\text{app}} [\text{Cu}^{\text{II}}\text{X}_2/\text{L}] \Rightarrow \{\text{M} \cdot \text{s}^{-1}\} = k_{\text{comp}}^{\text{app}} \{\text{M} \cdot \text{cm}^2/\text{cm}^3\} \Rightarrow k_{\text{comp}}^{\text{app}} = \{\text{cm} \cdot \text{s}^{-1}\} \quad (\text{A-V-6})$$



$$R_{\text{disp}} = \frac{S}{V} k_{\text{disp}}^{\text{app}} [\text{Cu}^{\text{I}}\text{X/L}]^2 / [\text{L}] \Rightarrow \{\text{M} \cdot \text{s}^{-1}\} = k_{\text{disp}}^{\text{app}} \{\text{M} \cdot \text{cm}^2/\text{cm}^3\} \Rightarrow k_{\text{disp}}^{\text{app}} = \{\text{cm} \cdot \text{s}^{-1}\} \quad (\text{A-V-8})$$



$$R_{\text{a0}} = \frac{S}{V} k_{\text{a0}}^{\text{app}} [\text{RX}] \Rightarrow \{\text{M} \cdot \text{s}^{-1}\} = k_{\text{a0}}^{\text{app}} \{\text{M} \cdot \text{cm}^2/\text{cm}^3\} \Rightarrow k_{\text{a0}}^{\text{app}} = \{\text{cm} \cdot \text{s}^{-1}\} \quad (\text{A-V-10})$$



$$\frac{k_{\text{a0}}^{\text{app}}}{k_{\text{d0}}^{\text{app}}} = \frac{k_{\text{a}}}{k_{\text{d}}} \frac{k_{\text{comp}}^{\text{app}}}{k_{\text{disp}}^{\text{app}}} \Rightarrow \frac{\{\text{cm} \cdot \text{s}^{-1}\}}{k_{\text{d0}}^{\text{app}}} = \left\{ \frac{\text{M}^{-1}\text{s}^{-1} \text{ cm} \cdot \text{s}^{-1}}{\text{M}^{-1}\text{s}^{-1} \text{ cm} \cdot \text{s}^{-1}} \right\} \Rightarrow k_{\text{d0}}^{\text{app}} = \{\text{cm} \cdot \text{s}^{-1}\} \Rightarrow R_{\text{d0}} = \frac{S}{V} [\text{R}^\bullet][\text{Cu}^{\text{I}}\text{X/L}]/[\text{L}] \quad (\text{A-V-12})$$

Scheme A-V-2. Reactions involving Cu species and the derivation of dimensions of rate

coefficients.

Kinetic models and rate coefficients in DMSO with MBrP as the initiator and Me₆TREN as the ligand are provided in Table A-V-1. Since comproportionation, disproportionation, Cu⁰ activation, and Cu^I deactivation are surface related heterogeneous reactions; the dimensions shown in Table A-V-1 for the corresponding rate coefficients (k_{comp}^{app} , k_{disp}^{app} , k_{a0}^{app} , and k_{d0}^{app}) include surface area to volume ratio, and these dimensions are different from k_{a1}^{app} and k_{d1}^{app} . In order to relate classical kinetics under homogeneous conditions and to conduct simulations of such systems, those rate coefficients should be multiplied by the ratio of copper surface area to the reaction volume. As shown in an earlier study, the rate of comproportionation does not depend on [L], while the rate of disproportionation is reciprocal to [L].²⁶² This work will show that the rate of the activation of alkyl halides by Cu⁰ does not vary with [L], indicating that the reverse reaction, deactivation by Cu^I, should scale inversely with [L].

Table A-V-1. Kinetic model and rate constants for model reactions at 25 °C

Reaction	Rate constant	Reference
$R-X + Cu^I X/L \rightarrow R^\bullet + Cu^{II} X_2/L$	$k_{a1}^{app} = 3.2 \times 10^2 \text{ M}^{-1} \text{ s}^{-1}$	this work (Figure A-V-1)
$R^\bullet + Cu^{II} X_2/L \rightarrow R-X + Cu^I X/L$	$k_{d1}^{app} = 1.4 \times 10^6 \text{ M}^{-1} \text{ s}^{-1}$	this work (Figure A-V-1), ref ²⁶⁶
$R-X + Cu^0 + L \rightarrow R^\bullet + Cu^I X/L$	$k_{a0}^{app} = 1.8 \times 10^{-4} \text{ cm s}^{-1}$	this work (Figure A-V-4 & Figure A-V-6)

$R^{\bullet} + Cu^I X/L \rightarrow R-X + Cu^0 + L$	$k_{d0}^{app} = 1.6 \times 10^{-2} \text{ cm s}^{-1}$	$k_{d0}^{app} = k_{a0}^{app} \times K_{disp}^L / K_{ATRP}$ <i>a</i>
$Cu^0 + Cu^{II} X_2/L + L \rightarrow 2Cu^I X/L$	$k_{comp}^{app} = 9.0 \times 10^{-4} \text{ cm s}^{-1}$	ref ^{262, 266}
$2Cu^I X/L \rightarrow Cu^0 + Cu^{II} X_2/L + L$	$k_{disp}^{app} = 2.0 \times 10^{-5} \text{ cm s}^{-1}$	ref ²⁶²
$R^{\bullet} + R^{\bullet} \rightarrow R-R$	$k_t = 1.7 \times 10^9 \text{ M}^{-1} \text{ s}^{-1}$	ref ^{64b}

^a $K_{disp}^L = 2.2 \times 10^{-2}$, $K_{ATRP} = 2.3 \times 10^{-4}$.^{262, 266} The value of k_{d0}^{app} was calculated using the principle of microscopic reversibility.^{7a}

Cleaning the Surface of Cu⁰ Wire. One of the key components of RDRP in the presence of Cu⁰ is the nature of the Cu⁰ itself, which can be in the form of wires, powders, nanopowders, etc. The smaller the particles the higher the surface area, and importantly, the more difficult it can be to accurately measure the surface area. In this series of experiments Cu⁰ wires are used, since the surface area of a wire can be determined precisely, to give accurate rate coefficients, which are surface to volume independent. As highlighted in the literature, there are different methods that can be used to treat the Cu⁰ wire, including the treatment with hydrazine.²⁶⁷ In this work, washing with HCl in methanol was used to remove the oxide layer from the surface. The solubility of both Cu^I and Cu^{II} oxides in HCl is well-known,²⁶⁸ and confirmed in Figure A-V-1. However, to compare kinetics, two RDRP reactions in the presence of Cu⁰ were performed, under the same conditions, except that in one case the Cu⁰ wire was washed with HCl in methanol, and in the other case the wire was treated with hydrazine, following the method of Percec *et al.*²⁶⁷ The results in Figure A-V-2, show that both methods of treating the Cu⁰ wire gave similar results,

indicating that washing Cu⁰ wire with HCl in methanol is an appropriate method of removing Cu oxides from the surface.

Measurement of k_{a1}^{app} and determination of k_{d1}^{app} . The parameter k_{a1}^{app} can be measured using a nitroxide, or other radical scavenger, to rapidly trap any radicals formed by activation of alkyl halides by Cu^I species. With less active species, the evolution of Cu^{II} can be followed by periodic measurements using a conventional UV-Vis spectrometer, whereas faster reactions require stopped flow techniques.²⁶⁵ Typically, activation rate coefficients have been measured in acetonitrile,^{94c, 265} however, solvent polarity affects the catalyst activity.^{64b} Recently, an electrochemical method was developed to measure the activation rate coefficient of EBiB by Cu^I/Me₆TREN complex in DMSO and acetonitrile.²⁶⁴ These measurements showed very large activation rate coefficients by the Cu^I/L species of $k_{a1} = 8.7 \times 10^4 \text{ M}^{-1} \text{ s}^{-1}$ for EBiB activated by Cu^I/Me₆TREN in DMSO. In this paper, the activation rate coefficient of MBrP by Cu^IBr/Me₆TREN was directly measured based on a total Cu^I species in DMSO using stopped flow techniques. The experimental data, and fitted exponential decay are shown in Figure A-V-1, providing an activation rate coefficient of $k_{a1}^{app} = 3.2 \times 10^2 \text{ M}^{-1} \text{ s}^{-1}$ for MBrP activated by the Cu^I/Me₆TREN complex in DMSO. This value is smaller than reported in ref²⁶⁴, due to lower reactivity of MBrP than EBiB and the fact that the total concentration of Cu^I species was taken into account. The deactivation rate coefficient was determined from the value $K_{ATRP} = 2.3 \times 10^{-4}$, and the relationship $k_{d1}^{app} = k_{a1}^{app} / K_{ATRP}$, giving a value of $k_{d1}^{app} = 1.4 \times 10^6 \text{ M}^{-1} \text{ s}^{-1}$. The activation of alkyl halides by Cu^I/Me₆TREN is very fast, as confirmed by the rapid decay of absorption, which was completed in less than 2 s (Figure A-V-1). A

similar analysis conducted in MA/DMSO = 2/1 (v/v) gave an activation rate coefficient of $k_{a1}^{app} = 2.0 \times 10^2 \text{ M}^{-1} \text{ s}^{-1}$ (Figure A-V-2).

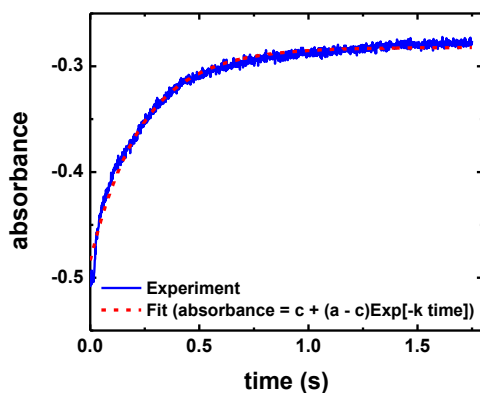


Figure A-V-1. Time resolved conversion of $[\text{Cu}^{\text{I}}]$ to $[\text{Cu}^{\text{II}}]$, ($[\text{Cu}/\text{Me}_6\text{TREN}]_0 = 0.33 \text{ mM}$), due to activation of MBrP (13.3 mM) and trapping of the generated radicals with TEMPO (13.3 mM) followed at 350 nm. Blue: experimental data; red: mono-exponential fit to the experimental data. The function, $\text{absorbance} = c + (a - c)\text{Exp}^{(-k \text{ time})}$ was fitted to the decay profile, with fitted parameters of $a = -0.484$, $c = -0.282$, and $k = 4.22 \text{ s}^{-1}$.

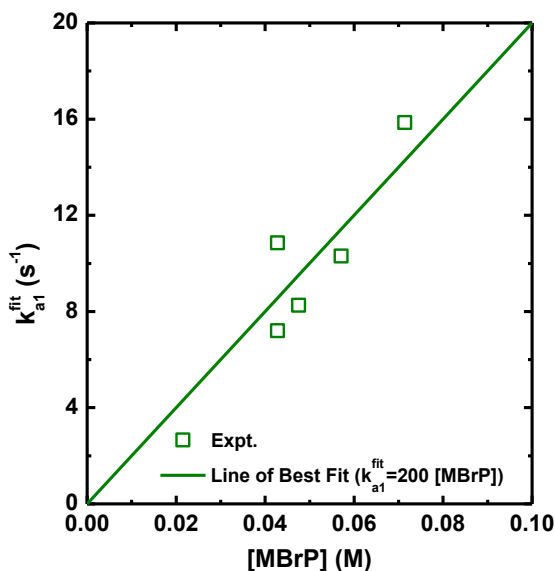


Figure A-V-2. Results of several stopped flow experiments followed at 780 nm in MA/DMSO = 2/1 (v/v). Stock solutions of $[MBrP]_0 = 142.7$ mM, $[CuBr]_0 = 6.34$ mM were used with an excess of TEMPO. Results of fitting gave $k_{a1}^{app} = 2.0 \times 10^2 \text{ M}^{-1} \text{ s}^{-1}$. Here k_{a1}^{fit} is the value of k fitted to the data.

Measurement of k_{a0}^{app} in a model system. The activation rate coefficient of EBiB by Cu^0 , measured in the presence of pentamethyldiethylenetriamine (PMDETA) and an excess of nitroxide radicals in DMSO was reported by Nicolas *et al.* to be $6.3 \times 10^{-5} \text{ s}^{-1}$.²⁶³ If one normalizes this value with Cu^0 surface area and the reaction volume (total volume of 5.67 mL with a Cu^0 surface area of 1.42 cm^2 , determined from the mass of Cu^0 (80 mg), the density of Cu^0 (8.96 g/cm^3), and the diameter of the wire (0.25 mm)), this value becomes $2.5 \times 10^{-4} \text{ cm s}^{-1}$.²⁶³ In their earlier work, Nicolas *et al.*,²⁶³ demonstrated that activation by Cu^0 was much slower than activation by Cu^I/Me_6TREN , implying that once the alkyl halide was activated by Cu^0 , the $Cu^I Br/Me_6TREN$ formed in that reaction rapidly

reacted with a second alkyl halide, generating a second radical and $\text{Cu}^{\text{II}}\text{Br}_2/\text{Me}_6\text{TREN}$. These radicals either terminated or could be trapped, leading to a buildup of $\text{Cu}^{\text{II}}\text{Br}_2/\text{Me}_6\text{TREN}$.

In this Appendix, experiments were designed to measure the activation rate coefficient of alkyl halides, particularly MBrP, by Cu^0 in the presence of Me_6TREN , in the absence of nitroxide radicals. The conditions employed in these model systems were designed to provide the smallest experimental error in the measurement, therefore, conditions were chosen to force almost all the formed radicals to terminate. This gave the largest change in the concentration of MBrP and highest accuracy, although in a typical polymerization, the reaction would be ceased at much shorter reaction times and run at much lower surface area Cu^0 , so that only a small fraction of the alkyl halide would be lost in termination reactions. Furthermore, although the model experiments studied here forced the termination of all the alkyl halide, the kinetic parameters were typically extracted only from the early phase of the reaction, where the concentration of Cu^{II} was sufficiently low, to minimize the influence of Cu^{II} deactivation and comproportionation. In all cases, the principle of halogen conservation dictates that any halogen end-groups lost by termination must be transferred to either soluble Cu^{I} or Cu^{II} species.^{260a}

Kinetic measurements of the activation rate coefficient of alkyl halides by Cu^0 (k_{a0}^{app}) were performed in 7 mL of DMSO using Cu^0 wire ($l = 4$ cm, $S = 1.27$ cm², $S/V = 0.18$ cm⁻¹), MBrP as the alkyl halide and an excess of Me_6TREN as the ligand. As shown in the literature,²⁶⁹ the rate of the polymerization is proportional to the square root of the surface area of the Cu^0 , therefore, powders with a smaller particle size give a faster rate of

polymerization, but also higher rates of termination, than wires with a lower surface area. However, it is difficult to accurately measure the surface area of powders with non-uniform surface and particle size,^{269a} or Cu⁰ nanopowders generated by disproportionation.²⁷⁰ Therefore, in these experiments, Cu⁰ wire is used to obtain kinetic parameters, which are subsequently corrected for the Cu⁰ surface area to reaction volume, to give accurate rate coefficients. In all cases, the surface area of the Cu⁰ wire was a good approximation to the total surface area of Cu⁰ in solution. This can be seen in the experiments of Percec *et al.*²⁷¹ who found that the polymerization continued, but the rate decreased by a factor of *ca.* 10 when the stirrer bar with the Cu⁰ wire wrapped around was lifted out of the reaction mixture. By the square root dependence of the polymerization rate on the surface area of Cu⁰ in solution, this indicates that the surface area of Cu⁰ in the solution, not attached to the wire itself is approximately 1% of the surface area of the Cu⁰ wire. This indicates that the Cu⁰ wire surface area is an excellent approximation to the total surface area of Cu⁰ in the solution. Figure A-V-3a shows the evolution of the concentrations of the Cu^{II}Br₂/Me₆TREN with time, as measured by UV/Vis/NIR spectroscopy and MBrP, as measured by NMR. As seen in the left plot in Figure A-V-3, initially the concentration of MBrP decreased, while the concentration of Cu^{II} increased. The maximum concentration of Cu^{II} was less than half of [MBrP]₀, and the maximum occurred at the same time as when almost all the initiator was consumed. After all the initiator was consumed, the concentration of Cu^{II} started to decrease, due to comproportionation.²⁶²

Figure A-V-3b shows the same data plotted as a semilogarithmic plot for the consumption of MBrP, and the production of Cu^{II}Br₂/Me₆TREN, assuming that activation

by Cu^0 was the rate limiting step.²⁶³ In that case, the plot of $\ln([\text{MBrP}]_0/([\text{MBrP}]_0 - 2[\text{Cu}^{\text{II}}\text{Br}_2/\text{Me}_6\text{TREN}]_t))$ should be linear with the same slope as the plot of $\ln([\text{MBrP}]_0/[\text{MBrP}]_t)$. In the simplest case, the slope of $\ln([\text{MBrP}]_0/[\text{MBrP}]_t)$ corresponds to $2(S/V) \times k_{a0}^{\text{app}}$ since each activation by Cu^0 forms a radical and a $\text{Cu}^{\text{I}}/\text{Me}_6\text{TREN}$ species. The intermediate $\text{Cu}^{\text{I}}/\text{Me}_6\text{TREN}$ activates a second alkyl halide, which forms a second radical, and both the radicals ultimately terminate, giving $\text{Cu}^{\text{II}}\text{Br}_2/\text{Me}_6\text{TREN}$. This implies the loss of MBrP occurs at twice the rate of increase of $\text{Cu}^{\text{II}}\text{Br}_2/\text{Me}_6\text{TREN}$, which is why the plot of $\ln([\text{MBrP}]_0/([\text{MBrP}]_0 - 2[\text{Cu}^{\text{II}}\text{Br}_2/\text{Me}_6\text{TREN}]_t))$ should be similar to the slope of $\ln([\text{MBrP}]_0/[\text{MBrP}]_t)$. The data show an initial linear plot, which increases in curvature due to a progressive buildup of Cu^{I} species via comproportionation, similar to the data of Nicolas *et al.*²⁶³

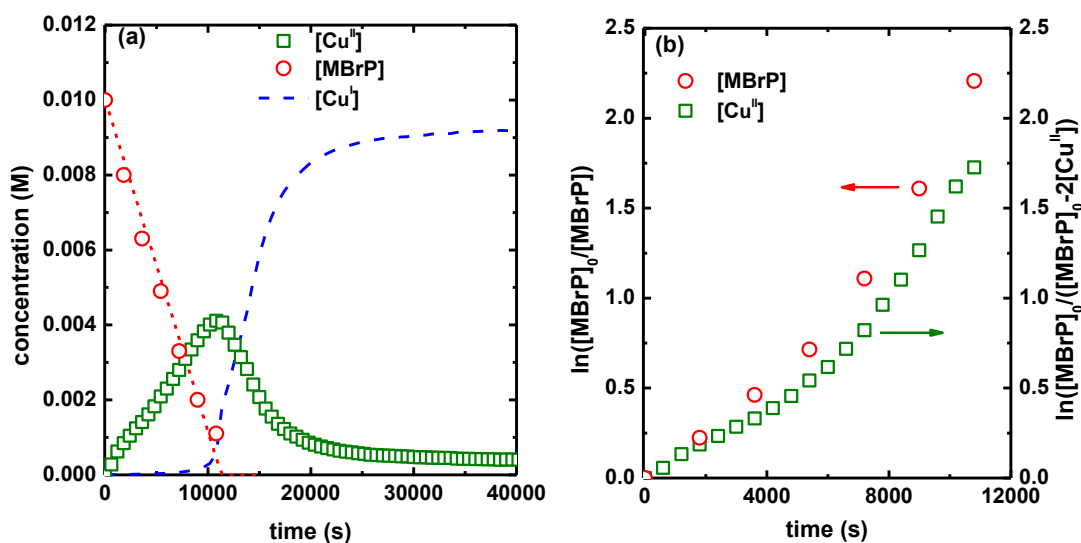


Figure A-V-3. (a) Time-evolution of $[\text{Cu}^{\text{II}}]$ and $[\text{MBrP}]$ measured by UV/Vis/NIR spectrum and GC, respectively $[\text{MBrP}] + [\text{Cu}^{\text{I}}]$ was calculated as $[\text{MBrP}]_0 - 2[\text{Cu}^{\text{II}}]$ because of halogen conservation. (b) Plot of $\ln([\text{MBrP}]_0/[\text{MBrP}]_t)$ vs. time and

$\ln([MBrP]_0/([MBrP]_0 - 2[Cu^{II}Br_2/Me_6TREN]))$ vs. time. Conditions: 25 °C; $[Me_6TREN]_0/[MBrP]_0 = 15 \text{ mM}/10 \text{ mM}$ in DMSO; $V = 7 \text{ mL}$; Cu^0 wire $l = 4 \text{ cm}$, $S = 1.27 \text{ cm}^2$, $S/V = 0.18 \text{ cm}^{-1}$.

The semilogarithmic plot of $[MBrP]$ vs. time is nearly linear, up to a value of *ca.* 0.7, or over the first 5400 s, indicating a relatively constant loss of MBrP due to activation and termination. Similarly, the $[Cu^{II}Br_2/Me_6TREN]$ vs. time semilogarithmic plot is linear up to a value of *ca.* 0.6, or within the first 5400 s. Then it accelerated due to comproportionation, consuming a small fraction of $Cu^{II}Br_2/Me_6TREN$ before the majority of the MBrP was consumed. From the consumption of MBrP the slope of the semilogarithmic plot is $1.3 \times 10^{-4} \text{ s}^{-1}$, over the range 0 to 5400 s, which provides a Cu^0 activation rate coefficient of $3.6 \times 10^{-4} \text{ cm s}^{-1}$. Similarly, from the generation of Cu^{II} , the slope of the semilogarithmic plot $9.6 \times 10^{-5} \text{ s}^{-1}$, over the range 0 to 5400 s, providing an activation rate coefficient of $2.6 \times 10^{-4} \text{ cm s}^{-1}$. This value is similar to the one reported by Nicolas *et al.*²⁶³ of $2.5 \times 10^{-4} \text{ cm s}^{-1}$,²⁶³ despite the fact that the initiator and ligand used in this study and in their study were different. After almost all the MBrP was consumed, the concentration of Cu^{II} species decreased to a low level. This decrease in the concentration of Cu^{II} resulted from comproportionation, which also occurred before all the initiator was consumed. However, the activation by Cu^0 and Cu^I and radical termination reactions were faster than comproportionation. Significant changes in the Cu^0 surface area can be ruled out, since the study of Nicolas *et al.*²⁶³ demonstrated that the same Cu^0 wire used into two subsequent reactions gave exactly the same results. The data in Figure A-V-3 showed a buildup of Cu^{II} species until the MBrP is consumed, which implies that the

comproportionation/disproportionation equilibrium can only be established after all the initiator is consumed. This is similar to the competitive equilibria phenomena outlined in various RDRP systems.²⁷²

General methodology for determining k_{a0}^{app} . As shown above, the rate coefficient k_{a0}^{app} can be measured by either the loss of alkyl halide or the accumulation of soluble Cu species, since the accumulation of Cu^I plus Cu^{II} must equal the consumption of Cu⁰, by the conservation of Cu atoms. Both methods give comparable values of the rate coefficient, particularly when the loss of alkyl halide was less than ~50% ($\ln([MBrP]_0/[MBrP]_t) < 0.75$). Since it was easier to measure the concentration of Cu^{II} spectroscopically, the Cu^{II} concentration was measured in all subsequent experiments to determine k_{a0}^{app} .

The change of soluble Cu species is given by:

$$\frac{d([Cu^I] + [Cu^{II}])}{dt} = \frac{S}{V} k_{a0}^{app} [R-X] + \frac{S}{V} k_{comp}^{app} [Cu^{II}] - \frac{S}{V} k_{d0}^{app} \frac{[Cu^I][R^\bullet]}{[L]} - \frac{S}{V} k_{disp}^{app} \frac{[Cu^I]^2}{[L]} \quad (\text{A-V-13})$$

since activation by Cu^I and deactivation by Cu^{II} do not change the overall Cu concentration. In equation (A-V-13), [R-X] is the concentration of all alkyl halides, [R[•]] is the concentration of all propagating radicals, [Cu^I] is the concentration of all Cu^I species, [Cu^{II}] is the concentration of all Cu^{II} species, and [L] is the ligand concentration.

The reactions involving Cu⁰ depend on surface area, therefore the ratio of Cu⁰ surface

area to total reaction volume is an important parameter that appears in the rates of each reaction step. The first paper of this series showed that comproportionation dominates disproportionation, in DMSO and mixtures of MA and DMSO. Also, the decrease of $[\text{Cu}^{\text{II}}]$ species after the consumption of the alkyl halide, as shown in Figure A-V-3, confirms that comproportionation dominates disproportionation. This implies that the final term can be safely neglected. Furthermore, deactivation by Cu^{I} species contributes very little in both SARA ATRP and SET-LRP models and can be neglected. Additionally, in the early phase of the reaction, the concentration of Cu^{II} species is much lower than $[\text{MBrP}]$, indicating that comproportionation should be slower than activation by Cu^0 . Therefore, at relative low consumption of the alkyl halide, *i.e.*, when $[\text{Cu}^{\text{II}}]$ is much less than half the value at the maximum, the activation by Cu^0 should be faster than comproportionation. This implies that in this early phase of the overall reaction, the change in soluble Cu species is predominantly given by the rate of activation by Cu^0 . Under these assumptions, equation (A-V-13) can be simplified to:

$$\frac{d([\text{Cu}^{\text{I}}] + [\text{Cu}^{\text{II}}])}{dt} = \frac{S}{V} k_{\text{a0}}^{\text{app}} [\text{R-X}] \quad (\text{A-V-14})$$

This equation can be rewritten as:

$$\frac{d[\text{Cu}^{\text{II}}]}{dt} \left(1 + \frac{d[\text{Cu}^{\text{I}}]}{d[\text{Cu}^{\text{II}}]}\right) = \frac{S}{V} k_{\text{a0}}^{\text{app}} [\text{R-X}] \quad (\text{A-V-15})$$

Once the ATRP equilibrium is established, the $[\text{Cu}^{\text{I}}]/[\text{Cu}^{\text{II}}]$ ratio should follow equation (A-V-16):

$$\frac{[\text{Cu}^{\text{I}}]}{[\text{Cu}^{\text{II}}]} = \frac{1}{K_{\text{ATRP}}} \frac{[\text{R}^\bullet]}{[\text{R-X}]} \quad (\text{A-V-16})$$

Therefore, because of a relatively constant radical and alkyl halide concentration,

$$\frac{d[\text{Cu}^{\text{I}}]}{d[\text{Cu}^{\text{II}}]} = \frac{[\text{Cu}^{\text{I}}]}{[\text{Cu}^{\text{II}}]} = \frac{1}{K_{\text{ATRP}}} \frac{[\text{R}^\bullet]}{[\text{R-X}]}, \text{ and consequently,}$$

$$\frac{d[\text{Cu}^{\text{II}}]}{dt} \left(1 + \frac{[\text{Cu}^{\text{I}}]}{[\text{Cu}^{\text{II}}]}\right) = \frac{S}{V} k_{\text{a0}}^{\text{app}} [\text{R-X}] \quad (\text{A-V-17})$$

In model systems in DMSO, the value of K_{ATRP} is very high at 2.3×10^{-4} ,²⁶⁶ which implies that at typical radical concentrations of 10^{-8} M and 10 mM concentrations of the alkyl halide, $[\text{Cu}^{\text{II}}]$ is 230 times higher than $[\text{Cu}^{\text{I}}]$. Therefore, in the model experiments conducted in pure DMSO, almost all the increase in soluble Cu species is in the form of Cu^{II} , therefore equation (A-V-17) can be simplified to allow to be determined from the initial slope of $[\text{Cu}^{\text{II}}]$ with time:

$$\frac{d[\text{Cu}^{\text{II}}]}{dt} = \frac{S}{V} k_{\text{a0}}^{\text{app}} [\text{R-X}] \quad (\text{A-V-18})$$

In an actual polymerization, the radical concentration can be determined from the consumption of monomer, since $d[\text{M}]/dt = -k_p[\text{R}^\bullet][\text{M}]$. At a constant radical concentration, the slope of the semilogarithmic plot of monomer conversion vs. time is proportional to the radical concentration, since $d\ln[\text{M}]/dt = -k_p[\text{R}^\bullet]$, providing a value of $[\text{R}^\bullet]$. The values of $[\text{R}^\bullet]$, $[\text{R-X}]$ and the K_{ATRP} value can be substituted into equation 16 to determine the $[\text{Cu}^{\text{I}}]/[\text{Cu}^{\text{II}}]$ ratio. Therefore, the activation rate constant can be determined from the slope of $[\text{Cu}^{\text{II}}]$ vs. time using equation (A-V-17).

Model study in DMSO with different lengths of Cu⁰ wire. Measurements of k_{a0}^{app} were performed in DMSO using Cu⁰ wire of different lengths (16, 4 and 2 cm, *i.e.*, $S = 5.04, 1.27$ and 0.64 cm^2 , respectively), MBrP as the initiator in the presence of an excess of Me₆TREN ligand. As highlighted above, at sufficiently low consumption of MBrP, the value of k_{a0}^{app} can be determined from the rate of consumption of the initiator and is the same as the value of k_{a0}^{app} determined from the generation of Cu^{II}. Therefore, for convenience, the Cu^{II} concentration, rather than the consumption of MBrP, was measured.

Figure A-V-4a shows the increase in the concentration of Cu^{II} with time during the early period of the reaction, and Figure A-V-4b shows the slope, $d[\text{Cu}^{\text{II}}]/dt$, proportional to the surface area. The full evolution of the $[\text{Cu}^{\text{II}}]$ profile over time is shown in Figure A-V-5, and each curve is qualitatively similar to that shown in Figure A-V-3a. Interestingly, the evolution of $[\text{Cu}^{\text{II}}]$ with time is approximately linear, even when a significant amount of the alkyl halide has been consumed. This is caused by the contribution of comproportionation, increasing at a rate comparable to the decrease in Cu⁰ activation. This interesting feature, unique to DMSO, was reported by Nicolas *et al.*²⁶³ In this case the decrease of activation rate caused by the decrease in the concentration of the alkyl halide, is compensated by an increase in $[\text{Cu}^{\text{I}}]$ formed by comproportionation. A value of the Cu⁰ activation rate coefficient (corrected for surface to volume dimensions) can be determined from the slope of $d[\text{Cu}^{\text{II}}]/dt$, using equation (A-V-18). The calculated values are $k_{a0}^{app} = 2.1 \times 10^{-4}, 2.4 \times 10^{-4}$ and $1.9 \times 10^{-4} \text{ cm s}^{-1}$, for 2, 4 and 16 cm ($S = 0.64, 1.27, 5.04 \text{ cm}^2$) of Cu⁰. They are in good agreement with the values measured from the semilogarithmic plots in

Figure A-V-3b.

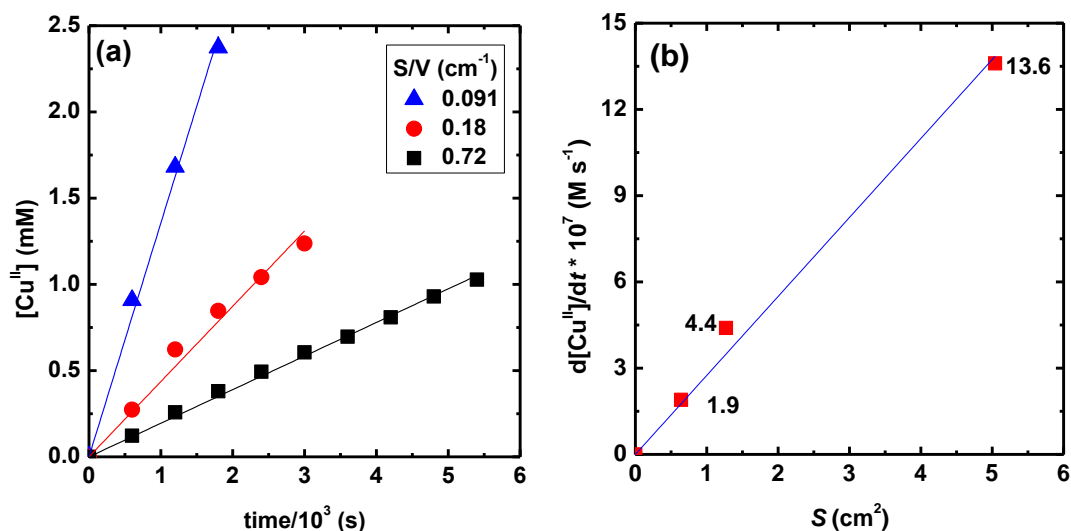


Figure A-V-4. Plots of (a) $[\text{Cu}^{\text{II}}]$ with time; and (b) $d[\text{Cu}^{\text{II}}]/dt$ vs. Cu^0 wire surface area for model reaction between Cu^0 wire ($d = 1$ mm) and 10 mM MBrP in the presence of 15 mM Me_6TREN in 7 mL DMSO at 25 °C. The lengths of Cu^0 wire were 2, 4 and 16 cm ($S = 0.64$, 1.3, 5.0 cm^2 , $S/V = 0.091$, 0.18, 0.72 cm^{-1}), giving $k_{a0}^{\text{app}} = 2.1 \times 10^{-4}$, 2.4×10^{-4} and 1.9×10^{-4} cm s^{-1} , respectively.

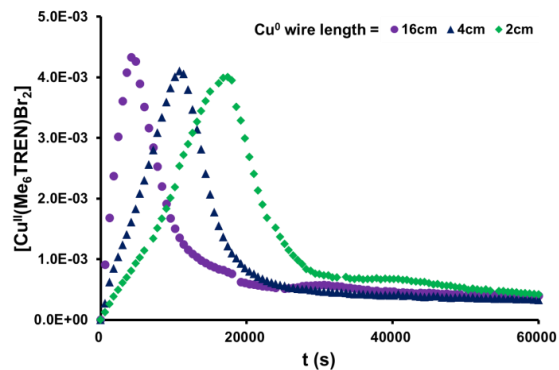


Figure A-V-5. Plots of $[\text{Cu}^{\text{II}}]$ vs. time for model reaction between Cu^0 wire ($d = 1$ mm)

and 10 mM MBrP in the presence of 15 mM Me₆TREN in 7 mL DMSO. The lengths of Cu⁰ wire were 2, 4 and 16 cm ($S = 0.64, 1.27, 5.04 \text{ cm}^2$).

Model study on the effect of different ratios of ligand to MBrP in DMSO. In the absence of ligand, the activation of MBrP by zero valent metals is very slow but it is strongly accelerated when ligand is present.^{251b} Figure A-V-6a shows the results of the kinetic measurements with different initial concentrations of ligand, performed with 4 cm Cu⁰ and $[\text{Me}_6\text{TREN}]_0/[\text{MBrP}]_0 = X \text{ mM}/10 \text{ mM}$ ($X = 20, 10, 5, 4, 2.5, 1$) in 7 mL DMSO. When $[\text{Me}_6\text{TREN}]_0/[\text{MBrP}]_0 > 0.4$ (Figure A-V-6a), the evolution of $[\text{Cu}^{\text{II}}]$ shows a maximum, after which time it decreases due to a progressive (although slow) comproportionation reaction. In these three systems, with excess ligand, $[\text{Cu}^{\text{II}}]$ decreased after reaching the maximum value and the final Cu^{II} concentration directly depended on the initial ligand concentration. Figure A-V-6b shows that in the presence of a sufficient concentration of ligand, it had a small influence on the initial slope of $[\text{Cu}^{\text{II}}]$ vs. time, indicating that k_{a0}^{app} was not affected by $[\text{Me}_6\text{TREN}]_0$. The k_{a0}^{app} value calculated from Figure A-V-4b and Figure A-V-6b gave an average value of $k_{a0}^{\text{app}} = 1.8 \times 10^{-4} \text{ cm s}^{-1}$. The initial rate of increase of $[\text{Cu}^{\text{II}}]$ is similar, regardless of the concentration of Me₆TREN, except for the 1 mM case. This is important since many polymerizations use a $[\text{Me}_6\text{TREN}]_0$ between 2 and 5 mM, indicating that the red and green traces are the monomer free analogues of typical polymerization conditions. Interestingly, the increase in the rate of Cu^{II} formation with higher ligand concentrations, followed by a plateau, is similar to the experiments of Percec *et al.* which show an increase in polymerization rate, followed by a plateau observed in the polymerization rate.²⁷³ This behavior was described by Nicolas *et*

al. as ligand adsorption onto the Cu^0 surface, first followed by reaction of the alkyl halide with the ligand coated Cu surface, as per Eley–Rideal kinetics.²⁶³

The reactions with higher concentrations of ligand showed a larger decrease of $[\text{Cu}^{\text{II}}]$ than those with lower concentrations of the ligand. This observation agrees with prior comproportionation/disproportionation equilibrium studies, which showed that the equilibrium shifted from Cu^{II} towards Cu^{I} with higher ligand concentrations.²⁶² However, at $[\text{Me}_6\text{TREN}]_0/[\text{MBrP}]_0 < 0.4$ (Figure A-V-6a), no maximum in the concentration of Cu^{II} was detected which indicates that efficient comproportionation requires the presence of sufficient ligand to be available to bind all soluble Cu^{II} and Cu^{I} species, because ligand binds much stronger to the Cu^{II} species than to the Cu^{I} species.^{30a, 274} At low concentrations of ligand, the system could contain a mixture of both $\text{Cu}^{\text{II}}\text{Br}_2/\text{Me}_6\text{TREN}$ and $\text{Cu}^{\text{II}}\text{Br}_2$, and therefore the concentration of total Cu^{II} species measured by UV/Vis/NIR is less precise than when it was measured with higher ligand concentrations. In order to confirm this trend experiments were conducted to measure the effect of ligand concentration on activation rate coefficient, activation experiments in DMSO with 1 cm of Cu^0 , of diameter 1 mm were performed in 10 mL of DMSO ($S/V = 0.033 \text{ cm}^{-1}$). The results of the series with lower S/V ratio give the same conclusions, as those with higher S/V ratio.

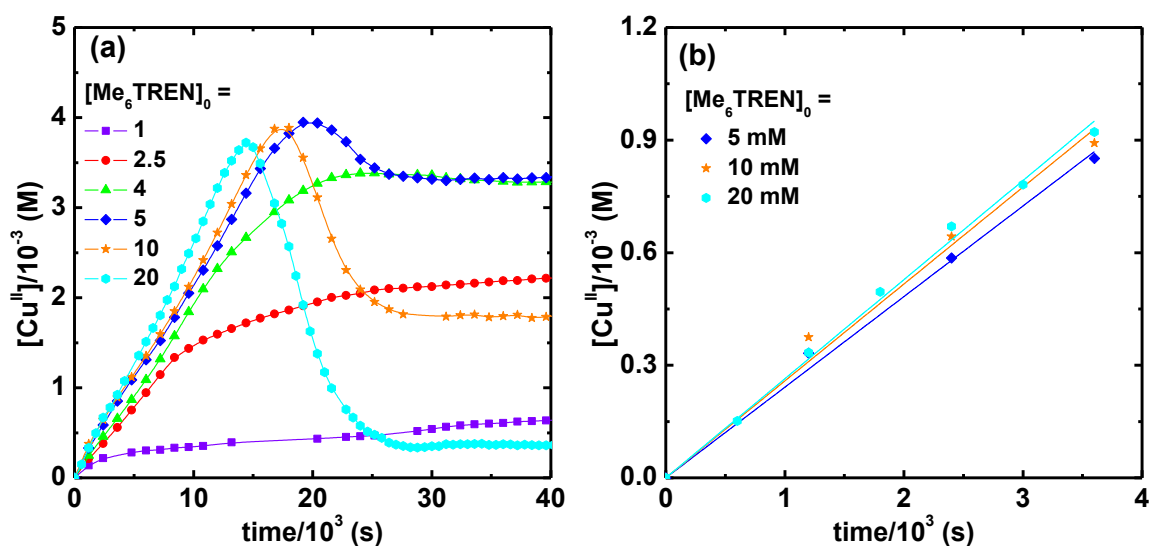


Figure A-V-6. Model reactions of 4 cm Cu^0 wire ($S = 1.27 \text{ cm}^2$) with 10 mM MBrP in the presence of different concentration of Me_6TREN (1 ~ 20 mM) in 7 mL DMSO at 25 °C ($S/V = 0.18 \text{ cm}^{-1}$). (a) Evolution of $[Cu^{II}]$ in all six experiments. (b) The initial plots of the three experiments with highest $[Me_6TREN]_0$, giving $k_{a0}^{app} = 1.3 \times 10^{-4}$, 1.4×10^{-4} and $1.4 \times 10^{-4} \text{ cm s}^{-1}$.

In real polymerization systems of acrylates, the ratio of initial concentrations of alkyl halide to ligand exceeds value of 10 and the reactions are typically stopped when the consumption of alkyl halide is very low ($< 3\%$). Therefore, the ratio of ligand to soluble Cu ratio remains relatively high.

Measurement of k_{a0}^{app} during polymerization. Four SARA ATRP experiments were performed in both MeCN and DMSO, with both TPMA and Me_6TREN ligands to measure the activation rate coefficient of Br-terminated poly(methyl acrylate) by Cu^0 . SARA ATRP of MA was performed in MA/DMSO = 1/1 (v/v) with the ratio

$[MA]_0/[MBrP]_0/[Me_6TREN]_0 = 200/1/0.1$, in the presence of 1 cm Cu^0 wire with $d = 0.25$ mm with a total volume of 10 mL. The concentration of Cu^{II} increased linearly with time and reached $[Cu^{II}] = 0.18$ mM after 150 min, which was 150 times lower than the initial concentration of MBrP, and approximately 15 times lower than the initial concentration of Me_6TREN . This implies that the loss of bromine functionality from both small molecule and polymeric species was below 3%, indicating high chain end functionality. Under these conditions, of a well-controlled polymerization, the contribution of comproportionation should be minimal, due to the low concentration of Cu^{II} relative to MBrP. Furthermore, since the ratio of $[L]/([Cu^{II}] + [Cu^I])$ was greater than 10/1, the extent of disproportionation should be negligible, in the polymerization medium, indicating that $[Cu^{II}]$ can safely be used to determine k_{a0}^{app} .²⁶²

Under these conditions, comproportionation was slower than activation by Cu^0 . A linear first order kinetic plot up to 40% monomer conversion is shown in Figure A-V-7b. The values of $[R^\bullet] = 3.9 \times 10^{-9}$ M was calculated from the slope $d\ln[M]/dt = -k_p[R^\bullet]$ and the known value of $k_p = 15600 \text{ M}^{-1} \text{ s}^{-1}$ at 25 °C. A value of $[Cu^{II}]/[Cu^I] = 22$ was calculated using equation (A-V-16), based on values $[MBrP]_0 = 0.0278 \text{ M}$, and $K_{ATRP} = 3.1 \times 10^{-6}$.²⁶⁶ This value for $[Cu^{II}]/[Cu^I]$ was used in equation (A-V-17), to calculate $k_{a0}^{app} = 1.0 \times 10^{-4} \text{ cm s}^{-1}$. The k_{a0}^{app} measured in a polymerization was similar to the one measured in the model system, validating the use of model systems to characterize polymerization systems.

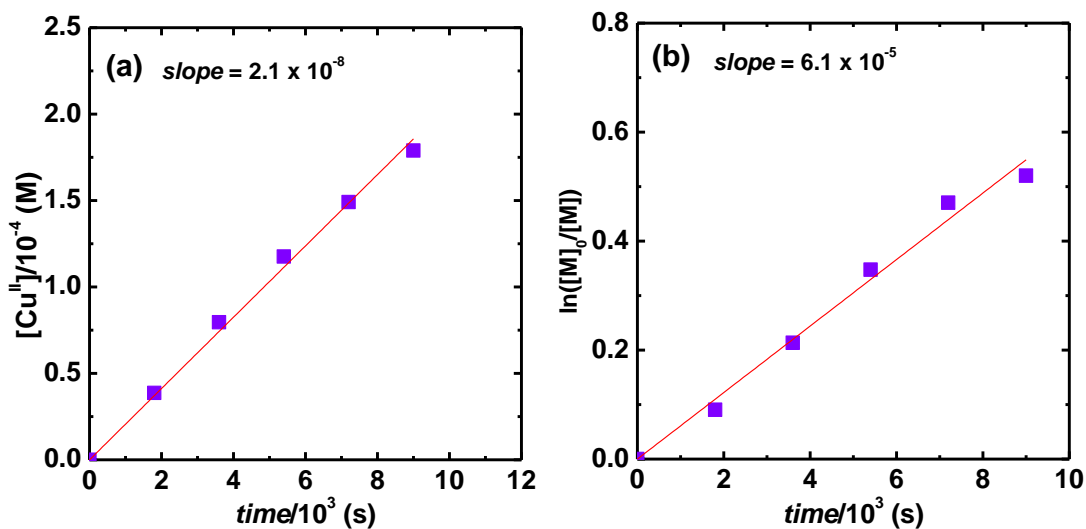


Figure A-V-7. Plots of (a) $[\text{Cu}^{\text{II}}]$ with time; and (b) $\ln([M]_0/[M])$ vs. time in SARA ATRP in MA/DMSO = 1/1 (v/v) with the ratio of reagents $[\text{MA}]_0/[\text{MBrP}]_0/[\text{Me}_6\text{TREN}]_0 = 200/1/0.1$, at 25 °C, in the presence of Cu^0 wire ($d = 0.25 \text{ mm}$, $l = 1 \text{ cm}$), the total volume 10 mL, $[\text{MBrP}]_0 = 0.0278 \text{ M}$, $S = 7.95 \times 10^{-2} \text{ cm}^2$, and $S/V = 7.95 \times 10^{-3} \text{ cm}^{-1}$.

It is important to note that the buildup of Cu^{II} during a polymerization originates from termination reactions and can be quantified, following the principle of halogen conservation.^{260a} If $[\text{Cu}^{\text{I}}] \ll [\text{Cu}^{\text{II}}]$, essentially all halogen atoms lost from the chain ends must be transferred to Cu^{II} species. Therefore, the rate of Cu^{II} formation corresponds to twice the rate of loss of chain end functionality, the latter is given by $-d[\text{P}_n\text{-X}]/dt$. Values of k_t^{app} can be calculated from equation (A-V-19), knowing the rate of Cu^{II} formation:

$$-\frac{d[\text{P}_n\text{-X}]}{dt} = 2\frac{d[\text{Cu}^{\text{II}}]}{dt} = 2k_t^{\text{app}}[\text{R}^\bullet]^2 \quad (\text{A-V-19})$$

Interestingly, a value of $k_t^{\text{app}} = 1.4 \times 10^9 \text{ M}^{-1} \text{ s}^{-1}$ was calculated from the slope

$d[\text{Cu}^{\text{II}}]/dt = 2.1 \times 10^{-8} \text{ M s}^{-1}$ experimentally measured by UV-Vis spectroscopy and $[\text{R}^\bullet] = 3.9 \times 10^{-9} \text{ M}$, as shown in Figure A-V-7a-b. This value $k_t^{\text{app}} = 1.4 \times 10^9 \text{ M}^{-1} \text{ s}^{-1}$ is higher than the value for conventional radical termination.²⁷⁵ Recent reports showed a possibility of additional termination events induced by copper species.²⁷⁶

Similar experiments were performed with different ligands and solvents. The rate coefficient of activation of MBrP by Cu^0 were $k_{a0}^{\text{app}} = 3 \times 10^{-4} \text{ cm s}^{-1}$ (Me_6TREN , MeCN), $6 \times 10^{-5} \text{ cm s}^{-1}$ (TPMA, DMSO) and $2 \times 10^{-4} \text{ cm s}^{-1}$ (TPMA, MeCN) (Table A-V-2). The k_{a0}^{app} values in the presence of TPMA were calculated using equation (A-V-17), since the fraction of Cu^{I} could not be neglected.

In all cases, the similarity and relatively low values for k_{a0}^{app} showed that Cu^0 reacted slowly with the alkyl halide in both DMSO and MeCN , and in the presence of both ligands Me_6TREN and TPMA. The activity of Cu^0 with Me_6TREN was ~ 1.5 larger than with TPMA and it was also ~ 3.5 larger in MeCN than in DMSO . Interestingly, both the solvent and ligand had a smaller effect on k_{a0}^{app} than on k_{a1}^{app} .^{16, 64b, 94c} Although the conditions used for the polymerization and for model reactions were quite different, they provided very similar values of k_{a0}^{app} . In model studies a much larger surface area was used in order to accelerate and more precisely measure formation of Cu^{II} . The S/V ratios were approximately 1-2 orders of magnitude lower in a polymerization, than those used in the model systems, to minimize termination.

Table A-V-2. Rate coefficient of activation of PMA-Br by Cu⁰.^a

solvent	ligand	K_{ATRP}	$-\text{dln}[M]/\text{dt}$ (s ⁻¹)	$[\text{Cu}^{\text{I}}]/[\text{Cu}^{\text{II}}]$	$\text{d}[\text{Cu}^{\text{II}}]/\text{dt}$ (M s ⁻¹)	k_{a0}^{app} (cm s ⁻¹)
MA/DMSO	TPMA	2.2×10^{-7}	4.9×10^{-5}	0.5	8.5×10^{-9}	5.8×10^{-5}
MA/DMSO	Me ₆ TREN	3.2×10^{-6}	6.1×10^{-5}	0.05	2.1×10^{-8}	1.0×10^{-4}
MA/MeCN	TPMA	2.5×10^{-8}	2.4×10^{-5}	2	1.6×10^{-8}	2.3×10^{-4}
MA/MeCN	Me ₆ TREN	3.2×10^{-7}	9.2×10^{-5}	0.06	4.3×10^{-8}	3.2×10^{-4}

^a SARA ATRP of MA in different solvents and with different ligands with the ratio of reagent $[\text{MA}]_0/[\text{MBrP}]_0/[\text{Me}_6\text{TREN}]_0 = 200/1/0.1$, MA/solvent = 1/1 (v/v), at 25 °C, in the presence of 1 cm Cu⁰ wire with $d = 0.25$ mm and the total volume 10 mL, $[\text{MBrP}]_0 = 0.0278$ M, $S = 7.95 \times 10^{-2}$ cm², $S/V = 7.95 \times 10^{-3}$ cm⁻¹. k_{a0}^{app} values were calculated based on equations 16-17, $k_p = 1.6 \times 10^4$ M⁻¹ s⁻¹,²⁷⁷ and K_{ATRP} values were from ref²⁶⁶.

Three additional experiments of SARA ATRP of MA were performed in MA/DMSO = 1/1 (v/v) with Me₆TREN using different lengths of Cu⁰ wire ($d = 0.5$ mm, $l = 0.5$, 1 and 2 cm) and the total reaction volume of 10 mL, with the ratio of reagents $[\text{MA}]_0/[\text{MBrP}]_0/[\text{Me}_6\text{TREN}]_0 = 200/1/0.1$. The accumulation of Cu^{II} increased linearly with the surface area of Cu⁰, which indicated that the activation of alkyl halides by Cu⁰ is proportional to the surface area, Figure A-V-8. In all cases the ratio of $[\text{Cu}^{\text{II}}]/[\text{Cu}^{\text{I}}]$ was larger than 5. The k_{a0}^{app} values were calculated as 1.0×10^{-4} , 9×10^{-5} and 1.2×10^{-4} cm s⁻¹ for 0.5, 1 and 2 cm Cu⁰ wire, respectively. An average value of k_{a0}^{app} based on these four experiments in Table A-V-2 and Figure A-V-8 was calculated to be 1.0×10^{-4} cm s⁻¹ for SARA ATRP of MA in MA/DMSO = 1/1 (v/v) at 25 °C with Me₆TREN as the ligand.

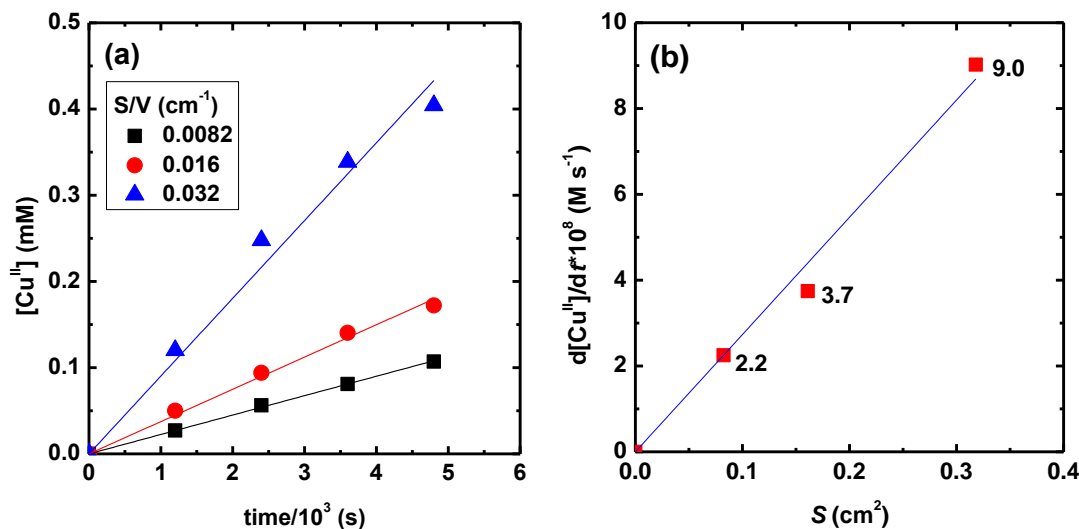


Figure A-V-8. Plots of (a) $[\text{Cu}^{\text{II}}]$ with time; and (b) $d[\text{Cu}^{\text{II}}]/dt$ vs. Cu^0 wire surface area for SARA ATRP of MA in 10 mL MA/DMSO = 1/1 (v/v) with the ratio of reagents $[\text{MA}]_0/[\text{MBrP}]_0/[\text{Me}_6\text{TREN}]_0 = 200/1/0.1$, at 25 °C, in the presence of different length of Cu^0 wire ($d = 0.5$ mm, $l = 0.5$, 1 and 2 cm, $S = 0.082$, 0.16 and 0.32 cm^2 , $S/V = 0.0082$, 0.016, and 0.032 cm^{-1}). $k_{a0}^{\text{app}} = 1.0 \times 10^{-4}$, 9.1×10^{-5} and 1.2×10^{-4} cm s^{-1} , respectively. The average value of k_{a0}^{app} for the four experiments in Table A-V-2 and Figure 8 is 1.0×10^{-4} cm s^{-1} .

Kinetics of Cu^0 activation measured by electrochemistry. Electrochemistry was used as a complementary method to measure the activation rate coefficient of alkyl halides by Cu^0 . In this system, a copper plated electrode with known surface area was used to study MBrP activation in the presence of a solution Me_6TREN in DMSO. Initially, cyclic voltammetry was applied to a solution of $[\text{Cu}^{\text{II}}\text{Br}_2/\text{Me}_6\text{TREN}]_0 = 15$ mM, $[\text{TBAClO}_4] = 0.2$ M in DMSO with a total volume 25 mL (30 μL of DMF was used as internal standard for NMR), at $T = 60$ °C. The cyclic voltammogram, illustrated in Figure A-V-10a, showed

a typical $\text{Cu}^{\text{II}}/\text{Cu}^{\text{I}}$ couple at 0.025 V with respect to $\text{Ag}/\text{AgI}/\text{I}^-$, as a continuous trace. The second dashed trace shows a second irreversible cathodic peak at more negative potential, which corresponds to the reduction of Cu^{I} to Cu^0 . Thus, a more reducing potential of -0.6 V vs. $\text{Ag}/\text{AgI}/\text{I}^-$ was applied to prepare a Cu^0 working electrode with a surface area 4.5 cm^2 . The surface roughness could increase the surface area beyond the 4.5 cm^2 of the foil, due to the deposition process. The Pt foil electrode before and after deposition of Cu is shown in Figure A-V-9. When the current decreased to very low values, the reaction mixture became colorless and most of copper was deposited on the electrode. During the deposition, a charge of 46 C, *i.e.*, 0.48 mmol of electrons, were passed. Since the deposition of Cu^0 from Cu^{II} requires two electrons, this result implies that 0.24 mmol of Cu were deposited on the electrode. Using the density of Cu of 8.96 g/cm^3 , the area occupied by a single Cu atom on the surface should be $5.2 \times 10^{-16} \text{ cm}^2$, which implies that a monolayer 4.5 cm^2 surface should consist of 8.7×10^{15} Cu atoms, or, 1.4×10^{-8} mol of Cu atoms. Therefore, there should be approximately 17000 monolayers of Cu deposited on the Pt foil electrode.

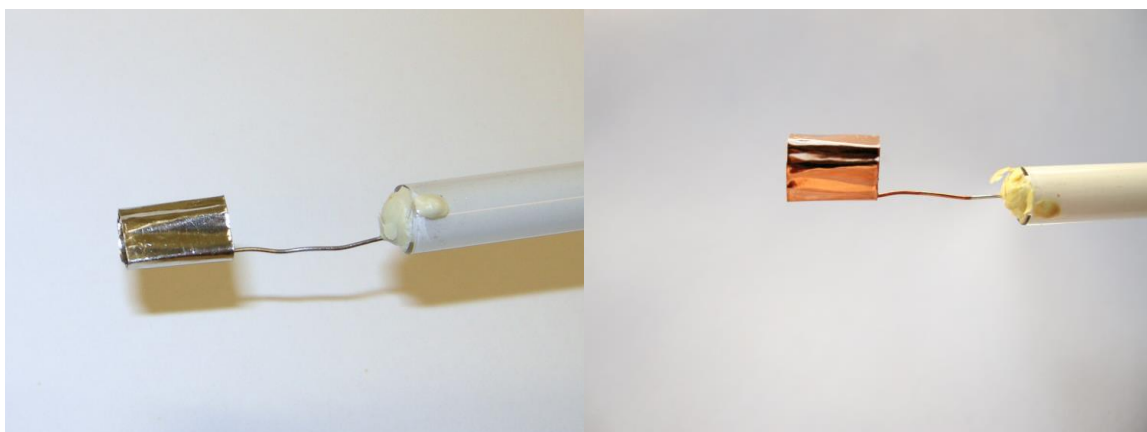


Figure A-V-9. Pt foil electrode of area 4.5 cm^2 before (left) and after Cu^0 deposition (right)

under the conditions: $[\text{Cu}^{\text{II}}\text{Br}_2/\text{Me}_6\text{TREN}]_0 = 15 \text{ mM}$, $[\text{TBAClO}_4] = 0.2 \text{ M}$ in a total volume 25 mL (30 mL of DMF used as internal standard for NMR), at $T = 60 \text{ }^\circ\text{C}$ in DMSO.

The temperature was subsequently decreased to $T = 25 \text{ }^\circ\text{C}$, and a potential of -0.7 V was applied, to force any Cu^{I} formed in the activation experiment to be reduced back to Cu^0 . Once the temperature and potential were stabilized, the MBrP was added, $[\text{MBrP}]_0 = 11 \text{ mM}$. The consumption of initiator is shown as a semilogarithmic plot in Figure A-V-10b. The slope of the semi-logarithmic plot is $6 \times 10^{-5} \text{ s}^{-1}$. The slope of the semilogarithmic plot, equal to $(S/V) \times k_{a0}^{\text{app}}$, gave a value for $k_{a0}^{\text{app}} = 3 \times 10^{-4} \text{ cm s}^{-1}$, which is similar, although larger than the values measured without electrochemistry. This larger value of k_{a0}^{app} is most likely because in the electrochemical experiments, some of the $\text{Cu}^{\text{I}}/\text{L}$, generated by the reaction between an alkyl halides and Cu^0 , activated a second alkyl halide before being reduced back to Cu^0 .

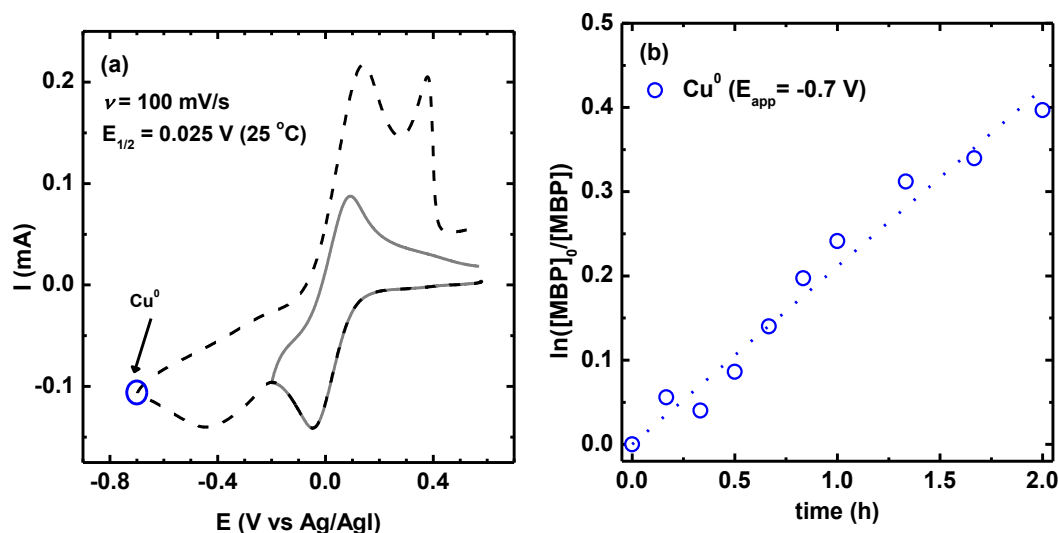


Figure A-V-10. Electrochemical measurement of the activation of alkyl halides by Cu^0 . (a) Cyclic voltammogram of a DMSO solution of $[\text{Cu}^{\text{II}}\text{Br}_2/\text{Me}_6\text{TREN}]_0 = 15 \text{ mM}$, $[\text{TBAClO}_4] = 0.2 \text{ M}$ in a total volume of 25 mL (30 μL of DMF was used as internal standard for NMR), at $T = 60 \text{ } ^\circ\text{C}$, with sweep rate $\nu = 100 \text{ mV/s}$. The continuous trace illustrates the $\text{Cu}^{\text{I/II}}$ couple only, the dashed trace shows a wider sweep range, including the $\text{Cu}^{0/\text{I}}$ couple. The potential used in the Cu^0 activation experiment is highlighted. (b) Semilogarithmic plot for the consumption of the initiator over time at the applied potential of -0.7 V (vs. Ag/AgI/I $^-$), $[\text{MBrP}]_0 = 11 \text{ mM}$, $[\text{Me}_6\text{TREN}]_0 = 15 \text{ mM}$, $T = 25 \text{ } ^\circ\text{C}$, using a 4.5 cm^2 Cu deposited electrode, $S/V = 0.18 \text{ cm}^{-1}$.

Similar results were obtained when the DMSO was replaced by $\text{MA/DMSO} = 2/1$ (v/v), *i.e.*, under polymerization conditions using $E_{\text{app}} = -0.5 \text{ V}$ (vs. Ag/AgI/I $^-$). As shown in Figure A-V-11, the reaction initiated by MBrP took 2.5 h to reach *ca.* 70% conversion. Very high molecular weight polymers were formed, $M_n > 100000$, and $M_w/M_n > 2$, indicating a poorly controlled polymerization. The values of M_n vs. conversion shown in

Figure A-V-11 were used to estimate the amount of newly generated chains, *i.e.* the amount of consumed MBrP, giving a value of $k_{a0}^{app} = 9.0 \times 10^{-5} \text{ cm s}^{-1}$, assuming, due to very low concentration of Cu^{II} , termination predominantly by coupling and no intermittent deactivation.

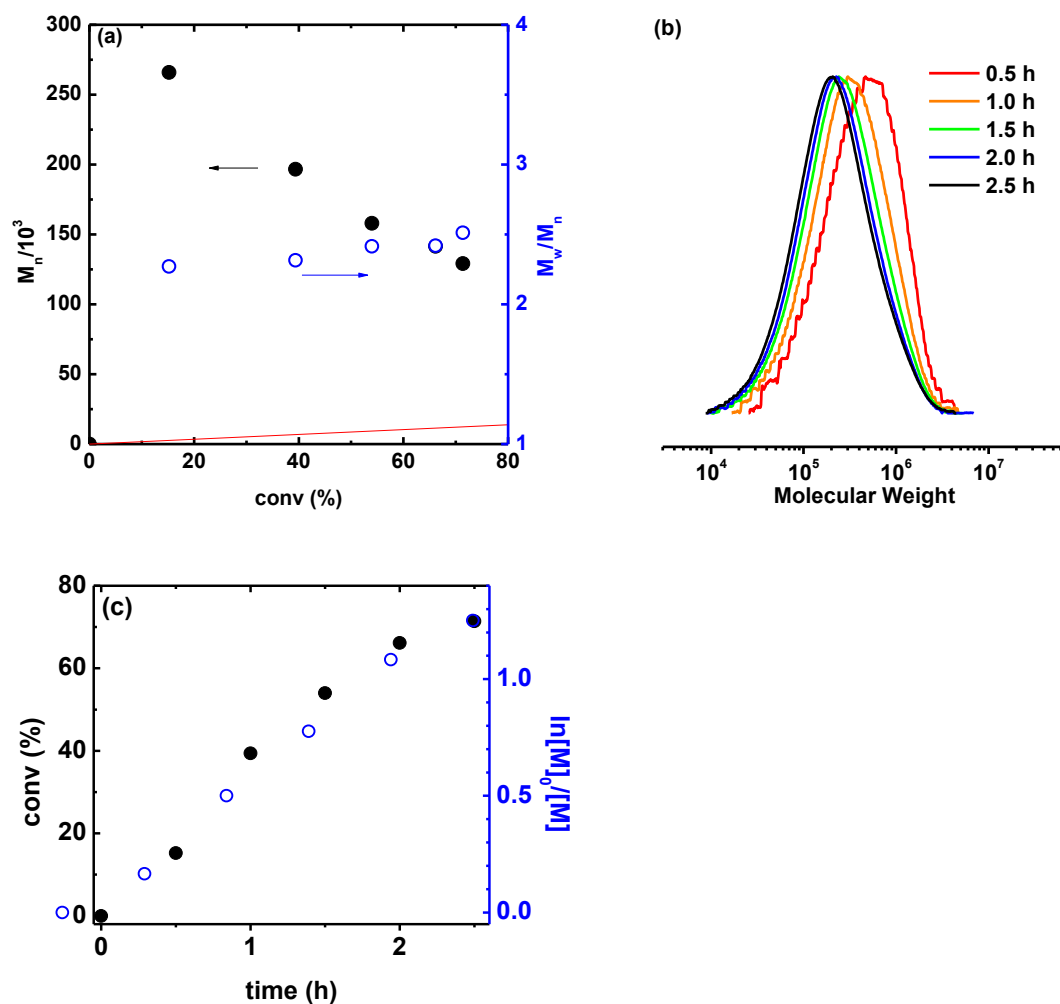


Figure A-V-11. Polymerization of MA under electrochemical conditions, with activation of alkyl halides by Cu^0 . Cu^0 was deposited onto the Pt electrode ($A = 4.5 \text{ cm}^2$): $[\text{Cu}^{\text{II}}\text{Br}_2/\text{Me}_6\text{TREN}]_0 = 15 \text{ mM}$, $[\text{TBAClO}_4] = 0.2 \text{ M}$ in a total volume 25 mL, at $T = 40 \text{ }^\circ\text{C}$,

$E_{app} = -0.6 \text{ V}$ (vs. $\text{Ag}/\text{AgI}/\text{I}^-$) for 22 h. Polymerization conditions: $[\text{MA}]_0/[\text{MBP}]_0/[\text{Me}_6\text{TREN}]_0 = 200/1/0.5$, $[\text{TBAClO}_4] = 0.2 \text{ M}$ in a total volume 21 mL ($[\text{MA}]_0 = 7.4 \text{ M}$), $T = 25 \text{ }^\circ\text{C}$, $E_{app} = -0.5 \text{ V}$ (vs. $\text{Ag}/\text{AgI}/\text{I}^-$). (a) M_n and M_w/M_n values vs. conversion, solid red line shows predicted M_n with complete initiation (b) evolution of MWD, (c) monomer conversion and $\ln([\text{M}]_0/[\text{M}])$ vs. time (solid points are conversion and hollow points are $\ln([\text{M}]_0/[\text{M}])$).

Comparison of measured k_{a0}^{app} values. A summary of all measured values of k_{a0}^{app} is given in Table A-V-3. All values are in the range $5 \times 10^{-5} - 3 \times 10^{-4} \text{ cm s}^{-1}$, and no experiments gave an induction period. Generally, measurements conducted by following $[\text{MBrP}]$ gave larger values than by those following $[\text{Cu}^{\text{II}}]$ (entries 1-3). The following trends can be observed: (i) presence of less polar MA decreased values of k_{a0}^{app} *ca.* 2 times (entry 1, 4-5); (ii) activation in MeCN was faster than in DMSO (entry 5, 6); (iii) activation in the presence of TPMA was slower than with Me_6TREN (entry 5-8). Nevertheless, the differences are relatively small and all activation rate coefficients, using both commercially available Cu^0 wires or freshly deposited Cu^0 electrodes, are in the order of $k_{a0}^{app} = 10^{-4} \text{ cm s}^{-1}$, similar to values reported for other ligands and alkyl halides using nitroxide trapping.²⁶³ The agreement between these results, using different kinetic techniques and experiments, shows the consistency of the measured values of k_{a0}^{app} .

Table A-V-3. Summary of all measured rate coefficient of activation of $\text{MBrP}/\text{PMA-Br}$

by Cu⁰ at 25 °C.

Entry	Solvent	Ligand	Method	Conditions	k_{a0}^{app} (cm s ⁻¹)
1	DMSO	Me ₆ TREN	Conventional/ [Cu ^{II}] measured	[MBrP] ₀ = 10 mM, [Me ₆ TREN] ₀ = 1 - 20 mM	1.8 × 10 ⁻⁴ (average value)
2	DMSO	Me ₆ TREN	Conventional/ [MBrP] measured	[MBrP] ₀ = 11 mM, [Me ₆ TREN] ₀ = 15 mM	3.6 × 10 ⁻⁴
3	DMSO	Me ₆ TREN	Electrochemical/ [MBrP] measured	[Cu ^{II} Br ₂ /Me ₆ TREN] ₀ = 15 mM, [TBAClO ₄] = 0.2 M before deposition, then [MBrP] ₀ = 11 mM	3 × 10 ⁻⁴
4	MA/DMSO = 2/1 (v/v)	Me ₆ TREN	Electrochemical/ M_n & c measured	[MA] ₀ /[MBrP] ₀ /[Me ₆ TREN] ₀ = 200/1/0.5, [TBAClO ₄] = 0.2 M	9 × 10 ⁻⁵
5	MA/DMSO = 1/1 (v/v)	Me ₆ TREN	Conventional/ [Cu ^{II}] measured	[MA] ₀ /[MBrP] ₀ /[Me ₆ TREN] ₀ = 200/1/0.1	1.0 × 10 ⁻⁴
6	MA/MeCN = 1/1 (v/v)	Me ₆ TREN	Conventional/ [Cu ^{II}] measured	[MA] ₀ / [MBrP] ₀ /[Me ₆ TREN] ₀ = 200/1/0.1	3.2 × 10 ⁻⁴
7	MA/MeCN = 1/1 (v/v)	TPMA	Conventional/ [Cu ^{II}] measured	[MA] ₀ /[MBrP] ₀ /[TPMA] ₀ = 200/1/0.1	2.3 × 10 ⁻⁴
8	MA/DMSO = 1/1 (v/v)	TPMA	Conventional/	[MA] ₀ /[MBrP] ₀ /[TPMA] ₀ = 200/1/0.1	5.8 × 10 ⁻⁵

As discussed earlier, in the above calculations the surface of the Cu⁰ wire was taken to be the only source of Cu⁰ in solution. This is justified, on several grounds. In the experiments used to extract rate coefficients, there was a significant excess of ligand to soluble Cu species. As shown in the work of Percec *et al.*,²⁷⁸ and in our previous paper,²⁶² when there is a significant excess of ligand to soluble Cu species, the extent of disproportionation is negligible. Furthermore, the reaction medium can also affect the extent of disproportionation, and as shown in our earlier paper,²⁶² in pure DMSO the extent of disproportionation is minimal (*ca.* 95% of soluble Cu is Cu^I) and in the polymerization medium containing a mixture of MA and DMSO the extent of disproportionation is even lower (>97% of soluble Cu is Cu^I). Therefore, the amount of Cu⁰ particles generated by disproportionation is small in these experiments, and in polymerizations where there is a large excess of ligand to soluble copper. Furthermore, the experiment of Percec *et al.*²⁷¹ confirms that the 99% of the Cu⁰ surface area is attached to the Cu⁰ wire, since the polymerization rate drops to 10%, after the wire is lifted out of solution. As discussed above, the decrease in the polymerization to 10% of the original value corresponds to 1% of the original surface area of Cu⁰. These factors justify the use of surface area of the copper wire, as the total surface area in solution. Using the typical Cu⁰ activation rate coefficient of MBrP in DMSO, $k_{a0}^{app} = 1.8 \times 10^{-4} \text{ cm s}^{-1}$, and the value of $k_{a1}^{app} = 3.2 \times 10^2 \text{ M}^{-1} \text{ s}^{-1}$ for the activation of MBrP by Cu^IBr/Me₆TREN in DMSO, an estimate of the equivalent activities can be performed. In particular, the overall activity of 1 mM of Cu^I/Br/Me₆TREN is k_{a1}^{over}

$$= k_{a1}^{app} \times [\text{Cu}^{\text{I}}/\text{Me}_6\text{TREN}] = (3.2 \times 10^2) \times (1 \times 10^{-3}) = 3.2 \times 10^{-1} \text{ s}^{-1}.$$

For Cu⁰ to have the

same activity as this solution of Cu^I/Me₆TREN, *i.e.* $k_{a1}^{over} = k_{a0}^{over}$, a ratio of $S/V = k_{a0}^{over} / k_{a0}^{app} = (3.2 \times 10^{-1}) / (1.8 \times 10^{-4}) = 1.8 \times 10^3 \text{ cm}^{-1}$ is needed. Assuming that 7 mL of solvent is used, the surface area of Cu⁰ needed is $S = S/V \times V = 1.8 \times 10^3 \times 7 = 1.3 \times 10^4 \text{ cm}^2$. If the diameter of the Cu⁰ wire is $d = 0.025 \text{ cm}$, this gives a length of Cu⁰ needed to match the activity of 1 mM Cu^I/Br/Me₆TREN of $l = S / (2 \times \pi \times d/2) = 1.3 \times 10^4 / (2 \times \pi \times 0.025/2) = 1.6 \times 10^5 \text{ cm} \approx 2 \text{ km}$, neglecting the contribution from the small ends of the cylinder. This implies that an extremely long length of almost 2 km of Cu⁰ wire, of diameter $d = 0.025 \text{ cm}$, in 7 mL of solvent is needed to match the activity of 1 mM Cu^I/Br/Me₆TREN, which illustrates the very high activity of Cu^I compared to typical Cu⁰ wires. However, considering the surface occupied by an atom of Cu⁰, of $5.2 \times 10^{-16} \text{ cm}^2$, a surface area of 1 cm² contains 1.9×10^{15} atoms. The activity of 1 cm² of Cu⁰ in 1000 mL of solvent is $k_{a0}^{over} = S/V \times k_{a0}^{app} = 1/1000 \times 1.8 \times 10^{-4} = 1.8 \times 10^{-7} \text{ s}^{-1}$, which is equivalent to an activity of $1.8 \times 10^{-7} / 1.9 \times 10^{15} = 9.4 \times 10^{-23} \text{ s}^{-1}$ per Cu⁰ atom on the surface. As discussed above, the activity of a 1 mM solution of Cu^I/Me₆TREN is $k_{a1}^{over} = 3.2 \times 10^{-1} \text{ s}^{-1}$, however, 1 L of a 1 mM Cu^I/Me₆TREN contains, $\text{concentration} \times V \times N_A = (1 \times 10^{-3}) \times (1 \times 100) \times 6.022 \times 10^{23} = 6.022 \times 10^{20}$ molecules of Cu^I/Me₆TREN, leading to an activity of $3.2 \times 10^{-1} / 6.022 \times 10^{20} = 5.3 \times 10^{-22} \text{ s}^{-1}$ per Cu^I/Me₆TREN in solution. Therefore, both Cu⁰ and Cu^I/Me₆TREN have similar activities on a per atom basis, although the relatively low number of Cu⁰ species on the surface of Cu⁰ gives Cu⁰ a much lower overall activity than Cu^I. A more detailed examination of the contributions from Cu⁰ and Cu^I, and other reactions is given in the next section.

Simulation of the model system in DMSO. To evaluate the validity of the kinetic model and corresponding (apparent) rate coefficients shown in equations (A-V-1) to (A-V-6), computer simulations were performed based on the apparent rate coefficients measured in these model systems, and kinetic parameters from Table A-V-1. The time evolution of [MBrP] and [Cu^{II}] are shown in Figure A-V-12a. The agreement between the simulated and experimental values confirms the validity of the kinetic model. These simulations included all the reactions that occur in a real polymerization except propagation, although they were extended to much longer times when all alkyl halides were consumed, followed by predominant comproportionation. The agreement between these simulations and experimental data for the model system allow these simulations to be extended to real polymerizations, as will be presented in the third paper of this series.²⁷⁹

Figure A-V-12b shows the rates of all relevant reactions, until nearly complete alkyl halide consumption: activation by Cu⁰ and Cu^I, deactivation by Cu^{II} and Cu^I, biradical termination, comproportionation, and disproportionation. As shown in Figure A-V-12b the rate of activation by Cu^I is greater by more than 2 orders of magnitude than the rate of activation by Cu⁰, during essentially the entire reaction, implying that over 99% of activation occurs *via* Cu^I. This difference is even larger under conditions corresponding to real polymerization, when the fraction of terminated chains is smaller and the ATRP equilibrium is rapidly established, as illustrated by nearly identical rates of activation by Cu^I and deactivation by Cu^{II}. Very interestingly, the rate of termination is equal to the sum of rates of activation by Cu⁰ and comproportionation. Initially, rates of radical termination and activation by Cu⁰ are nearly identical, indicating that when comproportionation is slow,

termination is compensated by Cu^0 activation. Subsequently, the comproportionation rate becomes faster than that of supplemental activation. Eventually, the rate of comproportionation equals the rate of termination until essentially all of the alkyl halide is consumed. Furthermore, the rate of comproportionation is more than 2 orders higher than the rate of disproportionation during the first 20000 s, and after 35000 s the rate of disproportionation approaches the rate of comproportionation. Disproportionation is slower, albeit nonzero under these conditions, which can explain the small amount of precipitate observed in the recent disproportionation experiments reported by Percec *et al.*,^{271, 280} however, activation by Cu^{I} clearly dominates the small extent of disproportionation. Under these polymerization-like conditions in DMSO the simulation results show that comproportionation contributed more than disproportionation in RDRP in DMSO in the presence of Cu^0 , and activation of alkyl halides by Cu^{I} dominates activation of alkyl halides by Cu^0 . This indicates that Cu^{I} is the major activator of alkyl halides, and Cu^0 acts as a supplemental activator and reducing agent, which is consistent with SARA ATRP but not SET-LRP.

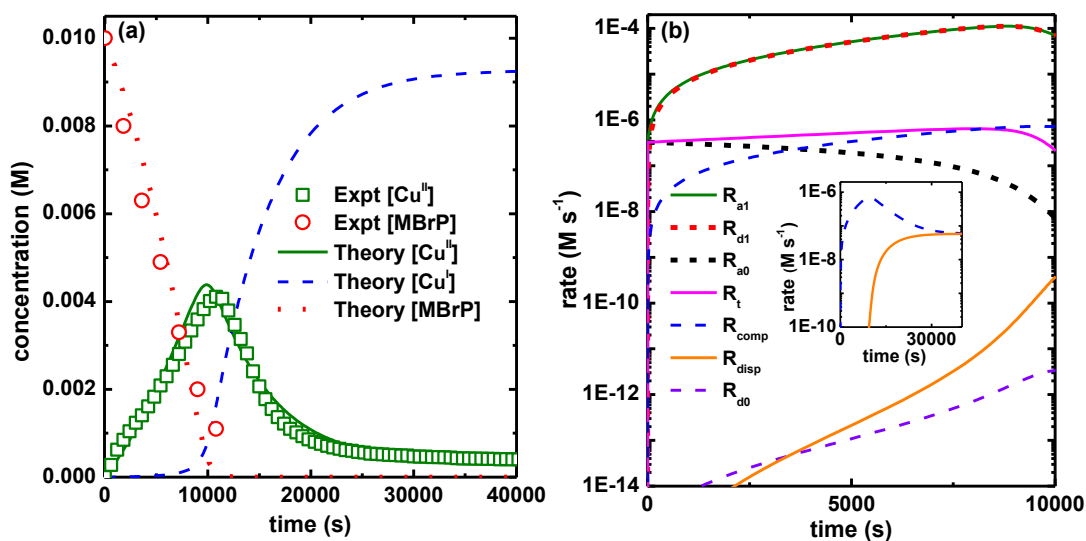


Figure A-V-12. Experimental and simulation results for a model reaction between 4 cm Cu^0 wire ($S = 1.27 \text{ cm}^2$) and 10 mM MBrP in the presence of 15 mM Me_6TREN in 7 mL DMSO ($S/V = 0.18 \text{ cm}^{-1}$). Solid points represent experimental data and dash lines follow simulation results. (a) concentrations of MBrP , Cu^{I} and Cu^{II} ; (b) rates of all relevant reactions from 0 to 10000 s, and the inset showing the comproportionation/disproportionation rates from 0 to 40000 s.

A-V. 3. Summary

The activation rate coefficients of alkyl bromides by Cu^0 , k_{a0}^{app} , were studied by following the concentration of the alkyl bromide and the evolution of the concentration of Cu^{II} species. Cu^{II} was formed by the activation of alkyl bromides by Cu^0 , followed by the subsequent rapid activation of a second alkyl bromide with the resulting Cu^{I} . Disproportionation was slow and was dominated by comproportionation in DMSO . Activation increased with the surface area of Cu^0 . The surface/volume independent

activation rate coefficient for MBrP by Cu^0 in DMSO at 25 °C was determined as $k_{a0}^{app} = 1.8 \times 10^{-4} \text{ cm s}^{-1}$. The presence of MA monomer reduced the value of $k_{a0}^{app} = 1.0 \times 10^{-4} \text{ cm s}^{-1}$ for MBrP in MA/DMSO = 2/1 (v/v) at 25 °C. The measured k_{a0}^{app} and k_{a1}^{app} (with Cu^I) values were used to compare the relative rates of activation of alkyl halides by Cu^0 and $\text{Cu}^I\text{Br}/\text{Me}_6\text{TREN}$, showing that the contribution of the $\text{Cu}^I\text{Br}/\text{Me}_6\text{TREN}$ to activation of alkyl halides exceeds 99%. This indicates that every time an alkyl halide is activated by Cu^0 , concurrently, there are more than 100 activations of alkyl halides by $\text{Cu}^I/\text{Me}_6\text{TREN}$. Because of the fact that the ATRP equilibrium is maintained during the entire process, activations by Cu^I is compensated by deactivation by Cu^{II} , which allows the active radical to be exchanged between the different alkyl halides. This indicates that activation by Cu^0 is the rate-limiting step in a typical polymerization. In DMSO, comproportionation is much faster than disproportionation but initially it is slower than activation by Cu^I . These observations invalidate two fundamental SET-LRP assumptions: instantaneous disproportionation of Cu^I and exclusive activation with Cu^0 species. Thus, the copper mediated RDRP in the presence of Cu^0 , i.e., so called SET-LRP, proceeds through the ATRP equilibrium with predominant ISET activation by very active Cu^I species, with Cu^0 acting as both a supplemental activator and a reducing agent, following SARA mechanism.

A-V. 4. Experimental Section

Materials. Cu^0 (wire, diameter 1.0 mm, 99.9+%, Aldrich) was washed with methanol/HCl first and then with fresh methanol before use. Methyl 2-bromopropionate (MBrP, 98%, Aldrich), tris(2-pyridylmethyl)amine (TPMA, 99%, ATRP Solutions), tris[2-

(dimethylamino)ethyl]amine (Me₆TREN, 99%, ATRP Solutions), DMSO (99+%, Aldrich), acetonitrile (MeCN, 99.8%, Aldrich), N,N-dimethylformamide (DMF, >99%, Aldrich), tetrabutylammonium perchlorate (TBAClO₄, 98%, Aldrich), copper(II) trifluoromethanesulfonate (Cu^{II}(OTf)₂, 98%, Aldrich) and tetraethylammonium bromide (TBABr, 99%, Aldrich) were used as received. MA (99+%, Aldrich) was passed over basic alumina to remove inhibitor/antioxidant.

Characterization. All spectroscopic measurements were performed on a Varian Cary 5000 UV/Vis/NIR spectrometer. Gas chromatography (GC) measurements were carried out with SHIMADZU GC-17A. ¹H NMR (500 MHz) spectra were taken on a Bruker Avance 300 spectrometer using CDCl₃ or deuterated DMSO as a solvent. All cyclic voltammograms were recorded with a Gamry Reference 600 potentiostat. Stopped flow apparatus consisted of a BioLogic Science Instruments MOS450 monochromator, equipped with a 150W Xe lamp and a photomultiplier 400, and a SFM20 stopped-flow module, equipped with two 10 mL gastight Hamilton syringes. Data acquisition and preliminary analysis was done with Bio-Kine 4.2. All measurements were performed at 25 °C in degassed DMSO in a FC15 cuvette with an optical path length of 15 mm. For every measurement, a total volume of 0.24 mL was pushed through the cuvette with a flow-rate of 7 mL/s.

Measurement of activation rate coefficient for MBrP in DMSO and in MA/DMSO = 2/1 (v/v). For the measurements, a 20 mM MBrP solution in DMSO and a 1 mM solution of Cu^IBr/Me₆TREN with 20 mM 2,2,6,6-tetramethylpiperidiny-1-oxy (TEMPO) solution in DMSO were prepared. The first syringe contained the 1 mM solution of

Cu^IBr/Me₆TREN, and the second syringe contained a 20 mM MBrP/TEMPO solution. All solutions and syringes were degassed by repeated freeze-thaw cycles before and after addition of the respective compound. The k_{a1}^{app} value was determined as $3.2 \times 10^2 \text{ M}^{-1} \text{ s}^{-1}$ in pure DMSO. A similar procedure was performed to measure the activation rate coefficient of MBrP by Cu^IBr/Me₆TREN in a solution of MA/DMSO = 2/1 (v/v), giving an activation rate coefficient $k_{a1}^{app} = 2.0 \times 10^2 \text{ M}^{-1} \text{ s}^{-1}$.

General procedures for model study of k_{a0}^{app} in DMSO. In a typical experiment, a selected length of Cu⁰ wire ($l = 4 \text{ cm}$, $d = 1.0 \text{ mm}$) was placed in a Schlenk flask connected to a quartz cuvette and the flask was evacuated and then backfilled with nitrogen. Nitrogen purged DMSO (6.1 mL), a DMSO solution of Me₆TREN (0.3 mL, $3.6 \times 10^{-1} \text{ M}$), and a DMSO solution of MBrP (0.6 mL, $1.3 \times 10^{-1} \text{ M}$) were then sequentially injected into the flask via syringes. After the addition of the initiator, the progress of the reaction was monitored by UV/Vis/NIR spectroscopy. A similar experiment was performed using deuterated DMSO, with small samples taken at periodic times to measure the loss of MBrP by NMR.

General procedures for measurement of k_{a0}^{app} during polymerization. Degassed MA (5 mL) and DMSO or MeCN (5 mL) was transferred *via* degassed syringes to a Schlenk flask in the presence of 1 cm Cu⁰ wire ($d = 0.25 \text{ mm}$) and 6.4 mg Me₆TREN or 8.1 mg TPMA, which was thoroughly purged by flushing with nitrogen. 31.0 μL MBrP was added *via* a microsyringe. UV/Vis/NIR spectra were recorded every 20 min. The Cu^{II} concentration was determined by the absorbance at 960 nm ($\varepsilon = 460 \text{ M}^{-1} \text{ cm}^{-1}$), and the

concentration of monomer was measured by integration of a signal between 1610 and 1625 nm.

Electrochemical model study of k_{a0}^{app} for MBrP in DMSO. In a typical experiment electrolysis was carried out and recorded with a Gamry Reference 600 potentiostat. Prior to each polymerization, the working and counter electrodes (Pt plate electrode ($A = 4.50 \text{ cm}^2$) and Pt mesh electrode, respectively) were cleaned thoroughly with methanol, THF, and acetone, submerged briefly in a fresh solution of HCl/HNO₃ (3/1 by volume), rinsed with deionized water, and dried before use. The Ag/AgI/I⁻ electrode was prepared and used as a reference electrode, separated from the reaction solutions by a salt bridge. All reactions were conducted in a 7-neck pear shaped jacket electrochemical cell (EC cell) maintained at 25 °C under a slow nitrogen purge. A 1.7 g of TBAClO₄ was placed in EC cell, and a 24.6 mL of nitrogen bubbled DMSO and 30 µL of DMF (as a ¹H NMR internal standard) were transferred to EC cell by nitrogen purged gas tight syringes. To this solution was added 375 µL of a 1 M solution of Cu^{II}(OTf)₂/Me₆TREN/2TBABr ([Cu^{II}Br₂/Me₆TREN]₀ = 15 mM, in the final solution). The solution was heated to 60 °C with an applied potential of -0.6 V for 12 hours (vs. Ag/AgI/I⁻) to deposit Cu⁰ onto a Pt plate electrode. Subsequently, the temperature was reduced to 25 °C, and the initiator (MBrP, 31 µL, 11 mM) was added to the solution with an applied potential of -0.7 V. Samples were withdrawn periodically for ¹H NMR (500MHz) to measure the conversion of MBrP.

Electrochemical model study of k_{a0}^{app} for MBrP in MA/DMSO. Cu⁰ deposition onto the Pt plate electrode was carried out as described above over 22 hours. The Cu⁰ deposited

electrode was cleaned with methanol and THF, and transferred immediately to the next polymerization reactor. 1.44 g of TBAClO₄ (0.2 M) was placed in an electrochemical cell and degassed MA (14 mL) and DMSO (6.8 mL) were transferred *via* degassed syringes to the EC cell. The electrochemical cell was fitted with the working electrode with Cu⁰ deposited on it, Ag/AgI/I⁻ reference electrode, and Pt mesh counter electrode separated from polymerization solution. Before injection of Me₆TREN and MBrP, the potential was set to -0.5 V vs. Ag/AgI/I⁻. 104 μL of Me₆TREN and 87 μL of MBrP were added to the reaction mixture. The monomer consumption was measured by GC and molecular weight was characterized by GPC with PMMA standards.

Estimation of k_{a1}^{app} in DMSO. The activation rate coefficient was estimated by fitting the stopped flow absorbance data in a solution of [Cu^I/Me₆TREN]₀ = 0.33 mM, [MBrP]₀ = 13.3 mM, [TEMPO]₀ = 13.3 mM. Figure A-V-5 shows the raw experimental absorbance trace, and the fitted function, absorbance = $c + (a-c)\text{Exp}^{(-k \text{ time})}$ with fitted parameters of $a = -0.484$, $c = -0.282$, and $k = 4.22 \text{ s}^{-1}$. After dividing the fitted value of k by [MBrP]₀ = 0.0133 M, an activation rate coefficient of $k_{a1}^{app} = 3.2 \times 10^2 \text{ M}^{-1} \text{ s}^{-1}$ was calculated.

Measurement of Cu⁰ activation rate coefficients at different ligand concentrations and a low surface to volume ratio. In addition to measurements with 4 cm Cu⁰ wire ($d = 1 \text{ mm}$) in 7 mL of DMSO ($S/V = 0.18 \text{ cm}^{-1}$), a series of activation experiments were performed using 1 cm Cu⁰ wire ($d = 1 \text{ mm}$) in 10 mL of DMSO ($S/V = 0.033 \text{ cm}^{-1}$). This series of experiments was performed with [MBrP]₀ = 27.8 mM, and [Me₆TREN]₀/[MBrP]₀ = 1, 0.5 and 0.1. In each case, the initial evolution of Cu^{II} with time was essentially linear

(< 10% MBrP conversion). The slopes of Cu^{II} evolution with time were found to be $5 \times 10^{-8} \text{ M s}^{-1}$, $7 \times 10^{-8} \text{ M s}^{-1}$, $8 \times 10^{-8} \text{ M s}^{-1}$ for ligand to MBrP ratios of 0.1, 0.5 and 1.0, respectively. Using equation (A-V-18), the following rate coefficients were calculated: $k_{a0}^{app} = 5 \times 10^{-5} \text{ cm s}^{-1}$, $8 \times 10^{-5} \text{ cm s}^{-1}$, and $8 \times 10^{-5} \text{ cm s}^{-1}$ for ligand to MBrP ratios of 0.1, 0.5, 1.0, respectively.

Estimation of k_{a0}^{app} for PMA-Br macroinitiator in MA/DMSO = 1/1 (v/v) solution by electrochemistry. A negative potential applied in electrochemical experiments reduced essentially all Cu^{II} and Cu^I species to Cu⁰, preventing establishment of an ATRP equilibrium and efficient deactivation by Cu^{II}. Therefore, under such conditions in MA polymerization is initiated by MBrP activated by Cu⁰, initially resulting in formation of high molecular weight polymers with molecular weight decreasing with conversion, as shown in Figure A-V-11. Based on molecular weight evolution with conversion, the value of k_{a0}^{app} was determined using the following equation, assuming no intermittent deactivation and termination by coupling:

$$DP_n = 2 \frac{[M]_0 - [M]_t}{[R-X]_0 - [R-X]_t} = 2 \frac{[M]_0 conv}{[R-X]_0 - [R-X]_t} \quad (\text{A-V-20})$$

where [M] is the concentration of monomer, [R-X] is the concentration of initiator, *conv* is the monomer conversion, and *t* is the reaction time. Assuming that only a small number of chains have been formed and terminated ($[R-X]_0 - [R-X]_t \sim \ln([R-X]_0/[R-X]_t)$) and that two propagating radical undergo termination by coupling rather than reversible deactivation, the equation can be further simplified to:

$$DP_n = \frac{M_n}{MW_{MA}} = 2 \frac{[M]_0 conv}{k_{a0}^{app} \frac{S}{V} [R-X]_0 t} \quad (\text{A-V-21})$$

where M_n is the experimentally measured number average molecular weight and MW_{MA} is the molecular weight of the MA monomer unit. This allows k_{a0}^{app} to be estimated by the following equation:

$$k_{a0}^{app} = 2 \frac{V}{S} \frac{MW_{MA}}{M_n} \frac{[M]_0 conv}{[R-X]_0 t} \quad (\text{A-V-22})$$

The data in Figure A-V-11 by using equation (A-V-22) provide a value of $k_{a0}^{app} = (9 \pm 2) \times 10^{-5} \text{ cm} \cdot \text{s}^{-1}$.

Computer Simulations. PREDICI[®] (v 6.3.2) was used for all kinetic modeling to obtain time-dependent concentrations of all species, and rates of the various reactions.

A-V. 5. References

1. (a) Wang, J. S.; Matyjaszewski, K., *Macromolecules* **1995**, *28* (23), 7901-7910; (b) Wang, J. S.; Matyjaszewski, K., *J. Am. Chem. Soc.* **1995**, *117* (20), 5614-5615; (c) Matyjaszewski, K.; Xia, J. H., *Chem. Rev.* **2001**, *101* (9), 2921-2990; (d) Matyjaszewski, K., *Macromolecules* **2012**, *45* (10), 4015-4039; (e) Kamigaito, M.; Ando, T.; Sawamoto, M., *Chem. Rev.* **2001**, *101* (12), 3689-3745; (f) Matyjaszewski, K.; Tsarevsky, N. V., *Nature Chemistry* **2009**, *1* (4), 276-288.
2. (a) Braunecker, W. A.; Matyjaszewski, K., *Prog. Polym. Sci.* **2007**, *32* (1), 93-146; (b) Jenkins, A. D.; Jones, R. G.; Moad, G., *Pure Appl. Chem.* **2010**, *82* (2), 483-491.
3. (a) Jakubowski, W.; Matyjaszewski, K., *Angew. Chem.-Int. Edit.* **2006**, *45* (27), 4482-4486; (b) Jakubowski, W.; Min, K.; Matyjaszewski, K., *Macromolecules* **2006**, *39* (1), 39-45.
4. (a) Wang, Y.; Zhang, Y. Z.; Parker, B.; Matyjaszewski, K., *Macromolecules* **2011**, *44* (11), 4022-4025; (b) Zhang, Y.; Wang, Y.; Matyjaszewski, K., *Macromolecules* **2011**, *44*, 683-685; (c) Zhang, Y. Z.; Wang, Y.; Peng, C. H.; Zhong, M. J.; Zhu, W. P.; Konkolewicz, D.; Matyjaszewski, K., *Macromolecules* **2012**, *45* (1), 78-86.

5. (a) Magenau, A. J. D.; Strandwitz, N. C.; Gennaro, A.; Matyjaszewski, K., *Science* **2011**, 332 (6025), 81-84; (b) Bortolamei, N.; Isse, A. A.; Magenau, A. J. D.; Gennaro, A.; Matyjaszewski, K., *Angew. Chem.-Int. Edit.* **2011**, 50 (48), 11391-11394.
6. (a) Tasdelen, M. A.; Uygün, M.; Yagci, Y., *Macromol. Chem. Phys.* **2011**, 212 (18), 2036-2042; (b) Fors, B. P.; Hawker, C. J., *Angew. Chem.-Int. Edit.* **2012**, 51 (35), 8850-8853; (c) Mosnáček, J.; Ilčíková, M., *Macromolecules* **2012**, 45 (15), 5859-5865; (d) Konkolewicz, D.; Schröder, K.; Buback, J.; Bernhard, S.; Matyjaszewski, K., *ACS Macro Lett.* **2012**, 1219-1223.
7. Jakubowski, W.; Kirci-Denizli, B.; Gil, R. R.; Matyjaszewski, K., *Macromol. Chem. Phys.* **2008**, 209 (1), 32-39.
8. Abreu, C. M. R.; Mendonça, P. V.; Serra, A. C.; Popov, A. V.; Matyjaszewski, K.; Guliashevili, T.; Coelho, J. F. J., *ACS Macro Lett.* **2012**, 1 (11), 1308-1311.
9. (a) Guliashevili, T.; Mendonça, P. V.; Serra, A. C.; Popov, A. V.; Coelho, J. F. J., *Chem. Eur. J.* **2012**, 18 (15), 4607-4612; (b) Hornby, B. D.; West, A. G.; Tom, J. C.; Waterson, C.; Harisson, S.; Perrier, S., *Macromol. Rapid Commun.* **2010**, 31 (14), 1276-1280.
10. Matyjaszewski, K.; Coca, S.; Gaynor, S. G.; Wei, M.; Woodworth, B. E., *Macromolecules* **1997**, 30 (23), 7348-7350.
11. Percec, V.; Guliashevili, T.; Ladislav, J. S.; Wistrand, A.; Stjern Dahl, A.; Sienkowska, M. J.; Monteiro, M. J.; Sahoo, S., *J. Am. Chem. Soc.* **2006**, 128 (43), 14156-14165.
12. (a) Matyjaszewski, K.; Nakagawa, Y.; Jasieczek, C. B., *Macromolecules* **1998**, 31 (5), 1535-1541; (b) Xia, J.; Gaynor, S. G.; Matyjaszewski, K., *Macromolecules* **1998**, 31 (17), 5958-5959.
13. Rosen, B. M.; Percec, V., *Chem. Rev.* **2009**, 109 (11), 5069-5119.
14. (a) Wang, Y.; Zhong, M.; Zhang, Y.; Magenau, A. J. D.; Matyjaszewski, K., *Macromolecules* **2012**, 45, 8929-8932; (b) Zhong, M.; Matyjaszewski, K., *Macromolecules* **2011**, 44 (8), 2668-2677.
15. Nguyen, N. H.; Levere, M. E.; Kulis, J.; Monteiro, M. J.; Percec, V., *Macromolecules* **2012**, 45 (11), 4606-4622.
16. Matyjaszewski, K.; Tsarevsky, N. V.; Braunecker, W. A.; Dong, H.; Huang, J.; Jakubowski, W.; Kwak, Y.; Nicolay, R.; Tang, W.; Yoon, J. A., *Macromolecules* **2007**, 40 (22), 7795-7806.
17. Wang, Y.; Zhong, M.; Zhu, W.; Peng, C.-H.; Zhang, Y.; Konkolewicz, D.; Bortolamei, N.; Isse, A. A.; Gennaro, A.; Matyjaszewski, K., *Macromolecules* **2013**, 46 (10), 3793-3802.
18. Harisson, S.; Couvreur, P.; Nicolas, J., *Macromolecules* **2012**, 45 (18), 7388-7396.
19. Bell, C. A.; Bernhardt, P. V.; Monteiro, M. J., *J. Am. Chem. Soc.* **2011**, 133 (31), 11944-11947.
20. (a) Pintauer, T.; Braunecker, W.; Collange, E.; Poli, R.; Matyjaszewski, K., *Macromolecules* **2004**, 37 (8), 2679-2682; (b) Tang, W.; Kwak, Y.; Braunecker, W.; Tsarevsky, N. V.; Coote, M. L.; Matyjaszewski, K., *J. Am. Chem. Soc.* **2008**, 130 (32), 10702-10713.
21. Wang, Y.; Kwak, Y.; Buback, J.; Buback, M.; Matyjaszewski, K., *ACS Macro Lett.* **2012**, 1367-1370.
22. Bortolamei, N.; Isse, A. A.; Di Marco, V. B.; Gennaro, A.; Matyjaszewski, K., *Macromolecules* **2010**, 43 (22), 9257-9267.

23. Braunecker, W. A.; Tsarevsky, N. V.; Gennaro, A.; Matyjaszewski, K., *Macromolecules* **2009**, *42* (17), 6348-6360.
24. Nguyen, N. H.; Percec, V., *Journal of Polymer Science Part A: Polymer Chemistry* **2010**, *48* (22), 5109-5119.
25. (a) Abbott, A. P.; Capper, G.; Davies, D. L.; McKenzie, K. J.; Obi, S. U., *Journal of Chemical & Engineering Data* **2006**, *51* (4), 1280-1282; (b) Habbache, N.; Alane, N.; Djerad, S.; Tifouti, L., *Chemical Engineering Journal* **2009**, *152* (2-3), 503-508; (c) Majima, H.; Awakura, Y.; Yazaki, T.; Chikamori, Y., *Metallurgical Transactions B* **1980**, *11* (2), 209-214; (d) Palmer, D. A., *Journal of Solution Chemistry* **2011**, *40* (6), 1067-1093.
26. (a) Nguyen, N. H.; Rosen, B. M.; Lligadas, G.; Percec, V., *Macromolecules* **2009**, *42* (7), 2379-2386; (b) Lligadas, G.; Rosen, B. M.; Bell, C. A.; Monteiro, M. J.; Percec, V., *Macromolecules* **2008**, *41* (22), 8365-8371.
27. Jiang, X.; Rosen, B. M.; Percec, V., *Journal of Polymer Science Part A: Polymer Chemistry* **2010**, *48* (2), 403-409.
28. Levere, M. E.; Nguyen, N. H.; Sun, H.-J.; Percec, V., *Polym. Chem.* **2013**, *4* (3), 686-694.
29. (a) Konkolewicz, D.; Sosnowski, S.; D'hooge, D. R.; Szymanski, R.; Reyniers, M.-F.; Marin, G. B.; Matyjaszewski, K., *Macromolecules* **2011**, *44* (21), 8361-8373; (b) D'Hooge, D. R.; Konkolewicz, D.; Reyniers, M.-F.; Marin, G. B.; Matyjaszewski, K., *Macromol. Theory Simul.* **2012**, *21* (1), 52-69.
30. Nguyen, N. H.; Jiang, X.; Fleischmann, S.; Rosen, B. M.; Percec, V., *Journal of Polymer Science Part A: Polymer Chemistry* **2009**, *47* (21), 5629-5638.
31. Tsarevsky, N. V.; Braunecker, W. A.; Matyjaszewski, K., *J. Organometal. Chem.* **2007**, *692* (15), 3212-3222.
32. (a) Smith, G. B.; Russell, G. T.; Heuts, J. P. A., *Macromol. Theory Simul.* **2003**, *12* (5), 299-314; (b) Johnston-Hall, G.; Monteiro, M. J., *J. Polym. Sci. Part A: Polym. Chem.* **2008**, *46* (10), 3155-3173.
33. Schroder, K.; Konkolewicz, D.; Poli, R.; Matyjaszewski, K., *Organometallics* **2012**, *31* (22), 7994-7999.
34. Horn, M.; Matyjaszewski, K., *Macromolecules* **2013**, *46* (9), 3350-3357.
35. Buback, M.; Kurz, C. H.; Schmaltz, C., *Macromol. Chem. Phys.* **1998**, *199* (8), 1721-1727.
36. Rosen, B. M.; Jiang, X.; Wilson, C. J.; Nguyen, N. H.; Monteiro, M. J.; Percec, V., *Journal of Polymer Science Part A: Polymer Chemistry* **2009**, *47* (21), 5606-5628.
37. Zhong, M.; Wang, Y.; Krys, P.; Konkolewicz, D.; Matyjaszewski, K., *Macromolecules* **2013**, *Submitted*.
38. Levere, M. E.; Nguyen, N. H.; Leng, X.; Percec, V., *Polym. Chem.* **2013**, *4* (5), 1635-1647.

Appendix VI

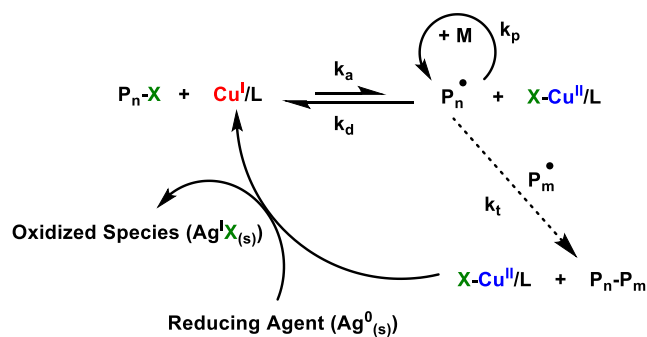
A Silver Bullet: Elemental Silver as an Efficient Reducing Agent for Atom Transfer Radical Polymerization of Acrylates*

A-VI. 1. Introduction

Since the conception of reversible deactivation radical polymerization (RDRP) in the 1990s, these types of methodologies have revolutionized polymer chemistry.^{2c, 281} Particularly, RDRP techniques have allowed for the synthesis of polymers with very narrow molecular weight distributions (MWDs), predetermined molecular weights (MWs), and remarkable conservation of chain-end functionality, previously only achievable *via* ionic polymerization.²⁸² Atom transfer radical polymerization (ATRP) is among the most commonly utilized RDRP methods.^{1d, 61a, 89d, 180d, 283} In addition to nitroxide mediated polymerization (NMP)^{59b, 284} and reversible addition-fragmentation chain transfer polymerization (RAFT),^{91e, 285} ATRP achieves its control of polymer chain growth and architecture through a transition metal catalyzed activation/deactivation redox cycle of alkyl halides and alkyl radicals, respectively.^{1e, 286} Traditionally, a large concentration of transition metal catalyst was required to successfully conduct an ATRP due to unavoidable radical termination resulting in a buildup of deactivator species, consistent with the persistent radical effect.^{1e, 125} However, within the past decade the use of reducing agents has allowed for a decrease in the initial amount of metal catalyst necessary for an efficient

*Work in this appendix was published and partially reformatted based on the following manuscript: Williams Valerie A.; Ribelli, Thomas G.; Chmielarz, Pawel; **Park, Sangwoo**; Matyjaszewski, Krzysztof *J. Am. Chem. Soc.* **2015**, 137, 1428

ATRP down to the ppm level.^{1c} Regeneration of the activator species from a deactivator complex is facilitated through a variety of different methods, including the addition of azo radical initiators (Initiators for Continuous Activator Regeneration, ICAR ATRP)^{65b} or chemical reducing agents (Activator Regenerated by Electron Transfer, ARGET ATRP),^{80, 287} use of electrical current (*e*ATRP ATRP)¹⁰ or light (photoATRP),^{81, 70d, 253c, 288} or addition of zerovalent metals (Supplemental Activator and Reducing Agent, SARA ATRP) (Scheme A-VI-1).^{109, 289} Zerovalent metals were first applied to ATRP processes in 1997,^{25a} where Cu⁰ (or Fe⁰) was used both to reduce Cu^{II} deactivator complexes to Cu^I activator species *via* comproportionation and directly activate alkyl halide species in solution. In SARA ATRP (also known as SET-LRP), Cu⁰ plays an active role in radical generation and plausible radical termination.^{289a, 290} Therefore, a reducing agent that acts *via* single-electron transfer and is inert to radical generation and termination has long been sought after, but other metals such as Fe⁰, Mg⁰, or Zn⁰ operate *via* a SARA mechanism.²⁹¹ In this Appendix, the use of Ag⁰ as a previously unexplored ARGET reagent.



Scheme A-VI-1. Proposed mechanism of ATRP in the presence of Ag⁰.

The use of elemental silver as a reducing agent is attractive for many reasons. Silver

has only two readily attainable oxidation states (0 and +1), so reduction with Ag^0 would likely be a single-electron process.²⁹² Both Ag^0 and the proposed oxidized species ($\text{Ag}^{\text{I}}\text{X}$) are insoluble in most reaction media, which would simplify purification processes and lessen product contamination by transition metals, as well as open the possibility of application on an industrial scale.²⁹³ Lastly, Ag^0 is relatively inert toward typical polymerization reagents, which could minimize or eliminate undesirable radical generation or termination events that are commonly observed in SARA ATRP and other reduced-catalyst techniques.^{289a} Herein, the use of Ag^0 as a heterogeneous reducing agent for copper-mediated ATRP is investigated.

A-VI. 2. Results and Discussion

The rate-determining step in many ATRP processes with low catalyst loading is the (re)generation of a low-valent activator species.^{65b} Therefore, it is of great importance to determine the efficiency of this (re)generation process in new ATRP systems. To achieve this, the heterogeneous reduction of $\text{Cu}^{\text{II}}\text{Br}_2/\text{TPMA}$ (TPMA = tris(2-pyridylmethyl)amine)²⁹⁴ by Ag^0 in polymerization media was monitored as a function of time. Alkyl halide initiator was excluded from these reactions to allow for simple and quantitative determination of reduction rates. As one of the most commonly used ligands for Cu-mediated ATRP, TPMA was chosen for the high activity and stability of its copper complexes under these reaction conditions. It was observed that Ag^0 readily reduced $\text{Cu}^{\text{II}}\text{Br}_2/\text{TPMA}$ to the Cu^{I} activator species, which could then enter into the ATRP equilibrium in the presence of alkyl halide initiator (Scheme A-VI-1).^{65b} In the absence of initiator, equilibrium between $\text{Ag}^0/\text{Cu}^{\text{II}}$ and $\text{Ag}^{\text{I}}/\text{Cu}^{\text{I}}$ was achieved after 90 min (Figure A-

VI-1). It should be noted that copper complexes with both Me₆TREN and PMDTA as ligands (Me₆TREN = tris[2-(dimethylamino)ethyl]amine; PMDTA = *N,N,N',N',N''*-pentamethyldiethylenetriamine) were successfully reduced by Ag⁰ as well, highlighting the large scope of this new methodology. To establish the efficacy of Ag⁰ as a heterogeneous reducing agent for ATRP, the polymerization of *n*-butyl acrylate (BA) was carried out at 50 °C. Under these conditions, 62% monomer conversion was observed after 2 h at 200 ppm initial CuBr₂/TPMA catalyst loading (Figure A-VI-2). MW was in very good agreement with theoretical values throughout the reaction, increasing linearly with conversion, and at 62% monomer conversion, gel permeation chromatography (GPC) analysis revealed a very low dispersity value of $\bar{D} = 1.03$, among the lowest reported for copper-mediated ATRP of acrylates. At higher conversion, a decrease in reaction rate was observed, but good control over polymerization was maintained at all reaction times (Figure A-VI-3). This low dispersity value likely indicates that Ag⁰ is not active in the generation or termination of radicals, and rather acts solely as a reducing agent. Accordingly, polymerization of BA in the absence of CuBr₂ did not occur over 2 h whereas, in the presence of CuBr₂/TPMA, 50% monomer conversion was attained after 2 hours. Thus, if activation occurred with Ag⁰, it was slow enough relative to Cu^I activation to be kinetically negligible. Additionally, although radical-radical termination reactions are unavoidable in any RDRP, it is possible that the presence of Ag⁰ may suppress alternative termination pathways such as Cu^I catalytic radical termination, which has been shown to be a dominant mode of radical termination in some Cu-based ATRP reactions of acrylates.^{290a}

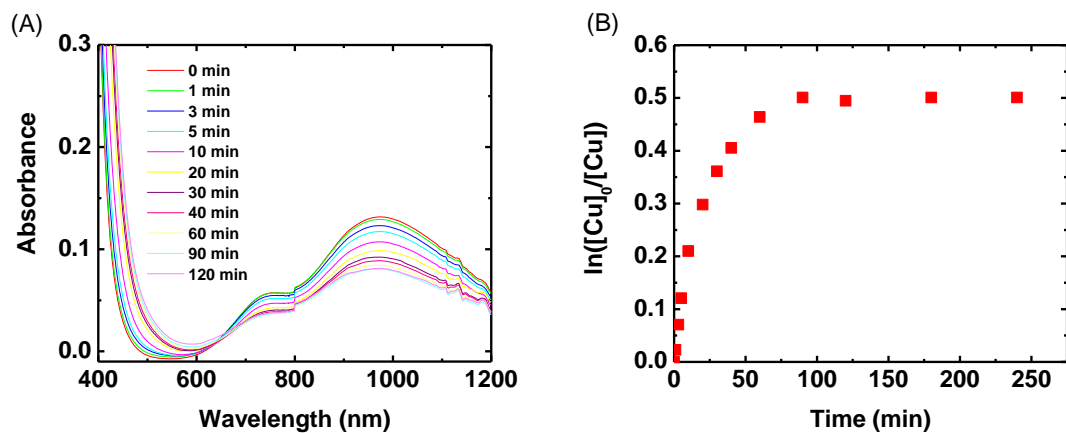
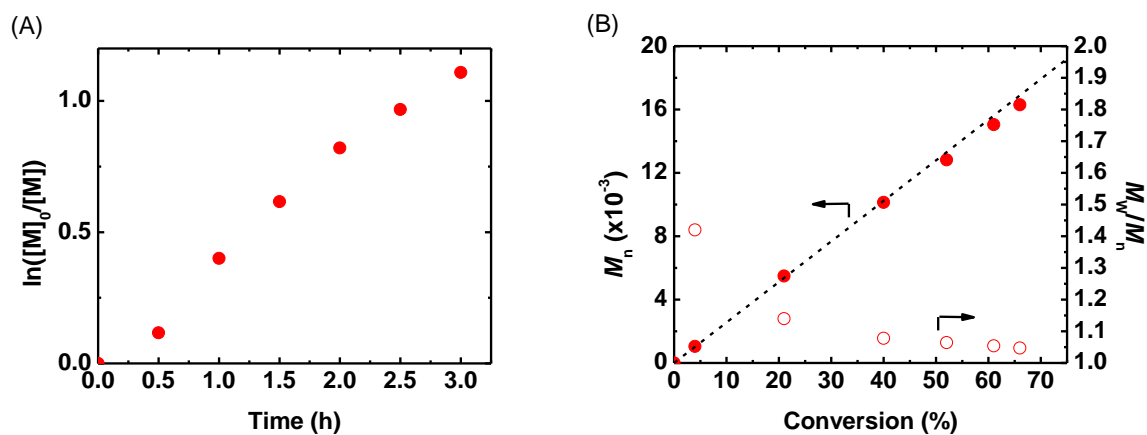


Figure A-VI-1. (A) UV-Vis-NIR spectra and (B) semi-log plot of $[Cu^{II}]$ in the reduction of $CuBr_2$ with Ag^0 in the absence of alkyl halide initiator. Reaction conditions: $[BA]_0/[CuBr_2]_0/[TPMA]_0 = 200/0.04/0.08$ with $[BA]_0 = 3.49$ M in DMF at $25^\circ C$, in the presence of 2 cm Ag^0 wire ($d = 2$ mm, $A = 1.3$ cm²; $V_{tot} = 10$ mL).



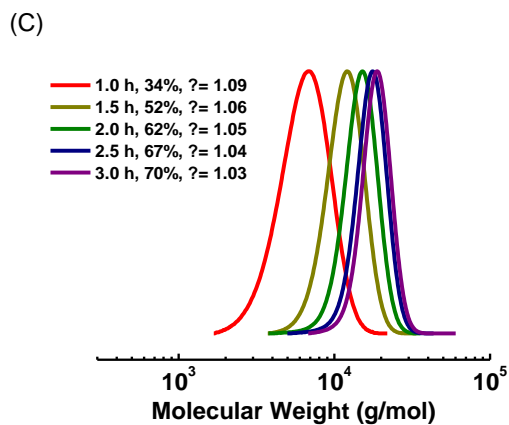
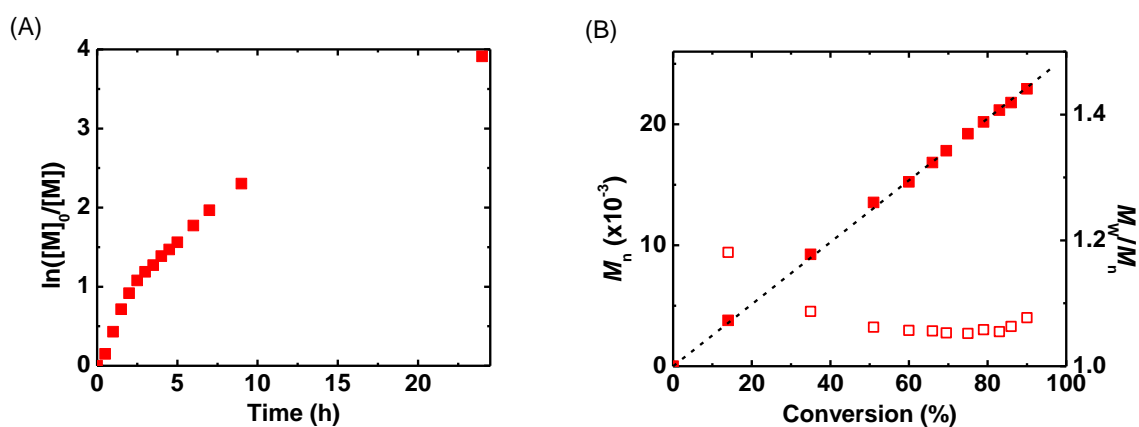


Figure A-VI-2. (A) Kinetics, (B) evolution of M_n and M_w/M_n with conversion, and (C) GPC traces for the polymerization of BA in DMF. Reaction conditions: $[BA]_0/[EBiB]_0/[CuBr_2]_0/[TPMA]_0 = 200/1/0.04/0.08$ with $[BA]_0 = 3.49$ M in DMF at 50 °C, in the presence of 5 cm Ag^0 wire ($d = 2$ mm, $SA = 3.2$ cm²; $V_{tot} = 10$ mL; $S/V = 0.32$ cm⁻¹).



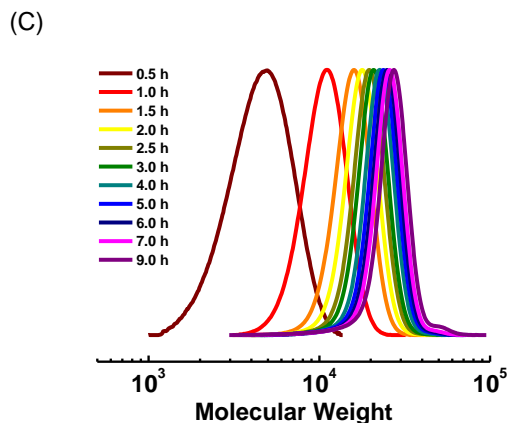


Figure A-VI-3. (A) Kinetics, (B) evolution of M_n and M_w/M_n with conversion, and (C) GPC traces for the polymerization of BA in DMF, run to long reaction times. Reaction conditions: $[BA]_0/[EBiB]_0/[CuBr_2]_0/[TPMA]_0 = 200/1/0.04/0.08$ with $[BA]_0 = 3.49$ M in DMF at 50 °C, in the presence of 5 cm Ag^0 wire ($d = 2$ mm, $SA = 3.2$ cm²; $V_{tot} = 10$ mL; $S/V = 0.32$ cm⁻¹).

Because silver is a relatively expensive reducing agent as compared to alternatives such as copper or ascorbic acid, the minimization of the amount of Ag^0 wire used is highly desired. Five separate experiments were conducted with varying amounts of silver wire: 10, 5, 2, 1, and 0.5 cm (silver surface area to solution volume ratio (S/V) = 0.64, 0.32, 0.13, 0.07 and 0.04 cm⁻¹, respectively). Figure A-VI-4A illustrates the polymerization kinetics of these five reactions. As the surface area of silver was decreased, the rate of polymerization similarly declined, suggesting the involvement of silver in the rate-determining step of the reaction. MW increased linearly with conversion (Figure A-VI-4b), and was nearly identical to theoretical MW. MWDs were independent of silver surface area and remained low, with $\bar{D} = 1.02$ at 75% monomer conversion (2 cm Ag^0 wire).

Importantly, because reaction rate was dependent on the S/V and not on the total amount of silver used, the reaction rate could feasibly be increased by either increasing the surface area of silver or decreasing the total reaction volume.

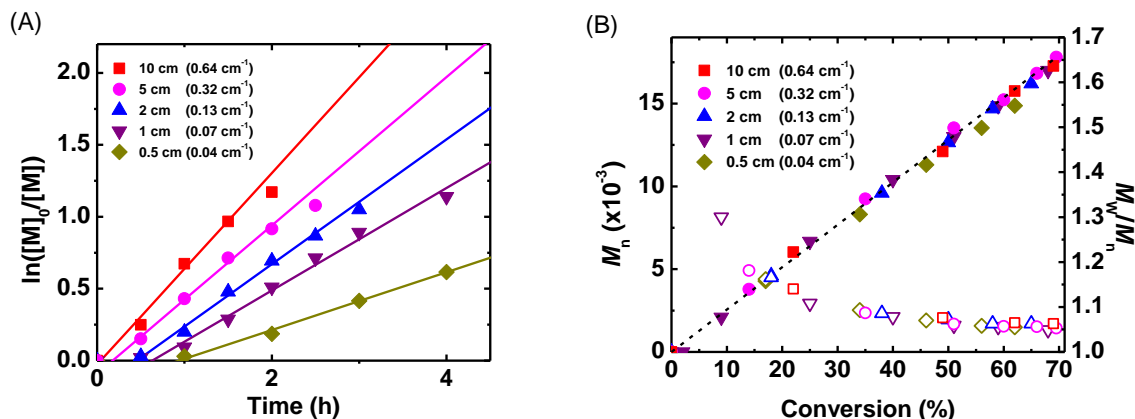


Figure A-VI-4. (a) Kinetics and (b) evolution of M_n and M_w/M_n with conversion in the ATRP of BA with various S/V of silver. Reaction conditions: $[BA]_0/[EBiB]_0/[CuBr_2]_0/[TPMA]_0 = 200/1/0.04/0.08$ with $[BA]_0 = 3.49$ M in DMF at 50°C , in the presence of 0.5-10 cm Ag^0 wire ($d = 2$ mm, $SA = 0.4 - 6.4$ cm^2 ; $V_{\text{tot}} = 10$ mL; $S/V = 0.04 - 0.64$ cm^{-1}).

Fortunately, use of large amounts of silver is still experimentally reasonable due to the high reusability of the metal. Indeed, one of the greatest advantages of a heterogeneous system is the potential reusability of the reagents,²⁹³ as demonstrated below. A single piece of silver wire was used without treatment in five sequential polymerizations of BA, and results are illustrated in Figure A-VI-5. The rate of polymerization does not change significantly over each cycle, and MW values match up well to theoretical values over all cycles. Most importantly, a high degree of control over polymerization was consistently

maintained, with $D = 1.05$ in all reactions. This result suggests that coating of the silver surface by either polymer or initial reagents is minimal and does not notably affect subsequent reactions.

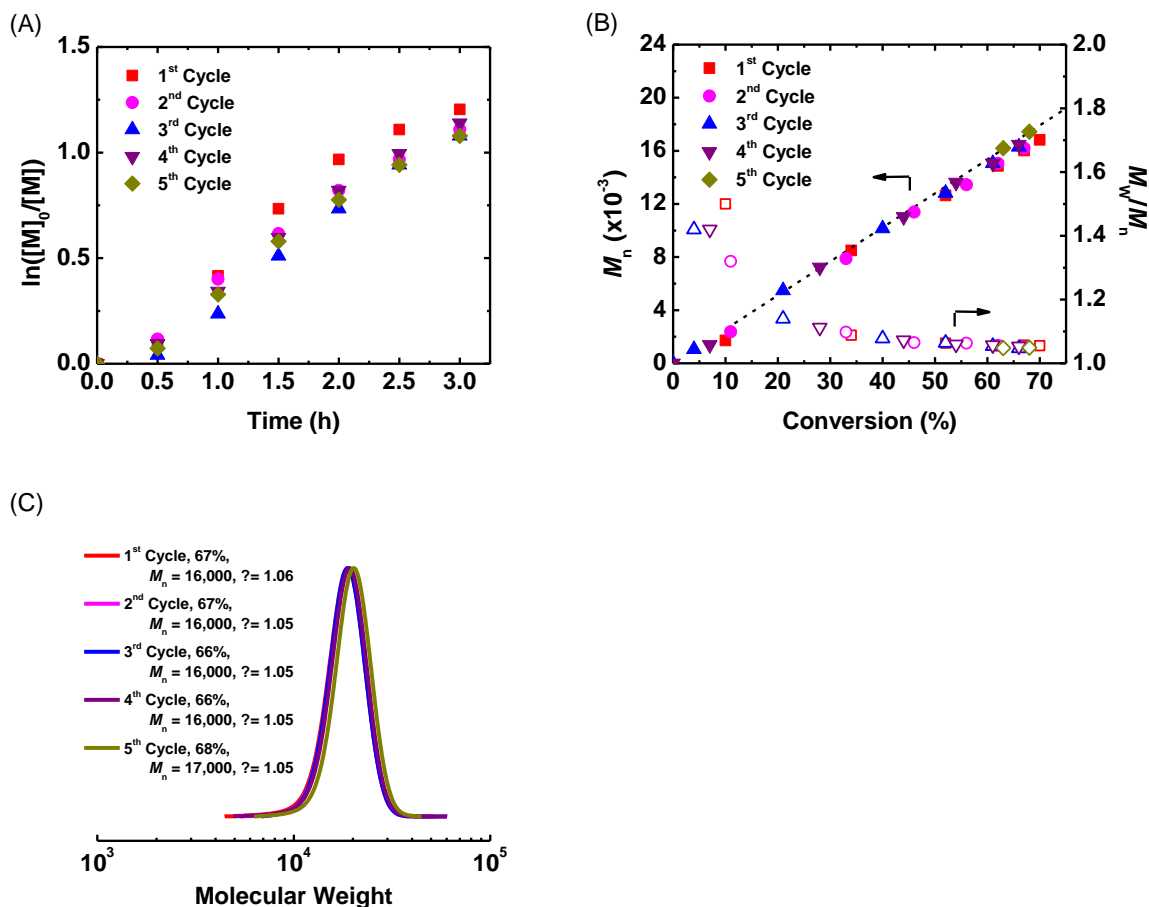


Figure A-VI-5. (A) Kinetics, (B) evolution of M_n and M_w/M_n with conversion in the ATRP of BA, and (C) GPC traces at ~67% conversion for 5 sequential polymerizations with reused silver wire. Reaction conditions: $[BA]_0/[EBiB]_0/[CuBr_2]_0/[TPMA]_0 = 200/1/0.04/0.08$ with $[BA]_0 = 3.49$ M in DMF at 50 °C, in the presence of 5 cm Ag^0 wire ($d = 2$ mm, $SA = 3.2$ cm²; $V_{tot} = 10$ mL).

It is also desirable to decrease the amount of catalyst necessary for reaction, so five different polymerizations were run with various initial $\text{CuBr}_2/\text{TPMA}$ catalyst loadings (Figure A-VI-6).^{99a, 295} As observed previously,²⁹⁶ decrease of catalyst concentration resulted in a reduction of reaction rate and a slight broadening of MWD. However, at all catalyst concentrations linear increase of M_n with conversion was observed, with experimental values matching up well to theoretical. Additionally, with catalyst loadings of down to 10 ppm $\text{Cu}^{\text{II}}\text{Br}_2$, at 62% monomer conversion $\bar{D} = 1.27$, indicating remarkably good control relative to comparable low-catalyst systems.

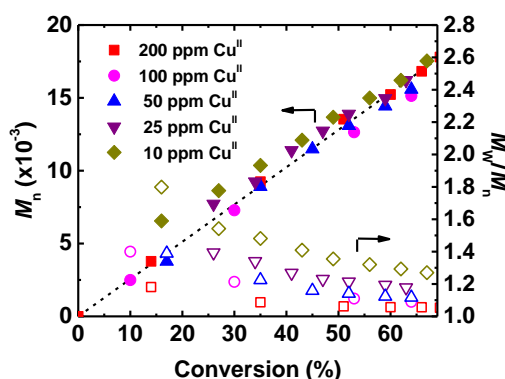


Figure A-VI-6. Evolution of M_n and M_w/M_n with conversion in the ATRP of BA with various initial concentrations of $\text{Cu}^{\text{II}}\text{Br}_2$. Reaction conditions: $[\text{BA}]_0/[\text{EBiB}]_0/[\text{CuBr}_2]_0/[\text{TPMA}]_0 = 200/1/x/2x$ ($x = 0.04, 0.02, 0.01, 0.005, 0.002$) with $[\text{BA}]_0 = 3.49 \text{ M}$ in DMF at 50°C , in the presence of 5 cm Ag^0 wire ($d = 2 \text{ mm}$, $\text{SA} = 3.2 \text{ cm}^2$; $V_{\text{tot}} = 10 \text{ mL}$).

To expand the scope of this methodology, polymerizations of tert-butyl acrylate (*t*BA) and methyl acrylate (MA) were carried out and for both acrylates 60% monomer conversion was achieved in under 2 h (Figure A-VI-7). MW was in good agreement with

theoretical values, indicating a high degree of livingness and preservation of chain-end functionality. A sample of P*t*BA ($M_n = 3,600$; $\bar{D} = 1.17$) was further studied by ^1H NMR spectroscopy and indicated $97 \pm 3\%$ retention of chain end functionality (Figure A-VI-8). This result suggested the possibility of facile and precise block copolymer synthesis, so chain extension from poly(*n*-butyl acrylate) (PBA) was carried out. PBA-Br ($M_n = 6,600$, $\bar{D} = 1.08$) was synthesized and purified according to the procedure given in the Experimental Section, and used as a macroinitiator in the subsequent polymerization of *t*BA. Monomer conversion as a function of time revealed pseudo-first-order kinetics, suggesting that a constant concentration of radicals was maintained throughout the reaction. Additionally, a linear increase in MW with conversion was observed while maintaining very narrow MWD, with $\bar{D} = 1.04$ (Figure A-VI-9). The GPC traces of chain extension shown in Figure A-VI-10 reveal very narrow MWD with minor low MW tailing at higher conversions, typical for this type of chain extension.^{260b} However, it should be noted that at lower monomer conversion ($> 50\%$), \bar{D} actually decreased upon chain extension from the PBA-Br macroinitiator, from $\bar{D} = 1.07$ to $\bar{D} = 1.02$ at 40% conversion. Thus, copper-catalyzed ATRP with Ag^0 is a very powerful method for the preparation of highly defined block copolymers.

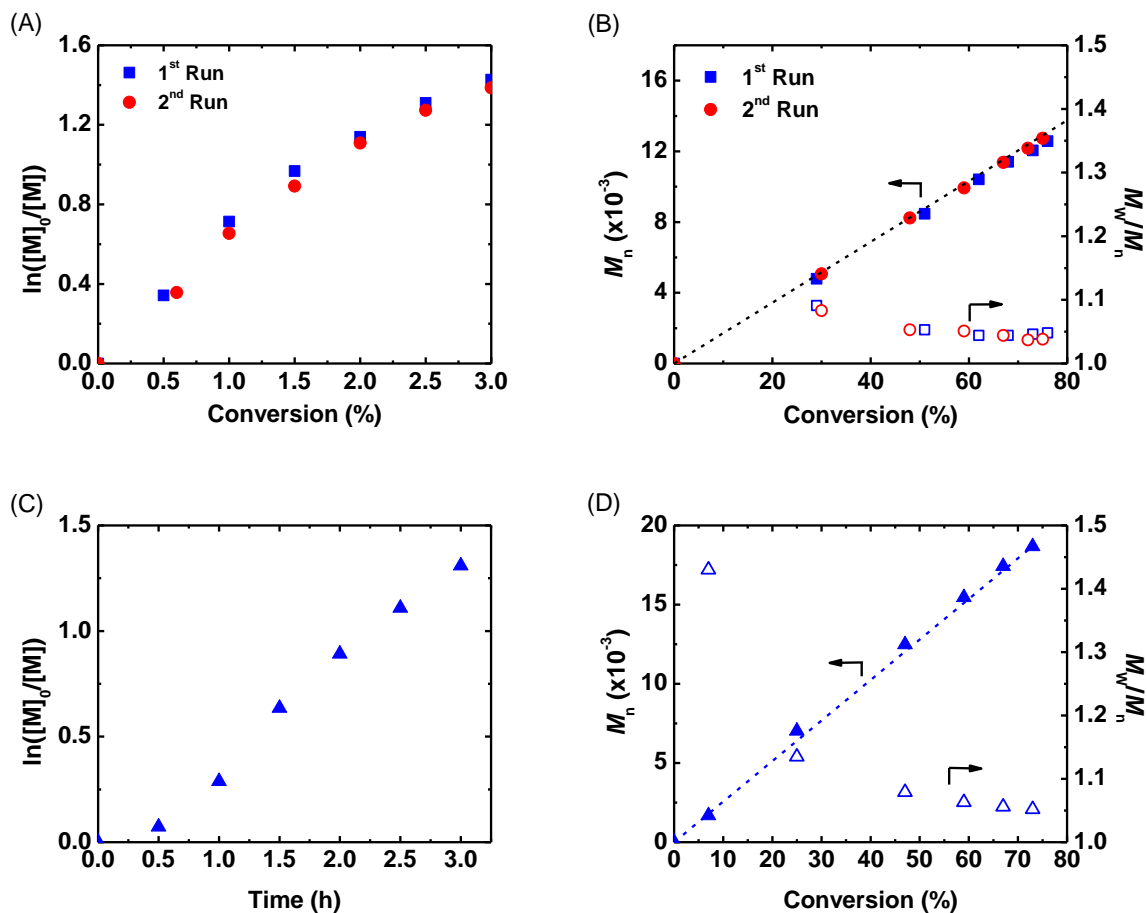


Figure A-VI-7. (A) Kinetics and (B) evolution of M_n and M_w/M_n with conversion for the polymerization of MA in DMF and (C) kinetics and (D) evolution of M_n and M_w/M_n with conversion for the polymerization of *t*BA in DMF. Reaction conditions: $[M]_0/[EBiB]_0/[CuBr_2]_0/[TPMA]_0 = 200/1/0.04/0.08$ with $[M]_0 = 3.49$ M in DMF at 50 °C, in the presence of 5 cm Ag^0 wire ($d = 2$ mm, SA 3.2 cm²; $V_{tot} = 10$ mL), M = MA or *t*BA.

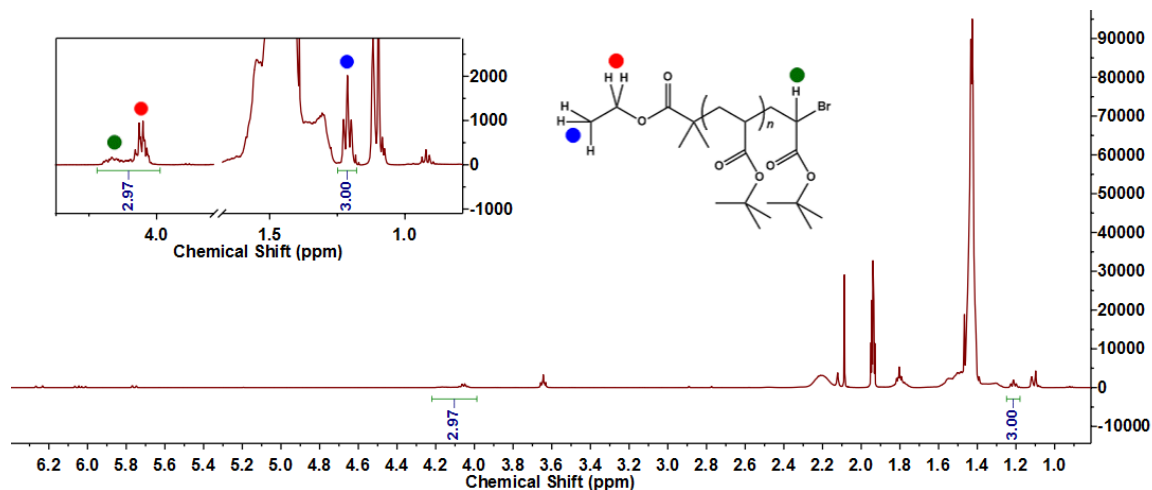


Figure A-VI-8. ^1H NMR spectrum of PtBA ($M_n = 3,600$, $\bar{D} = 1.17$) in CD_3CN . Inset: Regions containing resonances of interest. Conditions: 500 MHz, acquisition time = 5.5 s (sweep width = 12 ppm, centered at 5 ppm), delay = 15 s, number of scans = 128.

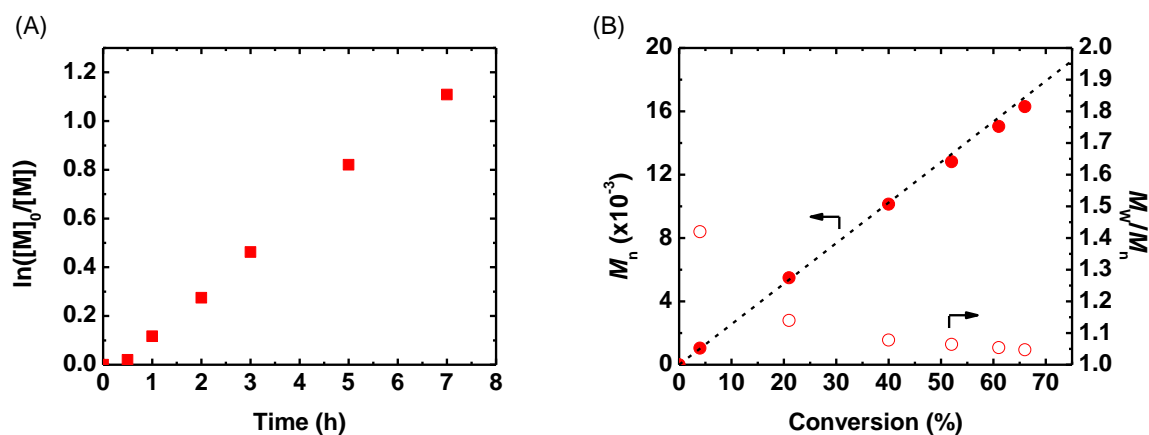


Figure A-VI-9. (A) Kinetics (B) evolution of M_n and M_w/M_n with conversion for the chain extension of $t\text{BA}$ from PBA-Br. Reaction conditions: $[t\text{BA}]_0/[PBA\text{-Br}]_0/[\text{CuBr}_2]_0/[\text{TPMA}]_0 = 1000/1/0.2/0.4$ with $[t\text{BA}]_0 = 3.49$ M in DMF at 50°C , in the presence of 5 cm Ag^0 wire ($d = 2$ mm, $\text{SA} = 3.2$ cm^2 ; $V_{\text{tot}} = 10$ mL).

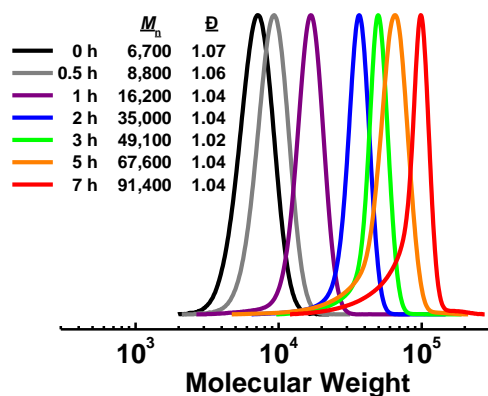


Figure A-VI-10. GPC traces for the chain extension from PBA-Br with *t*BA. Reaction conditions: $[tBA]_0/[PBA-Br]_0/[CuBr_2]_0/[TPMA]_0 = 1000/1/0.2/0.4$ with $[tBA]_0 = 3.49$ M in DMF at 50 °C, in the presence of 5 cm Ag^0 wire ($d = 2$ mm, $SA = 3.2$ cm²; $V_{tot} = 10$ mL).

A-VI. 3. Summary

A new copper-catalyzed ATRP system with elemental silver as the reducing agent was developed. Good control over polymerization of BA, *t*BA and MA was demonstrated with this methodology, with MW dispersity down to $\bar{D} = 1.03$. Monomer conversions of 60% were achieved in 1.5 – 2 h with 200 ppm $CuBr_2/TPMA$ catalyst loading, and MW of the resulting polymers were in good agreement with theoretical values. The same silver wire could be used for several sequential polymerizations without adverse effects on the polymer produced, and treatment of the silver was not required after each reaction. The amount of silver wire used in each reaction could be reduced to $l = 0.5$ cm, corresponding to a surface area-to-volume ratio of 0.04 cm⁻¹, without decrease in control. Polymerization of BA with 10 ppm $CuBr_2/TPMA$ catalyst loading afforded PBA with MW in excellent

agreement with theoretical values and $\bar{D} = 1.29$. Chain extension of a PBA-Br macroinitiator with *t*BA exhibited high chain-end functionality, and a PBA-*b*-P*t*BA-Br diblock copolymer was synthesized with $\bar{D} = 1.02$.

The use of silver as a reducing agent in ATRP represents a significant advance. As silver is a one-electron heterogeneous reductant, the side reactions that often hinder the efficacy of conventionalARGET ATRP reactions are minimized, and in contrast to the Cu⁰ used in traditional SARA ATRP reactions, Ag⁰ does not engender a buildup of reactive Cu^I through the course of reaction. As evidenced by the low \bar{D} values and high livingness observed here, silver likely does not act to generate nor terminate radicals in the system, thereby eliminating the side reactions observed in other ATRP processes which have previously led to some loss of chain-end functionality. As such, silver is an excellent reducing agent for highly controlled ATRP.

A-VI. 4. Experimental Section

Materials. *n*-Butyl acrylate (BA), *tert*-butyl acrylate (*t*BA), methyl acrylate (MA), ethyl α -bromoisobutyrate (EBiB) and copper (II) bromide (CuBr₂) were purchased from various suppliers. Monomers were passed through basic alumina to remove inhibitors and stored at 0 °C before use. Dimethylformamide (DMF) was purchased from Fisher and used without any purification, and silver wire (Alfa, Strem) was used without prior treatment unless otherwise noted. Tris(2-pyridylmethyl)amine (TPMA) was synthesized as according to literature procedures.²⁹⁴ All solvents and monomers were bubbled with dry N₂ gas for 30 minutes prior to use unless otherwise noted.

Measurements. Monomer conversion was determined by ^1H NMR in CDCl_3 using a Bruker Avance 300 MHz spectrometer with DMF ($\delta = 2.96, 2.88, (\text{CH}_3)_2\text{NCOH}$) as the internal standard.²⁹⁷ Number average molecular weight (M_n) and M_w/M_n values were determined by gel permeation chromatography (GPC) using PSS columns in THF at an eluent at a flow rate of 1 mL/min at 35 °C, calibrated to PMMA using DPE or toluene as an internal standard. The GPC system was composed of Waters 515 HPLC Pump and Waters 2414 Refractive Index Detector. Each sample was filtered over neutral alumina prior to analysis. A Mark-Houwink correction was applied to all samples to obtain the MW of PBA, *t*BA, or PMA with respect to the PMMA standard. UV-Visible Spectroscopy was performed on a Varian Cary 5000 UV-Vis-NIR spectrometer.

General polymerization procedure. (a) A 10 mL Schlenk flask was charged with Ag^0 wire ($d = 2$ mm, $l = 5$ cm) and stirbar, sealed, and evacuated and refilled with N_2 three times. Excess DMF and BA were independently deoxygenated by bubbling with N_2 for a minimum of 30 min, and 5.0 mL of each were added to the Schlenk flask *via* syringe. A stock solution of $\text{CuBr}_2/\text{TPMA}$ (140 μL of 0.05 M CuBr_2 and 0.10 M TPMA in DMF, 0.007 mmol CuBr_2 and 0.014 mmol TPMA), then EBiB (26 μL , 0.17 mmol), was added *via* syringe. The flask was again sealed and heated to 50 °C, and the reaction was monitored by GPC and ^1H NMR spectroscopy. **(b)** A 10 mL Schlenk flask was charged with Ag^0 wire ($d = 2$ mm, $l = 5$ cm) and stirbar, sealed, and evacuated and refilled with N_2 six times. A solution of $\text{CuBr}_2/\text{TPMA}$ (168 μL of 0.05 M CuBr_2 and 0.10 M TPMA in DMF, 0.008 mmol CuBr_2 and 0.017 mmol TPMA), EBiB (41 mg, 0.21 mmol), DMF (6.0 mL), and BA (6.0 mL, 42 mmol) was prepared and degassed *via* four freeze-pump-thaw cycles, and 10

mL of this solution was added to the reaction flask under N₂ *via* syringe. The flask was sealed and heated to 50 °C, and the reaction was monitored by GPC and ¹H NMR spectroscopy.

Chain extension of *t*BA from PBA-Br. A PBA-Br macroinitiator ($M_n = 6,600$ g/mol, $\bar{D} = 1.08$) was synthesized according to procedure (a) above and purified by precipitation in methanol/water (85/15 by v/v) three times, separating the polymer from the solution by centrifugation. The product was collected and dried under vacuum for 1 day. Silver wire ($d = 2$ mm, $l = 5$ cm) was placed in a Schlenk flask under N₂. The synthesized PBA-Br (320 mg, 0.0419 mmol) was dissolved in DMF (7 mL) and transferred to the reaction flask, and bubbled with N₂ for 30 minutes. Excess *t*BA was deoxygenated by bubbling with N₂ for 30 min and 7.0 mL (49 mmol) was added to the Schlenk flask *via* syringe, then the solution of CuBr₂/TPMA (195 μ L of 0.05 M CuBr₂ and 0.1 M TPMA in DMF, 0.01 mmol CuBr₂ and 0.02 mmol TPMA) was added. The flask was sealed and heated to 50 °C, and the reaction was monitored by GPC and ¹H NMR spectroscopy.

Reduction Kinetics of Cu^{II}Br₂ by Ag⁰. The reduction of Cu^{II}Br₂ by Ag⁰ was monitored by UV-Vis-NIR spectroscopy. The reaction was set up according to procedure (b), with the exclusion of EBiB initiator, and decrease in absorbance of the Cu^{II} *d-d* band at 930 nm was recorded as a function of time (Figure A-VI-1). A plot of $\ln([Cu^{II}]_0/[Cu^{II}])$ vs. time showed a pseudo-first-order initial reduction, followed by a decrease in reduction rate until a constant Cu^{II} concentration was observed after *ca.* 90 minutes.

Reaction with Initiator. The polymerization of BA was carried out according to

procedure (b). As discussed in the main text, 62% monomer conversion was observed after 2 h, with $\bar{D} = 1.03$ after 2 h. Kinetic and GPC data are shown in Figure A-VI-2.

High Conversion Experiments. To explore the polymerization at high conversions, the ATRP of BA was run for 9 h, achieving 90% monomer conversion. Although reaction rate slowed down after approximately 60% conversion, the polymerization was highly controlled at longer reaction times, as illustrated by kinetic and MW data in Figure A-VI-3. At high conversion (~90%) a slight increase in \bar{D} was observed corresponding to the appearance of a small high MW shoulder, presumably due to radical termination, as shown in the GPC traces.

Ag⁰ as a Reducing Agent Only. The polymerization of BA was attempted in the presence (RA) and absence (SARA) of CuBr₂ catalyst. The reaction was set up according to procedure (a), with the exclusion of CuBr₂ catalyst (SARA), and reaction progress was monitored by ¹H NMR spectroscopy. As illustrated in Figure A-VI-11, 50% BA conversion was observed in the presence of CuBr₂ catalyst. However, in the absence of CuBr₂ no monomer conversion was observed after 2 hours, suggesting that if a supplemental activation process was occurring with silver, it was much slower than activation by copper.

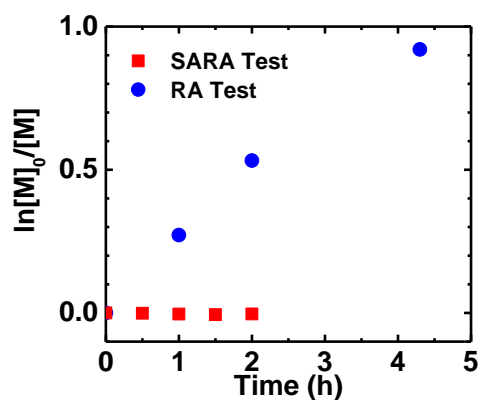


Figure A-VI-11. Polymerization of BA in the presence (RA) and absence (SARA) of CuBr_2 catalyst. Reaction conditions: **SARA**: $[\text{BA}]_0/[\text{EBiB}]_0/[\text{TPMA}]_0 = 160/1/0.018/0.036$ with $[\text{BA}]_0 = 3.49$ M in DMF at 50°C , in the presence of 10 cm Ag^0 wire ($d = 1$ mm, $\text{SA} = 3.2$ cm 2); **RA**: $[\text{BA}]_0/[\text{EBiB}]_0/[\text{CuBr}_2]_0/[\text{TPMA}]_0 = 160/1/0.018/0.036$ with $[\text{BA}]_0 = 3.49$ M in DMF at 50°C , in the presence of 10 cm Ag^0 wire ($d = 1$ mm, $\text{SA} = 3.2$ cm 2).

Ag^0 Wire Length. The polymerization of BA was carried out according to procedure (b) with 5 different lengths of Ag^0 wire (10, 5, 2, 1, and 0.5 cm) corresponding to SA/V values of 0.64, 0.32, 0.13, 0.07 and 0.04 cm $^{-1}$, respectively, and results are given in Figure A-VI-4. GPC traces as a function of reaction progress for $l = 0.5$ cm are given in Figure A-VI-12.

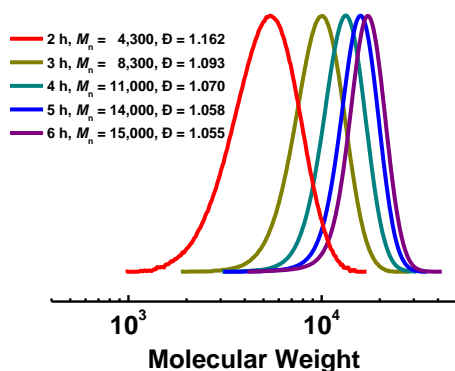


Figure A-VI-12. GPC traces as a function of reaction progress for the polymerization of BA in DMF with low S/V of silver. Reaction conditions: $[BA]_0/[EBiB]_0/[CuBr_2]_0/[TPMA]_0 = 200/1/0.04/0.08$ with $[BA]_0 = 3.49$ M in DMF at 50 °C, in the presence of 0.5 cm Ag^0 wire ($d = 2$ mm, $SA = 0.4$ cm²; $V_{tot} = 10$ mL; $S/V = 0.04$ cm⁻¹).

Ag^0 Reuse. The polymerization of BA was carried out according to procedure (b) using the same length of Ag^0 wire for five sequential reactions (Figure A-VI-5). Between each reaction, the Ag^0 was rinsed gently with acetone and allowed to air-dry. Figure A-VI-13 shows the silver wire before reaction and after each sequential polymerization. The loss of luster upon reaction likely correlates to reaction of Ag^0 atoms at the surface of the wire. Accordingly, Ag^0 mass lost was measured for the first cycle at 70% monomer conversion, in which the wire mass decreased by 2 mg, corresponding to consumption of 0.019 mmol Ag^0 or 2.6 Ag^0 per $CuBr_2$.

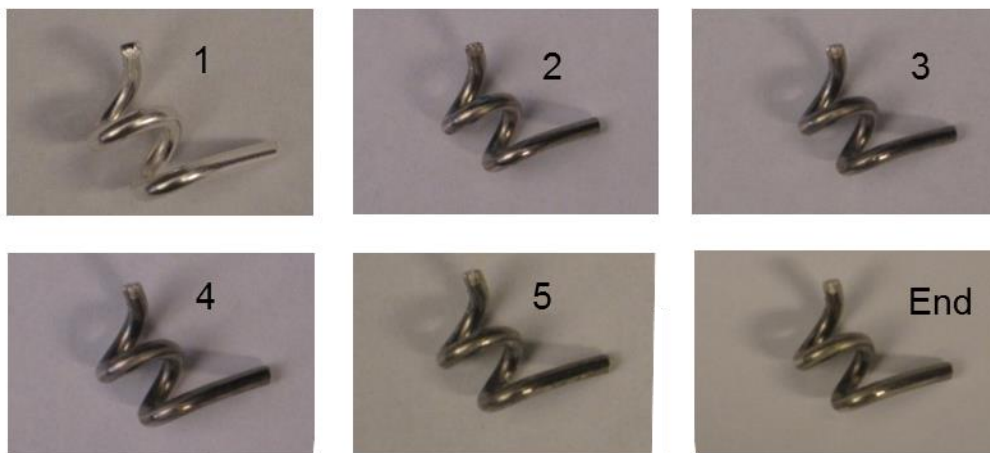


Figure A-VI-13. Photographs of Ag^0 before reaction (1) and after each polymerization (2 – End). Reaction conditions: $[\text{BA}]_0/[\text{EBiB}]_0/[\text{CuBr}_2]_0/[\text{TPMA}]_0 = 200/1/0.04/0.08$ with $[\text{BA}]_0 = 3.49 \text{ M}$ in DMF at 50°C , in the presence of 5 cm Ag^0 wire ($d = 2 \text{ mm}$, $\text{SA} = 3.2 \text{ cm}^2$; $V_{\text{tot}} = 10 \text{ mL}$).

Low Copper Concentration Experiments. The polymerization of BA was carried out according to procedure (b) at different initial CuBr_2 catalyst loadings. The kinetic data for the reactions are shown in Figure A-VI-14, and MW data are given in Figure A-VI-6. Within error, the rate of polymerization with 10 and 25 ppm CuBr_2 were the same, and at higher CuBr_2 concentrations the reaction rate increased with increasing catalyst concentration as expected.

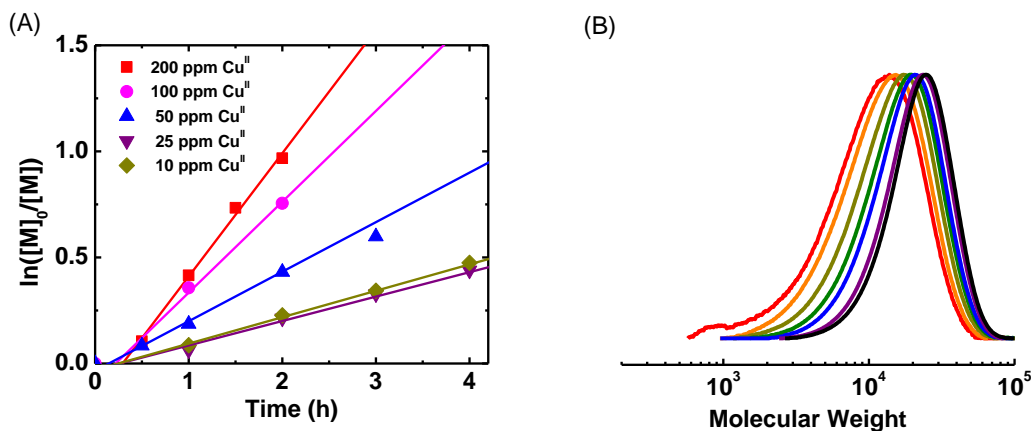


Figure A-VI-14. (A) Kinetic data for the polymerization of BA in DMF with various initial concentrations of $\text{Cu}^{\text{II}}\text{Br}_2$ and (B) GPC traces for the polymerization of BA with 10 ppm catalyst loading. Reaction conditions: $[\text{BA}]_0/[\text{EBiB}]_0/[\text{CuBr}_2]_0/[\text{TPMA}]_0 = 200/1/x/2x$ ($x = 0.04, 0.02, 0.01, 0.005, 0.002$) with $[\text{BA}]_0 = 3.49 \text{ M}$ in DMF at 50°C , in the presence of 5 cm Ag^0 wire ($d = 2 \text{ mm}$, $\text{SA} = 3.2 \text{ cm}^2$; $V_{\text{tot}} = 10 \text{ mL}$).

MA and *t*BA Polymerizations. To expand the accessible substrate scope, the polymerization of MA and *t*BA were carried out according to procedure (b). Kinetic and GPC data are given in Figure A-VI-7, and indicate fast pseudo-first-order kinetics with a high degree of livingness for both monomers.

Determination of Chain-End Retention by ^1H NMR Spectroscopy. A low MW sample of *Pt*BA was prepared according to procedure (b), with $M_n = 3,600$ and $D = 1.17$. The ^1H NMR spectrum of the polymer was acquired in CD_3CN as shown in Figure A-VI-8. The resonances corresponding to both the initiator-derived methylene protons (red circle) and chain-end methine proton (green circle) appear as overlapping signals at approximately 4.1 ppm. However, integration of the initiator-derived methyl protons (blue circle) vs. the

combined methylene and methane protons indicates ~ 97% chain-end retention.

Chain-Extension Experiments. Chain extension of *t*BA from a PBA-Br macroinitiator was carried out according to procedure (c). Kinetic and MW data are given in Figure A-VI-9, and GPC traces of the chain extension are shown in Figure A-VI-10.

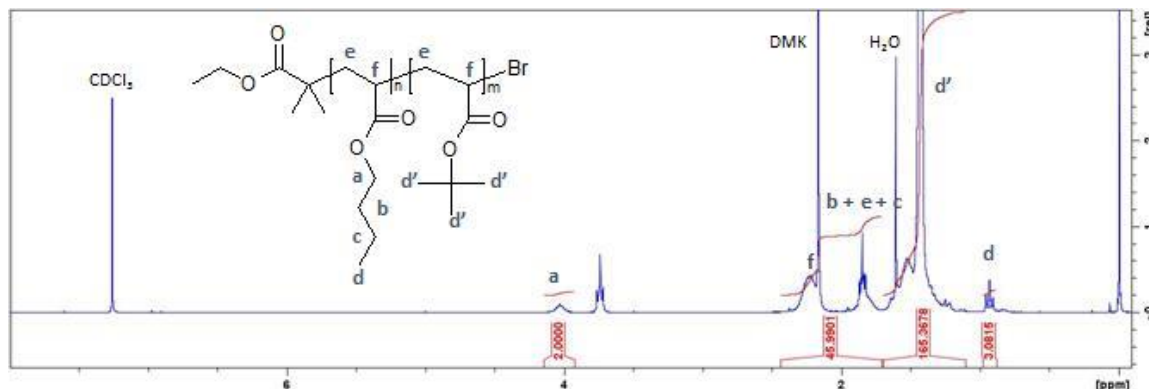


Figure A-VI-15. ^1H -NMR spectrum of PBA-*b*-PtBA block copolymer after purification.

A-VI. 5. References

1. (a) Matyjaszewski, K.; Davis, T. P., *Handbook of Radical Polymerization*. Wiley-Interscience: Hoboken, 2002; (b) Goto, A.; Fukuda, T., *Prog. Polym. Sci.* **2004**, 29 (4), 329-385; (c) Braunecker, W. A.; Matyjaszewski, K., *Progress in Polymer Science* **2007**, 32 (1), 93-146.
2. (a) Szwarc, M., *Nature* **1956**, 178, 1168-9; (b) Smid, J.; Van Beylen, M.; Hogen-Esch, T. E., *Progress in Polymer Science* **2006**, 31 (12), 1041-1067.
3. (a) Wang, J.-S.; Matyjaszewski, K., *Journal of the American Chemical Society* **1995**, 117 (20), 5614-15; (b) Kato, M.; Kamigaito, M.; Sawamoto, M.; Higashimura, T., *Macromolecules* **1995**, 28 (5), 1721-1723; (c) Patten, T. E.; Xia, J.; Abernathy, T.; Matyjaszewski, K., *Science (Washington, D. C.)* **1996**, 272 (5263), 866-868; (d) Matyjaszewski, K.; Xia, J., *Chemical Reviews* **2001**, 101 (9), 2921-2990; (e) Kamigaito, M.; Ando, T.; Sawamoto, M., *Chem. Rev.* **2001**, 101 (12), 3689-3745; (f) Matyjaszewski, K.; Tsarevsky, N. V., *J. Am. Chem. Soc.* **2014**, 136 (Copyright (C) 2014 American Chemical Society (ACS). All Rights Reserved.), 6513-6533; (g) Matyjaszewski, K.; Tsarevsky, N. V., *Nature Chemistry* **2009**, 1 (4), 276-288.
4. (a) Nicolas, J.; Guilleaume, Y.; Lefay, C.; Bertin, D.; Gigmes, D.; Charleux, B., *Progress in Polymer Science* **2013**, 38 (1), 63-235; (b) Grubbs, R. B., *Polymer Reviews*

- 2011**, *51* (2), 104-137; (c) Sciannamea, V.; Jérôme, R.; Detrembleur, C., *Chemical Reviews* **2008**, *108* (3), 1104-1126; (d) Poli, R.; Allan, L. E. N.; Shaver, M. P., *Prog. Polym. Sci.* **2014**, *39* (10), 1827-1845.
5. (a) Chiefari, J.; Chong, Y. K.; Ercole, F.; Krstina, J.; Jeffery, J.; Le, T. P. T.; Mayadunne, R. T. A.; Meijs, G. F.; Moad, C. L.; Moad, G.; Rizzardo, E.; Thang, S. H., *Macromolecules* **1998**, *31* (16), 5559-5562; (b) Moad, G.; Rizzardo, E.; Thang, S. H., *Australian Journal of Chemistry* **2012**, *65* (8), 985-1076; (c) Moad, G.; Rizzardo, E.; Thang, S. H., *Accounts of Chemical Research* **2008**, *41* (9), 1133-1142; (d) Ran, J.; Wu, L.; Zhang, Z.; Xu, T., *Prog. Polym. Sci.* **2014**, *39* (1), 124-144; (e) Moad, G.; Rizzardo, E.; Thang, S. H., *Polymer* **2008**, *49* (5), 1079-1131; (f) Quinn, J. F., *Chemical communications (Cambridge, England)* **2001**, (11), 1044; (g) Hardy, C. G.; Zhang, J.; Yan, Y.; Ren, L.; Tang, C., *Prog. Polym. Sci.* **2014**, *39* (10), 1742-1796; (h) Ahmed, M.; Narain, R., *Prog. Polym. Sci.* **2013**, *38* (5), 767-790.
6. (a) Matyjaszewski, K., *Macromolecules* **2012**, *45* (10), 4015-4039; (b) Ayres, N., *Polymer Reviews* **2011**, *51* (2), 138-162.
7. Fischer, H., *Chem. Rev.* **2001**, *101* (12), 3581-3610.
8. Tsarevsky, N. V.; Matyjaszewski, K., *Chemical Reviews (Washington, DC, United States)* **2007**, *107* (6), 2270-2299.
9. Matyjaszewski, K.; Jakubowski, W.; Min, K.; Tang, W.; Huang, J.; Braunecker, W. A.; Tsarevsky, N. V., *Proceedings of the National Academy of Sciences* **2006**, *103* (42), 15309-15314.
10. (a) Jakubowski, W.; Matyjaszewski, K., *Angew. Chem. Int. Ed.* **2006**, *45* (27), 4482-4486; (b) Chan, N.; Cunningham, M. F.; Hutchinson, R. A., *Macromol. Chem. Phys.* **2008**, *209* (17), 1797-1805.
11. Magenau, A. J. D.; Strandwitz, N. C.; Gennaro, A.; Matyjaszewski, K., *Science* **2011**, *332* (6025), 81-84.
12. (a) Ribelli, T. G.; Konkolewicz, D.; Bernhard, S.; Matyjaszewski, K., *Journal of the American Chemical Society* **2014**, *136* (38), 13303-13312; (b) Tasdelen, M. A.; Uygün, M.; Yagci, Y., *Macromolecular Chemistry and Physics* **2010**, *211* (21), 2271-2275; (c) Tasdelen, M. A.; Uygün, M.; Yagci, Y., *Macromolecular Rapid Communications* **2011**, *32* (1), 58-62; (d) Mosnáček, J.; Ilčíková, M., *Macromolecules* **2012**, *45* (15), 5859-5865; (e) Konkolewicz, D.; Schröder, K.; Buback, J.; Bernhard, S.; Matyjaszewski, K., *ACS Macro Letters* **2012**, *1* (10), 1219-1223; (f) Anastasaki, A.; Nikolaou, V.; Zhang, Q.; Burns, J.; Samanta, S. R.; Waldron, C.; Haddleton, A. J.; McHale, R.; Fox, D.; Percec, V.; Wilson, P.; Haddleton, D. M., *Journal of the American Chemical Society* **2014**, *136* (3), 1141-1149.
13. (a) Konkolewicz, D.; Wang, Y.; Zhong, M.; Krys, P.; Isse, A. A.; Gennaro, A.; Matyjaszewski, K., *Macromolecules* **2013**, *46* (22), 8749-8772; (b) Guliashvili, T.; Mendonça, P. V.; Serra, A. C.; Popov, A. V.; Coelho, J. F. J., *Chemistry – A European Journal* **2012**, *18* (15), 4607-4612; (c) Rosen, B. M.; Percec, V., *Chem. Rev.* **2009**, *109* (11), 5069-5119.
14. Matyjaszewski, K.; Coca, S.; Gaynor, S. G.; Wei, M.; Woodworth, B. E., *Macromolecules* **1997**, *30* (23), 7348-7350.
15. (a) Wang, Y.; Soerensen, N.; Zhong, M.; Schroeder, H.; Buback, M.; Matyjaszewski, K., *Macromolecules* **2013**, *46* (3), 683-691; (b) Konkolewicz, D.; Wang, Y.; Krys, P.;

- Zhong, M.; Isse, A. A.; Gennaro, A.; Matyjaszewski, K., *Polym. Chem.* **2014**, 5 (15), 4396-4417.
16. Zhang, Y.; Wang, Y.; Matyjaszewski, K., *Macromolecules* **2011**, 44, 683–685.
17. (a) Riedel, S.; Kaupp, M., *Coordination Chemistry Reviews* **2009**, 253 (5–6), 606-624; (b) Tarsey, A. R., *Journal of Chemical Education* **1954**, 31 (7), 375.
18. Lucarelli, C.; Vaccari, A., *Green Chemistry* **2011**, 13 (8), 1941-1949.
19. (a) Canary, J. W.; Wang, Y.; Roy, R.; Lawrence, Q.; Miyake, H., Tris[(2-Pyridyl)methyl] Amine (TPA) and (+)-Bis[(2-Pyridyl)methyl]-1-(2-Pyridyl)-Ethylamine (α -Metpa). In *Inorganic Syntheses*, John Wiley & Sons, Inc.: Hoboken, NJ, 2007; pp 70-75; (b) Britovsek, G. J. P.; England, J.; White, A. J. P., *Inorg. Chem.* **2005**, 44 (22), 8125-8134.
20. (a) Shen, Y.; Tang, H.; Ding, S., *Prog. Polym. Sci.* **2004**, 29 (10), 1053-1078; (b) Mueller, L.; Matyjaszewski, K., *Macromol. React. Eng.* **2010**, 4 (3-4), 180-185.
21. Pintauer, T.; Matyjaszewski, K., *Chemical Society Reviews* **2008**, 37 (6), 1087-1097.
22. Zhong, M.; Matyjaszewski, K., *Macromolecules* **2011**, 44 (8), 2668-2677.
23. Fulmer, G. R.; Miller, A. J. M.; Sherden, N. H.; Gottlieb, H. E.; Nudelman, A.; Stoltz, B. M.; Bercaw, J. E.; Goldberg, K. I., *Organometallics* **2010**, 29 (9), 2176-2179.

Appendix VII

Synthesis of β -cyclodextrin-based star polymers *via* a simplified electrochemically mediated ATRP*

A-VII. 1. Introduction

Atom transfer radical polymerization (ATRP) is one of the most versatile reversible deactivation radical polymerization (RDRP) methods, permitting control over macromolecular topology.^{1a-c, 2b-d, 14c, 15, 89, 253c, 298} During the past few years, various poly(meth)acrylates, poly(meth)acrylamides, polystyrenes, and polyacrylonitrile were successfully prepared by ATRP with relatively narrow molecular weight distribution (M_w/M_n , MWD) and targeted degrees of polymerization (DP).^{1a, 3a, 3c, 3e, 23d, 89b, 90c, 90d, 299}

Star polymers, consisting of multiple arms linked to a central core, have attracted significant attention, because of their branched architecture, globular shape, and chemically crosslinked structure.^{42a-d, 300} One approach to prepare star polymers *via* ATRP is the core-first technique, which involves the use of a multifunctional initiator, which predetermines the number of arms in the star polymer by the number of initiating sites on the initiator. In addition, the star polymers can easily introduce next segment by chain extension of ω -chain ends (at periphery of the stars) and the final products can be easily purified.^{300a, 301} β -Cyclodextrin (β -CD) is a cyclic oligosaccharide consisting of seven glucose units linked by α -1,4-glucosidic bonds with seven primary and fourteen secondary hydroxyl groups.³⁰²

*Work in this appendix was published and partially reformatted based on the following manuscript: Chmielarz, Paweł; **Park, Sangwoo**; Sobkowiak, Andrzej; Matyjaszewski, Krzysztof *Polymer* **2016**, 88, 36

The core can be used for selective modification of the hydroxyl groups. Therefore β -CD is an excellent candidate, among molecules of cyclical structure, for synthesis of star polymers *via* the core-first approach.³⁰²⁻³⁰³

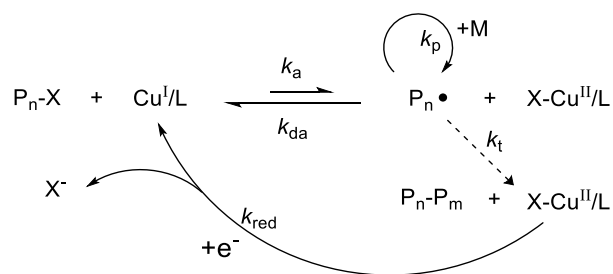
Amphiphilic star polymers composed of poly(*n*-butyl acrylate) (PBA) arms covalently linked to a β -CD core are especially interesting, because they can be potentially used in biomedical applications, such as target drug delivery system. Furthermore PBA is an industrially important polymer because of its low glass-transition temperature, durability, and potential use as a soft segment in thermoplastic elastomers.^{258, 304}

Previously using a β -CD macroinitiator, star polymers composed of poly(methyl methacrylate),^{301b, 305} poly(*tert*-butyl acrylate),^{303c, 306} poly(2-(dimethylamino)ethyl methacrylate),^{303f, 303h, 303j} poly((2-hydroxy-3-(2-aminoethyl) amino)propyl methacrylate),^{303h} polyacrylamide,³⁰² poly(*N*-isopropylacrylamide),³⁰³ⁱ poly(*N*-(3-(dimethylamino)propyl) methacrylamide),^{303h} or poly((2-(methacryloyloxy)ethyl) trimethyl ammonium)^{303a, 303h, 307} were synthesized using ATRP, but synthesis of β -CD-PBA has not yet been reported. Furthermore, in all cases rather high catalyst loadings, *ca.* 4,000–130,000 ppm as a molar ratio of catalysts to monomer (590–19,000 ppm (by wt)), were used for the star synthesis.^{301b, 302-303, 303c, 303f, 303h-j, 305, 307}

The advent of new low catalyst ATRP systems, that use parts per million (ppm) concentrations of catalyst, such as activators regenerated by electron transfer (ARGET) ATRP,⁹⁷ initiators for continuous activator regeneration (ICAR) ATRP,^{5a} supplemental activator and reducing agent (SARA) ATRP³⁰⁸ and photoinduced ATRP^{8e} offer more environmentally benign and industrially scalable reaction conditions for the synthesis of

polymers prepared by ATRP, but also provides an option to prepare polymers with designed dispersity, defined by the catalyst concentration.^{89b}

More recently, a novel ATRP process termed electrochemically mediated ATRP (*e*ATRP) was developed.^{10-11, 13b, 23b, 23d, 41a, 43b, 96b, 309} It has same advantages for synthesis of complex polymeric architectures, for example star polymers.^{13b} Based on the mechanism of *e*ATRP, the ratio of the concentration of $\text{Cu}^{\text{I}}/\text{L}$ to $\text{X-Cu}^{\text{II}}/\text{L}$ can be precisely controlled by the applied current (I), and potential (E) at the electrode surface.¹¹ Consequently, the concentration of the radical species required to propagate and form polymeric chains by reacting with monomers (M), and the efficiency of deactivation back to the dormant species ($\text{P}_n\text{-X}$) can be controlled, Scheme A-VII-1.^{309b}

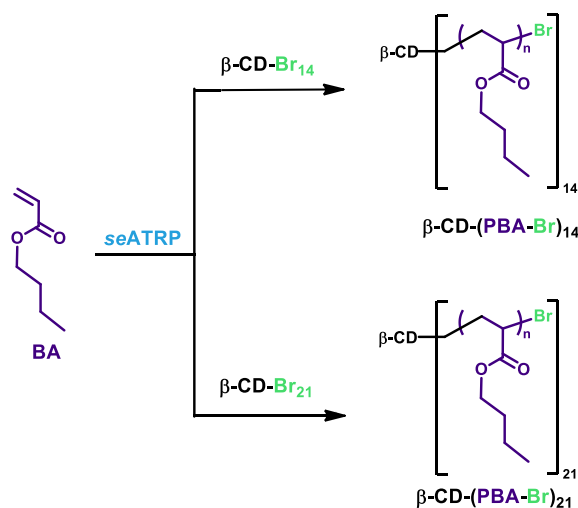


Scheme A-VII-1. Mechanism of *e*ATRP. Reprinted with permission from reference.¹¹

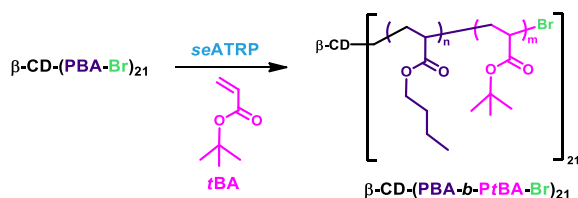
However, there are some limitations related to the reaction setup of the initial *e*ATRP procedure. Recently,^{309b} significant simplifications of the procedures used for an *e*ATRP were reported: the use of a sacrificial counter electrode that allowed elimination of the requirement for separation of electrode compartments and the polymerization under either potentiostatic and galvanostatic conditions.

In this Appendix, the first example of the preparation of both 14-arm and 21-arm β -

cyclodextrin (β -CD) based PBA stars by *e*ATRP using simplified electrochemically mediated ATRP (*se*ATRP), under both potentiostatic and pseudo-galvanostatic conditions (Scheme A-VII-2). Polymerization conditions were optimized to provide fast reactions while employing low catalyst concentrations and preparation of polymers with narrow molecular weight distributions. In addition, utilizing high ω -chain end functionalities of the star polymers (at the star periphery), well-defined block star copolymers, β -CD-PBA-*Pt*BA were successfully prepared by *se*ATRP (Scheme A-VII-3).



Scheme A-VII-2. Synthesis of β -CD-PBA star polymers *via se*ATRP.

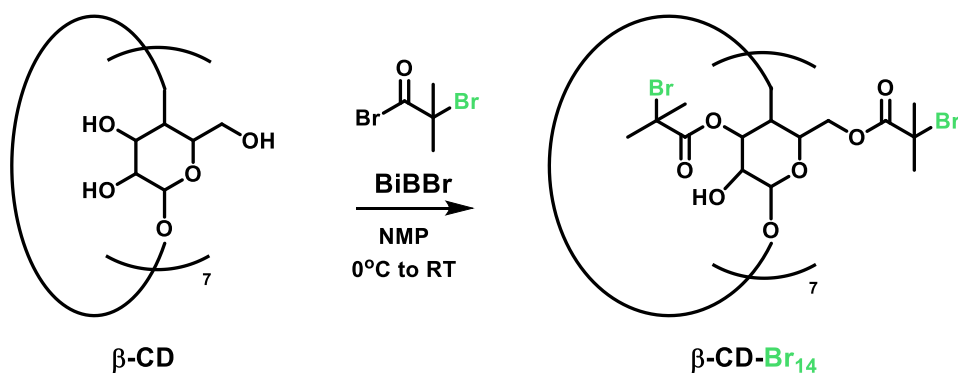


Scheme A-VII-3. Synthesis of β -CD-(PBA-*b*-*Pt*BA)₂₁ star block copolymers *via se*ATRP.

A-VII. 2. Results and Discussion

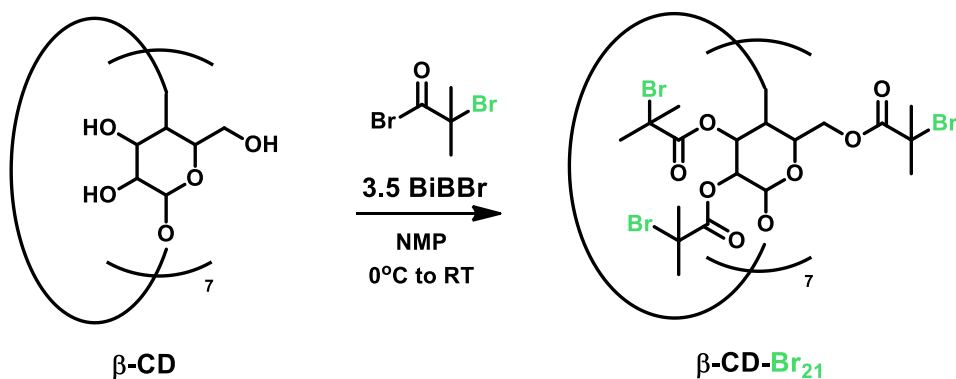
Motivated by the excellent control of various β -CD star polymers prepared by ATRP with high amounts of Cu catalyst complexes (typically > 4,000 ppm), we aimed to achieve similar levels of control using only 50 ppm (40 ppm (wt)) of $\text{Cu}^{\text{II}}/\text{L}$ in solution, following the *se*ATRP procedure under potentiostatic or pseudo-galvanostatic conditions. First, a β -CD-Br ATRP initiator with 14 -Br atoms tethered to the core was synthesized by esterification of a fraction of the hydroxyl groups on β -CD with BrIBr (Scheme A-VII-4), according to the procedures reported by Zhang et al.³¹⁰ The composition was confirmed by ^1H NMR (Figure A-VII-1). Additionally, a β -CD- Br_{21} initiator was prepared according to the procedure reported by Li et al.³¹¹ (Scheme A-VII-5), and the composition was also confirmed by ^1H NMR (Figure A-VII-2). The use of the functionalized β -CD's as core molecules, with a well-defined number of initiating groups, allows predetermination of the number of arms in star polymers.

Table A-VII-1 summarizes the results of the star polymers synthesis using the β -CD based macroinitiators (β -CD- Br_{14} , $M_n = 3,230$, $M_w/M_n = 1.05$ and β -CD- Br_{21} , $M_n = 4,260$, $M_w/M_n = 1.06$) under both potentiostatic and galvanostatic conditions.



Scheme A-VII-4. Synthesis of β -CD- Br_{14} ATRP initiator. Reaction conditions: [β -CD (per

$-\text{OH})]/[\text{BriBBr}] = 1/1$, $V_{\text{tot}} = 59 \text{ mL}$, $[\beta\text{-CD}]_0 = 0.04 \text{ M}$ in NMP.



Scheme A-VII-5. Synthesis of $\beta\text{-CD-Br}_{21}$ ATRP initiator. Reaction conditions: $[\beta\text{-CD}]$ (per $-\text{OH})]/[\text{BriBBr}] = 1/3.5$, $V_{\text{tot}} = 90 \text{ mL}$, $[\beta\text{-CD}]_0 = 0.03 \text{ M}$ in NMP.

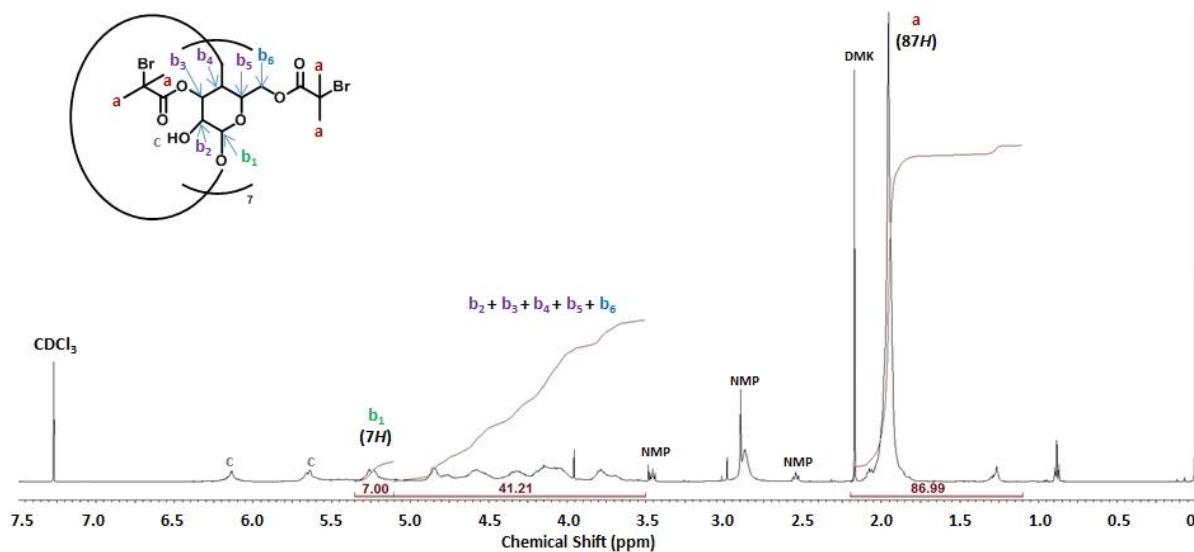


Figure A-VII-1. ^1H -NMR analysis of $\beta\text{-CD-Br}_{14}$ ($M_n = 2,930$, $D = 1.05$, 90% purity) after purification (in CDCl_3).

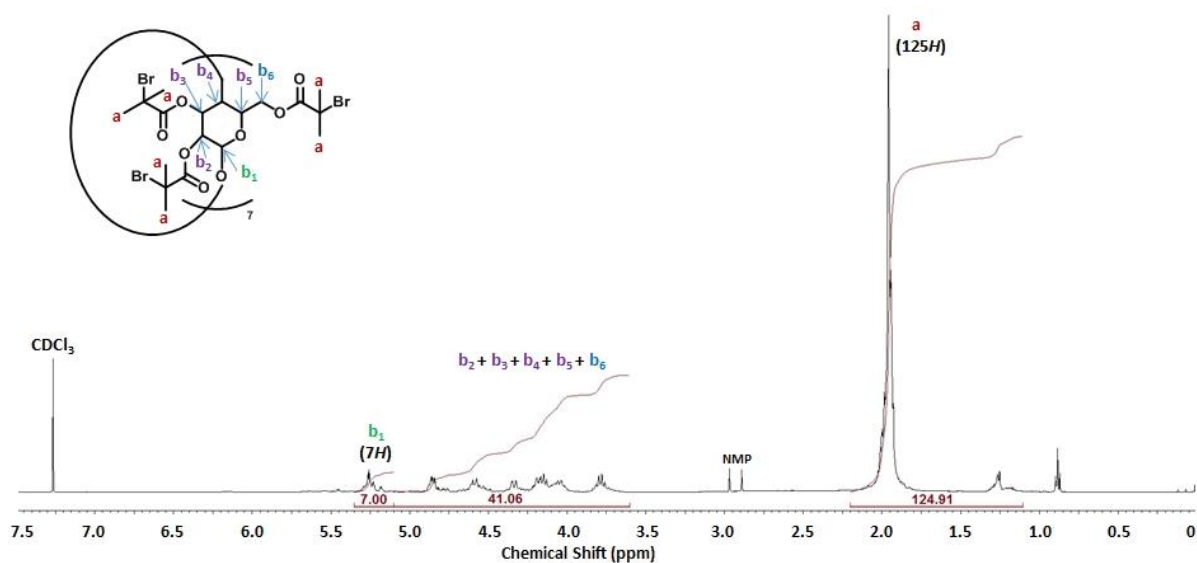


Figure A-VII-2. ^1H -NMR analysis of β -CD-Br₂₁ ($M_n = 4,260$, $D = 1.06$, 98% purity) after purification (in CDCl_3).

Table A-VII-1. Summary of β -CD-PBA synthesis by *e*ATRP and *se*ATRP.

entry	$[\text{M}]/[\text{I}]/$ $[\text{Cu}^{\text{II}}\text{Br}_2/2\text{TPMA}]$	$E_{\text{app}}^{\text{a}}$	$k_{\text{p}}^{\text{app}}$ $(\text{h}^{-1})^{\text{b}}$	conv $(\%)^{\text{b}}$	DP_{app} $(\text{per arm})^{\text{b}}$	$M_{\text{n,theo}}$ $(\times 10^{-3})^{\text{c}}$	$M_{\text{n}}^{\text{app}}$ $(\times 10^{-3})^{\text{d}}$	$M_{\text{w}}/M_{\text{n}}^{\text{d}}$
1	85/1 ^e /0.0085	$E_{\text{pc}}-80 \text{ mV}$	0.412	71	60	111.8	86.2	1.10
2	85/1 ^e /0.0085	<i>Galvanostatic Conditions</i> ^f	0.380	68	58	107.6	84.0	1.11
3	85/1 ^e /0.0085	$E_{\text{pc}}-80 \text{ mV}$	0.551	81	69	126.3	97.2	1.09
4	85/1 ^e /0.0085	<i>Galvanostatic Conditions</i> ^g	0.547	80	68	124.7	99.7	1.10
5	85/1 ^e /0.0064	$E_{\text{pc}}-80 \text{ mV}$	0.377	67	57	105.6	80.2	1.08
6	85/1 ^e /0.0043	$E_{\text{pc}}-80 \text{ mV}$	0.236	51	43	80.7	64.2	1.07
7	85/1 ^h /0.0043	$E_{\text{pc}}-80 \text{ mV}$	0.279	57	49	135.0	169.5	2.93

8	85/1 ^h /0.0043	E_{pc} -50 mV	0.251	54	46	128.4	89.5	1.27
9	85/1 ^h /0.0043	E_{pc} -20 mV	0.230	50	43	118.8	86.2	1.18
10	85/1 ^h /0.0043	Galvanostatic	0.219	48	41	115.0	84.3	1.18
		Conditions ⁱ						
11	60/1 ^j /0.0030	E_{pc} -35 mV	0.511	64	38	218.4	148.1	1.24
12	60/1 ^j /0.0030	Galvanostatic	0.466	61	36	212.9	140.2	1.23
		Conditions ^k						

Conventional *e*ATRP under potentiostatic conditions (WE = Pt mesh, CE = Pt mesh separated from the reaction solution by the supporting electrolyte saturated Tylose gel placed in a glass tube equipped with a glass frit, RE = saturated calomel electrode (SCE)): entry 1; *e*ATRP under galvanostatic conditions (WE and CE without RE): entry 2; *se*ATRP under potentiostatic conditions (WE = Pt mesh, CE = Al wire ($l = 10$ cm, $d = 1$ mm), RE = SCE): entries 3, 5–9, and 11; *se*ATRP under galvanostatic conditions: entry 4, 10, and 12. ^a E_{app} were selected based on CV analysis ($v = 100$ mV/s); ^bMonomer conversion, apparent propagation constants (k_p^{app}), and apparent practical degree of polymerization of monomer unit per arm (DP_{app}) were determined by NMR; ^c $M_{n,th} = ([M]_0/[MI]_0) \times \text{conversion} \times M_{monomer} + M_{initiator}$; ^dapparent M_n and MWD were determined by THF GPC with PS standard curves; ^eI = β -CD-Br₁₄ (calculated per 14 Br); ^f $I_{app} = -0.14, -0.08,$ and -0.07 mA for each steps; ^g $I_{app} = -0.28, -0.15, -0.78,$ and -0.06 mA for each steps; ^hI = β -CD-Br₂₁ (calculated per 21 Br); ⁱ $I_{app} = -0.31, -0.11, -0.06,$ and -0.04 mA for each steps; ^jI = β -CD-(PBA-Br)₂₁ (calculated per 21 Br); ^k $I_{app} = -0.23, -0.12, -0.05,$ and -0.03 mA for each steps. General reaction conditions: $T = 50$ °C; $V_{tot} = 20$ mL; [BA] = 3.6 M (except entries 11–12: [*t*BA] = 3.4 M); [β -CD-Br₁₄] = 3.1 mM, [β -CD-Br₂₁] = 2.0 mM, [β -CD-(PBA-Br)₂₁] = 2.7 mM; [Cu^{II}Br₂/2TPMA] = 0.36 mM (except entry 5 = 0.27 mM, entries 6–10 = 0.18 mM, and entries 11–12 = 0.17 mM). Supporting electrolyte concentration

(tetrabutylammonium perchlorate, TBAP) = 0.2 M.

Simplification of the setup for an electrochemically mediated ATRP reaction.

Electrochemically mediated ATRP was carried out under potentiostatic conditions with a Pt mesh WE, Pt mesh CE, and SCE RE (Table A-VII-1, entry 1, Figure A-VII-3, Figure A-VII-4, Figure A-VII-5a, and Figure A-VII-6). Prior to conducting a polymerization, the $E_{1/2}$ values for $\text{Cu}^{\text{II}}\text{Br}_2/2\text{TPMA}$ complex (which are reported in the Supporting Information (Figure A-VII-4)), were determined in the absence and presence of the $\beta\text{-CD-Br}_{14}$ multifunctional initiator. On the basis of these results, the applied potential (E_{app}) was selected as $E_{\text{app}} = \text{cathodic peak potential } (E_{\text{pc}}) - 80 \text{ mV}$. The polymerization of BA by *e*ATRP showed good evolution of molecular weight (MW), close to theoretical values, while maintaining narrow molecular weight distributions (Figure A-VII-3b and Figure A-VII-5a). The differences between theoretical and measured MW originate the differences in hydrodynamic radius of star and linear polymer standards for GPC.

The preparation of star homopolymers with PBA arms under pseudo-galvanostatic conditions was also carried out and the results are reported in Table A-VII-1, entry 2, Figure A-VII-3, Figure A-VII-5b, and Figure A-VII-6. The applied currents (I_{app}) were determined by the polymerizations conducted under potentiostatic conditions (Table A-VII-1, entry 1). On the basis of the preparative electrolysis results (Figure A-VII-3a), the total charge passed was calculated according to a previously published procedure.^{309b} It was observed that in Figure A-VII-3a the current decreased; it was probably caused by the formation of an oxidized species. The most probably explanation is to assumed, that the traces of oxygen were leaked through the glass frit of Pt mesh counter electrode in to the

reaction mixture. The increase of the current was so small, that it did not influenced the main reaction. The rate of polymerization (R_p) showed a slight decrease from values observed under potentiostatic conditions, cf. values of k_p^{app} ; Table A-VII-1, entries 2 vs. 1. However, nearly identical first-order kinetic plots were observed (Figure A-VII-6), and GPC analysis indicated similar MW evolution, indicating similar initiation efficiency, and formation of uniform star molecules (narrow MWD, Figure A-VII-3b).

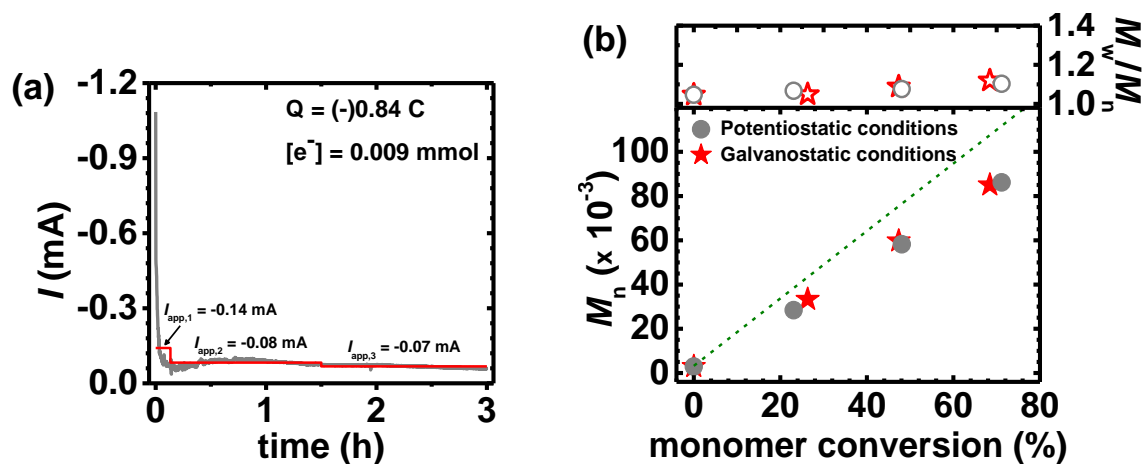


Figure A-VII-3. Multi-step preparative electrolysis for galvanostatic *e*ATRP; (a) preparative electrolysis results from potentiostatic conditions (grey line) and applied current (red line), and (b) M_n and M_w/M_n versus monomer conversion by potentiostatic and galvanostatic conditions.

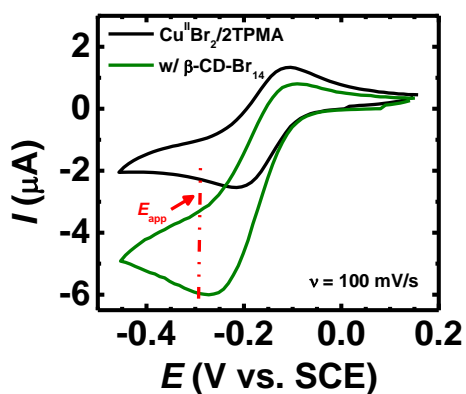
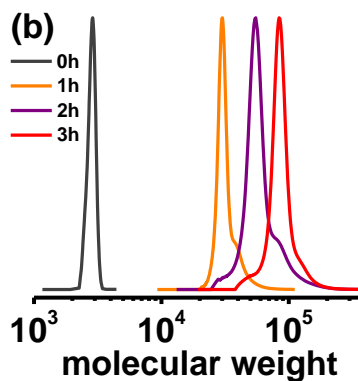
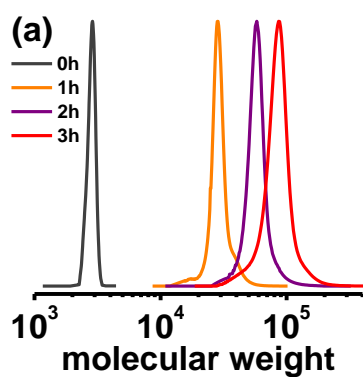
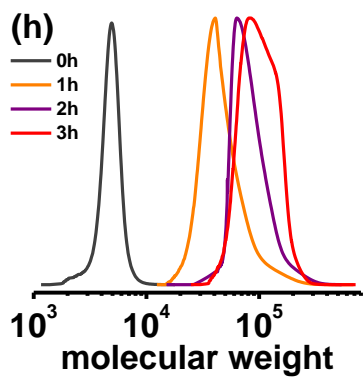
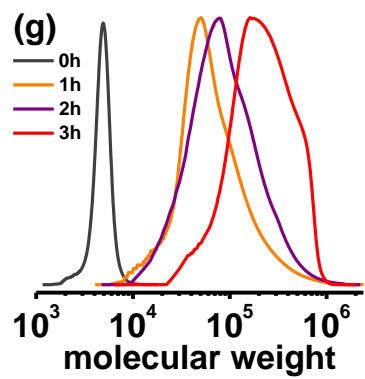
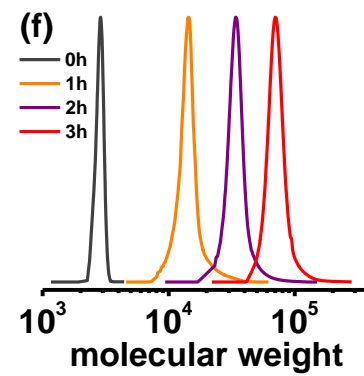
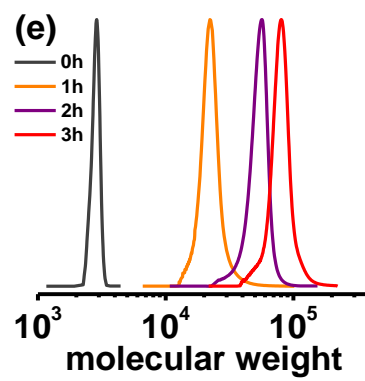
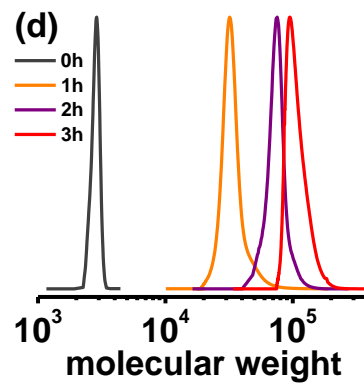
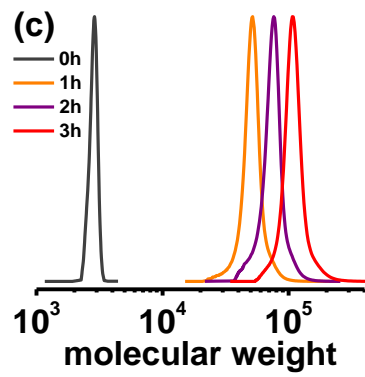


Figure A-VII-4. Cyclic voltammetry results of $\text{Cu}^{\text{II}}\text{Br}_2/2\text{TPMA}$ alone (black) and in the presence of $\beta\text{-CD-Br}_{14}$ (green). The arrow indicates the applied potential during electrolysis. Measurement conditions: $[\text{BA}]/[\beta\text{-CD-Br}_{14} \text{ (per } -\text{Br})]/[\text{Cu}^{\text{II}}\text{Br}_2/2\text{TPMA}] = 85/1/0.0085$, $[\text{BA}] = 3.6 \text{ M}$, $[\text{Cu}^{\text{II}}\text{Br}_2/2\text{TPMA}] = 0.36 \text{ mM}$, $T = 50 \text{ }^\circ\text{C}$, $[\text{TBAP}]_0 = 0.2 \text{ M}$, $V_{\text{tot}} = 20 \text{ mL}$.





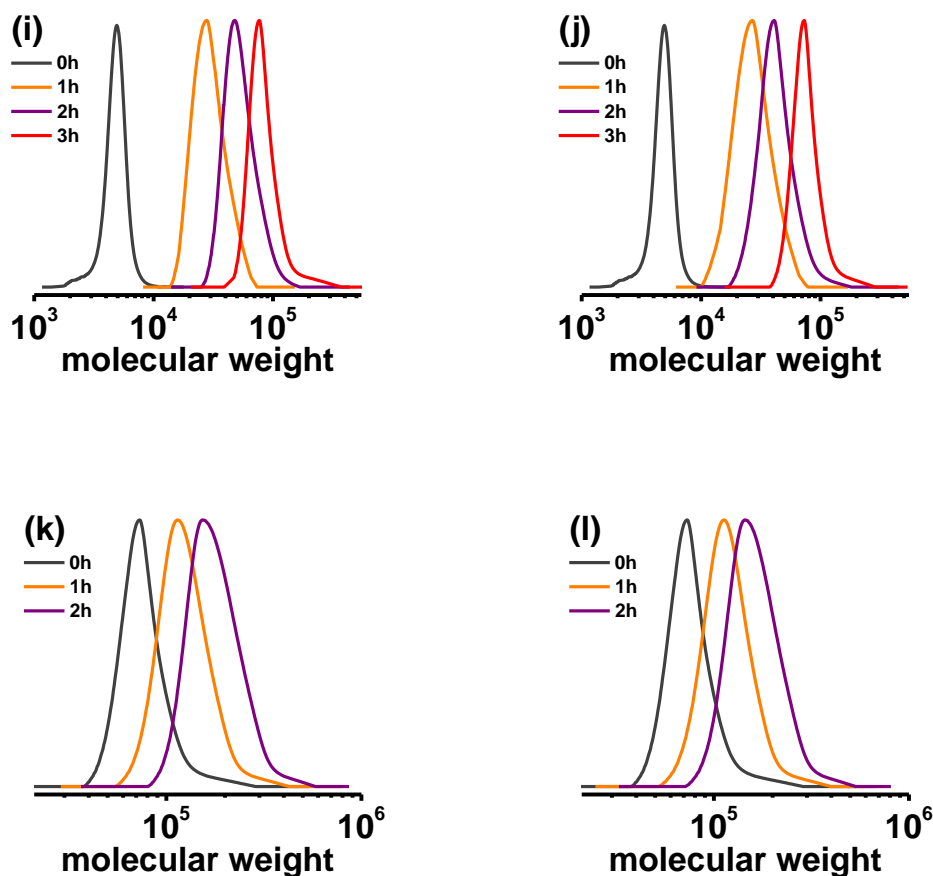


Figure A-VII-5. GPC traces of BA polymerization in the presence of β -CD-Br₁₄ under different conditions: potentiostatic *e*ATRP (a), galvanostatic *e*ATRP (b), potentiostatic *se*ATRP (c), galvanostatic *se*ATRP (d); GPC traces during the potentiostatic *se*ATRP as a function of [Br-Cu^{II}/2TPMA] concentration ((c) 100 ppm, (e) 75 ppm, and (f) 50 ppm). GPC traces of BA polymerization in the presence of β -CD-Br₂₁ under different conditions: potentiostatic *se*ATRP as a function of E_{app} ((g) E_{pc} -80 mV, (h) E_{pc} -50 mV, and (i) E_{pc} -20 mV); galvanostatic *se*ATRP (j). GPC traces of *t*BA polymerization in the presence of β -CD-(PBA-Br)₂₁ under different conditions: potentiostatic *se*ATRP (k); galvanostatic *se*ATRP (l).

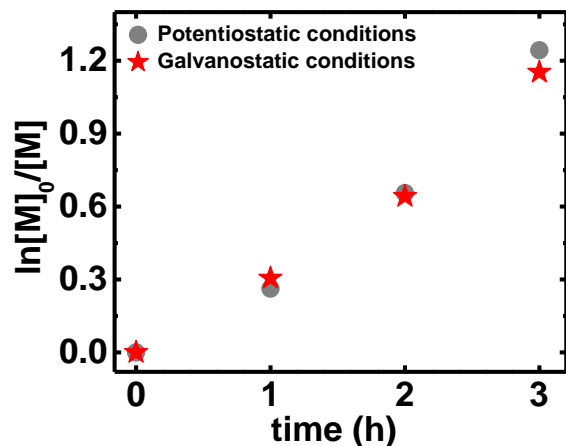


Figure A-VII-6. First-order kinetic plots by potentiostatic and galvanostatic *e*ATRP.

Reaction conditions: $[\text{BA}]/[\beta\text{-CD-Br}_{14} \text{ (per -Br)}]/[\text{Cu}^{\text{II}}\text{Br}_2/2\text{TPMA}] = 85/1/0.0085$, $[\text{BA}] = 3.6 \text{ M}$, $[\text{Cu}^{\text{II}}\text{Br}_2/2\text{TPMA}] = 0.36 \text{ mM}$, $T = 50 \text{ }^\circ\text{C}$, $[\text{TBAP}]_0 = 0.2 \text{ M}$, $V_{\text{tot}} = 20 \text{ mL}$, $E_{\text{app}} = E_{\text{pc}} - 80 \text{ mV (vs. SCE)}$.

The results of a simplified polymerization under potentiostatic conditions with a Pt mesh WE, a sacrificial Al CE, and SCE RE are shown in Table A-VII-1, entry 3, and in Figure A-VII-4c, Figure A-VII-6, and Figure A-VII-7. A first-order kinetic plot was also observed (Figure A-VII-8), with linear MW evolution and even narrower MWD (Figure A-VII-7b). Four constant I_{app} values were used for the polymerization under galvanostatic conditions; $I_{\text{app},1} = (-) 0.28 \text{ mA}$ (for 0 to 0.13 h), $I_{\text{app},2} = (-) 0.15 \text{ mA}$ (for 0.13 to 0.88 h), $I_{\text{app},3} = (-) 0.08 \text{ mA}$ (for 0.88 to 1.63 h), and $I_{\text{app},4} = (-) 0.06 \text{ mA}$ (for 1.63 to 3 h) where negative values indicate the cathodic currents (Table A-VII-1, entry 4, Figure A-VII-5d, Figure A-VII-7, and Figure A-VII-8). The values for MW evolution and MWD observed for *se*ATRP under galvanostatic conditions were compared to polymerizations conducted under potentiostatic conditions, Figure A-VII-7b, and were almost identical. The ^1H NMR

spectrum shown in Figure A-VII-9 confirms the structure of β -CD-PBA star polymer obtained through *se*ATRP under galvanostatic conditions (Table A-VII-1, entry 4).

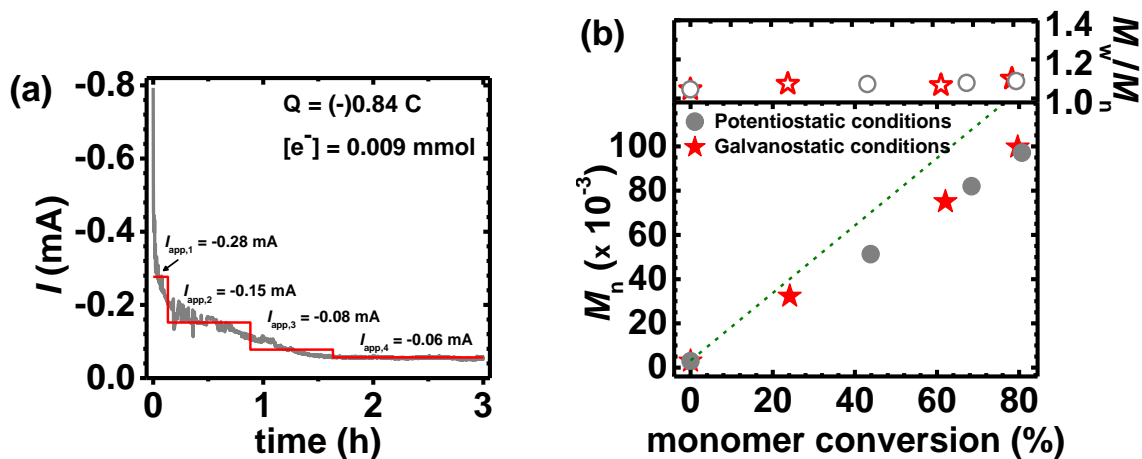


Figure A-VII-7. Multi-step preparative electrolysis for galvanostatic *se*ATRP; (a) preparative electrolysis results from potentiostatic conditions (grey line) and applied current (red line), and (b) M_n and M_w/M_n versus monomer conversion by potentiostatic and galvanostatic conditions.

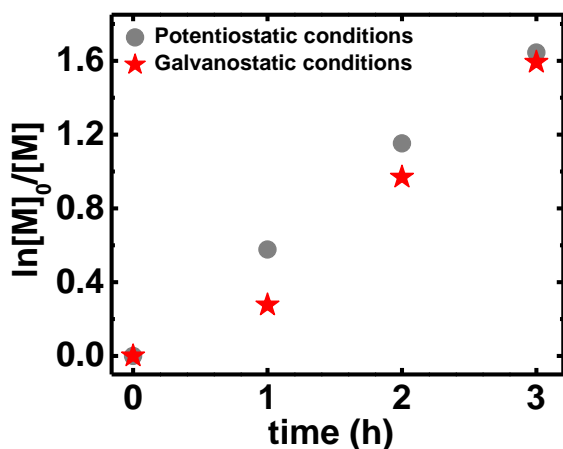


Figure A-VII-8. First-order kinetic plots by potentiostatic and galvanostatic *se*ATRP.

Reaction conditions: $[BA]/[\beta\text{-CD-Br}_{14} \text{ (per -Br)}]/[\text{Cu}^{\text{II}}\text{Br}_2/2\text{TPMA}] = 85/1/0.0085$, $[BA]$

= 3.6 M, $[\text{Cu}^{\text{II}}\text{Br}_2/2\text{TPMA}] = 0.36 \text{ mM}$, $T = 50 \text{ }^\circ\text{C}$, $[\text{TBAP}]_0 = 0.2 \text{ M}$, $V_{\text{tot}} = 20 \text{ mL}$, $E_{\text{app}} = E_{\text{pc}} - 80 \text{ mV}$ (vs. SCE).

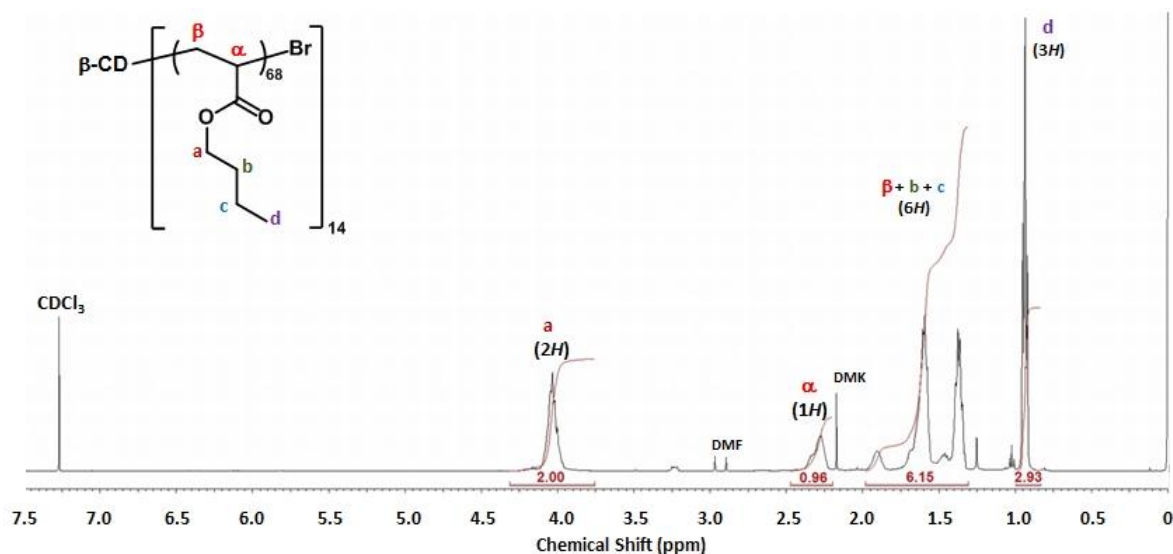
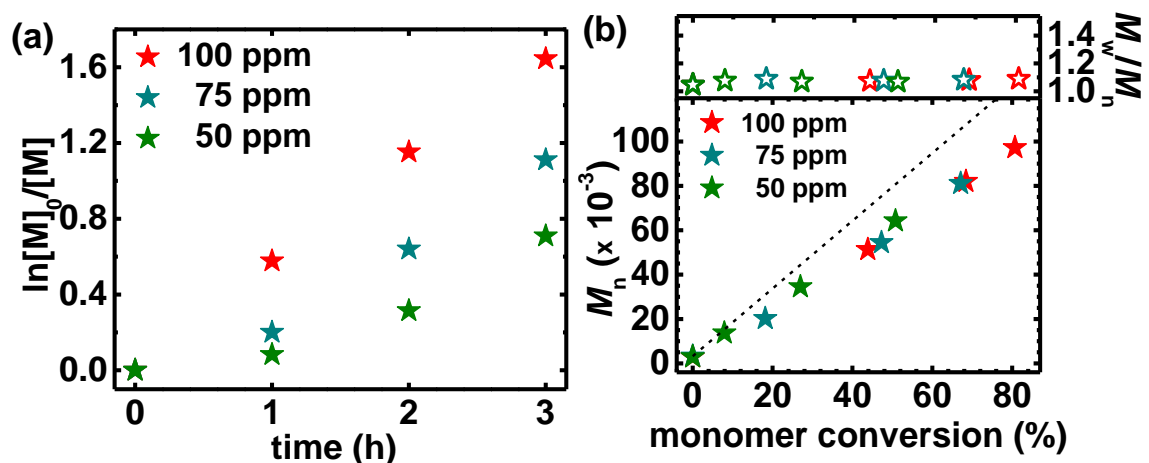


Figure A-VII-9. ^1H -NMR spectrum of CD star homopolymers with PBA arms ($\beta\text{-CD-}(\text{PBA}_{68})_{14}$); $M_n = 124,700$, $D = 1.10$) after purification (in CDCl_3). Table A-VII-1, entry 4.

Influence of the concentration of the catalyst complex. The next series of polymerizations were designed to examine the influence of the concentration of Cu/TPMA within *se*ATRP. Three polymerizations were conducted using different $[\text{X-Cu}^{\text{II}}/\text{L}]_0$, ranging from 100 to 25 ppm (Table A-VII-1, entries 3, 5, 6, Figure A-VII-5c, e, f, and Figure A-VII-10). Higher concentrations of copper catalyst should yield faster R_p in electrochemically mediated ATRP methods, because R_p is proportion to the square root of $[\text{X-Cu}^{\text{II}}/\text{L}]$ according to the equation defined as $R_p = k_p[\text{M}][\text{P}\cdot] = k_p[\text{M}]K_{\text{ATRP}} \frac{[\text{P-X}][\text{Cu}^{\text{I}}/\text{L}]}{[\text{X-Cu}^{\text{II}}/\text{L}]}$,¹¹ where $[\text{P}\cdot] = \sqrt{\frac{k_{\text{red}}[\text{X-Cu}^{\text{II}}/\text{L}]}{k_t}}$ ^{11, 66d, 80} (k_{red} denote reduction rate constant). Similar to literature accounts,^{66d, 80} it was observed that as the initial $[\text{X-Cu}^{\text{II}}/\text{L}]_0$

increases, the rate of polymerization increases with an approximately square root dependence on the catalyst concentration (Figure A-VII-10d). Briefly, a polymerization with 100 ppm catalyst concentration was 1.5 times faster (compare k_p^{app} ; Table A-VII-1, entry 3 vs. 5) than with 75 ppm catalyst and 2.3 times faster than with 50 ppm catalyst (compare k_p^{app} ; Table A-VII-1, entry 3 vs. 6). An increase in R_p reflects a higher $[P^*]$, which is a result of faster reduction rates generating more $\text{Cu}^{\text{I}}/\text{L}$. Moreover, as Figure A-VII-10b illustrates, there is an almost linear increase in MW with respect to conversion for all reactions and a slight decrease in the MWDs with lower $[\text{X}-\text{Cu}^{\text{II}}/\text{L}]_0$ (compare M_w/M_n ; Table A-VII-1, entries 3, 5, and 6). This observation is opposite to that supported by the equation describing the distribution of molecular weights of polymer¹¹: $\frac{M_w}{M_n} = 1 + \left(\frac{k_p[\text{P-X}]}{k_{\text{da}}[\text{Cu}^{\text{II}}]} \right) \left(\frac{2}{p} - 1 \right)$ (where p denotes monomer conversion), which indicates higher $[\text{X}-\text{Cu}^{\text{II}}/\text{L}]$ should produce polymers with lower M_w/M_n values from an increased rate of deactivation and fewer monomer additions within each activation–deactivation cycle.



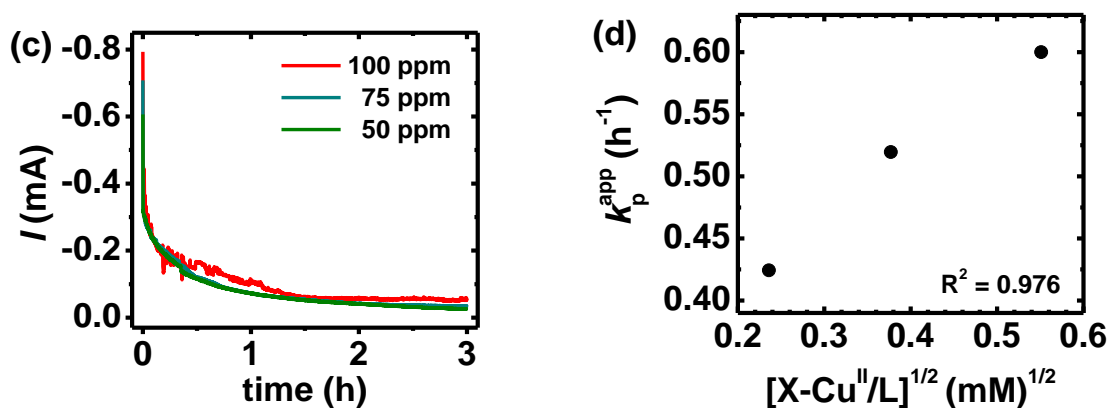
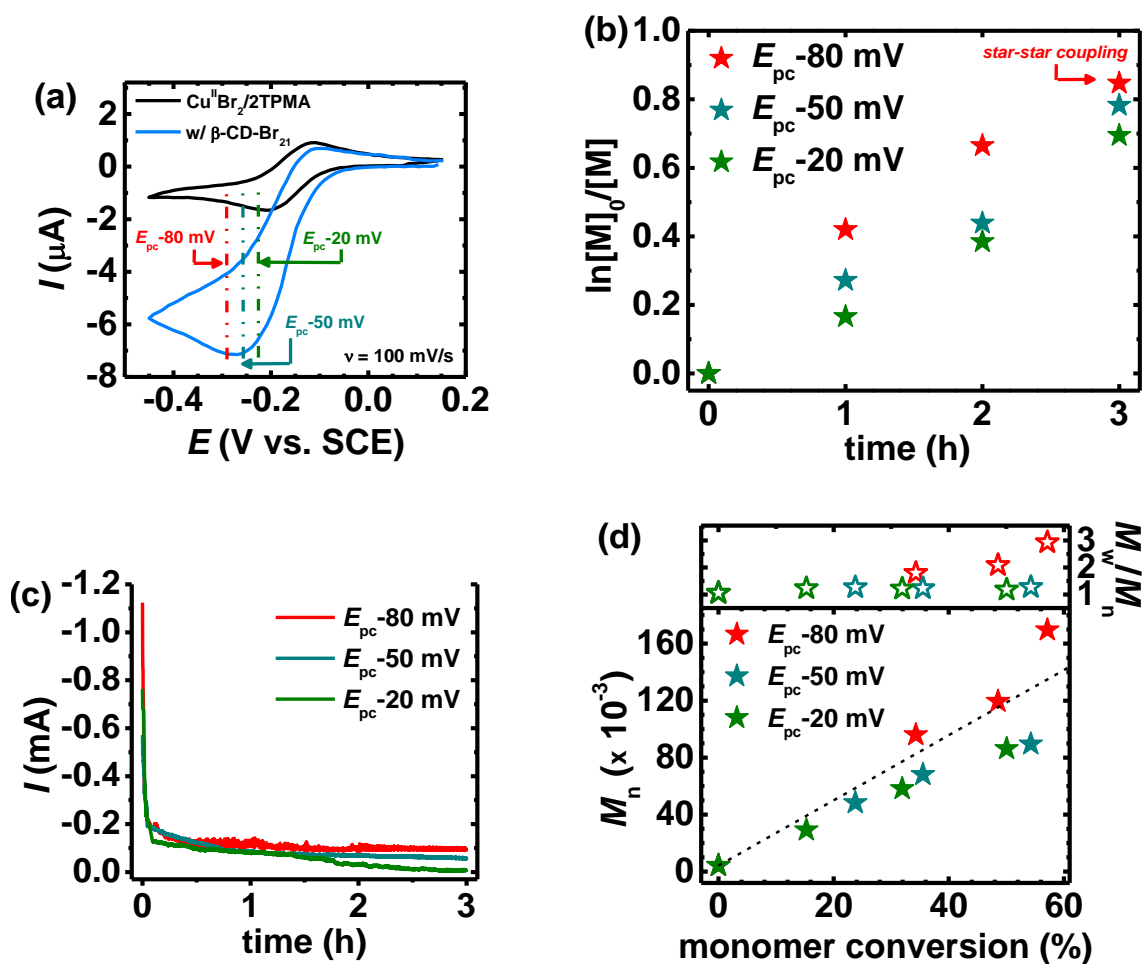


Figure A-VII-10. Synthesis of β -CD-PBA star polymers as a function of $[\text{Br-Cu}^{\text{II}}/2\text{TPMA}]$. (a) First-order kinetic plot of monomer conversion versus time, (b) evolution of M_n and M_w/M_n versus monomer conversion, (c) Current profile versus time, and (d) apparent polymerization rate coefficient (k_p^{app}) versus the square root of the $\text{X-Cu}^{\text{II}}/\text{L}$ concentration ($[\text{X-Cu}^{\text{II}}/\text{L}] = 0.36, 0.27$, and 0.18 mM). Reaction conditions: $[\text{BA}]/[14\text{Br-}\beta\text{-CD (per -Br)}]/[\text{Cu}^{\text{II}}\text{Br}_2/2\text{TPMA}] = 85/1/x$, $[\text{BA}] = 3.6$ M, $T = 50$ °C, $[\text{TBAP}]_0 = 0.2$ M, $V_{\text{tot}} = 20$ mL, $E_{\text{app}} = E_{\text{pc}} - 80$ mV (vs. SCE), $x = 0.0085, 0.0064$, and 0.0043 corresponding to 100, 75, and 50 ppm, respectively.

Furthermore, 40 ppm (by wt) concentration of catalyst complex generated transparent solutions and represents a 15–475 fold decrease in total Cu catalysts relative to previous reports where the concentration of Cu/L used in ATRP varied between *ca.* 590 and 19,000 ppm (by wt).

Influence of applied potential. After establishment of the optimal catalyst complex concentration, a series of polymerizations were carried out to examine the influence of the applied overpotential [$\eta = E_{\text{app}} - E_{1/2}$; $E_{1/2} = (E_{\text{pc}} + E_{\text{pa}})/2$] on the polymerization behavior

(Table A-VII-1, entries 7–9, Figure A-VII-5g–i, and Figure A-VII-11). Control over the rate of polymerization was evaluated by applying different constant potentials E_{app} . Three E_{app} values were selected: $E_{\text{pc}}-80$ mV, $E_{\text{pc}}-50$ mV, and $E_{\text{pc}}-20$ mV (Figure A-VII-11a). Faster R_p was observed when more negative potentials were applied. The fastest apparent propagation rate constant was observed for 0.279 h^{-1} ($E_{\text{pc}}-80$ mV). The R_p was 1.2 times faster than when $E_{\text{pc}}-20$ mV was applied, Figure A-VII-11b.



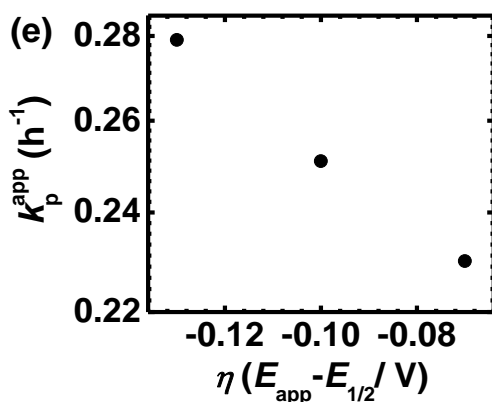


Figure A-VII-11. R_p as a function of applied potential during synthesis of β -CD-PBA star polymers. (a) Cyclic voltammetry of $\text{Cu}^{\text{II}}\text{Br}_2/2\text{TPMA}$ with and without initiator (lines indicate E_{app}), (b) first-order kinetic plots for different E_{app} values, (c) Current profile versus time, (d) M_n and M_w/M_n versus monomer conversion, and (e) apparent polymerization rate coefficient (k_p^{app}) versus the overpotential (η). Reaction conditions: $[\text{BA}]/[21\text{Br-}\beta\text{-CD (per -Br)}]/[\text{Cu}^{\text{II}}\text{Br}_2/2\text{TPMA}] = 85/1/0.0043$, $[\text{BA}] = 3.6 \text{ M}$, $[\text{Cu}^{\text{II}}\text{Br}_2/2\text{TPMA}] = 0.18 \text{ mM}$, $T = 50 \text{ }^\circ\text{C}$, $[\text{TBAP}]_0 = 0.2 \text{ M}$, $V_{\text{tot}} = 20 \text{ mL}$, $E_{\text{app}} = E_{\text{pc}} - 80 \text{ mV}$, $E_{\text{pc}} - 50 \text{ mV}$, and $E_{\text{pc}} - 20 \text{ mV}$ (vs. SCE).

More negative η values produced larger initial currents, indicative of a faster rate of reduction. In essence, faster rates of reduction provide a higher $[\text{Cu}^{\text{I}}/\text{L}]$ and, therefore, faster polymerization, due to higher $[\text{P}^\bullet]$. The magnitude of stationary current values, reflect the relative activator regeneration rates and hence termination rates, therefore, a more negative η leads to a higher R_p and stationary current, resulting in more termination.¹¹ Controlled polymerization behavior was confirmed in case of more positive applied potentials ($E_{\text{pc}} - 50 \text{ mV}$ and $E_{\text{pc}} - 20 \text{ mV}$) by a linear increase of M_n with conversion, while

producing a monomodal population of polymers with relatively low M_w/M_n values (Table A-VII-1, entries 8,9 and Figure A-VII-5h, i). Significantly higher M_w/M_n values were observed at the most negative applied potential (Table A-VII-1, entry 7, Figure A-VII-5g). The observed increase in M_w/M_n can be related to a more pronounced star-star coupling. Comparing polymerization using β -CD-Br₁₄ with polymerization using β -CD-Br₂₁ initiator (compare M_w/M_n ; Table A-VII-1, entry 6 vs. 8), the coupling reaction was observed in case of the second one, which is caused by sterically congestion of growing chains and might have on account of higher change to star-star intermolecular X-linking. Termination between growing arms can happen in the intermolecular and intramolecular mode. The former will lead to star-star coupling, the latter to less uniform growth of arms. Intramolecular coupling was mainly diminished by low radical concentration. Usually it can be evidenced by bimodal MWD of arms of stars.^{298c} In the case of presented results the % of chains terminated by radical means could be estimated according to the formulae (Dead Chain Fraction defined as $DCF = ([D]/[P-X]_0) \times 100\%$ ^{260b} where $[D] = k_t[P^\bullet]^2 t$ ($[D]$ denotes concentration of terminated chains, t denote reaction time), $k_t = 1.0 \times 10^8 \text{ M}^{-1}\text{s}^{-1}$,³¹² $[P^\bullet] = d\ln[M]/dt(k_p)^{-1}$, $k_p = 2.77 \times 10^4 \text{ M}^{-1}\text{s}^{-1}$).³¹³ The calculated values are well below 1%, so the bimodality cannot be detected by GPC, even if termination will be 100% of coupling (Table A-VII-2). It is also possible that there would be even less coupling and the disproportionation could not be detected by GPC.³¹⁴ Probability of the intramolecular termination of acrylates can be enhanced due to a close proximity of radicals but also can be diminished due to radical segregation.³¹⁵ Therefore subsequent reactions were performed with more negative E_{app} ($E_{pc} - 50 \text{ mV}$ and $E_{pc} - 20 \text{ mV}$ respectively) while targeting polymerizations with limited monomer conversion, thereby further suppressing

the intermolecular termination reactions between growing arms, and subsequent star-star coupling.

Table A-VII-2. Calculation of Dead Chain Fraction (DCF) for *e*ATRP/*se*ATRP of BA and *t*BA.

Entry (according to Table A-VII-1)	[P•] ×10 ⁸) ^a	(M [D] ×10 ⁴) ^b	(M [P-X] ₀ (mM)	DCF (%) ^c
1	0.413	0.184	3.1	0.59
2	0.381	0.157	3.1	0.51
3	0.553	0.330	3.1	1.06
4	0.549	0.320	3.1	1.05
5	0.378	0.154	3.1	0.50
6	0.237	0.060	3.1	0.20
7	0.098	0.010	3.1	0.03
8	0.280	0.085	2.0	0.42
9	0.252	0.068	2.0	0.34
10	0.231	0.057	2.0	0.29

11	0.220	0.052	2.0	0.26
12	0.496	0.177	2.7	0.66
13	0.453	0.147	2.7	0.55

^aThe radical concentration $[P^\bullet]$ calculated according to the equation defined as^{260b} $[P^\bullet] = \left(\frac{d\ln[M]}{dt}\right)(k_p)^{-1}$ where $\frac{d\ln[M]}{dt}$ values were calculated from the kinetic $\ln([M]_0/[M])$ -time graphs (k_p^{app} in Table A-VII-1), $k_p = 2.77 \cdot 10^4 \text{ M}^{-1}\text{s}^{-1}$ (except entries 12–13: $k_p = 2.86 \cdot 10^4 \text{ M}^{-1}\text{s}^{-1}$);³¹⁶ ^bThe concentration of terminated chains $[D]$ was calculated according to the equation defined as $[D] = k_t[P^\bullet]^2 t$ where t (denote reaction time) = 10,800 s (except entries 12–13: $t = 7,200 \text{ s}$), $k_t = 1.0 \cdot 10^8 \text{ M}^{-1}\text{s}^{-1}$; 312 °DCF = $\left(\frac{[D]}{[P-X]_0}\right) \cdot 100\%$.^{260b}

Synthesis of 21-arm star block copolymers. The preparation of CD star homopolymers with 21 arms of PBA under pseudo-galvanostatic conditions was carried out and the results are reported in Table A-VII-1, entry 10, Figure A-VII-12, Figure A-VII-5j and Figure A-VII-13. Nearly identical first-order kinetic plots were observed, and GPC analysis indicated narrow MWD (Figure A-VII-13 b-c). The ¹H NMR spectrum, shown in Figure A-VII-12, confirms the structure of β-CD-PBA star polymer obtained through *se*ATRP under pseudo-galvanostatic conditions (Table A-VII-1, entry 10). The chemical shifts, 0.80–1.03 ppm, 1.34–2.00 ppm, 2.16–2.55 ppm, and 3.75–4.30 ppm, are mainly attributed by the $-CH_3$ (d), $-CH_2-$ (β + b + c), $-CH-$ (α), and $-OCH_2-$ (a) groups of the PBA units in the arms, respectively, indicating the presence of PBA chains.

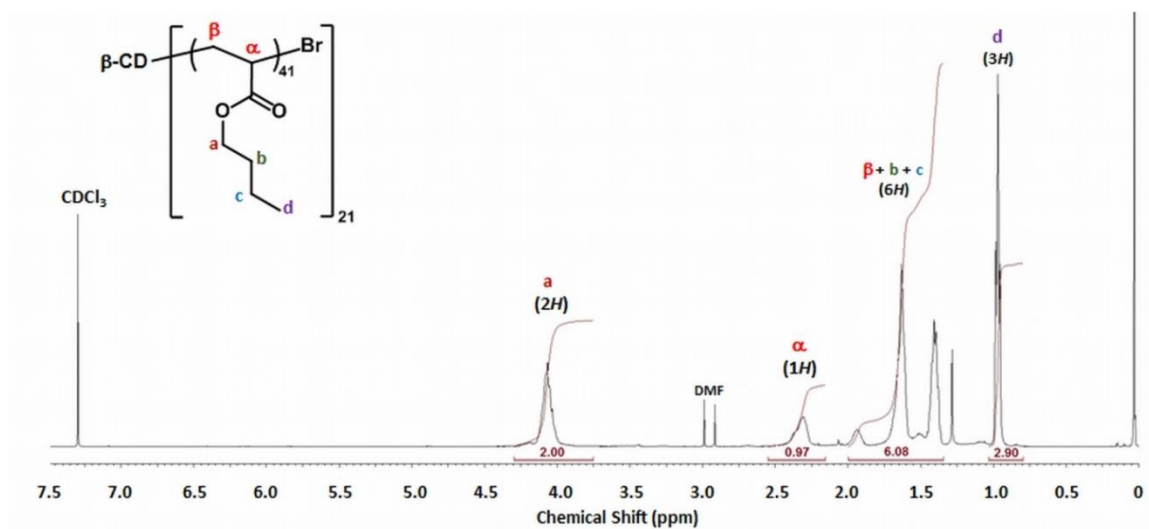
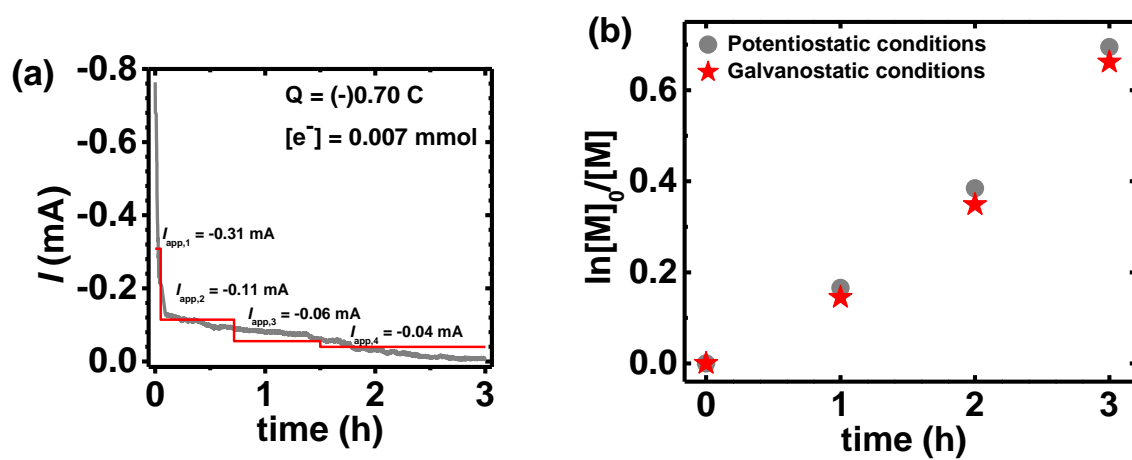


Figure A-VII-12. ¹H-NMR spectrum of CD star homopolymers with PBA arms (β -CD-(PBA₄₁)₂₁); $M_n = 115,000$, $D = 1.18$) after purification (in CDCl₃). Table A-VII-1, entry 10.



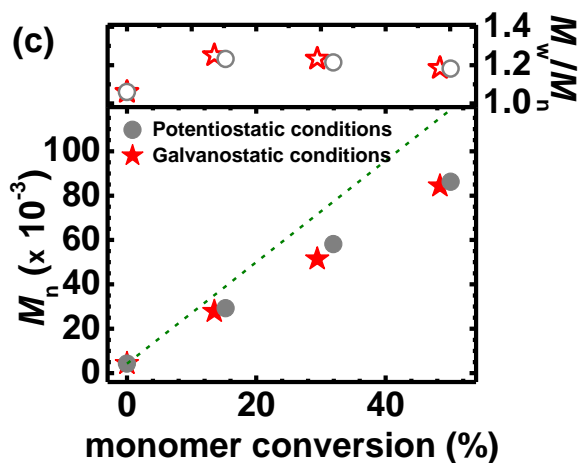


Figure A-VII-13. Multi-step preparative electrolysis for galvanostatic *se*ATRP; (a) preparative electrolysis results from potentiostatic conditions (grey line) and applied current (red line), (b) first-order kinetic plot of monomer conversion versus time, and (c) M_n and M_w/M_n versus monomer conversion by potentiostatic and galvanostatic conditions. Reaction conditions: $[BA]/[21Br-\beta-CD \text{ (per } -Br)]/[Cu^{II}Br_2/2TPMA] = 85/1/0.0043$, $[BA] = 3.6 \text{ M}$, $[Cu^{II}Br_2/2TPMA] = 0.18 \text{ mM}$, $T = 50 \text{ }^\circ\text{C}$, $[TBAP]_0 = 0.2 \text{ M}$, $V_{tot} = 20 \text{ mL}$.

The synthesis of star block copolymers under potentiostatic and pseudo-galvanostatic conditions was carried out (Table A-VII-1, entries 11 and 12, Figure A-VII-14, Figure A-VII-5k, l, and Figure A-VII-15). Close to identical first-order kinetic plots were observed, and GPC analysis indicated narrow MWD (Figure A-VII-15b-c) confirming that the halogen end groups were preserved during the *se*ATRP of BA. The 1H NMR spectrum shown in Figure A-VII-14 confirms the structure of β -CD-PBA-*Pt*BA star block copolymer obtained through *se*ATRP under galvanostatic conditions (Table A-VII-1, entry 12). The chemical shifts, 1.34–2.00 ppm, and 2.16–2.55 ppm, are mainly attributed to the $-CH_2-$ (β'), $-CH_3$ (e), and $-CH-$ (α') groups of the *Pt*BA units in the arms, respectively, indicating

the presence of PtBA chains.³¹⁷

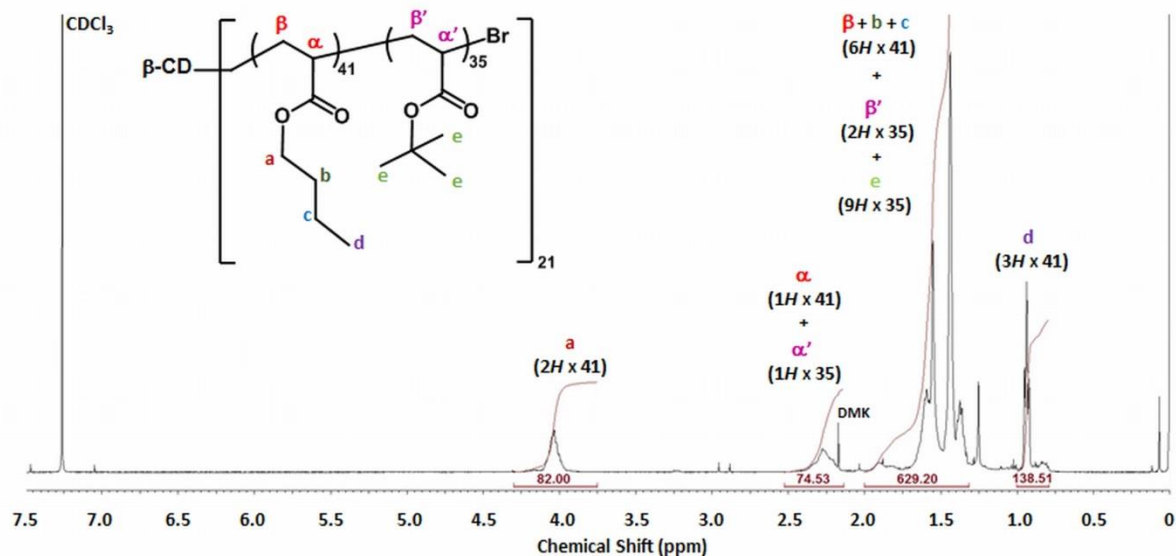
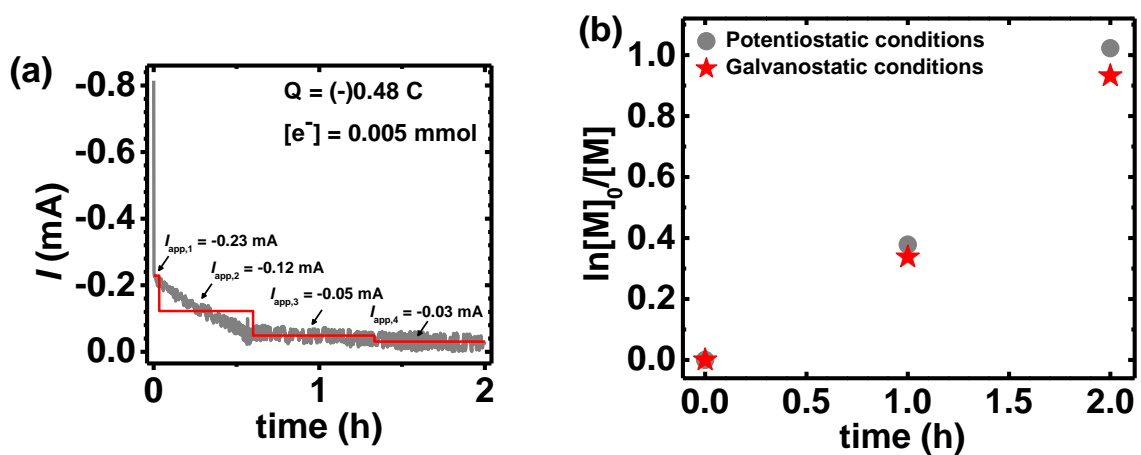


Figure A-VII-14. ^1H -NMR spectrum of star block copolymer ($\beta\text{-CD}-(\text{PBA}_{41}\text{-PtBA}_{35})_{21}$); $M_n = 212,900$, $D = 1.23$) after purification (in CDCl_3).



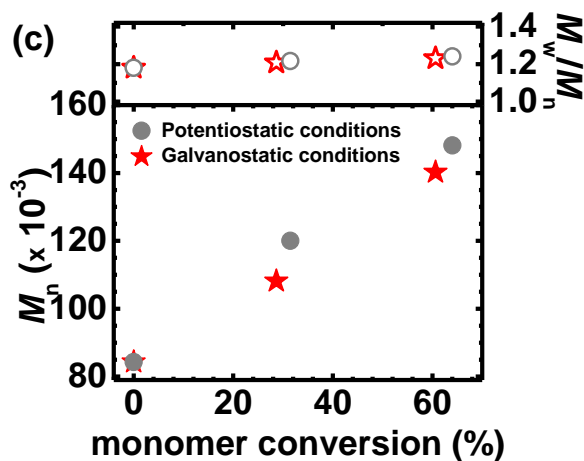


Figure A-VII-15. Multi-step chronoamperometry for galvanostatic *se*ATRP; (a) chronoamperometry results from potentiostatic conditions (grey line) and applied current (red line), (b) first-order kinetic plot of monomer conversion versus time, and (c) M_n and M_w/M_n versus monomer conversion by potentiostatic and galvanostatic conditions. Reaction conditions: $[tBA]/[\beta\text{-CD-(PBA-Br)}_{21} \text{ (per -Br)}]/[\text{Cu}^{\text{II}}\text{Br}_2/2\text{TPMA}] = 60/1/0.003$, $[tBA] = 3.4 \text{ M}$, $[\text{Cu}^{\text{II}}\text{Br}_2/2\text{TPMA}] = 0.17 \text{ mM}$, $T = 50 \text{ }^\circ\text{C}$, $[\text{TBAP}]_0 = 0.2 \text{ M}$, $V_{\text{tot}} = 20 \text{ mL}$.

Analysis of the arm length of star (co)polymers. In order to determine the actual arm length of obtained star polymers and copolymers, and thus the initiation efficiency (f_i), the arms were cleaved from the core by acid solvolysis of the ester groups.³¹⁸ The results of the molecular weight determinations and the comparison with the expected values are summarized in Table A-VII-3. The obtained polymer stars with homopolymer or di-block copolymer arms showed monomodal GPC eluograms (Figure A-VII-16) and their molecular weight distributions are narrow ($D < 1.32$; Table A-VII-3, entries 4, 11 and 13), indicating that radical coupling reactions are negligible. These results confirm the well-controlled *se*ATRP of BA/*t*BA as well as the formation of a well-defined (co)polymer

stars. As expected, the initiation efficiency (and blocking efficiency) of analyzed acrylates were close to 100% (Table A-VII-3, entries 4, 11 and 13).³¹⁹

Table A-VII-3. Results from the arms cleaved from the star (co)polymers in order to investigate initiation efficiency (f_i).

Entry (according to Table A-VII-1)	$DP_{n,arm,theo}^a$	$M_{n,arm,app}$ ($\times 10^{-3}$) ^b	$DP_{n,arm,app}^c$	M_w/M_n^b	f_i (%) ^d
4	68	8.9	69	1.28	98
11	41	5.4	42	1.31	98
13	36	4.8 (10.0) ^e	37	1.30	97

^aTheoretical (expected) degree of polymerization per arm from monomer to initiation site ratio and monomer conversion: $DP_{n,arm,theo} = (\text{conversion} \times [M]_0)/[MI]_0$, where $[M]_0$ and $[MI]_0$ are the initial monomer and initiation site concentrations, respectively;³¹⁹ ^bapparent M_n and MWD were determined by THF GPC with PS standard curves; ^capparent (experimental) degree of polymerization of one arm from dividing $M_{n,arm,app}$ by the molar mass of the polymer's repeating unit: $DP_{n,arm,app} = M_{n,arm,app}/M_{monomer}$,^{318b, 319} ^defficiency of initiation determined as: $f_i = (DP_{n,arm,theo}/DP_{n,arm,app}) \times 100\%$,^{298c, 318-319} ^eapparent M_n was determined by THF GPC and reduced by the value of PBA (from entry 11).

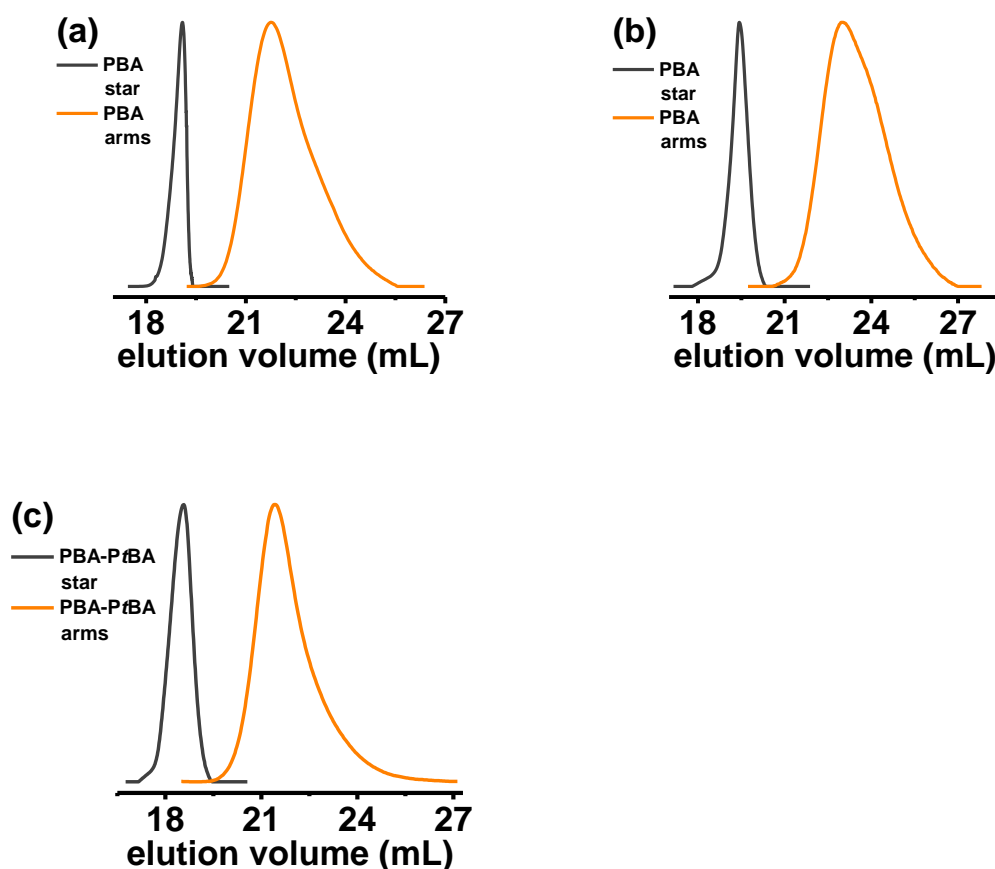


Figure A-VII-16. GPC traces of (a) β -CD-(PBA)₁₄ and the corresponding cleaved PBA arms (Table A-VII-1 and Table A-VII-3, entry 4), (b) β -CD-(PBA)₂₁ and the corresponding cleaved PBA arms (Table A-VII-1 and Table A-VII-3, entry 11), (c) β -CD-(PBA-*Pt*BA)₂₁ and the corresponding cleaved PBA-*Pt*BA arms (Table A-VII-1 and Table A-VII-3, entry 13).

A-VII. 3. Summary

β -cyclodextrin (β -CD) core macroinitiators were synthesized and employed for the preparation of well-defined star polymers with poly(*n*-butyl acrylate) (PBA) arms utilizing a simplified electrochemically mediated atom transfer radical polymerization (*se*ATRP)

procedure with low concentrations of catalyst, as low as 50 ppm of added Cu^{II} species. This appears to be the first report using *se*ATRP for the polymerization of *n*-butyl acrylate as hydrophobic arms from a modified β -CD as the hydrophilic macroinitiator. The use of a simplified multi-step current pseudo-galvanostatic technique provided identical results to polymerizations carried out under potentiostatic conditions, providing star-shaped polymers with molecular weight evolution close to theoretical values while generating stars with narrow molecular weight distribution. The rate of the polymerizations (R_p) under pseudo-galvanostatic conditions was controlled by applying less negative E_{app} , thereby suppressing intermolecular termination *via* a chain coupling process, and subsequent star-star coupling. Chain extension of the initially formed star polymer with *t*BA, confirmed the preservation of terminal halogen end group during the *se*ATRP of acrylates. The readily purified star polymers obtained by this procedure had a hydrophilic β -CD core with the potential to form inclusion complexes with small organic compounds. These new amphiphilic star polymers are promising precursors for polyelectrolyte star polymers, with potential application in biomedical application field.

A-VII. 4. Experimental Section

Materials. β -Cyclodextrin (β -CD, $M_n = 1,135$), 2-bromoisobutyl bromide (BriBBR, 98%), *N*-methyl-2-pyrrolidone (NMP, > 99%), dichloromethane (DCM, > 99.5%), *n*-hexane (95%), sodium bicarbonate (> 99.7%), tetrabutylammonium perchlorate (TBAP, > 98%), tetrabutylammonium hexafluorophosphate (TBAPF₆), copper(II) bromide ($\text{Cu}^{\text{II}}\text{Br}_2$, 99.9%), and methylated cellulose (Tylose, MH=300) were purchased from Aldrich. *N,N*-dimethylformamide (DMF, 99.9%) was purchased from Acros. These reagents were used

without further purification. Tris(2-pyridylmethyl)amine (TPMA) was prepared according to a previously published procedure and stored under Argon prior to use.¹⁰³ *n*-Butyl acrylate (BA, > 99% from Aldrich) and *tert*-butyl acrylate (*t*BA, > 99% from Aldrich) were passed through a column filled with basic alumina prior to use to remove any inhibitor. Platinum (Pt) wires and Pt gauge mesh were purchased from Alfa Aesar. Prior to each polymerization, the working and counter electrodes were cleaned thoroughly with organic solvents, submerged briefly in fresh aqua regia, rinsed with deionized water, and dried in an oven. The Pt disk (3 mm diameter, Gamry) was first polished on microcloth (Buehler) with Gamma micropolish deagglomerated alumina suspension (0.05 μm , Buehler) for 5 min. Following this, the electrode was rinsed with pure water and dried with air and argon for future use. All cyclic voltammetry (CVs) and preparative electrolysis were conducted in a Jacketed Dr. Bob's electrochemical cell kit (Gamry).

Analysis. ^1H NMR spectra in CDCl_3 used for calculation of monomer conversion were measured using Bruker Avance 500 MHz spectrometer at 25 $^\circ\text{C}$. Molecular weights and molecular weight distributions were determined by GPC (Polymer Standards Services (PSS) columns (guard, 10^5 , 10^3 , and 10^2 \AA), with THF eluent at 25 $^\circ\text{C}$, flow rate 1.00 mL/min, and with a differential refractive index (RI) detector (Viscotek, T60A). The apparent molecular weights and dispersity (M_w/M_n) were determined with a calibration based on PS standards using TRISEC software from Viscotec Corporation. All CVs and preparative electrolysis were recorded on a Metrohm Autolab potentiostat (AUT84337) using GPES software from EcoChemie B. V. Corporation. The electrolysis were carried out under Ar atmosphere using a Pt disk for CV, ($A = 0.071 \text{ cm}^2$) and Pt mesh for

preparative electrolysis, ($A \approx 6 \text{ cm}^2$) working electrodes. The Pt mesh counter electrode was prepared using a glass frit and a salt bridge made of Tylose gel saturated with TBAPF_6 to separate the cathodic and anodic compartments. The Al sacrificial anode was a wire ($l = 10 \text{ cm}$, $d = 1 \text{ mm}$), which was washed with acetone and THF, followed by direct immersion in the reaction mixture. Values for all potentials applied for preparative electrolysis were established from CV measurements at a 100 mV/s scan rate using SCE (Gamry) reference electrode. During *e*ATRP and *se*ATRP procedures, a condenser was connected to the reaction cell and the temperature was maintained at 50°C using a circulating thermostat (VEB MLW Inc., U7C).

Synthesis of the $\beta\text{-CD-Br}_{14}$ macroinitiator. The $\beta\text{-CD-Br}_{14}$ ATRP initiator was prepared by reacting $\beta\text{-CD}$ ($M_n = 1,135$) with BrIBr in NMP according to the procedure described in reference ³¹⁰ (Scheme A-VII-4) and was characterized by ^1H NMR. 3 g (2.6 mmol) of $\beta\text{-CD}$ was dissolved in 30 mL of NMP in a reaction flask, which was then cooled to 0°C . A solution of BrIBr (6.9 mL, 55.5 mmol) in NMP (20 mL) was slowly added to the flask then the reaction mixture was stirred for 48 h at room temperature. The resulting brown solution was purified by dialysis against water (Spectra/Por dialysis membrane, MWCO 1000, Spectrum Laboratories Inc.) and the crude product obtained by precipitation against *n*-hexane. The resulting yellow powder was dissolved in DCM and subjected to sequential extraction with saturated sodium bicarbonate aqueous solution and pure water. The organic layer was collected and any residual water removed using MgSO_4 . The obtained organic layer was concentrated in a vacuum oven and crystallized to produce a white product. The resulting powder was dried overnight under vacuum (8.81 g, yield

78.25%). According to ^1H NMR analysis, provided in Fig. S1, the major product has 14–Br functionalities. The degree of substitution of the hydroxyl groups on the outside surface of β -CD was determined by the area ratio of the methyl protons at the region of δ 1.10–2.20 ppm (87H) and acetal protons at the region of δ 5.10–5.35 ppm (7H).

Synthesis of the β -CD-Br₂₁ macroinitiator. The β -CD-Br₂₁ ATRP initiator was prepared to target a star-shaped polymer with 21 arms and was prepared by reacting β -CD ($M_n = 1,135$) with BrIBr in NMP (Scheme A-VII-5) according to procedure described in reference.³¹¹ The final product was characterized by ^1H NMR. A 3 g (2.6 mmol) sample of β -CD was dissolved in 30 mL of NMP in a reaction flask that was then cooled to 0 °C. A solution of BrIBr (24.0 mL, 194.3 mmol) in NMP (34 mL) was slowly added to the flask then the reaction mixture was stirred for 96 h at room temperature. The resulting brown solution was purified in the same manner as the β -CD-Br₁₄ macroinitiator. The final white powder was dried overnight under vacuum (7.89 g, yield 70.01%). According to ^1H NMR analysis, provided in Figure A-VII-2, the major product has over 99.1% functionalization efficiency, *i.e.* 21–Br functionalities. The degree of substitution of the hydroxyl groups on the outside surface of β -CD was determined by the area ratio of the methyl protons at the region of δ 1.10–2.20 ppm (125H) and acetal protons at the region of δ 5.10–5.35 ppm (7H).

Preparation of Cu^{II}Br₂/2TPMA stock solutions. Stock solutions of Cu^{II}Br₂ (0.11 g, 0.25 mmol) and TPMA (0.29 g, 0.5 mmol) were prepared in dry DMF (total volume = 5 mL), as previously described in reference^{309c}. The prepared Cu^{II}Br₂/TPMA solutions (50 mM) were used as catalyst precursors for *e*ATRP and *se*ATRP.

Synthesis of β -CD-PBA₁₄ star polymers by *e*ATRP/*se*ATRP under potentiostatic

conditions. TBAP (1.37 g, 4 mmol) was placed in an electrolysis cell maintained at 50 °C under a slow Ar purge. Then, 10 mL of Ar purged BA (73 mmol), DMF (7.9 mL) and 0.15 mL of Ar purged $\text{Cu}^{\text{II}}\text{Br}_2/2\text{TPMA}$ stock solution (0.05 M in DMF) were added to the reaction cell. The CV was recorded with Pt disk working electrode (WE), SCE reference electrode (RE), and Pt mesh/Al wire counter electrode (CE) to determine the applied potential ($E_{\text{app}} = E_{\text{pc}} - 80 \text{ mV}$). Subsequently a solution of 198 mg of $\beta\text{-CD-Br}_{12}$ (0.06 mmol) in 2 mL of DMF was injected into the reaction solution and the CV was measured to confirm an increased cathodic response. Then the Pt mesh WE, Pt mesh/Al wire CE, and SCE RE were prepared and immersed in the polymerization solution and the selected potential was applied using the preparative electrolysis method with stirring during the polymerization. Samples were withdrawn periodically to follow monomer conversion, using ^1H NMR. Afterward, the products were purified by precipitation against MeOH/water (9/1) mixture, collected and dried under vacuum. Then the M_n and M_w/M_n were determined by GPC measurements (with PS standard curve).

Synthesis of $\beta\text{-CD-PBA}_{14}$ star polymers by *e*ATRP/*se*ATRP under galvanostatic conditions. The initial *e*ATRP/*se*ATRP polymerization was carried out under potentiostatic conditions and the passed charge value, was determined by utilizing the EcoChemic GPES program and the proper applied current values were calculated based on $I = Q/s$ for each step. An identical reaction mixture was prepared and *e*ATRP/*se*ATRP was carried out under galvanostatic conditions under multiple sequential applied currents (*e*ATRP: $I_{\text{app},1} = (-) 1.14 \text{ mA}$ (0.13 h), $I_{\text{app},2} = (-) 0.08 \text{ mA}$ (1.37 h), $I_{\text{app},3} = (-) 0.07 \text{ mA}$ (1.5 h); *se*ATRP: $I_{\text{app},1} = (-) 0.28 \text{ mA}$ (0.13 h), $I_{\text{app},2} = (-) 0.15 \text{ mA}$ (0.75 h), $I_{\text{app},3} = (-) 0.08 \text{ mA}$

(0.75 h), $I_{app,4} = (-) 0.06$ mA (1.37 h)). Samples were withdrawn periodically to follow the monomer conversion, using ^1H NMR. The products were purified by precipitation against MeOH/water (9/1) mixture, collected and dried under vacuum. The M_n and M_w/M_n were determined by GPC measurements (with PS standard curve).

Synthesis of β -CD-PBA₂₁ star polymers by *se*ATRP under potentiostatic conditions. TBAP (1.37 g, 4 mmol) was placed in an electrolysis cell maintained at 50 °C under a slow Ar purge. Then, 10 mL of Ar purged BA (73 mmol), DMF (7.9 mL) and 0.07 mL of an Ar purged $\text{Cu}^{\text{II}}\text{Br}_2/2\text{TPMA}$ stock solution (0.05 M in DMF) were added to the reaction cell. The CV was recorded using a Pt disk working electrode (WE), a SCE reference electrode (RE), and an Al wire counter electrode (CE) for determining the appropriate applied potentials ($E_{app} = E_{pc} - 80$ mV, $E_{pc} - 50$ mV, or $E_{pc} - 20$ mV). A solution of 174 mg of β -CD-Br₂₁ (0.04 mmol) in 2 mL of DMF was injected to the reaction solution and the CV was measured to confirm an increased cathodic response. Then the Pt mesh WE, Pt mesh/Al wire CE, and SCE RE were prepared and immersed in the polymerization solution and the selected potential was applied using the preparative electrolysis method with stirring during the polymerization. Samples were withdrawn periodically to follow the monomer conversion, using ^1H NMR. The products were purified by precipitation against MeOH/water (9/1) mixture, collected and dried under vacuum. The M_n and M_w/M_n were determined by GPC measurements (with PS standard curve).

Synthesis of β -CD-PBA₂₁ star polymers by *se*ATRP under galvanostatic conditions. The initial *se*ATRP polymerization was carried out under potentiostatic conditions and the passed charge value, was determined by utilizing the EcoChemie GPES

program and the proper applied current values were calculated based on $I = Q/s$ for each step. An identical reaction mixture was prepared and *se*ATRP was carried out under multiple applied currents ($I_{app,1} = (-) 0.31$ mA (0.05 h), $I_{app,2} = (-) 0.11$ mA (0.67 h), $I_{app,3} = (-) 0.06$ mA (0.78 h), $I_{app,4} = (-) 0.04$ mA (1.50 h)). Samples were withdrawn periodically to follow the monomer conversion, using ^1H NMR. The products were purified by precipitation against MeOH/water (9/1) mixture, collected and dried under vacuum. The M_n and M_w/M_n were determined by GPC measurements (with PS standard curve).

Chain extension of a β -CD-(PBA-Br) $_{21}$ star macroinitiator with *t*BA. For the two-step method, the β -CD-(PBA-Br) $_{21}$ macroinitiator was prepared by *se*ATRP under galvanostatic conditions. Polymerization conditions: $[\text{BA}]/[\beta\text{-CD-Br}_{21}]/[\text{Cu}^{\text{II}}\text{Br}_2/2\text{TPMA}] = 85/1/0.0043$, $[\text{BA}] = 3.6$ M in DMF, $[\text{Cu}^{\text{II}}\text{Br}_2/2\text{TPMA}] = 0.18$ mM, $[\text{TBAP}]_0 = 0.2$ M, $E_{app} = E_{pc} - 20$ mV (vs. SCE), $T = 50$ °C, WE = Pt mesh, CE = Al wire, and RE = SCE. The polymerization was stopped after 3 h of reaction. The *se*ATRP method was also used for the chain extension of the β -CD-(PBA-Br) $_{21}$ macroinitiator with *t*BA. Polymerization conditions: $[t\text{BA}]/[\beta\text{-CD-Br}_{21}]/[\text{Cu}^{\text{II}}\text{Br}_2/2\text{TPMA}] = 60/1/0.003$, $[t\text{BA}] = 3.4$ M in DMF, $[\text{Cu}^{\text{II}}\text{Br}_2/2\text{TPMA}] = 0.17$ mM, $[\text{TBAP}] = 0.2$ M, $E_{app} = E_{pc} - 35$ mV (vs. SCE), $T = 50$ °C, WE = Pt mesh, CE = Al wire ($l = 10$ cm, $d = 1$ mm), and RE = SCE. The polymerization was continued for 2 h. An identical reaction mixture was prepared and *se*ATRP was carried out under multiple applied currents ($I_{app,1} = (-) 0.23$ mA (0.03 h), $I_{app,2} = (-) 0.12$ mA (0.57 h), $I_{app,3} = (-) 0.05$ mA (0.73 h), $I_{app,4} = (-) 0.03$ mA (0.67 h)). In both cases samples were withdrawn periodically to follow the monomer conversion, using ^1H NMR. The products were purified by precipitation against MeOH/water (9/1) mixture, collected and dried

under vacuum. The M_n and M_w/M_n were determined by GPC measurements (with PS standard curve).

Solvolysis of arms of star polymers. The arms of star polymers were cleaved by acid solvolysis according to procedure described in reference.³¹⁸ It has been previously demonstrated that complete cleavage of the polymer side chains occurs under these conditions and that the identity of the ester functionalities of each monomer unit is preserved.³²⁰ Therefore, the star sample (50 mg) was dissolved in THF (1 mL) and *n*-butanol (16 mL). Concentrated sulfuric acid (0.2 mL) was added, and the solution was heated at 100 °C for 7 days. The solvent was removed under vacuum, and the remaining residue was dissolved in CHCl_3 (4 mL). After extracting with water (1.5 mL), the organic layer was isolated, solvent was removed under vacuum. The resulting polymer obtained from the cleavage reaction was dried under vacuum for 3 days and then characterized by GPC to examine the growth of the polymer arms with monomer conversion.

A-VII. 5. References

1. (a) Kato, M.; Kamigaito, M.; Sawamoto, M.; Higashimura, T., *Macromolecules* **1995**, 28 (5), 1721-1723; (b) Wang, J. S.; Matyjaszewski, K., *J Am Chem Soc* **1995**, 117 (20), 5614-5615; (c) Shah, R. R.; Merreceyes, D.; Husemann, M.; Rees, I.; Abbott, N. L.; Hawker, C. J.; Hedrick, J. L., *Macromolecules* **2000**, 33 (2), 597-605; (d) Matyjaszewski, K.; Xia, J. H., *Chem Rev* **2001**, 101 (9), 2921-2990; (e) Coessens, V.; Pintauer, T.; Matyjaszewski, K., *Prog. Polym. Sci.* **2001**, 26 (3), 337-377; (f) Perruchot, C.; Khan, M. A.; Kamitsi, A.; Armes, S. P.; von Werne, T.; Patten, T. E., *Langmuir* **2001**, 17 (15), 4479-4481; (g) Cheng, G.; Böker, A.; Zhang, M.; Krausch, G.; Müller, A. H. E., *Macromolecules* **2001**, 34 (20), 6883-6888; (h) Edmondson, S.; Osborne, V. L.; Huck, W. T. S., *Chem. Soc. Rev.* **2004**, 33 (1), 14-22; (i) Venkatesh, R.; Yajjou, L.; Koning, C. E.; Klumperman, B., *Macromolecular Chemistry and Physics* **2004**, 205 (16), 2161-2168; (j) Ohno, K.; Morinaga, T.; Koh, K.; Tsujii, Y.; Fukuda, T., *Macromolecules* **2005**, 38 (6), 2137-2142; (k) Braunecker, W. A.; Matyjaszewski, K., *Progress in Polymer Science* **2007**, 32 (1), 93-146; (l) Tsarevsky, N. V.; Matyjaszewski, K., *Chemical Reviews (Washington, DC, United States)* **2007**, 107 (6), 2270-2299; (m) Meng, T.; Gao, X.; Zhang, J.; Yuan, J.; Zhang, Y.;

- He, J., *Polymer* **2009**, *50* (2), 447-454; (n) di Lena, F.; Matyjaszewski, K., *Prog. Polym. Sci.* **2010**, *35* (8), 959-1021; (o) Lee, H.-i.; Pietrasik, J.; Sheiko, S. S.; Matyjaszewski, K., *Prog. Polym. Sci.* **2010**, *35* (1-2), 24-44; (p) Lee, S. H.; Dreyer, D. R.; An, J.; Velamakanni, A.; Piner, R. D.; Park, S.; Zhu, Y.; Kim, S. O.; Bielawski, C. W.; Ruoff, R. S., *Macromolecular Rapid Communications* **2010**, *31* (3), 281-288; (q) Matyjaszewski, K., *Isr. J. Chem.* **2012**, *52* (3-4), 206-220; (r) Siegwart, D. J.; Oh, J. K.; Matyjaszewski, K., *Prog. Polym. Sci.* **2012**, *37* (1), 18-37; (s) Mosnáček, J.; Ilčíková, M., *Macromolecules* **2012**, *45* (15), 5859-5865; (t) Krol, P.; Chmielarz, P., *Prog Org Coat* **2014**, *77* (5), 913-948; (u) Matyjaszewski, K.; Tsarevsky, N. V., *J. Am. Chem. Soc.* **2014**, *136* (Copyright (C) 2014 American Chemical Society (ACS). All Rights Reserved.), 6513-6533.
2. (a) Qiu, J.; Matyjaszewski, K., *Macromolecules* **1997**, *30* (19), 5643-5648; (b) Teodorescu, M.; Matyjaszewski, K., *Macromolecules* **1999**, *32* (15), 4826-4831; (c) Matyjaszewski, K.; Jo, S. M.; Paik, H.-j.; Shipp, D. A., *Macromolecules* **1999**, *32* (20), 6431-6438; (d) Wang, X. S.; Armes, S. P., *Macromolecules* **2000**, *33* (18), 6640-6647; (e) Kowalewski, T.; Tsarevsky, N. V.; Matyjaszewski, K., *J Am Chem Soc* **2002**, *124* (36), 10632-10633; (f) Hester, J. F.; Banerjee, P.; Won, Y. Y.; Akthakul, A.; Acar, M. H.; Mayes, A. M., *Macromolecules* **2002**, *35* (20), 7652-7661; (g) Qin, S.; Qin, D.; Ford, W. T.; Resasco, D. E.; Herrera, J. E., *J Am Chem Soc* **2004**, *126* (1), 170-176; (h) Eugene, D. M.; Grayson, S. M., *Macromolecules* **2008**, *41* (14), 5082-5084; (i) Wang, D. P.; Clough, S. J.; Zhao, Y. F.; Korban, S. S.; Sundin, G. W.; Toth, I. K. In *REGULATORY GENES AND ENVIRONMENTAL REGULATION OF AMYLOVORAN BIOSYNTHESIS IN ERWINIA AMYLOVORA*, International Society for Horticultural Science (ISHS), Leuven, Belgium: 2011; pp 195-202; (j) Sui, Y.; Wang, Z.; Gao, X.; Gao, C., *Journal of Membrane Science* **2012**, *413-414*, 38-47; (k) Wever, D. A. Z.; Raffa, P.; Picchioni, F.; Broekhuis, A. A., *Macromolecules* **2012**, *45* (10), 4040-4045; (l) Liu, Q.; Singh, A.; Lalani, R.; Liu, L., *Biomacromolecules* **2012**, *13* (4), 1086-1092; (m) Chmielarz, P.; Park, S.; Simakova, A.; Matyjaszewski, K., *Polymer* **2015**, *60*, 302-307.
3. (a) Hadjichristidis, N.; Pitsikalis, M.; Pispas, S.; Iatrou, H., *Chem. Rev.* **2001**, *101* (12), 3747-3792; (b) Vamvakaki, M.; Hadjiyannakou, S. C.; Loizidou, E.; Patrickios, C. S.; Armes, S. P.; Billingham, N. C., *Chemistry of Materials* **2001**, *13* (12), 4738-4744; (c) Gao, H.; Matyjaszewski, K., *Progress in Polymer Science* **2009**, *34* (4), 317-350; (d) Setijadi, E.; Tao, L.; Liu, J.; Jia, Z.; Boyer, C.; Davis, T. P., *Biomacromolecules* **2009**, *10* (9), 2699-2707; (e) Blencowe, A.; Tan, J. F.; Goh, T. K.; Qiao, G. G., *Polymer* **2009**, *50* (1), 5-32; (f) Schmidt, B. V. K. J.; Rudolph, T.; Hetzer, M.; Ritter, H.; Schacher, F. H.; Barner-Kowollik, C., *Polymer Chemistry* **2012**, *3* (11), 3139-3145; (g) Li, Y.; Guo, H.; Zheng, J.; Gan, J.; Zhang, Y.; Guan, X.; Wu, K.; Lu, M., *RSC Advances* **2014**, *4* (97), 54268-54281; (h) Wu, W.; Wang, W.; Li, J., *Progress in Polymer Science* **2015**, *46*, 55-85.
4. (a) Zhang, X.; Xia, J.; Matyjaszewski, K., *Macromolecules* **2000**, *33* (7), 2340-2345; (b) Ohno, K.; Wong, B.; Haddleton, D. M., *Journal of Polymer Science Part A: Polymer Chemistry* **2001**, *39* (13), 2206-2214; (c) Suzuki, A.; Nagai, D.; Ochiai, B.; Endo, T., *Journal of Polymer Science Part A: Polymer Chemistry* **2005**, *43* (22), 5498-5505; (d) Liu, J.; Liu, H.; Jia, Z.; Bulmus, V.; Davis, T. P., *Chemical Communications* **2008**, (48), 6582-6584.
5. Li, S.; Xiao, M.; Zheng, A.; Xiao, H., *Materials Science and Engineering: C* **2014**, *43*, 350-358.

6. (a) Li, J.; Xiao, H.; Kim, Y. S.; Lowe, T. L., *Journal of Polymer Science Part A: Polymer Chemistry* **2005**, *43* (24), 6345-6354; (b) Zhao, Y.; Chen, Y.; Chen, C.; Xi, F., *Polymer* **2005**, *46* (15), 5808-5819; (c) Karaky, K.; Reynaud, S.; Billon, L.; François, J.; Chreim, Y., *Journal of Polymer Science Part A: Polymer Chemistry* **2005**, *43* (21), 5186-5194; (d) Zhang, Z.-X.; Liu, X.; Xu, F. J.; Loh, X. J.; Kang, E.-T.; Neoh, K.-G.; Li, J., *Macromolecules* **2008**, *41* (16), 5967-5970; (e) Dong, Y.-Q.; Dong, B.-T.; Du, F.-S.; Meng, J.-Q.; Li, Z.-C., *Polymer* **2009**, *50* (1), 125-132; (f) Xu, J.; Liu, S., *Journal of Polymer Science Part A: Polymer Chemistry* **2009**, *47* (2), 404-419; (g) Schmalz, A.; Hanisch, M.; Schmalz, H.; Müller, A. H. E., *Polymer* **2010**, *51* (6), 1213-1217; (h) Li, J.; Guo, Z.; Xin, J.; Zhao, G.; Xiao, H., *Carbohydrate Polymers* **2010**, *79* (2), 277-283; (i) Mauricio, M. R.; Otsuka, I.; Borsali, R.; Petzhold, C. L.; Cellet, T. S. P.; Carvalho, G. M. d.; Rubira, A. F., *Reactive and Functional Polymers* **2011**, *71* (12), 1160-1165; (j) Xiu, K. M.; Yang, J. J.; Zhao, N. N.; Li, J. S.; Xu, F. J., *Acta Biomaterialia* **2013**, *9* (1), 4726-4733; (k) Huang, B.; Chen, M.; Zhou, S.; Wu, L., *Polymer Chemistry* **2015**, *6* (21), 3913-3917; (l) Pan, Y.; Xue, Y.; Snow, J.; Xiao, H., *Macromolecular Chemistry and Physics* **2015**, *216* (5), 511-518.
7. (a) Matyjaszewski, K.; Nakagawa, Y.; Jasieczek, C. B., *Macromolecules* **1998**, *31* (5), 1535-1541; (b) Zhang, H.; Van Der Linde, R., *Journal of Polymer Science Part A: Polymer Chemistry* **2002**, *40* (21), 3549-3561.
8. Nafee, N.; Hirose, M.; Loretz, B.; Wenz, G.; Lehr, C. M., *Colloids and Surfaces B: Biointerfaces* **2015**, *129*, 30-38.
9. (a) Pang, X.; Zhao, L.; Akinc, M.; Kim, J. K.; Lin, Z., *Macromolecules* **2011**, *44* (10), 3746-3752; (b) Pang, X.; Zhao, L.; Han, W.; Xin, X.; Lin, Z., *Nat Nano* **2013**, *8* (6), 426-431; (c) Yang, D.; Pang, X.; He, Y.; Wang, Y.; Chen, G.; Wang, W.; Lin, Z., *Angewandte Chemie* **2015**, *127* (41), 12259-12264; (d) Zheng, D.; Pang, X.; Wang, M.; He, Y.; Lin, C.; Lin, Z., *Chemistry of Materials* **2015**, *27* (15), 5271-5278; (e) Jiang, B.; Pang, X.; Li, B.; Lin, Z., *J Am Chem Soc* **2015**, *137* (36), 11760-11767.
10. Deng, J.; Liu, X.; Ma, L.; Cheng, C.; Shi, W.; Nie, C.; Zhao, C., *ACS Applied Materials & Interfaces* **2014**, *6* (23), 21603-21614.
11. Jakubowski, W.; Matyjaszewski, K., *Angew Chem Int Edit* **2006**, *45* (27), 4482-4486.
12. Matyjaszewski, K.; Jakubowski, W.; Min, K.; Tang, W.; Huang, J. Y.; Braunecker, W. A.; Tsarevsky, N. V., *P Natl Acad Sci USA* **2006**, *103* (42), 15309-15314.
13. Siegwart, D. J.; Wu, W.; Mandalaywala, M.; Tamir, M.; Sarbu, T.; Silverstein, M. S.; Kowalewski, T.; Hollinger, J. O.; Matyjaszewski, K., *Polymer* **2007**, *48* (25), 7279-7290.
14. Konkolewicz, D.; Schroder, K.; Buback, J.; Bernhard, S.; Matyjaszewski, K., *Acs Macro Lett* **2012**, *1* (10), 1219-1223.
15. (a) Magenau, A. J. D.; Strandwitz, N. C.; Gennaro, A.; Matyjaszewski, K., *Science* **2011**, *332* (6025), 81-84; (b) Bortolamei, N.; Isse, A. A.; Magenau, A. J. D.; Gennaro, A.; Matyjaszewski, K., *Angew Chem Int Edit* **2011**, *50* (48), 11391-11394; (c) Magenau, A. J. D.; Bortolamei, N.; Frick, E.; Park, S.; Gennaro, A.; Matyjaszewski, K., *Macromolecules* **2013**, *46* (11), 4346-4353; (d) Li, B.; Yu, B.; Huck, W. T. S.; Liu, W.; Zhou, F., *J. Am. Chem. Soc.* **2013**, *135* (5), 1708-1710; (e) Park, S.; Cho, H. Y.; Wegner, K. B.; Burdyska, J.; Magenau, A. J. D.; Paik, H. J.; Jurga, S.; Matyjaszewski, K., *Macromolecules* **2013**, *46* (15), 5856-5860; (f) Li, B.; Yu, B.; Zhou, F., *Macromolecular Rapid Communications* **2013**, *34* (3), 246-250; (g) Jin, G.-P.; Fu, Y.; Bao, X.-C.; Feng, X.-S.; Wang, Y.; Liu, W.-H., *J Appl Electrochem* **2014**, *44* (5), 621-629; (h) Plamper, F. A., *Colloid and Polymer*

- Science* **2014**, 292 (4), 777-783; (i) Park, S.; Chmielarz, P.; Gennaro, A.; Matyjaszewski, K., *Angew. Chem., Int. Ed.* **2015**, 54 (8), 2388-2392; (j) Chmielarz, P.; Krys, P.; Park, S.; Matyjaszewski, K., *Polymer* **2015**, 71, 143-147; (k) Chmielarz, P.; Sobkowiak, A.; Matyjaszewski, K., *Polymer* **2015**, 77, 266-271.
16. Zhang, M.; Xiong, Q.; Wang, Y.; Zhang, Z.; Shen, W.; Liu, L.; Wang, Q.; Zhang, Q., *Polymer Chemistry* **2014**, 5 (16), 4670-4678.
17. Li, J.; Xiao, H., *Tetrahedron Lett.* **2005**, 46 (13), 2227-2229.
18. (a) Chan, N.; Cunningham, M. F.; Hutchinson, R. A., *Macromolecular Chemistry and Physics* **2008**, 209 (17), 1797-1805; (b) Magenau, A. J. D.; Kwak, Y.; Matyjaszewski, K., *Macromolecules* **2010**, 43 (23), 9682-9689.
19. Zhong, M.; Matyjaszewski, K., *Macromolecules* **2011**, 44 (8), 2668-2677.
20. (a) Barth, J.; Buback, M.; Hesse, P.; Sergeeva, T., *Macromolecules* **2010**, 43 (9), 4023-4031; (b) Nikitin, A. N.; Hutchinson, R. A., *Macromolecular Theory and Simulations* **2006**, 15 (2), 128-136.
21. Buback, M.; Kurz, C. H.; Schmaltz, C., *Macromolecular Chemistry and Physics* **1998**, 199 (8), 1721-1727.
22. Yamago, S., *Chem Rev* **2009**, 109 (11), 5051-5068.
23. Nakamura, Y.; Lee, R.; Coote, M. L.; Yamago, S., *Macromolecular Rapid Communications* **2016**, n/a-n/a.
24. Dervaux, B.; Junkers, T.; Schneider-Baumann, M.; Du Prez, F. E.; Barner-Kowollik, C., *Journal of Polymer Science Part A: Polymer Chemistry* **2009**, 47 (23), 6641-6654.
25. Williams, V. A.; Ribelli, T. G.; Chmielarz, P.; Park, S.; Matyjaszewski, K., *J. Am. Chem. Soc.* **2015**, 137 (4), 1428-1431.
26. (a) Sumerlin, B. S.; Neugebauer, D.; Matyjaszewski, K., *Macromolecules* **2005**, 38 (3), 702-708; (b) Neugebauer, D.; Sumerlin, B. S.; Matyjaszewski, K.; Goodhart, B.; Sheiko, S. S., *Polymer* **2004**, 45 (24), 8173-8179.
27. Plamper, F. A.; Becker, H.; Lanzendörfer, M.; Patel, M.; Wittemann, A.; Ballauff, M.; Müller, A. H. E., *Macromolecular Chemistry and Physics* **2005**, 206 (18), 1813-1825.
28. Xia, J. H.; Matyjaszewski, K., *Macromolecules* **1999**, 32 (8), 2434-2437.
29. Börner, H. G.; Beers, K.; Matyjaszewski, K.; Sheiko, S. S.; Möller, M., *Macromolecules* **2001**, 34 (13), 4375-4383.

Appendix VIII

Phototunable Supersoft Elastomers using Coumarin Functionalized Molecular Bottlebrushes for Cell-Surface Interactions Study*

A-VIII. 1. Introduction

Elastomers can reversibly extend up to several times of their original lengths.¹ The most common method of preparing elastomers is light crosslinking of polymers with low glass transition temperatures. Elastomers have a typical Young's modulus value at around 1 MPa. Even though such soft materials are useful for various applications, even softer materials are also in demand.² Supersoft elastomers are about 2 to 3 orders of magnitude softer than regular elastomers with a Young's modulus value at a level of kilopascals (kPa).³ Such elastomeric materials can be obtained by swelling lightly crosslinked elastomers with solvents. However, these systems show low stability since gradually evaporating solvent will decrease the softness of the material. In addition, solvent may contaminate its surroundings and decrease the practical application of the material, especially when interfacing with biomolecules. One solution to this problem is swelling the lightly crosslinked polymer network not with a solvent, but with covalently attached low glass transition temperature (T_g) short polymer chains. Such architecture can be formed either by crosslinking molecular bottlebrushes bearing soft, low T_g side chains,⁴ or by grafting such side chains to/from a preformed loosely cross-linked network.⁵ Backbones of the

*Work in this appendix was published and partially reformatted based on the following manuscript: Mukumoto, Kosuke; Averick, Saadyah E.; Park, Sangwoo; Nese, Alper; Mpoukouvalas, Anastasia; Zeng, Yukai; Koynov, Kaloian; Leduc, Philip R.; Matyjaszewski, Krzysztof *Macromolecules* **2014**, 47, 7852

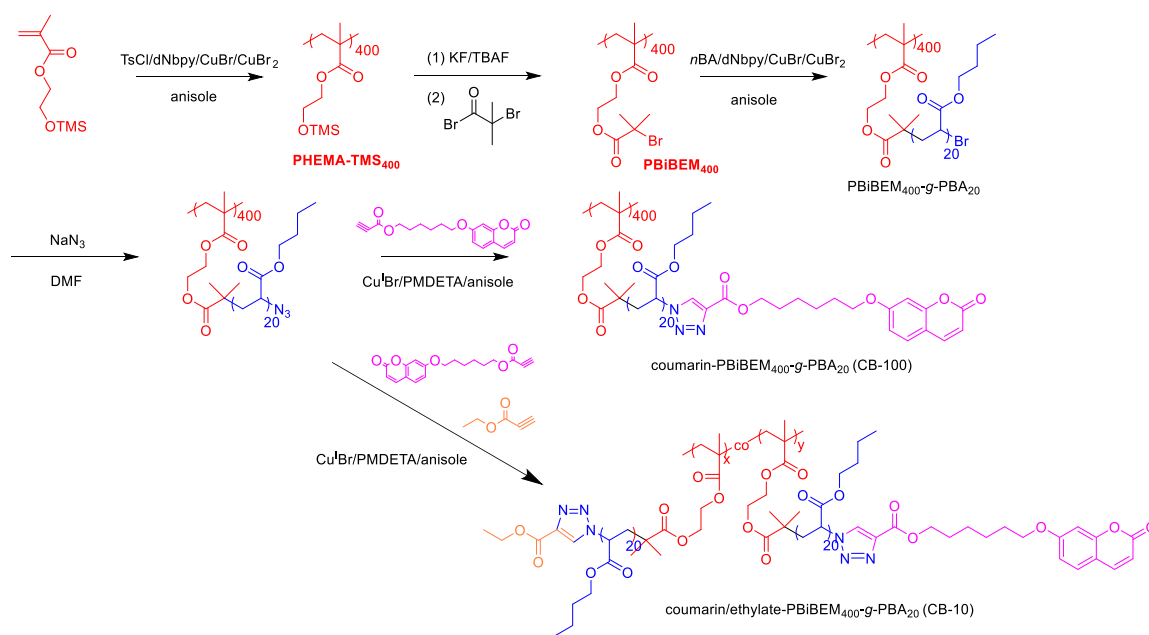
molecular bottlebrushes have an extended conformation as a result of the repulsion between the densely grafted side chains.⁶ Bottlebrushes have several potential applications including high aspect ratio nanowires,⁷ nanotubes and hollow objects,⁸ photonic crystals,⁹ molecular tensile machines,¹⁰ surfactants,¹¹ and nanoporous materials.¹² Molecular bottlebrushes have been successfully prepared by atom transfer radical polymerization (ATRP),¹³ by reversible addition–fragmentation chain-transfer polymerization (RAFT) polymerization^{9c, 14} and ring-opening metathesis polymerization (ROMP).^{9a, 9b, 15}

Coumarin and its derivatives can participate in [2+2] cyclization if irradiated at a light wavelength above 300 nm and in retrocyclization at a light wavelength below 300 nm.¹⁶ Crosslinking of coumarin units was successfully applied for preparation of various macromolecular architectures¹⁷ such as thermoplastic elastomers,¹⁸ and nanogels,¹⁹ and materials for optical data storage.²⁰ In this project, coumarin was selected to introduce reversible photocrosslinkable functionality at the periphery of the molecular bottlebrushes. The photocrosslinking method allowed solvent free preparation of supersoft elastomers, advantageous for the polymer film coatings for bio-related applications. In this Appendix, a new approach to prepare supersoft elastomers with tunable softness by using a coumarin based photocrosslinker is reported. Softness changes of the materials of only several kPa in the supersoft elastomeric region can affect the cell adhesion behavior.

A-VIII. 2. Results and Discussion

Synthesis. Molecular bottlebrushes with coumarin chain end functionalities were prepared by following the synthetic route shown in Scheme A-VIII-1. The PHEMA-TMS

macroinitiator was prepared by ATRP and the protected TMS groups were removed and converted to ATRP initiators. The polymers were characterized by gel-permeation chromatography (GPC) and ^1H NMR (Figure A-VIII-4). Molecular bottlebrushes were prepared by grafting poly(*n*-butyl acrylate) (PBA) side chains from a methacrylate backbone and GPC traces showed good molecular weight (M_n) evolution (Figure A-VIII-5). M_n molecular weight distribution (M_w/M_n) of polymers with two different contents of coumarin units are given in Table A-VIII-1 and gel-permeation chromatography (GPC) traces of the backbone and brushes are illustrated in Figure A-VIII-1.



Scheme A-VIII-1. Schematic illustration of synthesis of molecular bottlebrushes with coumarin chain end functionality.

Table A-VIII-1. Molecular weight and molecular weight distribution characterization of

bottlebrushes.

brush	$M_n \times 10^{-6}$ ^{a)}	M_w/M_n ^{b)}	DP_{BB}/DP_{SC} ^{c)}	molar % of incorporated coumarin ends groups ^{d)}
CB-100	2.38	1.62	400/20	100
CB-10	2.82	1.21	400/20	10

^{a)} M_n based on MALLS in THF using $dn/dc = 0.069$ ml/g; ^{b)} M_w/M_n based on GPC in THF for PMMA standards; ^{c)}Degree of polymerization of backbone (DP_{BB}) and side chains (DP_{SC}); ^{d)}The ratio of incorporated coumarin in side chain ends calculated by 1H NMR.

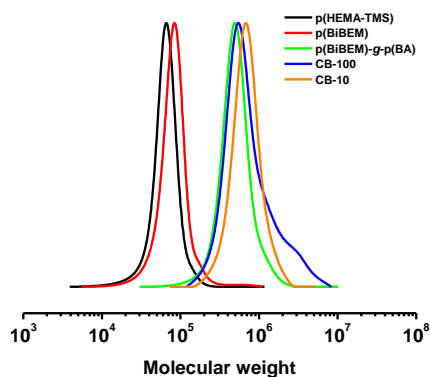


Figure A-VIII-1. GPC traces of the backbone and the resulting molecular bottlebrushes.

Br-chain ends at the brush side chains were replaced with azide groups for the subsequent azide-alkyne cycloaddition reaction (click).²¹ Backbone of the molecular bottlebrushes had an average degree of polymerization (DP) of 400 and the PBA side chains had a DP of 20. Molecular bottlebrushes were reacted with NaN_3 in DMF to replace Br-chain ends with azide functionality. Successful azidation reaction was confirmed by

Fourier transform infrared spectroscopy (FT-IR) spectra where a distinct azide peak appeared at 2150 cm^{-1} (Figure A-VIII-2).

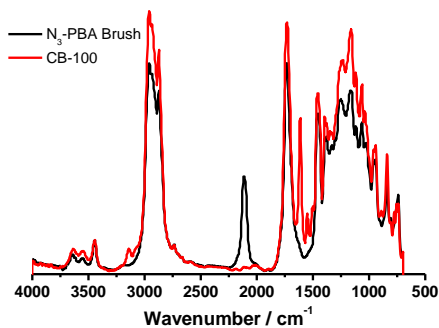


Figure A-VIII-2. FT-IR spectra of coumarin functionalized PBA bottlebrush (CB-100, red line) and azide functionalized PBA bottlebrushes (N₃-PBA, black line).

Coumarin units were incorporated by click reaction of azides with alkynes containing coumarin functionality. To study the effect of coumarin content on elastomeric behaviors, molecular bottlebrushes with 100% (CB-100) and 10% (CB-10) functionalized coumarin chain ends were prepared, from the same PBA brush (Table A-VIII-1). CB-100 was prepared by reacting azide chain end functionalized molecular bottlebrushes with excess of alkyne-coumarin. For the synthesis of CB-10, ethyl propiolate / coumarin alkyne ratio of 9/1 was used. The ratio of incorporated coumarin group at side chain ends was estimated by integration ratio of protons of [coumarin]/[methyl group of BA] in ^1H NMR spectra (Figure A-VIII-6). Ethyl propiolate and alkyne coumarin have similar reactivity toward azide. For both CB-100 and CB-10, complete disappearance of azide peaks at 2150 cm^{-1} was observed. GPC analysis indicated a slight increase of MWs after functionalization due

to the incorporation of coumarin groups. Dimerization/oligomerization could occur under ambient light condition. In case of CB-100, GPC traces showed more pronounced high MW shoulder. Further characterization was carried out by GPC with multiangle laser light scattering (MALLS) detector using $dn/dc = 0.069$ (the same dn/dc as for PBA). The MW of CB-100 was slightly lower than that of CB-10, plausibly because dn/dc values could be affected by the coumarin moieties (Table A-VIII-1).

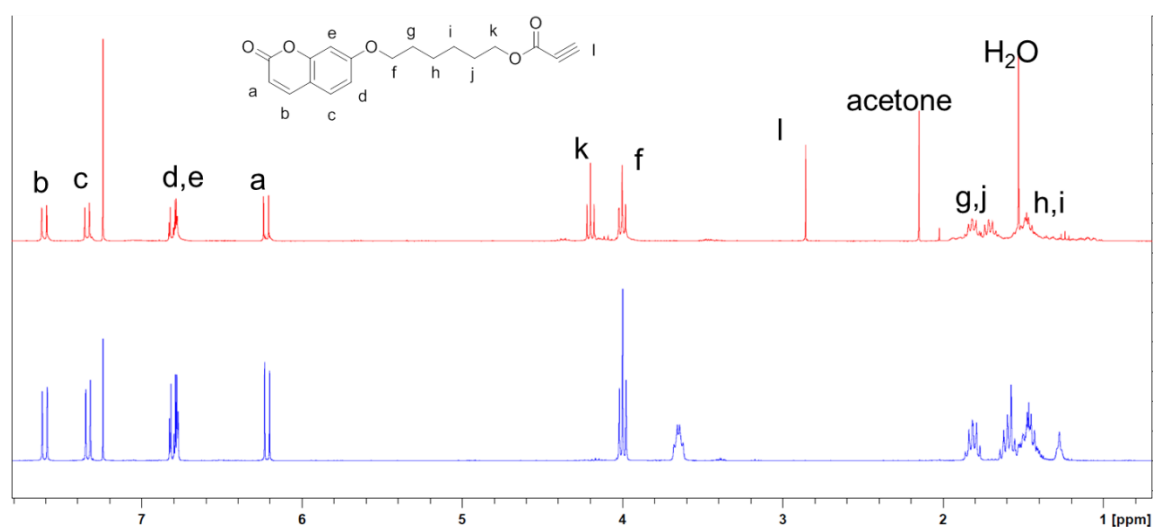


Figure A-VIII-3. ^1H NMR spectra of (red) the purified alkyne coumarin and (blue) 7-(6-hydroxyhexyl)oxycomarin.

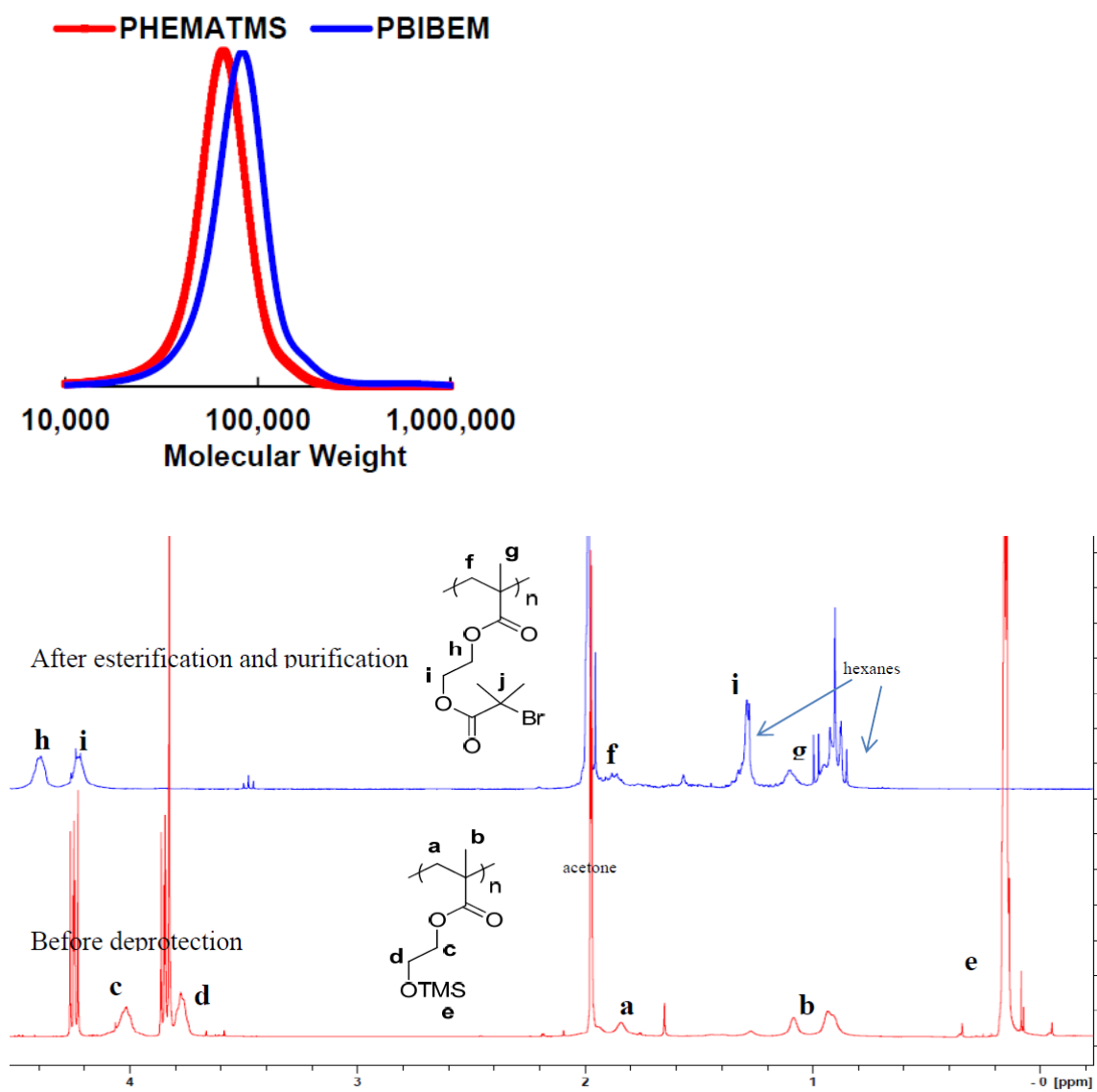


Figure A-VIII-4. GPC traces and ^1H NMR spectra of the PHEMA-TMS and PBiBEM.

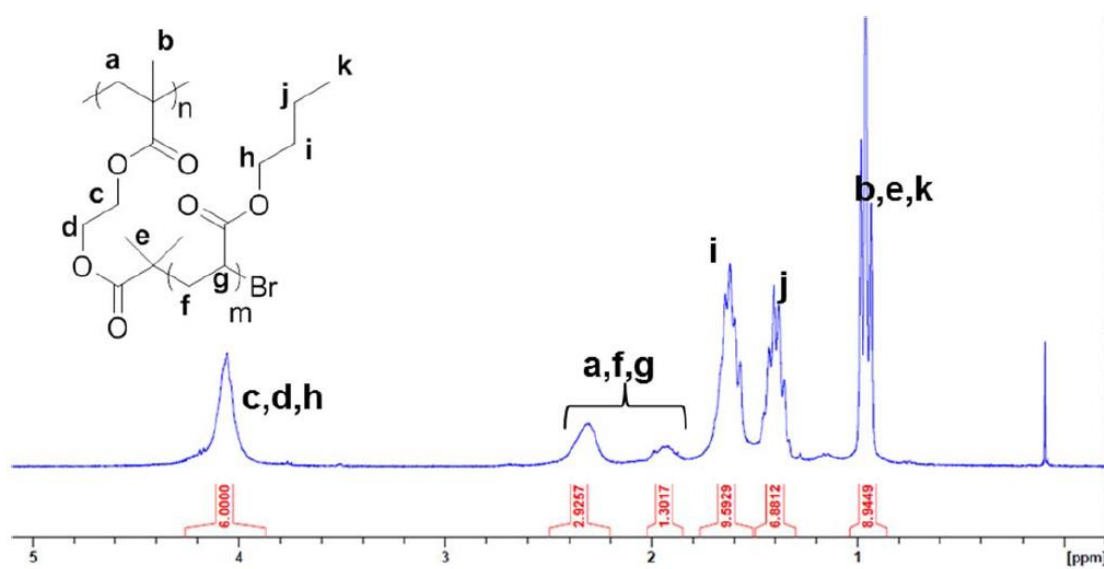
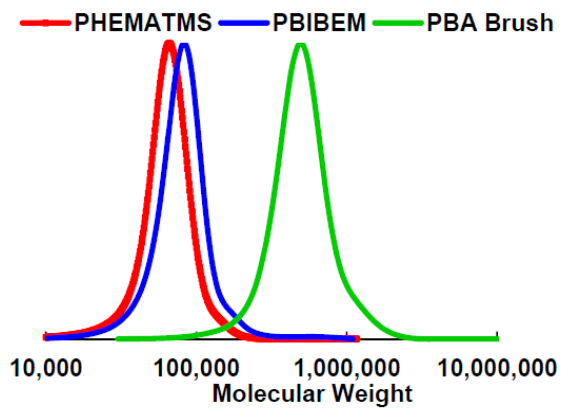


Figure A-VIII-5. GPC trace and ¹H NMR spectrum of PBA bottlebrushes.

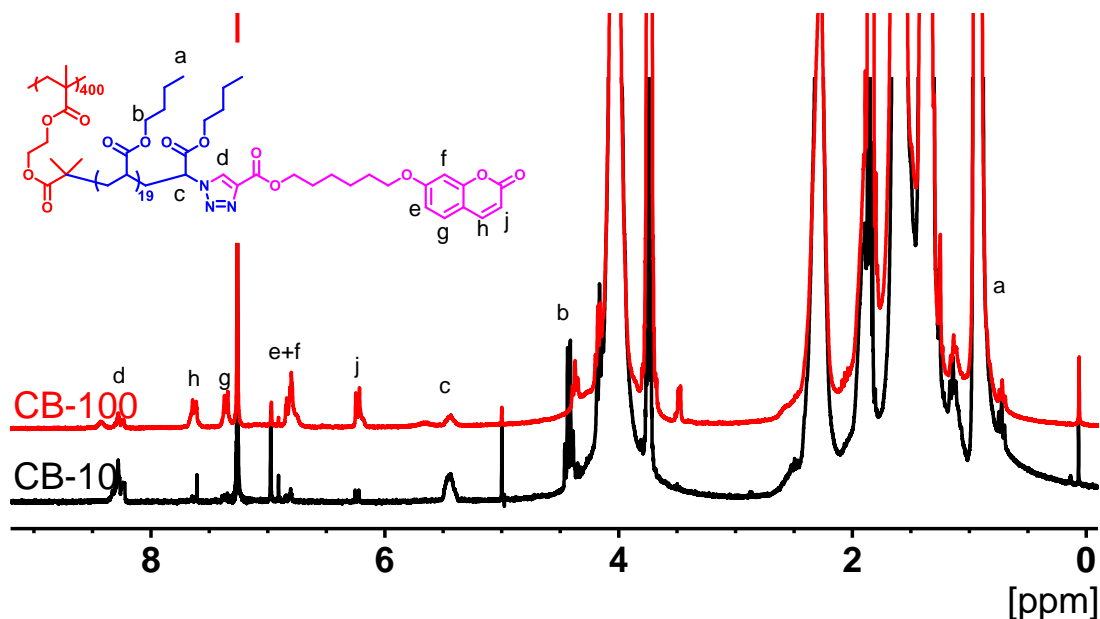


Figure A-VIII-6. ^1H NMR spectra of CB-100 and CB-10.

Photocrosslinking/scission studies. Photocrosslinking and photoscission of coumarin chain end functionalized molecular bottlebrushes were monitored by UV-vis spectrometry. Thin films of CB-100 and CB-10 were spread on quartz cells and irradiated with UV light at 320 nm to crosslink *via* coumarin dimerization. Samples were periodically characterized by UV-vis spectra (Figure A-VIII-7). The single coumarin adsorption peak at 320 nm decreased with irradiation time as dimerization proceeded. Complete dimerization took longer for CB-10 than for CB-100, since the concentration and the accessibility of the coumarin units were lower.

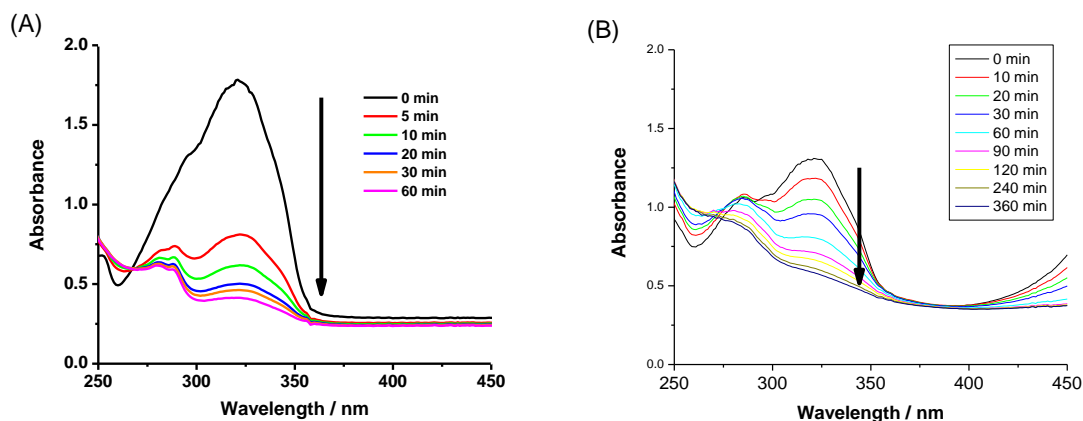


Figure A-VIII-7. UV-vis spectra of CB-100 (A) and CB-10 (B) as thin films after irradiation with UV light (320 nm), arrows indicate progressive decreasing coumarin peak intensities.

Crosslinked samples were subsequently irradiated with 254 nm UV light for photoscission to occur. Samples were again periodically characterized by UV-vis spectra to monitor the scission process (Figure A-VIII-8). For both CB-100 and CB-10, the peak at 320 nm increased. However, an extra peak at 280 nm appeared for CB-10 which might be due to a side reaction as a result of longer irradiation time (360 vs. 60 min) during earlier crosslinking reactions at 320 nm light exposure.

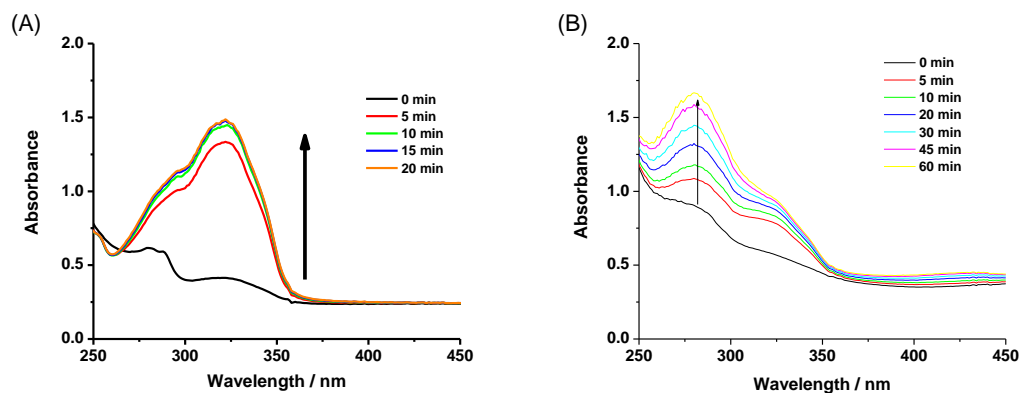


Figure A-VIII-8. UV-vis spectra of CB-100 (A) and CB-10 (B) as thin films after irradiation with UV light (254 nm) after the sample was irradiated with UV light at 320 nm, arrows indicate progressive increasing coumarin peak intensities.

CB-100 crosslinking's Photoreversibility was studied (Figure A-VIII-9). More than 90% of the coumarin was dimerized at the first cycle and around 80% photoscission occurred at every cycle. Photoscission at 254 nm was observed to be a dynamic equilibrium, with both crosslinking and scission reactions. However, the intensity of a peak of 320 nm progressively decreased due to side reactions during photocrosslinking and photoscission.²²

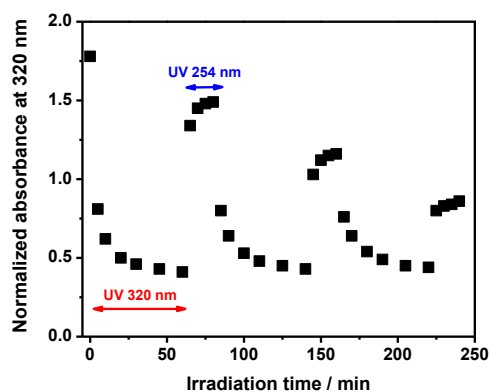


Figure A-VIII-9. Normalized absorbance at 320 nm of CB-100 as a function of irradiation time with UV of 320 nm and 254 nm.

Mechanical properties *via* DMA. Dynamical mechanical analysis (DMA) was used to characterize the mechanical properties of the prepared coumarin-functionalized molecular brushes and to evaluate the possibility for tuning of these properties by UV irradiation. Representative results in form of temperature dependences of the storage modulus (G') and the loss modulus (G'') parts of the shear modulus of CB-100 are shown in Figure A-VIII-10 and the individual curves are shown in Figure A-VIII-12. Frequency sweeps of G' and G'' measured at different temperatures and arranged in master curves are shown in Figure A-VIII-11. The sample before UV irradiation shows a behavior largely dominated by the PBA, *i.e.* it exhibits a single glass transition around $-35\text{ }^{\circ}\text{C}$ and starts flowing ($G'' > G'$) at rather low temperature of $\sim 0^{\circ}\text{C}$. However, upon irradiation with 320 nm UV light, the material becomes crosslinked, as evident from the appearance of a rubbery plateau of G' at high temperatures (Figure A-VIII-10A and Figure A-VIII-11). Furthermore, it was observed that photocrosslinking time has a direct influence on the

mechanical properties of the material. After photocrosslinking for 60 min, the sample becomes harder, with value of the storage modulus G' in the rubbery plateau region of 6.8 kPa compared to 3.6 kPa, after 5 min of irradiation. Such an increase in the elastic modulus value is consistent with the increase in the crosslinking density, as observed from UV-vis analysis (Figure A-VIII-7A). It is important to emphasize that the measured values of the elastic moduli are in a few kPa range, which are characteristic for supersoft elastomers.^{4b}

⁵ The change of G' of CB-10 by UV irradiation was smaller than that of CB-100 due to lower crosslinking density *via* dimerization. Dimerization can occur *via* intramolecular or intermolecular reaction. The increase in plateau moduli indicate some contribution of the intermolecular cross-linking, although the relatively small rise suggests the presence of the intramolecular process.

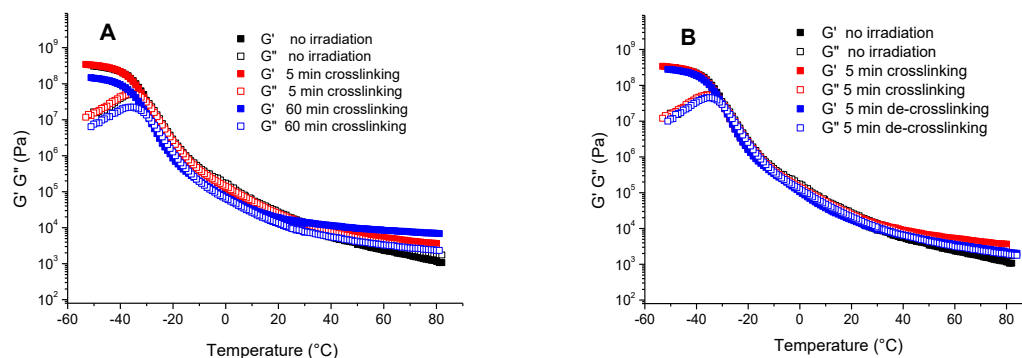


Figure A-VIII-10. Temperature dependence of the shear moduli G' and G'' of the CB-100 molecular bottlebrushes. Effect of (A) photocrosslinking time and (B) comparison of photocrosslinking and photoscission on mechanical properties.

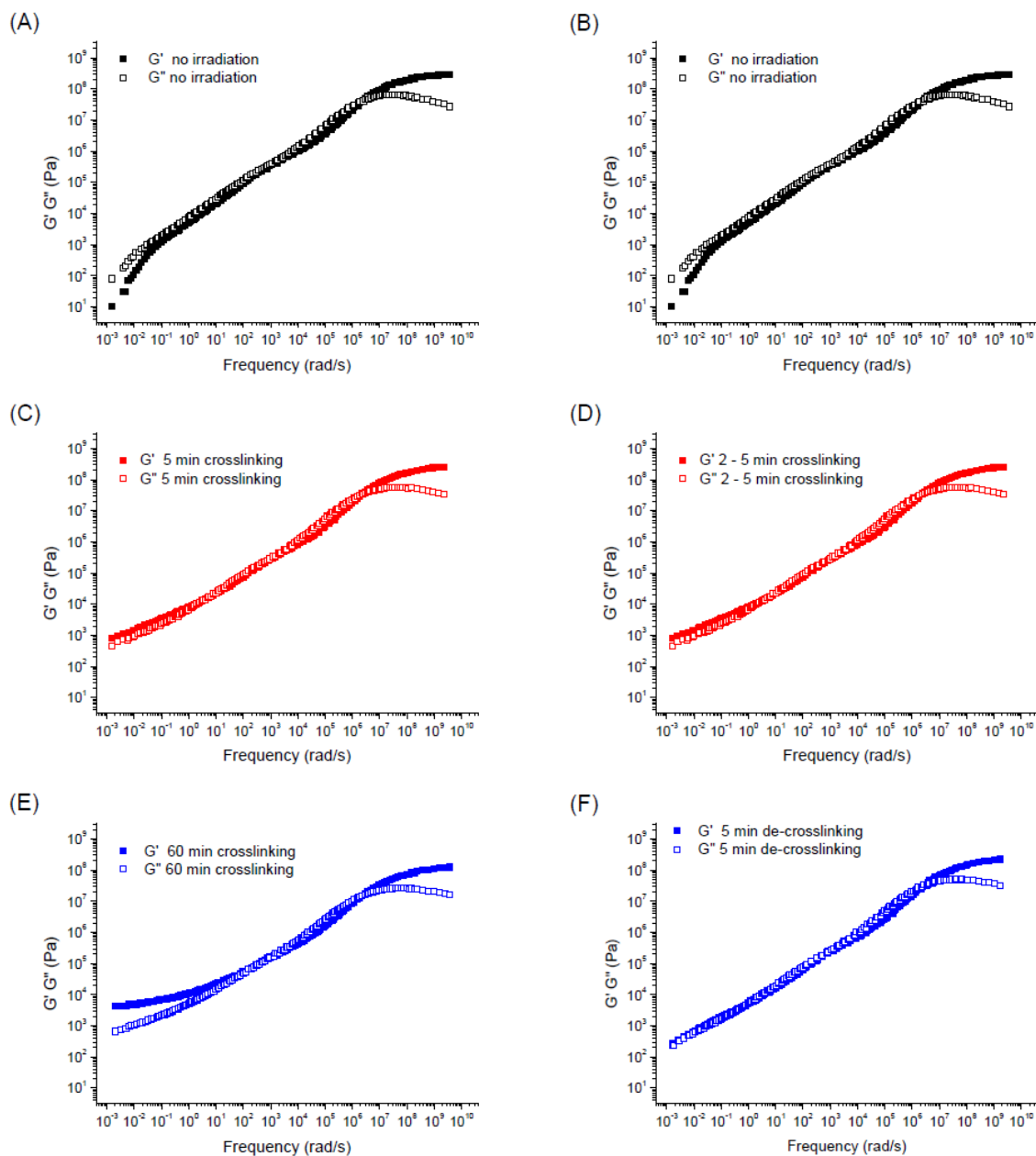


Figure A-VIII-11. Reduced frequency plots for the shear storage G' and loss G'' moduli of the CB-100 molecular bottlebrushes. Comparison of photocrosslinking (A, C, and E), and photoscission (B, E, and F). The reference temperature was 20 °C.

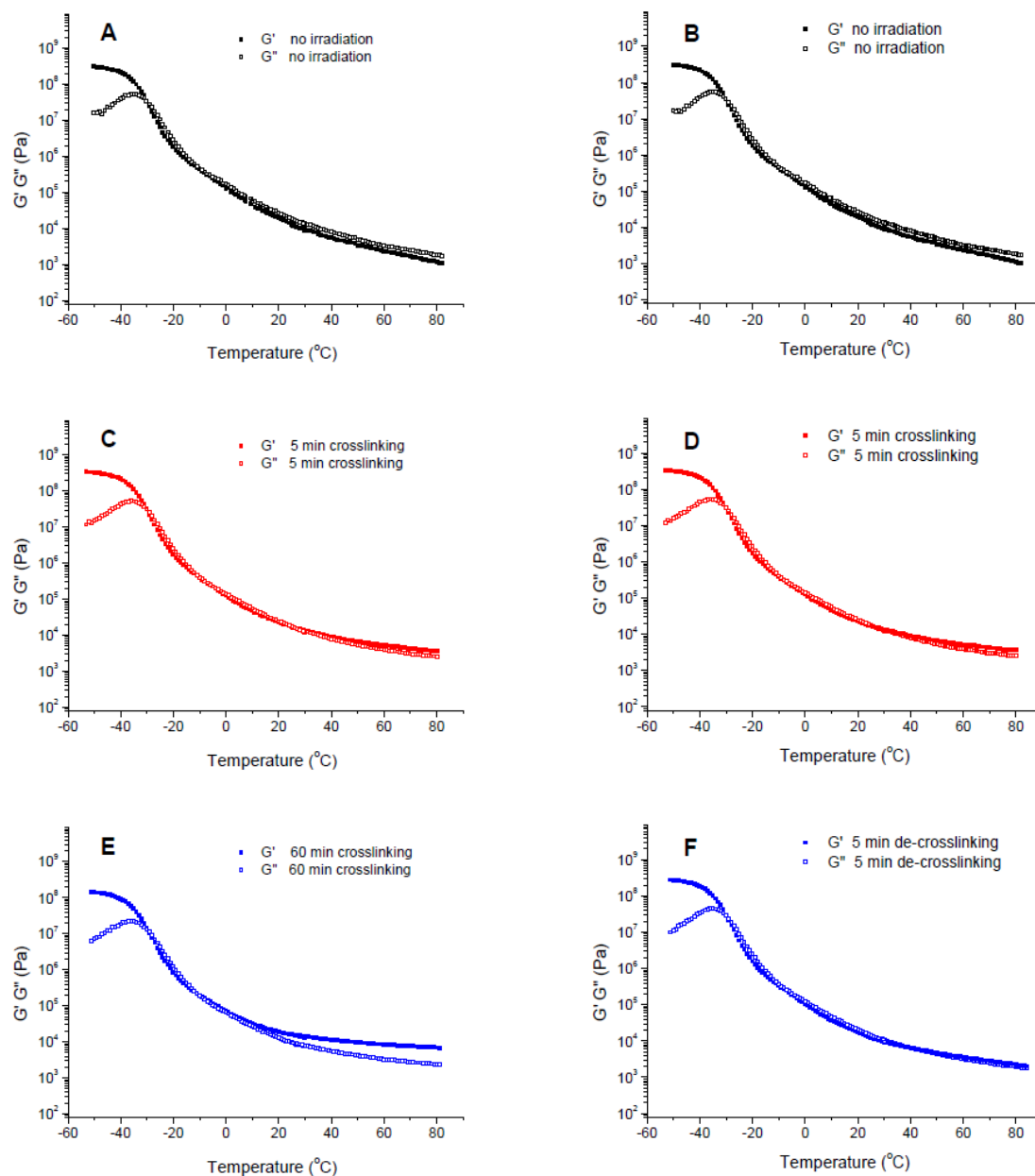


Figure A-VIII-12. Temperature dependence of the shear storage and loss moduli G' and G'' of the CB-100 molecular bottlebrushes. Effect of photocrosslinking time (A, C, and E) and comparison of photocrosslinking and photocrosslinking (B, D, and F) on mechanical properties.

Figure A-VIII-10B shows the effect of the photoscission of the dimerized coumarin units on the mechanical properties of the supersoft elastomers. CB-100, photocrosslinked *via* 5 min irradiation with 320 nm UV light, was then exposed for 5 min to 254 nm UV light for photoscission. The G' value in the rubbery plateau decreased from 3.6 kPa down to around 2 kPa, confirming a decrease in the crosslinking density due to photoscission of dimerized coumarin units. The sample did not flow at high temperatures (Figure A-VIII-10B and Figure A-VIII-11), indicating that some crosslinks still remained, in accordance with the UV-vis spectroscopy analysis that showed a photoscission efficiency of 80% (Figure A-VIII-9).

Cell adhesion and cytotoxicity studies. To study the ability for the photocrosslinkable bottlebrushes to be used as a support for cells, NIH 3T3 cells were grown on pristine CB-100 and photocrosslinked CB-100 spin casted surfaces, respectively. Live/dead cell assays were carried out with two polymer modified surfaces and control surface (cell cultivate polystyrene (PS) substrate). After 1 and 2 days of cell culture, the results showed that live to dead cell ratios of the modified surfaces were similar to the control experiments, indicating the polymer surfaces were nontoxic to the cultivated cells (Figure A-VIII-13 and Figure A-VIII-14).

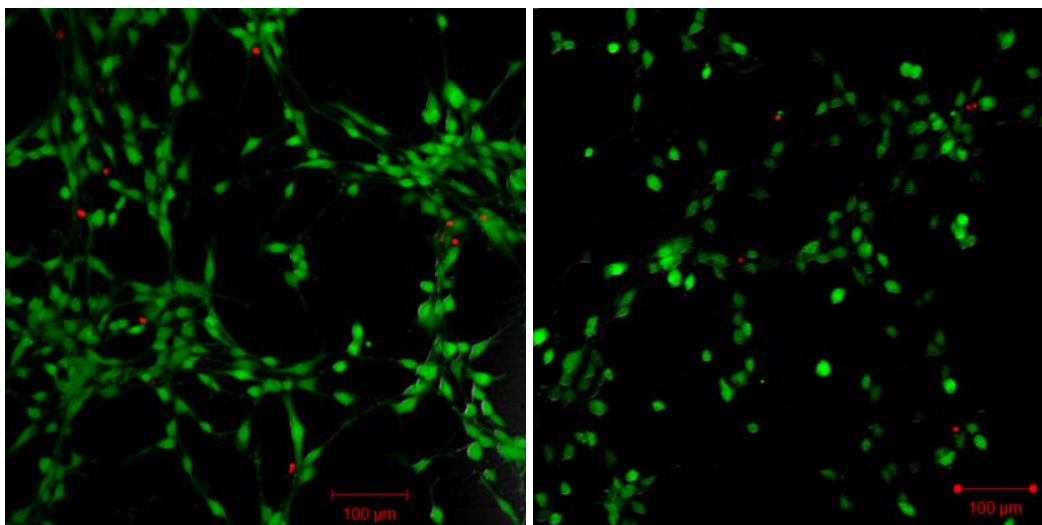


Figure A-VIII-13. Representative fluorescent images of NIH 3T3 fibroblasts cultured on pristine (left) and photocrosslinked (right) CB-100 coated substrates. The cytotoxicity of the cells was determined through a live/dead assay where the cells that show green fluorescence are living cells and the cells are dead with red fluorescence.

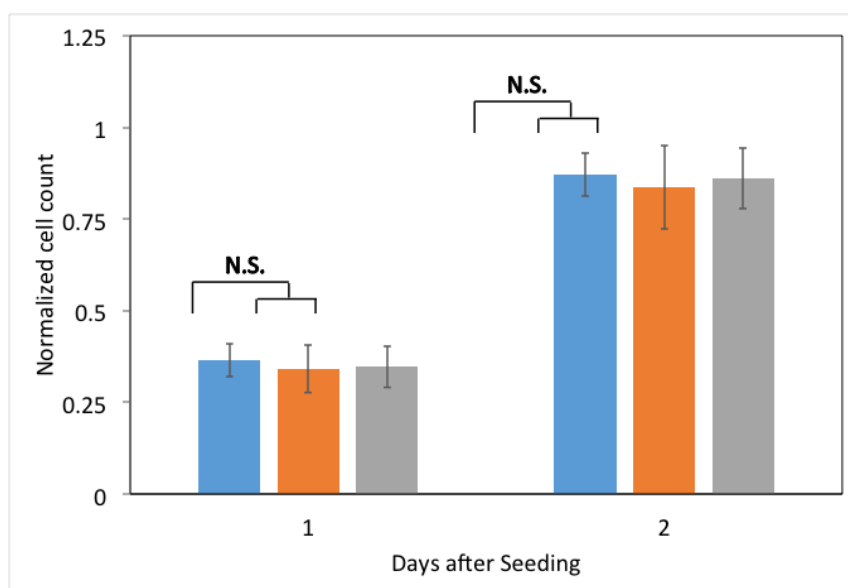


Figure A-VIII-14. NIH 3T3 fibroblasts growth on the CB-100 compared to controls.

Normalized cell count based on the absorbance readings from the MTT assay for cells grown on cover slips (control-blue), and soft (orange) and stiff (grey) CB-100 coated glass cover slips, 1 and 2 days after cell seeding. The values were normalized with respect to the well with the highest absorbance reading in the control on Day 2. Bars denote standard deviation ($n = 24$). Using student's t-tests, the differences between the controls and the coumarin brushes were not statistically significant (N.S.) ($P > 0.1$). The cell growth was the same on the CB-100 as the controls showing their ability to enable cell growth.

The cell–substrate interactions were further studied on pristine and photocrosslinked CB-100 coated surfaces using SEM and differential interference contrast microscopy (Figure A-VIII-15 to Figure A-VIII-18). The seeded cells were spread and efficiently attached to either PS or glass cell cultivated control substrates (Figure A-VIII-17 and Figure A-VIII-18). A similar phenomenon was observed using photocrosslinked CB-100 surfaces (Figure A-VIII-15C-D, and Figure A-VIII-16B) where the population of spread cells was larger than that of aggregated cell islets. On the other hand, cells incubated on pristine CB-100 mostly aggregated as islets (Figure A-VIII-15A-B, and Figure A-VIII-16A). These responses could be due to the softness of the polymeric surfaces, yet there could be other factors of these interactions that are important, including subtle morphological alterations, such as the mesh size of the loose network. These alterations would affect spreading through the focal adhesion complex formation, including through proteins such as transmembrane integrins, vinculin, and talin. The cells could potentially reach a substrate beneath a very soft (fluid-like) pristine CB-100. Similar results were previously reported for different substrates interacting with cells.²³ Thus, cells may not be

able to effectively adhere to soft and fluid-like surfaces of pristine CB-100. The crosslinked bottlebrush network with a smaller mesh size and a slightly harder surface may provide multiple sites that enable the seeded cells to adhere more efficiently through their focal adhesion complexes.

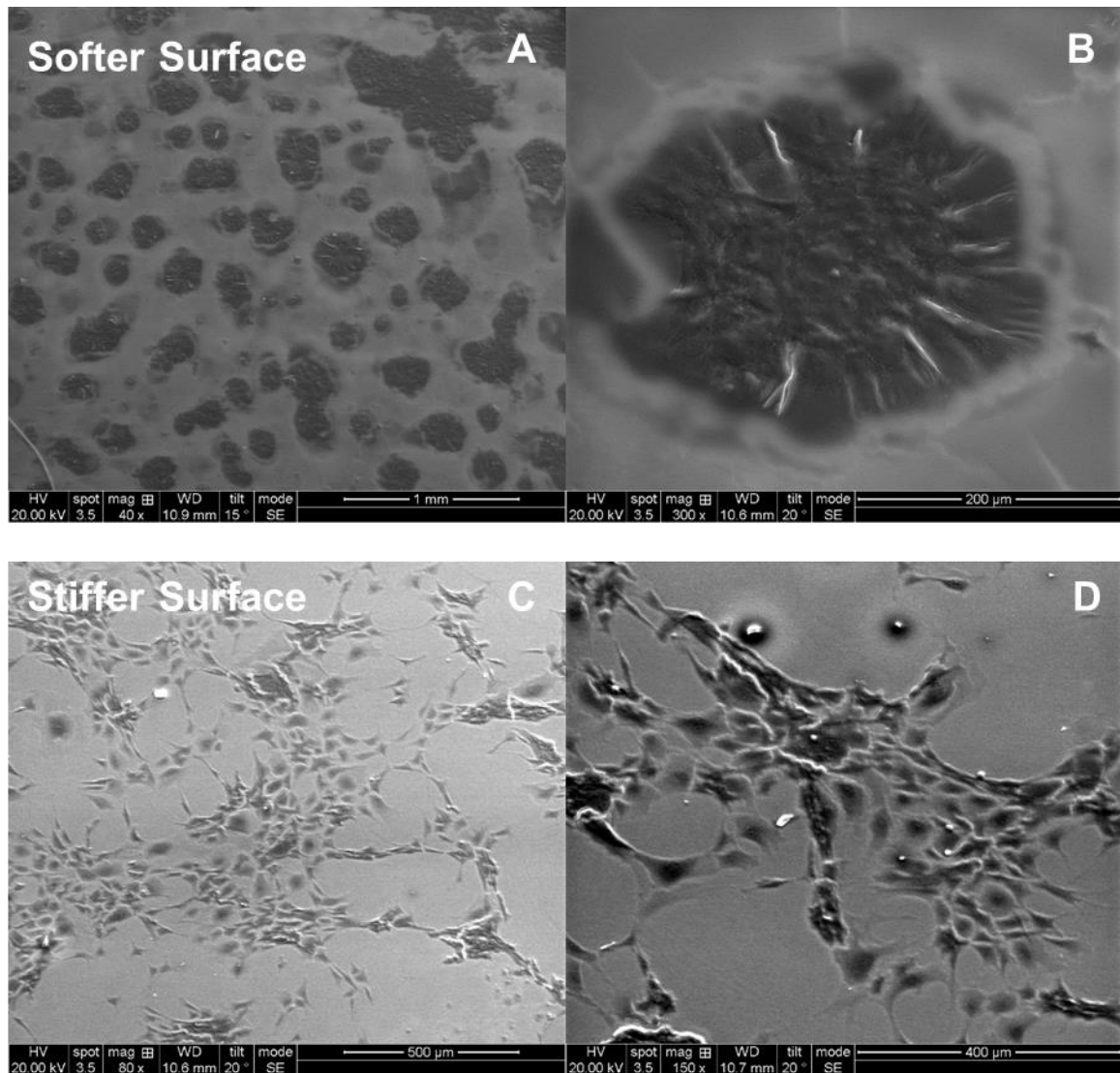


Figure A-VIII-15. Cell adhesion behavior on the softer surface (pristine brushes, A and B) and stiffer surface (crosslinked brushes, C and D).

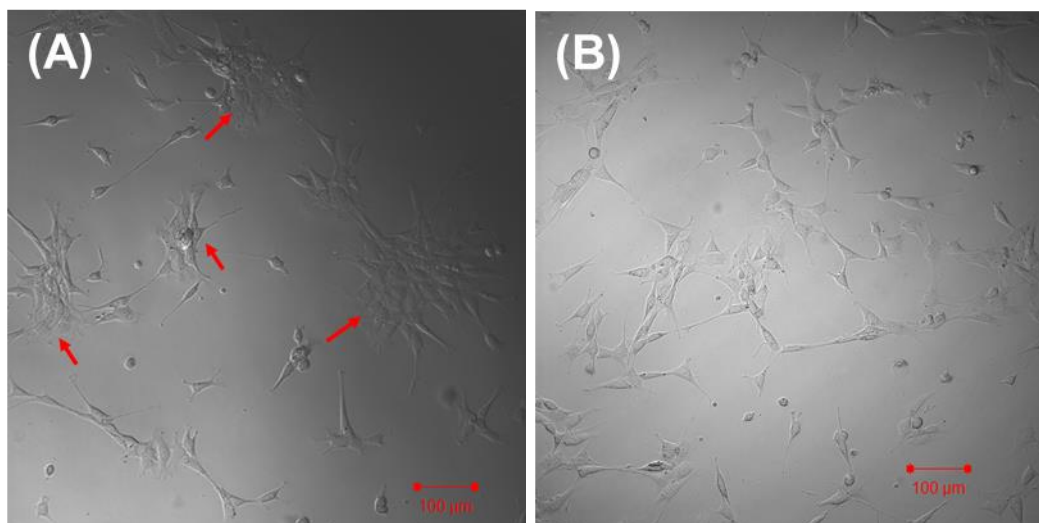


Figure A-VIII-16. Differential interference contrast microscopy images of the NIH 3T3 cells on the pristine (A, arrows indicate aggregating cells) and photocrosslinked (B) CB-100 coated substrates.

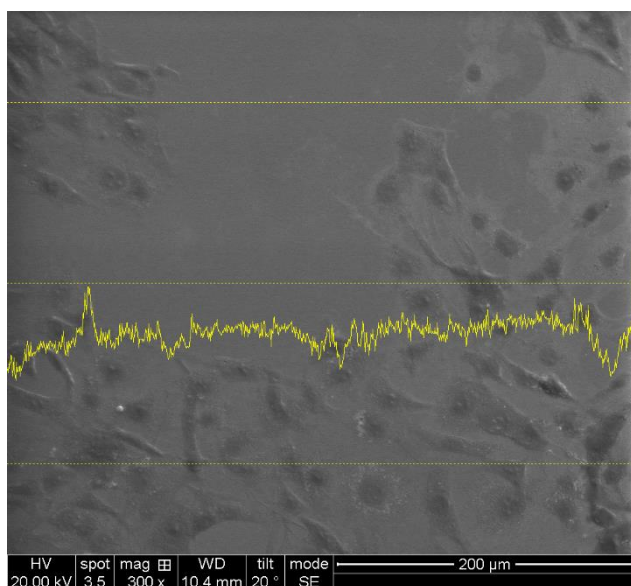


Figure A-VIII-17. SEM images of the NIH3T3 cells on glass substrate (control

experiments).

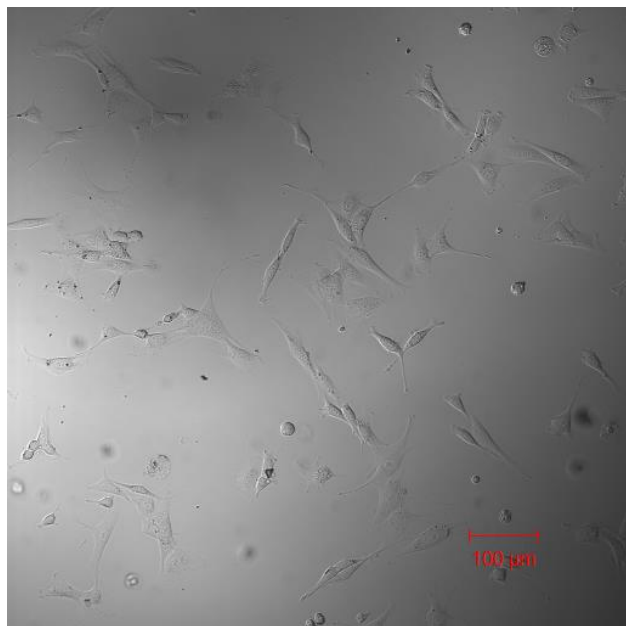


Figure A-VIII-18. Differential interference contrast microscopy images of the NIH 3T3 cells on polystyrene (petri dish) substrate (control experiments).

A-VIII. 3. Summary

Molecular bottlebrushes with coumarin chain end functionalities were successfully synthesized by ATRP and post-polymerization modification reactions. Photocrosslinking of molecular bottlebrushes resulted in supersoft elastomeric materials as confirmed by dynamic mechanical analysis. The elastic modulus can be tuned by photocrosslinking and photoscission of coumarin units *via* UV irradiation. Resulting materials were biocompatible and potentially can be used to investigate cell behavior on surfaces and morphology with variable softness by UV irradiation.

A-VIII. 4. Experimental Section

Materials. The inhibitor was removed from 2-(trimethylsilyloxy)ethyl methacrylate (HEMA-TMS, Scientific Polymer Products) and *n*-butyl acrylate (BA, Aldrich) by passing them through a column filled with basic alumina. CuBr (98%, Acros) was purified by stirring with glacial acetic acid followed by filtering and washing the resulting solid with isopropanol. Live/Dead stain for assessing cell viability was purchased from Invitrogen. All other reagents and solvents were purchased from Aldrich and used as received without further purification.

Measurements. The apparent molecular weights and molecular weight distributions of the synthesized polymers were characterized using a size exclusion chromatography system, consisting of a Waters 510 HPLC pump, three Waters UltraStyragel columns (10^2 , 10^3 , and 10^5 Å), and a Waters 410 differential refractive index detector, with a THF flow rate of 1.0 mL/min. Poly(methyl methacrylate) was used as calibration standards employing WinGPC software from Polymer Standards Service (PSS). ^1H NMR spectra were collected in CDCl_3 at 30 °C using a Bruker 300 MHz spectrometer. UV-visible spectra were recorded using an Agilent 8453 UV-visible spectrophotometer. A Carl Zeiss LSM 510 Meta NLO Confocor 3 inverted spectral confocal microscope was used to characterize cell growth and biocompatibility. Scanning electron microscopy (SEM, JEOL JSM-6060) was used for cell adhesion behavior on to the photocrosslinker bottlebrush surfaces.

Dynamic mechanical analysis (DMA). Dynamic mechanical analyses were performed using an Advanced Rheometric Expansion System (ARES) equipped with a force-rebalanced transducer. Plate-plate geometry with plate diameters of 6 mm was used.

The gap between the plates was approximately 0.5 mm. Experiments were performed under dry nitrogen atmosphere. Shear deformation was applied under conditions of controlled deformation amplitude that was kept in the range of the linear viscoelastic response of the studied samples. The isochronal temperature dependencies of G' and G'' were determined at $\omega = 10$ rad/s.

Procedure for synthesis of 7-(6-hydroxyhexyl)oxycoumarin. 7-hydroxycoumarin (1.0 g, 6.2 mmol), 6-bromohexanol (1.4 g, 7.4 mmol) were dissolved in a mixture of acetonitrile and DMF (15 mL, 2/1 (by v/v)), in a round bottom flask. Potassium carbonate (1.3 g, 9.3mmol) and potassium iodide (1.2 g, 7.4 mmol) were added to the solution. After the mixture was refluxed for 20 h, the solution was filtrated to remove the solid. The filtrate was dissolved with ethyl acetate and the organic phase was washed with brine four times. After drying on anhydrous magnesium sulfate, the solvent was evaporated and the residue was dissolved with a small amount of chloroform. The product was precipitated from solution into hexanes. The pure white yellow powder product was obtained (yield: 1.4 g, 83 %). The product was further characterized by ^1H NMR (Figure A-VIII-3 below).

Procedure for synthesis of alkyne coumarin. 7-(6-hydroxyhexyl)oxycoumarin (6.4 g, 24 mmol) was dissolved in dichloromethane (50 mL) with propiolic acid (1.7 g, 24 mmol). The mixture of N,N'-dicyclohexylcarbodiimide (5.0 g, 24 mmol) and 4-dimethylaminopyridine (0.3 g, 2.4 mmol) in 50 mL of dichloromethane was slowly added to the previous reaction flask and stirred overnight. After the reaction, the residual solvent was removed by evaporation and the product was purified by silica gel chromatography (eluent; chloroform/MeOH = 100/2). The purified product was a yellow viscous liquid

(yield: 3.0 g, 40%). The compound was characterized by ^1H NMR (Figure A-VIII-3 above).

Procedure for azidation of the PBA-Br side chains. The PBA brush -Br (0.2 g, 0.7×10^{-1} mmol of PBA-Br group, $\text{DP}_{\text{PBA}} = 20$, prepared by following a published procedure²⁴⁾ and sodium azide (50 mg, 7.7×10^{-1} mmol) were dissolved in 15 mL DMF. The mixture was stirred at room temperature overnight. The reaction mixture was transferred to a membrane (MWCO = 3500) and dialysis was performed in 1 L THF for 24 h to replace DMF with THF for easier precipitation. Then, the solution was precipitated into MeOH/water = 7/3 mixture twice. The polymer was separated and dried under vacuum.

Procedure for synthesis of PBA molecular bottlebrushes with coumarin chain ends. The PBA brush with azide chain end functionality (0.1 g, 3.6×10^{-2} mmol of PBA- N_3 group, $\text{DP}_{\text{PBA}} = 20$), alkyne coumarin (23 mg, 7.2×10^{-2} mmol), and *N,N,N',N',N''*-pentamethyldiethylenetriamine (PMDETA, 1.6 mg, 9.4 μmol) were dissolved with 5 mL anisole and the reaction mixture was degassed four times in freeze-pump-thaw cycles. During the third cycle, the flask was filled with nitrogen and CuBr (1.3 mg, 9.4 μmol) was added to the frozen mixture. The flask was sealed and filled with nitrogen. The mixture was stirred at room temperature for 15 h. The reaction was stopped by opening the flask to air and the reaction mixture was concentrated by evaporating the solvent. The polymer was purified by precipitation into methanol. The polymer was separated and dried under vacuum. The successful reaction was confirmed by the appearance of the coumarin peaks at the NMR traces (Figure A-VIII-6) and the disappearance of the azide peak at the IR spectra (Figure A-VIII-2).

Determining coumarin chain-end functionalities. The coumarin chain-end functionalities were determined by ^1H NMR, compared to the proton near the triazole peak (Figure A-VIII-6, c peak, $1H$) and coumarin peak (j , $1H$) from coumarin. The NMR results of CB-100 showed the peak ratio j/c as 0.98 ± 0.02 , nearly complete conversion of coumarin. In case of CB-100, the ratio showed 0.09 ± 0.01 , which indicated that ca. 9% of chain-ends were converted to coumarin.

Procedure for cytotoxicity measurements. To quantify the growth of cells on the softer and stiffer coumarin PBA brush polymers, a methylthiazol tetrazolium (MTT) assay were used (Figure A-VIII-14). Drops of the polymer solution in toluene (10 wt% polymers) were spin coated on 22×22 mm glass coverslips at 500 rpm for 30 sec and incubated overnight in an 80°C oven. For the stiffer polymers, the coverslips were irradiated with UV light at a wavelength of 320 nm for 60 min. The coverslips were then placed in 24 well plates and sterilized by rinsing with 70% ethanol solution before washing with phosphate buffered saline twice. NIH 3T3 cells were then seeded in each well at a density of 3×10^4 cells per well in 10% fetal bovine serum supplemented Dulbecco's Modified Eagle's Medium (DMEM) and cultured in the incubator overnight. To conduct the MTT test, 10 μL of the MTT reagent (ATCC) was added to each well at 24 h and 48 h after seeding. The American Type Culture Collection (ATCC) protocol was followed and the cells were incubated for 2 to 4 h until the purple precipitate was visible. Then 100 μL of MTT detergent reagent (ATCC) was added to each well at room temperature for 2 h. Using a plate reader, the absorbance at 570 nm was recorded for cells plated on glass coverslips (control), and on glass coverslips coated with the soft and stiff coumarin brush polymer

films at 1 and 2 days after the cells were seeded. The absorbance readings for all the wells were normalized with respect to the well with the highest absorbance reading in the control case on Day 2. The images were then captured using a Zeiss confocal microscope using fluorescent excitation according to manufactures instructions. On Day 1, the average normalized cell count for the control, and the soft and stiff CB-100 films were 0.365, 0.342 and 0.347, respectively, with standard deviations of 0.046, 0.066 and 0.057, respectively ($n = 24$). On Day 2, the average normalized cell count for the control, and the soft and stiff CB-100 films were 0.870, 0.836 and 0.860, respectively, with standard deviations of 0.059, 0.114 and 0.082, respectively ($n = 24$). Student's t-tests were conducted on these datasets. On Day 1, the average normalized cell count for the control compared to that of the soft and stiff coumarin brush films had two-tailed P values of 0.168 and 0.235, respectively, and thus are not statistically significant (as $P > 0.1$). On Day 2, the average normalized cell count for the control compared to the soft and stiff CB-100 films had two-tailed P values of 0.201 and 0.63 respectively. The differences are not statistically significant (as $P > 0.1$). Overall, there is no statistical difference in cell viability and proliferation of cells grown on the glass cover slips, when compared to cells grown on the soft and stiff CB-100 polymers. Therefore, this quantitative data supports that CB-100 polymers are useful in cell culture applications.

A-VIII. 5. References

1. Mark, J. E., *Prog. Polym. Sci.* **2003**, 28 (8), 1205-1221.
2. Terentjev, E. M., *Nature Materials* **2002**, 1 (3), 149-150.
3. Addad, J. P. C., *Physical properties of polymeric gels*. J. Wiley: 1996.

4. (a) Neugebauer, D.; Zhang, Y.; Pakula, T.; Sheiko, S. S.; Matyjaszewski, K., *Macromolecules* **2003**, *36* (18), 6746-6755; (b) Pakula, T.; Zhang, Y.; Matyjaszewski, K.; Lee, H. I.; Boerner, H.; Qin, S. H.; Berry, G. C., *Polymer* **2006**, *47* (20), 7198-7206.
5. Mpoukouvalas, A.; Li, W. W.; Graf, R.; Koynov, K.; Matyjaszewski, K., *ACS Macro Letters* **2013**, *2* (1), 23-26.
6. (a) Zhang, M.; Mueller, A. H. E., *J. Polym. Sci., Part A: Polym. Chem.* **2005**, *43* (16), 3461-3481; (b) Sheiko, S. S.; Sumerlin, B. S.; Matyjaszewski, K., *Prog Polym Sci* **2008**, *33* (7), 759-785; (c) Lee, H.-i.; Pietrasik, J.; Sheiko, S. S.; Matyjaszewski, K., *Prog Polym Sci* **2010**, *35* (1-2), 24-44; (d) Rzaev, J., *Acs Macro Letters* **2012**, *1* (9), 1146-1149.
7. (a) Djalali, R.; Li, S.-Y.; Schmidt, M., *Macromolecules* **2002**, *35* (11), 4282-4288; (b) Zhang, M.; Teissier, P.; Krekhova, M.; Cabuil, V.; Mueller, A. H. E., *Prog. Coll. Polym. Sci.* **2004**, *126*, 35-39; (c) Yuan, J.; Xu, Y.; Walther, A.; Bolisetty, S.; Schumacher, M.; Schmalz, H.; Ballauff, M.; Mueller, A. H. E., *Nat. Mater.* **2008**, *7* (9), 718-722.
8. (a) Cheng, C.; Khoshdel, E.; Wooley, K. L., *Macromolecules* **2007**, *40* (7), 2289-2292; (b) Huang, K.; Rzaev, J., *J. Amer. Chem. Soc.* **2009**, *131* (19), 6880-6885; (c) Mullner, M.; Yuan, J. Y.; Weiss, S.; Walther, A.; Fortsch, M.; Drechsler, M.; Muller, A. H. E., *J. Amer. Chem. Soc.* **2010**, *132* (46), 16587-16592; (d) Ling, J.; Zheng, Z.; Köhler, A.; Müller, A. H. E., *Macromol. Rapid Commun.* **2014**, *35* (1), 52-55.
9. (a) Jha, S.; Dutta, S.; Bowden, N. B., *Macromolecules* **2004**, *37* (12), 4365-4374; (b) Xia, Y.; Kornfield, J. A.; Grubbs, R. H., *Macromolecules* **2009**, *42* (11), 3761-3766; (c) Rzaev, J., *Macromolecules* **2009**, *42* (6), 2135-2141.
10. (a) Park, I.; Sheiko, S. S.; Nese, A.; Matyjaszewski, K., *Macromolecules* **2009**, *42* (6), 1805-1807; (b) Li, Y.; Nese, A.; Lebedeva, N. V.; Davis, T.; Matyjaszewski, K.; Sheiko, S. S., *J. Am. Chem. Soc.* **2011**, *133* (43), 17479-17484.
11. Fenyves, R.; Schmutz, M.; Horner, I. J.; Bright, F. V.; Rzaev, J., *J. Am. Chem. Soc.* **2014**, *136* (21), 7762-7770.
12. (a) Bolton, J.; Bailey, T. S.; Rzaev, J., *Nano Lett.* **2011**, *11* (3), 998-1001; (b) Wu, D. C.; Nese, A.; Pietrasik, J.; Liang, Y. R.; He, H. K.; Kruk, M.; Huang, L.; Kowalewski, T.; Matyjaszewski, K., *Acs Nano* **2012**, *6* (7), 6208-6214.
13. (a) Wang, J.-S.; Matyjaszewski, K., *Journal of the American Chemical Society* **1995**, *117* (20), 5614-15; (b) Cheng, G.; Böker, A.; Zhang, M.; Krausch, G.; Müller, A. H. E., *Macromolecules* **2001**, *34* (20), 6883-6888; (c) Börner, H. G.; Beers, K.; Matyjaszewski, K.; Sheiko, S. S.; Möller, M., *Macromolecules* **2001**, *34* (13), 4375-4383; (d) Matyjaszewski, K.; Xia, J., *Chem. Rev.* **2001**, *101* (9), 2921-90; (e) Sheiko, S. S.; Prokhorova, S. A.; Beers, K. L.; Matyjaszewski, K.; Potemkin, I. I.; Khokhlov, A. R.; Möller, M., *Macromolecules* **2001**, *34* (23), 8354-8360; (f) Matyjaszewski, K.; Qin, S.; Boyce, J. R.; Shirvanyants, D.; Sheiko, S. S., *Macromolecules* **2003**, *36* (6), 1843-1849; (g) Lee, H.-i.; Matyjaszewski, K.; Yu, S.; Sheiko, S. S., *Macromolecules* **2005**, *38* (20), 8264-8271; (h) Lee, H.-i.; Jakubowski, W.; Matyjaszewski, K.; Yu, S.; Sheiko, S. S., *Macromolecules* **2006**, *39* (15), 4983-4989; (i) Lee, H.-i.; Pietrasik, J.; Matyjaszewski, K., *Macromolecules* **2006**, *39* (11), 3914-3920; (j) Pietrasik, J.; Sumerlin, B. S.; Lee, R. Y.; Matyjaszewski, K., *Macromol. Chem. Phys.* **2007**, *208* (1), 30-36; (k) Tsarevsky Nicolay, V.; Matyjaszewski, K., *Chem. Rev.* **2007**, *107* (6), 2270-99; (l) Yamamoto, S.-i.; Pietrasik, J.; Matyjaszewski, K., *Macromolecules* **2007**, *40* (26), 9348-9353; (m) Matyjaszewski, K.; Tsarevsky, N. V., *Nature Chem.* **2009**, *1* (4), 276-288; (n) Matyjaszewski, K.,

- Macromolecules* **2012**, *45* (10), 4015-4039; (o) Matyjaszewski, K., *Isr. J. Chem.* **2012**, *52* (3-4), 206-220; (p) Bolton, J.; Rzaev, J., *Macromolecules* **2014**, *47* (9), 2864-2874; (q) Hadasha, W.; Klumperman, B., *Polymer International* **2014**, *63* (5), 824-834; (r) Matyjaszewski, K.; Tsarevsky, N. V., *Journal of the American Chemical Society* **2014**, *136* (18), 6513-6533; (s) Burdyńska, J.; Li, Y.; Aggarwal, A. V.; Höger, S.; Sheiko, S. S.; Matyjaszewski, K., *Journal of the American Chemical Society* **2014**, *136* (36), 12762-12770; (t) Banquy, X.; Burdyńska, J.; Lee, D. W.; Matyjaszewski, K.; Israelachvili, J., *Journal of the American Chemical Society* **2014**, *136* (17), 6199-6202; (u) Elsen, A. M.; Li, Y.; Li, Q.; Sheiko, S. S.; Matyjaszewski, K., *Macromolecular Rapid Communications* **2014**, *35* (2), 133-140; (v) Li, Y.; Nese, A.; Matyjaszewski, K.; Sheiko, S. S., *Macromolecules* **2013**, *46* (18), 7196-7201; (w) Sheiko, S. S.; Zhou, J.; Arnold, J.; Neugebauer, D.; Matyjaszewski, K.; Tsitsilianis, C.; Tsukruk, V. V.; Carrillo, J.-M. Y.; Dobrynin, A. V.; Rubinstein, M., *Nat Mater* **2013**, *12* (8), 735-740.
14. (a) Chiefari, J.; Chong, Y. K.; Ercole, F.; Krstina, J.; Jeffery, J.; Le, T. P. T.; Mayadunne, R. T. A.; Meijs, G. F.; Moad, C. L.; Moad, G.; Rizzardo, E.; Thang, S. H., *Macromolecules* **1998**, *31* (16), 5559-5562; (b) Nese, A.; Kwak, Y.; Nicolay, R.; Barrett, M.; Sheiko, S. S.; Matyjaszewski, K., *Macromolecules* **2010**, *43* (9), 4016-4019; (c) Zheng, Z.; Ling, J.; Müller, A. H. E., *Macromol. Rapid Commun.* **2014**, *35* (2), 234-241; (d) Nese, A.; Li, Y.; Averick, S.; Kwak, Y.; Konkolewicz, D.; Sheiko, S. S.; Matyjaszewski, K., *ACS Macro Lett* **2012**, *1* (1), 227-231.
15. Hadjichristidis, N.; Zhao, h.; Gnanou, Y., *Polymer Chemistry* **2014**.
16. Obi, M.; Morino, S.; Ichimura, K., *Chem. Mater.* **1999**, *11* (3), 656-664.
17. Trenor, S. R.; Shultz, A. R.; Love, B. J.; Long, T. E., *Chem. Rev.* **2004**, *104*, 3059.
18. Clarke, P. N.; Fawcett, J., *Macromolecules* **2014**, *47*, 1656-1663.
19. He, J.; Tong, X.; Zhao, Y., *Macromolecules* **2009**, *42* (13), 4845-4852.
20. Iliopoulos, K.; Krupka, O.; Gindre, D.; Salle, M., *J. Am. Chem. Soc.* **2010**, *132* (41), 14343-14345.
21. (a) Kolb, H. C.; Finn, M. G.; Sharpless, K. B., *Angew. Chem. Int. Ed.* **2001**, *40* (11), 2004-2021; (b) Golas, P. L.; Matyjaszewski, K., *Chem. Soc. Rev.* **2010**, *39* (4), 1338-1354.
22. (a) Chen, Y.; Geh, J.-L., *Polymer* **1996**, *37*, 4481-4486; (b) Nagata, M.; Yamamoto, Y., *J. Polym. Sci., Part A Polym. Chem.* **2009**, *47*, 2422-2433.
23. Gonzalez-Rodriguez, D.; Guevorkian, K.; Douezan, S.; Brochard-Wyart, F., *Science* **2012**, *338* (6109), 910-917.
24. Nese, A.; Sheiko, S. S.; Matyjaszewski, K., *Eur. Polym. J.* **2011**, *47* (5), 1198-1202.